

**FEASIBILITY STUDY
OF THE APPLICATION OF THE
ACOUSTIC EMISSION TECHNIQUE
TO CONCRETE BRIDGES**

Sabrina Colombo

PhD

The University of Edinburgh

May 2003



Declaration

I hereby declare that this thesis and the work discussed was carried out solely by Sabrina Colombo under the supervision of Prof. M.C. Forde and Prof. I.G. Main, unless otherwise stated within the text.

Sabrina Colombo

May 2003

Abstract

Bridges represent a national asset of functional and cultural significance. From the late 1960's to late 1970's the motorway construction boom gave rise to a large number of new concrete highway bridges, as concrete was perceived to be "maintenance free" and able to give bridges a 120 year life span. As a consequence, concrete bridges represent the majority of the UK motorways and trunk road bridge stock. Now that their average age is of the order of 25-35 years, they are starting to show signs of deterioration, demonstrating that the original construction expectation was too optimistic. The US bridge stock is older and faces a similar situation. Consequently, the necessity to monitor and verify the performance and safety for ongoing usage of concrete bridges is a matter of urgent concern. The strategy for the bridge authorities was to undertake an inspection and then to either "pass" or "fail" the bridge. Recently it became clear that bridges in visually good condition sometimes failed the inspection, thus the Highways Agency proposed the introduction of a third category of "monitoring" for those bridges that passed or failed the inspection by a small margin. This monitoring might be undertaken by non-destructive methods.

The purpose of this thesis is to assess the feasibility of the Acoustic Emission Technique as one of these methods. Acoustic emission testing was widely used in the nuclear and the oil industries to remotely monitor critical structures such as pressure vessels and storage tanks. Later on, the technique started to be used in seismic analysis and more recently in Japan to monitor concrete structures damaged from earthquakes. A detailed description of the AE method and principle is given.

This thesis addresses the issue of the feasibility of the Acoustic Emission Technique as a possible and effective way of monitoring the safety of concrete bridges. This includes an understanding of how to use and apply the method, a study of the different types of analyses and the finding of alternative ways to process and interpret the data. The key factors of an AE test are identified and discussed and a draft of an experimental protocol of AE application to concrete bridges structures is drawn. A conventional *b*-value analysis is proposed as a way to analyse data, and the AE source location analysis was investigated. A new parameter, named "relaxation ratio" is defined to characterize the damage of bridge beams. The potential of the SoundPrint system and the Moment Tensor method are studied. Finally, a field experiment was carried out to verify the feasibility of the application of the AE method to a real structure.

Acknowledgements

The undertaking of this thesis has not only given me the opportunity to improve my knowledge, but also to live and travel in different places, to meet several interesting people and therefore to grow and enrich myself both professionally and personally.

The work described in thesis was sponsored by the Highways Agency (London), Contract No.3/320, and its financial support is greatly acknowledged. Thanks are particularly due to P. Das and J. Halliday (H-A). A mention must be made of the Small Project Grants of the University of Edinburgh Development Trust and the Academic Frontiers Student Exchange Promotion Program Scholarship of the Japanese Ministry of Education and Culture, that supported the extra expenses for my travel and stay in Japan.

I wish to thank Professor Forde and Professor Main for their supervision and advice during the undertaking of the thesis, and Associate Professor Shigeishi for all his teaching and support during the three months I was in Japan. Thanks are due to Antonis (Dr. Giannopoulos) for his advice, especially on computing issues. I also wish to acknowledge the facilities and the technical and support staff of the University of Edinburgh (UK) and of the University of Kumamoto (Japan). A mention needs to be made of the technical help and resources provided by the Transport Research Laboratory (Crowthorne, England); I am particularly indebted to Mike Hill, for his helpfulness. Further thanks to all the postgraduates and undergraduates of the Institute for Infrastructure and Environment, that helped me during these three years.

I cannot singularly mention all my friends as that would add an extra chapter to the thesis, but my thanks to them all - you all contributed to this work - thankyou! Sankari deserves to be mentioned, as she had the incredible patience to read through the whole thesis and try to make my English "less Italianized" - thankyou very much! A final thanks goes to my family, for always being there when I needed them - "grazie!".

Contents

Declaration	i
Abstract	ii
Acknowledgements	iii
Contents	iv
Lists of Figures	viii
Lists of Tables	xvii
Notations	xvii
1 Introduction	1
2 Concrete Bridges	8
2.1 History, Development and Problems of Bridge Building	8
2.2 Bridge Maintenance and Monitoring	14
2.3 Assessment of Bridges in the UK	16
2.4 Summary	20
3 Acoustic Emission	21
3.1 General Overview	21
3.2 Acoustic Emission in Concrete	23
3.3 Acoustic Emission in Masonry	27
3.4 Acoustic Emission in Bridges	28
3.5 AE Standards and Procedures	30
3.6 Summary	33

4	General Theory	35
4.1	Principle-Definition	35
4.2	AE Waves and the AE Signal	36
4.3	AE Effects	38
4.4	AE Monitoring and Analysis	39
4.5	Concrete and Fracture Mechanics	40
4.6	The “ <i>b</i> -value”	43
4.7	AE Source Location	46
4.8	Relaxation Ratio	47
4.9	Moment Tensor	49
4.9.1	Statement of the Problem	49
4.9.2	Moment Tensor Theory	50
4.9.3	Moment Tensor Applications	59
4.10	Summary AE: Advantages and Drawbacks	61
5	Equipment and Experimental Procedure	63
5.1	Instrumentation	63
5.2	MISTRAS and DiSP Systems	64
5.3	SoundPrint System	68
5.4	AE Sensors	70
5.4.1	Types of Sensors	71
5.4.2	Mounting and Coupling of the Transducers	71
5.4.3	Sensor Calibration	81
5.4.4	Location of Sensors	82
5.5	PUNDIT Equipment	82
5.6	AE Experimental Procedure	83
5.7	Summary	85
6	Laboratory Experiments	87
6.1	Edinburgh Laboratory Experiments	87
6.2	TRL Experiments	97
6.3	Kumamoto Laboratory Experiments	109
6.4	Summary	122

7	Analysis and Results	123
7.1	<i>b</i> -value Study	123
7.1.1	<i>b</i> -value Analysis	123
7.1.2	<i>b</i> -value Conclusions	133
7.2	AE Source Location Study	135
7.2.1	AE Source Location Analysis	136
7.2.2	AE Source Location Conclusions	139
7.3	Quantitative Assessment	145
7.3.1	Relaxation Ratio Analysis	148
7.3.2	A proposed new procedure for evaluating bridge beams integrity by acoustic emissions	156
7.3.3	Comparison with the NDIS Procedure	157
7.3.4	Relaxation Ratio Conclusions	158
7.4	SoundPrint (SP) Study	161
7.4.1	The SoundPrint Analyst Processing Software	161
7.4.2	Small scale tests - Analysis and Results	162
7.4.3	Beam CF1 - Analysis and Results	170
7.4.4	Beam HB2 - Analysis and Results	174
7.4.5	Differences and/or Similarities between the PAC and SP systems	180
7.4.6	SP Conclusions	181
7.5	Preliminary Moment Tensor Study	183
7.5.1	Moment Tensor Analysis	184
7.5.2	Moment Tensor Conclusions	191
7.6	Summary	199
8	Boghall Bridge Monitoring	201
8.1	Boghall Bridge	201
8.2	Preliminary Investigation	203
8.3	Monitoring Description	203
8.4	Analysis	206
8.4.1	Cracks, Metereological and Displacements Measurements	206
8.4.2	Attenuation Study	207
8.4.3	AE Source Location - PAC Data	211

8.4.4	AE Source Location - SP Data	215
8.4.5	<i>b</i> -value Analysis	217
8.4.6	Old Monitoring Comparison	219
8.5	Conclusions	220
9	Overall Discussion	223
10	Overall Conclusions	227
10.1	Bridges	227
10.2	AE Method	227
10.3	Analysis	229
10.3.1	<i>b</i> -value Analysis	229
10.3.2	Source Location	229
10.3.3	Relaxation Ratio	230
10.3.4	SoundPrint	230
10.3.5	Moment Tensor Analysis	231
10.3.6	Full - Scale Field Test	232
10.4	Further Work	233
	References	235
	Appendix A – Design Calculations of RC beams	252
	Appendix B – Failure Load Calculations of Kumamoto Beams	255
	Appendix C – P-wave Velocity Calculations of Kumamoto Beams	257
	Appendix D – MATLAB Programs	261
	Appendix E – Publications and Certificates	298

List of Figures

2.1	Schematic representation of a typical Greek Temple and a Roman Arch. Note the similarity between the architrave (i.e. the beam resting across the tops of the columns) and the beams tested as described in Chapter 6.	9
2.2	Drawing showing the terminology used in relation to bridges.	10
2.3	Schematic representation of different types of arch.	11
2.4	Schematic representation of main types of bridge. Note the similarity with the Greek and Roman typology in Figure 2.1.	12
2.5	Failure by wind of the Tacoma Narrows Bridge, Washington - from [Mock, 1949].	14
2.6	UK trunk road types of bridges.	18
3.1	Classification of damage according to NDIS-2421 - from [Ohtsu et al., 2002].	33
3.2	Summarized representation of the milestones and significant development in AE research and application.	34
4.1	A schematic diagram of the AE Principle, from the AE source to the AE sensors and from the Digital Signal Processing (DSP) to the processing phase.	36
4.2	Representation of the Snell's Law and of waves generated at a solid-solid interface.	37
4.3	Schematic diagram of AE parameters. The diagram illustrates how the different attributes are measured.	40
4.4	Frequency-magnitude distribution as fracturing develops. Note the relationship between b -value (the slope of the line) and cracking.	45

4.5	Schematic representation of earthquake sequences and AE activity phases. Each individual diagram shows the number of events, as a function of time, with the vertical dotted line being the time of the mainshock.	49
4.6	Force couples and Double Couple Forces representation [Shearer, 1999].	51
4.7	Dislocation model for a model crack [Shigeishi and Ohtsu, 1998].	52
4.8	Eigenvalue decomposition of the Moment Tensor in a Double Couple (DC), Compensated Linear Vector Dipole (CLVD) and hydrostatic part - adapted from [Shigeishi and Ohtsu, 1998].	58
5.1	MISTRAS and DiSP systems.	65
5.2	PAC's AE sensors.	65
5.3	PAC's settings parameters.	68
5.4	SoundPrint System and sensor.	69
5.5	Photos of the equipment, hammer and ball bearing and concrete slab. .	74
5.6	Time Domain Signals of Superglue and Sticky Pads.	75
5.7	Concrete slab results: Time Domain (left) and Power spectral density (right) plots for the different couplant types, shown in comparison with each other.	77
5.8	Transducer mounting substances: Testing set up.	78
5.9	Concrete cube results: Time-Domain Signals for the three candidate couplants.	79
5.10	Concrete cube results: Power Spectral Density plots for the three candidate couplants.	80
5.11	Sensor Clamps.	81
5.12	Draft of the AE application protocol, showing the key steps and factors.	86
6.1	Phases of the beam making process.	88
6.2	Graphs of the two load cells calibration.	89
6.3	Load history of the beams of Edinburgh experiments.	91
6.4	Design details, test configuration and resonant sensor location (S1 to S8) of beam BF2.	92
6.5	Design details, test configuration and resonant sensor location (S1 to S8) of beam BF3.	92

6.6	Design details, test configuration and sensor location (resonant: S1 to S4 - broadband WD type: W1 to W8 - SoundPrint: SP1 to SP4) of beam BF4.	93
6.7	Design details, test configuration and sensor location (resonant: S1 to S4 - broadband WD type: W1 to W8 - SoundPrint: SP1 to SP4) of beam BF2c.	93
6.8	Design details, test configuration and sensor location (resonant: S1 to S4 - broadband WD type: W1 to W8 - SoundPrint: SP1 to SP4) of beam BF5.	94
6.9	Design details, test configuration and sensor location (resonant: S1 to S4 - broadband WD type: W1 to W8 - SoundPrint: SP1 to SP4) of beam BF6.	94
6.10	Photos of Edinburgh beams.	98
6.11	Final crack pattern of beam BF2.	99
6.12	Final crack pattern of beam BF3.	99
6.13	Final crack pattern of beam BF4.	99
6.14	Final crack pattern of beam BF2c.	99
6.15	Final crack pattern of beam BF5.	99
6.16	Final crack pattern of beam BF6.	100
6.17	Photos of Edinburgh beam failures. Note the visible shear dislocation of the grid pattern for test BF5.	100
6.18	Photo of instrumented beam CF1.	102
6.19	Photo of beam CF1 failure.	103
6.20	Design details, test configuration and sensor location (resonant: S1 to S6 - SoundPrint: SP1 to SP12) of beam CF1.	104
6.21	Design details, test configuration and sensor location (resonant: S1 to S8 - SoundPrint: SP1 to SP8) of beam HB2.	105
6.22	Load history of beam HB2.	107
6.23	Beam HB2. Test configuration and instrumentation.	108
6.24	Beam HB2. Shear Failure.	108
6.25	Phases of the casting of the beams in Kumamoto Laboratory.	111
6.26	Load history of the beams of Kumamoto beams experiments.	112

6.27	Design details, test configuration and broadband sensor location (UT-1000 type: U1 to U8) of beams K1 and K2.	113
6.28	Design details, test configuration and broadband sensor location (UT-1000 type: U1 to U8) of beam K3.	113
6.29	Design details, test configuration and broadband sensor location (UT-1000 type: U1 to U8) of beam K4.	113
6.30	Design details, test configuration and broadband sensor location (UT-1000 type: U1 to U8) of beam KL1.	114
6.31	Design details, test configuration and broadband sensor location (UT-1000 type: U1 to U8) of beam KL2.	114
6.32	Photo of instrumented beam at Kumamoto Laboratory.	116
6.33	Photos of failed beams at Kumamoto Laboratory.	117
6.34	Failure of a beam at Kumamoto Laboratory.	118
6.35	Set up of the concrete sample for the Moment Tensor test.	120
6.36	Failure the concrete sample for the Moment Tensor test.	120
7.1	Example of calculation of b -values for channel 2 during the loading cycle number 2. The graphs represent the log-frequency-magnitude chart with the best fitting curves shown as straight lines, and the best fitting slope or b -value shown.	125
7.2	b -value over time calculated with using groups of respectively 70 (blue line), 100 (red line) and 130 (green line) events.	126
7.3	b -value over time for channels 3 (top) and 7 (bottom) during load cycle number 2 - the load is shown by the dashed line with a scale shown on the vertical axis on the right. The localisation predicted on the basis of the minimum b -value is shown by the arrow. The bar errors of the statistical calculation in the b -value are shown.	128
7.4	Overlapping of b -value (blue line: left vertical axis) and normalised damage parameter (red dashed line: right vertical axis) for channels 3 (top) and 7 (bottom) during load cycle number 2. The bar errors of the statistical calculation of the b -value are shown.	129
7.5	Variation of the maximum and minimum b -value for channels 3 (top) and 7 (bottom) during all the cycles of the whole experiment. The vertical lines show the different identified cracking stages indicated by the arrows. 131	

7.6	A sketch of the fracture process developments during the different stages of the loading. The dotted line outlines the location of the steel reinforcement. Note the inclined shear cracks near the edges of the sample.	132
7.7	Frequency vs. Amplitude charts and corresponding b -values during the whole cycle number 2 for each channel.	133
7.8	Frequency vs. Amplitude charts and corresponding b -values during the whole cycle number 6 for each channel.	134
7.9	AE Source location results for beam BF2 and for cycle number 2. Each graph shows the amount of events (left column) and energy (right column) at each linear location along the beam, compared to the location of the macrocracks (upper diagram in each case) at the end of the specific cycle, with the dashed lines to aid comparison. The thick dark blue lines represent the new cracks, whilst the light blue lines indicate the presence or extension of pre-existing cracks. The position alongside the beam, expressed in meters, is shown on the horizontal axis. The green squares along the top of the horizontal axis represent the position of the transducers used to calculate the source location. . .	139
7.10	AE Source location results for beam BF2, for cycle numbers from 3 to 6, plotted as for Figure 7.9. The “oil” annotation refers to the technical problem described in section 6.1.	140
7.11	AE Source location results for beam BF2, for cycle numbers from 7 to 10, plotted as for Figure 7.9. The “oil” annotation refers to the technical problem described in section 6.1.	141
7.12	AE Source location results for beam BF3, for cycle numbers from 2 to 6, plotted as for Figure 7.9.	142
7.13	AE Source location results for beam BF3, for cycle numbers from 7 to 9, plotted as for Figure 7.9.	143
7.14	AE Source location results relative to the resonant sensors on beam BF6 for cycle numbers from 1 to 5, plotted as for Figure 7.9.	144
7.15	AE Source location results relative to the resonant sensors on beam BF6 for cycle numbers 6 and 7, plotted as for Figure 7.9.	145
7.16	AE Source location results relative to the broadband sensors on beam BF6, for cycle numbers from 1 to 5, plotted as for Figure 7.9.	146

7.17	AE Source location results relative to the broadband sensors on beam BF6, for cycle numbers 6 and 7, plotted as for Figure 7.9.	147
7.18	Relaxation ratio results of Group 1: beams BF2, BF3, BF4 and BF2c. The red line corresponds to a relaxation ratio equal to one. The dots represent the values of the relaxation ratio (on the vertical axis) for each relative number of cycle, that can be read on the horizontal axis.	150
7.19	Relaxation ratio results of Group 2: beams K1, K2, K3, K4, KL1 and KL2; plotted as for Figure 7.18.	151
7.20	Relaxation ratio results of Group 3: beams BF5 and BF6; plotted as for Figure 7.18.	152
7.21	NDSI assessment for beam BF4, using all data. The numbers indicate the loading cycle and the red lines define the different areas of damage.	158
7.22	NDSI assessment for beam BF4, using only channel 5 data. The numbers indicate the loading cycle and the red lines define the different areas of damage.	159
7.23	NDSI assessment for beam K2, using all data. The numbers indicate the loading cycle and the red lines define the different areas of damage.	159
7.24	NDSI assessment for beam K2, using only channel 5 data. The numbers indicate the loading cycle and the red lines define the different areas of damage.	160
7.25	SoundPrint Decision Tree.	163
7.26	Location of events recorded by the SoundPrint systemn on beams BF4 and BF5. The different colors indicate different loading cycles, whilst the diameter is proportional to the number of events.	164
7.27	Location of events recorded by the SoundPrint systemn on beams BF6 and BF2c. The different colors indicate different loading cycles, whilst the diameter is proportional to the number of events.	165
7.28	PAC AE location for the full test of beams BF4 and BF5.	167
7.29	PAC AE location for the full test of beams BF6 and BF2c.	168
7.30	AE location pattern emerging for beams BF4, BF6 and BF2c. The different colors indicate different loading cycles, whilst the diameter is proportional to the number of events.	169

7.31	Histogram representation of the recorded and located SP hits for beams BF4, BF5, BF6 and BF2c.	170
7.32	Histogram representation of located hits recorded by SoundPrint (SP), resonant (R6I) and broadband (WD) sensors.	171
7.33	Location of SP events during initial loading stage for beam CF1. The different colors indicate different loading stages.	171
7.34	Location of SP events during the whole experiment for beam CF1. The different colors indicate different loading stages.	172
7.35	Distribution of SP events for beam CF1.	173
7.36	Cumulative energy distribution for SP events for beam CF1.	174
7.37	PAC cumulative energy distribution for beam CF1.	175
7.38	Location of SP events during the whole experiment for beam HB2. The different colors indicate different loading stages.	175
7.39	Location of SP events during different load ranges for beam HB2.	176
7.40	Histogram representation of the cumulative energy of SP events for beam HB2.	177
7.41	Histogram representation of the cumulative energy of SP events as a function of load for beam HB2.	178
7.42	PAC energy as a function of location and loading cycle for beam HB2.	179
7.43	PAC energy as a function of load for beam HB2.	180
7.44	Arrival Time P_1 and First Motion Amplitude P_2 , from [Ohtsu and Shigeishi, 2002].	186
7.45	Output format of SiGMA results - the red comments have been added as further explanation.	188
7.46	Schematic diagram of the Moment Tensor procedure.	190
7.47	Moment Tensor results: First stage of the cracking on the sample. The red symbol represents a mixed-mode crack; the circle represents the crack surface, whilst the arrow indicates the P-axis, i.e. the direction of the crack extension. The white cylinders or circles represent the sensors. The grey circle and line indicates the hole and notch on the sample.	192
7.48	Moment Tensor results: Second stage of the cracking, plotted as in Figure 7.47. The different colors (red, green and blue) indicate different crack types (mixed-mode, tensile and shear).	193

7.49	Moment Tensor results: Third stage of the cracking, plotted as in Figure 7.48.	194
7.50	Moment Tensor results: Fourth stage of the cracking, plotted as in Figure 7.48.	194
7.51	Moment Tensor results: Fifth stage of the cracking, plotted as in Figure 7.48.	195
7.52	Moment Tensor results: Sixth stage of the cracking, plotted as in Figure 7.48.	195
7.53	Moment Tensor results: Seventh stage of the cracking, plotted as in Figure 7.48.	196
7.54	Moment Tensor results: Eighth stage of the cracking, plotted as in Figure 7.48.	196
7.55	Moment Tensor results: Final stage of the cracking, plotted as in Figure 7.48.	197
7.56	Failure of the sample used for the Moment Tensor analysis.	197
7.57	Moment Tensor results, first rotated view: final stage of the cracking, plotted as in Figure 7.48.	198
7.58	Moment Tensor results, second rotated view: final stage of the cracking, plotted as in Figure 7.48.	198
8.1	Boghall bridge: masonry and concrete side; pre-existing cracks.	202
8.2	Boghall bridge: plan view.	204
8.3	Boghall bridge. Location of sensors: Case 1 and 2.	207
8.4	Monitoring schedule and meteorological data.	208
8.5	Boghall bridge: crack width (left) and bridge displacements (right).	210
8.6	AE activity location: Noise study. The location along the beam is indicated on the x-axis in meters, whilst the green squares (on top) indicate the AE sensors.	212
8.7	Boghall bridge. AE source location for Case 1, plotted as for Figure 8.6.	213
8.8	Boghall bridge. AE source location for Case 2, plotted as for Figure 8.6.	214
8.9	Boghall bridge. AE source location for Case 3, plotted as for Figure 8.6.	216
8.10	Boghall bridge. Location of the SP events, for Case 1. The green triangles represent the SP sensors, while the red circles show the located AE sources.	217

8.11 Boghall bridge. Location of the SP events, for Case 2, plotted as for Figure 8.10.	218
8.12 Boghall bridge. Location of the SP events, for Case 3, plotted as for Figure 8.10.	218
8.13 Boghall bridge: Frequency-magnitude plots and resulting b -value estimated on Beam 1.	219
8.14 AE energy location: old monitoring results, plotted as for Figure 8.6. . .	220

List of Tables

2.1	UK trunk road bridge stock.	18
3.1	Acoustic Emission applications.	24
3.2	Summary of the features of AE applications to bridges.	31
5.1	Transducers Mounting Substances: Final Assessment Table.	79
6.1	Summarized description of the beams of Edinburgh experiments.	95
6.2	Summary of the AE setting values for Edinburgh experiments.	96
6.3	Summary of the AE setting values for TRL experiments.	109
6.4	Summarized description of the beams of Kumamoto experiments.	115
6.5	Summary of the AE setting values for Kumamoto experiments.	118
6.6	Summary of the AE setting values for the Moment Tensor experiment.	121
7.1	<i>b</i> -value quantitative results.	134
8.1	Boghall Bridge: Instruments Settings.	205
8.2	Boghall bridge: Results of attenuation study. The red values indicate the starting amplitude, whilst the blue values are the amplitude recorded by the near sensor. The drop of the amplitude is shown in brackets.	209
8.3	Boghall bridge: SP recorded and located signals.	215

Notation

AE ... Acoustic Emission

BS ... British Standard

JSNDI ... Japanese Society for Nondestructive Inspections

NDT ... Non Destructive Testing

PAC ... Physical Acoustic Corporation

RC ... Reinforced Concrete

SP ... SoundPrint

v_P, v_S, v_R ... velocity of P, S and Rayleigh wave

ρ ... density of the material

k ... Bulk modulus

R ... reflection coefficient

I ... acoustic impedance

L ... wavelength

f ... frequency

w ... crack width

M_L ... Richter magnitude

N ... incremental frequency

A_{max} ... maximum amplitude of a seismic trace

A_{dB} ... peak amplitude of an AE signal

b ... slope of the frequency-magnitude relation

S ... rupture area

Ib ... Improved b -value

G ... Green's function

\bar{f} ... unit force

t ... time

\bar{x} ... location vector

\bar{u} ... displacement vector

\bar{n} ... normal vector

\bar{b} ... dislocation vector

$S(t)$... source time function

F ... crack surface

T ... Green's function of the 2nd type

C ... elastic constant

C_s ... calibration coefficient

σ ... stress

ϵ ... strain

λ, ν ... Lamè constants

E ... static modulus

Chapter 1

Introduction

If it is true that rivers are the natural boundaries between and within countries, then bridges represent a line of communication between otherwise separated areas. Bridges make up part of the asset of a country with their importance lying both in their functional and cultural significance. The art of bridge building developed throughout the different historical periods, from the Roman to the Medieval Age, from the Renaissance to the Industrial Revolution and the Modern Age, with each era assuming varied characteristics. The development and use of new materials also played a fundamental role in determining the birth of new types of bridges. Consequently, several types of bridges stand nowadays, having different characteristics, exhibiting different problems and bear witness to the cultural and technical evolution that has occurred throughout the centuries.

From the late 1960's to late 1970's the motorway construction boom in the UK gave rise to a large number of new highway bridges. Concrete was mainly chosen as the building material as it was perceived to be "maintenance free" and was thought to give bridges a cost effective life span of 120 years. As a result, concrete bridges represent the majority of the UK motorway and trunk road bridge stock. As of now their average age is of the order of 25-35 years and they are starting to show signs of deterioration, due to varied construction defects and general wear and tear. The original designers' expectation thus has been demonstrated to be too optimistic. The US bridge stock is older and faces a similar situation with concrete road bridges that are typically 40 years old and are approaching the end of their useful life [Frangopol and Kong, 2001]. This problem does not only concern the UK and the US but it has even wider implications. Although different geographic areas have varied specific problems the over optimistic

belief in the “durability” of concrete has led to a widescale use of the material that has resulted in a global problem. Consequently, the necessity to monitor and verify the performance and safety for ongoing usage of concrete bridges is a matter of urgent concern.

Two key factors underly the issue of bridge monitoring. Firstly, there is the problem of how to assess the condition of a bridge in a cost-effective way and with the minimum possible traffic disruption. Secondly, the need to preserve the intended load carrying capacity of a bridge, while preserving the safety of the people using it, has to be considered. The necessity to bring all the trunk road structures up to the current standards set by an EU Directive that increased the load capacity of the trunk road bridges to 40 tonnes, further highlighted the matter [Hayter, 2000]. In order to tackle the problem the UK Department of Transport has developed and started programmes concerned with the inspection, assessment and strengthening of the bridges [Das, 2000], hoping to find alternative ways of solving the problem.

The strategy generally adopted by the bridge authorities was to undertake an inspection and then simply evaluate if a bridge either “passed” or “failed” that inspection. Different assessment codes were developed to evaluate the load carrying capacity of bridges and three levels of assessment were established: the first two consisting of structural and modeling calculations and the third one including an in situ investigation. The BD44 “Assessment of Concrete Highways Structures” [H-A, 2002] specifically refers to concrete bridges and is described in chapter 2. Recently it became clear that bridges in visibly good condition sometimes failed the inspection, suggesting that the assessment procedures were too conservative. As a consequence of the failure of an inspection, the Bridge Engineer is faced with one of the following options:

- closure of the bridge
- weight restriction
- lane closure

Thus bridges that may be in reasonably good condition are liable to have one of these options imposed upon them. All the above options are undesirable for both the bridge owner and the public. The Highways Agency thus proposed to “monitor” those bridges, provided that the monitoring procedure gave real confidence regarding its accuracy, i.e.

on the deterioration state and progress of the bridge. It was therefore proposed that this monitoring might be undertaken by non-destructive methods that could provide additional information which cannot be identified from visual inspection or standard instrumentation. The non-destructive methods most generally applied to concrete bridges include radar, radiography, ultrasonic and magnetic methods, thermography, the use of Schmidt Hammer and electrical instruments [Raina, 1994].

Non-destructive testing generally concerns evaluation, inspection, testing and characterization of a structure. The main advantage of non-destructive methods is that they allow a reliable knowledge of non-visible areas of the structure under study to be gained with zero or only a small amount of acceptable damage. On the other hand, these techniques need careful calibration and the processing and interpretation of the data is often not trivial. Having said this, each method has its specific application, advantages and drawbacks and a complementary use of different techniques is advisable. Once their use started and spread, the need for the development of standard procedures on their use arose as a natural consequence [ACI, 1998] [BS, 1986b] [BS, 1986a].

The Highways Agency has started to produce Advisory Notes on the different applications of these techniques. The work presented in this thesis was sponsored by the Highways Agency with the purpose to assess the feasibility of the Acoustic Emission Technique as a possible and effective way of monitoring the safety of concrete bridges. The final aim of this Highways Agency project would then be the delivery of a draft of an Advisory Note on the Acoustic Emission testing of concrete bridges. The rationale behind this choice lies in:

- the characteristics of the method itself and in its ability to be adapted to existing bridge types;
- the advantage of being able to detect early internal microcracking before it becomes visible, without any permanent damage to the structure;
- the minimal disruption to the traffic.

All the specific advantages and drawbacks of the Acoustic Emission method are discussed in more detail in chapter 4.

The Acoustic Emission technique derived its main principles from the theory of elastodynamics and seismology [Pazdera, 2001]. As for most of the other non-destructive methods, it was not initially developed for use in civil engineering.

Acoustic Emission testing was largely used in the nuclear and the oil industries to monitor remotely critical structures such as pressure vessels and storage tanks. It is in these fields that its major market and application still lies [Ohtsu, 1995]. Lately, the technique has started to be used in a broader range of fields such as in the research of material properties, fracture mechanics, rock corrosion studies, the aircraft industry and finally civil engineering. More recently in Japan, the Acoustic Emission method has started to be used to monitor concrete structures damaged from earthquakes. The specific application of the Acoustic Emission technique to concrete started in 1959 [Rusch, 1959].

This thesis addresses the issue of the feasibility of the Acoustic Emission technique by looking at how the method should be used and applied to concrete bridge beams, by studying different possible types of analysis and by trying to find alternative ways to process and interpret the data.

In order to achieve a multiple perspective, two different acoustic emission systems were used: the Physical Acoustic Corporation (PAC) system and the Pure Technologies Ltd (PTL) SoundPrint system. The different characteristics of the two systems were studied and discussed, providing a broader understanding of the factors involved and affecting an Acoustic Emission test. The original configuration of the SoundPrint system was developed to detect wire breaks in tendons in ungrouted ducts in parking structures, building and bridges - so the possibility to adapt the system in order to deal with the concrete fracture process and deterioration also represents an aim in itself.

The thesis reports on laboratory experiments on concrete specimens that provide evidence for configuring the monitoring systems in a quiet and controlled environment. The laboratory experiments were undertaken in three different laboratories: the Structures Laboratory of the University of Edinburgh (Scotland), the Transport Research Laboratory in Crowthorne (England) and the Structures Laboratory of Kumamoto University (Japan). They include both small and full scale tests which mainly involved the use of reinforced concrete beams differently designed in order to represent the behaviour of real concrete bridge beams. The fracture process of the concrete when deliberately loaded up to the point of deterioration was therefore investigated under controlled conditions, with the AE results compared to direct observation of structural damage.

On-site testing of a reinforced concrete bridge was then carried out to assess the effectiveness of the method on a real structure. The bridge, situated in the Scottish Borders, was a composite flat masonry arch/ reinforced concrete beams bridge. It was monitored using the two types of system for approximately ten days, focusing on its concrete beams.

In each use (laboratory and field) the Acoustic Emission test consisted of:

1. the acquisition of acoustic emission data
2. the processing and interpretation of acoustic emission data.

The first stage is of crucial importance as acquiring meaningful data is a key factor in obtaining useful information from the analysis. Acoustic Emission data can be acquired in different forms (i.e. simply as parameters or as entire waveforms) and using varied instrumentation settings and/or type of transducers, as described in Chapters 4 and 5. The choice of how to record the data, which type of sensor to use, where it has to be located, and finally how to set up the equipment is not a trivial matter. It depends on a combination of all these factors. The geometry, characteristics and material properties of the bridge have also to be considered, together with the specific problem that the Acoustic Emission test is addressing. Choosing only one of these factors incorrectly might totally compromise the success of the entire test. For this reason, particular attention has been put on this phase and as a result of the experiments and the field work that were undertaken, some key points are highlighted and discussed. This thesis shows the different features that influence an Acoustic Emission test, and provides guidelines for the use of this technique on concrete bridge beams including a draft test protocol for practical application.

The second stage of the thesis was to investigate the different types of analysis that can be carried out on the information gathered from the first phase of the AE technique. The data analysis is strongly influenced by the type of information that is required by the investigation. Global monitoring data and local monitoring data were taken into account; both parametric and waveforms analysis were considered and their relationship to the structural behaviour and the cracking process and damage of the concrete are discussed. Two parameters are often used to describe the frequency-energy distribution of acoustic energy radiated from a dynamically growing crack. These are the logarithm of the total log (event rate) - a - and the negative exponent b of the frequency magnitude

relation. Shiotani [Shiotani et al., 2001b] proposed a b -value analysis of AE data, hence a b -value analysis was carried out in the present work, as an alternative “local monitoring” way to process the data. In addition an analysis of the acoustic emissions source location as a way of “global monitoring” was investigated. The feasibility of the SoundPrint system to detect concrete cracking is studied and compared and contrasted with the PAC system. A new parameter (named the “relaxation ratio”) is proposed to quantitatively assess the state of damage of reinforced concrete bridge beams and compared to the assessment criterion developed by the JSCE [Ohtsu et al., 2002].

Japanese researchers are the current leaders in the use of Acoustic Emission testing, so I spent three months in Kumamoto University in Japan working with Assoc. Prof. M. Shigeishi and Prof. M. Ohtsu which allowed a critical understanding of their methodology. The period spent in Japan also enabled an investigation into the Moment Tensor method as an additional type of analysis. The Moment Tensor is proportional to the strain tensor of the local deformation of a given volume. The theory and the practical features on how a Moment Tensor experiment should be carried out are discussed and a preliminary analysis is presented.

Finally, conclusions about each type of analysis, their advantages and disadvantages are presented in order to provide guidelines on when and how they should be used. The proposed b -value analysis showed a good relationship between the b -value trend and the fracture process of a concrete beam, and it is published in:

- Colombo S., Main I.G., Forde M.C. (2003), Assessing Damage of Reinforced Concrete Beam using “ b -value” Analysis of Acoustic Emission Signals, Journal of Materials in Civil Engineering, ASCE, June 2003.

The AE sources location analysis showed the effectiveness of the AE energy as a parameter to indicate the structural damage of concrete bridge beams. Following this finding, the new parameter - the “relaxation ratio” - was defined based on the energy released during the loading and unloading phases of an AE test; its potential to assess the degree of damage of concrete beams was demonstrated and it is reported in:

- Colombo S., Main I.G., Forde M.C., Halliday J., Shigeishi M. (2003), AE Energy analysis on concrete bridge beams, NDT-CE Conference, BAM, Berlin, 16-19 September 2003, “to be published”.

Finally, results from the SoundPrint system appeared promising although further work

is needed and a critical understanding of the Moment Tensor was achieved.

A protocol for practical application was drafted and together with some of the above mentioned ways of analysis was successfully applied to an in-situ monitoring of a bridge, as reported in:

- Colombo S., Forde M.C., Halliday J., Kavanagh J., AE monitoring of concrete bridge beams in situ, *The Structural Engineer*, IstructE, “in press”.

A complete list of the publications derived from the work of this thesis is in Appendix E.

Chapter 2

Concrete Bridges

This chapter provides some background information about the development and actual state of bridges, with specific reference to concrete bridges. An overview on the issue of the maintenance, assessment and monitoring of bridges in the UK and elsewhere is also given.

2.1 History, Development and Problems of Bridge Building

The history of bridge building is influenced by many factors, such as the various types of arches and architectural style, environmental aspects and technological developments [Robins, 1948].

The beginnings and the evolution of bridges are a subject of speculation. The first foot-bridge was probably a simple tree trunk or a flat stone laid across a stream, many thousands of years ago. The sequential development of the early types of bridges is noticeable. From the crude *tree trunk* laid across a river it proceeds to the *stepping stones*, which are a line of stones separated from one another so as to afford passage by a normal step. Then the *clapper bridge*, a primitive bridge consisting of large, long simple slabs of stone laying between piers of piled rocks, principally found in stone areas. Finally came the *primitive suspension bridge* with a single cable made of cane, bamboo, birch, vines, twisted lianas or creepers [Beckett, 1969].

The ancient Greeks rarely built bridges. The great era of bridge building can be attributed to the Romans and started in 400/300 BC lasting till 200 AD. A schematic representation of a typical Greek and Roman structure is shown in Figure 2.1.

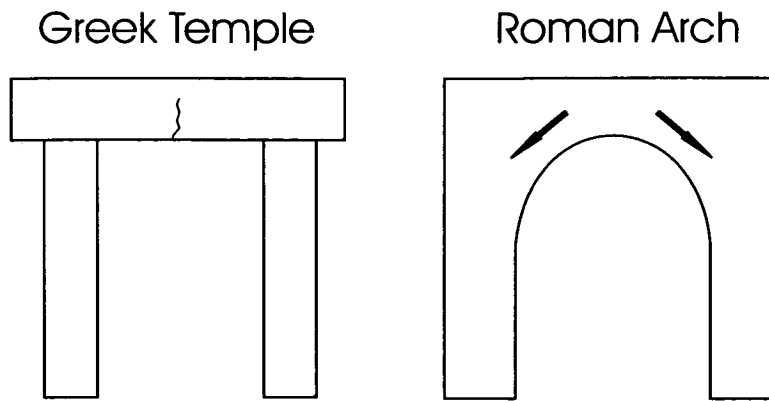


Figure 2.1: Schematic representation of a typical Greek Temple and a Roman Arch. Note the similarity between the architrave (i.e. the beam resting across the tops of the columns) and the beams tested as described in Chapter 6.

Though the Romans initially used timber, their later arch structures, aqueducts and bridges, were mainly made of stone or brick. The engineers made such technological advances that their work was close to perfection and can still be considered an outstanding model to follow nowadays. Many of the modern methods of construction were already known to Romans. They were accomplished brick-makers who built on a grand scale (arches with a span of 140 feet). One of their most important discoveries was the use of Pozzolana, a volcanic sand that when mixed with ordinary lime forms a hydraulic cement. Most of their construction consisted of whole or part “semi-circular arches” (Figure 2.3) that had the advantage that the arch stones used had the same dimensions making them easy to cut. The intrados and extrados of the arches were parallel, and the stones used as voussoirs were cut and fitted so perfectly, that there was no need for mortar at the connections (a visual explanation of the terminology related to bridges is given in Figure 2.2). The piers supporting the arches were very thick (on average about a third of the span) and each pier was strong enough to act as an abutment, so that if one arch was destroyed the neighbouring ones could still support themselves. Openings in the piers were quite common to reduce weight on the foundations and improve water flow in flood conditions. The weakest part of Roman bridges were the foundations which consisted of piles that were often too shallow and built without taking precautions to prevent them from being undermined by scour [O’Connor, 1993].

Following the fall of the Roman Empire, for nearly eight centuries the development

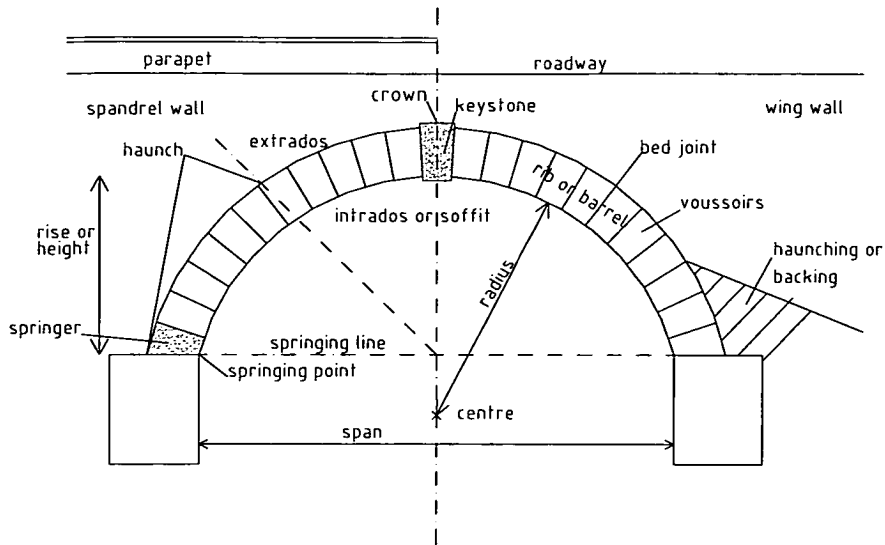


Figure 2.2: Drawing showing the terminology used in relation to bridges.

of bridge construction came to a halt and many of the Roman engineering skills were lost. Notwithstanding this, some technical innovations were developed, such as the use of the pointed Ogival (Figure 2.3) and the ribbed arch - a masonry bridge with independent ribs which considerably reduced the dead weight and the thrust on the piers, which could therefore be lighter [Liebenberg, 1992].

During the Middle Ages, there were two dominant types of bridge: the *war bridge*, a fortified bridge designed for defence, and the *chapel bridge*, built with chapels of different dedications and dimensions for the travellers safety and protection; they were often later addition to existing bridges. Medieval bridge foundations varied from stones simply dumped in the river to form a mound to the use of timber piles shod with iron, driven into the river bed. To protect the piers from the stress caused by the currents and from ice formation, around each foundation was built a “starling” - a protective barrier, triangular in shape with the apex of the triangle facing the flow of the stream and made up of half piles close together. The phenomenon or perhaps the legend of “Freres Pontifes”, also known as “Bridge Brothers” also occurred during the Middle Ages. They were a fraternity, perhaps of benedictines, consisting of devout men who looked after the welfare of travellers, by erecting shelters and hostels and by building and maintaining bridges. Later they were replaced by “private profit” organisations that erected fortifications and demanded exorbitant tolls of everyone who wanted to

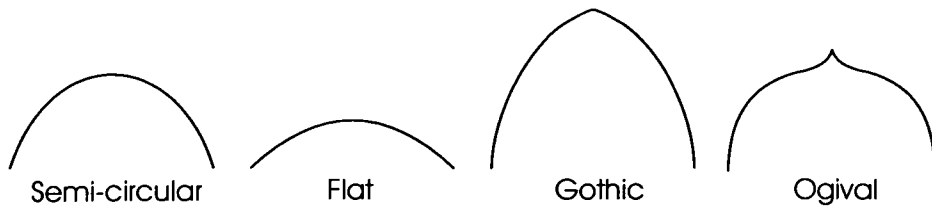


Figure 2.3: Schematic representation of different types of arch.

cross the river [Robins, 1948] [Colombo, 1999].

A new scientific approach to bridge design started during the Italian Renaissance in the 15th Century. The Renaissance was a great period of revival in art, science and architecture, during which there was an architectural rather than engineering emphasis on development. This resulted in the use of lighter piers whose thickness was one fifth the span length, but still proportioned to carry the entire arch thrust as if each single arch was acting alone. This heralded the use of the flat elliptical arch (Figure 2.3). The engineering and architecture of the Renaissance bridges was better than that of the Middle Ages [Robins, 1948] [Beckett, 1969].

The Industrial Revolution and the start of the Modern Age in the 18th Century led to fundamental changes in bridge building techniques on account of the availability of new materials, methods and machines. The Ecole des Pontes et Chaussées, formed in 1747, led to the development of balanced thrust arches and it is in the same Century that one finds the first use of iron for structures and the first cast-iron arch bridge. The “Father of Modern Bridge Building” was Jean Perronet, one of the greatest bridge engineers of the time. Impressed by the proportions of bridges in China, he had the idea of building very flat arches, where piers were designed to carry only their weight whilst the whole of the horizontal thrust was transmitted to the abutments at each end. This opened the way for flatter arches with high springings and piers of lesser thickness. Perronet discarded the use of abutment piers based on the principle that the lateral thrust components for two arches meeting at a pier may be balanced, leaving the pier under the action of vertical loads only.

Other new technological innovations in the 19th Century gave rise to the first steel bridge as well as to the cable stayed bridges and, more recently, the application of reinforced concrete to bridge construction. The 1990’s has finally shown a great revival of interest in masonry arches [Liebenberg, 1992].

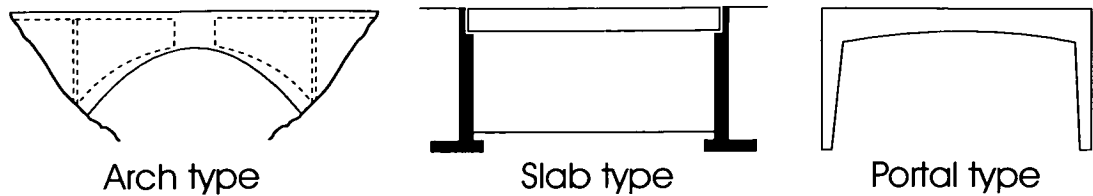


Figure 2.4: Schematic representation of main types of bridge. Note the similarity with the Greek and Roman typology in Figure 2.1.

From this brief review of bridge construction, it can be seen that the birth of reinforced concrete bridges is relatively recent. It was in fact only towards the end of the 19th century that reinforced concrete was applied to bridge construction. Although concrete bridges initially had mainly short spans, during the early decades of the 20th century concrete bridge building was expanded to medium span. The worldwide development of concrete bridges was then very rapid and it eventually led to prestressed and post-tensioned bridges, “father” of the pre-stressed concrete was in fact Eugene Freyssinet in the early 90’s [Encyclopedia, 1980].

Concrete bridges evolved into different types and forms and the following main categories can be identified:

- arch concrete bridges
- RC “slab” or “girder-slab” bridges
- portal frame
- prestressed and/or post-tensioned bridges.

and they are schematically illustrated in Figure 2.4 [Mock, 1949].

Bridges deteriorate due to several causes, such as inadequacy of design, overloading, chemical and atmospheric attacks, abnormal flood or earthquakes. Different categories of bridge manifest distinct kinds of distress, that can be identified as one of the following [Raina, 1994]:

- *cracking* - due to several causes, their significance depends on the genre of structure, the location and stability (i.e.: whether the length and width are increasing) of the crack;

- *scaling* - due to the freeze-thaw action, is exemplified by layers of concrete coming off the surface;
- *delamination* - a separation, parallel to the surface, of the concrete;
- *spalling* - presence of a depression due to separation and disintegration of concrete;
- *efflorescence* - the leaking of salt-dissolved moisture onto the concrete surface, indicating a porous or cracked concrete;
- *stains* - due to rust, indicating presence of metal corrosion;
- *hollow or dead sound* - noticed when tapping the concrete, indicating a low quality concrete, or presence of voids or delamination;
- *deformations* - due to a reaction of the material, to compressive failure or settlements of foundations;
- *excessive deflections* - due to structural problems, overload or creep behaviour.

Having said this, generally bridges in different geographic regions are exposed to varying environmental and geological conditions that affect their life and performance. Many of the Swiss bridges were built before 1973, when bridge waterproofing was introduced and thus are heavily subjected to winter salting corrosion. A survey of New Zealand bridges highlighted problems of expansion joints and spalled or cracked concrete. Bridge deck deterioration has been a significant problem in the United States together with the corrosion of the reinforcements. In Sweden, environmental conditions proved to be a major cause of bridge deterioration. Generally in North America and Northern Europe, the principal cause of concrete bridge deterioration was the corrosion of reinforcement due to chlorides [Mallet, 1994]. The laboratory work in this thesis will mainly address the cracking type of distress, whilst the field study will also refer to stains and deflections.

Depending on the class and degree of deterioration, a bridge can eventually fail. The collapses of the Tay (1879, UK) and Tacoma Narrows (1940, USA - see Figure 2.5) [Mock, 1949] bridges are probably two of the most famous examples of bridge failure, but they are not the only ones. Between the most sensational collapses it is possible to name: the Dee bridge (1847, UK), the Quebec bridge (1907, Canada),

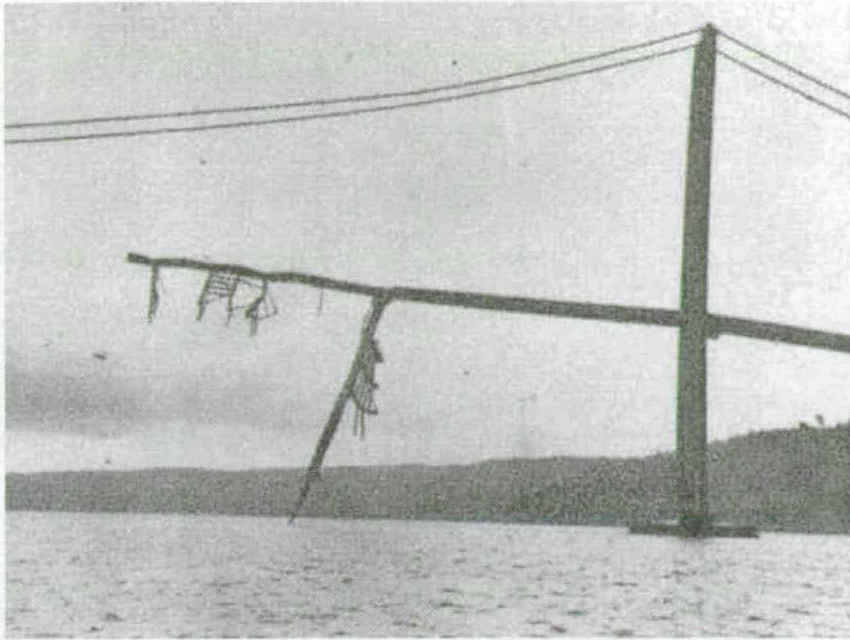


Figure 2.5: Failure by wind of the Tacoma Narrows Bridge, Washington - from [Mock, 1949].

the West Gate bridge (1970, Australia) and recently the Ponte de Ferro (Portugal) [Hansford et al., 2001]. Apart from the Tacoma Narrows, all these failures resulted in loss of human lives and the consequential social responsibility for a bridge engineer in these eventualities is inevitable [Raina, 1994]. The causes of such collapses are varying, going from nature's fury to weakness in original design for scour (which is today's most common reason for bridge failure). Errors do happen but some of these disasters could have been avoided - through improved engineering knowledge, better design codes and appropriate maintenance.

2.2 Bridge Maintenance and Monitoring

The use of the word "maintenance" in conjunction with bridges defines the work that has to be done to preserve the intended load carrying capacity of a bridge and the safety of the people using it [Raina, 1994]. Bridge engineering is not only about designing but also includes "looking after" and maintaining the service-life of bridges as well as repairing and strengthening them.

The process of maintenance differentiates between ordinary and major bridges

(i.e.: bridges that represent vital links) and between short-life elements (pavements, paint, joints) and long-life elements (deck, foundations, piers). The reasoning behind this is to identify the need for structural maintenance, rehabilitation and replacement and to provide guidelines and methodologies. The overall activity generally includes the followings steps [Raina, 1994]:

1. study of existing documentation;
2. visual detailed survey;
3. verification of the presence of damage and defects by carrying out appropriate in situ tests;
4. analysis and evaluation of the results of both visual and test inspections;
5. final decision process, to determine if or not the bridge, or some parts of it, need rehabilitation, repair or demolition and replacement;
6. design and evaluation of the repair work, if needed;
7. estimation of costs.

The Acoustic Emission technique could be used to detect and locate the areas of damage (step number 3), to monitor an existing damage as part of the rehabilitation decision (step number 5) [Sison et al., 1996] and to evaluate the success of repair work (step number 6) [Carter and Holford, 1998]. The procedure described above goes under the name of “*Bridge Management System*” (BMS) which stresses the importance of preventive maintenance in order to plan the eventual rehabilitation works in time and economically with the minimum disruption of traffic [Carter and Holford, 1996]. In order to achieve this, periodic bridge inspections are advisable, distinguishing between:

- routine inspection - a general, quick and broad visual inspection;
- detailed inspection - a survey with the aid of instrumentation;
- special inspection - to address a specific problem.

In the course of the maintenance procedure, there may be a period of time during which a bridge needs to be monitored to assess its performance and safety. Monitoring may involve laboratory and field tests and measurements of different factors [Raina, 1994]:

- strain measurements - using strain gauges or Demec gauges;
- deformation measurements - using laser devices;
- vibration measurements - using vibrating-wire-gauges;
- measurement of temperature effects, settlements, movements at hinges and so on - using specific instrumentation;
- measurements of corrosion potential - using permanent electrodes or probes.

No standard packages or procedure of monitoring exist [McGown et al., 2000], but several non-destructive techniques (NDT) can be used during the investigative step of the maintenance of concrete structures. They allow assessment of the conditions of the structure and the location of eventual defects and flaws. The most common methods applied to concrete include [Forde, 1992] [Bungey and Millard, 1996] [Woodward, 1989]:

- Schmidt Hammer - to measure the hardness of concrete surface;
- Magnetic Method - to determine the position of the reinforcements;
- Radar, Radiography and Ultrasonic Methods - to detect defects in the concrete;
- Thermography - to detect delamination and cracks;
- Electrical Instruments - to detect metal corrosion.

As each method has its specific application, a complementary use of these techniques is generally advisable. In more general terms, a bridge monitoring or inspection has to be approached as a comprehensive, multi-disciplinary, multi-stage task. The monitoring of the Kingston Bridge Complex in Glasgow represents a very good example of this principle [McGown et al., 2000].

The aim of this thesis is to test the Acoustic Emission technique as a relative new monitoring process and its potential application in both the detailed and specific inspections of a Bridge Management System.

2.3 Assessment of Bridges in the UK

Dependent on timely and adequate maintenance, the economic life of a bridge is estimated to be of approximately 120 years. After a period of negligence in the 1970s

(as a consequence of the oil crisis and thus the need to stop expensive large-scale works) there was a growing awareness of the necessity to safeguard and maintain the stock of bridges as part of the national asset. The concern about environmental and sustainability issues, started in the mid 1980s, highlighted this necessity [Mallet, 1994] [H-A, 2002].

In the UK several different authorities are charged with the responsibility for bridges. It was estimated in 1997, that there were 44,000 bridges in England. Estimating 150,000 pounds as the asset value for a bridge, this gives a total value of 6.6 billion pounds, without considering the rest of the UK [Young, 2000]. In 1987, England and Scotland started a 15-year rehabilitation programme for bridges on trunk roads. The cost of this programme was estimated at 1000 million pounds for the Dept. of Transport, and an additional 1000 million pounds for other authorities [Das, 2000]. The aim of the programme was to bring trunk road structures up to current standards, which had to satisfy the EU Directive which states that “bridges on principal routes, have to be capable of taking 40 tonne vehicles by 1 Jan 1999” [Hayter, 2000]. The programme was mainly concerned with the inspection, assessment and strengthening of the bridges [Das, 2000]. A “Steady State Assessment Programme” was planned which focused on maintaining safety, minimising expenditure over time, minimising disruption to users and minimising the impact on the environment [Finegan and Hogg, 2000].

WS Atkins Consultants, estimated that 10% of the Highways Agency bridges and 30% of other bridges would fail the assessment [Chubb, 2000]. This totals approximately 30,000 bridges, but as there were no reports of actual bridges failing in service, this suggested that the assessment standards were too conservative [Chubb, 2000]. As a result of this, particular emphasis was placed on increasing the accuracy of the assessment, so that the answer to whether a structure “is safe or not”, was not a simple “pass or fail” [Das, 2000]. Instead of the “*pass or fail*” results from the assessment procedures, a new “*pass, fail or monitor*” system has been suggested. The “*monitor*” category would then be applied when a bridge passes or fails by a small margin [Colombo et al., 2000]. In the latter case, Non-Destructive Testing (NDT) techniques can provide qualitative information, without great cost and disruption.

Information obtained from the different UK authorities about the trunk road stock of bridges showed that concrete bridges represent the majority of the trunk road asset (see Table 2.3 and Figure 2.3). As the average age of these bridges is now in the order

	England	London	Scotland	N. Ireland	Wales	TOT.
CONCRETE	7615	1265	1291	1495	N/A	11666
MASONRY	358	586	181	4160	N/A	5285
OTHERS	1771	442	332	845	N/A	3390

Table 2.1: UK trunk road bridge stock.

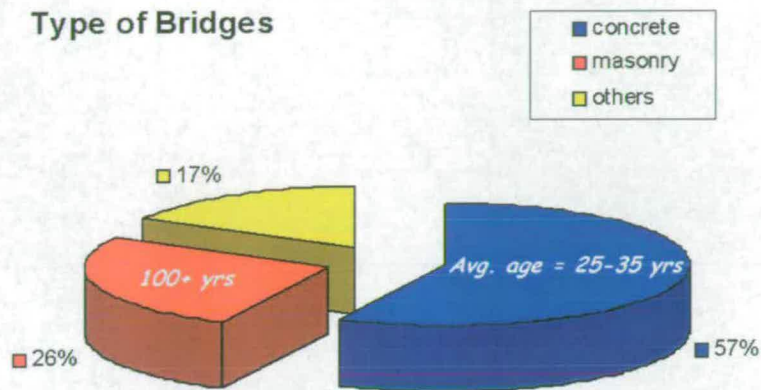


Figure 2.6: UK trunk road types of bridges.

of 25-35 years, they are starting to show signs of distress. Consequently, the necessity to monitor and verify their performance and safety is a matter of urgent concern.

If this is the actual situation in the UK, things are not very different in the rest of the world [Mallet, 1994]. Concrete bridges account for about 80% of the Swedish National Road stock. Two third of the highway bridges in the Czech Republic were built using concrete. A bridge survey in India showed that about 20% of their bridges were distressed. In the US in 1977 it was reported that more than one in six bridges were deficient [Mallet, 1994]. The situation has grown even worse with 29% of the bridges being ranked as structurally deficient or obsolete in 2001 [Frangopol and Kong, 2001]. The current bridge management system in the US is based on the assessment of the state of bridge elements, on the prediction of their deterioration and on a cost-benefit analysis of the eventual repair work. Generally the whole process is carried out during routine inspections in a qualitative and subjective way. The development of a quantitative, objective and affordable method is globally a high priority [Frangopol and Kong, 2001].

In Japan, several concrete structures were built since the 1950's and their

importance in the Japanese economy is unquestionable. Concrete was preferred to steel due to its higher expected durability, but due to the large number of concrete structures that had to be built, the engineers were too busy to verify all the details of the design and construction. As a result, many of the new structures started to deteriorate within 5 to 10 years and spalling of concrete from bridges has become a recent crucial problem [Uomoto, 2000].

Before the mid-19th Century, no analytical tools were available and the only way to assess the integrity of a bridge was based on visual inspection and intuitive judgement. For a long time, the assessment was considered a “special case” of the design and thus the same rules were applied. Then “Assessment Code BD21/84” represented a milestone in the start of introducing codes, which directly dealt with bridge assessment. Based on the Limit State Concept, the code dealt only with the Ultimate Limit State, but it was then amended in 1987 to include a serviceability Limit State and to be specifically applied to trunk road bridges. The code used safety factors as defined during the design stage and it proved to be too conservative. The design factors need to take into account variations of materials properties (which may conversely be measured during an inspection) and they generally have a low cost effect. Conversely, such factors can make the difference between the “pass” or “fail” result of an assessment. A new protocol BD44 was therefore produced in 1990, to be used for both old and new concrete bridges. The new code introduced the concept of “Worst Credible Strength”, i.e. when possible, values of strength obtained by tests on the actual material were used and in this case lower safety factors were applied [H-A, 2002]. The conventional assessment derived by this code identified four levels:

- Level 0 - Collecting information about the structure (previous existing records) and site inspection
- Level 1 - A standard assessment applying full safety factors, using the above collected information
- Level 2 - If a structure fails Level 1, a more sophisticated assessment is undertaken, involving modelling calculations
- Level 3 - If a structure fails Level 2, an in-situ investigation is carried out to obtain additional information for the assessment

The NDT techniques and the Acoustic method are then part of the last Level of assessment.

2.4 Summary

An overview of the history, development and actual conditions of concrete bridges was presented and discussed in this chapter. The analysis of the development of bridge building allowed an understanding of the significant role that bridges had and have in the society and highlighted the problems emerged during the past years till the present days. A discussion about the actual condition and assessment criteria in the UK was reported. The importance of correct maintenance, monitoring and assessment of the existing bridges was underlined, together with the need to develop new tools, techniques and protocols to support the Bridge Engineer during the diagnosis process and to improve his confidence.

It is in the light of this necessity that this thesis investigates the feasibility of the Acoustic Emission method to be one of these alternative tools. An overview of the history, development and applications of the Acoustic Emission technique is therefore presented in the following chapter.

Chapter 3

Acoustic Emission

This chapter gives an overview of the Acoustic Emission technique (AET), from its birth to the present time. After a general review of the development of the Acoustic Emission method (section 3.1), a detailed account on the use of Acoustic Emission testing of concrete is provided (section 3.2), from its first application [Rusch, 1959] till the present day.

Following the successful results obtained with civil engineering materials such as steel and concrete, an interest about the possibility to use the Acoustic Emission technique on masonry has recently arisen. As this appears to be one of the main future subject of research and application, a summary of the work done on this topic till the present time is also given (section 3.3).

As this thesis specifically deals with bridges, a review of the use of the Acoustic Emission technique on bridges is described (section 3.4). Finally, the state of the existing procedures and codes on the use of the Acoustic Emission testing is discussed (section 3.5).

3.1 General Overview

The Acoustic Emission technique was not originally born as a “civil engineering” tool. In fact, research about Acoustic Emission (AE) started in the middle of the 20th century in different fields such as seismology, mining [Miller et al., 1987], physics and metallurgy. The development of the technique itself was strongly linked and dependent on the improvements in technology and thus the opportunity to use instrumentation able to record a wider frequency range of signals [Williams, 1980].

Early examples of work concerning AE started in the 1930s and the first report on an acoustic emission experiment on the fracture of wood was published by F. Kishinouye in 1934 [Kishinouye, 1934]. Further work was carried out by L. Obert in 1941 [Obert, 1941]. Using vibration microphones to predict rock burst in mines, he discovered an increase of “disturbances” within 15 minutes of a rock burst that could be used as a warning of collapse to secure the safety of the miners. The following year, E.A. Hodgson reported a seismology analysis of waves generated by rock bursts in Ottawa [Hodgson, 1942].

Notwithstanding these earlier works, it is generally accepted that the concept of acoustic emission, as it is known today, started with the research of Josef Kaiser in the 1950s [von Kaiser, 1953] [Scott, 1991]. In that year Kaiser successfully submitted his PhD at the Technische Hochschule Munchen, signally the start of modern AE research. In his studies on metals (copper, steel, lead, zinc and aluminium) he developed the basis of modern AE technology and published the first comprehensive investigation on the phenomenon of AE in several different materials. During his research he provided a major contribution as he noticed the “irreversibility” of acoustic emissions, patented in 1952 and today known as the “Kaiser effect”, (see section 4.3) - i.e. emissions are not generated in a material until it is stressed beyond its maximum prior stress states [von Kaiser, 1953] [Henning, 1988].

After Kaiser’s research, several studies on AE on different materials started, although difficulties were encountered due to the fact that different materials exhibited different AE characteristics and no standards were available. Nevertheless, the researches continued - the location of the AE sources was achieved by adapting it from seismology (AE used to be described as “*microseismic activity*”) and the understanding and confidence in the method improved.

The first major application of the AET as non-destructive testing was in the aerospace and nuclear industries to monitor the presence and growth of cracks in pressure vessels [Green, 1970]. In the Spanner review article [Spanner, 1981] the predominance of the AE application to Chemical, Petroleum and Nuclear vessels, systems and components clearly appeared. Nowadays it is still in this field that the majority of the AET market lies.

A significant contribution to the development of the AE instrumentation and method was provided by the work of H.L. Dunegan and A.A. Pollock. During the

60s, Dunegan worked on the implementation and development of AE instrumentation [Dunegan and Tatro, 1967] and reported several experiments concerning the application of the Acoustic Emission method to the testing of metals [Dunegan et al., 1968] [Dunegan and Harris, 1969]. His studies proved the relationship between the generation of acoustic emissions and the plastic deformation of different metals and suggested the use of AET to proof test pressure vessels as he showed that flawed vessels generated AE earlier than unflawed vessels. Dunegan finally developed his own AE system and in 1968 he founded the Dunegan Research Corporation equipment manufacturer that was successively bought by the Physical Acoustic Corporation (see also section 5.2).

Pollock's work covered a wide range of areas, AE instrumentation and theory [Pollock, 1981] [Pollock, 1986] [Pollock, 1989], feasibility study of the frequency analysis of the AE waves [Stephens and Pollock, 1971] as well as a preliminary AE application to monitor a military steel bridge [Pollock and Smith, 1972]. He proposed varied practical applications of the AE method although their use was limited by the lack of specific equipment [Pollock, 1969].

From the 70s a large flourish of publications started [Nesvijski and Sarkis, 2000], and nowadays the Acoustic Emission technique is used in several different fields, as a research tool in the laboratory as well as to evaluate the safety of a system, a structure or their components [Scott, 1991] [Ono, 2000], during pre-service testing or in-service testing and monitoring [Spanner, 1981]. A more extensive review of the AE work in all its fields of application is beyond the aim of this thesis. More details are given in the next section with specific reference to concrete, whilst the varied AE applications are summarised in Table 3.1.

3.2 Acoustic Emission in Concrete

The earliest studies about AE on concrete mainly focused on the understanding of the AE characteristics and their relationship to concrete's properties. The Acoustic Emission research in concrete started in 1959 when Rusch reported preliminary observations about the noise produced by stressed concrete - showing that the internal structure of the concrete fractured when approximately 75% of the failure load was reached [Rusch, 1959].

The following year, l'Hermite published an extensive study on the change of volume

LABORATORY RESEARCH	SAFETY EVALUATION
<ul style="list-style-type: none"> - Material study and properties: <ul style="list-style-type: none"> metal alloy ceramics glass fiber reinforced concrete masonry ... - Corrosion study - Fracture and rock mechanics 	<ul style="list-style-type: none"> - Aircraft industry - Monitoring of glass reinforced plastic (GRP) tank and pressure vessels - Structural integrity evaluation of FRP and metal vessels, new and in service <ul style="list-style-type: none"> - Pipeline monitoring - Evaluation of storage tanks floor and walls <ul style="list-style-type: none"> - High pressure reactors - Leak detection - Detection of gas through valve-leakage in plant, refineries and offshore platform <ul style="list-style-type: none"> - Welding monitoring and control - Inspection of aerial lift mechanisms and cranes <ul style="list-style-type: none"> - Rocks and Seismology - Geotechnical Engineering <ul style="list-style-type: none"> - Hydrofracturing - Civil Engineering: bridges monitoring and wire break detection

Table 3.1: Acoustic Emission applications.

of concrete. During the investigation of the plastic concrete deformation he recorded, by simply using a microphone and an amplifier, the noise generated by the concrete sample under the effect of the load. He discovered that the recorded sound occurred and increased in correspondence to a significant longitudinal deformation in the concrete, a sudden increase in the Poisson's ratio and a sharp decrease in the velocity of wave propagation [L'Hermite, 1960].

A study on AE in mortar and concrete was undertaken in 1965 by Robinson [Robinson, 1965]. It showed that the Acoustic Emission method can provide information about the formation and propagation of small cracks, the load at which they occurred and the energy that they released. The latter proved to be dependent on the size and coarse aggregate concentrations.

In 1970, Wells designed an AE apparatus able to record acoustic emissions from small concrete samples in a range of frequency between 2 and 20 kHz [Wells, 1970]. In the same year, Green reported a comprehensive work on cylindrical concrete specimens and a model concrete pressure vessel. His studies showed that changes in the AE rate were the precursor of failure and that the Kaiser effect was valid. He also demonstrated the feasibility of the method to test concrete pressure vessels and to detect fluid leakage [Green, 1970]. The feasibility of AET as a non-destructive method to evaluate the safety of concrete was further demonstrated a few years later by McCabe [McCabe et al., 1976].

More references can be found in the bibliography published in 1986 by Drouillard. It contains a list of 76 references published in the world literature from 1959 to the date of the article on acoustic emission of concrete [Drouillard, 1986].

Work done in the 80s [Mindess, 1982] [Woodward, 1983] highlighted the necessity to develop an AE standard procedure and the difficulties arising from the data interpretation, but the "boom" of AE publications on concrete started in the 1990s.

A review was then carried out to gain a critical understanding of the types of analysis that had been used and investigated and thus to decide which ones were suitable to be adapted and/or implemented to be used in this thesis. Two main trends were identified during the course of the review: studies that took into consideration a waveform analysis of the AE signals and researches that focused instead on the investigation of parameters derived from the AE wave and their relationship with mechanical factors and/or structural behaviour of the concrete. The difference between

these two ways of approaching the data analysis is discussed in detail in section 4.4.

The waveform studies included attempts to relate frequency to the fracture stage process [Berthelot et al., 1993], to compare signals [Koppel and Vogel, 2000] and Moment Tensor Analysis. The Moment Tensor method developed by Ohtsu in Japan [Ohtsu, 2000] was applied during this thesis and it is described in detail in sections 4.9 and 7.5, but other studies on the Moment Tensor were also carried out elsewhere [Li and Xi, 1995] [Grosse et al., 1995] [Finck et al., 2002] with less sophisticated analyses. More recently, wavelet studies has been used to improve the signal-to-noise of AE data [Takemoto et al., 2000] [Grosse et al., 2002].

The second trend, concerning AE parametric analysis, appeared however to be predominant. A large selection of different parameters and/or their combination was applied throughout the years:

- AE rate [Li and Xi, 1995] [Ohtsu and Watanabe, 2001]
- AE counts [Moczko et al., 1995]
- AE energy [Bordyugov and Erminson, 1993] [Muravin and Lezvinsky, 1995] [Shiotani et al., 2001a] [Yuyama et al., 2000]
- AE events and hits [Shiotani et al., 2001a] [Kamada et al., 2000]
- damage parameter [Ohtsu and Iida, 2001]
- amplitude [Koppel and Vogel, 2000] [Keru et al., 2000]
- rise time and average frequency [Tsuji et al., 2000]
- b -value [Shiotani et al., 2000c]

A number of these parameters were considered during the data processing of this thesis; those only that led to successful and promising results, such as the b -value and the AE energy, are further discussed in the next chapters.

The application of both the waveform and parametric analysis varied from earlier studies on small plain concrete samples [Moczko et al., 1995] to RC beams [Roca, 1997] [Shigeishi, 1998] and slabs [Yuyama et al., 2000] to concrete piles [Shiotani et al., 2000a] and joints [Kamada et al., 2000] - mainly focusing on feasibility, cracking behaviour and damage estimation studies.

3.3 Acoustic Emission in Masonry

The encouraging and successful results obtained in concrete have drawn attention towards another civil engineering material, i.e. masonry. Moreover, the application of the Acoustic Emission technique to masonry turned out not to be trivial, due to the heterogeneity of the material and thus the significant wave attenuation caused by the presence of joints between bricks and/or stones.

The first preliminary work of AE on masonry was done by Leaird in 1984 [Leaird, 1984]. It consisted of an investigation of the feasibility to use a “pulse acoustic emission method” to assess the integrity of masonry walls. A few years later, in the early '90s a study was undertaken to show the potential of using AE activity, in terms of cumulative number of events, as a way to assess masonry arch bridges [Royles and Hendry, 1991].

No more studies were undertaken anywhere in the following nine years until Acoustic Emission testing was attempted on a stone masonry arch bridge [Shigeishi et al., 2001] confirming the possibility to record AE under traffic load on a real masonry structure. Following this work, Shigeishi carried out a basic study of the characteristics of AE on brick masonry [Shigeishi and Forde, 2001]. The results showed that the significant AE frequency spectrum in bricks lies in the range below 100kHz, similar to that of concrete. The location of AE sources proved to be possible and successfully indicative of different crack patterns. In the light of these results a comprehensive research on brick structures was presented at the EWGAE-2002 conference [Shinomiya et al., 2002]. The work identified the relationship between the stages of fracture in brick and the average frequency of the relative AE as well as the possibility to apply the damage assessment table proposed for concrete in the NDIS 2421 (herein described in section 3.5) to brick structures. The study included an in-situ monitoring of an arch railway bridge, in which the response of 15 kHz and 60 kHz resonant sensors were compared. The frequency range related to cracks was identified, showing that the 60 kHz resonant sensor provided the best accuracy in the AE location. All these studies started the understanding of the characteristics of AE in masonry structures and opened the way for future applications of the Acoustic Emission technique.

3.4 Acoustic Emission in Bridges

The development and progress of AE during the last decades posed the basis for the application of the Acoustic Emission technique to real structures. Experiments on beams belonging to and/or recovered from a bridge demolition or widening started in the eighties [Woodward, 1983] and were followed few years later by applications to in-service bridges.

The first application of AE testing on a real bridge dates back to 1971 [Pollock and Smith, 1972] when Pollock and Smith recorded AE data during the proof test of a military steel bridge. Their work showed a relationship between the AE results obtained from laboratory experiments and the AE signals recorded on the bridge.

The promising findings obtained from this work opened the way to further studies and applications that initially focused mainly on steel bridges. Efforts were particularly directed to eliminate the background noise, develop filters and locate and identify the AE sources relative to different types of damage [Sison et al., 1996]. A relationship between AE recorded data on bridges and the traffic volume, speed and weight was also found [Prine and Hopwood, 1985].

Since these early attempts, several applications of AET to steel bridges can be found. They addressed varied problems: the presence of cracking in girders and/or pin and web components [Sison et al., 1996]; the feasibility of bridge monitoring, the requirements and factors involved in it [Carter and Holford, 1998]; the detection of cracks in box girders [Watson et al., 2000]; the monitoring of fatigue cracks [Watson et al., 1999]; the classification of fatigue cracks into safety levels [Gong et al., 1992].

The successful results achieved on steel bridges, suggested the possibility to explore a further application to concrete bridge structures. The requirements and findings discovered on steel structures could not however be directly translated to concrete bridge applications. The wave attenuation in steel is generally low (especially in the absence of joints) and thus high frequency (100-300 kHz) signals can be recorded. Therefore, noise, which typically has a low frequency content can be easily eliminated [Carter and Holford, 1998]. Conversely, in concrete, due to its heterogeneity a significant attenuation issue (due to multiple scattering and intrinsic anelastic absorption) arises.

Initially, researches on concrete mainly focused on laboratory experiments and it is only recently that few studies were undertaken in real concrete structures. A study to detect cracks in prestressed concrete bridge was carried out in 1983 [Woodward, 1983]. A waveform analysis was performed on AE data collected on a 50 m span prestressed concrete bridge to investigate the characteristics of the noise generated by the traffic and thus the possibility to distinguish it from structural AE sources [Hick et al., 1992]. Measurements to evaluate the repair work done on an existing crack were also carried out.

A reinforced concrete beam cut out from a 60 year old bridge in Japan was tested, as an example of AET application to large civil structures [Shigeishi et al., 1999a]. This work demonstrated the relationship between laboratory experiments and the data collected on the bridge beam, suggesting the possibility to extend the use of the AE method to full scale structures.

In the past few years, AE was used to monitor a few concrete bridges in Japan. Two RC slabs of a highway bridge were monitored under live traffic load and the AE parametric analysis, in terms of hit number and energy, used to establish the most damaged slab [Yuyama and Li, 2000]. In the same year, the AE monitoring of an RC beam belonging to a railway bridge in service showed the absence in it of crack extensions [Watson et al., 1999].

As mentioned in section 2.3, part of the USA bridge stock faces a serious deterioration state. As a consequence, some RC beams from a bridge in New York State had to be removed and AE testing was performed, investigating the failure of the material from the AE activity location [Watson et al., 1999].

A further area of interest relates to concrete bridge joints. The monitoring of half joints on a concrete bridge on the M6 motorway, UK, was commissioned by WS Atkins to the PAC [Watson et al., 1999]. AE was used to classify the varied state of damage of eight joints, from a comparison between the amplitude and the location of the AE signals and the displacements of the joints.

Finally AE monitoring of a 45 year old reinforced concrete bridge was reported in 2002 [Shigeishi et al., 2002]. The monitoring was carried out under in-service traffic load as well as under an on-site loading test, establishing a relationship between the recorded emissions, the vehicles' speed and the measured strain.

Prestressed and post-tensioned bridges are exposed to the corrosion of their

wires. The SoundPrint system (described in detail in section 5.3) was specifically designed to detect wire breaks in ungrouted tendons. After successful laboratory trials [Cullington et al., 1999] [Paulson et al., 2001] it was then applied to bridge structures. The system is currently in use on three bridges in the UK - the railway viaduct in Huntingdon [Cullington et al., 1999], the Soar River Bridge [Fugro, 2000a] and the Mossband viaduct [Fugro, 2000b] - plus two bridges in France: the Saint Cloud viaduct and the Riviere d'Abord Bridge [Elliot et al., 2002].

The SoundPrint system was also tested on the Brox Whitestone suspension bridge in New York during the repair of broken wires, proving able to detect wire cuts with an accuracy of 220 mm [Elliot et al., 2002]. The system is also used on cable stay bridges to monitor the integrity of their wires. After a prototype installation on the Alex Fraser Bridge in Vancouver, a system is now permanently mounted on the Fred Hartman Bridge in Texas [Elliot et al., 2002].

Overall, a large variety of applications can be seen in the reported works of AE on bridges, both in terms of type of analysis and type of sensors - two main aspects of an AE test. A summary is shown in Table 3.2. It can be noted, that the author has not always specified the type of sensors that were used and that broadband and resonant sensors were used in equal measure. However a predominance of parametric analysis emerged clearly.

3.5 AE Standards and Procedures

One of the main obstacles to the application of the AET to bridge structures, lies in the lack of appropriate codes and standards that describe how the method should be used. A comprehensive and up-to-date work about the state of the AE standards and guidelines was reported by Brunner & Bohse [Brunner and Bohse, 2002]. The study took into consideration both national organisations, such as ISO (International Organisation for Standardisation), CEN (Comite Europeen de Normalisation), ASTM (American Society for Testing and Materials) and AFNOR (Association Francaise de Normalisation); and private institutions such as EWGAE (European Working Group on Acoustic Emission) and DGZfP (German Society for Non-Destructive Testing). The guidelines produced deal with terminology, measurement technique and calibration, plus few specific application procedures. Dissimilarities between the

REFERENCE	ANALYSIS	SENSORS
STEEL BRIDGES		
[Gong et al., 1992]	AE count rate	Resonant 200 kHz
[Carter and Holford, 1998]	AE Source Location AE amplitude	Resonant 30 kHz, 60 kHz and 150 kHz
[Watson et al., 2000]	AE Source Location AE events	N/A
CONCRETE BRIDGES		
[Woodward, 1983]	AE ring counts	Resonant 175 kHz
[Hick et al., 1992]	AE counts waveform analysis	N/A
[Shigeishi et al., 1999a]	AE Source Location AE events AE amplitude AE energy rise & duration time AE counts	Broadband UT-1000
[Shigeishi et al., 2002]	AE events AE energy	Broadband
[Watson and Cole, 2001]	AE Source Location	N/A
[Watson et al., 1999]	AE Source Location AE energy AE hits rate	N/A

Table 3.2: Summary of the features of AE applications to bridges.

standards produced by these organisations were highlighted, as well as the lack of a description of the general AE principles. Moreover, it was noted that a vast majority of the application codes deal with storage tanks and pressure vessels. The need to develop “International Uniformed” codes was strongly underlined and the necessity to expand the protocols to new AE applications, civil engineering structures being among them, emerged.

The above mentioned organisations did not include the committee of the Japanese Society for Nondestructive Inspections (JSNDI). Until recently however, the situation in Japan was very similar, with the AE existing standards concerning only the description of the AE instrumentation, generic analysis guidelines, sensor calibration and sensitivity and a single specific application to pressure vessels [Ohtsu and Yuyama, 2000].

The situation recently evolved, with the introduction by the JSNDI of a criterion based on the Kaiser Effect to quantitatively assess concrete structures [Ohtsu et al., 2002]. The criterion is based on the definition of two parameters:

$$\text{Load ratio} = \frac{\text{load at the onset of AE activity in the subsequent loading}}{\text{the previous load}}$$

$$\text{Calm ratio} = \frac{\text{the number of cumulative AE activities during the unloading process}}{\text{total AE activity during the last loading cycle up to the maximum}}$$

The *Load ratio* is based on the concept of Kaiser Effect (more details about the Kaiser effect are in section 4.3). As the effect is associated with structural stability, a ratio greater than 1 is an indication of a structure in good condition, whilst a value less than 1 suggests the presence of damage. The generation of AE activity during unloading is also an indication of structural instability, as in a structure in good condition no acoustic emission are generally recorded in the unloading phase. On the basis of a combination of the two parameters a classification is now recommended by NDIS-2421, as shown in Figure 3.1. It has to be pointed out that the classification limits indicated by the dashed line should be determined in advance, based on preliminary tests, in order to be used for practical applications [Ohtsu et al., 2002].

The proposed assessment criterion by the Japanese represents a positive example of the future trend that the responsible organisations should follow, directing their attention towards new AE applications. The existence of quantitative codes would provide confidence about the validity of the AE method and highlights the necessity to produce guidelines on the use of AET on civil engineering structures. For this reason, a draft of a protocol about the AET application to concrete bridges was developed during the research of this thesis. It is presented in section 5.6.

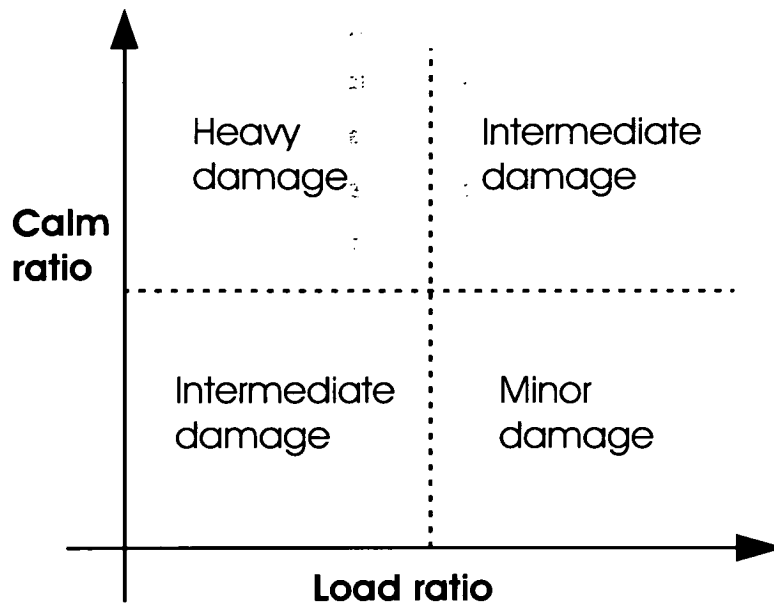


Figure 3.1: Classification of damage according to NDIS-2421 - from [Ohtsu et al., 2002].

3.6 Summary

This chapter provided background knowledge on the development and applications of the AE method, in order to obtain a general overview of the different features that the technique involves. Particular emphasis was placed in the discussion of the AE work on concrete and bridges as directly related to the objectives and aims of this thesis. For the same reason an analysis of the existing AE codes was reported. A summary of the review, in the light of the specific topic of this thesis is illustrated in Figure 3.2.

This chapter concludes the general background information at the basis of this thesis. The following chapters will then specifically deal with the main subject of the research, starting in the next chapter with its principles and theory.

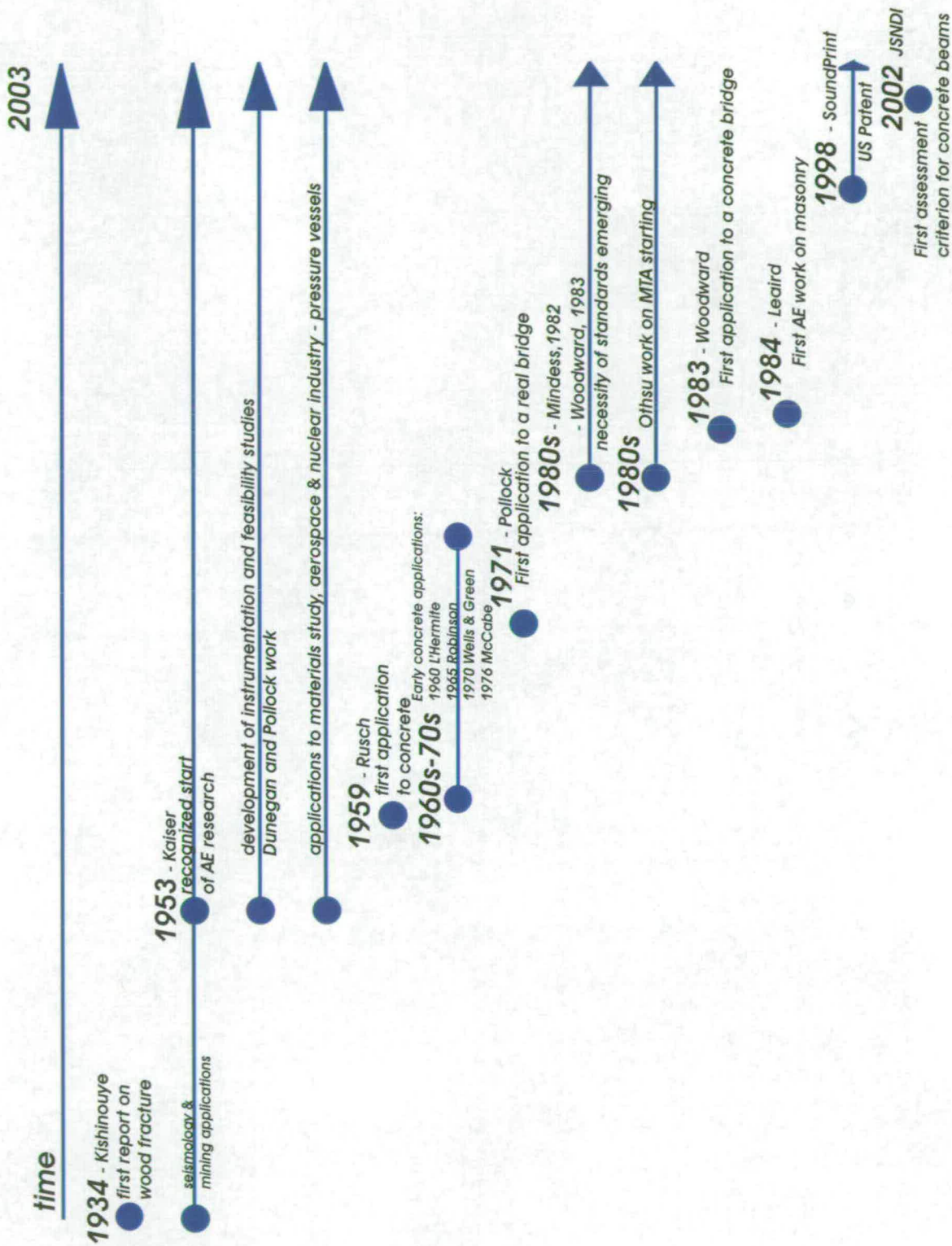


Figure 3.2: Summarized representation of the milestones and significant development in AE research and application.

Chapter 4

General Theory

4.1 Principle-Definition

The Acoustic Emission technique (AET) is a passive, non-intrusive, method that allows monitoring of concrete structures [Ohtsu, 1995]. Its basic principle, derived from the theory of elastic waves, is very similar to that used for earthquakes in seismology [Grosse, 2002]. However the AET works on a smaller geometric scale, generally on dynamic structures (e.g. bridges), and deals with higher frequencies.

The term Acoustic Emission encompasses all phenomena where elastic waves are generated by the release of energy from localised sources. According to the BS EN 1330-9:2000 [BS, 2000] Acoustic Emission is a “term used for transient elastic waves generated by the release of energy within a material or by a process”. In every solid body subjected to stress - the occurrence of cracking, corrosion, slip or friction is followed by a release of stored strain energy that generates elastic waves, which is referred to as acoustic emission. These waves propagate through the material and can then be detected and recorded by AE sensors, previously mounted on or embedded in the material. The detected wave is turned into an electrical signal by the sensor and can be subsequently analysed and interpreted. As the source of the AE energy comes solely from the elastic stress in the material a lack of stress will result in no emission [Roca, 1997] [Pazdera, 2001]. The stress determines the presence of strain, which can be either elastic or plastic. Acoustic Emission is associated with plastic permanent strain. The general principle of AE is illustrated in Figure 4.1.

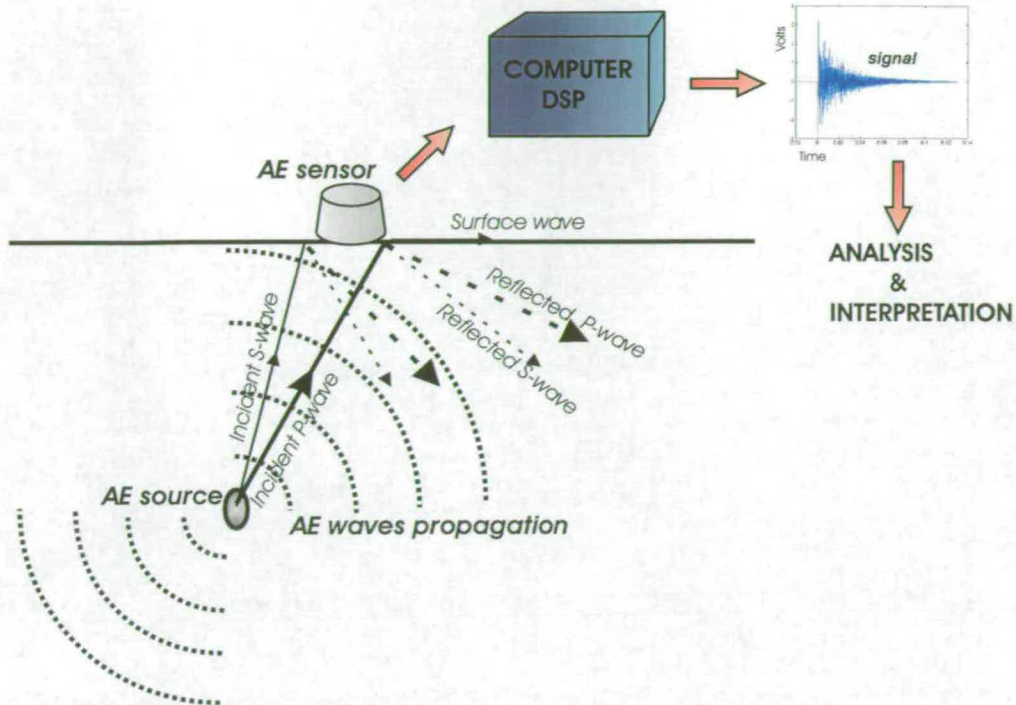


Figure 4.1: A schematic diagram of the AE Principle, from the AE source to the AE sensors and from the Digital Signal Processing (DSP) to the processing phase.

4.2 AE Waves and the AE Signal

Physically the AE waves consist of P-waves (longitudinal), S-waves (shear - transverse) and surface waves (Rayleigh waves), which are reflected and diffracted within the material [Ohtsu, 1995]. The direction of motion of longitudinal waves is identical to the direction of their propagation. They are the fastest propagating waves in an elastic body, are the first to arrive and are therefore called Primary waves (P-waves). Transverse waves travel perpendicular to the direction of the propagation, are slower and thus termed Secondary waves (S-waves). The P-waves are generally associated with the normal component of stress and then with a change of volume; unlike S-waves which are associated with the shear component of stress and therefore with an equivoluminal change. Rayleigh waves, v_R are the slowest waves; typically for a Poisson solid (i.e. $\mu = \lambda$) the velocity of the P-waves, v_P is approximately $\sqrt{3}$ the velocity of the S-waves, v_S [Sheriff and Geldart, 1995]; P-waves travel in concrete with a velocity between 3000-4800 m/sec, comparable to that in limestones or carbonate-cemented sandstones in geological formations. The velocity provides an indication about the quality of the

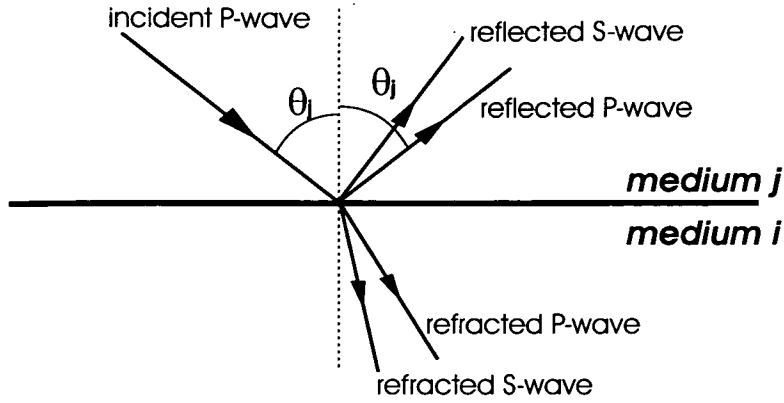


Figure 4.2: Representation of the Snell's Law and of waves generated at a solid-solid interface.

material, lower velocity indicating a lower quality. The different velocities of the elastic waves are summarised in the following equations:

$$v_P = 3000 - 4800 \text{ m/sec} = \sqrt{3}v_S \quad (4.1)$$

$$v_R \leq v_S \leq v_P \quad (4.2)$$

The velocity of the P-waves can moreover be expressed in terms of the Bulk (k) and shear (μ) moduli as [Sheriff and Geldart, 1995]:

$$v_P = \sqrt{\frac{(k + \frac{4}{3}\mu)}{\rho}} = \sqrt{\frac{(\lambda + 2\mu)}{\rho}} \quad (4.3)$$

where ρ is the density of the material.

During their travel, when the elastic waves meet a boundary (e.g. a different material) their energy is redistributed between P and S waves and the waves themselves are transmitted, reflected and refracted according to the *Snell's Law*:

$$\frac{\sin\theta_j}{v_j} = \text{constant} \quad (4.4)$$

where j is the relevant parameter for the j^{th} layer. E.g. if the Angle of Incidence = θ_j and v_j = velocity of the layer containing the incident wave, then the Angle of Reflection is also θ_j (Figure 4.2).

For normal incidence, using the constraints of continuity of displacement and stress at the boundary, it is possible to show that the reflection coefficient R between two

media is:

$$R = \frac{\text{Reflected amplitude}}{\text{Incident amplitude}} = \frac{I_2 - I_1}{I_2 + I_1} \quad (4.5)$$

where I is the Acoustic Impedance defined as $I = \text{Density} \times \text{Velocity}$. For non-normal incidence, the equation for $R(\theta)$ can be found in [Sheriff and Geldart, 1995], p.73.

The AE signal is a combination of all these waves and depends on the source, the properties and geometry of the material as well as on the sensor response. All AE signals contain background noise due to electrical (e.g. electromagnetic interferences, noise generated by the system itself or cables, ...) and mechanical (e.g. test machine, frictional noise, human activity, ...) causes. Methods employed to reduce the noise include frequency or data analysis filtering, reducing the test sensitivity, use of anti-noise materials between the noise source and the sensor and use of differential sensors [Pazdera, 2001].

4.3 AE Effects

One of the first diagnostic effects in AE was discovered by Kaiser in the early 1950s [von Kaiser, 1953] and it is known as the “*Kaiser Effect*”. This states that, if stresses are applied, removed and then re-applied on a structure, no acoustic emissions occur until the maximum load of the previous stage is reached [von Kaiser, 1953] [Henning, 1988]. Therefore Acoustic Emission is irreversible, and this irreversibility or stress “memory” can be used to determine the magnitude of the previous stress to which the structure has been subjected [Roca, 1997].

The Kaiser Effect does not apply to all materials or material conditions [Muravin et al., 2000]. Several works by Yuyama *et al.* show that the Kaiser effect exists on concrete beams subjected to tensile cracking as long as the crack width is less than 0.15-0.20 mm. This effect breaks down, when shear cracks appear and start to play a primary role [Yuyama et al., 1994] [Yuyama et al., 1995b] [Yuyama et al., 1995a] [Yuyama et al., 1998].

Despite the Kaiser Effect, when the level of stress becomes high, acoustic emissions can start below the previous maximum load. This behaviour is called the “*Felicity Effect*” and the Felicity ratio is defined as:

$$\text{Felicity Ratio} = \frac{\text{load at which emissions start}}{\text{previous maximum load}} \quad (4.6)$$

Thus as a material approaches failure, the Felicity Ratio decreases [Pollock, 1989].

Finally a study by Nesvijski [Nesvijski, 1997] on concrete specimens showed that during tests AE activity decreased for a certain period, until a new increase occurred just before the failure. This phenomenon was named the “*Silence Effect*” and its duration the “*silence time*”. An explanation for this was proposed by Nesvijski [Nesvijski, 1997] based on the Griffith theory of fracture [Lawn, 1993]. According to this theory numerous small cracks are present during the initial stage of the fracture process giving rise to several AE sources. Afterwards, when the damage localizes, the cracks join up resulting in fewer AE sources and consequently less AE activity. This effect has also been shown on rocks, and explained by a time-dependent theory for crack growth by the stress corrosion mechanism [Main and Meredith, 1991].

4.4 AE Monitoring and Analysis

Two types of Acoustic monitoring are possible: “*global*” monitoring which is intended to yield general information on the whole structure and “*local*” monitoring which yields a more detailed understanding of a certain area of the structure [Colombo et al., 2002] - they can both be long or short term monitoring [Carter and Holford, 1998].

During an AE test is it possible to identify two main steps:

1. Acquiring AE data.
2. Processing/Analysing AE data

The first step is of crucial importance if the second step is to be successful. Only by recording good quality AE data is it possible to obtain meaningful results during the processing. On the other hand, the type and data that need to be acquired depend on the kind of analysis and information that are expected. The two steps are then mutually interdependent [Colombo and Forde, 2001].

The AE signals can be analysed in an analogue or digital manner. The analogue analysis consists of a parametric study, whilst the digital analysis comprises a waveform analysis. The parametric study is an analysis of several AE attributes or parameters (i.e.: amplitude, duration, AE counts, arrival time, rise time - see Figure 4.3), which can be correlated with the fracture process and/or with properties and behaviour of a structure. The waveform analysis looks at the characteristics of the whole AE wavetrain.

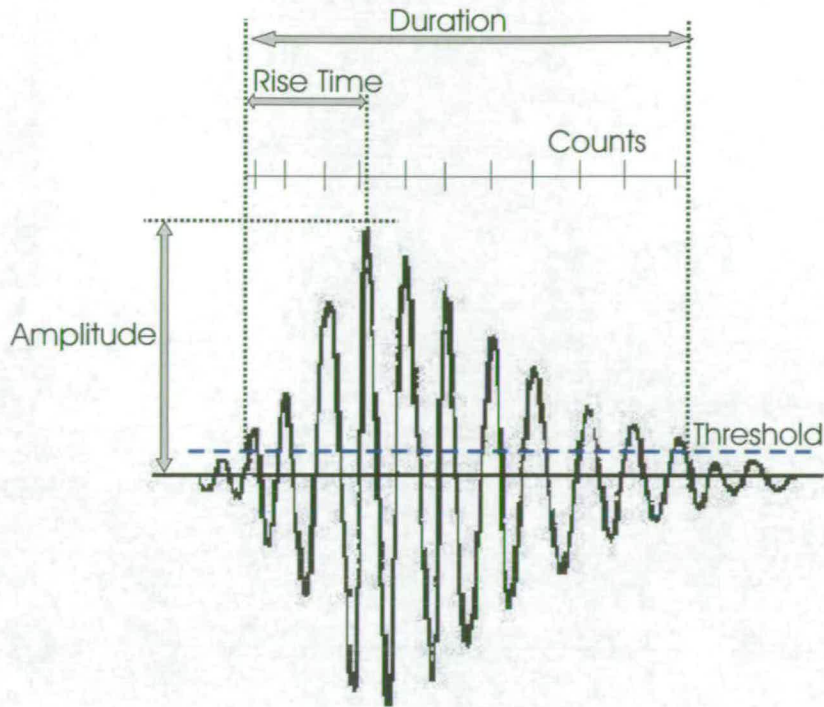


Figure 4.3: Schematic diagram of AE parameters. The diagram illustrates how the different attributes are measured.

Generally, the parametric analysis appears to be a quick and cost-effective method of monitoring structures, whilst the wave analysis is more time consuming. On the other hand the waveform analysis can provide more detailed information. It has been suggested that the parametric analysis could be used in the first instance to pinpoint the critical areas of a structure, followed by a subsequent waveform analysis on these areas [Colombo and Forde, 2001].

4.5 Concrete and Fracture Mechanics

Concrete can be defined as a proportional mixture of cement, aggregates, water and eventually admixtures [Neville, 1995]. Nowadays the most commonly used cement is Portland Cement which consists mainly of lime, silica, alumina and iron oxide. Aggregates can be natural (i.e.: belonging to the basalt, granite, quartzite and porphyry groups, ...) or artificial (i.e.: derived from industrial products) and they are generally classified as fine or coarse aggregates, depending on their size. Admixtures are chemical products added to specifically modify the properties of the concrete. The characteristics

of concrete depend on several factors, such as the properties of the constituent materials and their relative relationships, the water/cement ratio and the degree of compaction.

In terms of AE measurements, it is possible to refer to concrete as a homogeneous material. Heterogeneity depends on the relationship between the wavelength and the characteristic dimensions of the material; if the wavelength is larger than the sizes of the heterogeneous inclusions, then the effect of heterogeneity can be neglected [Roca, 1997]. In concrete, assuming a velocity (v) between 3000 and 4000 m/sec and a frequency range (f) just above 100 kHz, the wavelength (L) is:

$$L = \frac{v}{f} = \frac{4000}{150 * 10^3} = 0.027 \text{ m} = 27 \text{ mm} \quad (4.7)$$

which is greater than the normal “grain” size of concrete aggregates (20 mm). Having said that, it has to be pointed out that signal attenuation (defined as a loss of signal amplitude with increasing distance from the source) in concrete is a bigger problem compared to more homogeneous materials, such as metals.

In this thesis the fresh concrete used to cast the specimens in the laboratories of Edinburgh and Kumamoto Universities were obtained from an external supplier. This limited the range of properties of the available concrete. The concrete was poured and vibrated using an electrical poker in the laboratory. Details about the concrete used during the experiments are given in sections 6.1, 6.2 and 6.3.

As this thesis places emphasis on cracking, a brief overview of the fracture process is given. Different types of cracking can affect concrete, both in its fresh and hardened state. Non-structural cracks include plastic settlement and shrinkage, early thermal contraction, long-term drying shrinkage, crazing, corrosion of reinforcement, alkali-aggregate reaction, blister in, D-cracking [Neville, 1995]. Structural cracks are generally classified as shear cracks and tensile (bending) cracks; mixed-mode cracks [Shigeishi and Ohtsu, 1997] also occur. It is often useful to distinguish between *dead* or *dormant* cracks that do not open, close or extend and *live* cracks that do move [Raina, 1994].

Generally, materials fracture when their stress goes beyond a critical level; such stress is referred to as “*critical applied stress*”. Different materials fracture in different ways, due to a combination of several causes and this makes “critical applied stress” difficult to define. An in depth discussion on the different theories developed in fracture mechanics is beyond the aim of this thesis, but it is useful to define the three basic

modes of crack propagation [Lawn, 1993]:

- *Mode I* - opening mode, corresponding to a normal separation of the crack walls;
- *Mode II* - sliding mode, corresponding to a longitudinal shearing normal to the crack front;
- *Mode III* - tearing mode, corresponding to a lateral shearing parallel to the crack front.

Concrete, studies have shown that minute cracks exert an important influence on the behaviour of concrete and are largely responsible for its failure process [Robinson, 1965]. As these cracks are very small ($\leq 1 \text{ mm}$) they are usually referred as “microcracks” [Collact, 1985]. Conversely, easily visible cracks ($\geq 1 \text{ mm}$) can be referred to as “macrocracks” [Collact, 1985]. A microcracking event is the breaking of inter-molecular bonds; a collection of microcracks in close proximity, generally culminates with the formation of a macrocrack [Zietlow and Labuz, 1998]. Locating microcracks is generally a tedious and not trivial matter, especially if located in the interior of the material.

There is no universally accepted criterion to determine the tolerable limits of crack width w . A general guide can be defined for flexural cracks as follows [Raina, 1994]:

- fine cracks - $w \leq 0.3 \text{ mm}$ - there is no distress to the structure, but crack monitoring is recommended
- medium cracks - $0.3 \leq w \leq 0.5 \text{ mm}$ - there is a loss of structural capacity; monitoring and eventual repair is needed
- wide cracks - $w \geq 0.5 \text{ mm}$ - there is a serious loss of structural capacity and immediate repair is needed

The Acoustic Emission technique takes advantage of the release of energy associated with the formation and propagation of a microcrack. During this process part of the original strain energy is dissipated in the form of heat, mechanical vibrations and in the creation of new surfaces. The mechanical vibrations can be detected and recorded by an AE system.

The AE generation depends on both time and the amount of energy released from fracture events. Mori and Obata [Mori and Obata, 1988] studying the characteristics

of an AE source in a fatigue crack on a stainless steel sample, suggested the existence of two sources of acoustic emissions:

- a *cracking source* - at the tip of the crack and present only during loading;
- a *frictional source* - between crack faces, which emits both during loading and unloading.

Different types of cracks generate different types of AE signals with varying frequency ranges and amplitudes. These differences can be related to the degree of damage of the structure. Microcracks generate a large number of events of small amplitude whilst macrocracks generate fewer events but of larger amplitude. When the cracks open up, most of the energy is released and many small amplitude events are created. Furthermore, tensile cracks spawn large amplitude events whilst shear cracks create smaller amplitude signals [Li and Xi, 1995] [Iwanami et al., 1997].

In general, AE activity generated by crack nucleation and formation is defined as “*primary AE activity*”, whilst activity due to friction of pre-existing cracks is referred to as “*secondary AE activity*” [Shinomiya et al., 2002].

4.6 The “*b*-value”

In earthquake seismology, events of larger magnitude occur less frequently than events of smaller magnitude. This fact can be quantified in terms of a magnitude-frequency relationship, for which Gutenberg and Richter proposed the empirical equation:

$$\log_{10} N = a - bM_L \quad (4.8)$$

where M_L is the Richter magnitude of the events, N is the incremental frequency (i.e. the number of events with magnitudes in the range of $M_L \pm \Delta M/2$), and a and b are empirical constants [Shearer, 1999].

The Richter magnitude M_L is proportional to the logarithm of the maximum amplitude A_{max} recorded in a seismic trace, corrected for the attenuation in amplitude with distance due to wave propagation and inelastic absorption. The magnitude is proportional to the logarithm of source rupture area S :

$$M_L \propto \frac{2}{3}c \log_{10} A_{max} \propto \frac{2}{3}c \log_{10} S \quad (4.9)$$

where the factor c varies depending on the transducer. If the sensor is acting as a displacement transducer then $c = 1$; whilst if it is acting as a velocity transducer, $c = 1.5$; and finally $c = 3$ in the case of an accelerometer.

The same principle can be applied to the AE method to aid the study of the scaling of the “amplitude distribution” of the acoustic emission waves generated during the cracking process in the laboratory or in engineering structures. From the relationship (4.8), the b -value is the negative gradient of the log-linear AE frequency/magnitude plot and hence it represents the slope of the amplitude distribution. A study of amplitude distributions showed that different ranges of b -values were computed for different materials [Pollock, 1981]. Moreover, the b -value changes systematically with the different stages of fracture growth [Sammonds et al., 1994] and thus can be used to estimate the development of a fracture process. In terms of the AE technique, the Gutenberg-Richter formula can be modified as:

$$\log_{10} N = a - b' A_{dB} \quad (4.10)$$

where A_{dB} is the peak-amplitude of the AE events in decibels:

$$A_{dB} = 10 \log_{10} A_{max}^2 = 20 \log_{10} A_{max} \quad (4.11)$$

Comparing 4.9 and 4.11 the b -value obtained with this relationship should be multiplied by a factor of 20 to be comparable with the one used in seismology [Shiotani et al., 2001b].

In general terms, when distributed microcracks are occurring in the early stages of damage, the b -value is high and when the macrocracks begin to localise the b -value is low [Sammonds et al., 1994] (Figure 4.4).

Although the analysis of the b -value is well known in rock mechanics and seismology [Main, 1991] [Main et al., 1993], very little work has been done on concrete and civil engineering structures. In the work of Sammonds *et al.*, on damage evolution in rock, the trend of the b -value over time is plotted and a single minimum is observed just prior to dynamic failure. The decrease in b -value leads directly to dynamic failure immediately following minimum b -value [Sammonds et al., 1994].

An “improved” Ib -value was proposed and applied to the evaluation of slope failure by Shiotani *et al.* [Shiotani et al., 1994]. The Ib -value was defined as:

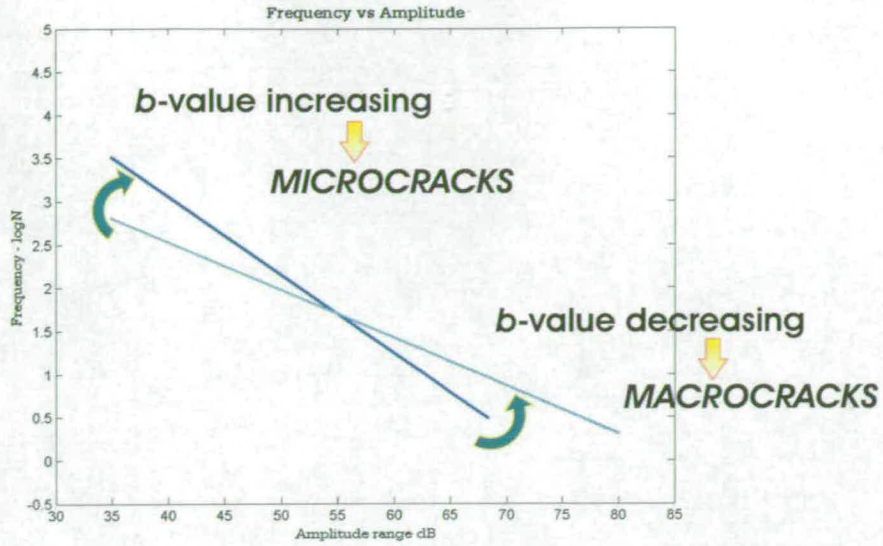


Figure 4.4: Frequency-magnitude distribution as fracturing develops. Note the relationship between b -value (the slope of the line) and cracking.

$$Ib = \frac{\log N(\mu - \alpha_1\sigma) - \log N(\mu - \alpha_2\sigma)}{(\alpha_1 + \alpha_2)\sigma} \quad (4.12)$$

where σ is the standard deviation, μ is the mean value of the amplitude distribution, α_1 is a coefficient related to the smaller amplitude and α_2 is a coefficient related to the fracture level. The variation of the Ib -value was found to be in significant agreement with the progressive failure of the slope model, suggesting that the Ib -value has the possibility to be a precursor for slope failure [Shiotani et al., 1994], just as it is in the laboratory to rock failure. The use of the improved Ib -value was later applied by Shiotani et al. [Shiotani et al., 2000b] to evaluate the fracture process in concrete. The work showed that the Ib -value analysis was successful in evaluating the fracture process of concrete specimens [Shiotani et al., 2000b].

In later chapters of this thesis a conventional b -value analysis is presented using the relationship 4.10 and assuming

$$b = b' * 20. \quad (4.13)$$

The trend of the b -value is also related to the damage parameter D . This parameter was derived from the study of Cox and Meredith on the microcrack formation in rock

[Cox and Meredith, 1993]. The accumulated state of damage in a material can be analysed in terms of acoustic emissions by defining a damage parameter:

$$D = \Sigma 10^{cm} \quad (4.14)$$

where m is the seismic magnitude and $c = 3$, where the instrument acts as an accelerometer (this will be demonstrated later during the analysis of data in section 7.1). In terms of AE, m can be computed as the AE event amplitude in $dB/20$. Such a parameter is proportional to the cube of the mean crack length [Cox and Meredith, 1993]. The parameter is descriptive of damage and thus by definition is related to the volume of the cracks, i.e. to a change of porosity in the concrete. The concrete fails due to dilatant cracking, just like rocks, although the evolution of the damage itself might be different for both materials [Costin, 1989].

4.7 AE Source Location

The analysis of the AE location consists of calculating the location of the AE sources in three dimensions from the compressional-wave arrival time at different transducer locations, using a least squares iterative inversion scheme. For beams a one-dimensional, linear location, is generally adequate. These source locations can then be related to the development or existence of defects in the structure. Such locations can be calculated in terms of AE hits (SoundPrint system), events or in terms of the energy associated with the events (PAC system). The location and its accuracy also depends on the type of signals that a system can record. The arrival time of higher amplitude signals is easier to identify and thus increases the precision of the source location. Details about the differences of the signals recorded by the PAC and the SoundPrint systems are given in sections 5.2 and 5.3.

According to the BS EN 1330-9:2000 [BS, 2000], hits, events and energy are defined as follows:

- *hit* - “detection of one burst signal on a channel”, where burst indicates an AE signal having an identifiable beginning and end;
- *event* - “physical phenomena giving rise to acoustic emission”, i.e.: a hit that was able to be located and therefore related to a physical cause;

- *signal energy* - “measurement of the relative energy of an acoustic emission burst”;
- *acoustic emission event energy* - “elastic energy released by an acoustic emission event”.

Nowadays different manufacturers of AE equipment may have different methods of calculating the AE energy, some of which may not correspond to the above definition.

Generally, the energy or power of a signal can be calculated using Parseval’s theorem, which in the time domain takes the form [Lynn and Fuerst, 1989]:

$$E = \frac{\sum_{i=1}^n s_i^2}{n} \quad (4.15)$$

where s_i is the value of the i^{th} time sample. The SoundPrint System, described in section 5.3, uses this type of calculation [Pure, 1996]. The PAC’s systems, described in section 5.2, developed a variation of this where energy is computed as follows [Colombo, 1999]:

$$PAC's \text{ ENERGY} = V(0) + V(1) + \dots + V(n) \quad (4.16)$$

where $V(n)$ is the voltage of the signal envelope at sampling $\#n$. As a result, the unit of the PAC’s energy is the voltage and it corresponds to:

$$1 \text{ AE energy unit} = 1/100,000 \text{ Volt}$$

Once the location of the sensors and the velocity of the P-wave is provided, the source location is computed completely automatically by the MISTRAS software (see 5.2). Some manual work is required by the SoundPrint software (see 5.3), but it requires only the location of the sensors as the wave velocity is determined automatically through an iterative method.

4.8 Relaxation Ratio

An AE test often consists of several load cycles on the material or structure of interest. Each cycle generally includes two phases: a loading phase and an unloading phase. During the undertaking of the experiments it was observed that during the early cycles of the tests, no or very low AE activity was recorded during the unloading of the specimens. This is consistent with the Kaiser effect for dilatant microcracks, and implies

that shear cracks do not form until near the macroscopic structural failure. The AE activity increased with the approach of failure and increasing damage of samples.

A parallel can be drawn with earthquake sequences, recognised in seismology. Earthquakes seldom occur as isolated events, they are made up of *foreshock* and *after-shock* sequences which are closely associated with a larger event called the mainshock. A schematic illustration can be seen in Figure 4.5. Aftershocks follow the mainshock and are linearly proportional to the area of the mainshock rupture. Aftershocks typically begin immediately after the mainshock over the entire rupture area and its surroundings, or are generally concentrated around the rupture perimeter or in locations where the mainshock has newly produced high concentrations of stress. Therefore it can be said that aftershocks are a process of relaxing stress concentrations caused by the dynamic rupture of the mainshock. Foreshocks are smaller earthquakes that precede the mainshock. They generally occur in the vicinity of the mainshock hypocentre and are probably a part of the nucleation process [Scholz, 2002].

Keeping earthquake sequences in mind the failure of a specimen, or accumulated damage at the end of a load cycle, can be considered as the mainshock. The foreshocks and aftershocks can be seen as the acoustic emissions generated respectively during the loading and unloading phases.

In the light of these preliminary observations, a “*relaxation ratio*” is proposed to quantify and compare the AE activity during the loading and unloading phases. At the time of these considerations, previous experiments have already been carried out, showing (see 7.2) that the AE energy seems to be the most effective parameter to describe the damage for a beam. Therefore the relaxation ratio is expressed in terms of energy and defined as:

$$RELAXATION\ RATIO = \frac{\text{average energy during unloading phase}}{\text{average energy during loading phase}} \quad (4.17)$$

where the average energy is calculated as the cumulative energy recorded (by the PAC’s equipment) for each phase divided by the number of recorded hits. A relaxation ratio greater than one implies that the average energy recorded during the unloading cycle is higher than the average energy recorded during the corresponding loading cycle, therefore the relaxation (aftershock) is dominant. Vice-versa, the loading (foreshock) is dominant.

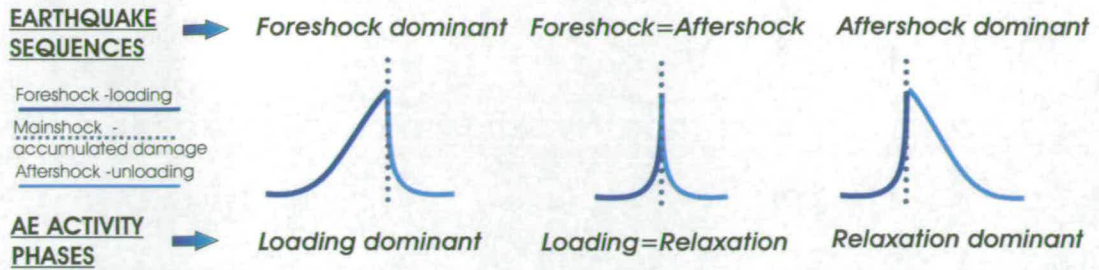


Figure 4.5: Schematic representation of earthquake sequences and AE activity phases. Each individual diagram shows the number of events, as a function of time, with the vertical dotted line being the time of the mainshock.

4.9 Moment Tensor

The Moment Tensor concept and representation was mainly used in seismology to model the mechanism of earthquakes [Manthei et al., 2001]. Although the mechanism of earthquakes and of AE sources are in principle the same, a major difference lies in the presence of tensile cracks in AE, that are conversely absent in earthquakes. For this reason, the theoretical treatment established in seismology had to be modified, including not only shear dislocation but also tensile dislocation [Ohtsu, 1991]. Different attempts have been made in this direction and a recognized leader of this is Prof. Masayasu Ohtsu (Kumamoto University, Japan) who developed a simplified and stable procedure to determine the moment tensor components [Ohtsu, 1987].

The aim of this section is to provide a critical overview and understanding of the moment tensor method developed by Ohtsu and of the basic theory behind it. Due to the complexity of the subject, this section is a summarized treatment and more details can be found in the papers that will be referenced. Any statement that does not specifically refer to a publication was derived from personal communications and discussions held with Prof. Ohtsu and Assoc. Prof. Shigeishi during the period spent at Kumamoto University in Japan.

4.9.1 Statement of the Problem

As explained in section 4.1, the presence in a structure of an AE source, at a vector location \bar{x}_0 at time t_0 , generates a displacement (i.e. a waveform) at a recording point \bar{x} at time t . In seismology, the source (e.g. a fault) is generically represented as an

internal force $\bar{f}(\bar{x}_0, t_0)$, and the displacement at the measured point $\bar{u}(\bar{x}, t)$ depends on the source and the structure. Such displacement is unique and describes the specific response of the structure where the response is defined by the Green's function $G(\bar{x}, t)$, which expresses the displacement in \bar{x} , due to a unit force applied in \bar{x}_0 [Shearer, 1999]. Therefore in general terms:

$$\bar{u}(\bar{x}, t) = G(\bar{x}, t) * \bar{f}(\bar{x}_0, t_0) \quad (4.18)$$

which is a linear equation and thus a displacement can always be calculated as a sum or superposition of different forces.

In a structure the momentum and angular momentum have to be conserved. Thus if there are internal forces they must act equally in opposing directions, giving rise to two possibilities: force couple and double couples (see Figure 4.6). Equation 4.18 can then be rewritten for force couples by the linear sum of each contribution:

$$u_i(\bar{x}, t) = G_{ij}(\bar{x}, t, \bar{x}_0, t_0) f_j(\bar{x}_0, t_0) - G_{ij}(\bar{x}, t, \bar{x}_0 - \bar{x}_k d, t_0) f_j(\bar{x}_0, t_0) \quad (4.19)$$

$$u_i(\bar{x}, t) = \frac{\delta G_{ij}(\bar{x}, t, \bar{x}_0, t_0)}{\delta x_k} f_j(\bar{x}_0, t_0) d \quad (4.20)$$

$$u_i(\bar{x}, t) = \frac{\delta G_{ij}(\bar{x}, t, \bar{x}_0, t_0)}{\delta x_k} M_{jk}(\bar{x}_0, t_0) \quad (4.21)$$

This final equation defines the Moment Tensor M_{jk} , which represents the internal forces at the source [Shearer, 1999]. To conserve angular momentum $M_{jk} = M_{kj}$ and if there is no volume change $\Sigma M_{ii} = 0$.

In an AE test, the displacement is what the sensors record and thus it is a known variable. Assuming that the Green's function for the structure under study is known as well, the problem consists in finding the components of the Moment Tensor that would allow one to specify the characteristic of the source. This is what is called an "inverse problem" [Ohtsu, 1984].

4.9.2 Moment Tensor Theory

The first step in the development of the Moment Tensor method, consists of defining the representation of the AE source, which in this specific case is a crack. It was found that the seismological use of pure double and couple forces, although it can be used as an analogy, cannot practically be applied to a tensile crack which has a finite volume

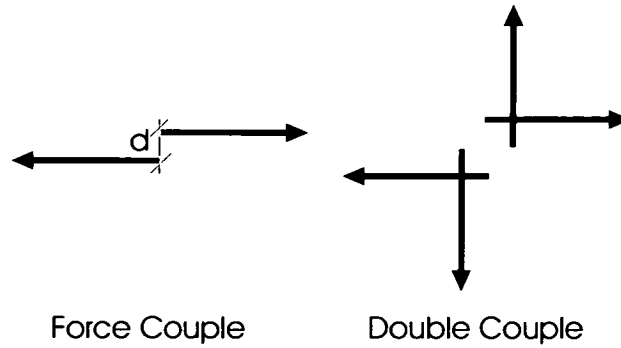


Figure 4.6: Force couples and Double Couple Forces representation [Shearer, 1999].

change due to the opening displacement [Ohtsu, 1999b]. The dislocation crack model is therefore adopted [Ohtsu, 1982], reasonably assuming the concrete as an homogeneous material (see section 4.5). According to this model, a crack is represented by two internal planes or crack surfaces, F^+ and F^- . Before the crack is formed the two planes are in coincident motion, whilst once the crack is present there is a dislocation between the two planes. To describe a crack is therefore to describe this dislocation and thus a crack is related to a displacement (and not to a force) that can be described using two vectors:

- \bar{n} = normal vector
- \bar{b} = dislocation vector or Burger's vector = $b\bar{l}$

where \bar{l} is the crack motion direction and \bar{b} can be described in terms of the displacement of the two surfaces as:

$$b_i(\bar{x}_0, t) = u_i^+(\bar{x}_0, t) - u_i^-(\bar{x}_0, t) \quad (4.22)$$

A representation of these vectors is given in Figure 4.7.

If α is the angle between the vectors \bar{b} and \bar{n} , then the following classification is derived [Ohtsu, 1987]:

- $\alpha = 0 = \textit{tensile crack}$
- $\alpha = 90^\circ = \textit{shear crack}$
- $\alpha \neq 0 \text{ and } \alpha \neq 90^\circ = \textit{mixed mode crack}$

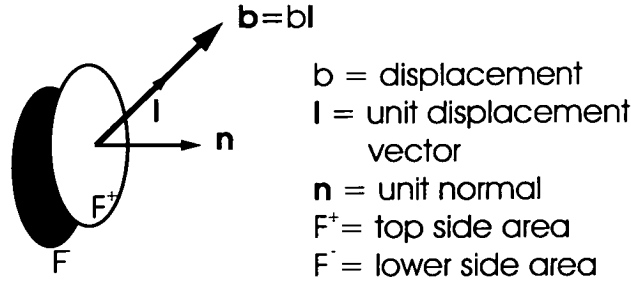


Figure 4.7: Dislocation model for a model crack [Shigeishi and Ohtsu, 1998].

The crack motion is both space and time dependent and is described by:

$$\bar{b}(\bar{x}_0, t_0) = b(\bar{x}_0)\bar{l}S(t) \quad (4.23)$$

where:

$b(x)$ is the magnitude of the crack

\bar{l} is the direction of the crack

$S(t)$ is the source-time function of the crack

As mentioned earlier, cracks generate a displacement \bar{u} that can be recorded by an AE sensor in a generic location \bar{x} at time t . From the theory of elastodynamics, a generic component of the displacement, derived by a crack can be mathematically expressed by two terms [Ohtsu, 1984]:

$$u_i(\bar{x}, t) = \int_S G_{ik}(\bar{x}, t, \bar{x}_0, t_0) * f_k(\bar{x}_0, t_0) dS + \int_S T_{ik}(\bar{x}, t, \bar{x}_0, t_0) * u_k(\bar{x}_0, t_0) dS \quad (4.24)$$

where the symbol “*” indicates the deconvolution integral, S is the boundary surface, G is the Green’s function, f is the applied force, u_k is the displacement at the source and T is the traction or Green’s function of the second type defined as:

$$T_{ik} = G_{ip,q}(\bar{x}, \bar{x}_0, t) C_{pqkl} n_l \quad (4.25)$$

where $G_{ip,q} = \frac{\delta G_{ip}(\bar{x}, \bar{x}_0, t)}{\delta x_q}$.

The first term of equation (4.24) describes the displacement due to an applied source force, i.e. $f(x_0, t_0)$ and it represents a balance of forces, whilst the second term defines the displacement generated by a discontinuity or a displacement, i.e. a crack [Ohtsu, 1984]. Generally one of the two terms dominates, so that when dealing with

cracks only the second term is normally considered [Ohtsu, 2002] and the boundary surface S is substituted by the internal crack surface F :

$$u_i(\bar{x}, t) = \int_F T_{ik}(\bar{x}, t, \bar{x}_0, t_0) * u_k(\bar{x}_0, t_0) dF = \int_F G_{ip,q}(\bar{x}, \bar{x}_0, t) C_{pqkl} n_l * u_k(\bar{x}_0, t_0) dF \quad (4.26)$$

and again:

$$u_i(\bar{x}, t) = \int_F C_{pqkl} G_{ip,q}(\bar{x}, \bar{x}_0, t) * [b(\bar{x}_0) l_k S(t)] n_l dF \quad (4.27)$$

$$u_i(\bar{x}, t) = G_{ip,q}(\bar{x}, \bar{x}_0, t) * C_{pqkl} l_k S(t) n_l \int_F b(\bar{x}_0) dF \quad (4.28)$$

$$u_i(\bar{x}, t) = G_{ip,q}(\bar{x}, \bar{x}_0, t) * C_{pqkl} l_k S(t) n_l V \quad (4.29)$$

$$u_i(\bar{x}, t) = G_{ip,q}(\bar{x}, \bar{x}_0, t) * M_{pq} S(t) \quad (4.30)$$

where:

- C_{pqkl} = elastic constant
- $G_{ip,q}(\bar{x}, \bar{x}_0, t)$ = spatial derivative of the Green's function that describes the elastodynamic field between \bar{x} and \bar{x}_0 , i.e. the propagation medium
- M_{pq} = Moment Tensor, that defines the kinematics of the crack, i.e. the crack type and orientation
- $S(t)$ = source-time function, that expresses the kinetics of the crack motion
- V = equivalent of source volume term, related to the rupture area F and the mean displacement b

In summary, the displacement (or waveform recorded by the AE sensor) depends on:

- the impulse response of the propagation medium - $G(\bar{x}, \bar{x}_0, t)$
- the source-time function - $S(t)$
- the crack orientation, size and mean displacement - M

From this mathematical definition the Moment Tensor can be expressed as [Ohtsu, 2002]:

$$M_{pq} = C_{pqkl} l_k n_l \Delta V \quad (4.31)$$

$$M_{pq} = [\text{elastic constant}] [\text{crack vector} \cdot \text{crack normal}] \Delta V \quad (4.32)$$

$$M_{pq} = [\text{elastic constant}] [\text{strain vector}] \Delta V \quad (4.33)$$

and thus is compatible to a stress tensor. As the Moment Tensor is defined by the product of the elastic constant [N/m^2] and the crack volume [m^3] this leads to the physical unit of a Moment [Nm] [Ohtsu, 2002]. For an isotropic material, the Moment Tensor components are defined as [Ohtsu, 1987]:

$$M_{pq} = \begin{bmatrix} m_{11} & m_{12} & m_{13} \\ m_{21} & m_{22} & m_{23} \\ m_{31} & m_{32} & m_{33} \end{bmatrix} = \begin{bmatrix} \lambda l_k n_k + 2\mu l_1 n_1 & \mu l_1 n_2 + \mu l_2 n_1 & \mu l_1 n_3 + \mu l_3 n_1 \\ \mu l_2 n_1 + \mu l_1 n_2 & \lambda l_k n_k + 2\mu l_2 n_2 & \mu l_2 n_3 + \mu l_3 n_2 \\ \mu l_1 n_3 + \mu l_3 n_1 & \mu l_3 n_2 + \mu l_2 n_3 & \lambda l_k n_k + 2\mu l_3 n_3 \end{bmatrix} \quad (4.34)$$

where λ and μ are Lamè constants and assuming $\lambda\mu = \epsilon$ the components of the tensor can be seen in relation to the elastodynamic expression:

$$\sigma_1 = (\lambda + 2\mu)\epsilon_1 + \lambda\epsilon_2 + \lambda\epsilon_3 = \lambda\epsilon_1 + \lambda\epsilon_2 + \lambda\epsilon_3 + 2\mu\epsilon_1 = \lambda(l_1 n_1 + l_2 n_2 + l_3 n_3) + 2\mu l_1 n_1 \quad (4.35)$$

$$\sigma_1 = \lambda l_k n_k + 2\mu l_1 n_1 \text{ with } k = 1, 2, 3 \quad (4.36)$$

As a consequence of the conservation of the angular moment, the components of the Moment Tensor are symmetrical and therefore only six are independent. If the Green's functions are known, therefore six or more recordings are needed to solve uniquely for M_{ij} . The diagonal components constitute dipole forces corresponding to a tensile crack opening in the three orthogonal directions. Off diagonal components represent a force couple corresponding to a shear crack [Ohtsu, 1987].

Ohtsu demonstrated [Ohtsu, 1982] the validity of applying the above theory derived from elastodynamics to AE. His study compared waveforms computed mathematically by applying the theory, with the waveforms recorded from concrete specimens and its results validated the use of the dislocation model to describe a crack. The study also assumed an initial theoretical expression for the source-time function $S(t)$, that is then compared with the $S(t)$ obtained by the deconvolution of the recorded waveforms. The good agreement obtained demonstrated the validity of the deconvolution process to obtain the source-time function of a crack. Therefore from equation (4.30), if the displacement is recorded by six sensors, to allow one to calculate the six independent components of the Moment Tensor, and if the Green's function of a structure is known, then a deconvolution can be applied and the crack motion described by $S(t)$ can be obtained and the source would then be completely defined.

During the study of 1982 [Ohtsu, 1982] Green's functions previously computed by other researchers in different fields were used. A later work [Ohtsu, 1984] addressed the specific issue of the determination of the Green's functions. Green's functions calculated for infinite space are not suitable to be applied to an AE study, because the waveforms are recorded by the AE sensor on a free-surface, i.e. the problem is related to a half-space [Ohtsu, 1984]. Based on the crack dislocation model, Fortran programs were developed [Ohtsu, 1984] that computed the necessary Green's functions and the Green's function of the second type for a tensile cracks and a slip. Simulated and experimentally detected waveforms were compared and shown to have a good agreement. It was also found that the value of the Poisson's ratio ν used in the calculations affected considerably the Green's function. The Poisson's ratio is in fact related to the Lamé constants according to [Ohtsu, 1999b]:

$$\lambda = \frac{2\mu\nu}{1 - 2\nu} \quad (4.37)$$

At this stage the validity of equation (4.30) has been proven and all the different factors have been addressed and defined. In summary:

- the use of elastodynamics theory was validated
- the validity of the dislocation model was proved
- the assumed source-time function was confirmed

- the Green's function could be mathematically generated if the elastic properties and geometry of the structure is known
- the displacement could be recorded by six AE sensors
- the components of the Moment Tensor were defined and could be calculated

The rigorous, general procedure described above is very complex so in applications some simplifying assumptions are made. The SiGMA procedure was therefore developed. SiGMA is the name given to a computer code, developed to automatically solve a simplified version of the problem. The SiGMA code uses only the first motion of the P-wave and assumes the far-field term of the Green's function dominates for homogeneous and isotropic materials [Ohtsu, 1991].

As equation (4.30) is time dependent, theoretically all the amplitudes of a waveform should be considered, but this would make the process too slow and expensive (it has to be remembered that at the time of the development of the method, the computers were not as advanced as today). The reason for the first simplification is due to the certainty that the first motion amplitude is related to a P-wave, to which the theory refers to. The P-waves are the fastest in a medium (section 4.1) and thus the first to arrive. Conversely, it is not possible to be sure of which type of wave the remaining amplitudes refer to.

The far-field approximation is based on the relationship between the propagating distance of the elastic waves and the characteristic dimension of the cracks. An AE wave has a typical duration of approximately 1 msec and in concrete can travel for several metres. The dimensions of the crack in concrete are known to be of the order of millimetres and thus the far-field approximation is reliably applicable [Ohtsu, 2002]. Applying the far-field approximation, the displacement is defined as:

$$u_i(\bar{x}, t) = -\frac{1}{4\pi\rho v_p^3} r_p r_q r_i \frac{1}{R} \frac{dS(t)}{dt} M_{pq} \quad (4.38)$$

where:

R is the distance between the AE source at point x_0 and the sensor at point x

ρ is the density of the material

v_p is the velocity of the P-wave

and r_i are the components of the vector \bar{r} indicating the direction of R . Note that in the far-field, the radiated displacement is proportional to the first derivative with respect to time of the source-time function.

Using the far-field term of the Green's function, the validated theoretical expression of $S(t)$, the waveforms recorded by six sensors and considering the effect of the reflection at the surface, the SiGMA code solves a set of linear equations derived from equation (4.30) that takes the following form [Ohtsu et al., 1998a]:

$$A(\bar{x}) = \frac{C_s Ref(\bar{l}, \bar{r}) r_p m_{pq} r_q}{R} \quad (4.39)$$

where:

A = amplitude of the first motion of the P-wave

R = distance between the AE source at point \bar{x}_0 and the sensor at point \bar{x}

C_s = calibration coefficient of the AE sensors, obtained prior to the analysis using a pencil-lead break at the known source position

\bar{r} = vector of components r_p and r_q indicating the direction of R

\bar{l} = vector indicating the direction of the sensor sensitivity

$Ref(\bar{l}, \bar{r})$ = reflection coefficient between vectors \bar{l} and \bar{r} as defined by the Snell's law in the generalised form of equation (4.4) and the Zooprutz equations in [Sheriff and Geldart, 1995].

Knowing the six values of the first motion amplitude from the waveforms recorded by six AE sensors, the SiGMA code solves the set of equations (4.39) and determines the six independent components of the Moment Tensor [Ohtsu, 1991].

Once the components of the Moment Tensor are known, they can be decomposed and expressed in a new form. It is possible to calculate the eigenvalues and eigenvectors of the Moment Tensor and obtain the components along the principal axis, as shown in the top half of Figure 4.8, where I, II and III represent the principal directions. From equation (4.34) the three eigenvalues result [Ohtsu, 2002]:

$$\text{maximum eigenvalue} = \mu \frac{(l_k n_k)}{((1 - 2\nu) + 1)} \quad (4.40)$$

$$\text{intermediate eigenvalue} = \frac{2\mu\nu(l_k n_k)}{(1 - 2\nu)} \quad (4.41)$$

$$\text{minimum eigenvalue} = \mu \frac{(l_k n_k)}{((1 - 2\nu) - 1)} \quad (4.42)$$

These components can, once again, be decomposed using a method proposed by Knopoff and Randall [Knopoff and Randall, 1970], according to which the configuration

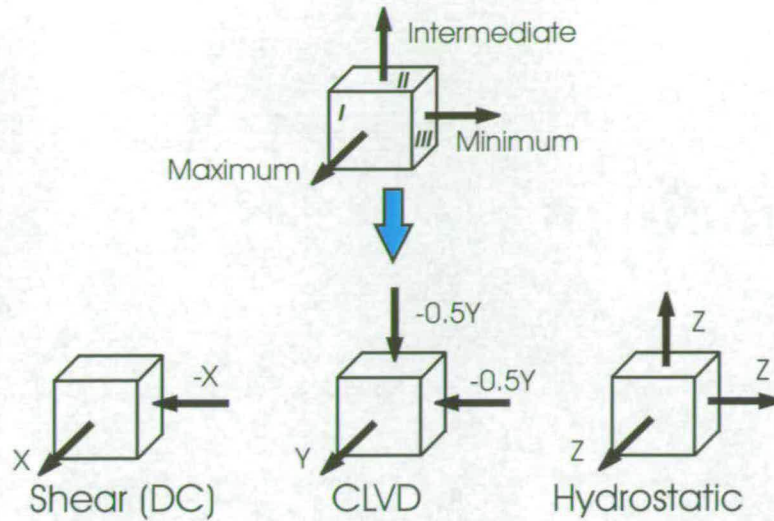


Figure 4.8: Eigenvalue decomposition of the Moment Tensor in a Double Couple (DC), Compensated Linear Vector Dipole (CLVD) and hydrostatic part - adapted from [Shigeishi and Ohtsu, 1998].

on the top of Figure 4.8 is equivalent to a new configuration (shown in the bottom half of Figure 4.8), which includes a Double Couple (DC) part, a compensated linear vector dipole (CLVD) part and an isotropic part [Ohtsu, 1991].

The SIGMA code utilizes this last decomposition and normalized the components by the previous maximum eigenvalue (equation 4.40) to obtain [Ohtsu, 1991]:

$$\text{maximum eigenvalue} = 1.0 = X + Y + Z \quad (4.43)$$

$$\text{intermediate eigenvalue} / \text{maximum eigenvalue} = 0 - 0.5Y + Z \quad (4.44)$$

$$\text{minimum eigenvalue} / \text{maximum eigenvalue} = -X - 0.5Y + Z \quad (4.45)$$

The code thus classified the type of crack according to the proportions of the components X , Y and Z . The ratio X denotes the contribution of the shear motion, whilst the $Y + Z$ shows the contribution of tensile motion, i.e. a shear crack corresponds to the case of $X = 1$, $Y = 0$, $Z = 0$ and a pure tensile crack has $X = 0$ [Ohtsu, 1991]. The following criteria was finally chosen [Munwam and Ohtsu, 1999]:

- shear ratio $X \leq 40\% \implies$ *TENSILE CRACK*
- shear ratio $40\% \leq X \leq 60\% \implies$ *MIXED CRACK*
- shear ratio $X \geq 60\% \implies$ *SHEAR CRACK*

Once the crack has been classified, its directions is derived by calculating the eigenvectors [Ohtsu, 1991]:

$$\text{eigenvector for the maximum value} = \bar{l} + \bar{n} \quad (4.46)$$

$$\text{eigenvector for the intermediate value} = \bar{l} \times \bar{n} \quad (4.47)$$

$$\text{eigenvector for the minimum value} = \bar{l} - \bar{n} \quad (4.48)$$

where “x” indicates the vector product.

A post-analysis procedure was also developed [Ohtsu et al., 1994] to validate the simplified solutions obtained by the SiGMA code. It consists of using the location and the Moment Tensor components obtained by running the SiGMA code, to synthesize theoretical waveforms. The SiGMA code is then re-applied to these waveforms and only the results for which the solutions of the two SiGMA code are in good agreement are accepted.

As a final comment it has to be pointed out that in theory, the Moment Tensor method could be applied to any material and structure as long as the hypothesis on which the method is based (homogeneity and isotropy of the material and far-field approximation) are respected and the material constants are accordingly modified.

The following section provides some practical requirements that should be observed during a Moment Tensor test as well as an overview of some applications of the method.

4.9.3 Moment Tensor Applications

Since its development, the Moment Tensor method has been used in Japan in several applications including in-situ hydro fracturing tests [Ohtsu, 1991], and several mortar, concrete and RC samples.

As a results of some of these applications, some practical requirements can be identified for concrete [Ohtsu et al., 1998a]:

- the AE sensors have to surround the area where the fracture process is expected spherically and direct radially
- to increase the accuracy of the source location, the sensors should be distributed asymmetrically

- in order to acquire valid data, the distance between an AE sensor and the AE source should be less than 1 m for typical frequencies of approximately few hundreds kHz.

The Moment Tensor method was applied to RC beams under static bending load [Shigeishi and Ohtsu, 1997] [Shigeishi et al., 1999b], and showed good agreement with the location, orientation and displacement vector of visible cracks. A higher AE activity was also recorded when a deformed steel reinforcement bar was used compared to normal steel reinforcement bars.

Two applications, on an L-shaped RC sample and on a notched rectangular beam, were also reported [Ohtsu et al., 1998a]. In the first case, resonant type sensors were used and approximately 1.8% of the initial recorded signals were successfully conducted through a Moment Tensor Analysis. In the second case, broadband sensors were adopted and the percentage increased to approximately 3.3%. Two reasons were given for the larger number of results obtained in the second case: the smaller size of the sample and the type of sensor, but no clear statement was made about the inappropriate use of resonant sensors. Further details about this issue are elaborated in section 7.5 - in a simple analogy here, we prefer a high fidelity (broadband) amplifier in our CD player to a narrow-band (resonant) one.

Experiments continued on three point bending tests on notched rectangular beams [Ohtsu et al., 1998b], until the percentage of results increased to approximately 10% during further experiments on concrete and mortar beams subjected to bending tests [Ohtsu, 1999a].

An extension of the SiGMA procedure was proposed [Shigeishi and Ohtsu, 1998] to evaluate the volume of micro-cracks forming on a cement-mortar plate, but the accuracy of the estimated volume could not be confirmed as the real volume of the internal micro-cracks could not be practically measured. The work on this implementation continued [Shigeishi and Ohtsu, 2001] on cement-mortar and concrete plate samples, estimating the damage parameters from the moment tensor components and comparing it with the calculated crack volume - a good agreement between the cracks volume and the damage was found.

4.10 Summary AE: Advantages and Drawbacks

The AE method has two main differences from the other non-destructive techniques: the signal has its origin in the material itself and not in an external source; it detects movements ($\frac{dx}{dt}$), not absolute geometrical discontinuities [Pollock, 1989]. Moreover the question of whether AE is completely non-destructive is often posed, since during testing it is often necessary to fracture the samples [Grosse, 2002]. There is damage to the structure, but the method does not compromise the integrity of the structure. In this sense the method can be regarded as non-destructive. To observe the evolution to destruction, in this thesis, the laboratory samples were loaded until they failed completely. This allows a prediction of total failure from data recorded in the early stages of damage. As with all NDT techniques the Acoustic Emission method has some advantages and some drawbacks. Advantages include:

1. The possibility to have continuous monitoring.
2. It requires only limited accessibility to the tested object; when working on a bridge, no lane closure is required during the setting up and the monitoring (if using normal traffic as load).
3. The instrumentation is relatively quick and easy to install and can be linked to a Modem to provide remote data collection.
4. It can be retrofitted to existing structures and adapted to existing types and is not invasive.
5. The AE technique can locate the sources generating the elastic waves (i.e.: the defect, cracks and so on) and can be used to predict crack locations, orientation and type before they are visible on the surface.
6. It can detect active flaws.

Drawbacks include:

1. AE systems are generally quite expensive.
2. The data analysis is not always trivial, requiring a skilled operator and lots of computer memory and disk space.

3. The emissions depend on the load configuration and on the material and are affected by inelastic attenuation and background acoustic noise.
4. Although the AE systems can locate defects and cracks they cannot determine the absolute size, only the latest crack growth increment.
5. A standardised procedure for civil engineering structures does not exist yet.

A significant part of this thesis was dedicated to overcome the drawbacks related to the data analysis by developing and proposing new and alternative ways of processing AE data (Chapter 7). The last of the above mentioned drawbacks have also been addressed and a standard protocol for AE application was drafted (section 5.6).

Chapter 5

Equipment and Experimental Procedure

This chapter deals with the first stage of AE testing, which concerns the acquisition of useful AE data, as defined in Chapter 1. The AE equipment is presented, with specific description of the two main systems used during the experiments - the PAC and the SoundPrint systems. Their relative softwares and the different parameters that need to be set up during an experiment are also discussed.

The AE sensors represent a crucial point during the acquisition phase of an AE experiment and emphasis was put in defining their characteristics and test requirements. The results of an experiment investigating the use of different sensors couplant materials are reported.

The PUNDIT apparatus is described as it was used to calculate the velocity of the elastic wave through the concrete specimens. This velocity was necessary for performing the AE source location (section 7.2). The specific values were not of interest although they are reported in the next chapter.

The key factors influencing an AE test are defined and a proposed protocol for AE application is drafted.

5.1 Instrumentation

The vast majority of the Acoustic Emission market is controlled by the Mistras Holdings Group (www.mistrasholdings.com), whilst a few other smaller companies (Valen - Germany, SoundPrint - Canada, NS - Japan...) make up the remainder. In this

study three AE systems have been used: the Mistras system, the DiSP system and the SoundPrint system. Their specific characteristics are described in the following sections.

The main AE instrumentation consists of a computer, a signal acquisition-processing device and a set of amplifiers and transducers. Although the settings differ for different systems, some common features can be highlighted, such as the “threshold” value and the “sample rate”.

An AE signal is recorded when it crosses the “threshold” value, a parameter set up by the operator on the instrumentation in order to avoid recording unwanted noise. If expressed in dB, a value between 30 and 45 dB is generally satisfactory for concrete, depending on the noise level of the surrounding environment.

In a Digital Signal Process (DSP) environment, a signal is defined only for particular instants in time, or *sampling instants*. Therefore an analog signal is digitised through the process of sampling, i.e.: the wave is represented by a series of samples at a fixed defined interval. The *Sampling Theorem* which defines how often a signal should be sampled states that: “An analog signal containing components up to some maximum frequency f_1 Hz may be completely represented by regularly-spaced samples, provided the sampling rate is at least $2f_1$ samples per second” [Lynn and Fuerst, 1989]. A lower sampling rate would lead to aliasing errors, i.e. part of the signal is falsely translated, and the frequency spectrum distorted with false low frequency signals included.

The settings used during the tests will be specified for each experiment.

5.2 MISTRAS and DiSP Systems

Both the MISTRAS-2001 (Massively Instrumented Sensor Technology for Received Acoustic Signals) and the DiSP are PAC’s (Physical Acoustic Corporation) systems (Figure 5.2). The PAC is the UK subsidiary of the Mistras Holdings Group.

The DiSP is the new advanced version of the MISTRAS system and they both work at frequencies above 25 kHz. Both are fully digital, multi-channel, computerized acoustic emission systems that can perform waveform and signal measurements and store and display recording data. The systems mainly consist of a Personal Computer, a circuit board, sensors, preamplifiers and coaxial cables [PAC, 1995]. The MISTRAS



Figure 5.1: MISTRAS and DiSP systems.



Figure 5.2: PAC's AE sensors.

and DiSP models owned by Edinburgh University have eight channels and four channels respectively. Two sets of sensors were also available at the University: eight broadband sensors (PAC WD) and eight resonant sensors (PAC R6I Resonant 60 kHz Integral sensor) (Figure 5.2). A different broadband model of sensors (PAC UT-1000) was used in Kumamoto University. The resonant sensors have an incorporated amplifier of 40 dB, whilst the broadband types use an external amplifier that can be set to 40 or 60 dB. The 40 dB option was adopted in all the experiments. Further details about the AE transducers are given in section 5.4.

The PAC's systems are equipped with software packages to collect and process

data. The MISTRAS software deals with AE parameters, whilst the MI-TRA (Mistras Transient Recorder and Analysis) software allows the user to perform AE waveform collection and analysis. Both the Mistras systems software run under MS-DOS, a new version of the parametric software is available for the DiSP system [PAC, 1995]. The data collected with one software can be replayed with the other software, as long as they are converted using some of the utilities available with the software itself. In the conversion process some of the features of the software are lost. An example of one of these cases is described in section 7.2.1.

The two software options need different settings to be set up before starting an experiment. When recording the AE data using the MISTRAS software, three specific parameters have to be defined in order to provide the software with the correct information to extract the AE parameters [PAC, 1995]:

- PDT - Peak Definition Time - it enables the system to determine the peak time (i.e. the rise time) of the signal; if it is too short, the software will choose an incorrect value of rise time. Generally it can be computed as:

$$PDT = D/C \quad (5.1)$$

where D represents the sensors' spacing and C is the velocity of the elastic waves.

- HDT - Hit Definition Time - it enables the system to determine the end of the recorded hit and on this basis to calculate all the AE parameters; it has to be set up long enough to include the whole signal but without overlapping two consecutive hits. It can be calculated as:

$$HDT = L/C \quad (5.2)$$

where L is the length of the structure under study and C is again the wave velocity.

- HLT - Hit Lockout Time - it is the time that the system uses after having recorded a signal, to set itself up and be ready to record the following hit; it can be set up as the largest allowed value (65534 μ s) in order to control the quantity of data to be acquired when a large amount is expected.

The quickest and most accurate way to choose the values of these settings is to collect some waveforms (using the MT-TRA software) from the area to be monitored and scan over their rise time and shape. An estimation of the rise time plus a margin

of error of approximately 50% gives the value of PDT. By looking at the tail of the signal and when it goes below the fixed threshold, the value of HDT can be estimated. Generally the values of PDT and HDT comply with the following relationship:

$$HDT \geq 2PDT$$

The above parameters can be seen in Figure 5.3 whilst the values used during the experiments described in this thesis are summarised in Tables 6.2 and 6.5. During the recording of the data using the MISTRAS software, all the sensors are automatically set up in an *independent* “trigger mode”, i.e. each channel has its own trigger. Conversely in the MI-TRA software the type of “trigger mode” can be determined by the operator: one can choose between the *independent* mode or a *synchronised* mode (i.e. when a hit triggers the first channel, all the remaining ones are also triggered automatically) in which the channels record waveforms generated from the same event are linked together. The MI-TRA software also allows one to define the “trigger source”, choosing between *External* - EXT, *Independent* - IND and *Digital* - DIG. The trigger source identifies the way in which the channels get triggered, i.e. from an external source; from a digital trigger where the trigger is automatically generated when the signal exceeds the specified threshold; from a internal trigger, when the recording is continuous, without waiting for any form of trigger [PAC, 1995]. Finally, a *pre-trigger time* has to be set up in both software. This value defines the amount of time of signal that the software records before the threshold is exceeded (Figure 5.3). The definition of the pre-trigger time and of the trigger mode has a significance when a Moment Tensor analysis has to be carried out as will be explained in section 7.5. The values adopted during the other types of analysis will be therefore omitted.

The MISTRAS software includes an option which, if selected, allows the user to collect waveforms together with the AE parameters. Enabling this option is fundamental if the data are expected to be replayed using the MT-TRA software, but it significantly increases the size of the acquired data file. A file containing only AE parameters data has a size generally less of 1Megabyte, whilst when waveforms are recorded, file sizes up to few hundred Megabyte can be reached.

An external zip drive or the Laplink software were used to transfer the data from the systems to other PCs for subsequent processing . The data were stored by the systems in a binary format, but it was possible to convert them to ASCII file using

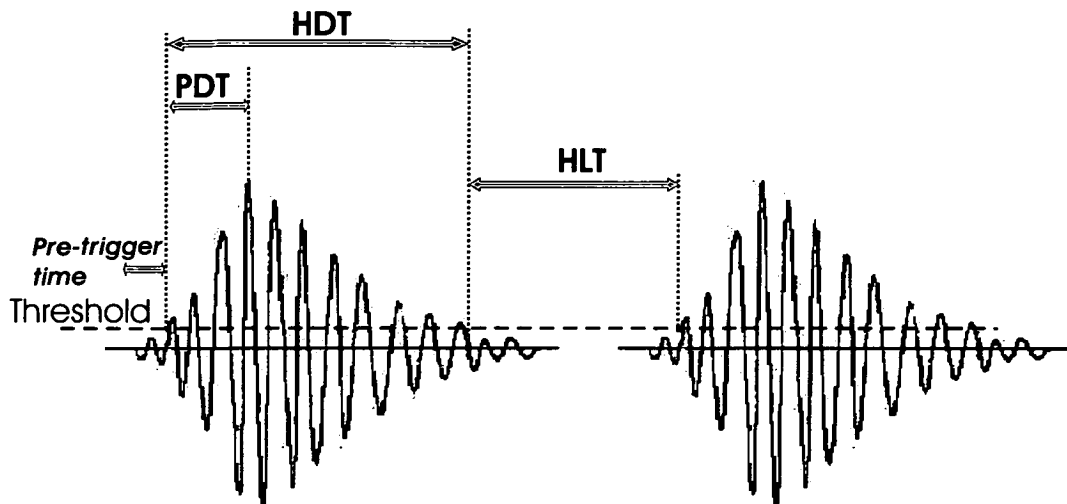


Figure 5.3: PAC's settings parameters.

specific software utilities. Once converted the file could be analysed and processed using MATLAB, taking advantage of its flexibility and advanced features.

The reliability of the system itself was checked by connecting an oscilloscope to the system. This allowed comparison of the waves on the two screens, which apart from small differences due to system or cable noise, were very similar.

5.3 SoundPrint System

The SoundPrint System (SP) was developed by Pure Technologies Ltd (Canada) for the detection of wire breaks in tendons in ungrouted ducts in parking structures, buildings and bridges [Paulson, 1998]. It is generally set up to operate in the frequency range from 0 to 25 kHz. The system (Figure 5.4) is composed of low-cost data acquisition and computing hardware, an array of sensors, standard TV cables (RG-6 with "F" connectors) and analytical and data management "SoundPrint SPDaq Software" [SoundPrint, 1996].

The sensors used during the experiments of this thesis are high-output unpowered, polyaxial piezo-electric accelerometers. They have a range of sensitivity to over 100kHz, but have a peak sensitivity between 5 and 10 kHz, corresponding to a wavelength between 0.8 and 0.4 m in concrete (applying equation 4.7).

A different software, the *SoundPrint Analyst*, allows (if installed on a PC together with an accompanying hardware key connected to the parallel port) a user to personally

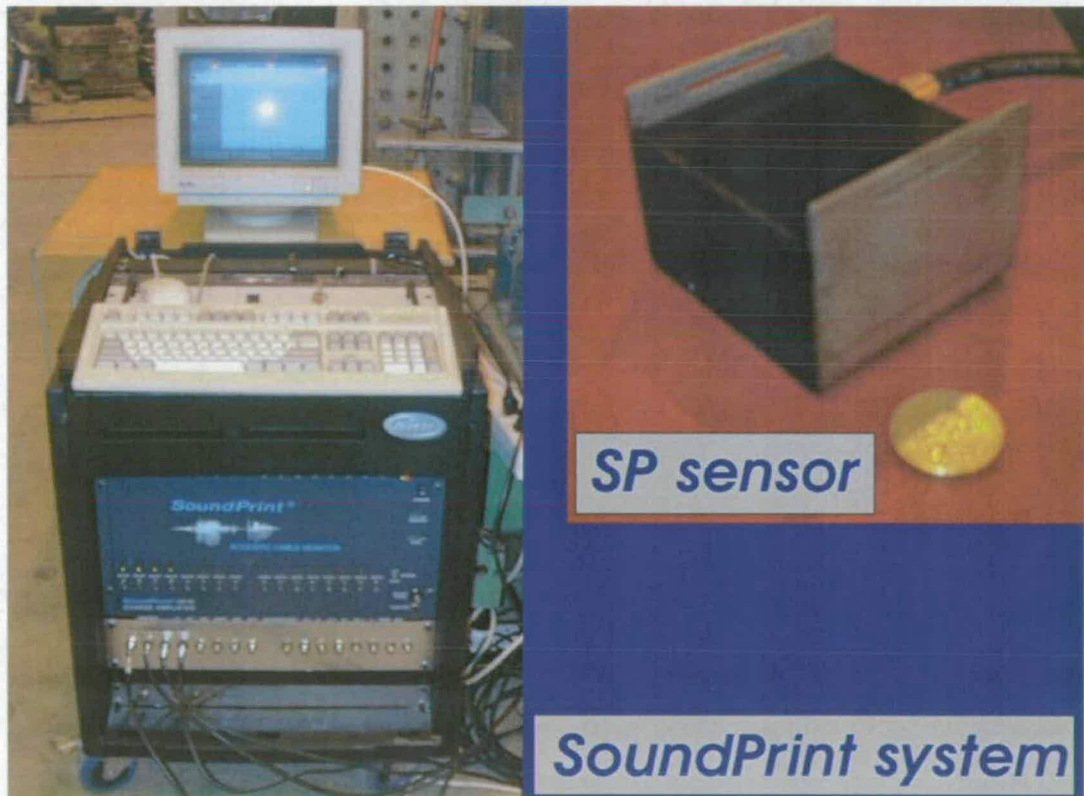


Figure 5.4: SoundPrint System and sensor.

analyse the recorded data [Pure, 1996]. As a second option, the data can be sent to the processing centre in Calgary by means of an Internet file transmission protocol [Cullington et al., 1999].

The commonly used SP system is optimised to detect tensile fractures in tendons. During this study however it was used to detect the formation and propagation of cracks which generate signals which have a much lower energy than a wire break. For this reason, the triggering of the system had to be modified.

In the SP system, the triggering is governed by two controls: the T-Mast and the threshold settings. The T-Mast is an analogue adjustment of a potentiometer, located in the front panel of the system. By turning it clockwise, it amplifies the trigger signal and consequently increases the system sensitivity. The threshold setting consists of a 3-digit thumb-wheel control on the top of the instrument. The hardware also has a delay setting which sets an interval time between two consecutive trigger events [Hill et al., 2002]. As the cracking process usually generates emissions at a high rate, the delay was always set to minimum.

5.4 AE Sensors

The AE sensors are piezoelectric crystal transducers that convert movement (a variation of pressure) into an electrical voltage. Physically, the transducers detect a movement that leads to a redistribution of the electrical charges inside the crystal resulting in a change in the voltage. A typical AE sensor transforms elastic vibrations of 10^{-9} mm amplitude into electrical signals of 10^{-6} V amplitude. A good sensor should have a high signal-to-noise (S/N) ratio [Ohtsu, 1995].

Two types of piezoelectric material are commonly used: quartz and polycrystalline ceramics. Quartz is a natural material that is considered the most stable and reliable of piezoelectric materials and it can be used over a relatively large temperature range with little loss of performance. Polycrystalline ceramic materials are man-made and a polarization process has to be carried out on them to force them to become piezoelectric. They are less reliable and more sensitive to temperature and electrical interference [PCB, 2000].

5.4.1 Types of Sensors

There are several types of AE sensors according to their different aims and applications. The choice of the appropriate transducer is an important matter in order to perform a successful AE test. The choice of the type of sensor depends on several factors:

- structure material, geometry and scale;
- working environment;
- type of data analysis which is required;
- sensitivity and frequency range of the transducer;
- signal attenuation.

During its propagation through the medium, the acoustic emission signal is attenuated. It was found that in concrete, for frequencies of about 100 kHz, after 1m the waves are attenuated by 50% [Ohtsu, 1995]. Higher frequencies have even greater attenuation. A large structure translates to a larger distance between the sensors and therefore a greater attenuation, so that only the lower frequencies are detectable. A small structure means a smaller distance between the sensors and then less attenuation, so that a larger range of frequencies can be detected [PAC, 2001]. In the light of these considerations, the sensor location and the dimensions of the structure that has to be analysed are important factors when choosing the appropriate type of sensor.

The main classification of transducers distinguishes between “resonant” or “broadband” sensors. Resonant transducers are more sensitive but only within a certain fixed frequency range. They are usually used for low frequencies when there is large attenuation and an analysis of the signal frequency spectrum is not required. The broadband sensors although less sensitive, react to a wider range of frequencies and allow a reliable frequency analysis [PAC, 1997a] [PAC, 2001]. On concrete, the working frequency range is normally up to few hundred kHz [Ohtsu, 1995].

5.4.2 Mounting and Coupling of the Transducers

The mounting of a sensor is an essential requirement in order to record good quality data. Firstly a good acoustic coupling between the sensor and the surface of the structure has to be ensured. To achieve this, the sensor surface needs to be smooth

and clean and the couplant material should be thin so as to fill any eventual air gaps [PAC, 1997a].

It is common practice to use Cyanoacrylate adhesive glue (e.g. Superglue), but during the experiments it was found difficult to remove the sensors.

The nature of the coupling substance affects the quality of the bond and has implications on the quality and reliability of the recorded signal. For this reason an experimental study of a range of materials that may be suitable as couplants was carried out. The following eight substances were selected, and the specific products were chosen to be representative of the commonly available brands of each substance:

- superglue - Cyanoacrylate Adhesive, manufactured by RS Components
- micro soft beads of wax
- general purpose light brown grease by RS Components
- plasticine - indicating the trademark used for soft modelling material (generally used by children); the “Humbrol” brand was specifically used during this experiment
- general purpose adhesive - manufactured by RS Components
- sealant - indicating a waterproof all purpose sealant; the Uni-bond - Henkel brand was specifically used
- adhesive pads - the “Pritt Sticky Pads” brand was specifically used
- Hot gluegun glue - indicating the hot glue commonly used in gluegun; the “Loctite” glue was specifically used

As the thickness of some of the substances also affects the response, three different thicknesses were considered in those cases: 2 mm, 5 mm and 8 mm.

Based on the problems encountered during the early AE tests, the following criteria were considered:

- quality of the received signal- e.g. the frequency content and the amplitude;
- adaptability to surface - e.g. ability of the substance to mould to the surface;

- repeatability - e.g. ability to produce the same quality of results during repeated tests;
- durability - e.g. ability of the substance to hold the transducer over time;
- ease of installation;
- ease of removal - e.g. time taken and effort required to remove the accelerometer from the surface and the couplant from the accelerometer, without the latter being damaged;
- location limitations - e.g. necessity of power supply that could limit the ease of use in some fieldwork;
- time for substance to set, if necessary;

It was decided not to use the AE sensors but a general accelerometer during the experiment. The reasons for this were:

- the PAC sensors do not exhibit a flat calibration curve;
- the SP sensors record signals that can only be used with the SoundPrint software, whose features did not suit this test;
- by using an accelerometer, the results would be applicable not only to AE but to any non-destructive technique which involves the use of transducers, such as sonic testing and tomography and pulse-impact echo.

The test was undertaken using an impact-echo system which tied into MATLAB. The impact echo technique consists of generating waves in a material through an impact applied by an external source, such as a hammer or a ball bearing [Sansalone and Streett, 1997]. The system used for this experiment had three channels: one recorded the hammer impulse, the remaining two recorded the signal detected by the accelerometers. The latter were connected to a pre-amplifier and through it to a switch box and then on to a laptop. The transducers were PCB Piezoelectric 308B15 accelerometers, which have a broadband frequency range of 1-3000 Hz. They weigh about 55 grams and use quartz as piezoelectric material; they are connected through coaxial cables and have a built in amplifier. A metal mounting base was used for their protection. A PCB 086B03 impulse hammer was used to generate the impacts at the

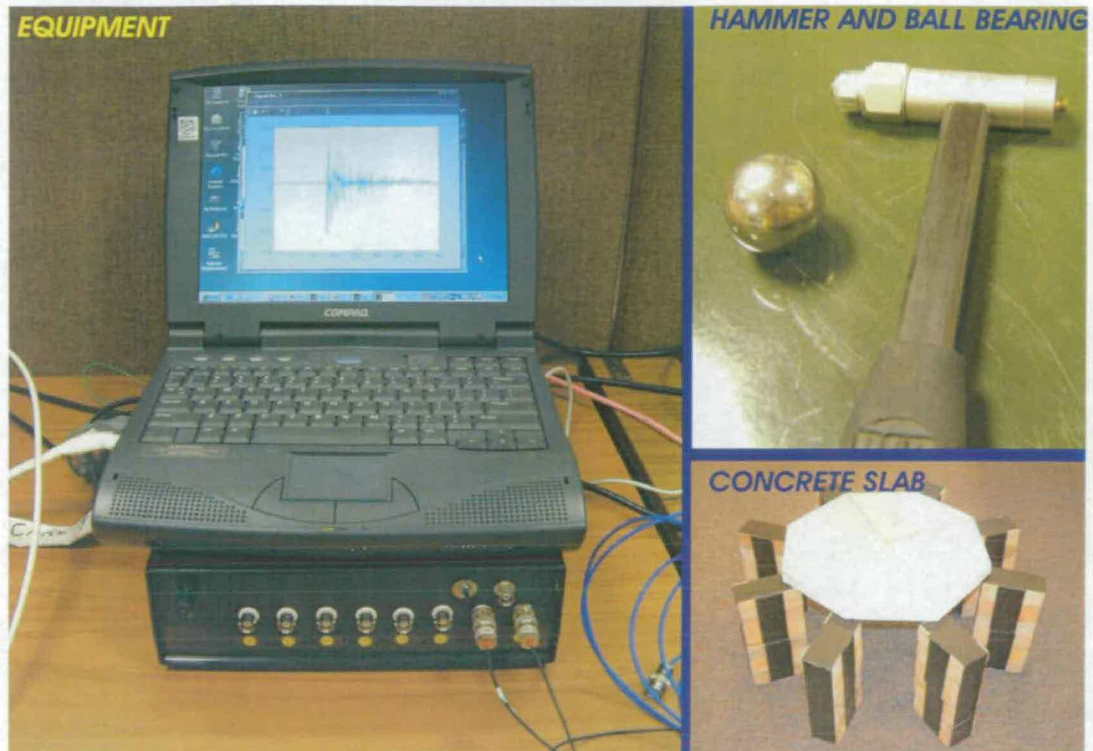


Figure 5.5: Photos of the equipment, hammer and ball bearing and concrete slab.

centre of the bottom of the slab. The hammer has a working frequency range from 0 to 8000 Hz and a resonant frequency at 31 kHz. Ten impacts were generated for each case in order to have a reliable sample of signals. An octagonal solid concrete plate, 25 mm thick and with a side of 150 mm, represented the propagating medium. The plate was supported on eight brick columns, one positioned at each corner of the plate. Photos of the equipment, hammer and the slab can be seen in Figure 5.5.

The two accelerometers were mounted on the slab in horizontal alignment; each was 100 mm from the centre. With this arrangement the accelerometers were equidistant from the impact point at the centre of the slab and equally positioned with respect to external boundaries. A photo of the set up can be seen in the left half of Figure 5.8.

A calibration was undertaken by mounting the two accelerometers with the same couplant and verifying that the recorded signals were identical.

The test consisted of three stages, during which the signals were compared in the Time-Domain and Frequency Domain. The comparison was carried out using the Signal Processing MATLAB toolbox that automatically performs the conversion from Time to Power spectrum. The power spectrum describes the distribution, over frequency,

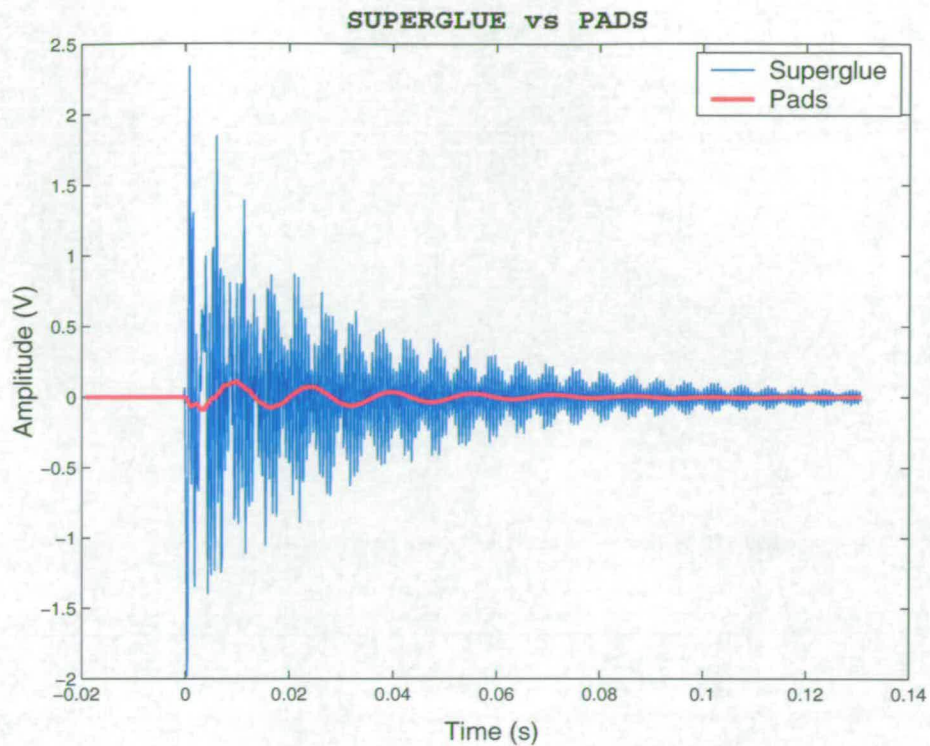


Figure 5.6: Time Domain Signals of Superglue and Sticky Pads.

of the power contains in the signal. Different methods can be used to estimate the power spectral density and The Welch's method available in MATLAB was used for the data of this experiment as it produced smoother plots. This method divides the time domain data into (possibly overlapping) segments, producing a power spectrum for each of them and then averages them to produce the final plot.

As a first stage two accelerometers were used simultaneously, one accelerometer was mounted as a "control", using superglue, whilst the other was mounted with different couplants that could then be compared against the "control" signal. The substances that provided a good signal with no major drawbacks were then advanced to the second stage of the investigation, where they were directly compared to each other.

The results of this first stage permitted the elimination of a few materials. The sticky pad couplant was excluded as the quality of the signal (see Figure 5.6) was exceptionally poor: both amplitude and number of peaks in the time domain are much lower than those in the superglue signal. As a result it was considered unnecessary to convert the signal to its Frequency Domain. Wax and grease were disqualified due to installation difficulties. In fact the use of wax was very impractical. The beads of wax

must be placed in position and melted using a heating source such as a cigarette lighter. This requires a large amount of heat for a considerable length of time and it can be extremely difficult to ensure that all the wax is fully melted. Once all the wax was in a liquid state and the heat source removed, the wax set very quickly. Therefore the accelerometer had to be placed in position accurately and almost instantly. In practice it was easy to fail to get the accelerometer mounted at all, it was difficult to mount it in the perfect position and impossible to adjust it once the wax had set. Finally, this whole process would be impossible to carry out on anything but a horizontal surface. The use of grease was also problematic, as its bonding characteristics were very poor, resulting in poor coupling of the accelerometer. Both the sealant and the general adhesive were finally eliminated due to their slow set up times. In both cases approximately twelve hours were required in order for the couplant to set properly. Moreover, significant time and effort had to be put in to removing the substances from the transducer and the concrete.

Three materials reached the second stage: superglue, 2 mm thick plasticine and gluegun glue.

By comparing the amplitude of the recorded waveforms and their frequency components, the Superglue always provided the best quality signal. The signal recorded using the gluegun glue (top graph of Figure 5.7) showed some losses of amplitude compared to the Superglue signal. Some losses can be also seen in the plasticine signal (the middle graph) when compared to the Superglue, although the plasticine performed better than the Gluegun glue (bottom graph). The following ranking in terms of signal quality was thus deduced:

1. superglue;
2. plasticine;
3. gluegun glue.

In the final stage a test on a cast concrete cube (150 mm) specimen was carried out using these couplants. A ball bearing (13 mm in diameter) attached by an elastic band to a frame that sat above the impact point, was used as an impact source. The frame was located such that the ball would strike the surface only once. This system set-up would ensure an adequate, constant and reproducible impact. Only one accelerometer at a time was used and this was mounted on the centre of one of the vertical sides of

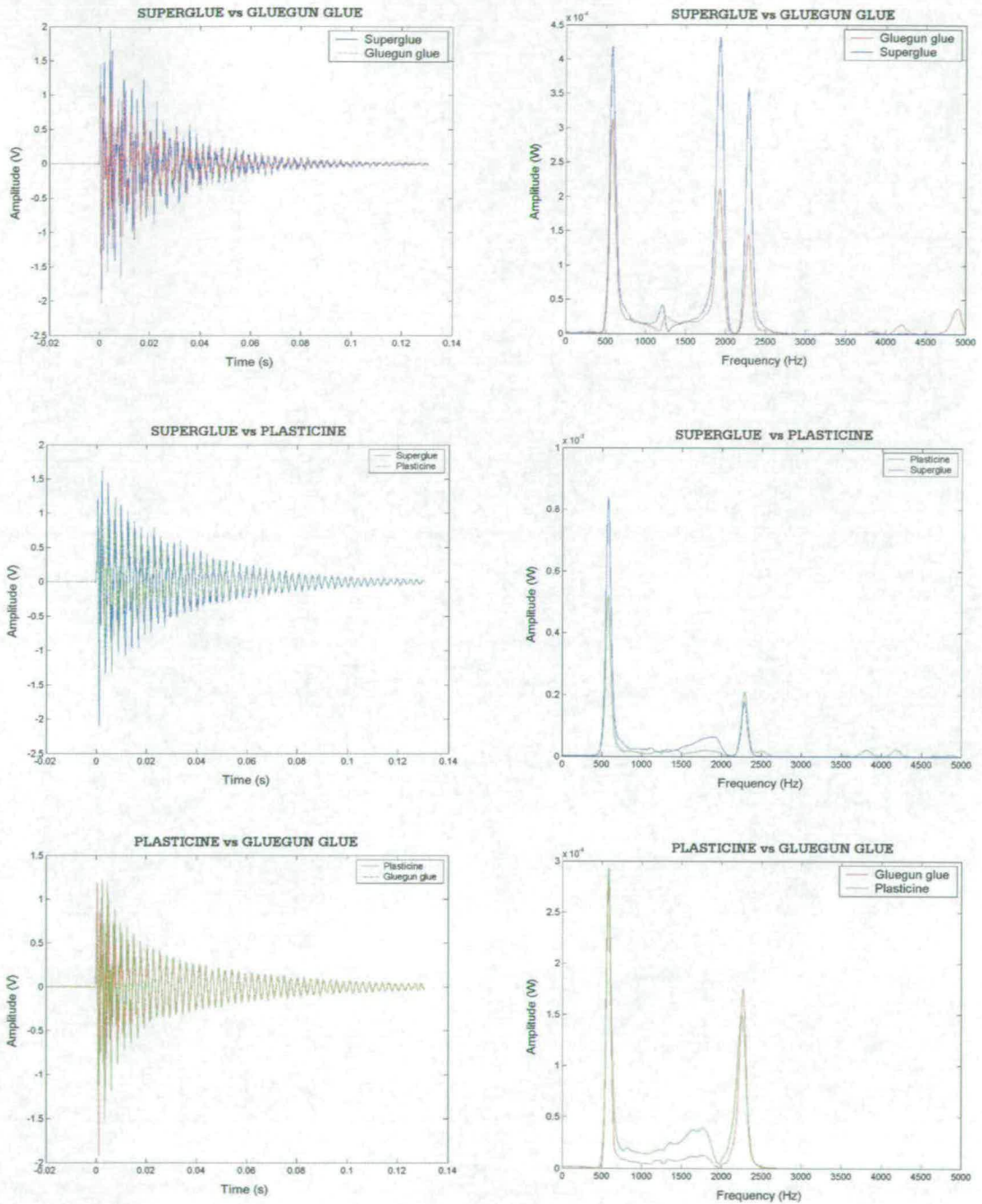


Figure 5.7: Concrete slab results: Time Domain (left) and Power spectral density (right) plots for the different couplant types, shown in comparison with each other.

the cube. This was due to the fact that an initial calibration using two accelerometers, showed significant differences between the recorded signals, probably caused by internal flaws or differences in the concrete. The test was repeated using two different cube faces and the setting of the experiment can be seen in the right photo of Figure 5.8.

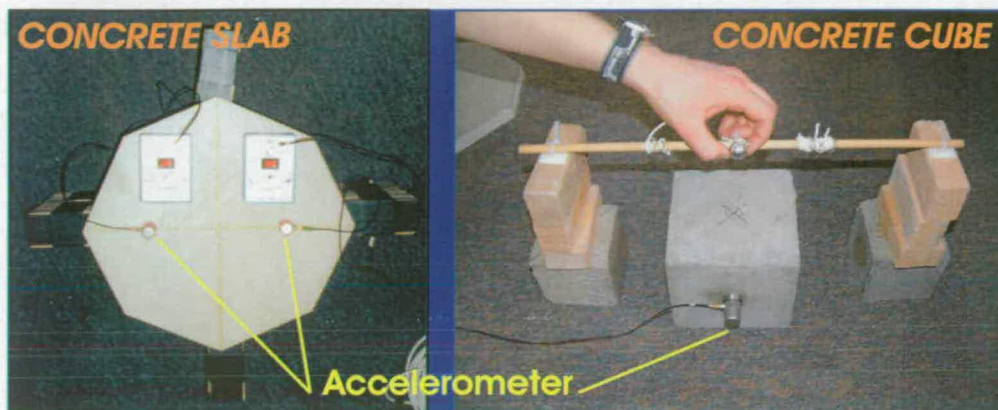


Figure 5.8: Transducer mounting substances: Testing set up.

The results (Figure 5.9 and 5.10), both in terms of time and frequency domain, showed that superglue provided by far the better signal, whilst the response of plasticine and gluegun glue were very similar to each other.

A final comparison table was produced (Table 5.4.2) assigning a value between 1 and 5 (5 = excellent; 1 = poor) to each of the previously mentioned criteria.

Overall, plasticine appeared to be the best material.

In the light of these results, plasticine was used in the following AE experiments. An exception was the tests carried out at Kumamoto University, where following the Japanese standard practice, bees wax was adopted. Bees wax was not considered in the above described couplant experiment and thus for the tests carried out in Edinburgh laboratory in the project, but it proved to be a valuable option, for the experiments carried out in Japan. However the necessity of warming it makes it unsuitable for large contact areas or on-site testing.

A second major factor to be considered when mounting the transducers is how well it is fixed to the surface of the tested material. For this purpose, the use of clamps was deemed advisable after the first experiments [Colombo et al., 2002]. Metal clamps were then designed to be used with the PAC R6I sensors and the SP accelerometers

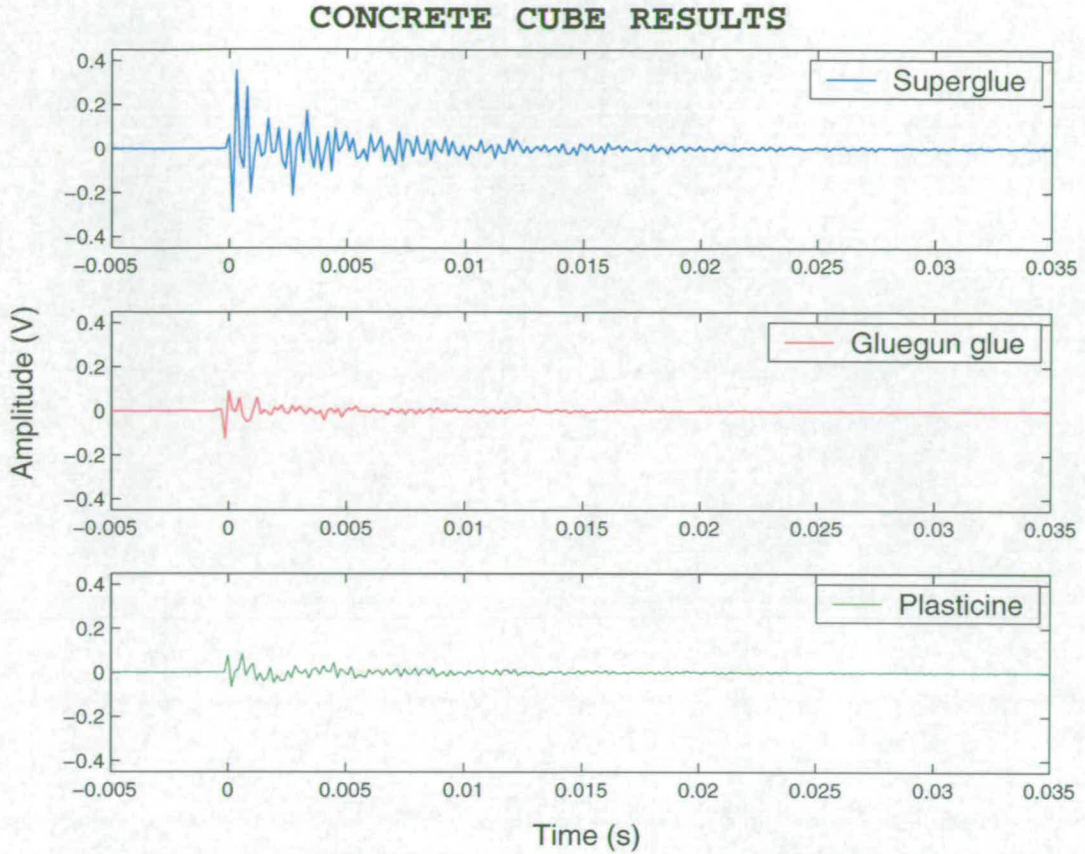


Figure 5.9: Concrete cube results: Time-Domain Signals for the three candidate couplants.

<i>Criteria</i>	<i>Superglue</i>	<i>Plasticine</i>	<i>Gluegun Glue</i>	<i>Grease</i>
Quality of received signal	5	3	2	2
Adaptability to surface	3	5	5	4
Repeatability	5	5	5	2
Durability	5	3	5	2
Ease of installation	4	4	3	2
Ease of removal	1	5	4	4
Location limitations	5	5	3	5
Time to set	3	5	4	4
<i>Total /40:</i>	31	35	32	25

Table 5.1: Transducers Mounting Substances: Final Assessment Table.

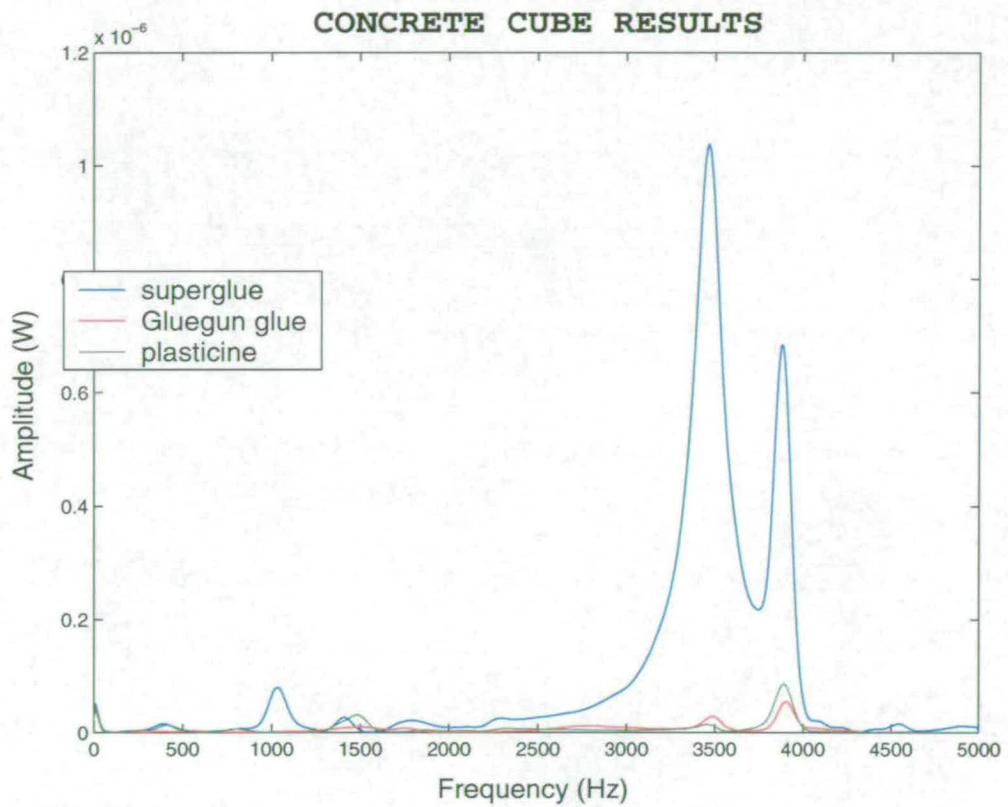


Figure 5.10: Concrete cube results: Power Spectral Density plots for the three candidate couplants.



Figure 5.11: Sensor Clamps.

throughout all the following experiments (Figure 5.4.2).

5.4.3 Sensor Calibration

The sensors should be calibrated at the beginning and at the end of the testing; an intermediate calibration, if possible, is also advisable, to ensure the correct performance throughout the whole test.

In the course of the experiments it was found that the Schmidt Hammer can be used as a quick and easy method to verify that all the transducers are working. The Schmidt Hammer is a spring controlled hammer; when it is pressed against the concrete surface its spring is automatically released, causing an impact that generates a high energy and easily detectable signal [Bungey and Millard, 1996]. Secondly a pencil lead break (BS EN 1330-9:2000) near each sensor provides confidence on the sensitivity of individual transducers. This stage is also used to define the threshold level of the instrumentation. This level should be high enough to eliminate the background noise whilst being able at the same time to detect the events generated by the pencil lead break.

The main drawback of this type of calibration, is that both the Schmidt Hammer and the pencil lead do not allow to have an exactly repeatable signal. Work has been undertaken at Cardiff University [Bradshaw et al., 2002] to develop a method of calibration using ball bearings but it has the major disadvantage that can be used only on horizontal surfaces, and therefore is not generally applicable to bridge structures where the beams are generally accessible at their side or underside.

5.4.4 Location of Sensors

The optimal location of the sensors (their distance apart and position) depends on the structure itself and the aim of the monitoring. If using resonant low frequency sensors, (60 kHz) a maximum interspace of two metres is usually reasonable. This distance has to be reduced by approximately half if using broadband sensors.

5.5 PUNDIT Equipment

To identify the location of the AE sources (see section 4.7) it is necessary to know the velocity of the P-waves through the concrete. A PUNDIT (Portable Ultrasonic Non-destructive Digital Indicating Tester) equipment was used for this purpose, at the beginning of each test, before starting loading the samples. The system generates a pulse from a transmitter transducer, transmits it through the concrete and receives it from a receiver transducer. The equipment measures and digitally displays the time taken for the pulse to travel from the transmitter to the receiver [Bungey and Millard, 1996].

From the experiment described above, plasticine appeared to be a good couplant material; it was therefore used with the PUNDIT instead of the commonly advised [Bungey and Millard, 1996] petroleum jelly or grease. An advantage of using plasticine instead of the commonly advised water pump grease is that plasticine stands the weight of the transducers better, making it easier to hold in place the transducers while the measurements are taken. The transducers always have to be initially calibrated using a reference bar so plasticine was used as the couplant during this calibration to ensure the reliability of the measurements. The velocity was thus measured by placing the two transducers (54 kHz) on the two sides of the concrete beam and recording the time displayed by the instrument. The velocity (v) was therefore calculated as:

$$v = d/t \quad (5.3)$$

where d was the width of the beam and t the recorded travel time. The measurements were repeated in different locations, always making sure that the pulse would not cross the reinforcement bars. A final average value of the velocity was then obtained for each tested beam and used for the AE source location.

5.6 AE Experimental Procedure

As previously mentioned, there is no standardised procedure in the UK for the application of the AET to civil engineering structures. In the light of the observations, results and experience gained throughout the undertaking of both the laboratory and the on-site tests, some key factors were identified. If correctly taken into consideration, before and during AE testing they lead to useful recorded AE data and therefore to a successful analysis and results. On this basis, a proposed standard experimental protocol was drawn, a draft of which is illustrated in Figure 5.12. Each single step is discussed below in more detail. It has to be pointed out, that the protocol provides general guidelines and that an experienced person should be required.

- *PRELIMINARY SURVEY* - When dealing with a real structure, a preliminary survey should always be carried out, including an investigation of the historical records, actual drawings and photos of the structure, records and maps of existing damage and previous monitoring data, if existing.
- *AIM OF THE TEST* - Although the specific problem of the structure under investigation might not be known, a general aim of the test should initially be defined. All the following factors and steps should then be evaluated on the basis of this aim. This does not necessary exclude the possibility of unexpected results during the test and the analysis.
- *CHOICE OF SENSOR* - The choice of the right type and model of sensors is fundamental to ensure that no vital information is lost due to an incorrect choice. The latter is mainly affected by the signal attenuation; the structure, its scale, geometry and material characteristics; the sensitivity and frequency range of the sensor; and the type of analysis. When a large sensor spacing is needed (i.e. during global monitoring) low frequency resonant sensors should be preferred, as they are less influenced by attenuation and they are more sensitive. On the other hand, if a frequency analysis or a Moment Tensor Analysis is required, the broadband type should be used. It should also be noted that the frequency range is normally up to a few hundred kHz.
- *SENSOR LOCATION* - The distance apart and position of the sensors depends on the structure itself and the aim of the monitoring. Global monitoring of

the whole structure generally implies a large spacing whilst local monitoring involves closer spacing concentrated on a smaller area. The available number of sensors is also an issue as in some cases the transducers are very expensive and therefore an optimum decision affects the cost-effectiveness of an investigation. Generally, a maximum interspace of two metres is reasonable when using resonant low frequency sensors (60 kHz). This distance has to be reduced to approximately half if using broadband sensors. The presence of pre-existing cracks or damage can affect the signal and its propagation and therefore has to be taken into account when deciding the sensor location.

- *SENSOR MOUNTING* - The mounting of the AE sensors affects the quality and quantity of data that will be recorded and therefore it has to be carefully considered. The choice of the right couplant is fundamental: while Cyanoacrylate adhesive glue can be very good for permanent monitoring, different substances have to be used when the sensors need to be removed. Plasticine (2 mm thick) proved to be a good alternative. The use of clamps to hold the sensors in place is also advisable, as well as cable ties to avoid interference deriving from electromagnetics induced in the cables by wind activity or cross-talk.
- *INSTRUMENTATION SETTINGS* - The settings of the AE instrumentation need to be determined. They specifically depend on the type of system, the software that is used - as previously discussed in this chapter. If the data are stored locally, the first check should consist of verifying the presence of enough disk space to store the data. Waveform data in particular generates large size data files. If the data are transferred to a data centre, the necessary connections have to be provided. Although the settings are decided at this stage, results and/or considerations arose during the following calibration and noise-attenuation study might give reason to modify these initial settings.
- *SENSOR CALIBRATION* - Once the sensors are chosen, located and mounted they need to be calibrated. The Schmidt Hammer is a quick and easy way to verify that all the transducers are functioning, whilst a pencil lead break (BS EN 1330-9:2000) near to each sensor provides confidence on the sensitivity of the transducers. The calibration should be done at the beginning, at the end and if possible in the middle of the test to assure the correct performance throughout

the whole test.

- *NOISE AND ATTENUATION STUDY* - When working in the field, a noise and attenuation study can provide useful preliminary information about the condition of the structure under investigation.
- *COMPLEMENTARY MEASUREMENTS AND ENVIRONMENT* - During AE testing, it may be useful to record additional information, such as displacement and/or strain. Although less important when working in a lab, the environment factor becomes important when monitoring on-site. Factors such as wind, temperature and rain can significantly affect the recording and should be recorded - as well as considered when setting the threshold value of the equipment. A threshold between 30 - 45 dB is generally appropriate for concrete. Possible external events that could generate signals similar to AE events should also be taken into consideration.

5.7 Summary

Detailed descriptions of the AE and PUNDIT equipment used during the experiments of this thesis were given in this chapter. The varied settings required during a test were discussed, as well as the different software that can be used in relation to each system. Different sets of AE sensors were used throughout all the tests, and their general as well as specific characteristics, were described.

An experiment carried out to investigate the different couplant materials that can be used to mount the AE sensors on the specimens was reported - plasticine appeared a valid choice.

The different features related to the acquisition of AE data that would lead to a successful analysis and results were identified and discussed. Some guidelines were provided and a draft protocol for AE application was proposed. The protocol is a result of the critical understanding of the equipments as well as of the experience gained throughout all the laboratory experiments and the field work. The next chapter describes the method and experimental design of the laboratory tests, whilst the in-situ application is reported in Chapter 8.

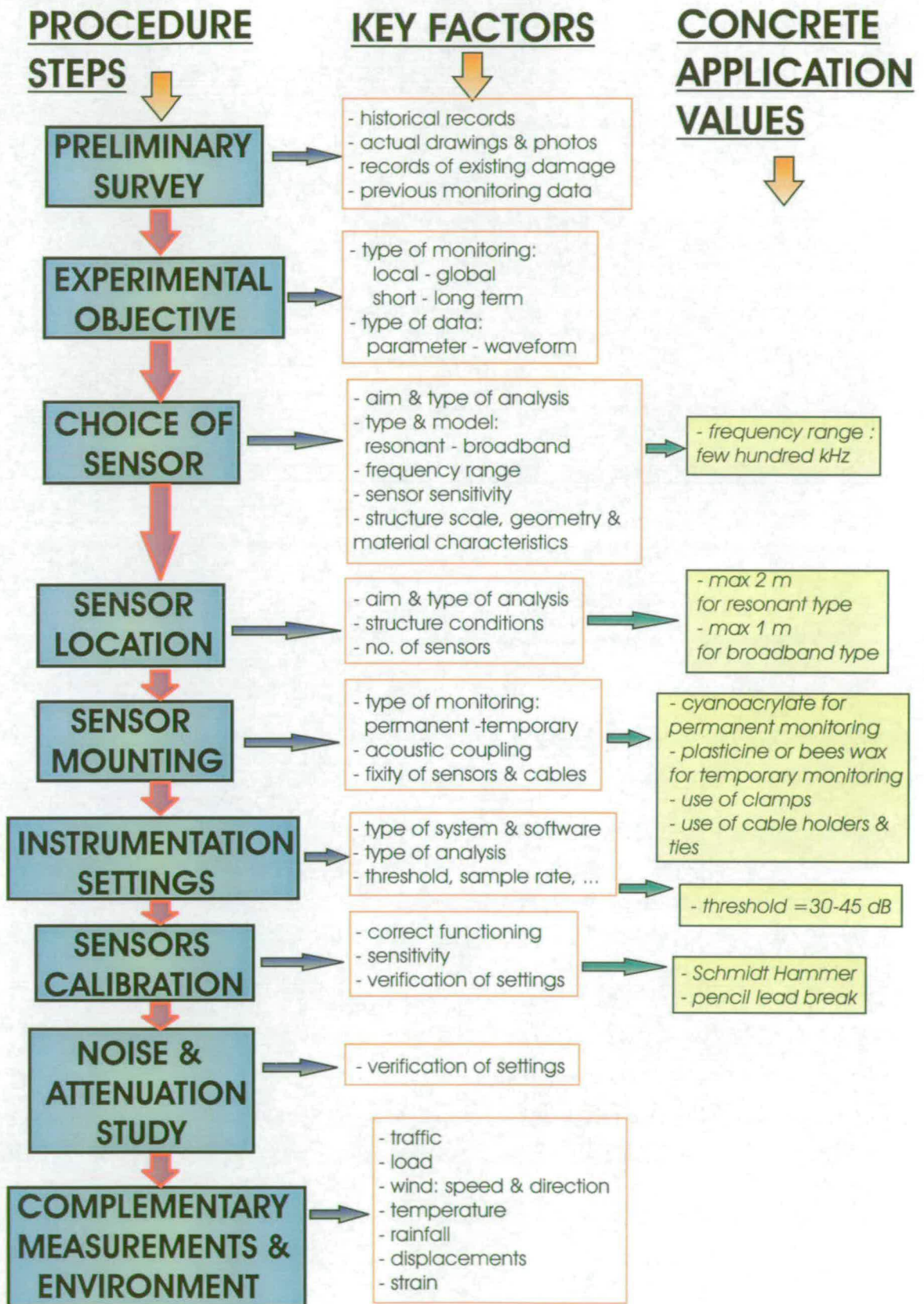


Figure 5.12: Draft of the AE application protocol, showing the key steps and factors.

Chapter 6

Laboratory Experiments

As part of this thesis, several laboratory experiments were carried out and the data obtained were processed differently depending on the data themselves and the aim of the analysis. For this reason, this chapter describes all the laboratory experiments whilst all the analyses are included in the following chapter with specific references to the relative specimens.

The experiments described here are divided according to the three different laboratories where they were performed: Edinburgh University (Scotland), Transport Research Laboratory (TRL, Crowthorne, England) and Kumamoto University (Japan). The experiments include both small scale and full scale tests and the most of them involve the use of reinforced concrete (RC) beams as specimens representative of the behaviour of concrete bridge beams. Load induced cracks were generated in these samples and the derived acoustic emissions were then recorded using different AE systems. Parameters such as strain, crack width and displacements were recorded as well - depending on the available laboratory facilities. Not all the recorded parameters proved to be relevant for the ensuing analyses; therefore only the most significant data will be shown. An experiment on a small concrete sample specifically related to the Moment Tensor Analysis was also carried out at Kumamoto University and its description is included in the relevant section.

6.1 Edinburgh Laboratory Experiments

Six RC beams were tested in the Structures Laboratory of the University of Edinburgh and they were named BF1 to BF6. Beam BF1 was considered as a trial whose utility

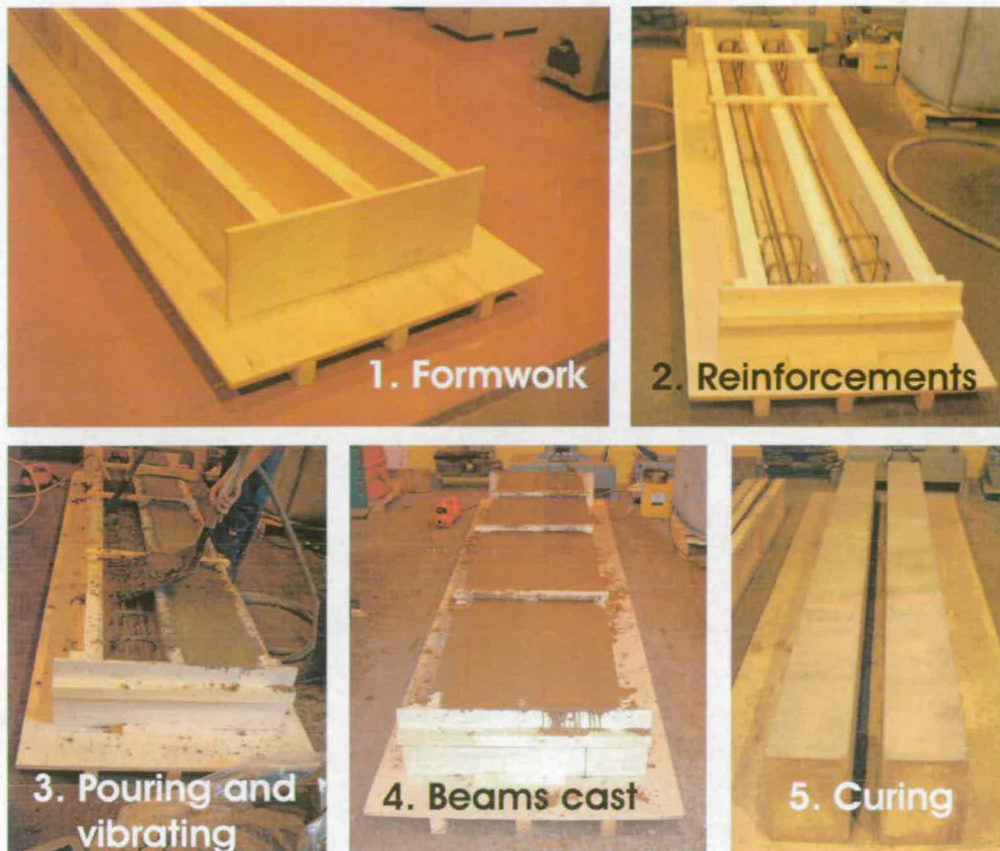


Figure 6.1: Phases of the beam making process.

lay in gaining an understanding of how to carry out the ensuing tests, so its results are not reported here. All beams were firstly designed then cast and cured for at least 28 days before testing. An example of the different steps is shown in Figure 6.1 that specifically refers to beams BF3 and BF4.

The design of all beams was based on BS 8110: Part 1: 1997. Except for beam BF6, all beams were designed to be under-reinforced, in order to be able to observe extensive cracking of the concrete and substantial deflections. The extensive cracking was expected to generate large amounts of acoustic emissions. Beam BF6 was designed with stirrups as bridge beams often have shear reinforcements. Examples of the design calculations can be found in Appendix A.

Both fresh concrete and reinforcement needed to make the beams were ordered from an external supplier. The steel bars were assembled according to the design and placed in the formwork that was previously made using plywood planks and timber. The concrete was poured into the oiled formwork and then vibrated using an electrical

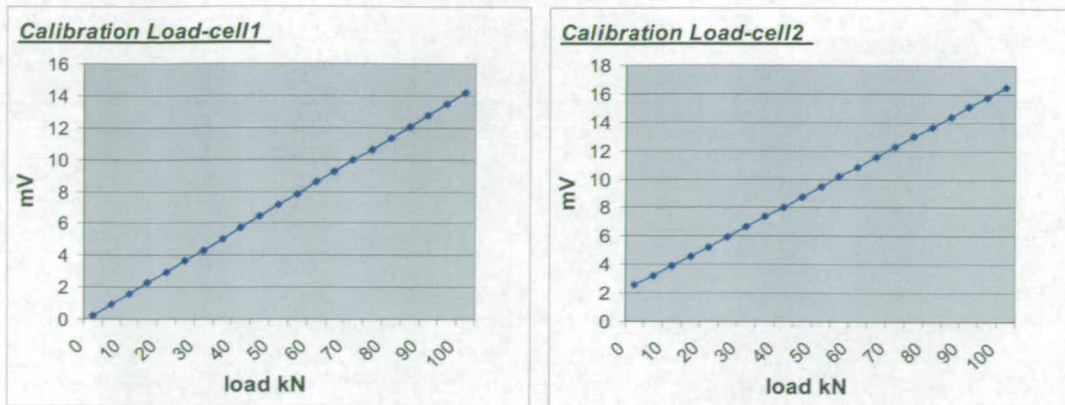


Figure 6.2: Graphs of the two load cells calibration.

poker. Cylinder and cubes were also cast and tested in compression according to BS 1881: Part 116: 1983 to estimate the concrete strength; an average value of 25 MPa was obtained.

During the tests all beams were simply supported using rollers positioned on the testing rig. The load was applied at two points that varied for the different specimens according to the type of failure that was to be achieved. Two hydraulic jacks were used to apply the load and a small layer of rubber material was placed under them during the test to reduce the noise generated by the jacks themselves. The load was applied in cycles of varying steps (generally determined on the basis of the calculated designed failure load) and measured via two 100kN load cells, connected to a voltmeter. Both load cells were initially calibrated and their calibration diagrams are shown in Figure 6.2. In the case of beams BF4, BF5 and BF6 a new connection made it possible to record the load using the MISTRAS system. A complete cycle usually consisted of four sequential phases :

- loading up phase
- gauge readings at constant load
- crack mapping at constant load
- unloading phase.

As a general rule, once the load reached the established value for that specific cycle, it was then held as long as the beam stabilised (i.e. no more acoustic emissions

were recorded). This was not done for beam BF3 where the load was held for about 1.5 hours to investigate any possible influence on the data due to the performing of a creep test. All beams were loaded up to failure, resulting in bending or shear depending on the beam design and load configuration. Beam BF2 although seriously damaged did not fail completely and the load could not be increased any further due to the limitations of the testing equipment. The beam was therefore re-tested (named BF2c) using a different load configuration that allowed generation of a higher stress level. The higher strength of beam BF2 was thought to be due to the fact that it was the only beam that was cured in a water tank. The different steps and cycles for each beam are schematically represented in Figure 6.3 where the time on the horizontal axis is merely representative, but the vertical axis is the absolute load. The beam design details, load configurations and type of failures are summarised in Table 6.1 and Figures 6.4 to 6.9.

Dial gauges were used to measure the displacements of the beams but they were not always able to provide useful information; better results were obtained for beams BF4, BF5, BF6 and BF2c where a digital dial gauge was used. A six inch Demec gauge was adopted to measure the strain in beams BF2 and BF3 but due to the formation of cracks the data cannot be considered as totally reliable (an imperial Demec gauge was available at the University of Edinburgh, whereas a metric Demec gauge was used later at TRL). The use of strain gauges was excluded as they are unable to stand the tensile stress that developed in the bottom part of the beam. Before starting each test, Pundit ultrasonic equipment was used to measure the velocity of elastic waves through the concrete (see section 5.5). The values of velocity obtained are summarized in Table 6.1.

During the tests the beams were monitored using different AE systems and a varying number and location of sensors. Beams BF2 and BF3 were tested using the MISTRAS system with eight resonant R6I sensors, whilst for all the remaining beams the MISTRAS system with WD broadband sensors, the DiSP system with R6I resonant sensors (see section 5.2) and the SoundPrint system were used. Recording was stopped when the cracks were mapped and the data were originally recorded as parameters, enabling the software waveforms recording option during the testing of beam BF2 and BF3 (see sections 5.2 and 4.4 for more details). The different sensor configurations are shown in Figures 6.4 and 6.7. A linear location alongside the beam was usually adopted. The particular location of the sensors and the recording of waveforms on beams BF2 and

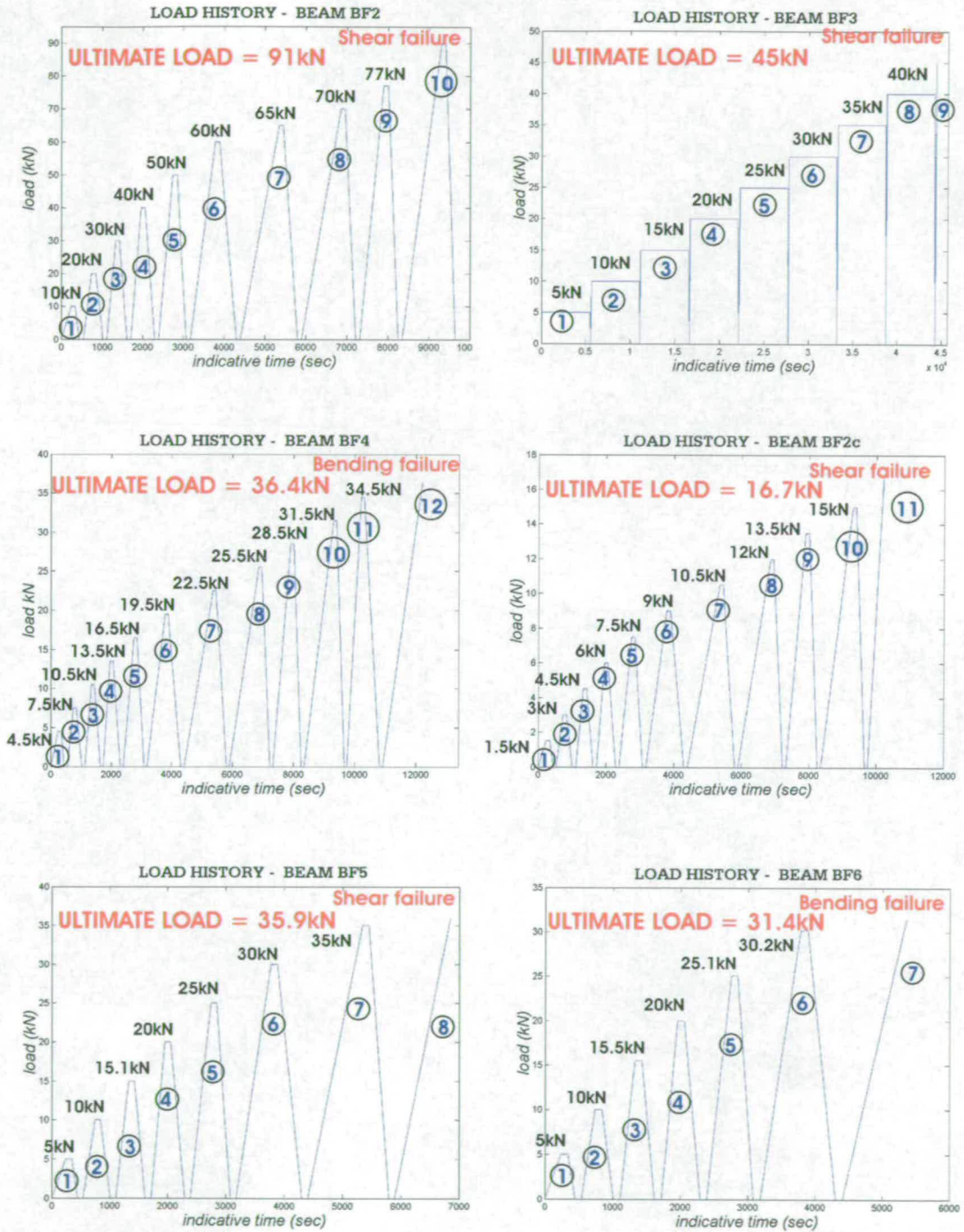


Figure 6.3: Load history of the beams of Edinburgh experiments.

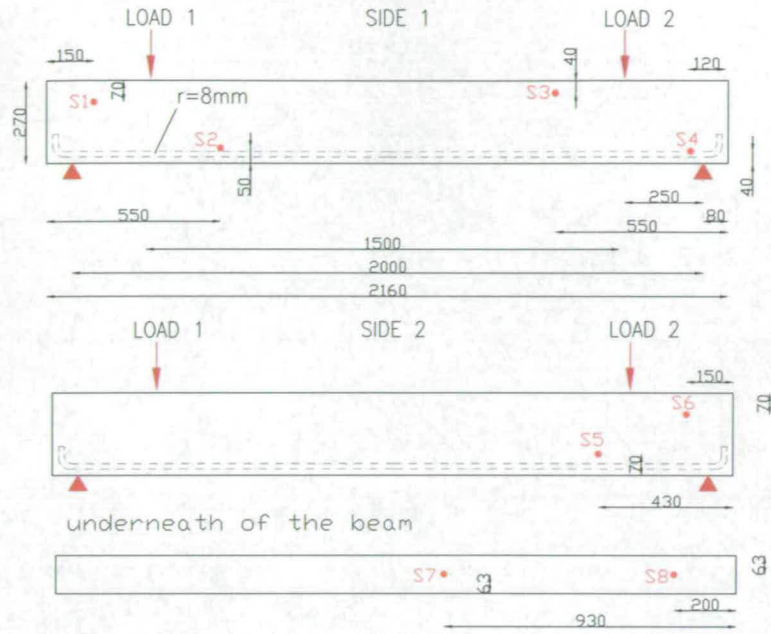


Figure 6.4: Design details, test configuration and resonant sensor location (S1 to S8) of beam BF2.

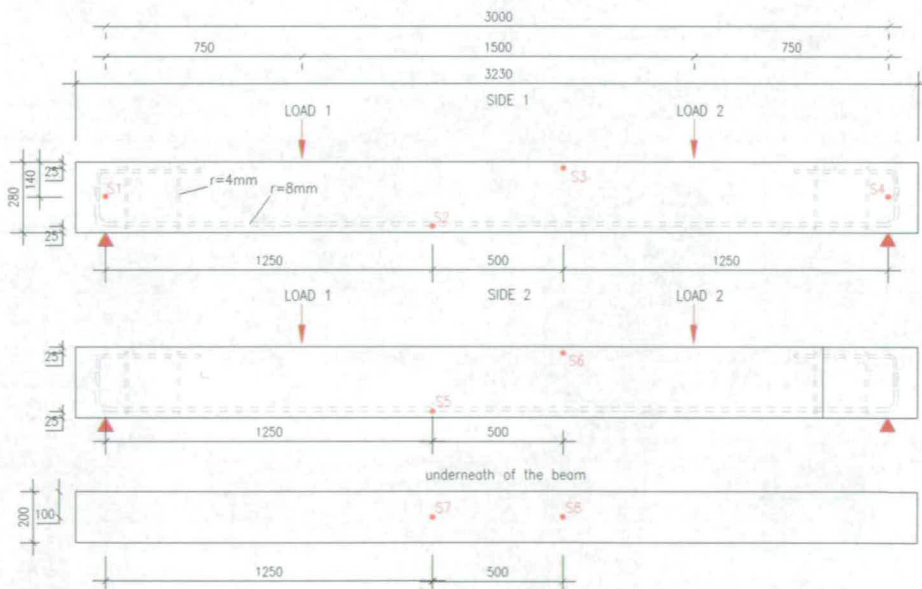


Figure 6.5: Design details, test configuration and resonant sensor location (S1 to S8) of beam BF3.

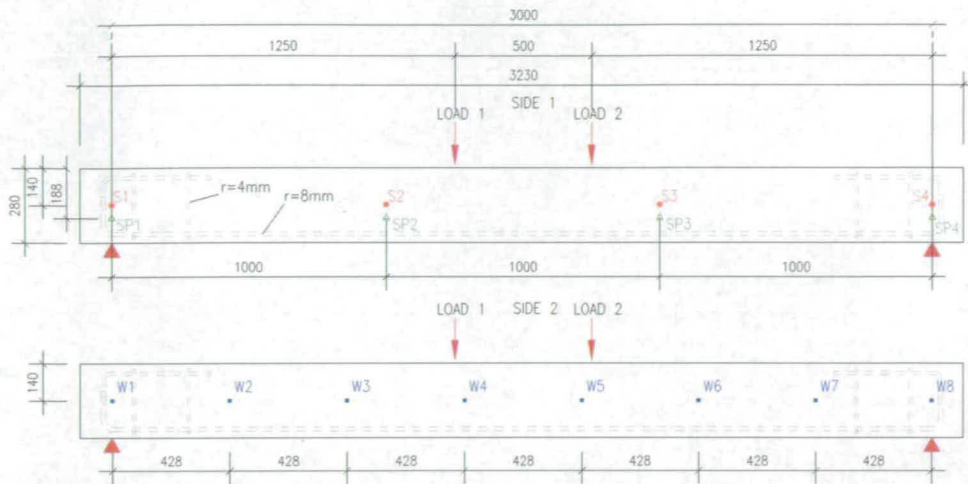


Figure 6.6: Design details, test configuration and sensor location (resonant: S1 to S4 - broadband WD type: W1 to W8 - SoundPrint: SP1 to SP4) of beam BF4.

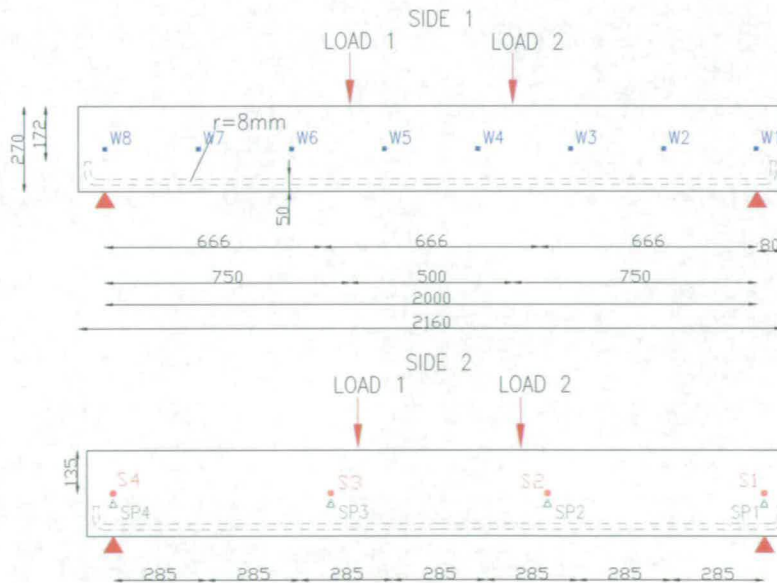


Figure 6.7: Design details, test configuration and sensor location (resonant: S1 to S4 - broadband WD type: W1 to W8 - SoundPrint: SP1 to SP4) of beam BF2c.

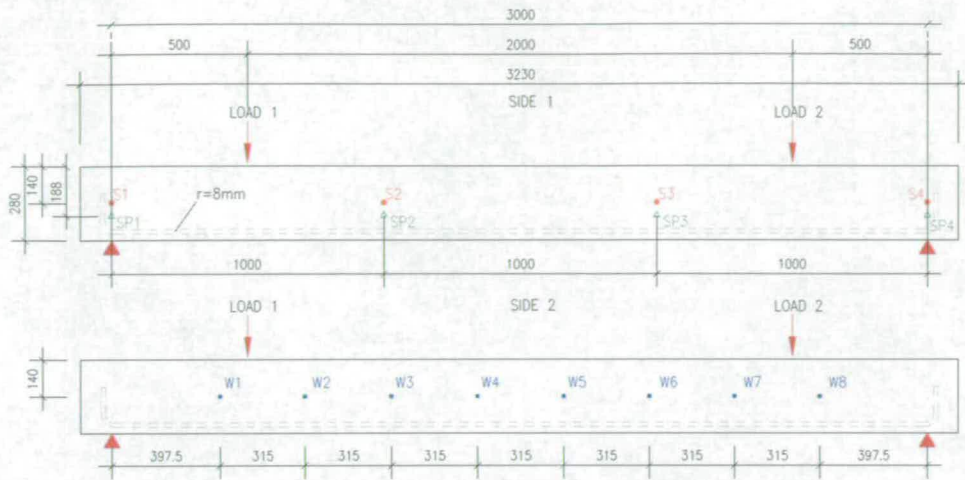


Figure 6.8: Design details, test configuration and sensor location (resonant: S1 to S4 - broadband WD type: W1 to W8 - SoundPrint: SP1 to SP4) of beam BF5.

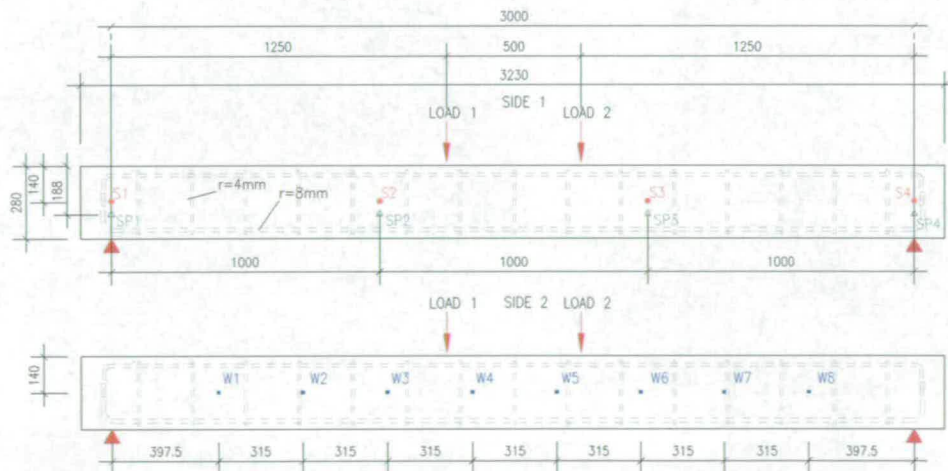


Figure 6.9: Design details, test configuration and sensor location (resonant: S1 to S4 - broadband WD type: W1 to W8 - SoundPrint: SP1 to SP4) of beam BF6.

	BF2	BF3	BF4	BF2c	BF5	BF6
Section	125x270mm	200x275mm	200x275mm	125x270mm	200x275mm	200x275mm
Span	2m	3m	3m	2m	3m	3m
Reinforcements	simply reinforced 1 ϕ 16mm	long. reinf. + shear links at the end 2 ϕ 16mm 4 ϕ 8mm	long. reinf. + shear links at the end 2 ϕ 16mm 4 ϕ 8mm	simply reinforced 1 ϕ 16mm	simply reinforced 2 ϕ 16mm	stirrups cage 4 ϕ 16mm 15 ϕ 8mm
Concrete strength	25MPa	25MPa	25MPa	pre-damaged	25MPa	25MPa
Wave velocity	3800m/sec	3700m/sec	3300m/sec	3300m/sec	3100m/sec	3100m/sec
No. of cycles	10	9	12	11	8	7
Load steps	10kN	5kN	3kN	1.5kN	5kN	5kN
Failure load	90kN	45kN	36.4kN	16.7kN	35.9kN	31.4kN
Failure type	shear	shear	bending	shear	shear	bending
Sensors used	R6I	R6I	R6I WD SP	R6I WD SP	R6I WD SP	R6I WD SP
Sensors spacing	varied 550-1000mm	varied 550-1250mm	1000mm 428mm 1000mm	666mm 285mm 666mm	1000mm 315mm 1000mm	1000mm 315mm 1000mm

Table 6.1: Summarized description of the beams of Edinburgh experiments.

	BF2	BF3	BF4		BF2c		BF5		BF6	
PAC SYSTEM										
Threshold	35dB	40dB	35dB		35dB		35dB		35dB	
Sample rate	1MHz	1MHz	1MHz		1MHz		1MHz		1MHz	
Hit Length	2K	2K	2K		2K		2K		2K	
Sensor type	<i>R6I</i>	<i>R6I</i>	<i>R6I</i>	<i>WD</i>	<i>R6I</i>	<i>WD</i>	<i>R6I</i>	<i>WD</i>	<i>R6I</i>	<i>WD</i>
PDT			500	500	500	500	500	500	500	500
HDT			1000	1000	1000	1000	1000	1000	1000	1000
HLT	65534	65534	65534	1000	65534	1000	65534	1000	65534	1000
Pre-trigger			512	512	512	512	512	512	512	512
SP SYSTEM										
T-Mast	-	-	max		max		max		max	
	-	-	clockwise		clockwise		clockwise		clockwise	
Threshold	-	-	999		999		999		999	
Sample rate	-	-	44.1kHz		44.1kHz		44.1kHz		44.1kHz	
Delay	-	-	minimum		minimum		minimum		minimum	

Table 6.2: Summary of the AE setting values for Edinburgh experiments.

BF3 derived from the intention, albeit unsuccessful, of attempting a Moment Tensor Analysis (see section 7.5). The sensors were mounted using plasticine and from beam BF2c to BF6 metal clamps were used to hold the resonant and SP sensors in place (see section 5.4); no clamps were needed for the broadband transducers due to their small dimensions and weight. The different settings and thresholds used are summarised in Table 6.2.

A technical problem occurred while testing beam BF2 as one of the jacks started leaking oil after cycle no.4. This affected the AE data and there were negligible emissions at this side of the beam during all the remaining cycles despite the visible appearance of cracks. The oil acted as a lubricant attenuating the friction and therefore influenced the recording of the acoustic emissions. As a result of this, during the subsequent analyses of BF2, the data coming from the “oiled” side of the beam

after cycle no.4 was ignored. Some of the full instrumented beams can be seen in Figure 6.10.

At the end of the loading phase of each cycle, the cracks were marked on the beams by drawing a line beside them as they appeared visibly. A number referring to the relative load cycle was written next to the mark. The final crack pattern and the failure of these beams can be seen in Figures 6.11, 6.12, 6.13, 6.14, 6.15, 6.16 and 6.17. Beam BF5 showed the presence of plastic shrinkage cracks on the concrete surface when it was removed from the mould. It was generally possible to identify the following stages of cracking:

- no cracks
- cracks forming
- no new cracks appearing but extending cracks and/or widening of the existing cracks
- failure.

6.2 TRL Experiments

Two full scale experiments were carried out at the Transport Research Laboratory (TRL) in Crowthorne (England) on beams named CF1 and HB2.

Beam CF1 was tested as part of a TRL project looking at cracking and failure loads of concrete bridges. The beam was designed and made by TRL personnel on the basis of a reinforced concrete slab deck from a demolished bridge (Thurloxtton underpass) which was tested by TRL in the mid 1990s [Hill et al., 2002].

The beam was 345 mm wide, with an overall height of 305 mm. It was 4.2 m long and reinforced with three 25 mm diameter mild steel bars. After having been cast, the beam was turned over through 180° so that it could be tested upside-down (i.e. with the tension zone at the top), in order to facilitate the monitoring of the cracks. The concrete compressive strength was 32 MPa and the beam was designed to fail in flexure. The velocity of the wave-propagation was calculated using the PUNDIT (see section 5.5) and an average value of 4118 m/sec was obtained. One side and half the top and

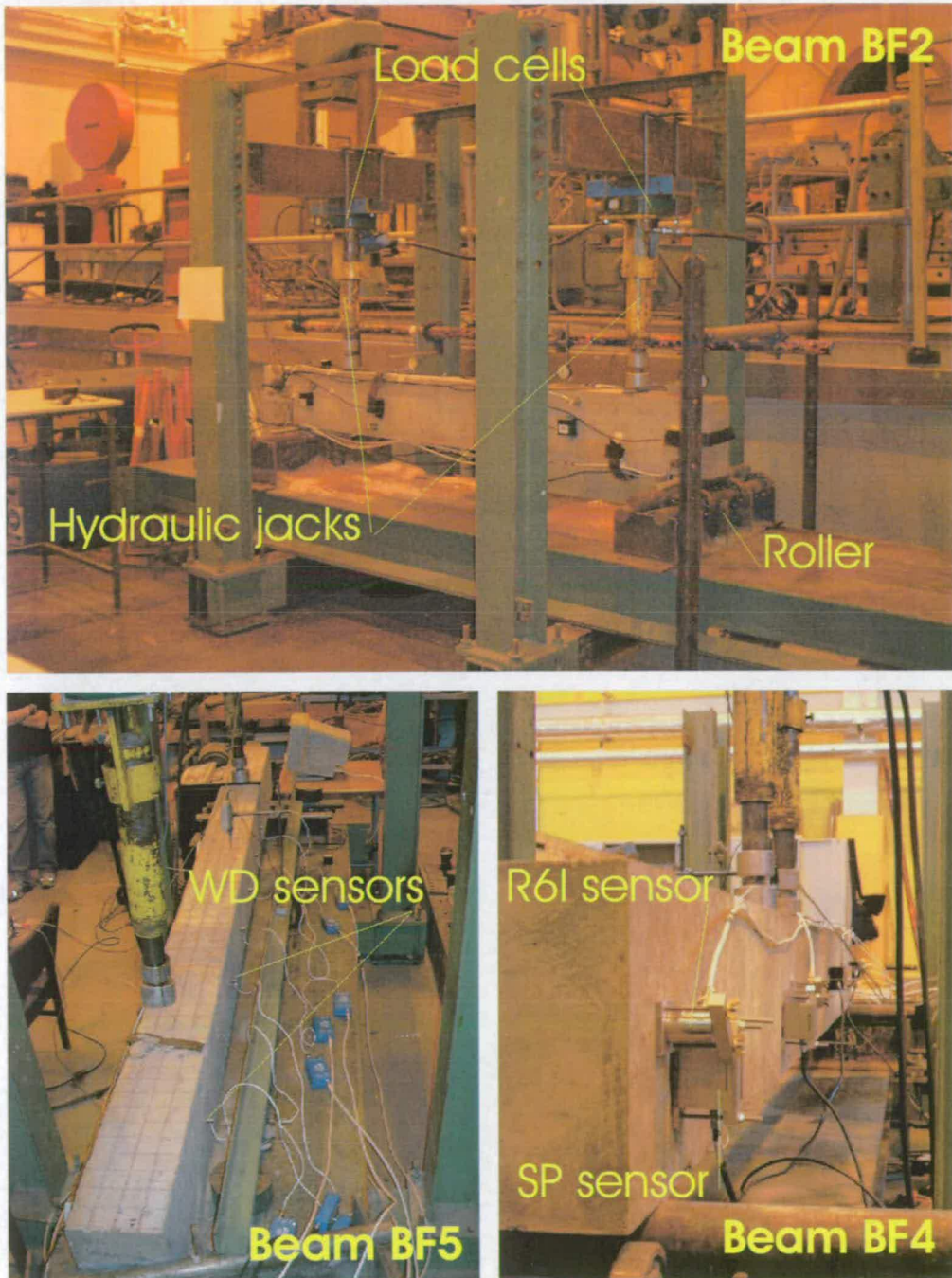


Figure 6.10: Photos of Edinburgh beams.

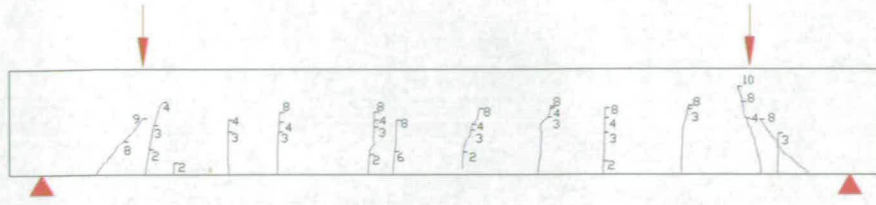


Figure 6.11: Final crack pattern of beam BF2.

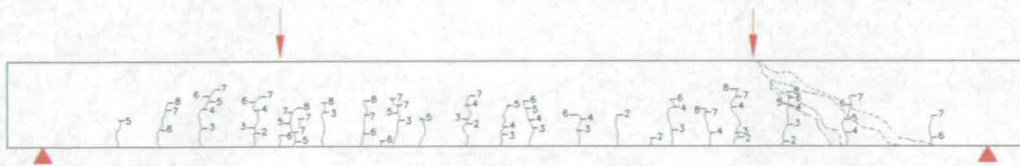


Figure 6.12: Final crack pattern of beam BF3.



Figure 6.13: Final crack pattern of beam BF4.

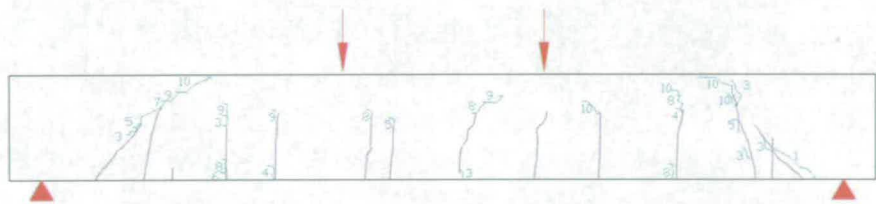


Figure 6.14: Final crack pattern of beam BF2c.

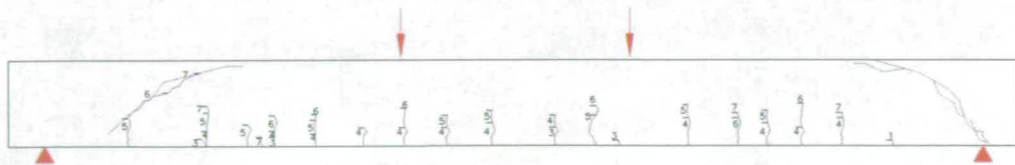


Figure 6.15: Final crack pattern of beam BF5.



Figure 6.16: Final crack pattern of beam BF6.



Figure 6.17: Photos of Edinburgh beam failures. Note the visible shear dislocation of the grid pattern for test BF5.

bottom faces of the beam were painted using watered down emulsion (water:paint ratio of 3:1) to compare the ability to see cracks on painted and unpainted surfaces.

One of the aims of this test was to load the beam simulating the real live loading a bridge beam is subjected to. For short-span bridges the live loads are governed by single axles and bogies traversing the span such that the load starts at zero and returns to zero after the passage of each axle. The dead load is uniformly distributed and has less influence than the live one. For long-span bridges it is the multiple-vehicle loading that prevails and thus the load corresponds to a distributed load for as long as the vehicles pass over the structure. As the vehicles move, the total load fluctuates and a moment envelope is produced. The dead load has a greater influence in the global behaviour of the bridge as well [Hill et al., 2002].

In order to simulate the real effect of a vehicle crossing a bridge, the load was applied and removed at seven different positions (W1 to W7) along the beam using hand-pump operated hydraulic jacks. A 75 mm full width metal plate coupled with a thin piece of plywood was used to obtain a better contact. The load was measured via 200 kN load cells connected to a Scorpio data logger. The beam was tested over a span of 3.8 m. As a consequence of the upside-down position of the beam, the self weight load was acting in reverse to the normal direction. To compensate for this, two corrections were applied. Firstly, during each single point loading, an adjusted load was applied to overcome the negative self-weight. Secondly at the end of the seventh load position, three point loads were applied at positions W2, W4 and W6 to model the positive self-weight and to allow the crack mapping. The final failure of the beam was reached through a series of ten cycles of three-point loadings (W2, W4 and W6) and it occurred at 107.5 kN.

The general load procedure can be summarized as follows:

- NSW - negative self-weight; no external load applied
- PW1-PW7 - single-point adjusted load applied at positions W1-W7; all positions were repeated for five levels of load: 9 kN, 14 kN, 23 kN, 50 kN and 80 kN
- PSW - positive self-weight; three point loads applied at W2, W4 and W6 to allow crack mapping under real dead load
- C - cyclic three point loads applied at W2, W4 and W6 applied and removed ten times until failure.

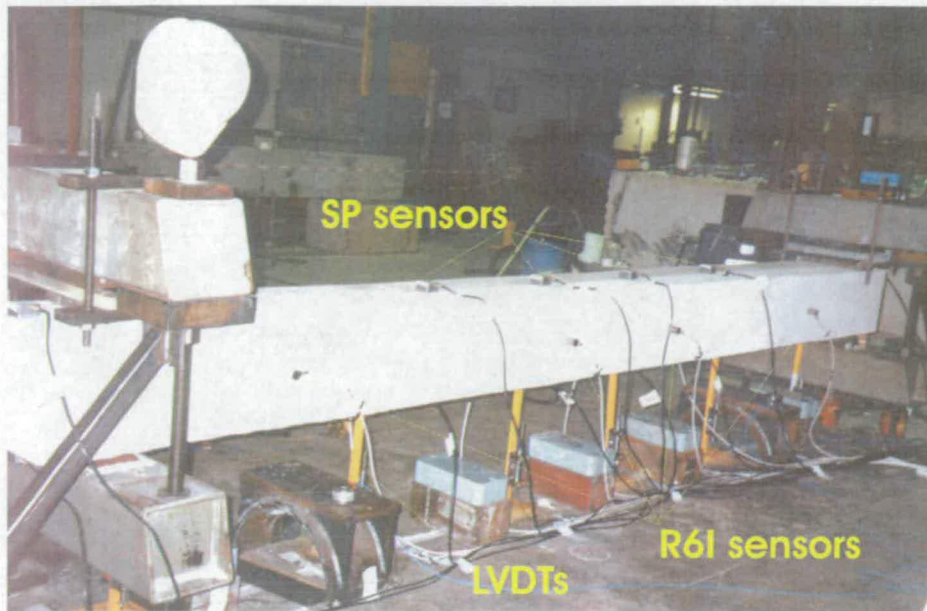


Figure 6.18: Photo of instrumented beam CF1.

The strain of the beam was measured using a 200 mm Demec gauge. Two lines of Demec positions were located on the tension face of the beam extending for almost its full length. A crack microscope (with a resolution of 0.01 mm) was used to measure the crack width. The cracks were mapped as described for the Edinburgh experiment. The crack map and width and the Demec readings were taken after each loading point was applied.

During the test the beam was monitored using two AE systems, the MISTRAS system in conjunction with six R6I sensors and the SP system with twelve transducers. Full details of the beam, instrumentation, failure, loading configuration and sensor positions are shown in Figures 6.18, 6.19 and 6.20.

Beam HB2 was tested as part of a TRL project looking at the behaviour and design criteria of hinge beam decks on concrete bridges, the so called “hinge beam bridges” [Hill et al., 2002].

In a cantilever span of this type of bridge it is possible to identify three distinct regions:

- the haunched region, where due to the great depth and fully effective tension steel, there should not be structural problems

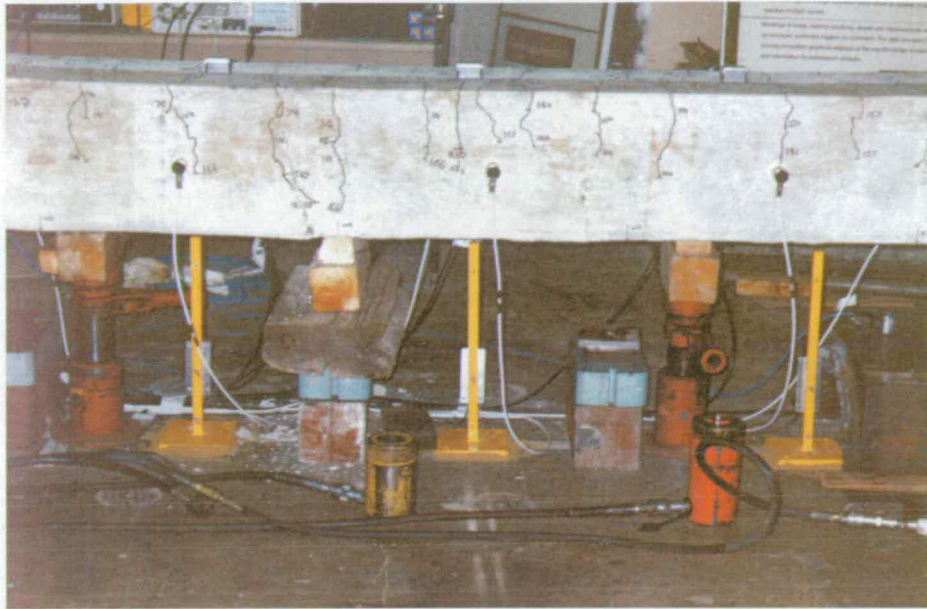


Figure 6.19: Photo of beam CF1 failure.

- the constant depth section, containing the main cantilever tension reinforcement; it carries the shear forces transmitted through the hinge
- the section adjacent to the hinge, where the great concentration of shear reinforcement should reassure against structural problems.

This experiment concerns the second of these regions.

The beam, designed and made at TRL, was based on the cantilever proportion of a motorway overbridge. It was cast in-situ and was about 8 m long, with a height of 524 mm at the hinge and 1300 mm at the haunch. The cross sectional dimensions were 524x524 mm at the constant depth section increasing to 524x1004 mm at the end of the haunch. The beam contained three layers (of six R25 bars) of tension reinforcements in the top flange. The hinge reinforcement consisted of three T20 bars bound by R6 sturrups; the main shear reinforcement over a length of 424 mm either side of the hinge was made up of six R8 bars. Design details are shown in Figure 6.21. The concrete compressive strength was 45 MPa and the velocity of the wave propagation, calculated using the PUNDIT equipment (see section 5.5) at the beginning of the test, was found to be approximately 4100 m/sec.

The beam was tested as a cantilever and the haunch end was tied down to the strong floor of the laboratory. A one point load was applied to the suspended span side

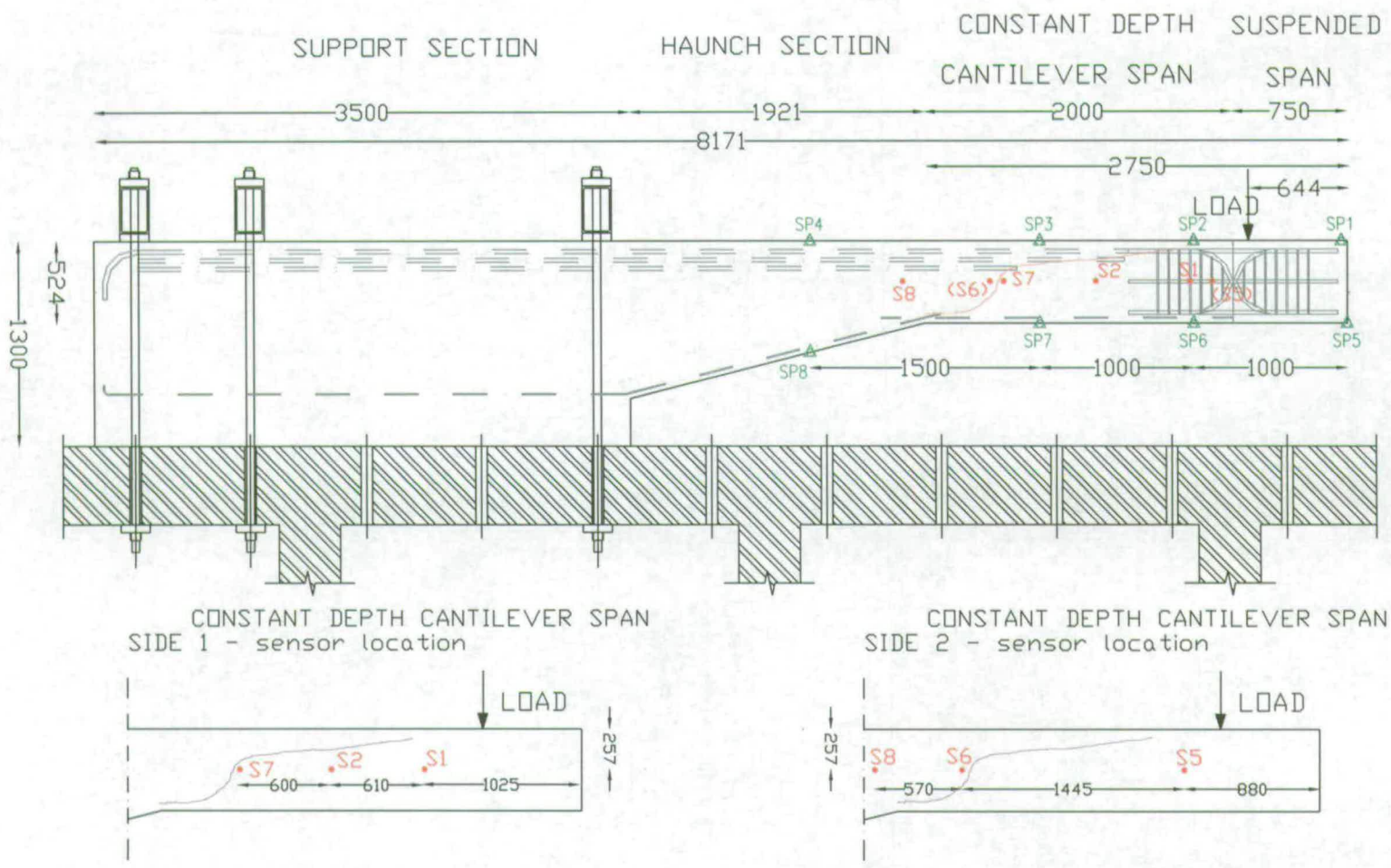


Figure 6.21: Design details, test configuration and sensor location (resonant: S1 to S8 - SoundPrint: SP1 to SP8) of beam HB2.

of the hinge with the aim of replicating the transfer of shear forces across the hinge that might occur as a vehicle passes over a real bridge.

The load was applied using a hollow column load cell, sandwiched between the hydraulic jack and a loading plate situated on the top of the beam. The first cycle was repeated a second time to allow extra measurements necessary for the specific TRL project. The general load cycle was composed of four sequential phases:

- loading up phase
- gauge readings
- crack mapping
- unloading phase.

The whole load history, as summarized in Figure 6.22, was:

- cycle 1:
 - loading up: $0 \xrightarrow{t_Q} 40$ kN, in steps of 10 kN
 - unloading: $40 \xrightarrow{t_Q} 0$ kN, in steps of 10 kN
- cycle 2:
 - as for cycle 1
- cycle 4:
 - loading up: $0 \xrightarrow{t_Q} 80$ kN, in steps of 10 kN;
 - unloading: $80 \xrightarrow{t_Q} 0$ kN, in steps of 10 kN;
- cycle 6:
 - loading up: $0 \xrightarrow{t_Q} 120$ kN, in steps of 20 kN;
 - unloading: $120 \xrightarrow{t_Q} 0$ kN, in steps of 20 kN;
- cycle 7:
 - loading up to failure, in steps of 20 kN;

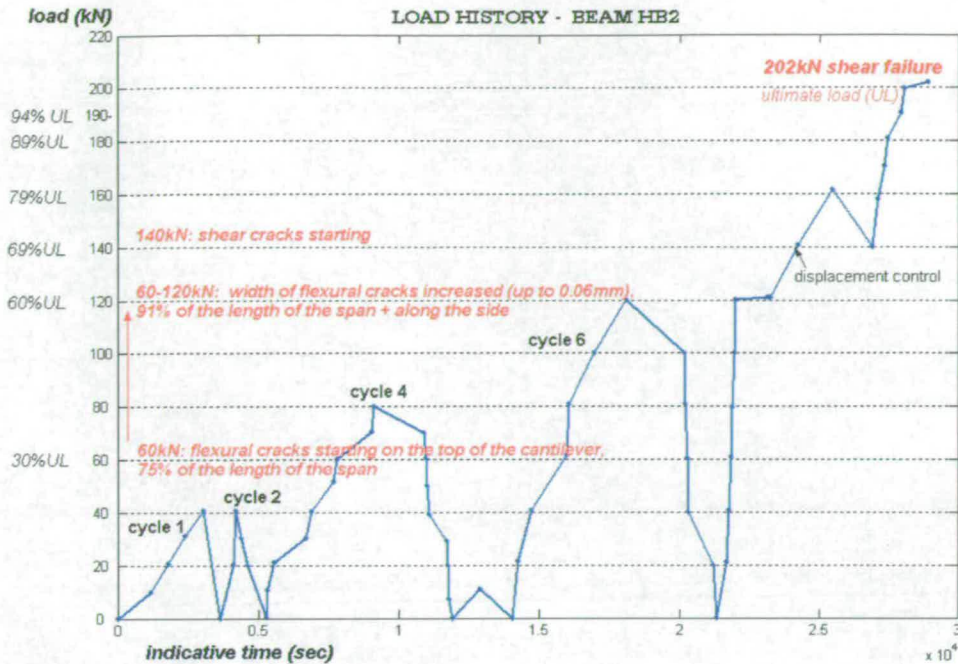


Figure 6.22: Load history of beam HB2.

During the last failure cycle the loading equipment was switched from load control to displacement control to provide better control over the failure. The beam failed at 202 kN in shear in the constant depth region, outside the densely reinforced hinge region as expected.

A four inch (no metric gauge of an equivalent size was available, so an Imperial gauge had to be used once again) Demec gauge was adopted to measure the strain in the area below the predicted crack and adjacent to the hinge. Ten LVDTs connected to a Scorpio data logger were used to measure the displacements along the length of the beam.

The crack mapping was carried out as previously described for the Edinburgh experiments. The first flexural cracks, which were found in the top surface of the cantilever section extending for about 75% of the length of the beam, appeared when the load reached 60 kN. The flexural cracks widened (up to 0.06 mm) with the increase in the load (from 60 to 120 kN), extending for about 91% of the length of the surface beam span and appearing also alongside the beam. Shear cracks started to appear when the load reached the value of 140kN.

During the tests the beam was monitored using the MISTRAS system in



Figure 6.23: Beam HB2. Test configuration and instrumentation.

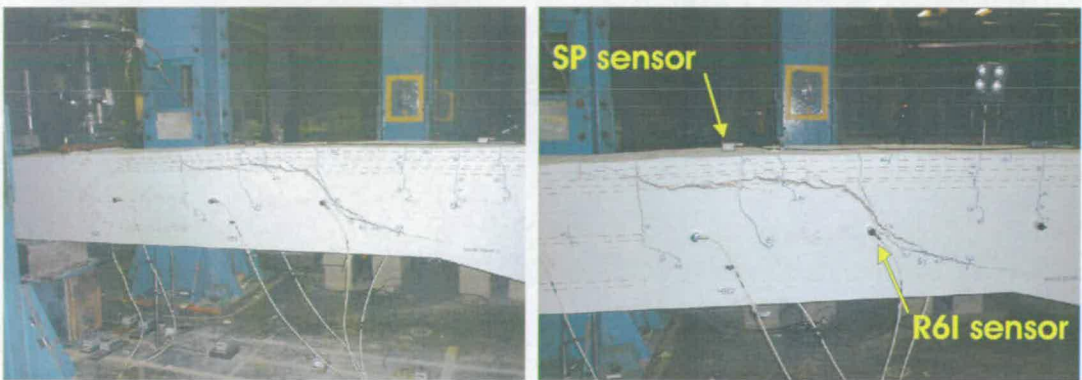


Figure 6.24: Beam HB2. Shear Failure.

conjunction with six R6I sensors and the SP system with eight transducers. Details of the instrumented beam, its failure and sensors' locations are shown in Figures 6.21, 6.23 and 6.24.

For both beams CF1 and HB2, all sensors were mounted using Cyanoacrylate adhesive glue. This did not cause any complication with relation to the SP transducers as they were left in place after the experiment, but it proved to be a problem during the removal of the PAC sensors. The sensors were so heavily glued that their removal proved to be troublesome and dangerous for the sensors themselves as they risked damage in the process. The location of the PAC sensors was determined, in both cases, by the intention to carry out a MTA. For the same reason the data was originally acquired as

Beam CF1		Beam HB2
	PAC SYSTEM	
varied 40-70dB	Threshold	varied 40-60dB
500kHz	Sample rate	500kHz
2K	Hit Length	2K
1100	Pre-trigger	1100
65534	HLT	65534
	SP SYSTEM	
3 oclock position	T-Mast	3 oclock position
N/A	Threshold	N/A
44.1kHz	Sample rate	44.1kHz
minimum	Delay	minimum

Table 6.3: Summary of the AE setting values for TRL experiments.

waveforms using the MT-TRA software (see section 5.2 and 7.5). The settings of the AE instrumentation for both beams are summarized in Table 6.3.

6.3 Kumamoto Laboratory Experiments

Six RC beams were tested in the laboratory of Kumamoto University in Japan and they were named K1, K2, K3, K4, KL1 and KL2. The main aim of the testing of these beams was to understand the Japanese methodology and to obtain more data for the Relaxation ratio analysis.

The beams were designed according to experiments previously performed in the laboratory and the dimensions were determined by the existing metal mould that could be used. Two types of beam were made in order to verify the influence of beam design on the results. Four beams were designed having stirrup cages (beams K1, K2, K3 and K4) whilst the remaining two beams were simply reinforced (beams KL1 and KL2). Due to the limited available time, rapid hardening concrete was used and as before the fresh concrete and the reinforcement were ordered from an external supplier. The longitudinal bars and the stirrups were bent and the stirrup cages assembled in the laboratory and the assemblies placed in the formwork (Figure 6.25). The concrete was

then poured and vibrated. Due to the particular characteristics of the rapid hardening concrete the beams were ready to be tested after a week. Cylinders were cast and tested in compression using four strain gauges. This allowed calculation of the strength and the static Young's Modulus E of the concrete and thus the velocity of the waves through the sample. Details of these calculations are in Appendix C. The strength of the concrete and the velocity of the waves were approximately 45.99 MPa and 3600 m/sec respectively. The quality of this concrete was higher than that used in the Edinburgh experiments. It has to be pointed out that the value of velocity cannot be compared directly with the velocity of the beams tested in Edinburgh and TRL. In these two cases, the velocity was calculated using the PUNDIT and therefore is related to a dynamic elastic modulus, whilst in the velocity calculations for the Kumamoto beams a static modulus was used.

During the tests, the beams were simply supported using rollers placed on the testing rig. The load was applied using a hydraulic jack and uniformly distributed on two points of the beam using a steel bar and two rollers. Different load configurations were applied and for each, the designed failure load was calculated (see Appendix B) and used to define the loading steps. All beams failed in bending with some shear damage appearing on beams K3, K4 and KL2. The loading procedure and the composition of the cycles were as previously described for the Edinburgh experiments. The different steps and cycles are described in Figure 6.26.

An LVDT was used to record the displacements in the middle span of the beams during the testing. Clipping crack gauges were also used to measure the width of the cracks. A gauge was generally placed on a crack thought to be representative of the cracking behaviour of the beam. The load, LVDT and clipping gauge were directly connected to the AE system, with reading of a sample every second. Thus no manual recordings were needed.

Drawings showing design details, load configuration and gauge positions of all beams are shown in Figures 6.27, 6.28, 6.29, 6.30, 6.31 and are summarized in Table 6.4.

During the test the beams were monitored using a DiSP AE system in conjunction with eight UT-1000 broadband transducers. The choice of the type of sensors was dictated by the availability in the Kumamoto laboratory. The sensors were mounted on the beam using bees wax according to the Japanese procedure. The sensors were



Figure 6.25: Phases of the casting of the beams in Kumamoto Laboratory.

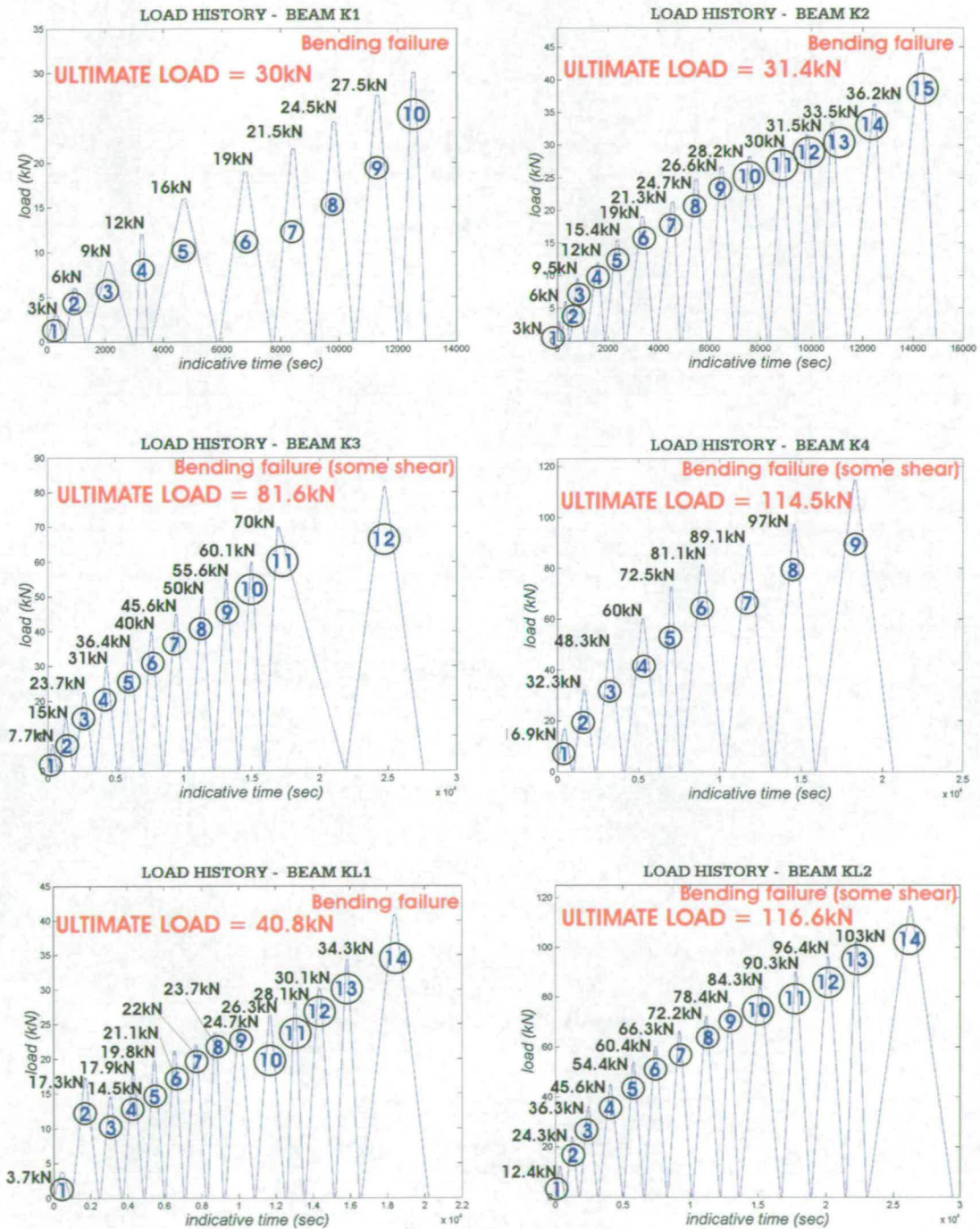


Figure 6.26: Load history of the beams of Kumamoto beams experiments.

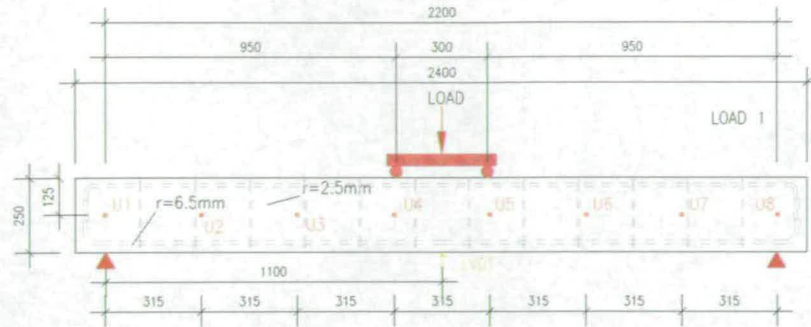


Figure 6.27: Design details, test configuration and broadband sensor location (UT-1000 type: U1 to U8) of beams K1 and K2.

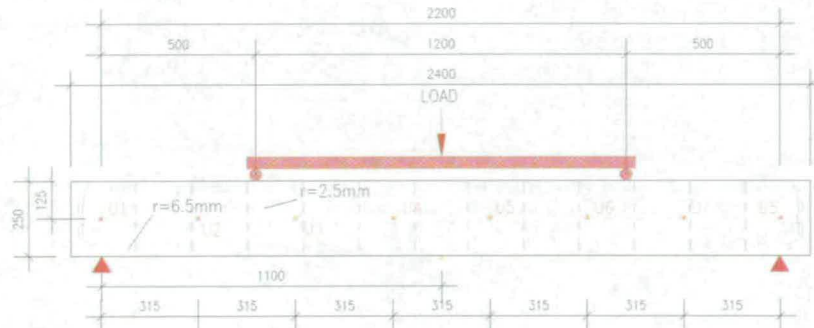


Figure 6.28: Design details, test configuration and broadband sensor location (UT-1000 type: U1 to U8) of beam K3.

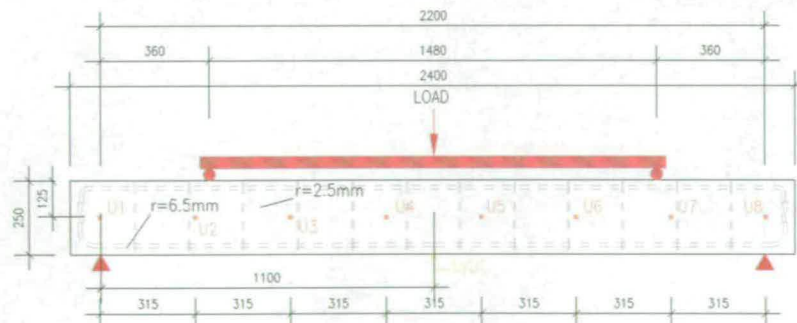


Figure 6.29: Design details, test configuration and broadband sensor location (UT-1000 type: U1 to U8) of beam K4.

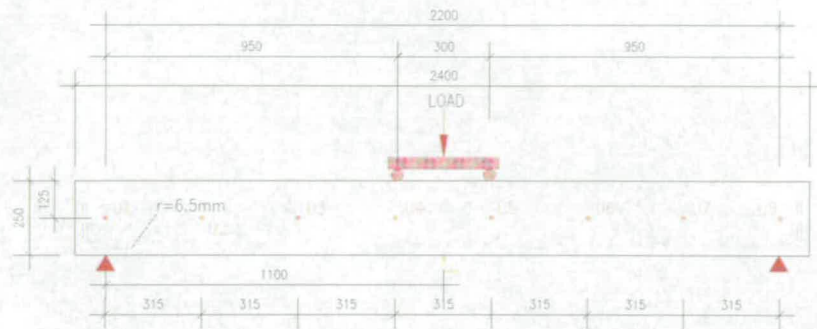


Figure 6.30: Design details, test configuration and broadband sensor location (UT-1000 type: U1 to U8) of beam KL1.

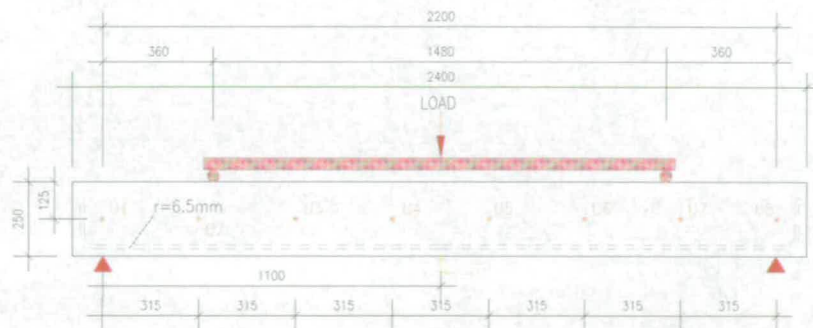


Figure 6.31: Design details, test configuration and broadband sensor location (UT-1000 type: U1 to U8) of beam KL2.

	K1	K2	K3	K4	KL1	KL2
Section	150x250mm	150x250mm	150x250mm	150x250mm	150x250mm	150x250mm
Span	2.2m	2.2m	2.2m	2.2m	2.2m	2.2m
Reinfor- cements	stirrups cage 4 ϕ 13mm 12 ϕ 5mm	stirrups cage 4 ϕ 13mm 12 ϕ 5mm	stirrups cage 4 ϕ 13mm 12 ϕ 5mm	stirrups cage 4 ϕ 13mm 12 ϕ 5mm	simply reinforced 2 ϕ 13mm	simply reinforced 2 ϕ 13mm
Concrete	45.99MPa	45.99MPa	45.99MPa	45.99MPa	45.99MPa	45.99MPa
Concrete type	rapid hardening	rapid hardening	rapid hardening	rapid hardening	rapid hardening	rapid hardening
Wave velocity	3600m/sec	3600m/sec	3600m/sec	3600m/sec	3600m/sec	3600m/sec
No. of cycles	10	15	12	9	14	14
Load steps	3kN	3kN	varied	varied 1.2-1.6kN	3.5kN	varied 1.2-1.6kN
Failure load	30kN	44kN	81.6kN	114.5kN	40.8kN	116.6kN
Failure type	bending	bending	bending some shear	bending some shear	bending	bending some shear
Sensors used	UT-1000	UT-1000	UT-1000	UT-1000	UT-1000	UT-1000
Sensors spacing	315mm	315mm	315mm	315mm	315mm	315mm

Table 6.4: Summarized description of the beams of Kumamoto experiments.

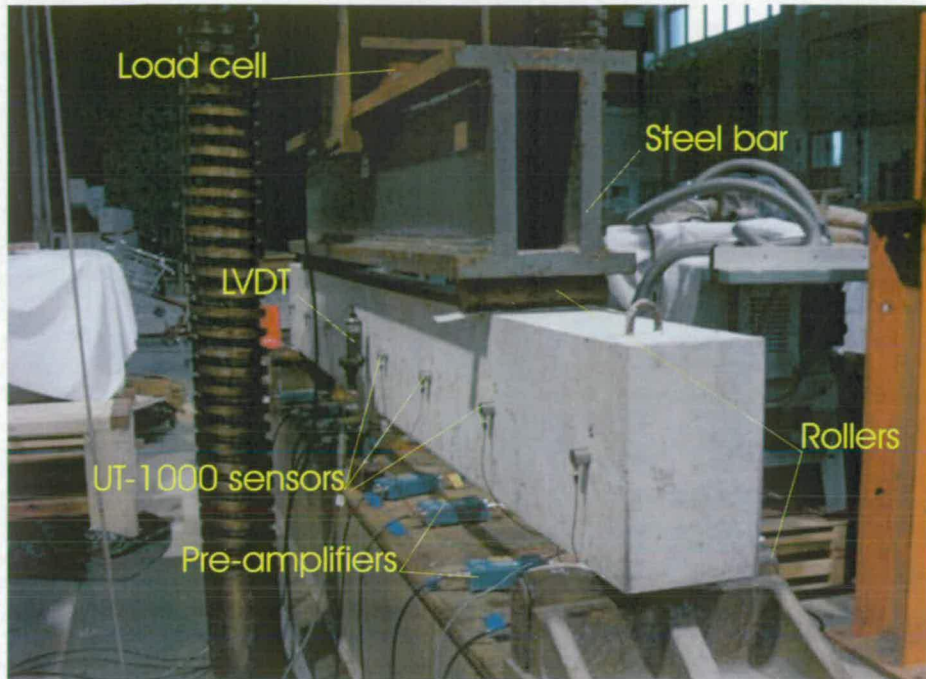


Figure 6.32: Photo of instrumented beam at Kumamoto Laboratory.

equally spaced alongside the beam and their exact location is shown in Figures 6.27, 6.28, 6.29, 6.30, 6.31, whilst Figure 6.32 is a photo of an instrumented beam and Table 6.5 summarizes the instrumentation settings. The data were recorded as parameters (see section 4.4).

During each cycle the cracks were marked as in the Edinburgh experiments although their exact pattern was of no specific interest for the purpose of these tests and it is therefore not shown here in detail. Depending on the load configuration the crack patterns appeared to be composed of pure bending cracks (beams K1, K2 and KL1) or of a predominance of bending cracks alongside the beam with few shear cracks appearing at the beam ends (beams K3, K4 and KL2). Photos of the failures are in Figures 6.33 and 6.34.

One of the main aims of the period spent in Japan was to understand how to perform a Moment Tensor experiment and analysis. To achieve this aim part of time was spent assisting the undertaking of Moment Tensor experiments on small concrete samples. The experiments were planned by Prof. M. Ohtsu and Assoc. Prof. M. Shigeishi of Kumamoto University and no personal claim is made on their originality or



Figure 6.33: Photos of failed beams at Kumamoto Laboratory.

	K1	K2	K3	K4	KL1	KL2
Threshold	40dB	43dB	43dB	43dB	43dB	43dB
Sample rate	1MHz	1MHz	1MHz	1MHz	1MHz	1MHz
Hit Length	2K	2K	2K	2K	2K	2K
PDT	500	500	500	500	500	500
HDT	1000	1000	1000	1000	1000	1000
HLT	1000	2000	1000	1000	1000	1000
Pre-trigger	512	512	512	512	512	512

Table 6.5: Summary of the AE setting values for Kumamoto experiments.

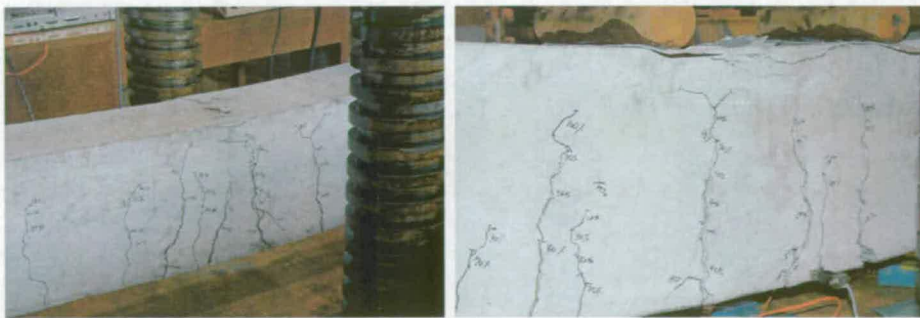


Figure 6.34: Failure of a beam at Kumamoto Laboratory.

results. They are considered merely as an example of how a Moment Tensor experiment should be carried out and to help in the understanding and provide explanations as to why previous attempts to carried out a Moment Tensor analysis in Edinburgh were unsuccessful. Having clarified this point, an explanation of the whole experiment and its aims are hereby given, although it is the section concerning the MTA that is of any interest with regards to this thesis.

The experiment was planned in order to use the MTA to confirm the results obtained by a crack propagation analysis carried out using the Boundary Element Method (BEM) and reported in [Farid, 2001] and [Farid and Ohtsu, 2002]. The analysis is still under development at Kumamoto University and this experiment was specifically planned to deal with the cracking generated by the corrosion of the concrete reinforcements.

Corrosion is one of the major cause of deterioration affecting RC structures. Carbon dioxide and chloride can penetrate through the pores of the concrete and annul the passivity of the steel that can then be subjected to corrosion. As a result of the corrosion and the corrosion products the volume of the steel increases and generates tensile stress in the sourrounding areas and thus cracks develop [Farid and Ohtsu, 2002].

The model developed at Kumamoto University showed that the corrosion of the rebars gives rise to different crack patterns depending on the thickness of the concrete cover [Farid, 2001]. Several concrete samples were made and set up to simulate the corrosion mechanism of the rebar. The specimens consisted of concrete notched slabs of varying dimensions and cover and a hole in place of the rebar. The tested slab was instrumented with four strain gauges around the rebar hole and a pressure gauge, which were all connected to a data logger. Six AE UT-1000 sensors were mounted on the sample and connected to the DiSP system. As an example of a Moment Tensor experiment, one sample is taken into consideration and its set up and failure are shown in the sketch of Figures 6.35 and 6.36. The settings used are summarized in Table 6.6 and their importance for the success of the analysis will be discussed in section 7.5.

The experiment consisted of pouring an expansive agent (dolomite paste) in the rebar hole of the concrete sample. This agent then expanded (over a period of about 12 hours) simulating the corrosion of a rebar and thus generating the cracking and failure of the sample. The pressure gauge, placed in the rebar hole before pouring the agent,

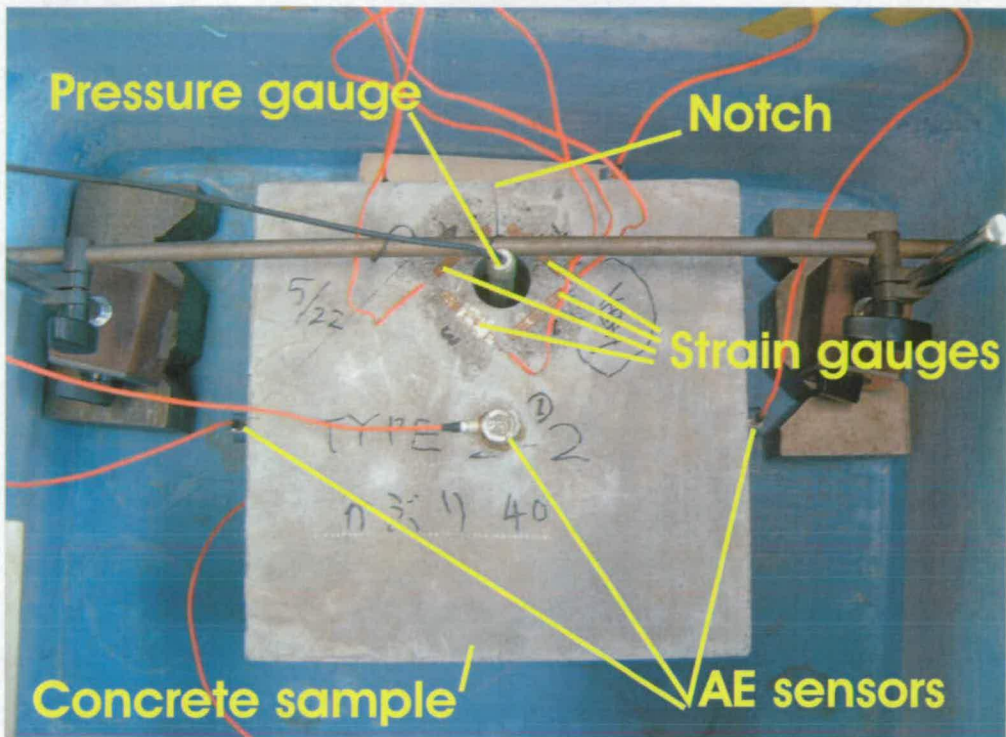


Figure 6.35: Set up of the concrete sample for the Moment Tensor test.

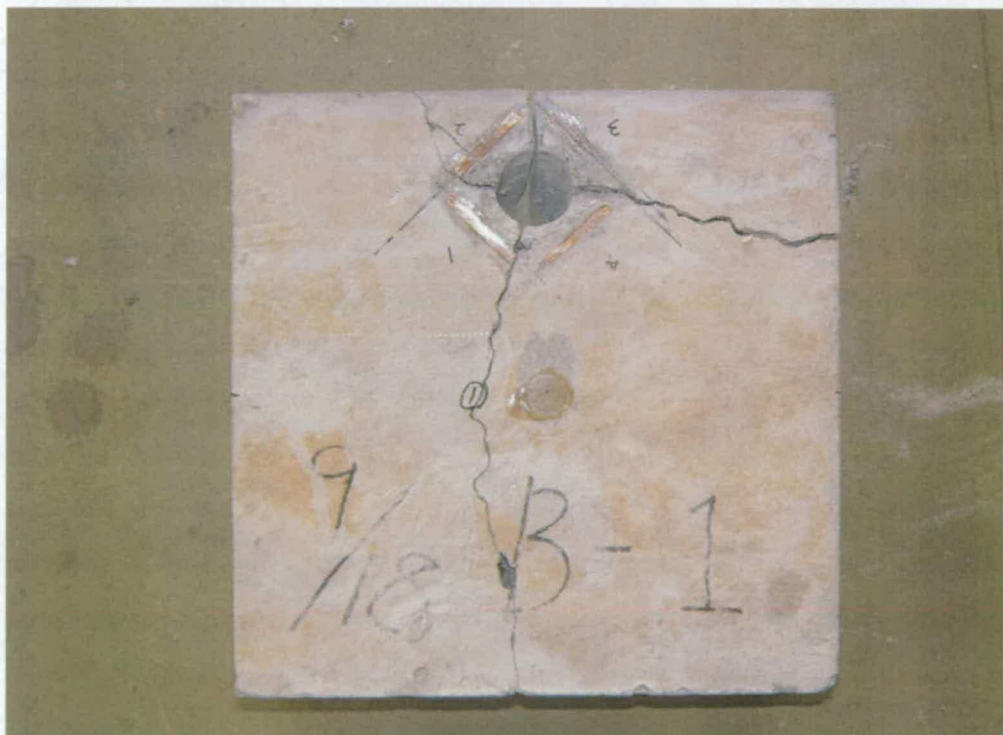


Figure 6.36: Failure of the concrete sample for the Moment Tensor test.

Moment Tensor Settings	
Threshold	40 dB
Sample rate	1 MHz
Hit Length	2K
Pre-trigger	-256
HLT	2000
Trigger Mode	SYN
Trigger source	5 EXT and 1 DIG

Table 6.6: Summary of the AE setting values for the Moment Tensor experiment.

measured the increase in pressure during the expansion process. During the expansion period, acoustic emissions were generated and recorded by the UT-1000 sensors in the form of waveforms using the MT-TRA software. A Moment Tensor Analysis was then performed on this data and it will be further discussed in section 7.5.

At this stage two key points have to be highlighted. Firstly the sensors were located asymmetrically. This method of placement helps and makes more precise the mathematical calculation of the sources performed by the software during a step of the successive MTA. This point was in fact reported in [Ohtsu et al., 1998a] and this location was adopted in the attempts of beams BF2 and BF3. Secondly, the use of the broadband sensors have to be highlighted. Discussions held with Assoc. Prof. Shigeishi proved that the use of broadband sensors is vital for the success of the Moment Tensor Analysis. Although there is no certainty about the motives behind it, a possible explanation is that the resonant sensors are sensitive to a narrow frequency range. Thus depending on their frequency range either low frequency slow motion signals or high frequency quick motion signals are detected, resulting in the loss of some information. The broadband sensors due to their wider frequency range can by comparison record the whole motion. No references to the specific need to use broadband sensors could be found in the literature but this is thought to be the main cause of the failure of the experiments attempted in Edinburgh and TRL.

6.4 Summary

This chapter provided a complete description of the method and experimental design adopted during the experiments. Overall, twelve small scale RC beams were designed and made and thirteen tests, as beam BF2 was tested twice, were carried out on them:

- BF1, BF2, BF3, BF2c, BF4, BF5, BF6 - at the University of Edinburgh
- K1, K2, K3, K4, KL1, KL2 - at Kumamoto University

Moreover, two full scale tests were undertaken at TRL on beams CF1 and HB2 and a small concrete sample was tested at Kumamoto University. The specimens were differently designed, instrumented and loaded, depending of the specific aim of the experiment. Different types of analysis were performed on the data collected during the tests and they are thus fully described and discussed in the following chapter.

Chapter 7

Analysis and Results

A significant portion of this thesis was dedicated to the investigation of different types of analysis of the AE data and sought alternative ways of processing and interpreting the data recorded during AE monitoring. This chapter includes the analyses that have been successfully carried out on the concrete specimens from the laboratory experiments described in the previous chapter. They include both “global” and “local” types of monitoring analysis and both parameter and waveform analyses (see section 4.4). A conventional b -value analysis is proposed and described and an analysis of the source location is presented, to process data obtained by a “local” and a “global” monitoring respectively. Its accuracy was assessed against the visible cracking on the specimen during the experiment. The introduction of a new parameter, the “relaxation ratio” described in section 4.8, is also proposed to assess the state of damage of RC beams and compared to the criteria proposed by the JSCE [Ohtsu et al., 2002]. The SoundPrint system was not originally developed to detect cracking in concrete (see section 5.3). For this reason particular emphasis has been placed on the data analysis collected by this technique. Finally, an example of Moment Tensor Analysis is described.

7.1 b -value Study

7.1.1 b -value Analysis

This section presents the results of a b -value analysis carried out on data recorded during the laboratory test on Beam BF2. Details about the b -value theory have been described in section 4.6. The b -value analysis is presented and proposed as a method to study the development of the fracture process of the concrete.

During the test it was possible to identify different stages of cracking:

- cycle 01: no cracks
- cycle 02 to cycle 05: cracks forming and the appearance of tensile cracks along the whole span of the beam
- cycle 06: appearance of shear cracks at the two ends of the beam
- after cycle 06: no new cracks growing; old cracks opened up

These stages had to be compared with the b -value analysis.

The raw data recorded with the MISTRAS system were processed using MATLAB software in order to carry out a b -value analysis. During all the processing the first cycle was ignored as the number of AE events was not significant. First, the range of amplitude was decided, starting from a threshold of 35 dB to a maximum of 100 dB in steps of 5 dB. Then the total number of events during a loading cycle were divided in groups. For each group the log-frequency-magnitude graph was plotted and their linear trend calculated using the least squares method of fitting curves. The slopes of the graphs represented the b -values. An example of some of these graphs and their relative b -values can be seen in Figure 7.1 where the b -value is calculated for groups of events during the whole cycle number 2. The graphs represent the log-frequency-magnitude chart and its relative curve fitting and b -value calculation for different groups of 100 events.

These b -values, during a whole cycle, were then plotted versus time (which corresponded to the final time in seconds of the time-range in which the relative group of events happened during the test). This was done for each loading cycle and for each channel. It was necessary to determine the number of events forming the groups on which the calculations were based. In order to do this, the whole calculation process was repeated using groups formed by different numbers of events. The trends of b -value values were then plotted for each case and overlapped. The results (see Figure 7.2) showed that using groups formed by a number of events between 70 and 130 did not substantially modify the final trend. It was then decided to use an intermediate value of 100 events. This whole process allowed verification that the choice of the number of events on which the b -value calculation would be based, did not affect the results.

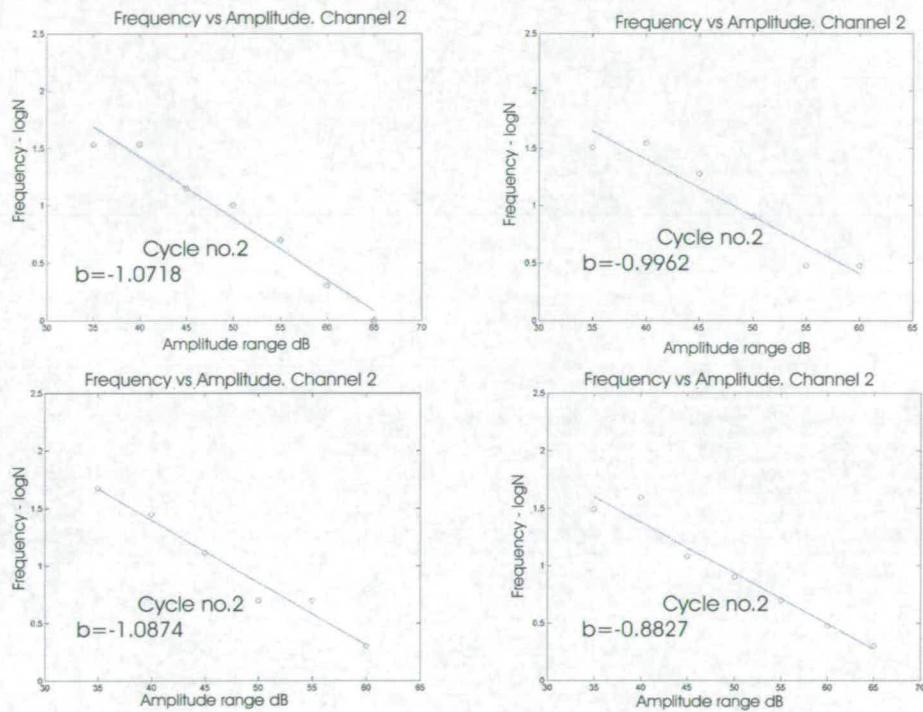


Figure 7.1: Example of calculation of b -values for channel 2 during the loading cycle number 2. The graphs represent the log-frequency-magnitude chart with the best fitting curves shown as straight lines, and the best fitting slope or b -value shown.

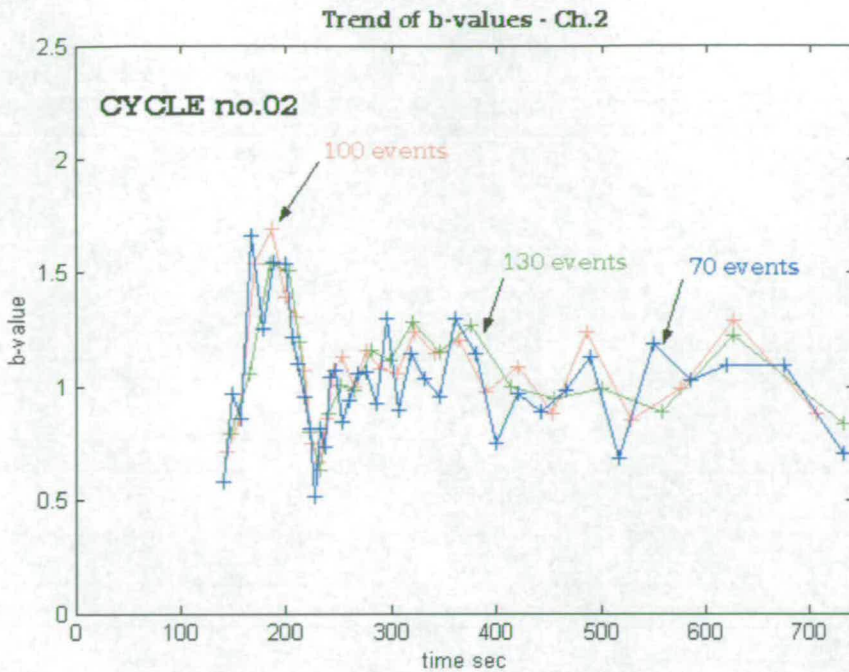


Figure 7.2: b -value over time calculated with using groups of respectively 70 (blue line), 100 (red line) and 130 (green line) events.

The trend of the b -value was then calculated and plotted for each cycle of the test and for each channel. The pattern was clearer in the early cycles when the cracks were forming. The presence of a large number of concentrated microcracks creates a clear pattern. However once the external macrocracks are formed (the beam is failing) the AE sources are fewer and more scattered so the pattern is less clear. This might imply that the analysis of the b -value is meaningful on sound structures as it provides information between the microcracking beginning up to the stage where macro fractures occur by localisation (i.e.: the number of microcracks is high and they join, thereby creating a localised macrocrack). The trend of the b -value for channels 3 and 7 during the second cycle of the test is shown in Figure 7.3; the load over time is shown on the same graph (dotted line) on the vertical axis on the right. The localisation predicted on the basis of the minimum b -value is shown by the arrow and the error bars of the statistical calculation are shown. As the two sensors were located respectively on the end and the middle area of the beam they can be considered as giving a whole representation of the full beam. Notwithstanding the presence of “fluctuations” in the trend (due to the presence of reinforcement bars in the concrete), it is possible to see

in both cases a pattern showing a decrease at the beginning (the dashed line in the chart) when the load is going up, and then a transient during the relaxation when the load is held constant. The b -value decrease corresponds then to the loading phase of the test, when the cracking is happening. The b -value reaches its minimum when the load and the damage on the beam are maximum. Its value can therefore be a good representation of what is really happening on the beam in the early stages of failure, when the beam is damaged but still structurally intact.

The b -value was also compared with the damage parameter D (see section 4.6). D was calculated for each loading cycle, using intervals of 100 events as for the b -value. The whole damage parameter was normalised to one, so that one was equal to the maximum damage at the end of each cycle. The results were compared with the b -value trend and they are shown in Figure 7.4 where the continuous line is the b -value trend, while the dotted line represents the damage parameter. On the graph the trend of the b -value, on the left vertical is overlapped with the trend of the normalised damage parameter, on the right vertical axis. The error bars of the statistical calculation are also shown. The graph shows how the minimum of the b -value corresponds to the sudden increase in the damage of the beam represented by the D parameter. Such an increase in damage corresponds to the final stage of the loading up when the visual observations during the experiment confirmed the appearance of cracking on the beam.

In a post-failure phase, the minimum and maximum value of the b -value were considered, for each cycle and for each channel. The trend of the range during the whole cycle and for each channel was then plotted. Due to the relationship mentioned earlier in the paper between the increasing and decreasing of b -value and the micro and macro cracking, the minimum b -value trend suggests macrocracks have formed, whilst the maximum b -value trend implies microcrack growth. The chart of the trend for channel 3 and channel 7 during the whole experiment is shown in Figure 7.5, where the vertical lines show the different cracking stages indicated by the arrows.

When examining the results for channel 3 (which is located near to the end of the beam (see Figure 6.4), the maximum trend is increasing from cycle number 2 to 3, implying that microcracks are forming. During the experiment it was actually in these early stages that the cracking appeared and could be mapped on the beam. A peak of

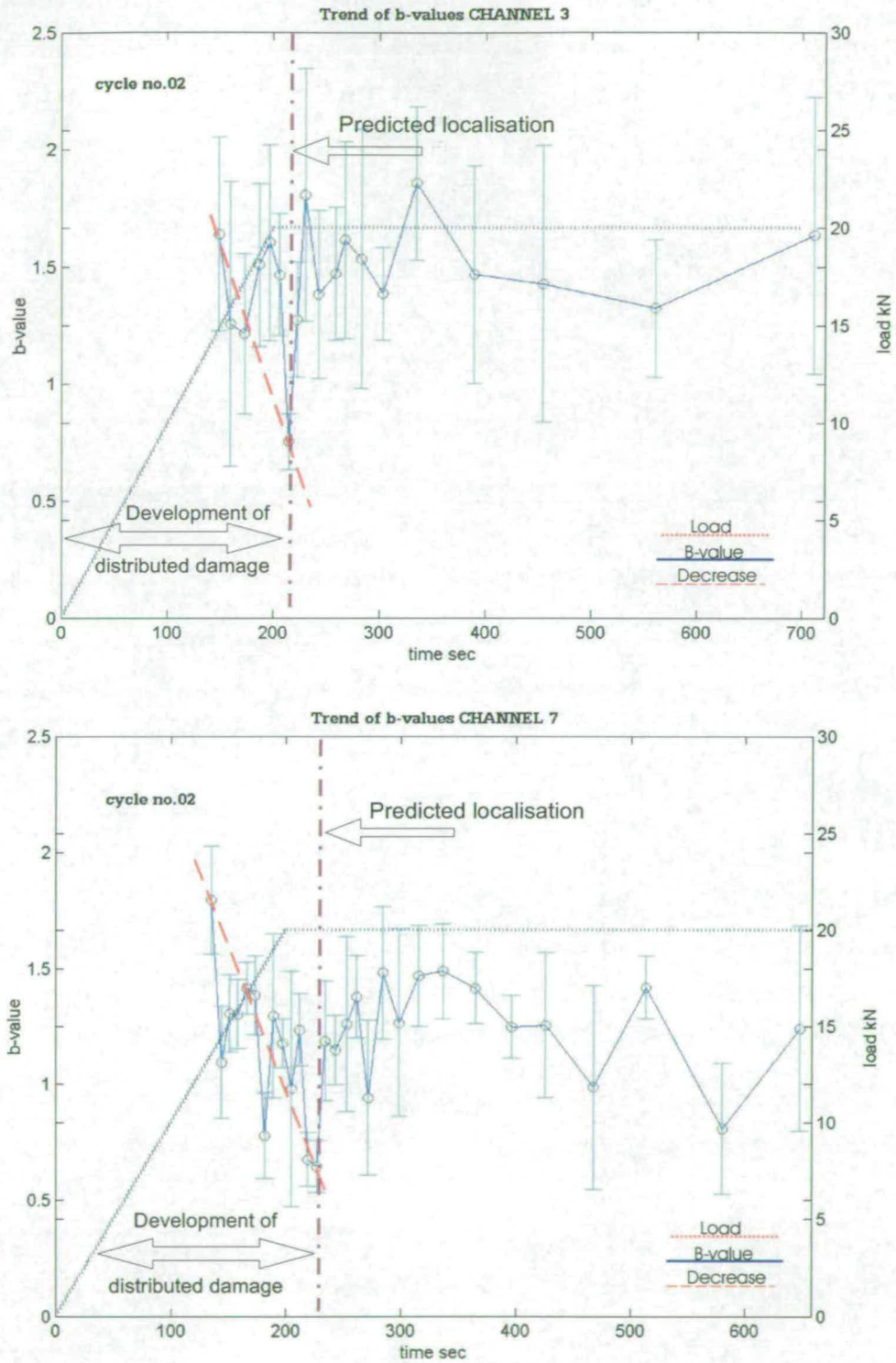


Figure 7.3: b -value over time for channels 3 (top) and 7 (bottom) during load cycle number 2 - the load is shown by the dashed line with a scale shown on the vertical axis on the right. The localisation predicted on the basis of the minimum b -value is shown by the arrow. The bar errors of the statistical calculation in the b -value are shown.

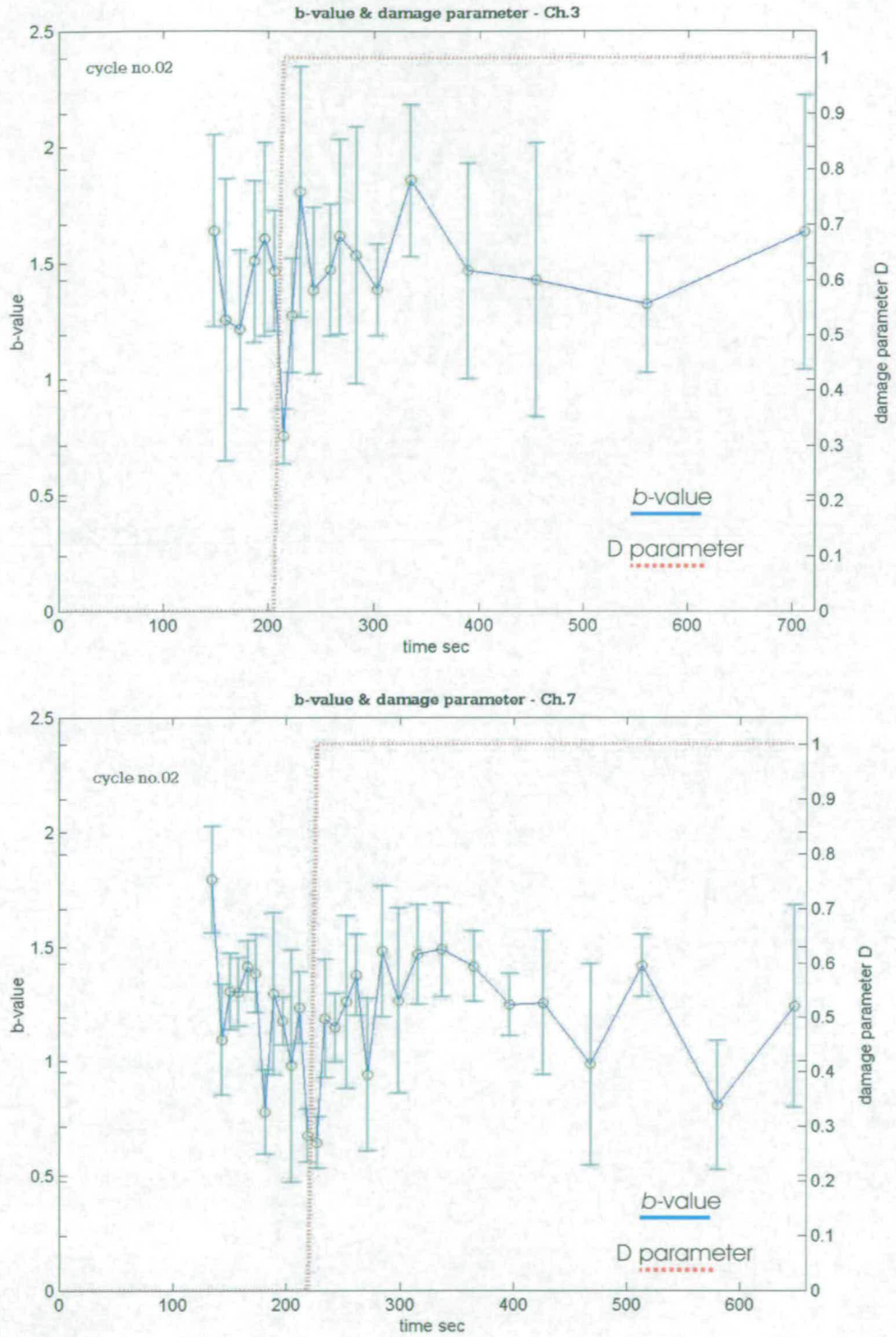


Figure 7.4: Overlapping of b -value (blue line: left vertical axis) and normalised damage parameter (red dashed line: right vertical axis) for channels 3 (top) and 7 (bottom) during load cycle number 2. The bar errors of the statistical calculation of the b -value are shown.

the trend appears in cycle number 9, which when correlated with the experiment was the point at which all the cracks were already formed. However, the shear cracks at the end of the beam were visibly opening up, just before the failure that happened in the following cycle. The minimum trend is decreasing in the early stages, reaching a minimum in cycle number 4, suggesting the existence of macrocracks. It was possible to observe that at this stage all the macrocracks had appeared on the beam. Therefore from this point onwards the minimum trend is constant as no major changes of damage could be observed on the beam. The b -value evolution is in good agreement with the damage observed independently on the beam.

Looking at the results for channel 7 (which is located in the middle of the beam), the maximum trend still decreases at the beginning, implying that microcracks are forming; once again this corresponds to the stage of the test when the microcracking was happening. After this phase, the trend remains constant as at this point the cracks could be seen uniformly spread along the beam. The peak at the end (shown in the results from channel 3) is unclear now, as this channel is located too far from the end of the beam where the shear cracks are opening to be affected strongly by them. The minimum trend is decreasing in the first cycle as macrocracks started to be visible on the beam and it stabilises afterwards when all the macrocracks had appeared on the beam and no more new cracks could be seen.

In both cases, three stages of the fracture process can be identified. A first stage is where the microcracks are dominant and the macrocracks are starting to appear. This corresponded to the early stages of loading when the cracking could be seen starting to appear on the beam. A second phase of constant range when the macrocracks are constant and uniformly distributed all along the beam can then be recognised during the middle phase of the loading when visually no new cracks could be seen appearing on the beam. After this stage the cracks do not grow towards the top part of the beam (as the concrete is in compression) so a last stage can be identified when the macrocracks are opening up as the beam is failing.

The crack pattern during these phases as it appeared on the beam is represented in Figure 7.6. The stress level related to the fracture stages could not be estimated exactly as the data obtained using a Demec gauge are not reliable once macrocracks appear.

Finally, the b -value was calculated considering all the events (instead of groups

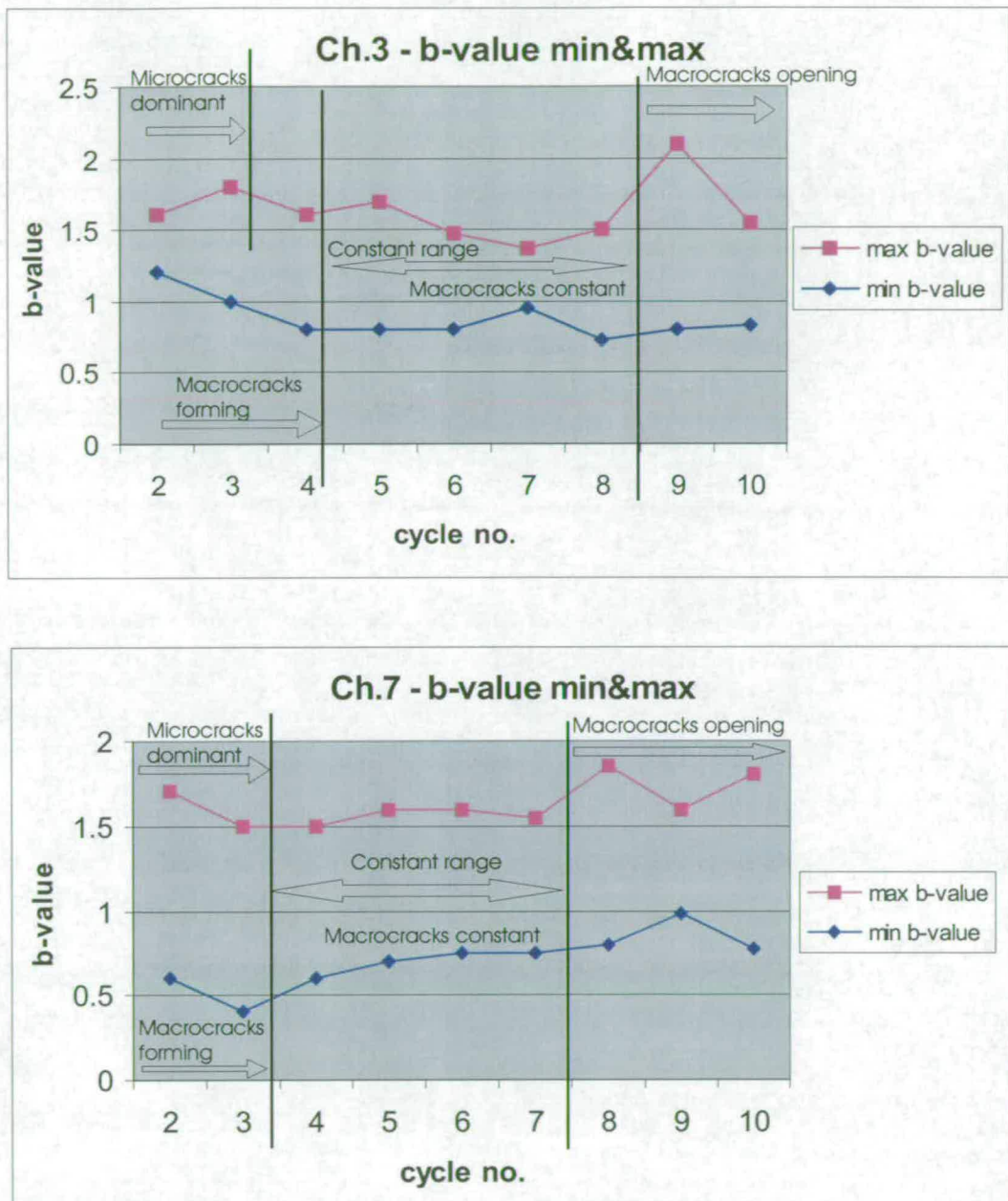


Figure 7.5: Variation of the maximum and minimum b -value for channels 3 (top) and 7 (bottom) during all the cycles of the whole experiment. The vertical lines show the different identified cracking stages indicated by the arrows.

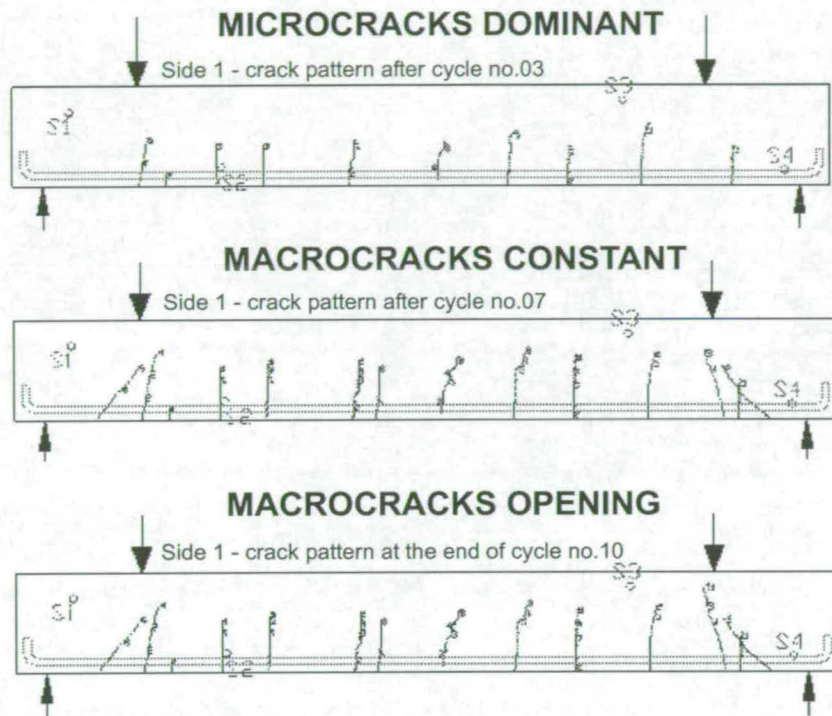


Figure 7.6: A sketch of the fracture process developments during the different stages of the loading. The dotted line outlines the location of the steel reinforcement. Note the inclined shear cracks near the edges of the sample.

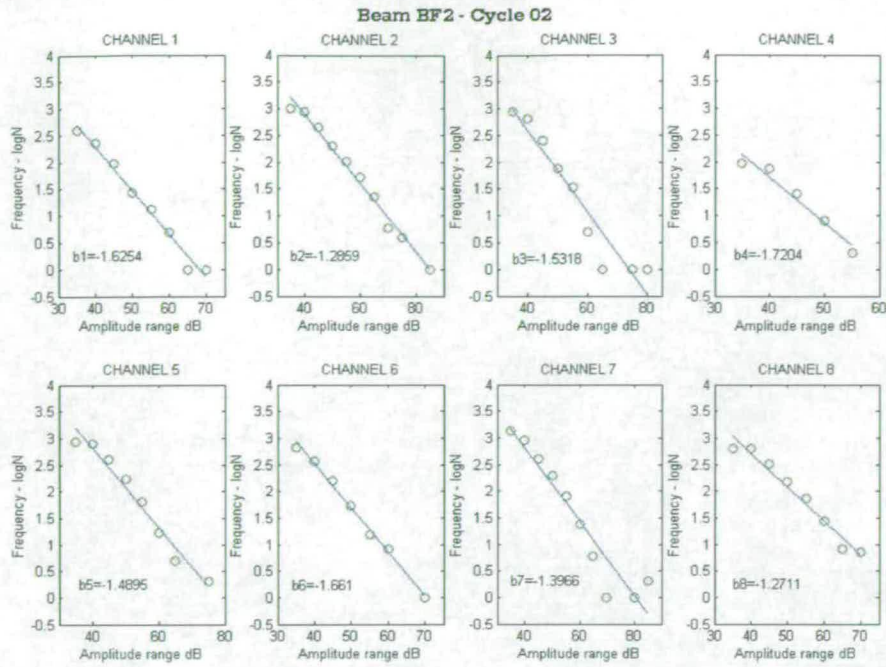


Figure 7.7: Frequency vs. Amplitude charts and corresponding b -values during the whole cycle number 2 for each channel.

of 100 events) of a whole cycle and for all channels, to compare the slopes of each channel. The results of these b -value calculations for two of the loading cycles (number 2 and number 6) are shown in Figures 7.7 and 7.8. By comparing the numerical values obtained in all cycles for all eight sensors with the location of the sensors themselves and the appearance of the cracks on the beam some quantitative considerations were drawn and they are summarized in Table 7.1. At this stage, the results confirm observations from earthquake aftershocks, slope stability studies and laboratory rock mechanics, that the b -value is (negatively) correlated with the degree of localisation of damage [Sammonds et al., 1994].

7.1.2 b -value Conclusions

A conventional b -value analysis was applied on the AE data obtained from the experiment on beam BF2. The trend of the b -value was then compared with the development of the fracture process of the beam observed during the experiment:

- A good relationship was found between the trend of the b -value and the microcracking and macrocracking appearance during the test.

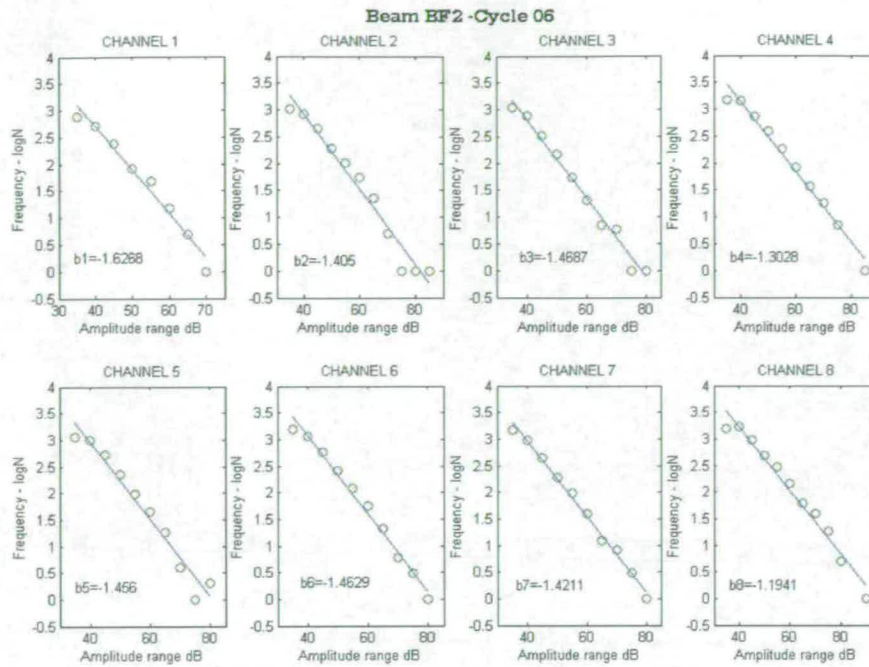


Figure 7.8: Frequency vs. Amplitude charts and corresponding b -values during the whole cycle number 6 for each channel.

b -value	Cracking process
$1.0 \leq b - \text{value} < 1.2$	Implies that the channel is very near to a large crack; i.e. macrocracks forming
$1.2 < b - \text{value} \leq 1.7$	Uniformly distributed cracking; i.e. macrocracks are constant
$b - \text{value} > 1.7$	Microcracks are dominant or macrocracks are opening

Table 7.1: b -value quantitative results.

- The results confirmed that the b -value is correlated to the fracture process of the concrete and to the degree of localisation of damage.
- The minimum b -value trend suggests the formation of macrocracks, whilst the maximum b -value trend implies microcrack growth.
- This study suggests that a b -value analysis could be used to interpret data obtained by “local monitoring” of concrete bridges, although further work is needed in order to consolidate the results that were found and to make the b -value suitable for practical use.

The significance of this analysis is that the b -value analysis possibly provides a tool to enable an engineer to diagnose the degree and type of degradation of a concrete beam from remote monitoring of sensors mounted on the structure. The specific practical application relates to the monitoring on concrete bridge beams. The installation of the AE monitoring on a bridge would provide information on changes in the cracking forming in the structure, although at this stage the monitoring should be applied continuously and at an early age of the structure to be effective. Table 7.1 summarizes the results in a quantitative way. Note that these values of b correspond to the relative ratio of source duration to recording frequencies that applied in the tests reported here.

7.2 AE Source Location Study

The b -value analysis described in the previous section has been proposed as a “local” monitoring process. Its use can be extended to global monitoring applications, as long as the structure under study is not too large. The b -value analysis is based on the amplitude of the recorded signals, so an increased spacing of the sensors (which would be necessary in a larger structure) would generate generally low amplitude signals, making any distinctions in terms of related cracking activity unlikely. The source location type of analysis was then considered as a possibility for “global” monitoring applications.

7.2.1 AE Source Location Analysis

This section presents the results of the AE source linear location carried out using the MISTRAS software, both in terms of AE events and AE energy (section 4.7) on the beams tested at Edinburgh Laboratory. The location of the AE activity was then compared to the crack pattern that was mapped on the beams during the experiments to verify their relationship.

In order for the data to be representative of a variety of situations, a set of cases was considered, choosing tested beams with different designs, load configuration, type of sensors and type of failure. Therefore among the beams tested at Edinburgh Laboratory and described in section 6.1, the following ones were chosen for this analysis:

- beam BF2
- beam BF3
- beam BF6

This range of samples embraces (see section 6.1):

- the two main types of failure: shear (BF2 and BF3) and bending (BF6)
- the two types of sensors: resonant (BF2, BF3, BF6) and broadband (BF6)
- different types of design: simply reinforced (BF2), simply reinforced with shear links at the end (BF3) and stirrups cage (BF6)

The results are shown in Figures 7.9 to 7.17 both in terms of AE events (left column) and of AE energy (right column). It has to be pointed out that the scale of the vertical axis changes for the different cycles and beams. This was because using the same scale for each of them would have obscured information in the early cycles, when the AE activity is significant but small compared to the last failing cycle, which has high AE activity. On the other hand, a comparison of the absolute values of activity of the different cycles or beams was not of interest and therefore the change of scale was not considered an issue.

Figures 7.9, 7.10 and 7.11 show the results relative to beam BF2 from loading cycle number 2 to 10. Cycle number 1 was ignored as no significant activity was recorded. After cycle number 4, only the right half of the beam should be considered as the presence of oil made the data of the other half unreliable (see section 6.1). A good

relationship can be seen between the AE events and the crack pattern mapped on the beam, but it should be noted that the correlation with the cracks is stronger in terms of energy than events. This was more apparent in the early cycles (from number 2 to number 4) where the events spread all along the beam, whilst the energy concentrated in areas where new cracks formed. This might be due to the fact that events generated by reflections, noise or interference can still be located but the energy associated with them is irrelevant. On the other hand, structurally meaningful events are characterised by a relatively large amount of radiated energy. It can also be observed that a high peak of located energy appeared in the middle of the beam in cycle number 5. Although no correlation could be seen with the cracks marked at the end of this cycle, in the following cycle a new crack appeared in this area. The high energy released by this crack was therefore recorded when the crack was internal and thus not visible to be marked in cycle number 5. After cycle number 6, the middle of the beam had become inactive, whilst a concentration of AE activity was recorded at the right supported end, where the beam failed in shear.

Figures 7.12 and 7.13 illustrate the results of the data recorded on beam BF3. Once again cycle number 1 was ignored as no significant activity was present so that the above mentioned figures include the source location of cycle number 2 to 6 and cycle number 7 to 9 respectively. Once again, the correlation between the located AE activity and the cracks is clearer in terms of energy than events, especially with reference to the newly appeared cracks. A clear example is given by cycle number 5. By looking at the events location it would appear that the beam has a constant behaviour along all its length. Conversely the energy location showed few peaks from the middle to the left side of the beam indicating the presence of particular activity and three new cracks had appeared in this region. The energy location during cycle number 7 finally revealed a sudden concentration of energy on the right end side of the beam, where the shear failure occurred in the following cycle.

Figures 7.14 and 7.15 describe the results obtained by carrying out the source location on the data recorded by the resonant sensors placed on beam BF6, from cycle number 1 to 5 and from number 6 to 7 respectively. As before, in the early cycles the located energy tended to identify few areas of damage, whilst the events showed a more uniformly distributed pattern. Overall, this case appeared less evident than the previous two. This is probably due to the fact that the bending generated more cracks

alongside the beam, affecting the precision of the source location algorithm. In order to calculate the AE sources, the software requires the user to introduce the velocity of the wave propagation, which is generally the velocity measured at the beginning of the test and it is considered to be uniform through the whole specimen. The presence of cracks formed during an experiment affect this velocity as the waves have to now travel a longer path through the air which fills the gap of the existing cracks. This decreases the propagation velocity and leads to the generation of more reflections and thus interference. Concentrations of cracks in specific areas also makes the assumed velocity variable through the sample. This explains why the pattern is generally more accurate during the early loading cycles when fewer cracks are present. In the graph relating to cycle number 6, an intense energy activity can be identified. This was shown to precede the bending failure which was reached in this zone in the following cycle.

The last two figures 7.16 and 7.17 still refer to beam BF6 but to the data recorded by the broadband sensors. The concentration of energy and the presence of energy peaks in corresponding to areas where new cracks appeared can again be observed. In cycle number 1 an energy peak on the left side of the beam (between 0.6 and 0.8 m) is present; a new crack can be seen near to this very position in the following cycle. The same situation can be observed in cycle number 3, where a first peak between 0.6 and 0.8 m and a second peak between 1.8 and 2 m corresponded to two new cracks formed in these areas in cycle 4. The less precise correlation of this case compared to cycle number is due to the previously explained reasons. Finally, the events located in cycle number 6 indicate a quite uniform AE activity along the entire length of the beam, whilst two peaks in the middle of the energy graph anticipated the beam failing in this area in the successive cycle.

It would have been interesting to undertake this type of analysis on the full scale tests on beam CF1 and HB2, but the recorded data were not suitable for this type of processing. These data were recorded using the MI-TRA software and later converted and exported into the MISTRAS software using a software utility. However on this newly created file the location function was disabled. The PAC manual [PAC, 1995] does not report any explanation on the matter. When recording with the MI-TRA software, the sensors were set as synchronised, i.e. as soon as a signal exceeds the threshold and triggers one sensor all the remaining sensors are contemporary triggered.

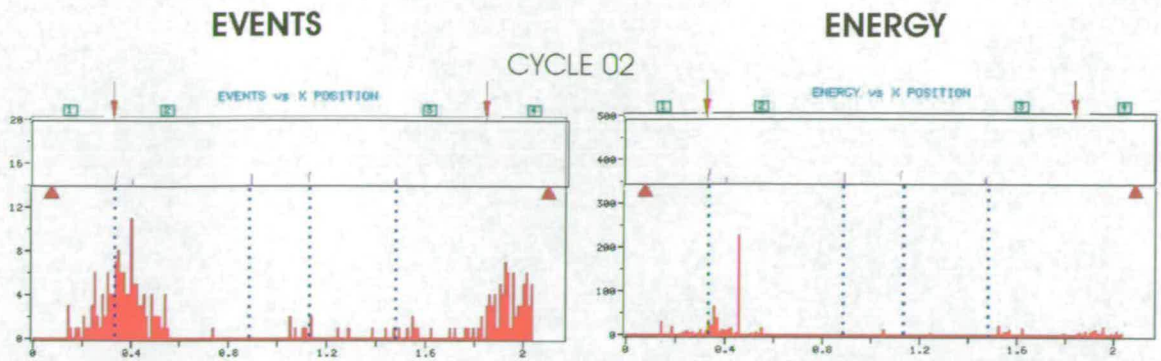


Figure 7.9: AE Source location results for beam BF2 and for cycle number 2. Each graph shows the amount of events (left column) and energy (right column) at each linear location along the beam, compared to the location of the macrocracks (upper diagram in each case) at the end of the specific cycle, with the dashed lines to aid comparison. The thick dark blue lines represent the new cracks, whilst the light blue lines indicate the presence or extension of pre-existing cracks. The position alongside the beam, expressed in meters, is shown on the horizontal axis. The green squares along the top of the horizontal axis represent the position of the transducers used to calculate the source location.

This is thought to make the software unable to automatically pick up the relative arrival times of the sensor which is necessary for the computation of the source location.

7.2.2 AE Source Location Conclusions

The AE source location analysis investigated the relationship between the located AE events and AE energy with the cracks appearing on the beams during the different loading cycles. The different cases studied gave rise to the same conclusions.

- A good relationship was observed between the located activity and the crack pattern mapped on the beams
- The precision of the location was higher in the early cycles when less cracks were present
- The AE activity - cracks correlation appears to be stronger in term of AE energy than AE events. This is more evident when related to the formation of new cracks
- The located energy often showed concentrations of activity where internal

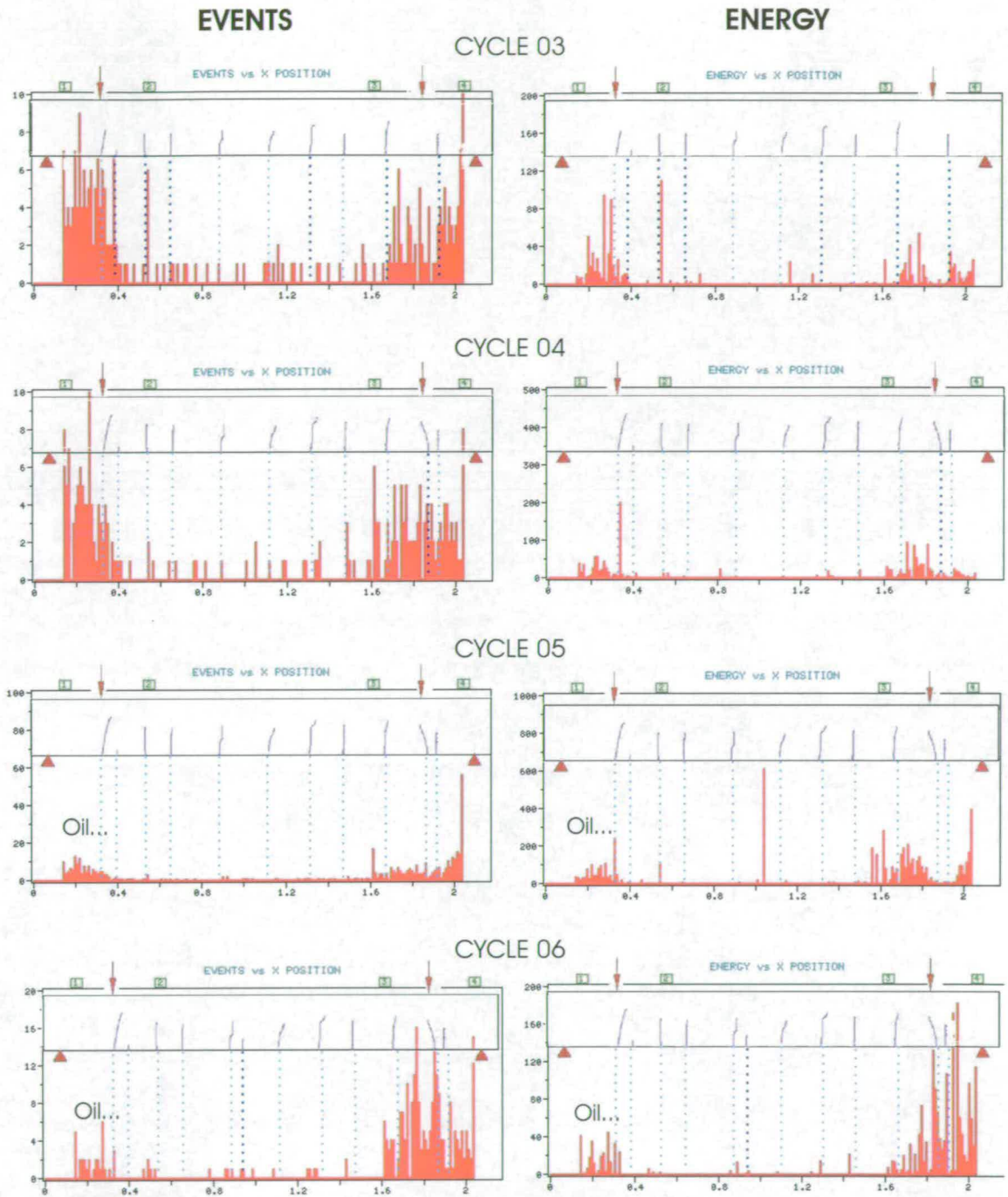


Figure 7.10: AE Source location results for beam BF2, for cycle numbers from 3 to 6, plotted as for Figure 7.9. The “oil” annotation refers to the technical problem described in section 6.1.

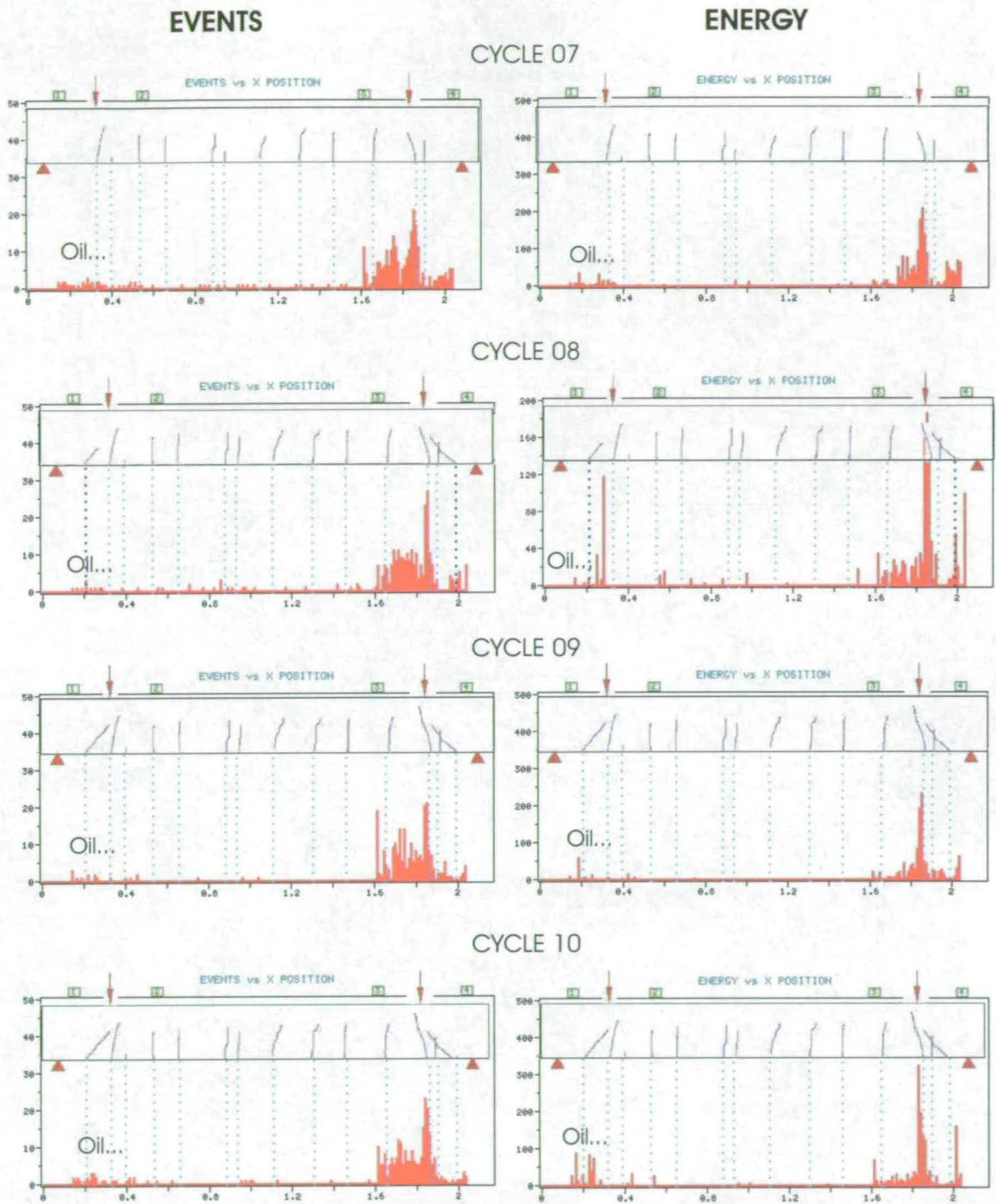


Figure 7.11: AE Source location results for beam BF2, for cycle numbers from 7 to 10, plotted as for Figure 7.9. The “oil” annotation refers to the technical problem described in section 6.1.

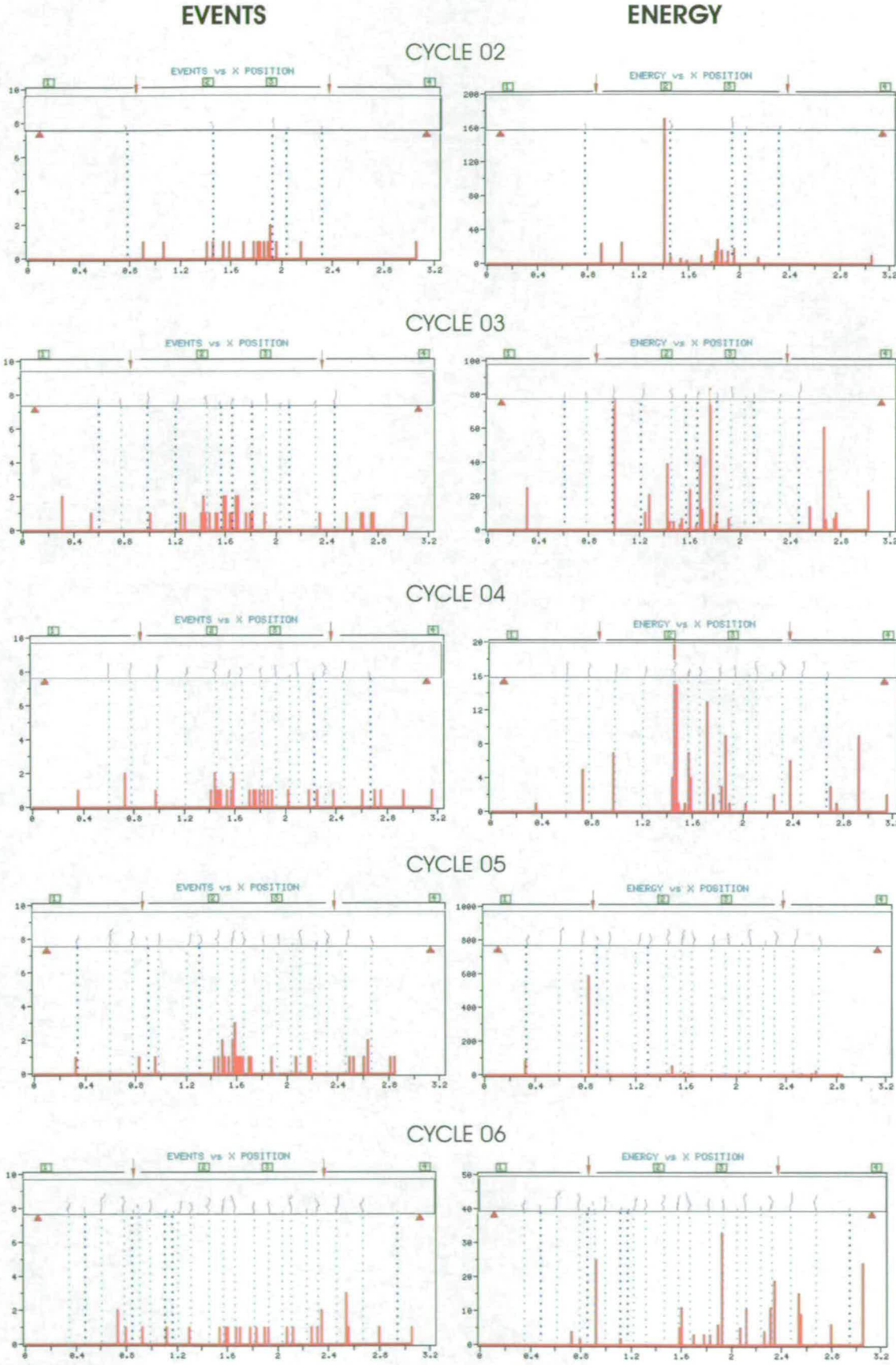


Figure 7.12: AE Source location results for beam BF3, for cycle numbers from 2 to 6, plotted as for Figure 7.9.

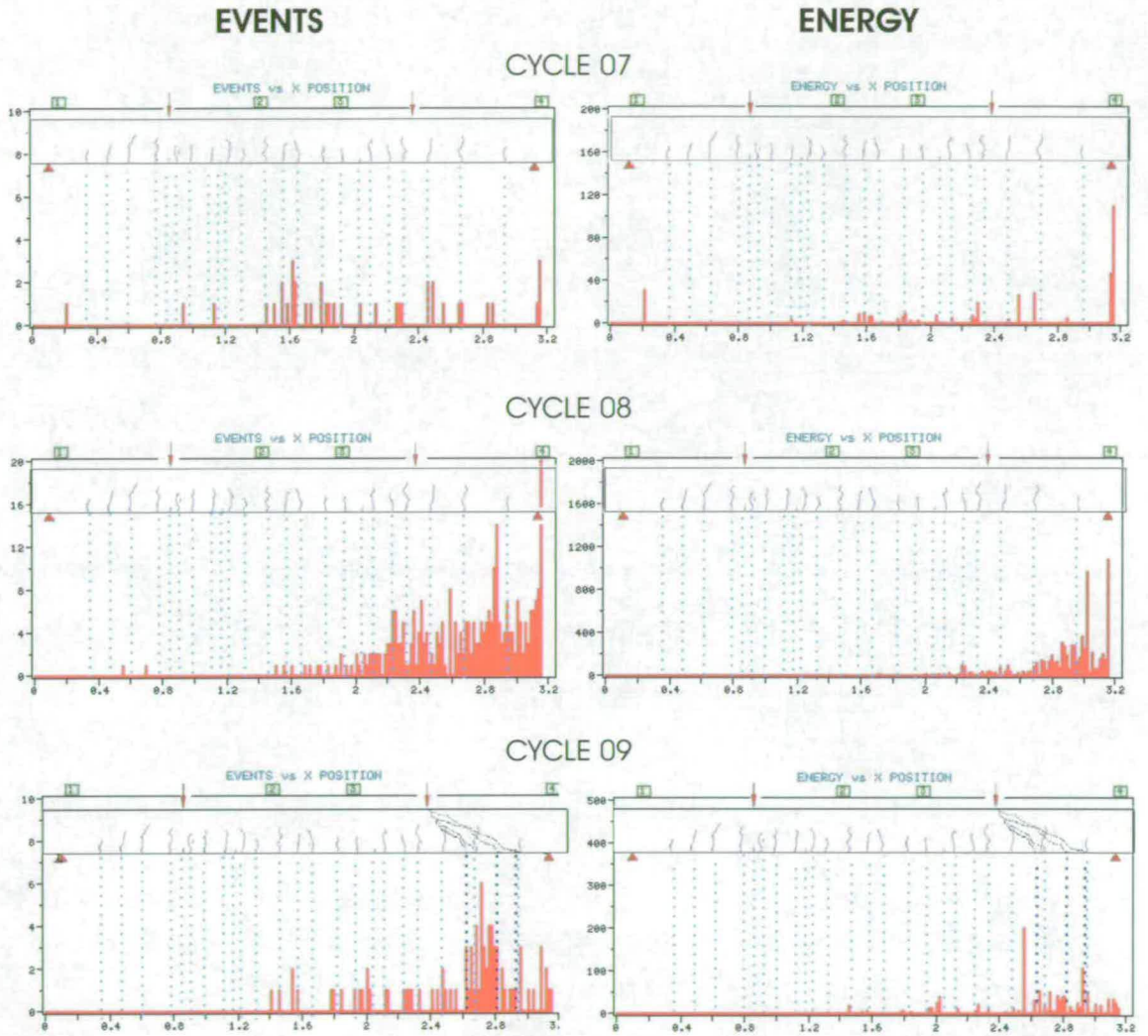


Figure 7.13: AE Source location results for beam BF3, for cycle numbers from 7 to 9, plotted as for Figure 7.9.

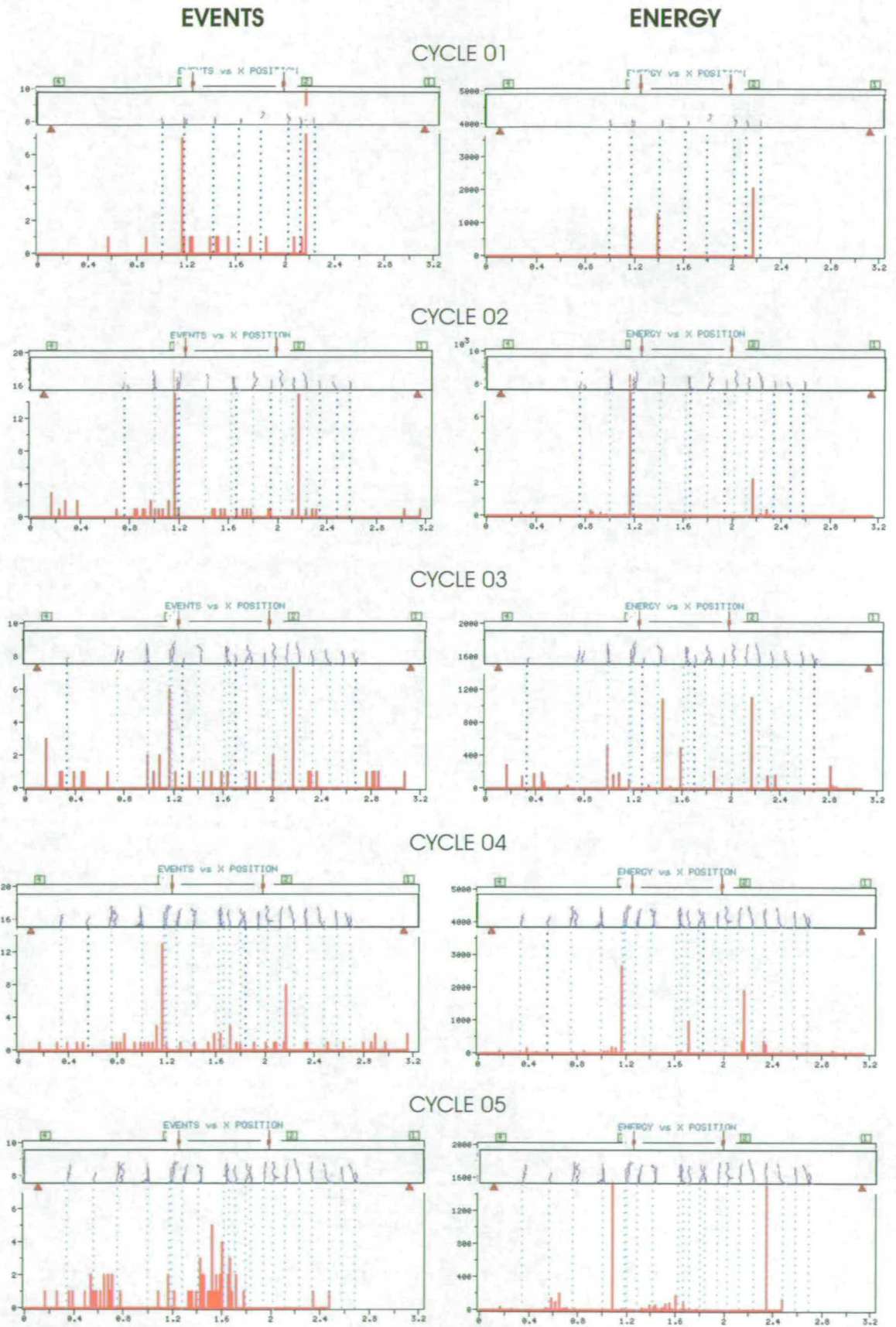


Figure 7.14: AE Source location results relative to the resonant sensors on beam BF6 for cycle numbers from 1 to 5, plotted as for Figure 7.9.

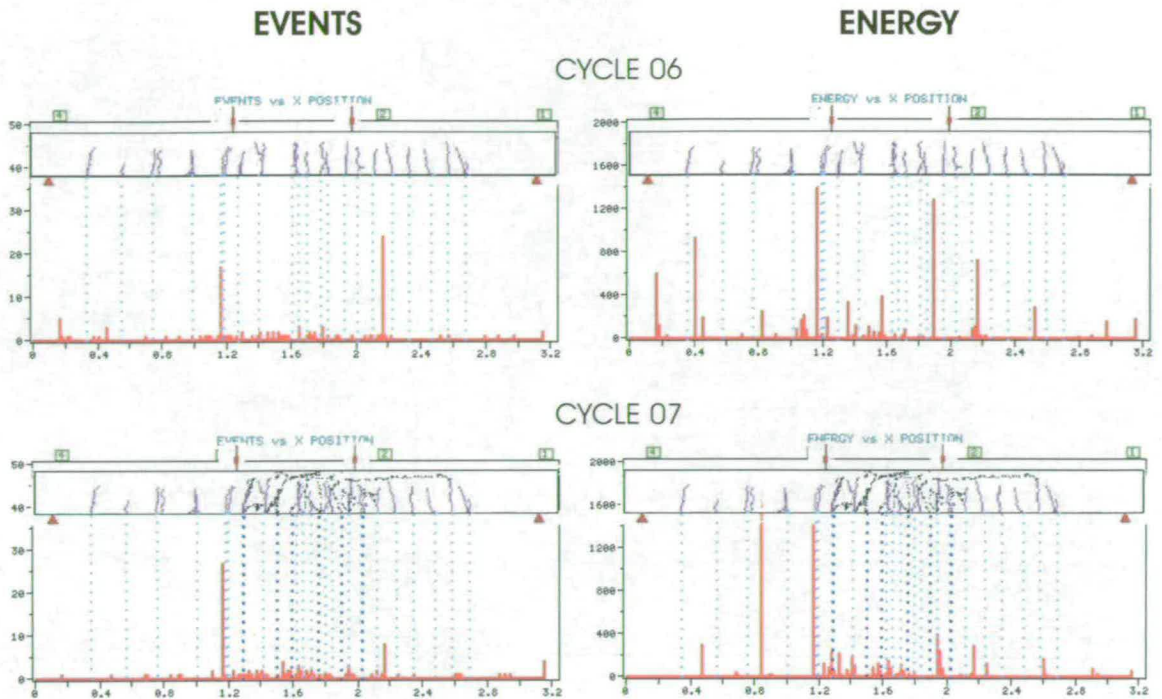


Figure 7.15: AE Source location results relative to the resonant sensors on beam BF6 for cycle numbers 6 and 7, plotted as for Figure 7.9.

non-visible cracks are present, which appeared during the subsequent loading cycle

- Concentrations of located AE energy can be considered a precursor of failure
- The energy can be considered as an effective parameter to indicate and anticipate the location of damage of a concrete structure.

In terms of practical application of this type of analysis it has to be pointed out that the location of the AE sources is a relatively quick type of processing that can be applied as a means of global monitoring and gives immediate and easy to interpret results. On the other hand it only provides a qualitative assessment of a structure and no quantitative information about the state of damage can be obtained.

7.3 Quantitative Assessment

The assessment of a bridge does not simply consist in determining if it is safe or not. During the evaluation of the safety of a bridge, it would be very useful for the bridge

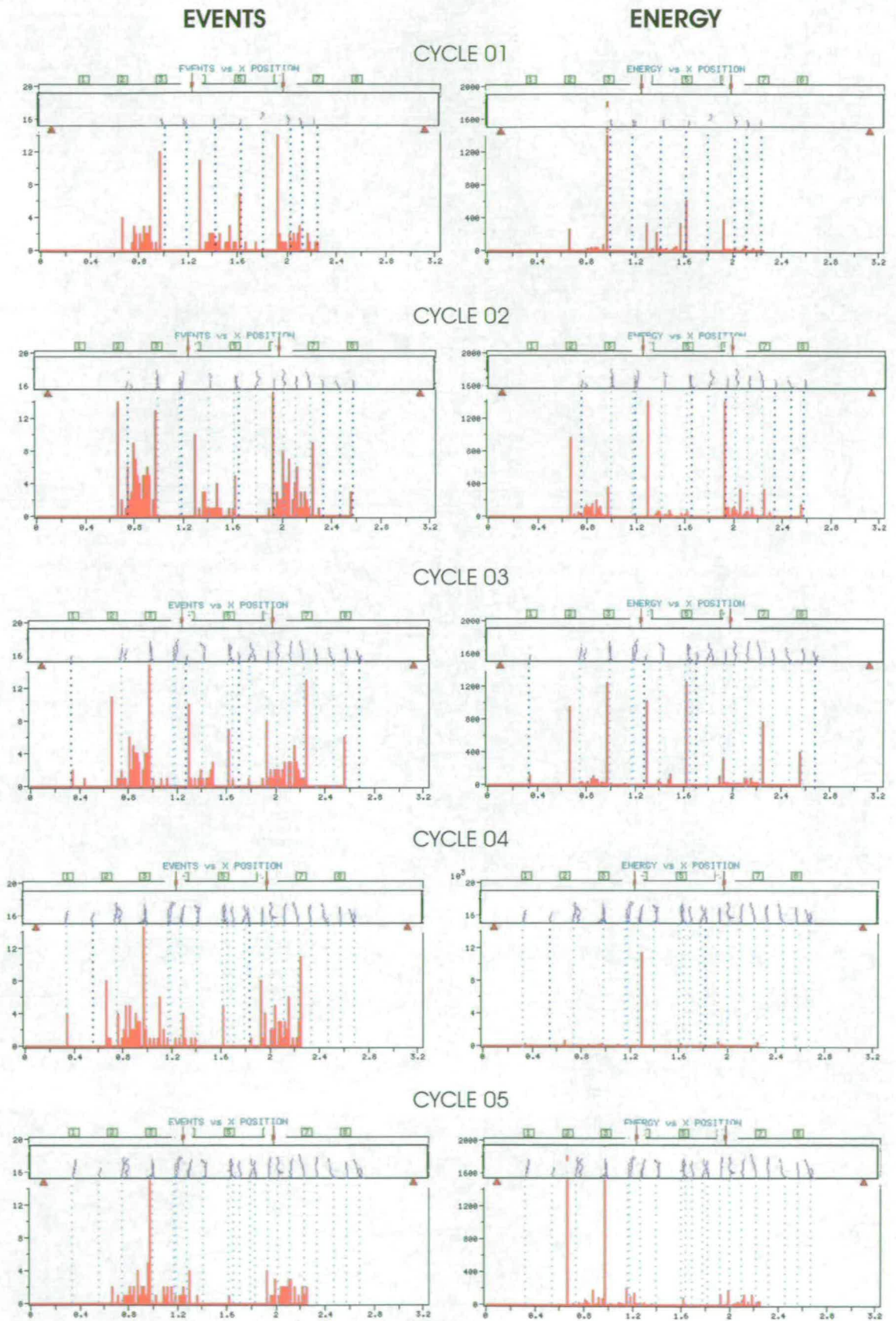


Figure 7.16: AE Source location results relative to the broadband sensors on beam BF6, for cycle numbers from 1 to 5, plotted as for Figure 7.9.

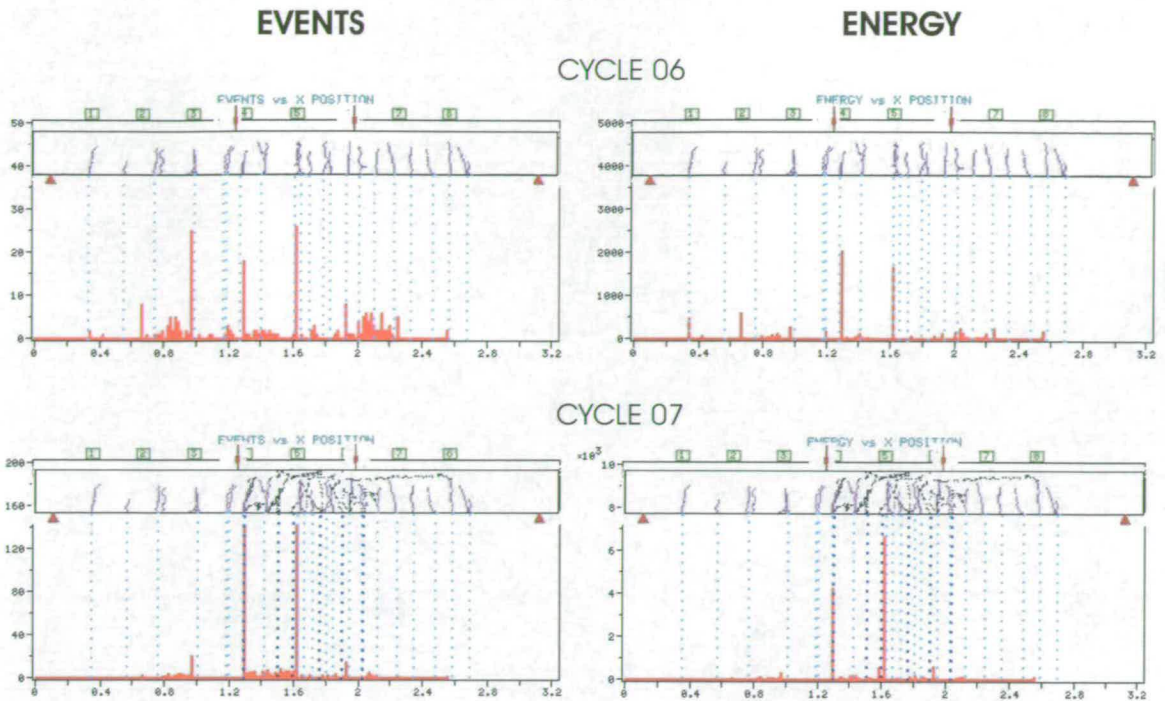


Figure 7.17: AE Source location results relative to the broadband sensors on beam BF6, for cycle numbers 6 and 7, plotted as for Figure 7.9.

engineer to be able to establish not only if the bridge is damaged, but also “how seriously” it is damaged. A quantitative way to assess the structural condition of a bridge is therefore highly desirable.

This issue was approached and a new type of parametric analysis of the AE data was developed, based on the concept of the “relaxation ratio” described in section 4.8.

This section describes this new method of analysis and presents the results obtained to date. In order to have results that would be representative of a significant range of cases (in terms of type of failure, design, load configuration, concrete properties and type of sensor) the PAC data related to all the beams tested in Edinburgh (i.e. beams BF2, BF3, BF2c, BF4, BF5 and BF6) and to all the beams tested in Kumamoto (i.e. beams K1, K2, K3, K4, KL1 and KL2) were considered. For beams BF2c, BF4, BF5 and BF6 the sets of data obtained from both the resonant and the broadband sensors were used, giving a total of sixteen sets of data. The reason for the use of such a large number of samples lies also in the fact that during the analysis some contradictory results were found. On the basis of the results, some preliminary conclusions are drawn and a criterion to assess concrete bridge beams is proposed and discussed. The Japanese

Society for Non-Destructive Inspection (NDIS) has itself proposed a criterion, based on the Kaiser effect, to quantitatively assess concrete beams. This criterion was described in detail in section 3.5 and here it is applied to some of the data to compare it with the alternative method developed and suggested here.

7.3.1 Relaxation Ratio Analysis

The initial idea that led to the development of this analysis derives from some observations made during the undertaking of the experiments. It was in fact noted that the AE activity recorded during the unloading phase of the loading procedure was increasing as the damage on the beam was progressing. In fact, AE activity observed during the unloading process is generally an indication of structural instability [Ohtsu et al., 2002] [Williams, 1980].

Generally in an AE test, the activity generated during the unloading of the sample is neglected. Conversely, the analysis presented here focuses on this particular activity and the relaxation ratio described in section 4.8 was defined specifically for this purpose. As mentioned in that section the decision to characterize the AE activity in terms of energy came from the results discussed in section 7.2.1 that showed how the energy is an effective parameter to identify the damage in a RC beam.

The duration of the different experiments and of the single loading and unloading phases that were analysed was varied and that could affect the results in terms of the comparison of the amount of recorded activity. For this reason the relaxation ratio was computed in terms of average energy.

The analysis consisted in calculating the value of the relaxation ratio for each loading cycle of a sample. The process was repeated for each of the previously mentioned specimens, for a total of sixteen different cases. These are divided in three main Groups.

The PAC original data were converted into ASCII files to be used in MATLAB, which was thus adopted to carry out the necessary calculations, as the average energy for each loading and unloading phase was computed by dividing the total cumulative energy for the total number of recorded hits. The data acquired by all the active channels were used, with the exception of beam BF2, for the reason explained in section 6.1. As a result of the above calculations, the value of the relaxation ratio for each cycle of each experiment was attained.

The final results of all the sixteen cases are shown in Figures 7.18, 7.19 and 7.20. The red horizontal line corresponds to a relaxation ratio equal to one. It therefore divides the area above the line, in which the relaxation phase is dominant, from the zone below the line - where the loading phase is dominant. According to the preliminary observations, a dominance of the relaxation phase would be indicative of increased damage of the beam.

Group 1 and 2

Group 1 includes the beams BF2, BF3, BF4 and BF2c, tested in Edinburgh. Their results are shown in Figure 7.18 and a common behaviour can be noted. Initially, the loading phase is dominant and the values of the relaxation ratio all lie below the horizontal red line. An inversion of trend then occurs when the load reached approximately 45% of the ultimate failure load of the specimen. The relaxation phase then becomes dominant. The data related to the resonant sensors on beam BF2c indicate the change of trend at a lower percentage (36.9%). This can be explained by the fact that the beam was pre-damaged. The resonant sensors might then be recording more activity and/or noise generated by the closing of the pre-existing cracks during the relaxation of the sample.

The general effect can be explained as a dominance of the primary AE activity (see section 4.5) during the early stages of the fracture process when the cracks are forming and thus the damage is still restricted. Conversely, once the damage has seriously progressed, the secondary AE activity due to the friction of the existing cracks starts to prevail - manifesting itself during the relaxation phase of the tests.

Group 2 includes the beams K1, K2, K3, K4, KL1 and KL2 tested in Kumamoto University and their results are illustrated in Figure 7.19. The data are more scattered and this is probably due to the fact that during these tests a higher threshold value was used (see Tables 6.2 and 6.5). The higher threshold generates a higher "signal to noise" ratio, resulting in the dispersion. However, no clear pattern can be identified in any of these six cases. In some graphs (beams K1, K4 and KL2), the relaxation ratio never exceeds the threshold value of one represented by the red line. In the remaining cases, some values go beyond the horizontal red line, but without a constant trend.

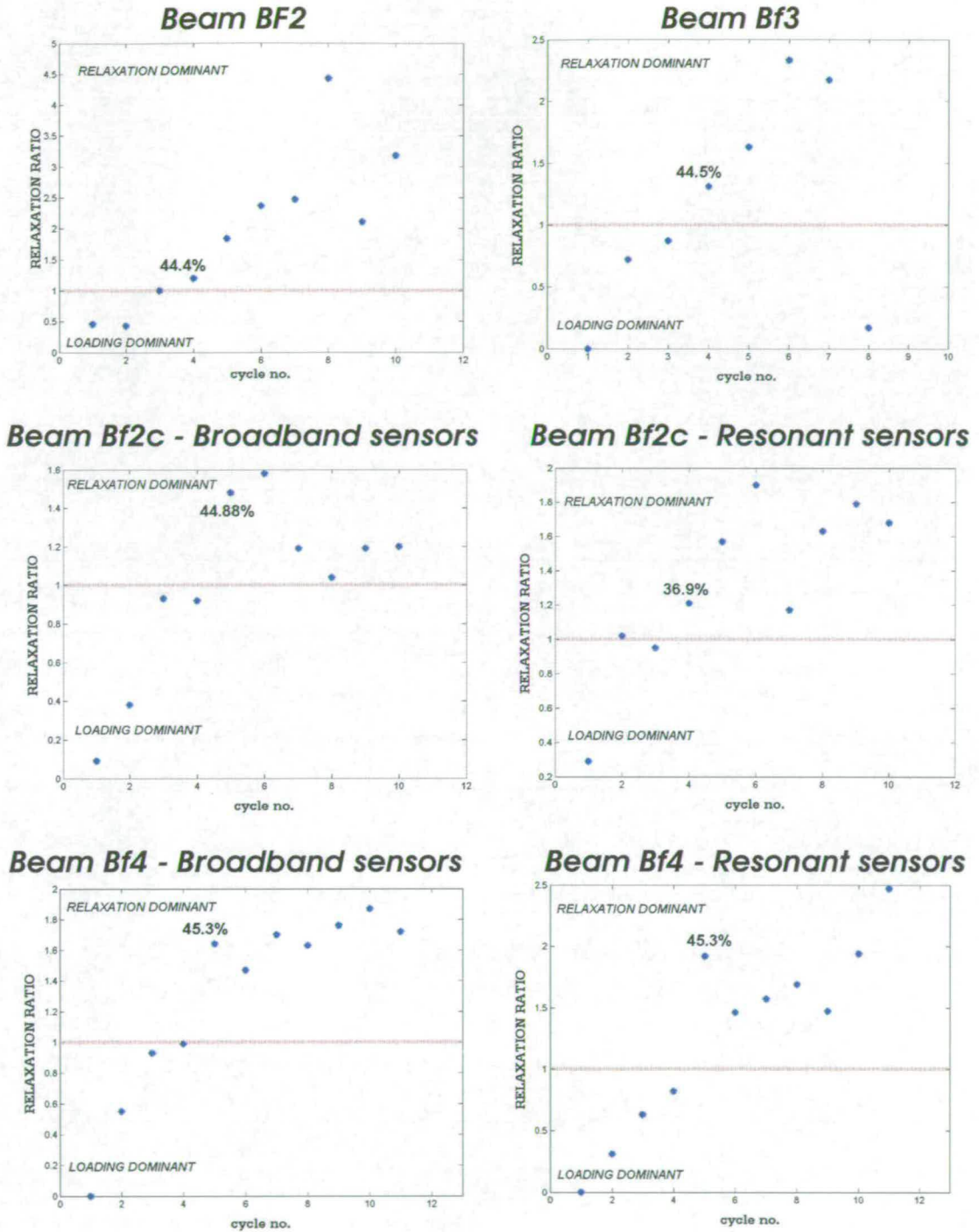


Figure 7.18: Relaxation ratio results of Group 1: beams BF2, BF3, BF4 and BF2c. The red line corresponds to a relaxation ratio equal to one. The dots represent the values of the relaxation ratio (on the vertical axis) for each relative number of cycle, that can be read on the horizontal axis.

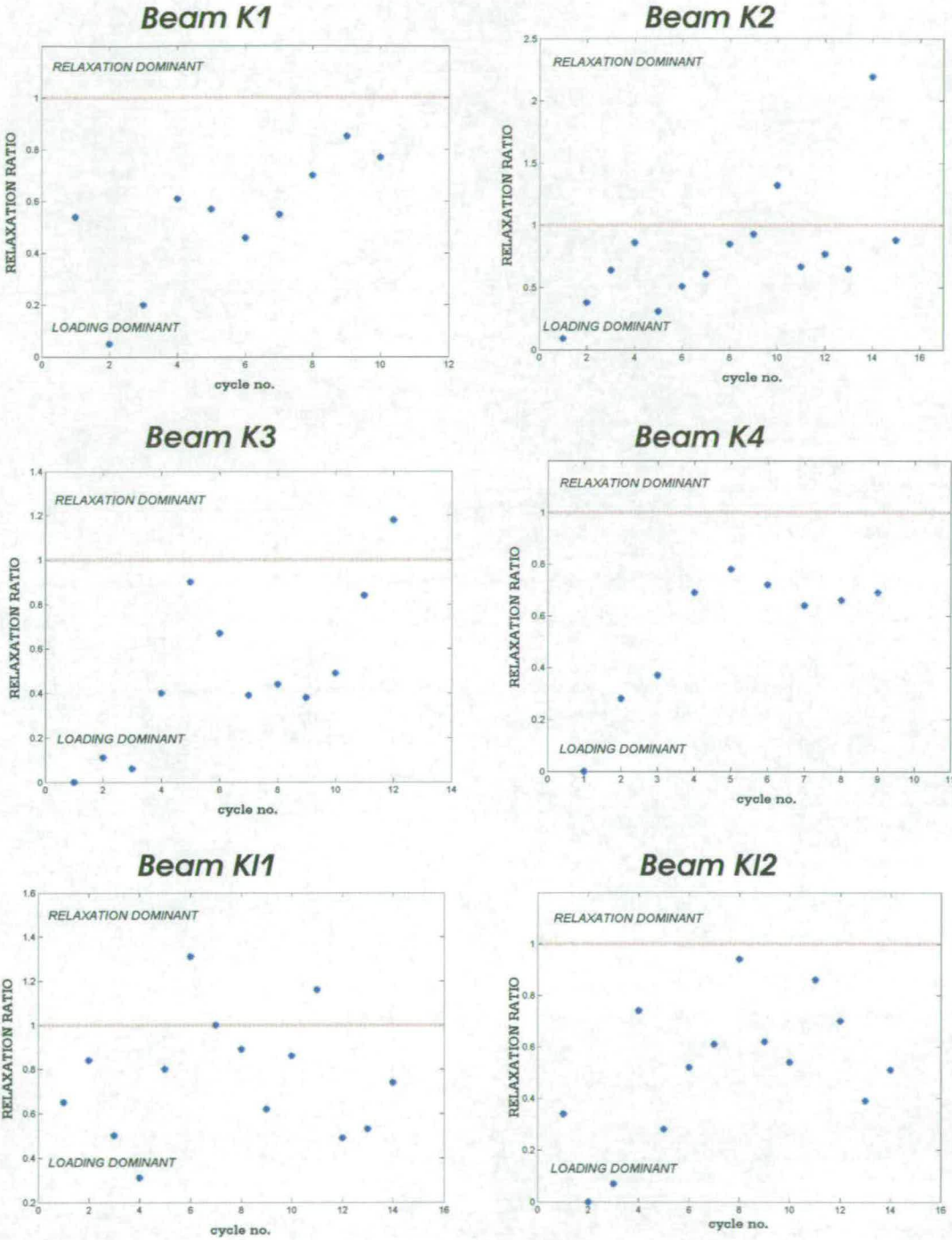


Figure 7.19: Relaxation ratio results of Group 2: beams K1, K2, K3, K4, KL1 and KL2; plotted as for Figure 7.18.

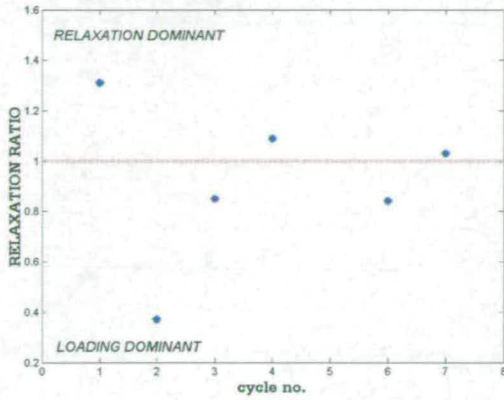
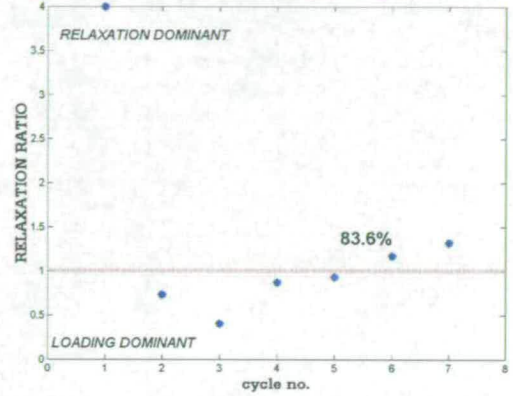
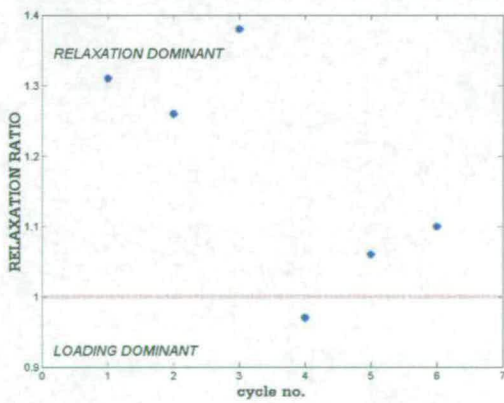
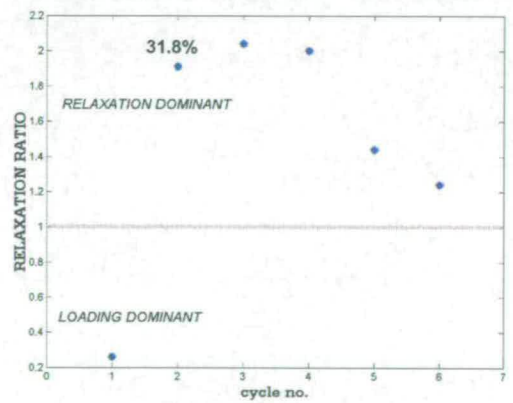
Beam Bf5 - Broadband sensors**Beam Bf5 - Resonant sensors****Beam Bf6 - Broadband sensors****Beam Bf6 - Resonant sensors**

Figure 7.20: Relaxation ratio results of Group 3: beams BF5 and BF6; plotted as for Figure 7.18.

Discrepancy between Group 1 and Group 2

From Tables 6.1 and 6.4, the main significant differences between the tests used in Figures 7.18 and 7.19 consisted of:

- type and model of the AE sensor
- dimensions, design and type of failure of the beams
- characteristics of the concrete

The difference in the type of sensor does not seem to be a likely cause as the results using two types of sensors (the R6I and the WD models) provided a similar pattern in the Edinburgh beams. Both the UT-1000 model used in the Kumamoto experiments and the WD model adopted in the Edinburgh tests were broadband type. The main difference between the two models lay in their operating frequency which is 100-1000 kHz for the WD model and 60-1000 kHz for the UT-1000 [PAC, 1997a]. The wider range of the UT-1000 implies that no vital information could have been lost in Figure 7.18, whilst being instead recorded by the WD type and may thus explain the difference in the results.

A similar conclusion can be drawn regarding the dissimilarities in design and dimensions. The beams tested in Edinburgh have different dimensions and types of reinforcement and this did not affect their results so it appears unlikely that it would do it for the beams tested in Kumamoto.

The last of the above mentioned possibilities is related to the characteristics of the Portland Cement concrete. The concrete used in Japan, due to time restrictions, was Rapid Hardening Portland type. This type of concrete develops strength more rapidly, due to a higher C_3S (tricalcium silicate) content and a higher fineness. In fact as the hydration during the last step in the manufacture of the cement starts at the surface of the cement particle, it is the total surface that gets hydrated. A higher degree of particle fineness for a given mass has a greater surface area, this implies more hydration and thus a rapid development of strength [Neville, 1995]. As the secondary AE activity recorded during the relaxation phase is due to the friction between the surfaces of the existing cracks, then a higher degree of particle fineness is expected to generate more friction (as there are more “contact points” from which the friction derives). This should then accentuate the predominance of the unloading

phase. On the other hand, the concrete used in Japan had a much higher strength and thus it cracked at a higher level of stress. AE derives from the energy released from the material, so it seems reasonable to expect that higher stress should release a higher amount of energy. This could therefore be the reason for the dominance of activity recorded during crack nucleation and formation, i.e. during the loading phase.

It has also finally to be pointed out that the load rates used in Edinburgh and Kumamoto were different. In both cases the load was applied and removed by manually turning a wheel on the loading machine. Due to the manual aspect involved, it was not possible to quantify the exact loading rate. An average value was then calculated by simply dividing the sum of the maximum load applied (and removed) in each cycle for of the duration time of each cycle. The case of beam BF3 was neglected as it was a creep test. An average value of approximately 0.06 – 0.07 kN/sec was found for the experiments carried out in Edinburgh, whilst a value of approximately 0.04 – 0.05 kN/sec was found in the experiments in Kumamoto. This could then have affected the generation of AE activity and therefore the results.

Group 3

To have a further confirmation, the data related to the beams BF5 and BF6 (Group 3) were analysed and the results are shown in Figure 7.20. To verify the influence of the load rate, the load was applied and removed as slowly as possible, within the limits of the test machine. The average value of load rate was in fact calculated as approximately 0.04 kN/sec.

By looking at the graphs referring to the resonant sensors, it is possible to note that a similar trend to the one observed in the previous Edinburgh experiments is present. The percentage of failure load to which the change of dominant phases occurs is however different, being 31.8% for beam BF6 and 83.6% for beam BF5. Looking at Table 6.1, the lower wave velocity measured on these beams seems to suggest a lower quality of the concrete compared to all previous cases. The characteristics of the concrete and the lower load rate might have influenced the results.

The results obtained from the data sets recorded by the broadband sensors did not reveal a clear pattern. The spacing of the sensors was fixed to be exactly the same as the sensors in Kumamoto. As a consequence, they did not cover the whole length of the beam and this might explain the discrepancy with the results from the data of the

resonant sensors.

Discussions

At this stage it appeared that two main causes affected the previous results:

- the loading rate
- the properties of the concrete

Very few references could be found in which the use of the AE activity during the relaxation phase of a test was considered significant and that would help in supporting and/or explaining the findings that have just been discussed. Although the AE activity was found to be dependent by the level of load [Yuyama et al., 2000], no specific reference to “loading rate” were found. Concerning the relationship between the concrete strength and the AE activity, Muravin [Muravin and Lezvinsky, 1995] stated that “. . . specimens with higher strength have higher median AE energy” but as he referred to experiments on hardening concrete the direct translation of this finding to cured concrete is questionable. On the same topic, Bordyugov and Erminson [Bordyugov and Erminson, 1993] did not find any significant relationship between the AE energy and the different strength of the plain concrete samples that were tested.

During the loading phase, when the cracks are in the initial stage of their growth, and thus the damage is starting and it is not yet structurally significant, they release high energy and a large number of events. Conversely, once the damage has progressed macrocracks have formed and opened up, generating fewer events. The primary AE activity is therefore dominant and the relaxation ratio value is less than one. In these circumstances, the friction between the surfaces of the cracks plays a dominant role during the unloading phase, when due to the relaxation the cracks close up. The secondary AE activity is then prevalent and the relaxation ratio value is greater than one.

With reference to the work of Mori and Obata [Mori and Obata, 1988], it could be said that in the loading phase the cracking sources prevail, whilst in the unloading phase the friction sources are dominant (see section 4.5). The explanation of the “silence effect” (see section 4.3) also states that when the damage increased and therefore is localized, there are fewer AE sources and then less activity. This leads to the “silence time”, i.e. to a period of absence of AE activity. The dominance of the unloading phase

corresponding to a relaxation ratio greater than one could thus be seen as corresponding to this stage of the fracture process.

7.3.2 A proposed new procedure for evaluating bridge beams integrity by acoustic emissions

Although at this stage the conclusions with this type of analysis are not definitive, the method appears very promising and suitable to practical application. Although many aspects need further investigation and therefore its application is for now merely hypothetical, the idea behind this way of processing the AE data is that it could be used during (or instead of) a full scale assessment load test on a real bridge.

A load test is generally intended to check the serviceability and working strength of a bridge. The full scale test consists in loading a bridge using fully loaded vehicles of known axle weights and spacings, concrete blocks of known weight, water tanks or hydraulic jacks. The load is generally applied in five equal increments (plus a final load that has to be maintained for 24 hours) until the elastic limit is reached and with a pause of about two hours between a load and the next one. After each increment, deflections, cracks pattern and width, and the strain are measured. The load is then removed in five equal decrements, always measuring the previous mentioned parameters. These tests can be very time consuming and expensive but sometimes are unavoidable [Raina, 1994].

A new procedure is here suggested using the AET and the relaxation ratio analysis. The assessment test would consist of gradually loading and unloading, alternatively, the bridge, whilst monitoring it with an AE system. The value of the load applied should be determined on the basis of the maximum expected load that the bridge has to carry. Values of approximately 45% of this expected load, which demonstrated a significant change of trend of the relaxation ratio in the earlier experiments at Edinburgh, could then be applied during the loading cycles. From the AE data, the relaxation ratio of each cycle should be calculated. A value greater than one would indicate heavy damage, whilst a value less than one would reassure the Engineer about the condition of the bridge and its capacity to hold the expected load. The need to gradually load and unload the bridge is highlighted and the use of hydraulic jacks might be suitable. When a source of water (i.e. a river) is available, a system of tanks in which the water could be pumped in and out could also be used.

The main advantage of this test would be:

- the AE system is relatively easy and quick to install
- the installation of the AE system would not cause any traffic disruption
- no need of additional instrumentation to measure strain or cracks would be necessary
- the analysis itself is reasonably easy and quick and the results very immediate
- no damage would be generated to the structure as the loading would not need to reach or exceed the maximum expected load capacity, thus it is safer than proof load testing

Further work is needed to obtain final conclusions and thus on the feasibility of this type of analysis and eventual test procedure. On site trials would also be indispensable.

7.3.3 Comparison with the NDIS Procedure

This section tests the feasibility of the procedure described above, using the quantitative assessment criterion proposed by the NDIS and described in section 3.5.

The NDIS criterion was successfully validated [Ohtsu et al., 2002] by experiments on RC beams, where the limits of the classification (i.e. the dashed line in figure 3.1 that defined the boundary of the area of damage) were fixed on the basis of the crack mouth opening displacement (CMOD). The data from the most active channel were used for the calculation.

Two significant cases were considered, beam BF4 for which the new procedure appeared to work (as for all the first set of the BF tests) and beam K2 for the K tests which in general were not successful (probably because of the different loading rate and concrete properties). The NDIS assessment procedure was carried out for both cases, using the data of the most active channel as well as the data relative to all the recording channels. The limits were determined graphically as the values of the CMOD were not available. The most active channel was number 5, for both beams.

The results are shown in Figures 7.21, 7.22 for test BF4, and 7.23 and 7.24 for test K2. The load ratio and the calm ratio are indicated on the horizontal and vertical axes respectively. The number inside the circle represents the corresponding loading cycle number. The areas of different damage are also indicated.

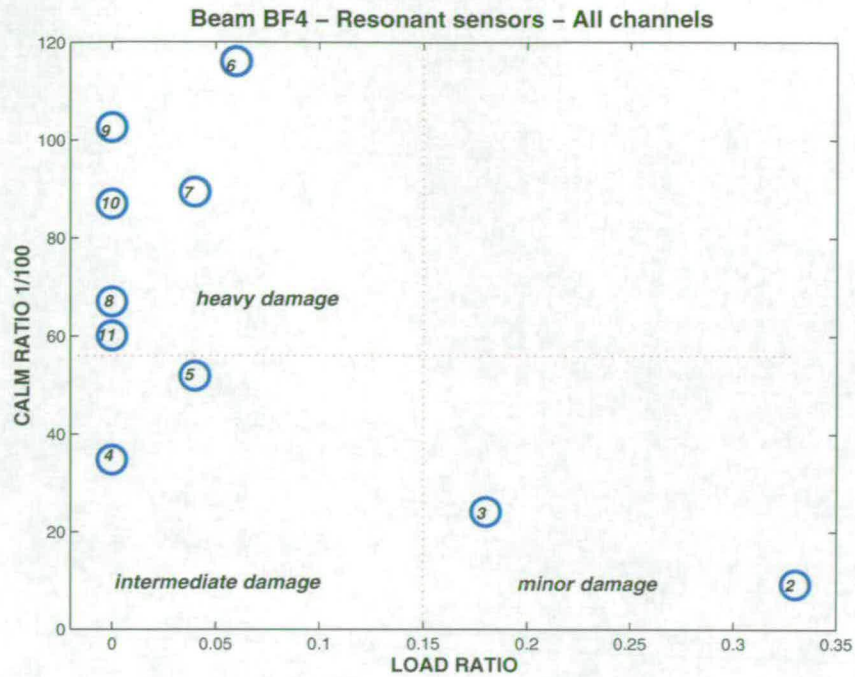


Figure 7.21: NDSI assessment for beam BF4, using all data. The numbers indicate the loading cycle and the red lines define the different areas of damage.

Although there is no significant difference (i.e. the area of damage in which the cycles fall, does not change) between the results obtained from data related to all channels and data related only to channel 5, the numerical values are different and the limits of the graph are subjected to changes. Moreover in beam K2, the value corresponding to the last cycle fell in the area of the graph related to intermediate damage.

For beam BF4, the change of trend during the relaxation analysis occurred during cycle number 5. It can be noted on the NDSI assessment table that that cycle corresponds to the last one falling into the intermediate damage area - after which serious damage takes place. The two results appear then to support each other.

7.3.4 Relaxation Ratio Conclusions

At this stage, preliminary conclusions can be drawn.

- The method of analysis seems to be very promising and able to define the state of damage of concrete beams. A structurally serious damage condition should in fact result in the relaxation phase being dominant and thus a relaxation ratio

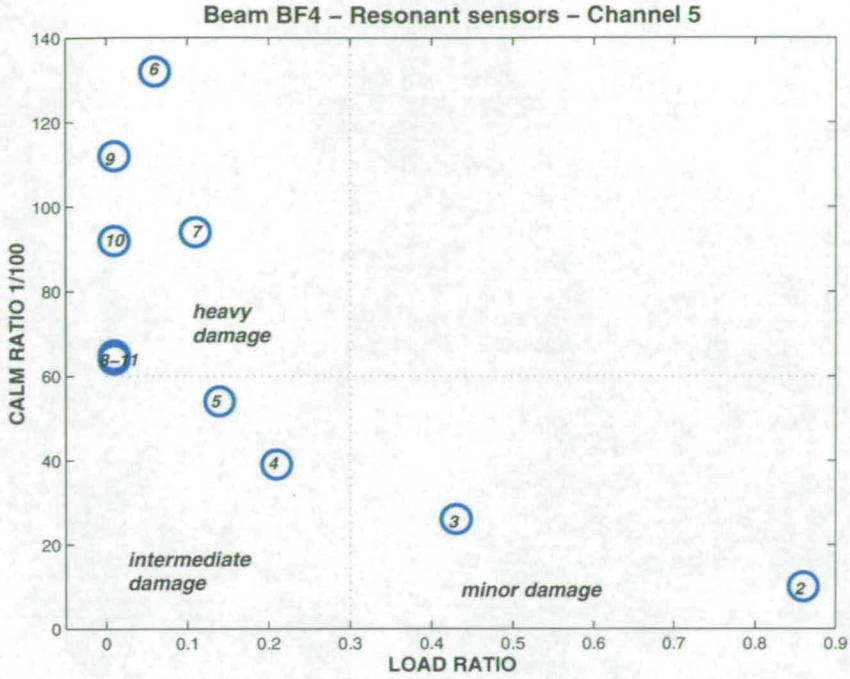


Figure 7.22: NDSI assessment for beam BF4, using only channel 5 data. The numbers indicate the loading cycle and the red lines define the different areas of damage.

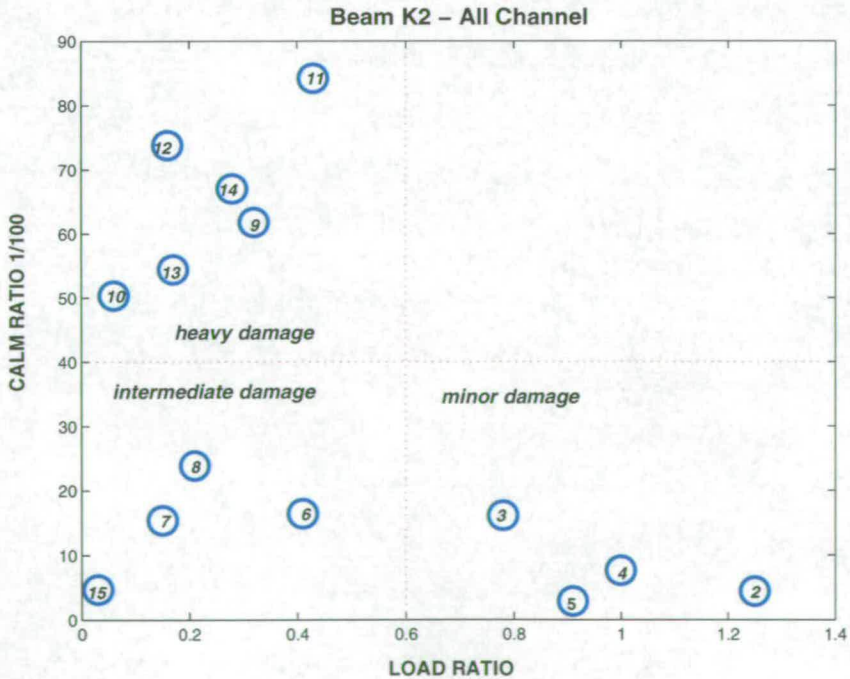


Figure 7.23: NDSI assessment for beam K2, using all data. The numbers indicate the loading cycle and the red lines define the different areas of damage.

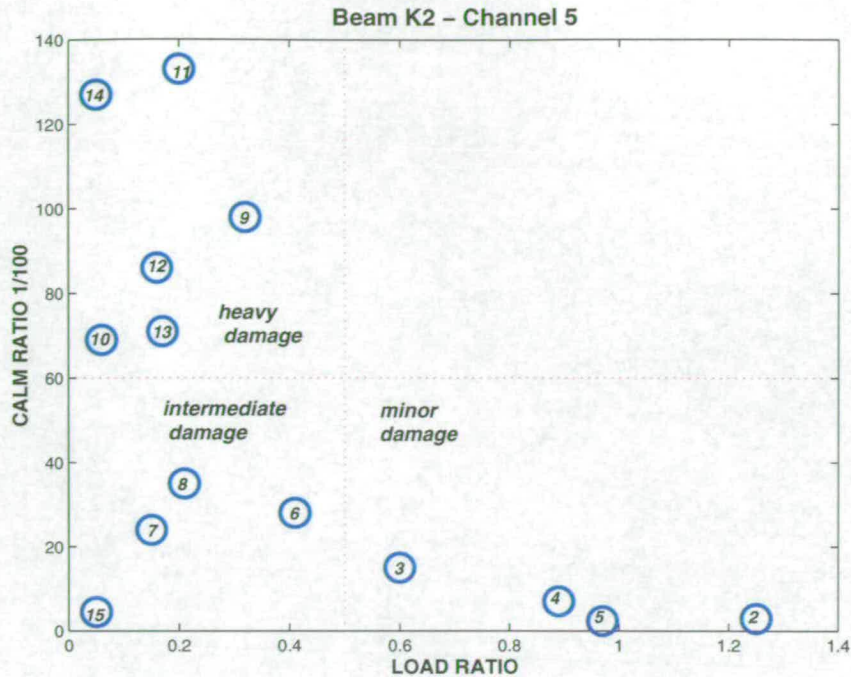


Figure 7.24: NDSI assessment for beam K2, using only channel 5 data. The numbers indicate the loading cycle and the red lines define the different areas of damage.

greater than one.

- However 10 of the 16 studied cases (i.e. 62.5%) showed a disagreement which is thought to be due to a combination of different properties of the concrete and loading rate adopted during the experiments.
- The successful results obtained at this stage were supported by the NDIS assessment procedure.
- A full load test procedure for a real bridge is suggested, on the basis of further analysis to further define the limits of the method.

Further experiments are needed to evaluate in which specific conditions the analysis is successful, to establish the limits of its application and the confirm the feasibility of this type of analysis. These experiments should consider a large variety of samples tested in different ways with one parameter changing at time. On site trials would also be indispensable.

7.4 SoundPrint (SP) Study

This section deals with the investigation of the data recorded with the SP system described in section 5.3.

The use of two independent AE systems (PAC and SP) allows a dual perspective on the feasibility of AE monitoring for assessing the integrity of bridges. Data obtained using the SP method from the small scale tests undertaken at Edinburgh University, and from the full scale tests carried out at TRL (and described in sections 6.1 and 6.2), are presented and interpreted in this section. From the Edinburgh data, only beams BF4, BF5, BF6 and BF2c are considered, as the SP system was not available during the experiments on the remaining beams. This set of samples provides information about both bending and shear failure cases, simply reinforced and doubly reinforced stirrups cage designed cases and the implications related to an application on a heavily pre-damaged beam (see Table 6.1). The SP data obtained by the full scale TRL tests were processed by the TRL personnel [Hill et al., 2002], and then made available for further discussions and comparison with the PAC data recorded during the same experiments.

As mentioned in section 5.3 the SP system was not originally designed for detecting cracking in concrete. The experiments have then to be considered as trials to evaluate the possibility and the performance of the current SP system towards this new task. No fundamental changes to the SP operation system were considered necessary at this stage, but some settings of the equipment were modified within their existing range, as specified in section 5.3.

7.4.1 The SoundPrint Analyst Processing Software

The data acquired by the SP system were not sent to the Pure Technologies headquarters in Calgary according to the standard SP procedure, but instead were stored and processed locally. However the SP Analyst software developed by Pure Technologies Ltd. was used to analyse the data recorded with the SP system.

The software allows one:

- to locate the events (manually or automatically), providing information about their accuracy
- to visualize the waveforms of the signal

- to visualize the frequency spectrum of the signals
- to show the energy of the event
- to create specific filters to discharge or keep only particular types of events
- to generate an automatic report about the results

Two points have to be highlighted. Firstly, the software deals with the events on a “single” base, i.e. it visualizes one event at a time. For this reason, Excel and/or Autocad have to be used subsequently to illustrate the totality of the results. Secondly, the software allows one to create a “Decision Tree” including several filters in order to classify different types of signals that have various characteristics. The filters can be manually defined, by specifying parameters such as: energy content, frequency range, time and so on.

A specific decision tree was used for the analysis of the data recorded during the small scale experiments. The tree was developed by Pure Technologies Ltd. on the basis of previous trials carried out by TRL and it needed to be validated on further data. The tree is illustrated in Figure 7.25. Its first step (corresponding to number 1 on the figure) divides all the signals into two groups according to their energy content. Events for which the signals of at least three channels have an energy content (calculated over a window of 0.15 sec) above 0 dB pass to step number 2. Step 2 consists in an automatic location of the signal and then a classification of such events as Schmidt Hammer Impact (number 2A on the figure) due to the calibration. The events whose energy does not meet the above described requirements are directed towards step number 3, which imposes a new energy condition. The events for which at least one sensor records an energy above -10 dB (that is the cut off value commonly used during instrument calibration) are automatically located (step 4) and therefore classified as a crack (step 4A). The events that did not reach the fixed energy threshold were instead classified as a small crack (step 5) and a manual location can be attempted on them.

7.4.2 Small scale tests - Analysis and Results

The SP system was used on four of the beams tested in Edinburgh, BF4, BF5, BF5 and BF2c. They include the cases of shear and bending failure as well as a test of the pre-damaged beam (see Table 6.1).

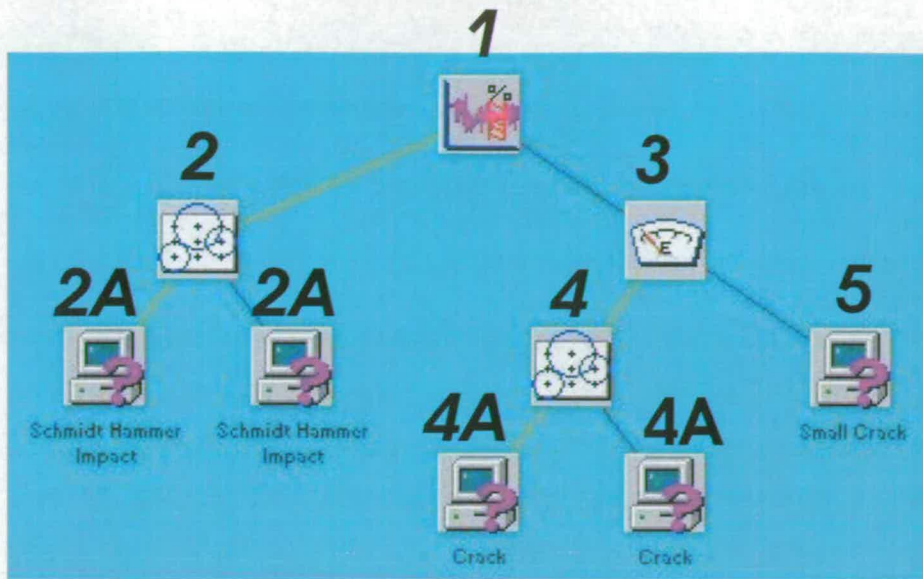


Figure 7.25: SoundPrint Decision Tree.

The analysis was carried out initially using the SoundPrint Analyst software and then Autocad, MATLAB and Excel to visualize the results. Firstly, a location of the AE events was attempted, using the Decision Tree discussed above. The tree classified approximately all the recorded events as small cracks, and therefore they had to be located manually. The results are shown in Figures 7.26 and 7.27.

These figures show the cracks as they appeared on one side of the beam (as the crack pattern was generally symmetrical) at the end of the test; the numbers indicate the exact cycle in which they appeared. The circles represent the located SP events; the different colours indicate the varied loading cycles as specified in the legend. The radius of the circles is proportioned to the number of events recorded in the same location. As the location algorithm was linear, all the events are on the same line, whilst on the figure they are represented in different levels to avoid overlapping that would have hidden some of the events.

On beam BF4 (top of Figure 7.26) two active areas can be identified, corresponding to the region where the bending moment was maximum; very few events were however located in the middle of the beam. The two active areas correspond to the peaks in Figure 7.28, which shows the PAC results.

On beam BF5 (bottom of Figure 7.26) it is not possible to identify a clear pattern. A larger concentration emerged towards the right end of the beam, where the sample



Figure 7.26: Location of events recorded by the SoundPrint system on beams BF4 and BF5. The different colors indicate different loading cycles, whilst the diameter is proportional to the number of events.

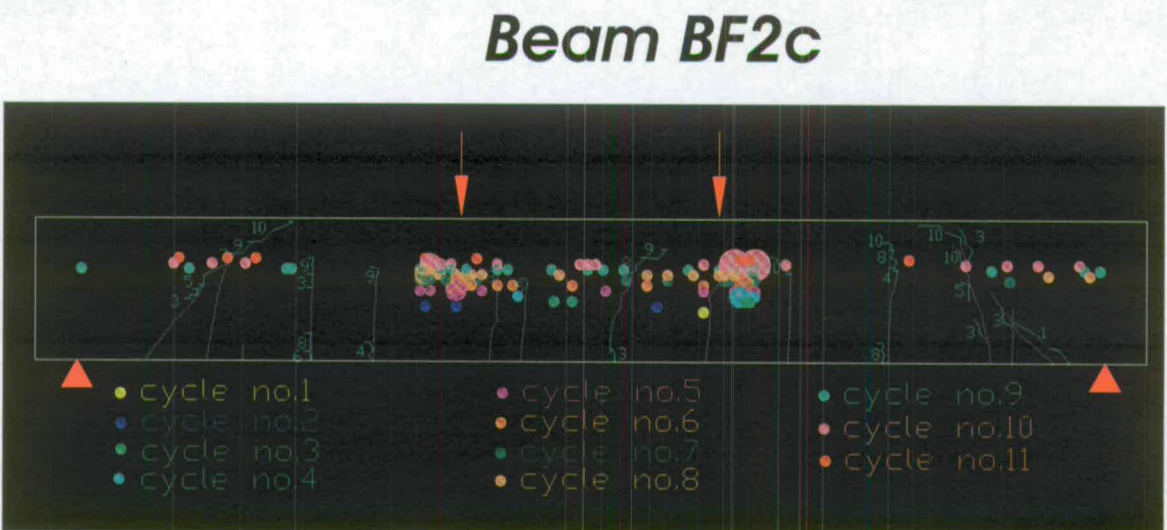
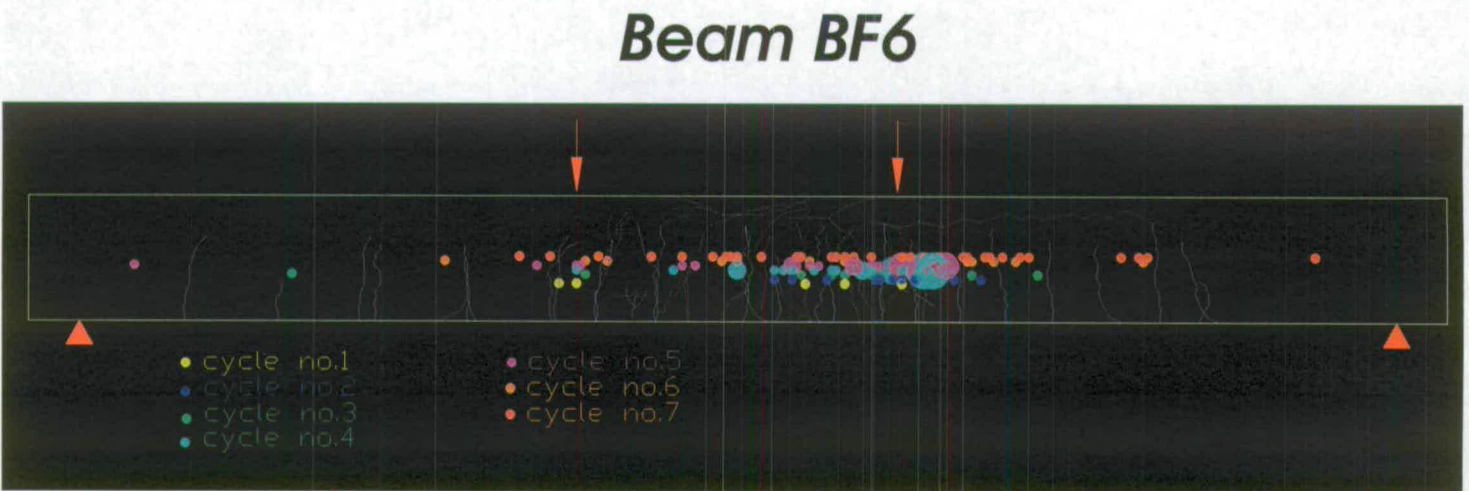


Figure 7.27: Location of events recorded by the SoundPrint system on beams BF6 and BF2c. The different colors indicate different loading cycles, whilst the diameter is proportional to the number of events.

failed in shear. A uniform distribution also emerged from the PAC results (Figure 7.28).

On beam BF6 (top of Figure 7.27) the activity resulting was concentrated in the middle region of the beam, where the majority of the cracks were visible and the beam finally failed in bending. In this case the cracks mapped on both sides of the beam are shown whilst the number of their relative cycle is omitted to make the drawing easier to read. A similar situation is found from the PAC results (Figure 7.29).

Finally, on the pre-damaged beam BF2c, three active areas were evident: two at the ends of the beam, where heavy shear damage was present and one in the middle of the beam. By comparison only two areas can be seen in the PAC results (Figure 7.29).

In all cases, acoustically active regions were identified, although on beam BF5 the pattern was not as evident as on the other beams. These regions corresponded to the areas of high structural stress and generally are similar to the areas identified by the PAC location. On the pre-damaged beam, the most active area appeared to be the middle of the specimen. The beam was heavily pre-damaged in shear and it is therefore possible that most of the activity derived from cracks growing in the middle of the beam, although the beam finally failed in shear.

The locations shown in Figures 7.26 and 7.27 include the events recorded during all the cycles and a pattern can be recognized for beams BF4, BF6 and BF2c. It was noted that for these beams, the pattern of AE activity emerged on cycles number 6, 3 and 6 respectively (Figures 7.30). These cycles corresponded to 53.6%, 49.4% and 53.4% of the ultimate load to which each beam failed. The SP activity was then able to give an early indication of where ultimately those beams were going to fail.

As mentioned earlier, the events had to be located using the manual option of the software. Not all the events could however be located. Figure 7.31 shows the relationship between the total number of recorded events and the events that were finally located for the four beams. Although there is not a clear pattern on the absolute percentage values of events that were located during the cycles, it can be noted that this percentage always decreased in the last two or three cycles. This was probably due to the fact that the large number of cracks present at this stage on the beam were an obstacle for the travelling of the elastic waves and this resulted in difficulties in locating

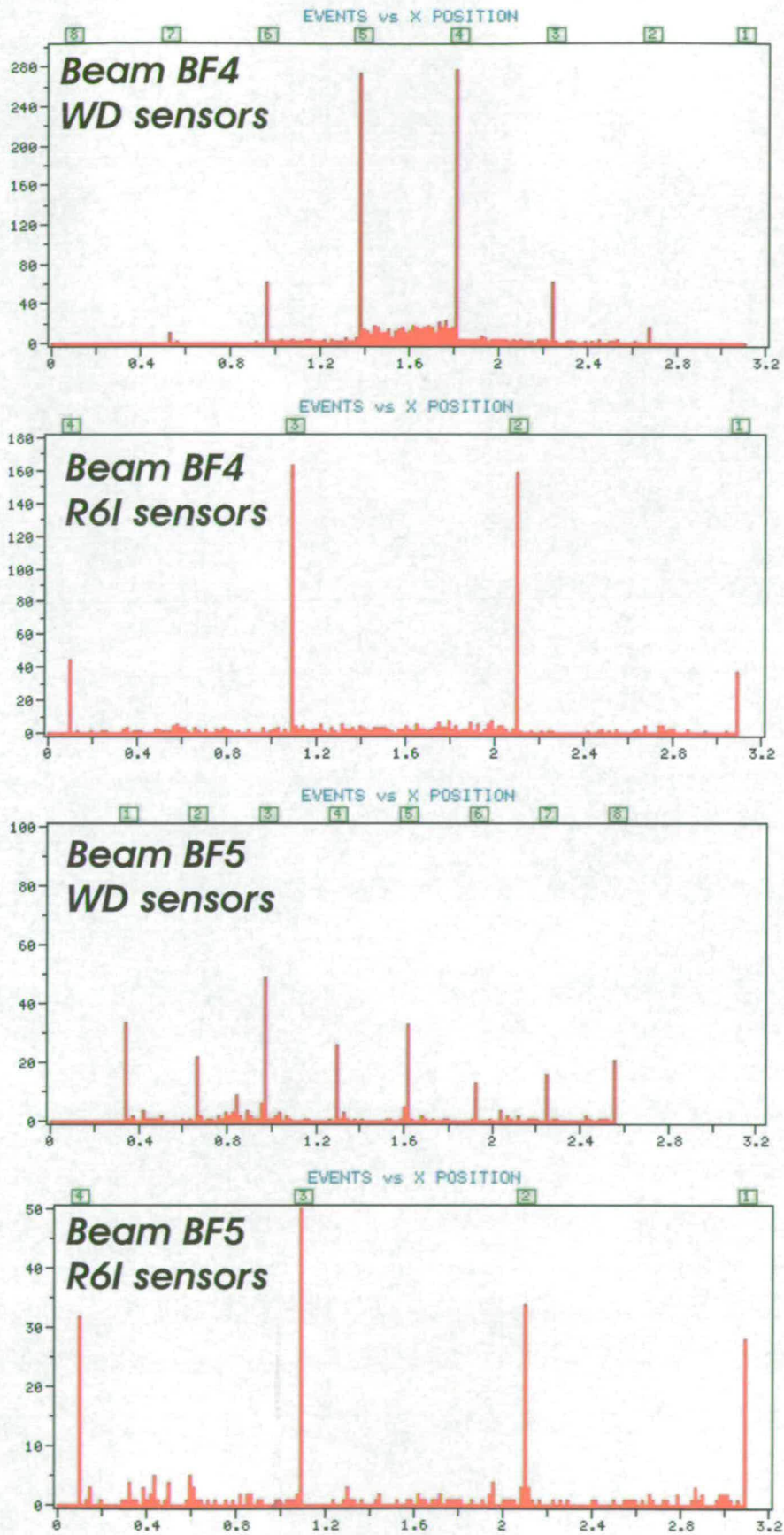


Figure 7.28: PAC AE location for the full test of beams BF4 and BF5.

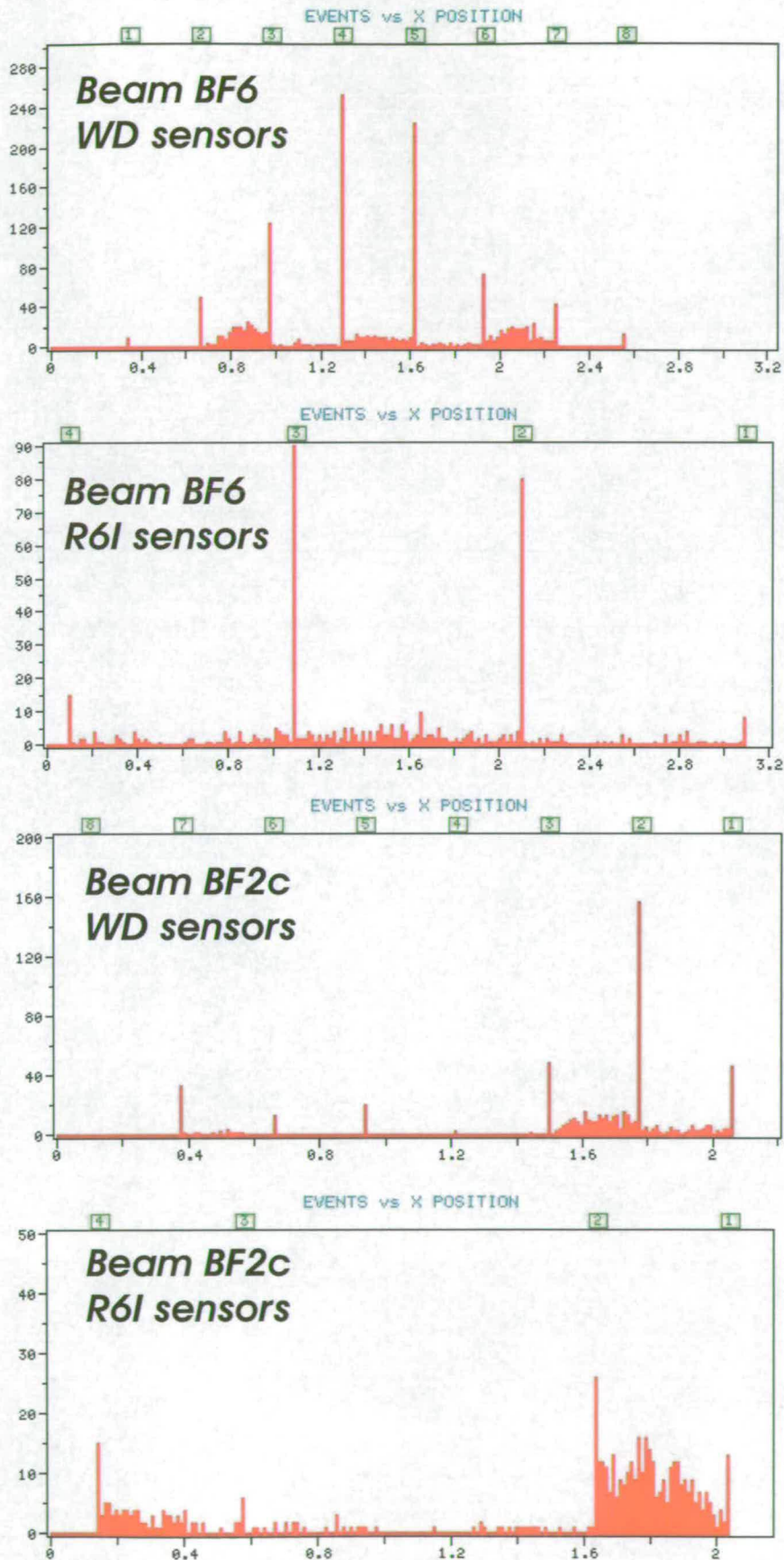


Figure 7.29: PAC AE location for the full test of beams BF6 and BF2c.

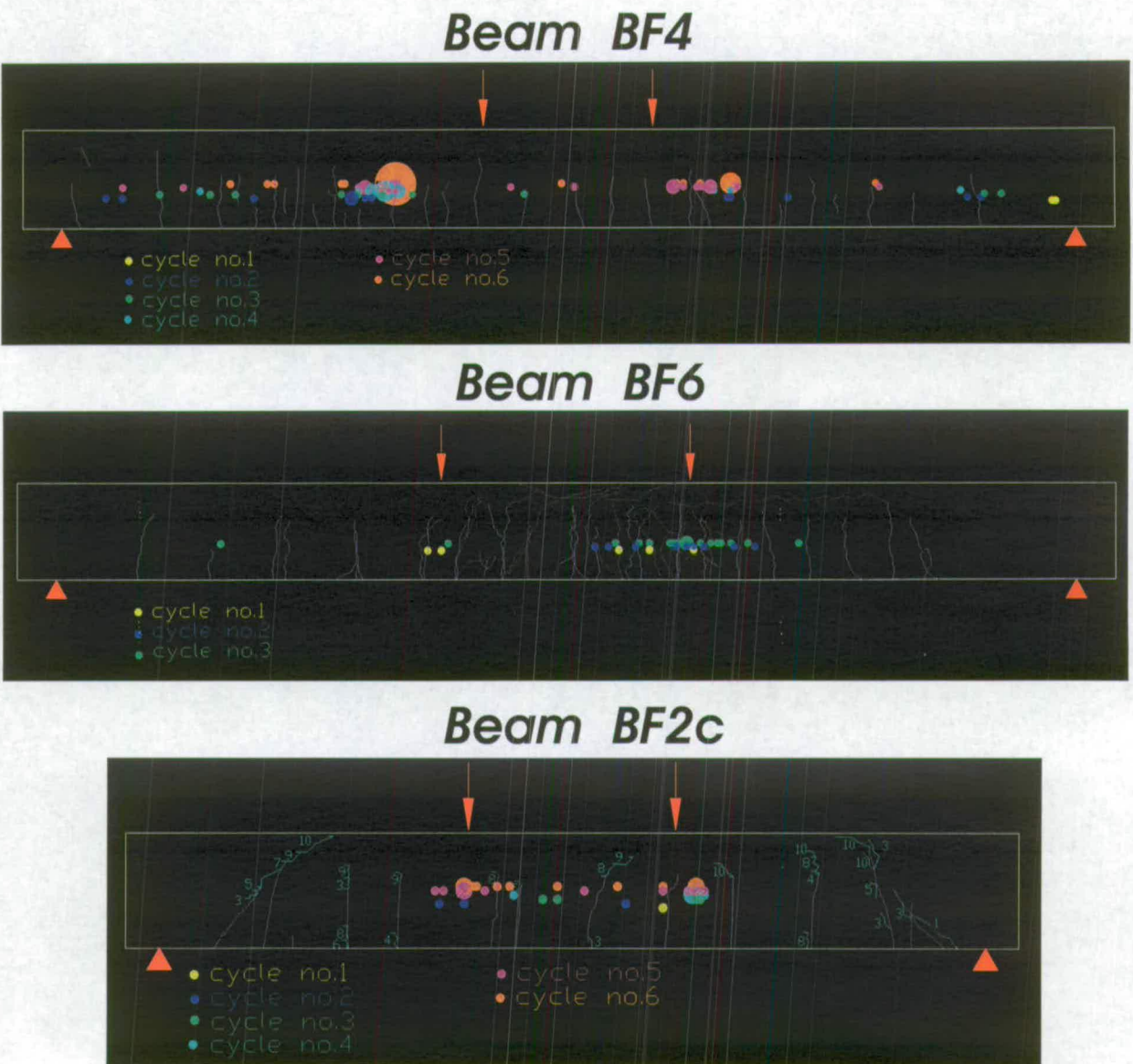


Figure 7.30: AE location pattern emerging for beams BF4, BF6 and BF2c. The different colors indicate different loading cycles, whilst the diameter is proportional to the number of events.

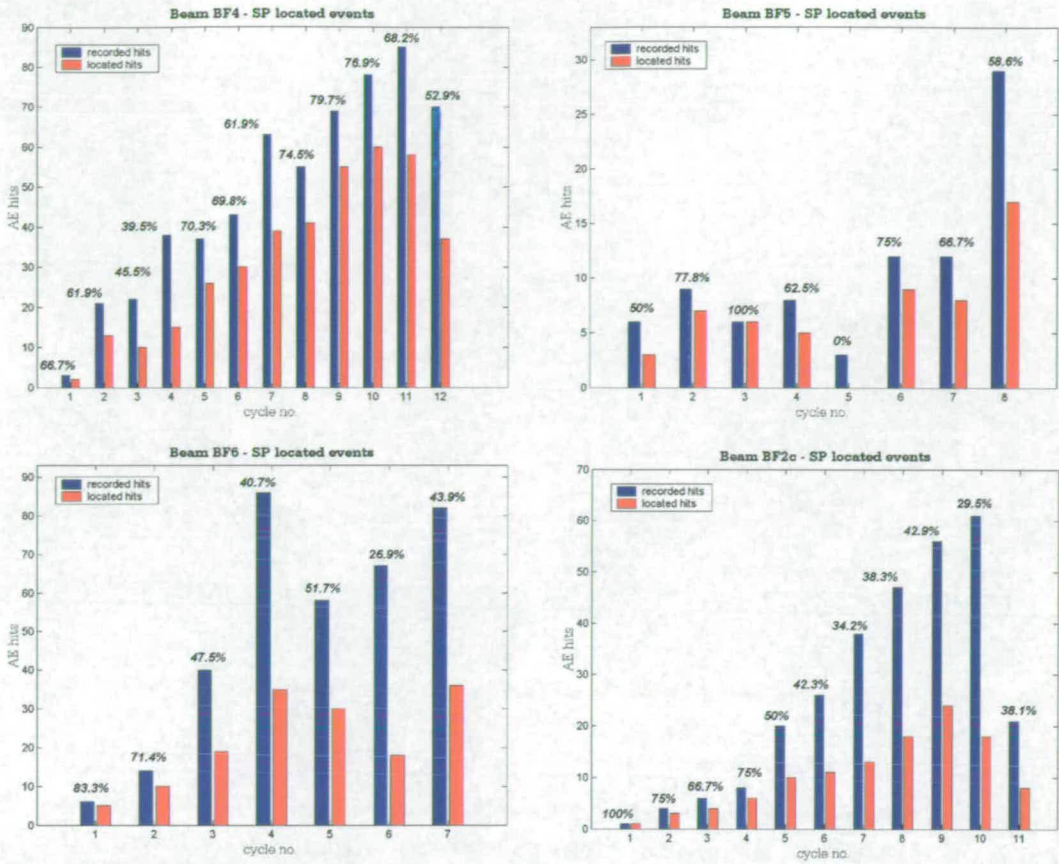


Figure 7.31: Histogram representation of the recorded and located SP hits for beams BF4, BF5, BF6 and BF2c.

the sources of such waves. A similar problem occurred during the location of the PAC data (see section 7.2.1) when it was noted that the accuracy of the location was affected by the amount of cracks. From Figure 7.32, the broadband sensors appeared to record a greater number of events.

7.4.3 Beam CF1 - Analysis and Results

The results of the automatic location of the events recorded by the SP system and performed by the Analyst software were illustrated using Excel in Figures 7.33 and 7.34.

In both cases it can be noted that some events were located outside of the beam. This was due to problems of accuracy. The events generated by cracking have a lower amplitude and energy than the ones deriving from the wire breaks for which the system

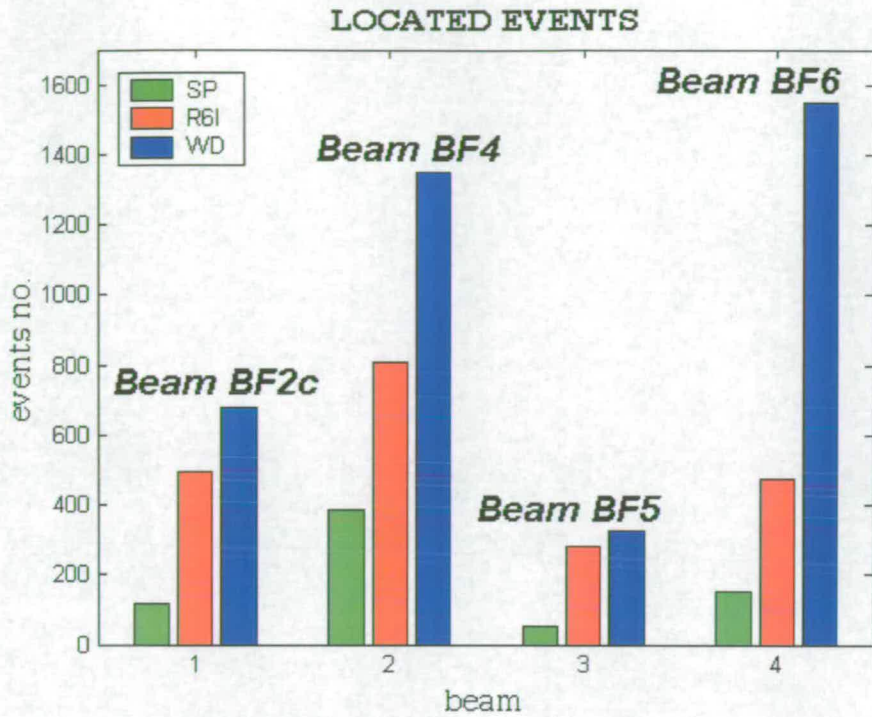


Figure 7.32: Histogram representation of located hits recorded by SoundPrint (SP), resonant (R6I) and broadband (WD) sensors.

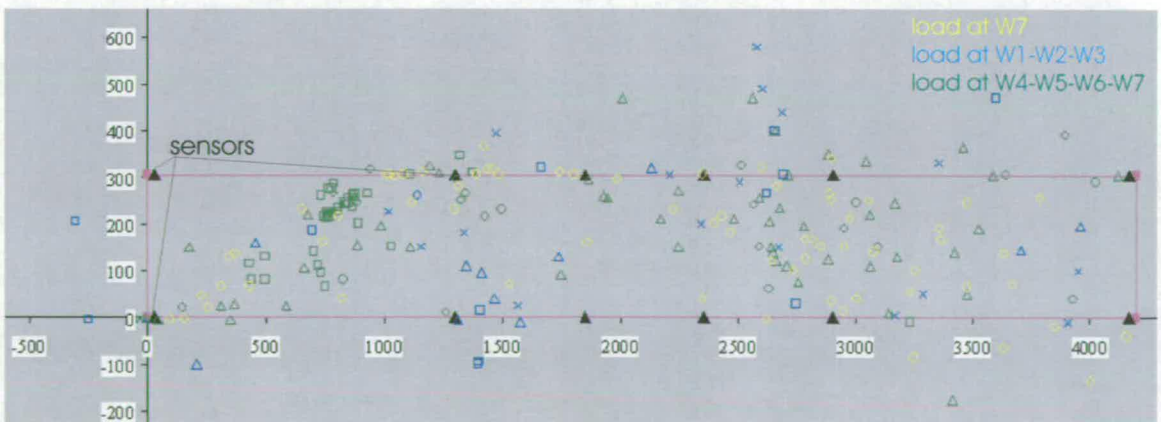


Figure 7.33: Location of SP events during initial loading stage for beam CF1. The different colors indicate different loading stages.

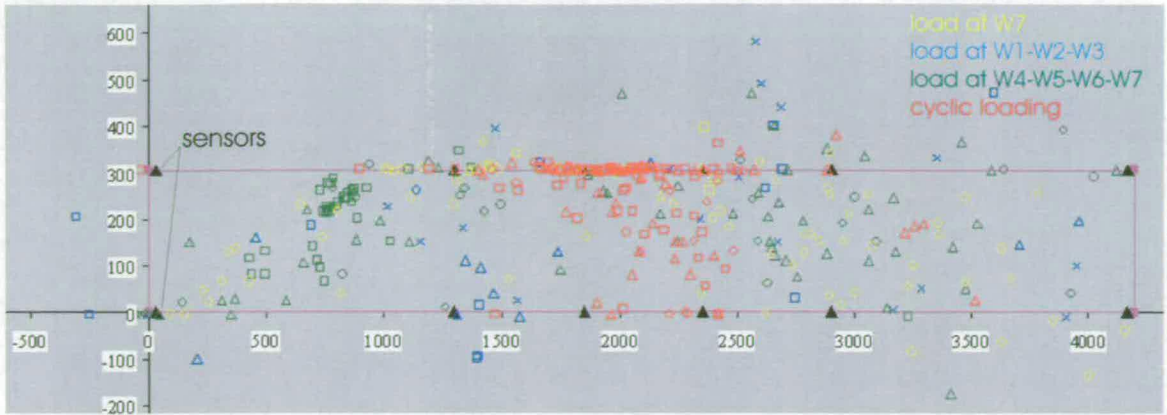


Figure 7.34: Location of SP events during the whole experiment for beam CF1. The different colors indicate different loading stages.

and the software were originally designed. This might explain the difficulty in the location process. A poorer location precision is more evident in the vertical than in the longitudinal direction, probably due to a closer spacing of the sensors.

Figure 7.33 shows the events recorded during the first stage of the loading, when the load was moved alongside the beam from position W1 to W7. At this stage it is not possible to identify a clear pattern of the acoustic emission sources.

Figure 7.34 comprises the recorded and located events during the whole experiment, with the red dots indicating the new events, i.e. the events acquired during the cycling load at mid-span and thus in the range between 90% and 100% of the ultimate load. In this case a cluster of events in the middle of the beam can be observed. The load applied at mid-span generated a high bending moment in this region and this explains the area of concentrated AE activity.

The two situations are illustrated on the same graph using a histogram representation, Figure 7.35, and a clearer pattern emerged. The graph indicates the number of located events on the vertical axis and their longitudinal position on the beam on the horizontal axis. If the red part of the histogram, related to the mid-span loading, was ignored, then most of the events during the first loading phase resulted in events generation at the two ends of the beam, the converse of what would be expected. In fact, during this loading phase, the cracks started to appear in the middle of the beam and then spread towards its ends; events would normally be expected from the middle of the beam.

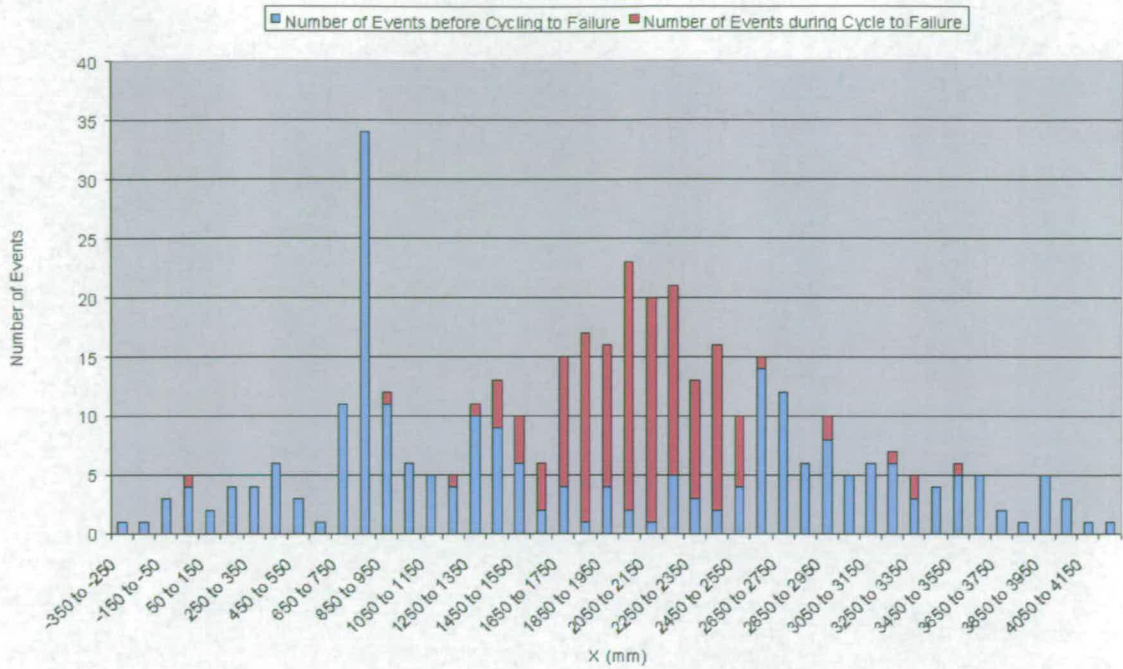


Figure 7.35: Distribution of SP events for beam CF1.

A similar situation is highlighted by the histogram representation of Figure 7.36, where the cumulative energy of all channels is computed (using equation 4.15) instead of the events. A lack of symmetry is also noted from this graph, as most of the energy seems to be recorded in the left half of the beam. Although the lack of symmetry might be a consequence of the complexity of the loading procedure, no plausible explanation could be found for the unexpected scarcity of events recorded at mid-span during the early stage of the loading.

A comparison with the PAC data was therefore carried out to validate the results and to establish if this unexpected behaviour was due to a real effect or it was a consequence of the system.

During the test on beam CF1, AE data were also independently recorded with the PAC MISTRAS System using the Mi-tra software, as described in section 6.2 and therefore analysed to compare and/or support the findings obtained with the SP system.

Before proceeding with the analysis of the PAC data, some observations need to be considered. During the recording phase, all the channels were synchronised. Therefore it does not make sense to analyse the data in terms of AE hits for each channel, as each

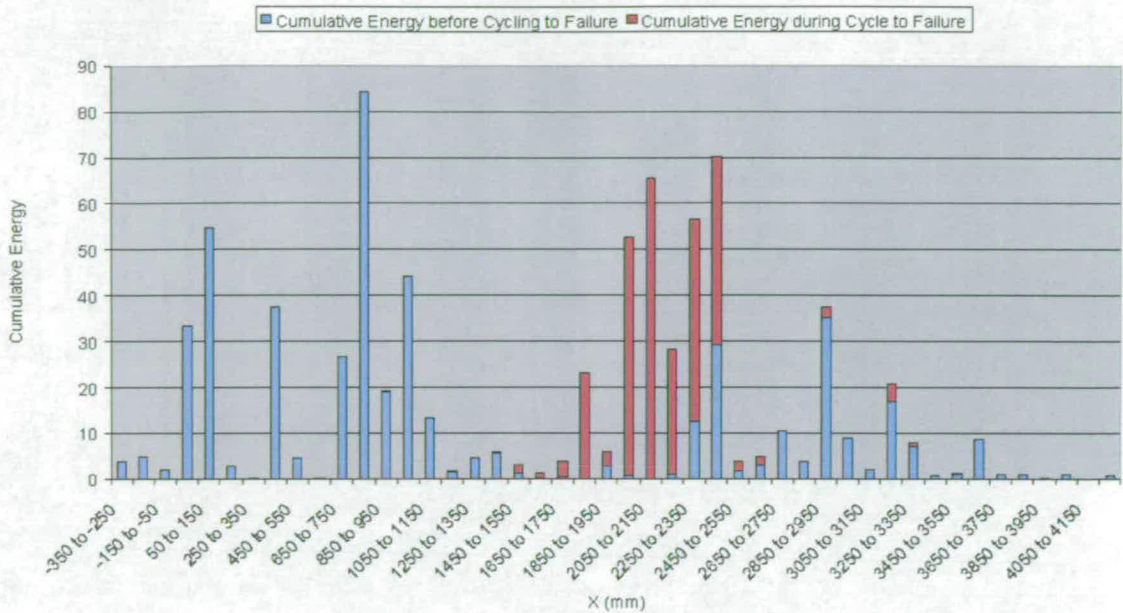


Figure 7.36: Cumulative energy distribution for SP events for beam CF1.

of them had recorded exactly the same number. The data had thus to be processed in terms of AE energy. For the same reason, the PAC software was not able to perform a location of the AE events. The only information about the location that we can obtain is in relation to the sensor position. An histogram representation of the cumulative PAC energy is shown in Figure 7.37, for both sides of the beam. The same lack of symmetry noted in Figure 7.36 can be seen in the PAC results, supporting the SP findings and thus implying that the SP results were not affected by the system. On side 1, the PAC results confirmed that the most of the energy during the first loading phase came from the end of the beam, conversely to what would be expected, but in agreement with the SP results. This comparison could not be done for side 2, as both sensors were in the middle of the beam.

7.4.4 Beam HB2 - Analysis and Results

As in the previous full scale test, the results of the automatic location performed by the Analyst software were processed using Excel.

Figure 7.38 illustrates the distribution of all events captured by the SP system during all load cycles. The thick black line indicates the final failure shear crack, the

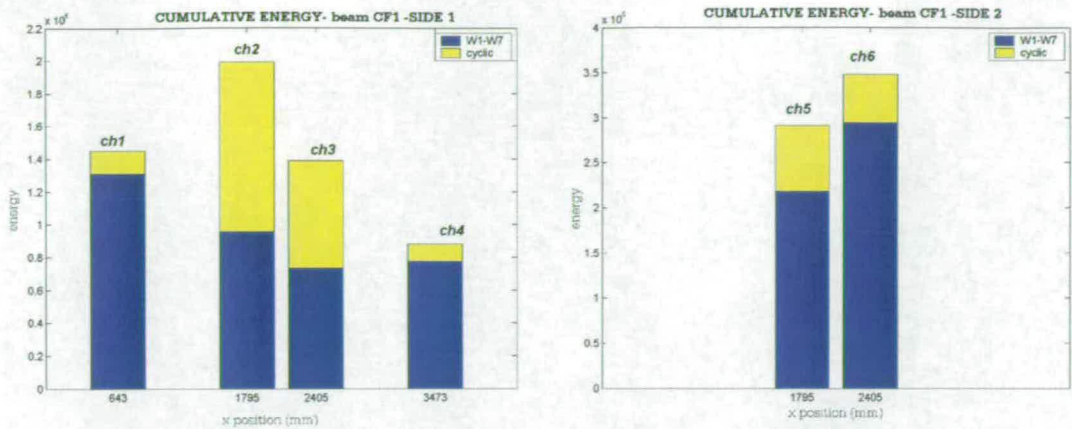


Figure 7.37: PAC cumulative energy distribution for beam CF1.

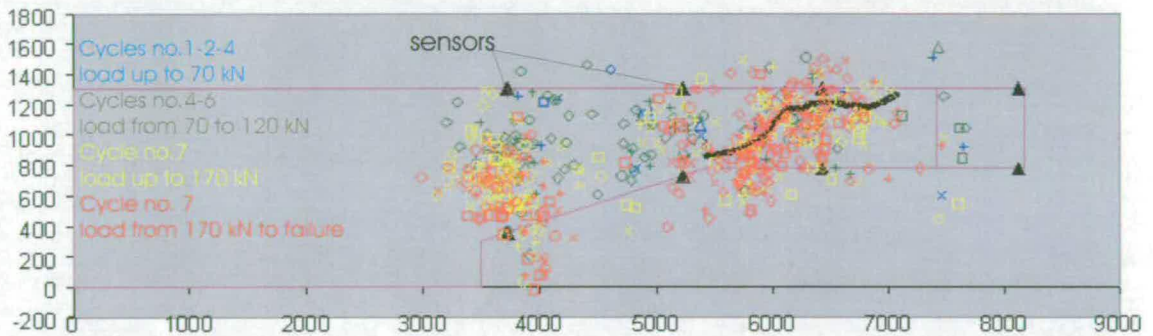


Figure 7.38: Location of SP events during the whole experiment for beam HB2. The different colors indicate different loading stages.

vertical and horizontal axis have different scales to ease the viewing of the located events; this results in a distortion of the proportion of the beam. The events are distinguished on the basis of the loading cycle in which they appeared and of the load range as well.

From Figure 7.38, two clusters of acoustic emission activity can be identified. The main cluster localized along the cantilever section where the shear failure eventually occurred. A second zone also appeared at the widest part of the haunch where due to the large distance from the load, the moment increased substantially, although no severe cracking was noted in this area. Both the active areas are therefore compatible with the structural behaviour of the beam. It might be noted that the location appears more precise along the horizontal than the vertical axis. This might be due to the close

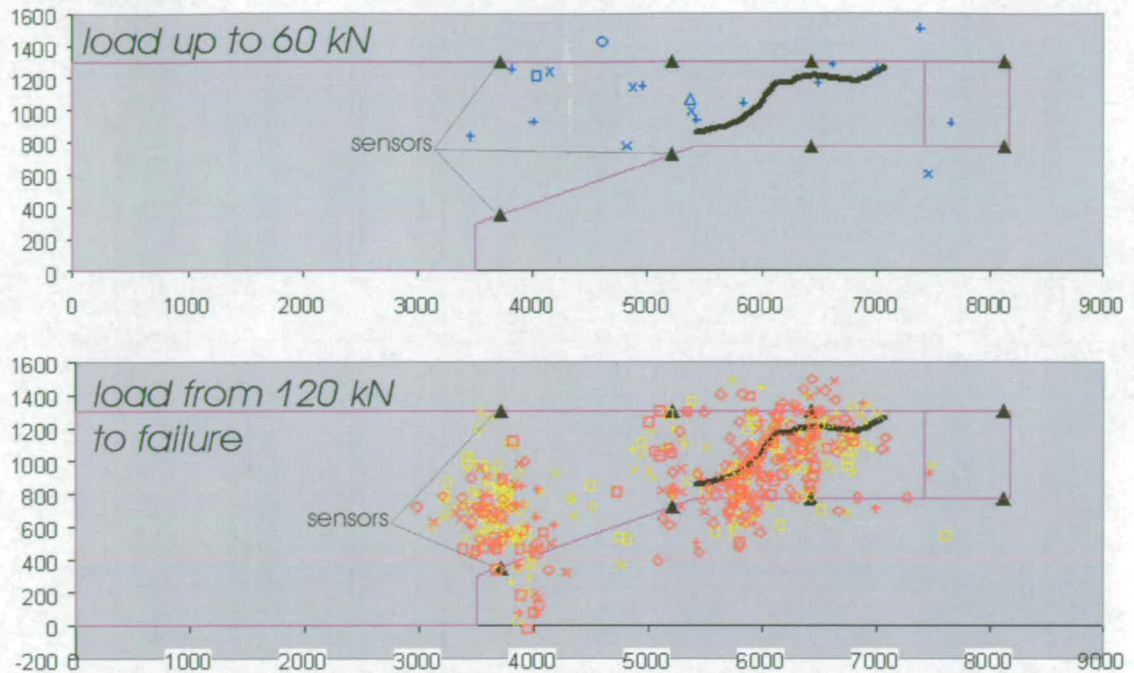


Figure 7.39: Location of SP events during different load ranges for beam HB2.

vertical spacing of the sensors.

Figure 7.39 shows the located events recorded during different ranges of load: from 0 to 60 kN (top) and from 120 kN to failure (bottom). During the first load interval, up to approximately 30% of the failure load (i.e. 202 kN), few events were identified. A pattern started to emerge, becoming clearer in the final stage when the events from 60% to 100% of the ultimate load are taken into consideration.

A clear space with no activity appeared between the two active regions. This might be due to the spacing of the sensors and a poor transmission of the signals throughout the forming of the cracks. On the other hand, this zone could be simply inactive, as the stress generated by either the bending moment and the shear force does not represent an issue.

An analysis of the energy was also carried out. The cumulative energy related by all the located events and recorded by all channels is shown in Figure 7.40, where the energy (calculated using equation 4.15) is indicated on the vertical axis and the location along the length of the beam is represented on the horizontal axis in mm. It is interesting to note that although the two previously pinpointed active regions can

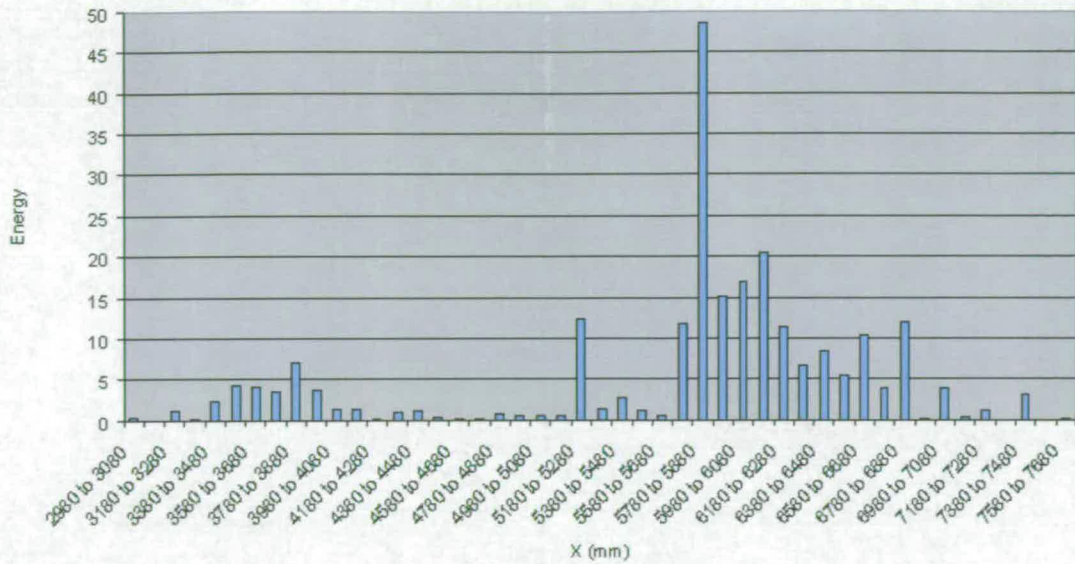


Figure 7.40: Histogram representation of the cumulative energy of SP events for beam HB2.

still be recognized, most of the energy was concentrated in the area of the shear failure (i.e. on the right side on the histogram). This indicates that although both regions were acoustically active and subjected to cracking, it was the one on the right that expressed the most serious energy structural damage and released the larger amount of AE energy. This finding supports the conclusions reached during the AE location study discussed in section 7.2 - that the energy is an effective parameter to identify the degree of damage of a structure.

In a later analysis, the energy was divided according to the magnitude of the load. The results are shown in Figure 7.41, where four ranges are adopted:

- from 0 to 120 kN
- from 120 to 158 kN
- from 158 to 190 kN
- from 190 kN to failure

It is clear that the most amount of energy was recorded during the last stage, i.e. when the load was over the last 5% of the ultimate load. This might represent a limitation of the SP system at this stage when monitoring a structure, as this is too late a stage

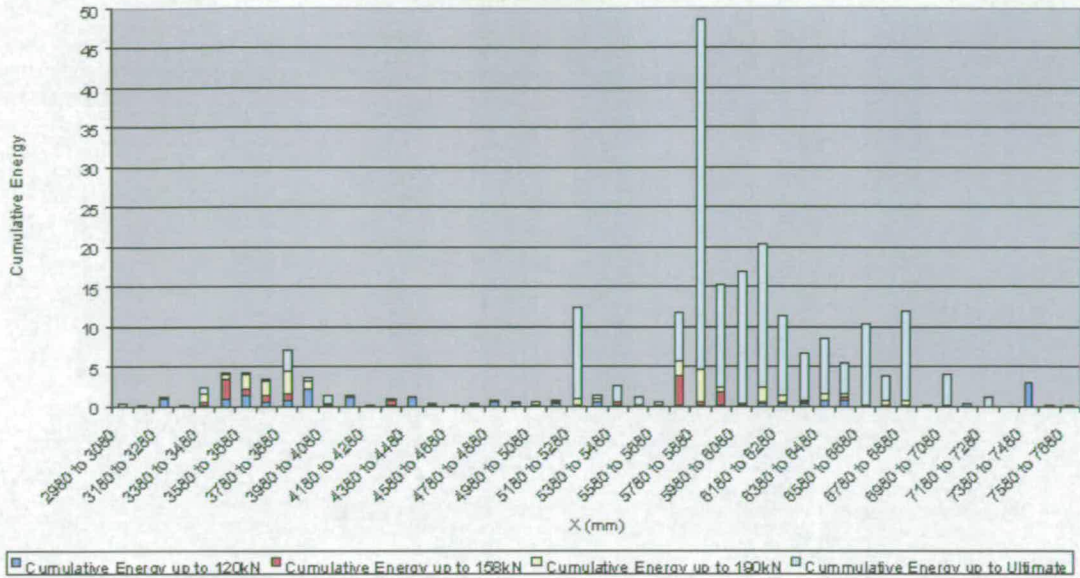


Figure 7.41: Histogram representation of the cumulative energy of SP events as a function of load for beam HB2.

to be effective as a warning of the ensuing failure.

During the test on the hinge beam HB2, AE data were also recorded with the PAC MISTRAS System using the Mi-tra software, as described in 6.2 and therefore analysed to compare with the findings obtained with the SP system.

For the same reasons discussed for beam CF1, the data had to be processed only in terms of AE energy and the only information about the location that we can obtain is in relation to the sensor position. Moreover, the threshold was not kept constant during the whole test. A 50 dB threshold was adopted during the first two loading cycles and then it was raised up to 60 dB during the last two. This created difficulties when comparing the data obtained from different cycles using the PAC software. To overcome the problem, the data were converted into ASCII format and MATLAB software was used to process the data. MATLAB allowed filtering of the data by imposing a 60 dB threshold to the whole data set. This made the comparison between different cycles reliable. Finally, in the light of further experiments (undertaken after the test on the beam HB2) it was established that 60 dB is a very high threshold to be used on concrete. The fact that the sensors were located quite close to each other and to the failure area may have reduced the problem, although this still means that some meaningful data

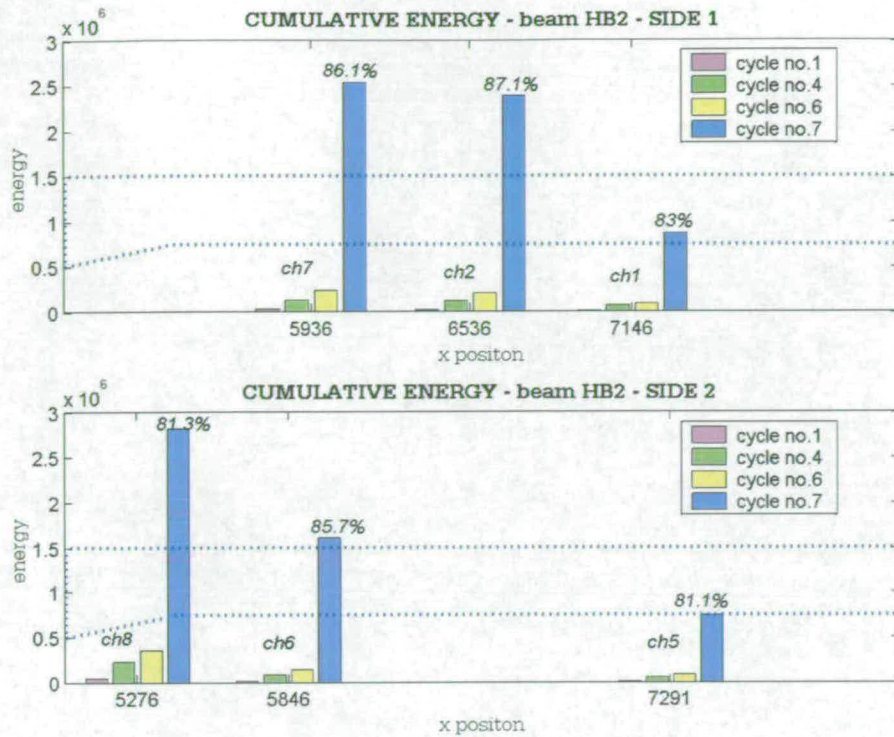


Figure 7.42: PAC energy as a function of location and loading cycle for beam HB2.

were probably lost.

An analysis of the AE energy recorded during the test was carried out. The energy was analysed as a function of location (i.e.: for each channel), of cycle and of load.

Figure 7.42 shows the energy associated with each channel on the two sides of the beam (the dotted line represents the beam itself) and as a function of the loading cycles. The shear failure region appears to be more active in terms of energy, especially in the left half-span. It is also shown that the largest amount of energy (over 80%) is released during the last cycle. Figure 7.43 considers the energy as a function of load intervals and it can be seen that most of the energy arises when the load is between 190 and 202 (failure load) kN. Very low energy was recorded up to 30% (i.e. 60 kN) of the ultimate load when no visible cracking had yet occurred. It has to be pointed out again that the high threshold probably prevented the recording of useful data, especially in the early cycles.

The results obtained with the PAC and the SP system can be compared. As the

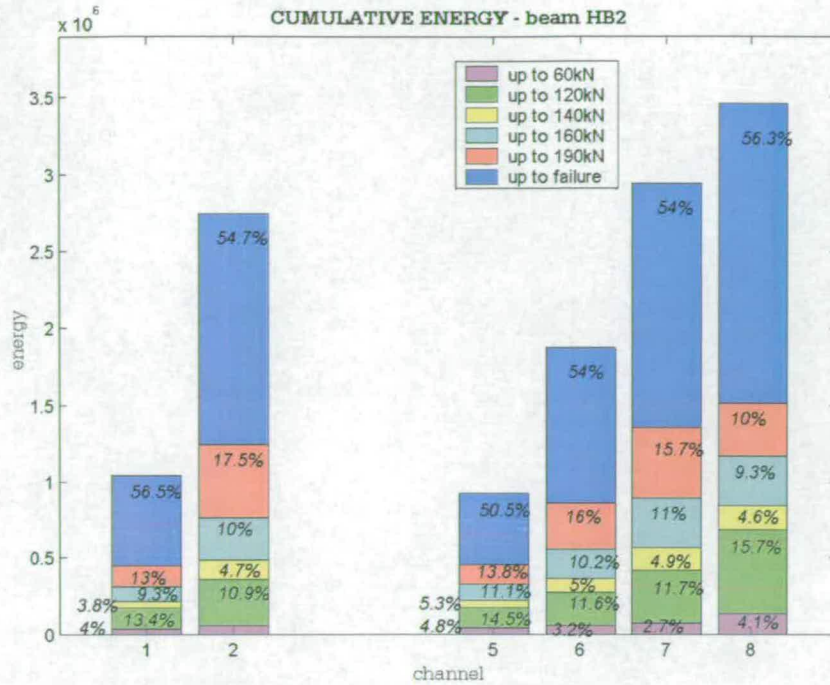


Figure 7.43: PAC energy as a function of load for beam HB2.

PAC sensors were all located on the cantilever span of the beam, only the results for this area can be compared with the SP conclusions. Figures 7.42 and 7.43 can be related respectively to Figures 7.40 and 7.41 that show the SP results. These show that most of the energy comes from the cantilever span cracked area. Moreover, most of the cumulative energy appeared when the load is up to 190 kN. At this stage of the analysis the results of the two systems were then in agreement.

7.4.5 Differences and/or Similarities between the PAC and SP systems

In the light of the experiments carried out and of the results that were obtained, some differences and similarities can be drawn concerning the PAC and the SP system.

- The PAC system is normally targeted to detect accumulating data arising from several sources and therefore to identify the presence of acoustically active regions.
 - The SP system is normally set up in order to record single “failure” events, and therefore to identify the occurrence and position of significant individual

events.

2.
 - The PAC system records the development of microcracks before they are visible.
 - The SP system detects large failure events, such as the sudden development of a large crack.
3.
 - The PAC system is intended as a general purpose equipment; its settings are therefore very flexible and the user is free to modify and adjust them according to his specific needs.
 - The SP system is generally set up by the company according to the required specific task, and the user only has the facility to change a limited number of parameters.
4.
 - Both systems are suitable for laboratory and field work.
5.
 - The filtering features of the SP system may in the future enable outputs similar to the MTA which can be carried out using the PAC system, as described in section 7.5. The location step is already covered by the software and it would be interesting to see if filters and decision trees could be developed in order to exactly distinguish between different types of cracks.
6.
 - During the data acquisition process, the PAC system allows filtering on frequency and amplitude.
 - During the data acquisition process, the SP system allows filtering on frequency, amplitude, energy content and time.
7.
 - The location process in the MISTRAS software is performed automatically in real-time by the software - all the events can be visualized on the same screen.
 - The location process in the SP system is performed automatically or manually, for single events.

7.4.6 SP Conclusions

The SP data recorded during small scale and full scale tests were analysed in order to evaluate the potential and capability of the system to detect cracking in concrete.

- In all the experiments the SP was able to record and thus locate AE events generated by concrete cracking.
- The pattern recognized in the SP activity location emerged at approximately 50-60% of the failure load of the samples, for the small scale tests as well as for the full scale test on beam HB2.
- In the small scale tests:
 - acoustically active regions could be identified
 - the location process was affected by the number of cracks, i.e. fewer events were located during the last cycles of the experiments, due to the presence, at this stage, of a large amount of cracks
 - the Decision Tree appeared to classify all the events recorded during the small scale tests as “small cracks”
 - the location of the events had to be done using the manual option of the SP software and it therefore proved to be very time consuming
- On beams CF1 and HB2 the accuracy of the longitudinal location was better than the vertical one.
- The differences and similarities of the SP and PAC systems were discussed:
 - both systems allow filtering and source location and are suitable for laboratory and field work
 - the PAC system is targeted to accumulating data, it records the early stage of microcracks and its settings are very flexible
 - the SP system is targeted to single signals, related to “failure” events and its settings are generally pre-defined
- On beam CF1:
 - events were recorded and successfully located in corresponding with the visible cracking
 - areas of high activity were identified in the centre of the beam during the mid-span loading, corresponding to the areas of maximum bending moment, as expected

- very few events were recorded in the central area of the beam before the cycling load.
- On beam HB2:
 - events were recorded and successfully located in corresponding with the observed cracking
 - the located events correctly identified active cracking areas
 - most of the events were located once the load was over 30% of the ultimate load
 - most of the energy occurred over the last 5% of the load to failure.
 - high energy characterized serious structural damage, in agreement with the findings described in section 7.2
- On beams CF1 and HB2, the results, in terms of energy, of the PAC and SP systems were in good agreement.

7.5 Preliminary Moment Tensor Study

The aim of a Moment Tensor Analysis (MTA) is to characterise the AE sources in terms of their location, type and orientation. The MTA presented in this chapter is based on the method developed by Ohtsu and described in section 4.9. This Moment Tensor method while widely used in Japan, has seen limited usage in the rest of the world, probably due to its complexity and the lack of a clear understanding of how the analysis is carried out in practical terms. This limited adoption worldwide is despite several publications on the subject, and could be due to the fact that they in fact mainly deal with the theory on which the method is based, rather than providing a practical explanation for the actual analysis procedure. This gap is only partially covered by the software manual [PAC, 1997b]. In fact it was not possible to achieve a clear, total understanding until the writer spent a period in Japan, and experiments were carried out there and discussions held with Prof. Ohtsu and Assoc. Prof. Shigeishi - without whom this section could not have been written.

This section firstly describes in detail each step that has to be followed in order for an MTA to be successful and it summarizes the whole procedure by drafting a protocol. Particular emphasis is placed on the steps that are not covered by the manual

or references. Only after having clarified the correct procedure, is the analysis of the experiments presented. The unsuccessful attempts that were carried out before the experience in Japan are discussed, explaining the reasons for their failure. In the light of the correct procedure the analysis of the Moment Tensor experiment undertaken at Kumamoto University and described in section 6.3 is presented. Data related to the experiment were made available for analysis and the results of one of the samples is shown here. It has to be stressed once again that the analysis presented here was aimed at attaining a critical understanding of the MTA. Final conclusions are drawn about the advantages and drawbacks of the method.

7.5.1 Moment Tensor Analysis

The Moment Tensor Analysis consists of several different steps that require the use of varied software. In order to complete the whole analysis, four software packages are needed:

- the PAC MT-TRA software, or its equivalent latest version DMT-TRA when the new DiSP system is used
- the PAC SiGMA 3D software
- Microsoft Excel
- a visualizing program, such as the Cosmo Player or the Cortona VRML Client 4.0 Web 3D viewer

To start the analysis, an input data file is needed. Although this point might be thought to be trivial, it is in fact vital for the success of the analysis. The data included in the file has to meet and to be recorded according to some specific requirements:

1. the data file has to have a .tda extension, i.e. the data has to be recorded as waveforms using the MT-TRA software
2. the waveforms have to be recorded with a pre-trigger value (see section 5.2) equal to at least 25% of the total waveform length; this is required by the software automatic algorithm to determine the background noise [PAC, 1997b]
3. six recording channels are required [PAC, 1997b] [Ohtsu et al., 1998a]
4. the trigger mode (see section 5.2) has to be set up as “SYN”

5. the trigger source (see section 5.2) has to be set up as “EXT” in five out of the six channels, whilst the sixth channel has to be set up as “DIG”. This sixth channel is chosen as the main trigger of the system and thus has to be placed in the proximity of the expected AE sources
6. the data file has to be placed in the same directory folder of the executable MT-TRA program

A few points have to be clarified. As mentioned in sections 4.9 and 6.3, the sensors have to be broadband type transducers and they have to act as a network of instruments, i.e. be distributed around the target area for a variety of the azimuths. Better results are obtained if the sensors are located asymmetrically and with a spacing less than 1 m [Ohtsu et al., 1998a]. According to the Moment Tensor manual [PAC, 1997b], the first of the above five conditions is not essential and the data could be recorded using the MISTRAS software as long as the waveform collection option is enabled (section 5.2); a utility can then be used to convert the file a second time. This method of processing was tried during one of the Edinburgh experiments, but as a consequence of this the MT-TRA software used during the successive step was continuously crashing, making it impossible to bring the analysis to an end. The use of this method is therefore not advised. The manual states that the trigger mode of the sensors has to be set as synchronized, but it does not give any particular requirement for the trigger source.

Before being able to characterize the AE sources, it firstly has to be located. Once the data have been correctly recorded, the first step consists in replaying the input file with the MT-TRA software and starting its Moment Tensor Analysis option by picking up the arrival time P_1 of the signals. These times are needed by the automated algorithm to perform the source location. The arrival time has to be picked up for each waveform and for each sensor. It is strongly recommended that the process is undertaken manually, as the automatic option of the software available appears to be unreliable.

At the same time, the amplitude of the first motion P_2 has to be picked up for each waveform and each channel; this value represents the amplitude defined in equation 4.39. For the reasons stated above this has to be again a manual process. The two

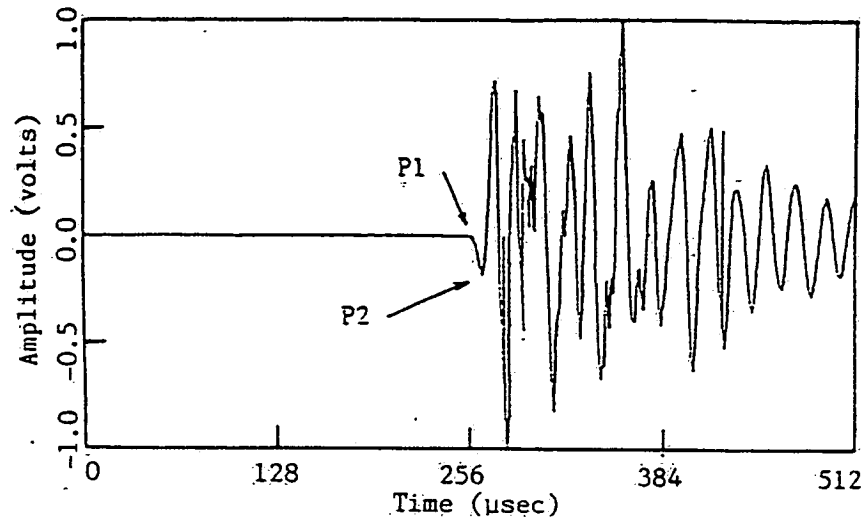


Figure 7.44: Arrival Time P_1 and First Motion Amplitude P_2 , from [Ohtsu and Shigeishi, 2002].

parameters, the arrival time and the amplitude of the first motion, are shown in Figure 7.44. At the end of the two processes the software generates a series of $.PTn$ file, one for each sensor, containing all of the values picked up.

A few practical factors need to be highlighted in relation to this step. The process of selecting the arrival time and the first motion amplitude has to be undertaken only for the waveforms that are judged to be “valid data”; i.e. the arrival time and the amplitude are clearly identifiable above the background noise in all the six channels. This makes the quantity and quality of the results dependent on the ability of the user to correctly select the data and choose the values. Both values do not have to be picked up for the waveforms whose peak amplitude exceeds 10 V, which is the limit value of the software window. Although the use of the mouse is available during the manual process its use is not recommended as it often causes the software to crash. Finally and occasionally not all the channels record the same number of hits, probably due to a fault in the software. This generates a delay in selecting the two values as it has to be done by groups of six signals belonging to the same hit.

Once the above step has been completed, the SiGMA software can be run. It requires the user to specify the location and direction of the sensors, and a value for the

Poisson's ratio and the P-wave velocity for the sample material studied. The previously created .PTn file is also required. The direction of the sensor has to be established in relation to a system of axis on the sample that has to be defined by following the "left hand rule".

The SiGMA 3D code runs in the DOS environment (a new Windows version has been developed at Kumamoto University, but at the moment it can only deal with a maximum of 1000 hits) in two phases. The first one calculates the location of the AE sources. If successful, the second stage can be run and it performs the calculation of the Moment Tensor components and the characterization of the located sources. The program has to be run for each hit for which the arrival time and the first amplitude were selected. The code finally generates:

- an output file *.00n* (containing the summarised results) for each of the hit signals successfully run through the two phases
- an *.chd* file with the latest run hit
- a final *.lst*
- an ASCII file that includes the results of the calculations for all these hits

The next step consists of checking if the results computed by the SiGMA code are correct. This is done by opening the *.lst* file with Excel and manually verifying that the location of the source fell inside the actual sample and that the relative calculated "mean" value (i.e. the normalized Z eigenvalue of equation 4.43) is positive. Due to its definition the Z eigenvalue can in theory have only one direction. All the results for which any of the two above conditions are not satisfied, are discarded. A new *.txt* file is then created containing only the valid results. An example of its format is shown in Figure 7.45.

The last step concerns the visualization of the obtained results. Until very recently, this was done by an additional SGMPLLOT program that would read the final output file, create a new file and send it to a printer that would then plot a 2D drawing of the results. The drawing illustrated the sample itself and the located sources using different symbols to differentiate between the type of cracks and arrows to indicate

```

*** AE Source Inversion SiGMA Solution List ***
" ( Date, 01-06-2003 Time, 13:42:58 )"

```

input settings

```

[ Channel Data List ]
ch. | Transducers Position | Transducers Direction | Arrival Time | Amplitude
    | x   y   z   | x   y   z   | (sec) | (volts)
B 1 | 0.000 0.000 0.075 | 0.0000 0.0000 -1.0000 | 0.100000E-04 | -0.0021
B 2 | -0.125 0.000 0.000 | 1.0000 0.0000 0.0000 | 0.100000E-05 | -0.0015
B 3 | 0.000 0.000 -0.075 | 0.0000 0.0000 1.0000 | 0.000000E+00 | -0.0006
B 4 | 0.125 0.000 0.000 | -1.0000 0.0000 0.0000 | 0.440000E-04 | -0.0015
B 5 | -0.063 0.125 0.025 | 0.0000 -1.0000 0.0000 | 0.320000E-04 | 0.0012
B 6 | 0.063 0.125 -0.025 | 0.0000 -1.0000 0.0000 | 0.790000E-04 | -0.0024

```

```

* Velocity of P-wave : 4000.0 (m/sec)
* Poisson's Ratio : 0.20000

```

input velocity & Poisson's ratio

```

[ Step 1 : AE Source Location ---> Completed ]
"Source ( x , y , z ) = ( -0.766 , -0.493 , -1.599 )"

```

Location Results

```

[ Step 2 : Moment Tensor Solution ---> Completed ]
***** MOMENT TENSOR *****
0.2166 0.3212 -0.1984
    1.0000 -0.4994
sym.      0.2585
*****

```

Moment Tensors Components

```

[ Step 3 : Eigen Value Analysis ---> Completed ]
    | max | mid | min
Eigen Value | 1.000 | 0.076 | -0.002
Eigen Vector x | 0.3094 | -0.9045 | 0.2935
Eigen Vector y | 0.8461 | 0.4027 | 0.3491
Eigen Vector z | -0.4340 | 0.1403 | 0.8899

```

Eigenvalues & Eigenvectors Results

```

< Composition Ratios of Eigen Value >
Shear : 7.81 % | CLVD : 56.39 % | Mean : 35.80 %

```

Decomposition of Eigenvectors

Figure 7.45: Output format of SiGMA results - the red comments have been added as further explanation.

their orientation. The major drawback of this method was that it would work only if a Japanese printer was used!

A recent implementation modifies this last step [Ohtsu and Shigeishi, 2002] and a new visualization system was developed using VRML (Virtual Reality Modeling Language) to illustrate the crack locations, types and orientations in a three dimensional way. In order to create the necessary *.vrmf* file for the visualization, a program in VBE (Visual Basic Editor) language has to be run in Excel. The program reads the final *.txt* file containing the valid results and converts it in the *.vrmf* file that can be viewed by an Internet 3D Viewer. The latest proposed viewer program is the Cortona VRML Client 4.0 that can be freely downloaded from the Internet and it shows a 3D image of the results (see Figures 7.47 to 7.58).

It has to be pointed out that the VBE program contains internal information about the geometry of the tested sample and the location of the sensors. Thus it has to be modified according to the varied samples that are used. Besides, at this stage, the existing code contains Japanese characters and it can only be run on a Japanese version of Excel!

All the above steps are summarized in a diagram in Figure 7.46.

A Moment Tensor Analysis was attempted on the data recorded from the TRL experiments and from the beams BF2 and BF3 at Edinburgh. In the TRL experiments the data were recorded using the MT-TRA software, whilst in the Edinburgh beams the data were recorded as parameters using the MISTRAS software and later on converted, leading to the problems explained earlier. All cases were unsuccessful. A follow up investigation showed that the settings used in terms of sensor locations and pre-trigger were correct. The sensors were set in the synchronised mode, following the instructions in the manual, and in all cases the resonant R6I transducers were used. The latter are assumed to be the substantial reason for the failures (see section 6.3 for more details).

A complete and successful MTA was carried out on the data of one of the samples tested at Kumamoto University and described in section 6.3. This analysis was performed following step by step the procedure previously discussed.

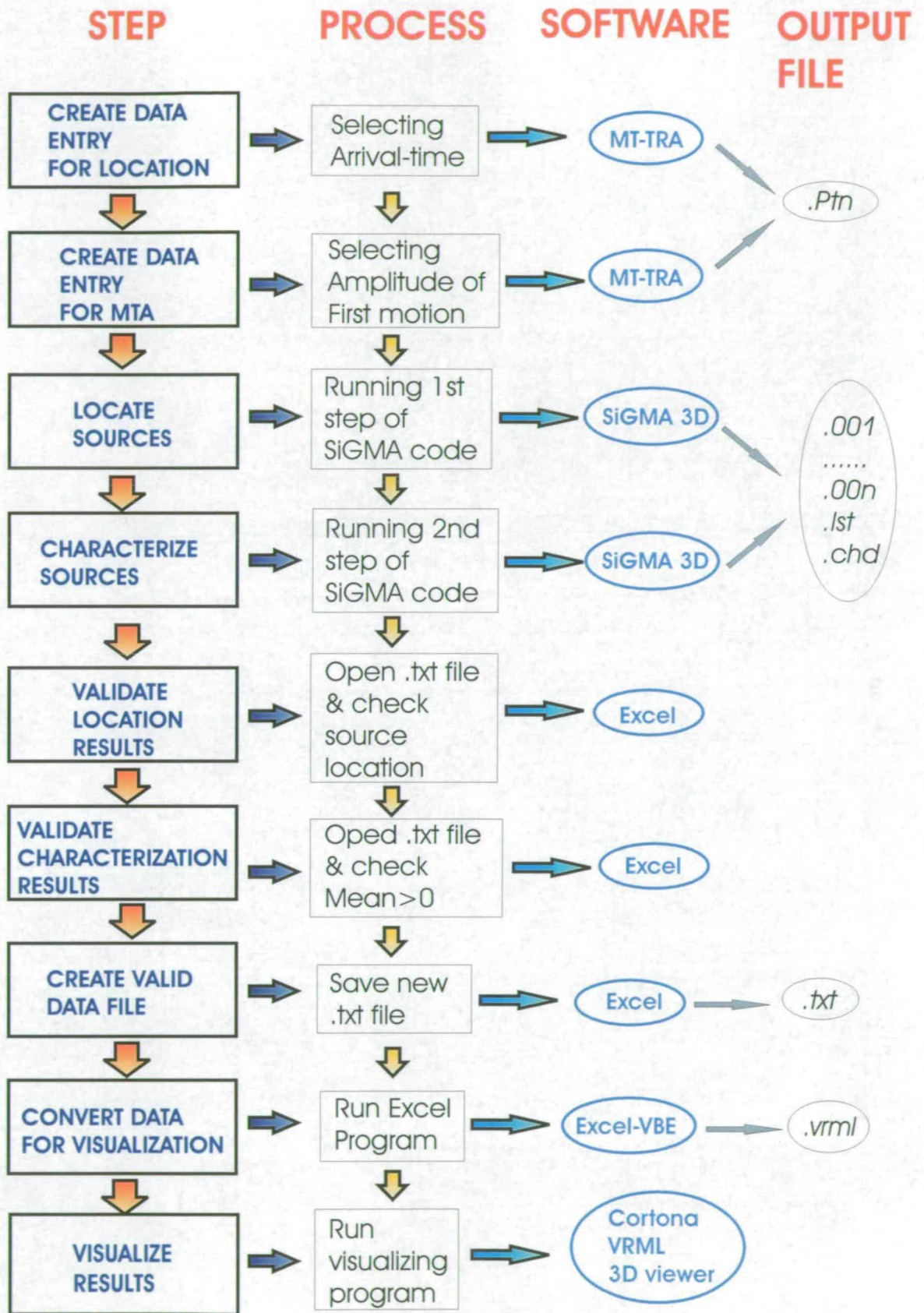


Figure 7.46: Schematic diagram of the Moment Tensor procedure.

The steps concerning the selection of the arrival times and of the first motion amplitude was very time consuming. Approximately 8500 hits were recorded on just one sample; multiplying this by the number of sensors leads to a total of approximately 51,000 signals that had to be manually scanned through. Approximately 700 of the total number of hits were judged to be “valid data” (i.e. 8.2%) and therefore for those the arrival time and first motion amplitude were selected and the SiGMA code was run. The process of verifying the SiGMA results eliminated approximately one third of them, resulting in approximately 6% of the initial recorded hits reaching the final step of the analysis. The final valid results are shown using the Cortona 3D viewer in Figures 7.47 to 7.55. The Figures show the sample itself, the location of the sensors in a white color, and the different types of located cracks. More specifically, the arrow vector indicates the crack motion vector, whilst the circular plate corresponds to the crack surface [Ohtsu and Shigeishi, 2002].

These figures give a clear example of the different phases of the cracking in time, with the main crack along the middle of the sample developing first and the lateral crack starting to form only later. The final stage (Figure 7.55) can then be compared with the photo of the failure of the sample in Figure 7.56 and a good agreement can be seen. The program allows a plan view of the results which can be conveniently rotated enabling one to have different views of the sample; examples of which are given in Figures 7.57 and 7.58.

7.5.2 Moment Tensor Conclusions

Attempts at undertaking an MTA were carried out on RC specimens tested at TRL and at Edinburgh University and they were all unsuccessful as the data were not recorded following the previously described procedure and therefore were not suitable for the MTA. The period spent in Japan allowed both a critical understanding of the reasons behind these failures and of the correct analysis procedure steps that have to be performed.

- The whole procedure of an MTA was discussed, summarized and applied to a concrete sample tested at Kumamoto University.
- The quality of the results obtained by the MTA was unquestionably high, providing complete information about the location, type and orientation of the

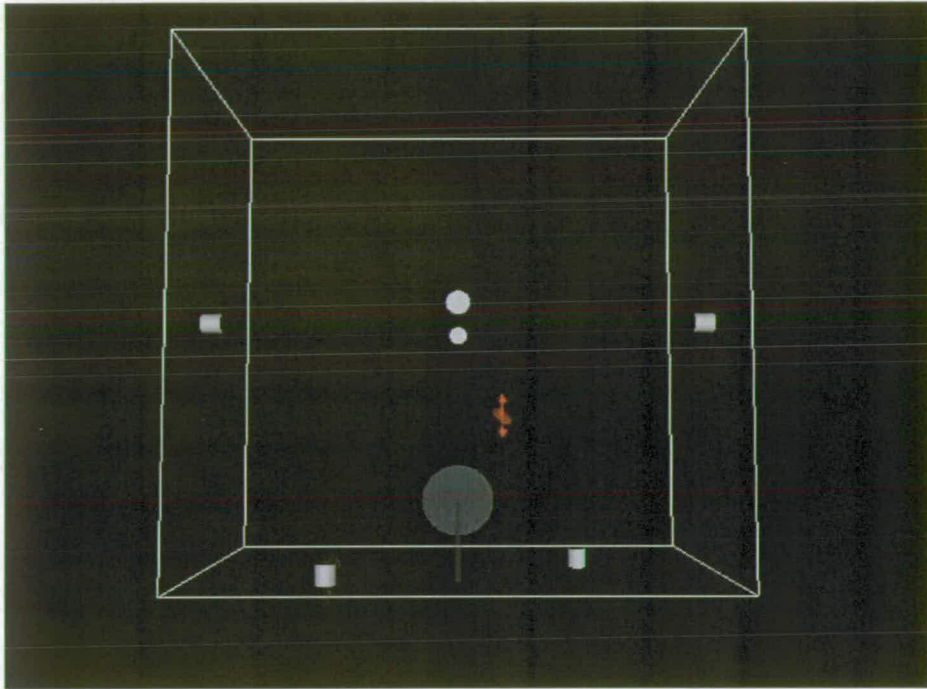


Figure 7.47: Moment Tensor results: First stage of the cracking on the sample. The red symbol represents a mixed-mode crack; the circle represents the crack surface, whilst the arrow indicates the P-axis, i.e. the direction of the crack extension. The white cylinders or circles represent the sensors. The grey circle and line indicates the hole and notch on the sample.

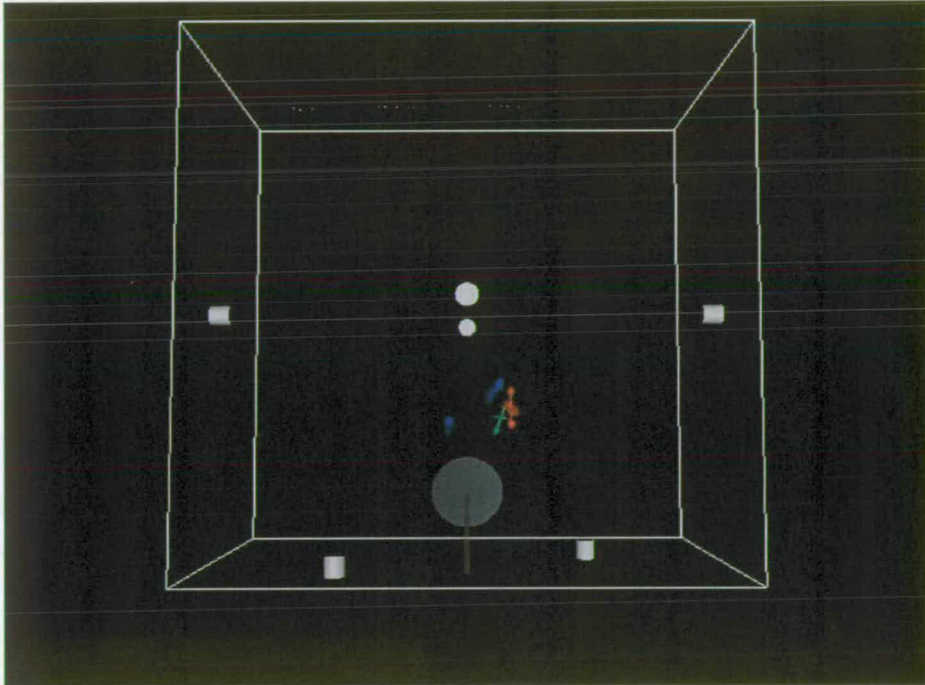


Figure 7.48: Moment Tensor results: Second stage of the cracking, plotted as in Figure 7.47. The different colors (red, green and blue) indicate different crack types (mixed-mode, tensile and shear).

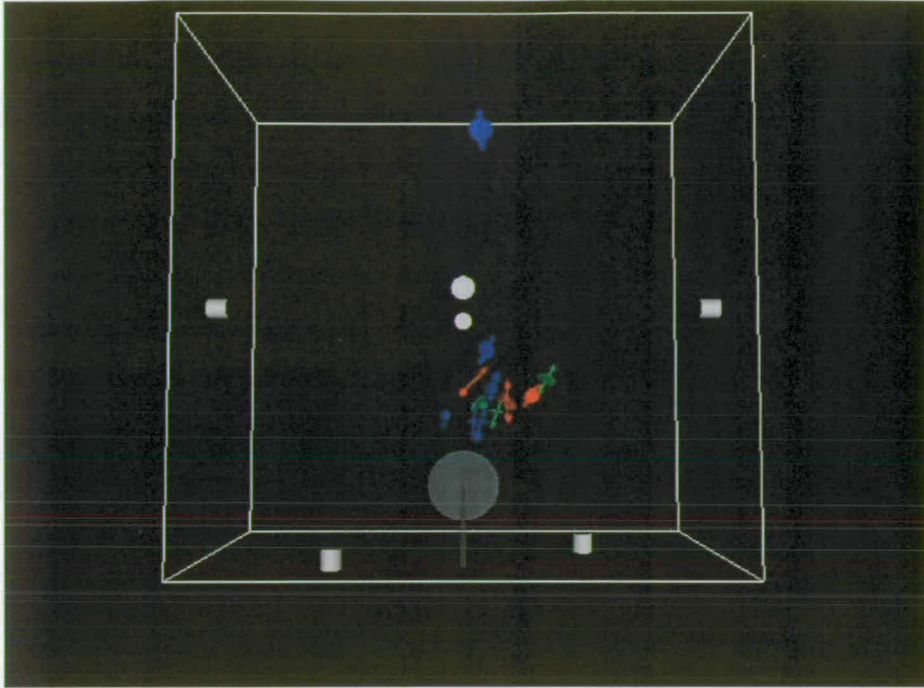


Figure 7.49: Moment Tensor results: Third stage of the cracking, plotted as in Figure 7.48.

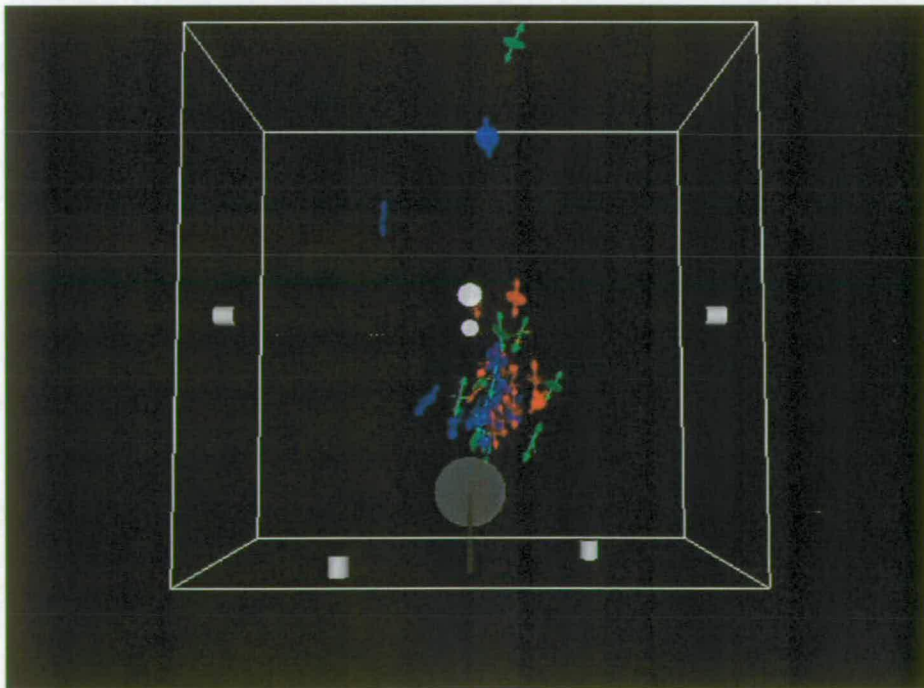


Figure 7.50: Moment Tensor results: Fourth stage of the cracking, plotted as in Figure 7.48.

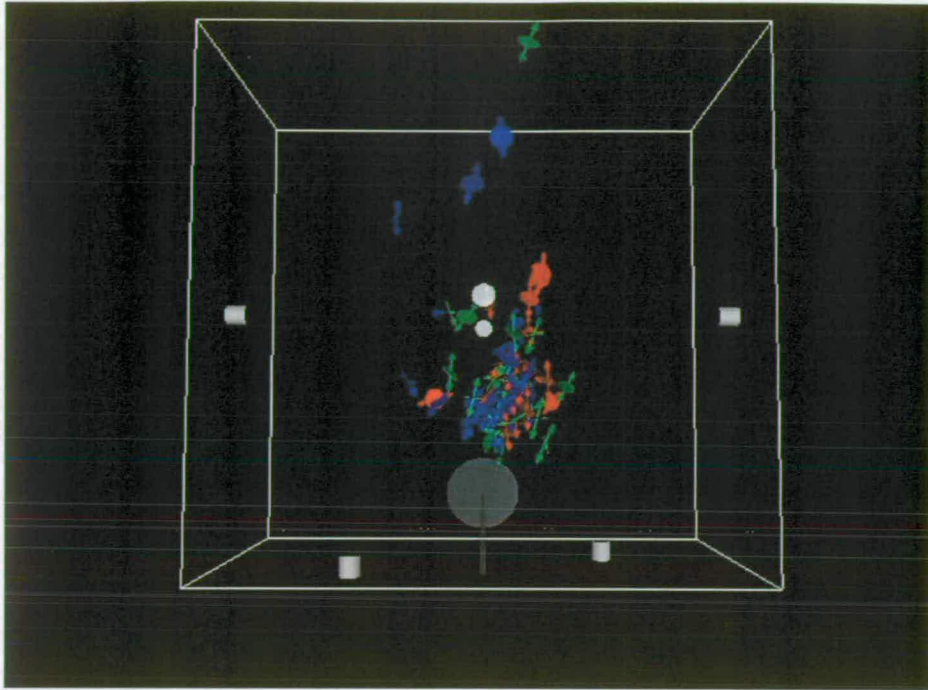


Figure 7.51: Moment Tensor results: Fifth stage of the cracking, plotted as in Figure 7.48.

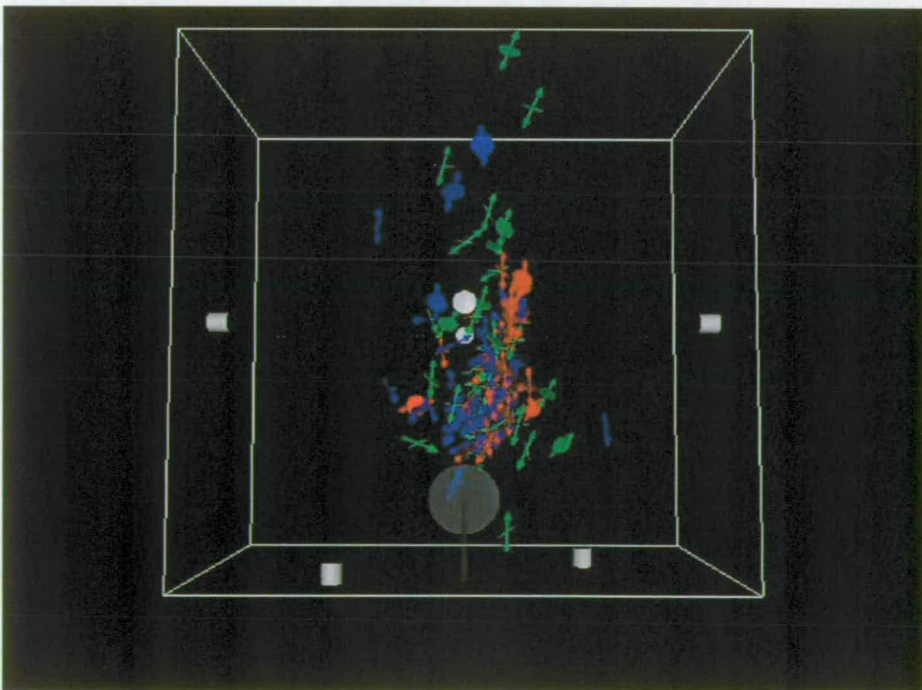


Figure 7.52: Moment Tensor results: Sixth stage of the cracking, plotted as in Figure 7.48.

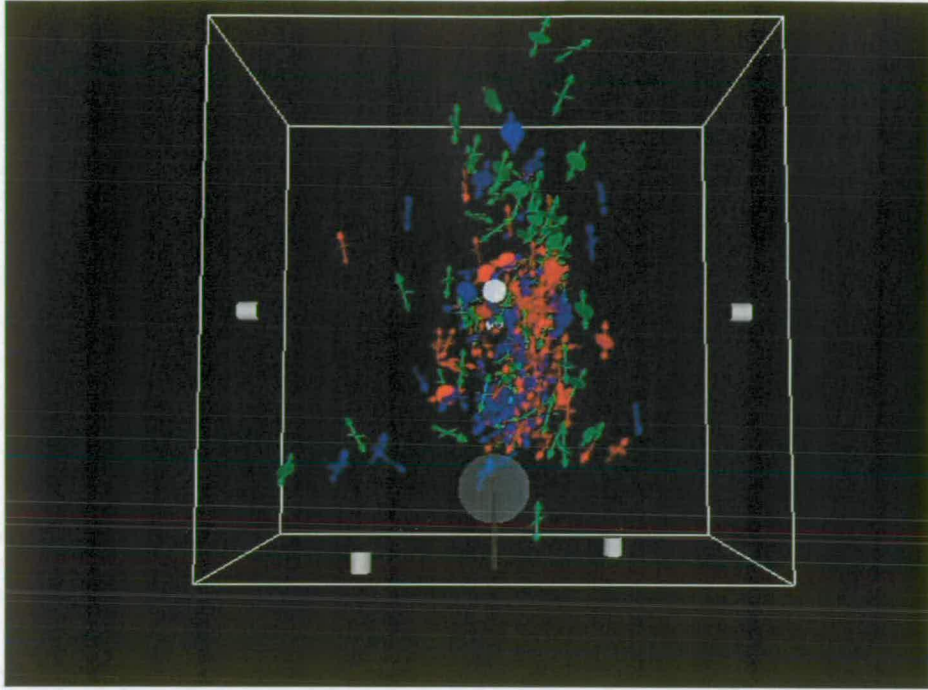


Figure 7.53: Moment Tensor results: Seventh stage of the cracking, plotted as in Figure 7.48.

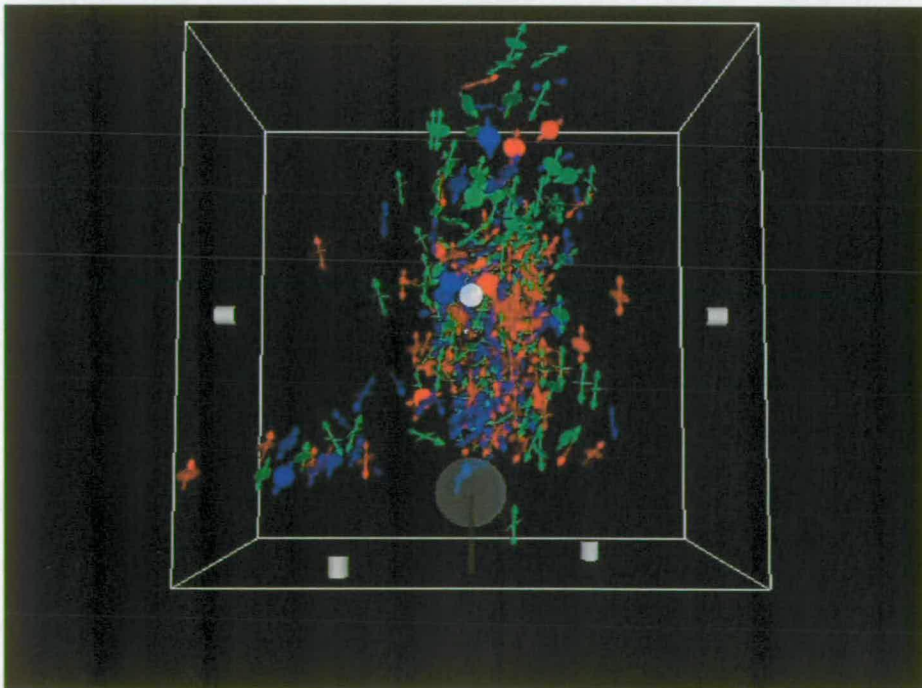


Figure 7.54: Moment Tensor results: Eighth stage of the cracking, plotted as in Figure 7.48.

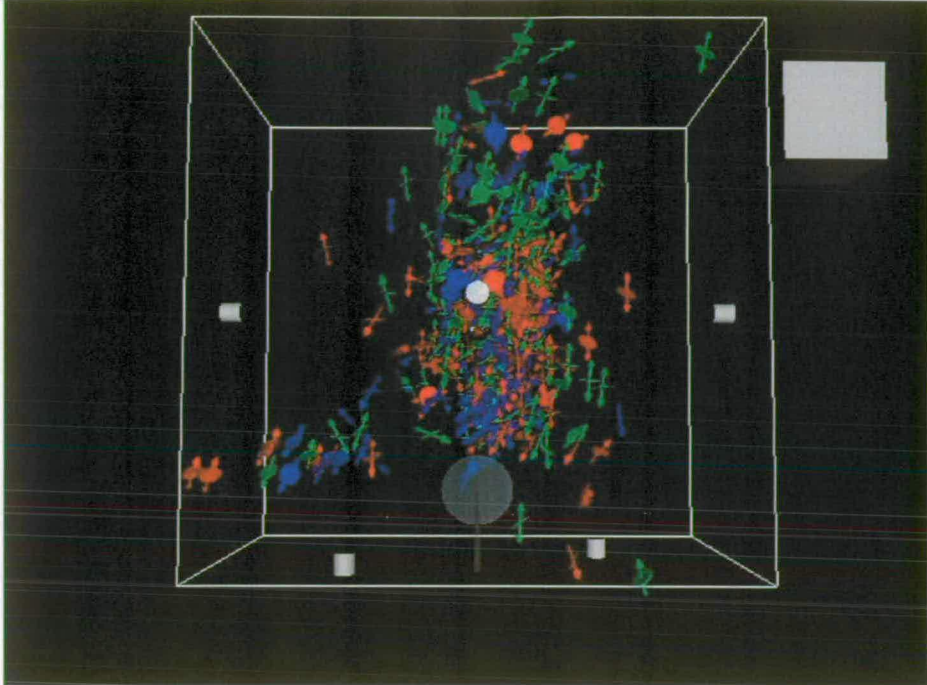


Figure 7.55: Moment Tensor results: Final stage of the cracking, plotted as in Figure 7.48.

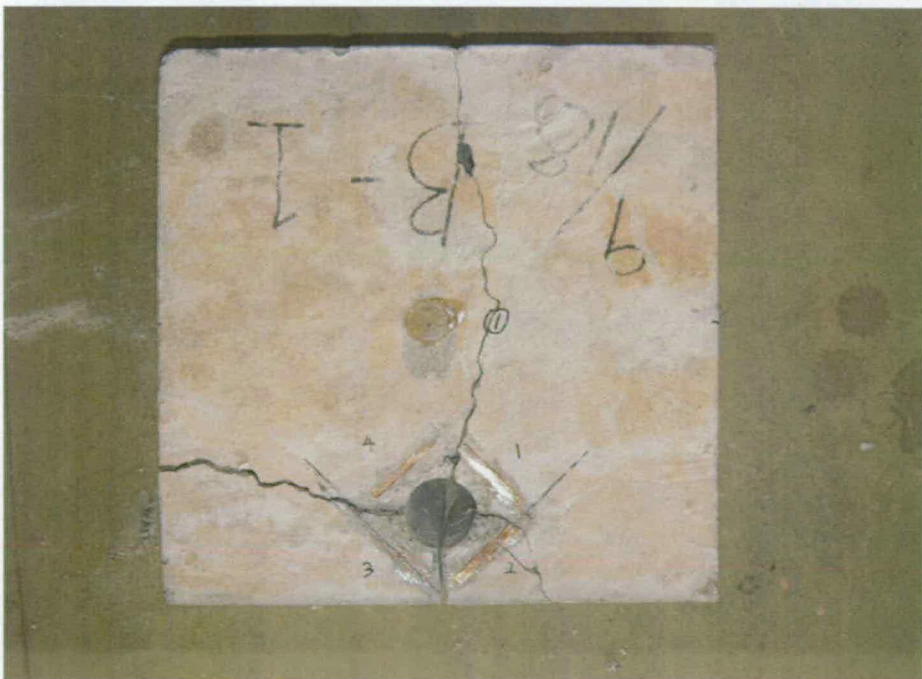


Figure 7.56: Failure of the sample used for the Moment Tensor analysis.

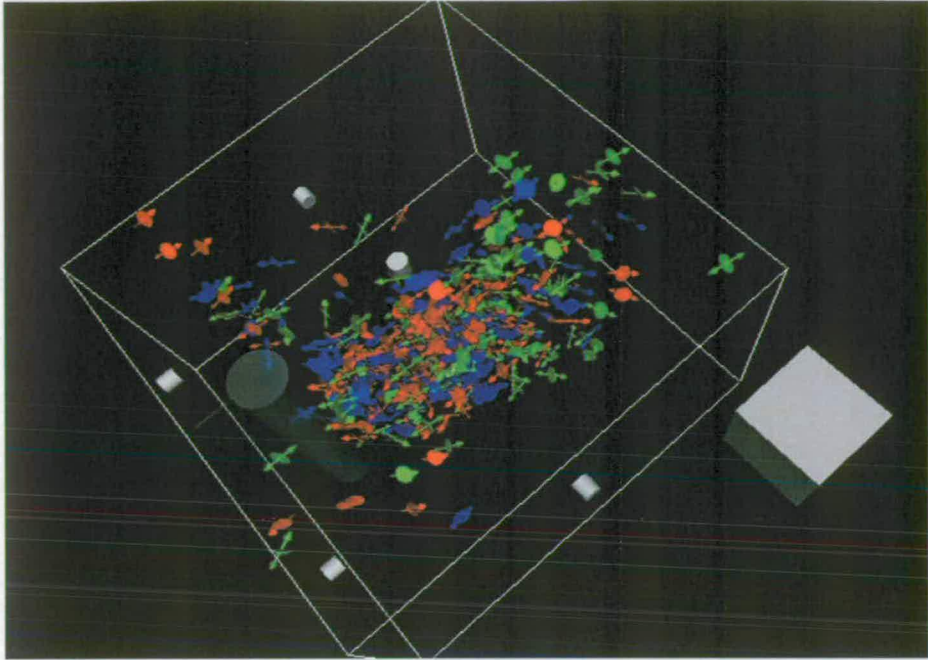


Figure 7.57: Moment Tensor results, first rotated view: final stage of the cracking, plotted as in Figure 7.48.

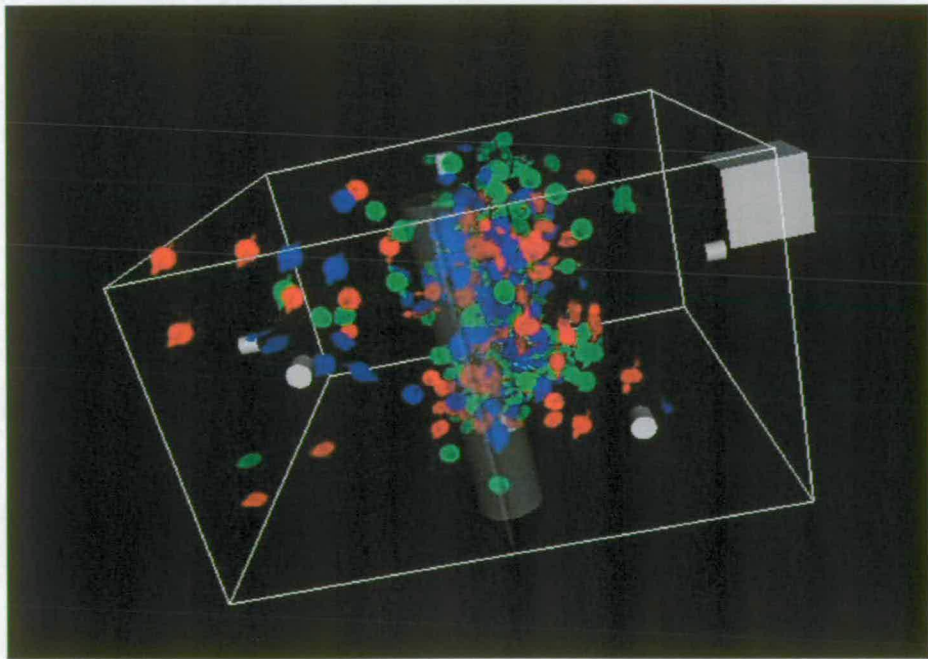


Figure 7.58: Moment Tensor results, second rotated view: final stage of the cracking, plotted as in Figure 7.48.

cracks.

- The results of the analysis were in good agreement with the failure observed on the sample, confirming the validity of this type of analysis.
- Over 90% of the initial data were disregarded during the analysis.
- The final step of the procedure that is needed to visualize the results is at this stage not compatible with non Japanese software, although further development to solve this issue is in progress.
- The analysis procedure is highly time consuming, as many steps have to be undertaken manually. This is considered to make this type of analysis “non-commercial”.
- Due to the manual aspects involved in some of the procedure steps, both the quantity and the quality of the results depends on the individual skills of the operator.
- During the data recording, one of the AE sensors has to be chosen as the main trigger and positioned near to the expected failure. This implies the need to correctly foresee where the failure of the sample or structure under study is going to happen.

7.6 Summary

This chapter presented different methods of processing AE data, in some cases adapted from existing procedures and in other cases newly proposed:

- a b -value analysis was proposed and showed a good agreement with the different cracking and damage appearing during the tests
- an AE source location analysis demonstrated the effectiveness of the AE energy as a parameter to identify and predict damage
- a Relaxation ratio analysis was developed and seemed very promising to define the degree of damage, although its results are affected by the loading rate and concrete properties

- a SoundPrint data analysis was undertaken and it showed the possibility to adapt the system to be used to detect concrete cracking
- a Moment Tensor analysis was carried out, its procedure was explained and its validity was demonstrated

Detailed conclusions about each method were described at the end of each study and their advantages and drawbacks were discussed. It has to be pointed out that these different types of analysis do not exclude each other but they have to be considered for use, when possible, in conjunction with one another in order to support each others results.

Both the PAC and SP location and the b -value analysis were then applied to a real structure, as described in the next chapter to test their validity on site. Overall discussions and conclusions about the different processing methods investigated is finally given in chapter 9 and 10 respectively.

Chapter 8

Boghall Bridge Monitoring

This chapter describes the field work element in the thesis. The monitoring of Boghall bridge was intended as a demonstration of global monitoring (see 4.4) and it was carried out in line with the procedure described in sections 2.2 and 5.6. The existing documentation was studied (section 8.1), a visual survey and verification of damage was performed (section 8.2) and based on the findings the monitoring was planned and undertaken. All the steps are herein presented and discussed.

8.1 Boghall Bridge

Boghall Bridge is located in the Scottish Borders, south of Carfraemill north-east of Lauder on the A697. The original bridge was a flat masonry arch built, according to the Council records, in 1793 using red sandstone blocks. Later on, the road was widened and a trapezoidal cast in-situ concrete slab, consisting of four beams, was placed alongside the masonry arch. The road orientation was also altered explaining the lack of alignment. Construction details of the bridge and its actual aspect can be seen in Figure 8.1 and 8.2.

The work described in this chapter focuses on the concrete side of the bridge. One of the main reasons this bridge was chosen was that it had been already monitored with AET back in 1999 [Shigeishi et al., 2001] allowing a comparison with the old data. As a result of the previous monitoring it was known that one of the concrete beams was visibly damaged and this was expected to give rise to interesting data. Finally, the reasonably small size of the bridge and its location in a traffic area which was safe, ensuring the security of the equipment, were further motivations behind the choice of



Figure 8.1: Boghall bridge: masonry and concrete side; pre-existing cracks.

Boghall bridge.

8.2 Preliminary Investigation

Initially a visual survey was undertaken. The most northerly of the four concrete beams (named Beam 1) shows extensive visible cracking on both sides, concentrated mainly on the eastern end of the beam (Figure 8.1). This cracking is probably due to unseen corrosion of the reinforcement, as iron staining can be observed clearly on the beam. According to the bridge documentation, there is no joint present at the interface between the masonry arch and the concrete slab, thus it can be supposed that water can penetrate freely and cause such corrosion. Salt, commonly spread on roads to avoid ice can also dissolve in water and infiltrate the bridge - accelerating the rate of corrosion. The other three beams appear to be in good condition. At the beginning of this preliminary investigation, it was decided to focus the monitoring on the visibly damaged beam (Beam 1) and the one in good condition beside it (named Beam 2).

The main objectives of this investigation were:

- to investigate the feasibility of the AE technique on a real concrete bridge
- to investigate the different factors that can influence the collection of AE data during in-situ monitoring, such as: wind, temperature, rain, traffic, displacements, presence of cracks, etc
- to compare the response from a beam in visibly poor condition to one that shows little deterioration and to gain an understanding of the bridge condition
- to compare the actual results with the findings obtained in the previous monitoring in 1999
- to verify the application of the SP system on a real concrete structure.

8.3 Monitoring Description

During the monitoring, different sets of data were recorded in order to obtain a comprehensive understanding of the bridge. A low scaffold platform was built over the stream, allowing one to be able to reach the underside of the bridge beams.

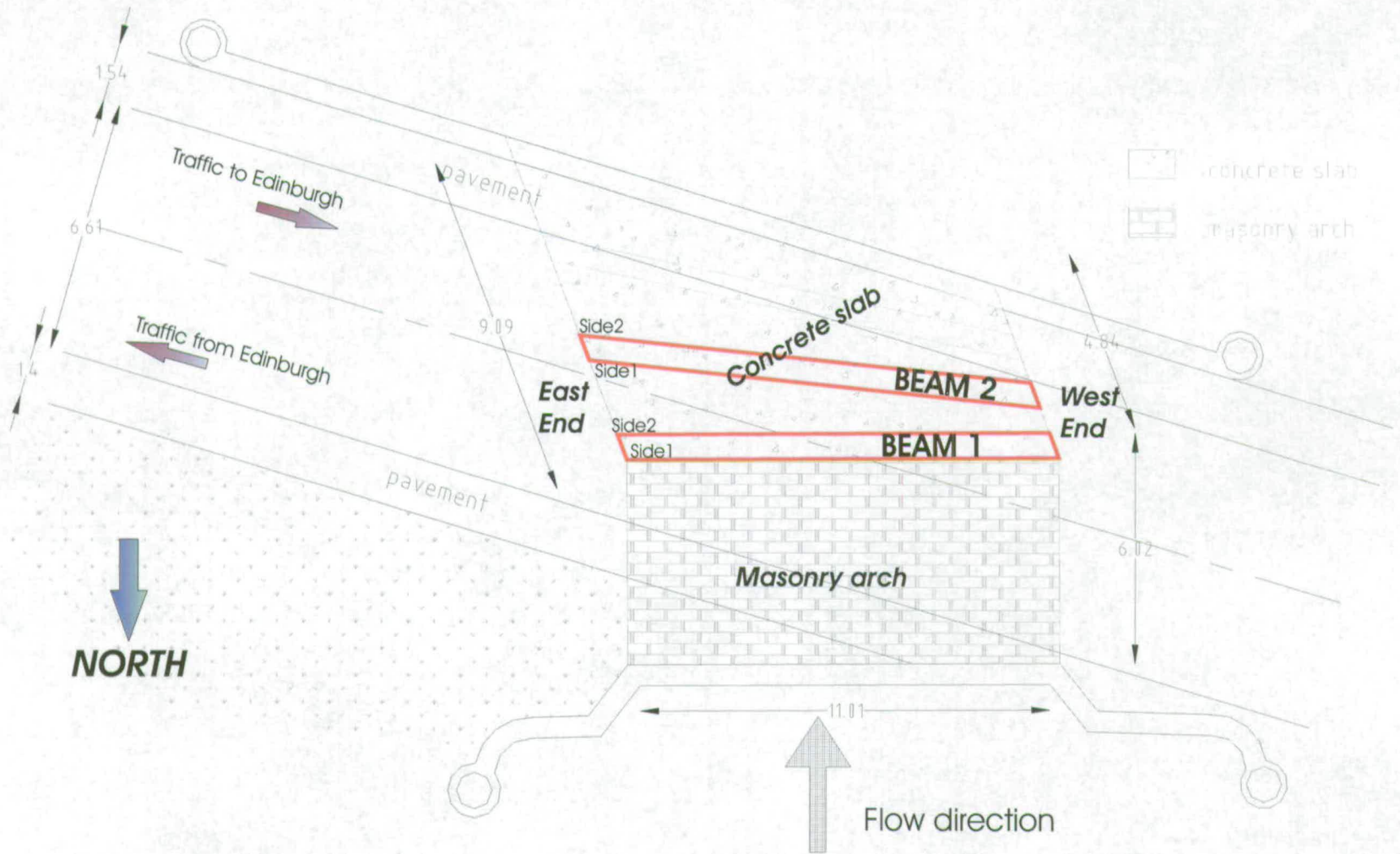


Figure 8.2: Boghall bridge: plan view.

MISTRAS		SoundPrint	
30 dB	Threshold	T-Mast	max clockwise position
		Analog	999
1MHz	Sample Rate	Sample Rate	44.1kHz
2K	Hit Length		
65534	HLT	Delay	minimum
500	PDT		
1000	HDT		

Table 8.1: Boghall Bridge: Instruments Settings.

Acoustic Emission data were recorded using two systems: the PAC MISTRAS equipment in conjunction with eight PAC R6I (Resonant 60kHz Integral) sensors and the SoundPrint system with eight transducers. The settings used for both systems are summarised in Table 8.1.

Pre-existing cracks can generate acoustic emissions (section 4.5) and their presence has to be taken into account. The cracks visible on Beam 1 were mapped and measured. Metal base points were positioned (in nine locations) on either side of the cracks and the distance between them measured using a digital Vernier caliper. This allowed recording of any variation in crack width throughout the whole monitoring. The length of the cracks was also recorded at the beginning and at the end of the study.

Excessive movements and vibrations of the bridge could affect the AE data by generating misleading signals. A laser vibrometer was used to measure the displacements of the bridge and it was set on the river bank with the laser pointing at the mid-span of Beam 1. The instrument allows displacement measurements to be made over a range of 0.08 microns to 80 mm with a frequency range of up to 1.5 GHz [Manual, 2002]. The laser vibrometer was connected to a data logger and to a laptop, where the data was recorded and stored using MATLAB software.

Acoustic emissions are generated by stress release deriving from an applied load (4.1). To avoid any road closure or disruption, passive monitoring was adopted using normal traffic conditions as a load to induce AE. A video camera was positioned on the deck of the bridge to film the flow of traffic during the monitoring period. The number of vehicles passing per minute for each thirty minutes period was established,

indicating the volume of traffic.

Previous studies, [Shigeishi et al., 2000] - [Shigeishi et al., 2001], showed that environmental factors can influence AE readings and so meteorological data was obtained from the Meteorological Office, Charterhall station, 23.1 Km east of Boghall bridge. Due to the distance of the meteorological station from Boghall Bridge, it was anticipated that the information might not be totally accurate, but would still provide an understanding of the meteorological condition. This information was then integrated with the field observations.

In the light of the experiment described in section 5.4.2 all the sensors were mounted on the surface of the beam using plasticine as an acoustic couplant and were held in place with metals clamps. The cables connecting the sensors to the acquisition system were secured using cable holders and ties to prevent movements and/or interference. Every day before recording commenced, the transducers were calibrated using a Schmidt Hammer and a pencil lead as described in section 5.4.3.

Three different cases were investigated. Firstly, the sensors were placed underneath Beam 1 (Case 1). Due to the poor quality data recorded using this location, the sensors were removed and located alongside Beam 1 on side 2 (Case 2). Finally (Case 3), half of the sensors were placed on Beam 1 (side 2) and the other half on Beam 2 (side 1), to compare the response of beams in different states of deterioration. The exact location of the sensors for Case 2 and Case 3 is shown in Figure 8.3. The bridge was monitored over a period of about 10 days. The exact monitoring time for each case is shown in Figure 8.4. The figure also includes a summary of the meteorological and traffic data.

8.4 Analysis

8.4.1 Cracks, Metereological and Displacements Measurements

The measurements showed that the cracks did not grow in length during the monitoring period. Little variation (Figure 8.5) in their width was recorded between the start and end of each day; and this small variation was probably due to temperature conditions or instrument inaccuracy. Only one discrepancy was noticeable - on the 23rd May 2002 - but it is believed to be due to an error in the reading as on the following day the recorded crack width had returned to the previously recorded value.

The laser measurements showed that the displacements were minute (about 1 mm)

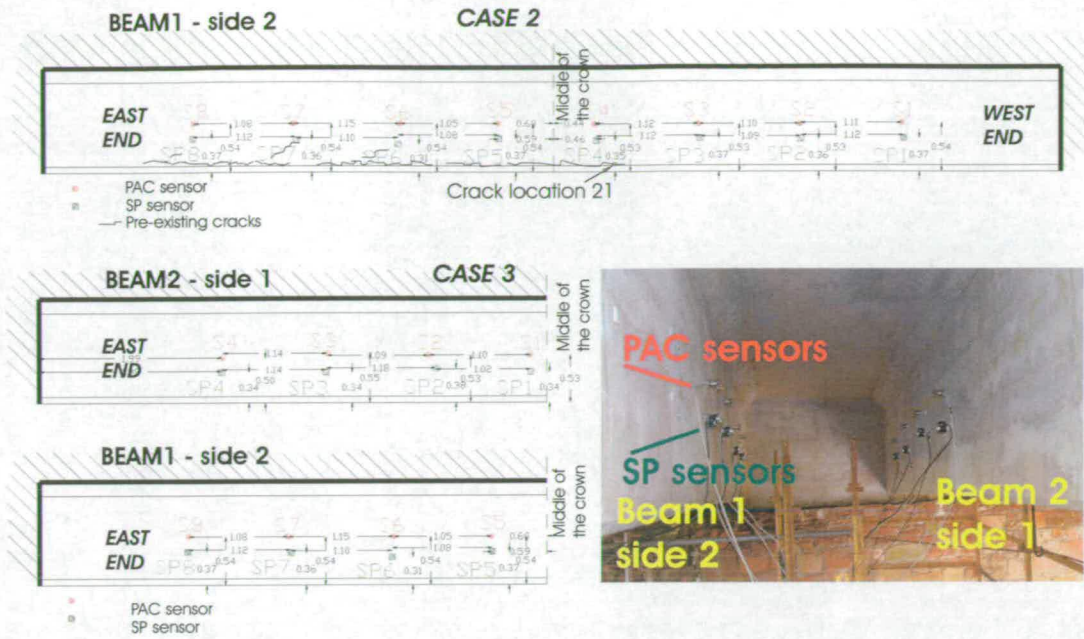


Figure 8.3: Boghall bridge. Location of sensors: Case 1 and 2.

and followed a regular trend (Figure 8.5). It can then be assumed that they did not affect the AE readings.

The data seemed not to be affected by the wind and the rain. This confirmed that the use of cable holders and ties was effective and the beams being at the centre of the structure resulted in them being protected from the direct action of the rain and wind.

8.4.2 Attenuation Study

In order to gain an understanding about the properties and uniformity of the concrete, a study of the AE signal attenuation and noise was undertaken.

The attenuation study consisted of an analysis of the amplitude of the signals generated by the pencil lead during the calibration of the sensors. The results are shown in Table 8.2.

The pencil lead was broken near to each sensor and it generated a signal that was recorded by the nearest sensor with an amplitude varying between 70 and 82 dB (the red values in the Table 8.2). In all cases, the signal was only able to reach the two sensors directly adjacent to the one near which the lead was broken. The amplitude of the signal when it reached these sensors is represented in the above mentioned table by the blue values.

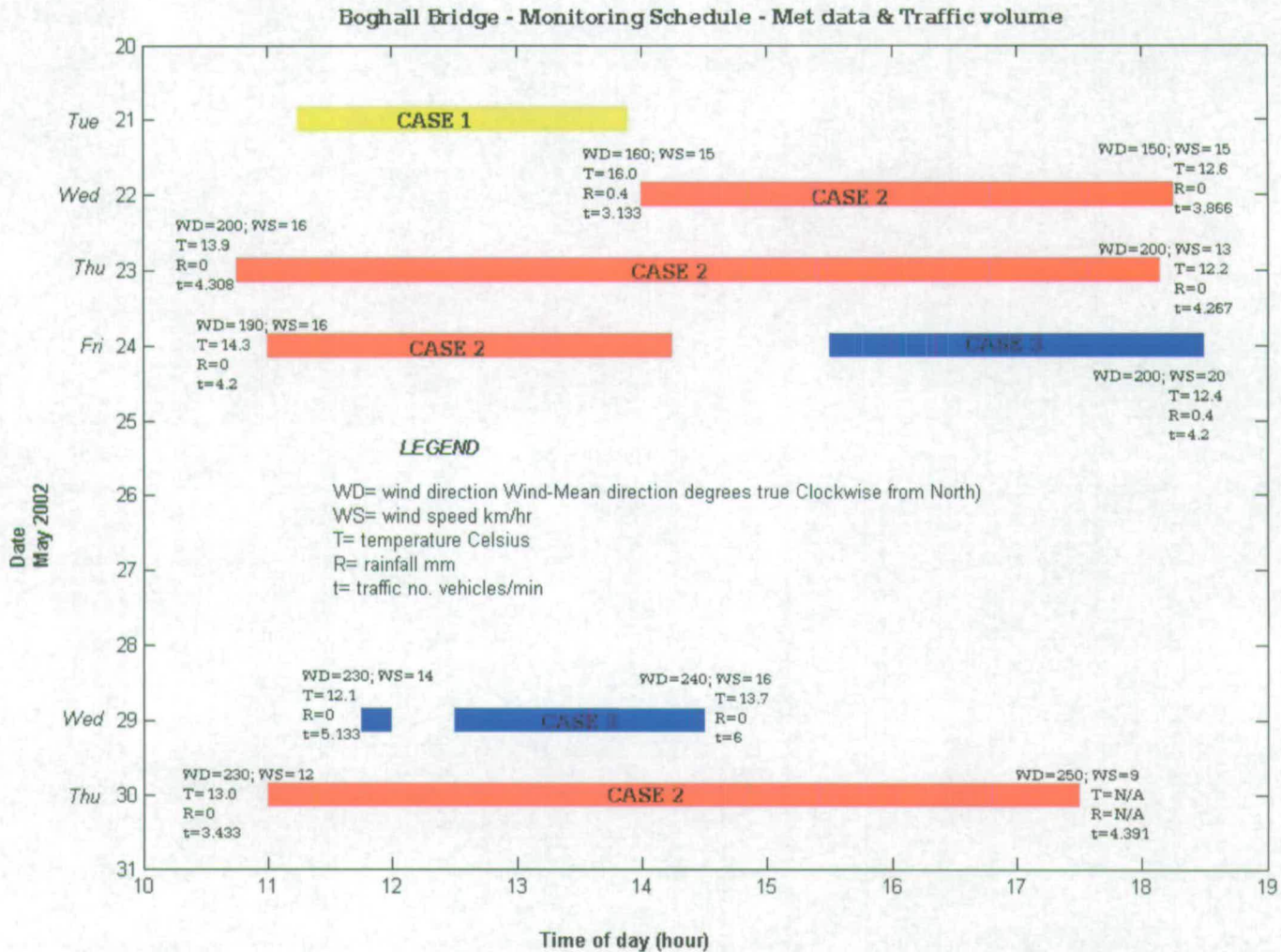


Figure 8.4: Monitoring schedule and meteorological data.

		EASTERN SIDE				WESTERN SIDE			
SENSOR INTERSPACE.		1.08m	1.15m	1.05m	1.04m	1.12m	1.10m	1.11m	
SENSOR NO.		8	7	6	5	4	3	2	1
S I G N A L								(34)	
								41 ← 75	
								(40) (41)	
								40 ← 80 → 39	
								(35) (31)	
								36 ← 71 → 40	
								(42) (32)	
								30 ← 72 → 40	
								(43) (36)	
								32 ← 75 → 39	
								(35) (36)	
								35 ← 70 → 34	
								(33) (35)	
								39 ← 72 → 37	
								(36) (38)	
								41 ← 77 → 39	
							(33) (36)		
							38 ← 71 → 35		
							(33) (34)		
							40 ← 73 → 39		
							(34) (36)		
							37 ← 71 → 35		
							(37) (41)		
							43 ← 80 → 39		
							(32) (33)		
							39 ← 71 → 38		
							(36) (40)		
							37 ← 73 → 33		
							(36) (41)		
							46 ← 82 → 41		
							(33)		
							76 → 43		

S
I
G
N
A
L

A
M
P
L
I
T
U
D
E

dB

Table 8.2: Boghall bridge: Results of attenuation study. The red values indicate the starting amplitude, whilst the blue values are the amplitude recorded by the near sensor. The drop of the amplitude is shown in brackets.

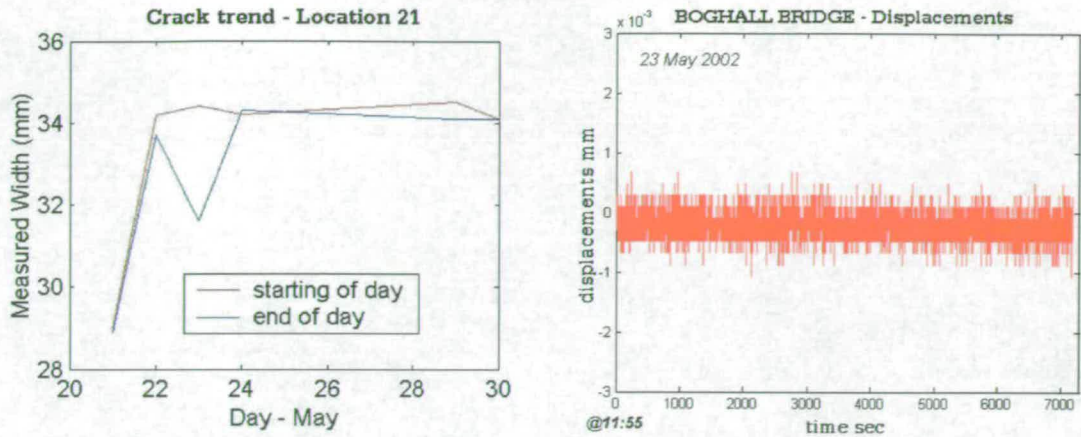


Figure 8.5: Boghall bridge: crack width (left) and bridge displacements (right).

By comparing the drop in the amplitude of the signals (values in brackets) it is possible to recognize two trends:

- in the western half of the beam (sensors 1 to 4) the average attenuation was approximately 35 dB over a distance of 1.10 m;
- in the eastern half of the beam (sensor 4 to 8) the average attenuation was approximately 38 dB over a distance of 1.10 m.

The attenuation appeared greater in the damaged eastern half of the beam, in agreement with the fact that the presence of cracks causes elastic scattering and anelastic absorption. This results in greater attenuation and then lower amplitude of the waves.

Although the threshold was fixed at 30 dB during the monitoring a 15 minutes test was carried out using the PAC system at the beginning or at the end of the day using a lower threshold of 25 dB, to verify if any information could be obtained about the noise level of the structure.

The location of the AE activity recorded during these tests is shown in Figure 8.6 both in terms of events and energy (see section 4.7). The graphs illustrate similar outputs. A few events, with no associated energy, were recorded - but only on the eastern side of Beam 1. This complied with what was expected, as the surfaces of the pre-existing cracks in that area are subject to friction that generates few acoustic

emissions which have low energy, resulting in the area being more noisy. No relevant data was obtained when the same study was carried out on Beam 2. A variation in the distribution of the noise level can then be indicative of a difference in the state of a structure.

8.4.3 AE Source Location - PAC Data

The analysis of the AE location consists of locating the AE sources. These sources can then be related to development or existence of crack patterns on the beams.

A linear location (alongside the beams) of the PAC data was carried out using the MISTRAS software (see section 4.7). The sources were located with reference to both the recorded events and energy but only the latter are shown here as previous results show that energy can be considered as the effective parameter to indicate the active damage of a structure (see section 7.2).

Case 1

On a bridge beam, it is the bottom part that is in tension and as a result this is the area where the cracks and the acoustic emissions are generally expected to develop. For this reason, in the first case study, all the sensors were placed underneath Beam 1. Very little AE activity was recorded and it was confined to the western area of the beam (Figure 8.7). This was thought to be due to the presence of the large visible cracks propagating alongside the eastern area. The existence of these cracks prevented the elastic waves from travelling through the concrete and reaching the sensors located on the underside of the beam. This led to the relocation of the sensors.

Case 2

With the second location of the sensors, Beam 1 was monitored for about four days and the results are shown in Figure 8.8. During three out of the four days, the data consistently showed that the majority of the AE activity was occurring on the western side of the beam. The cracks already visible on the eastern side generated acoustic emission but of lower energy as the opening up of existing cracks creates AE events of smaller amplitude and energy. Most of the energy is usually released during the formation and localisation of new microcracks (section 4.5). This suggests that the existing cracks on the western side are propagating towards the opposite side of the

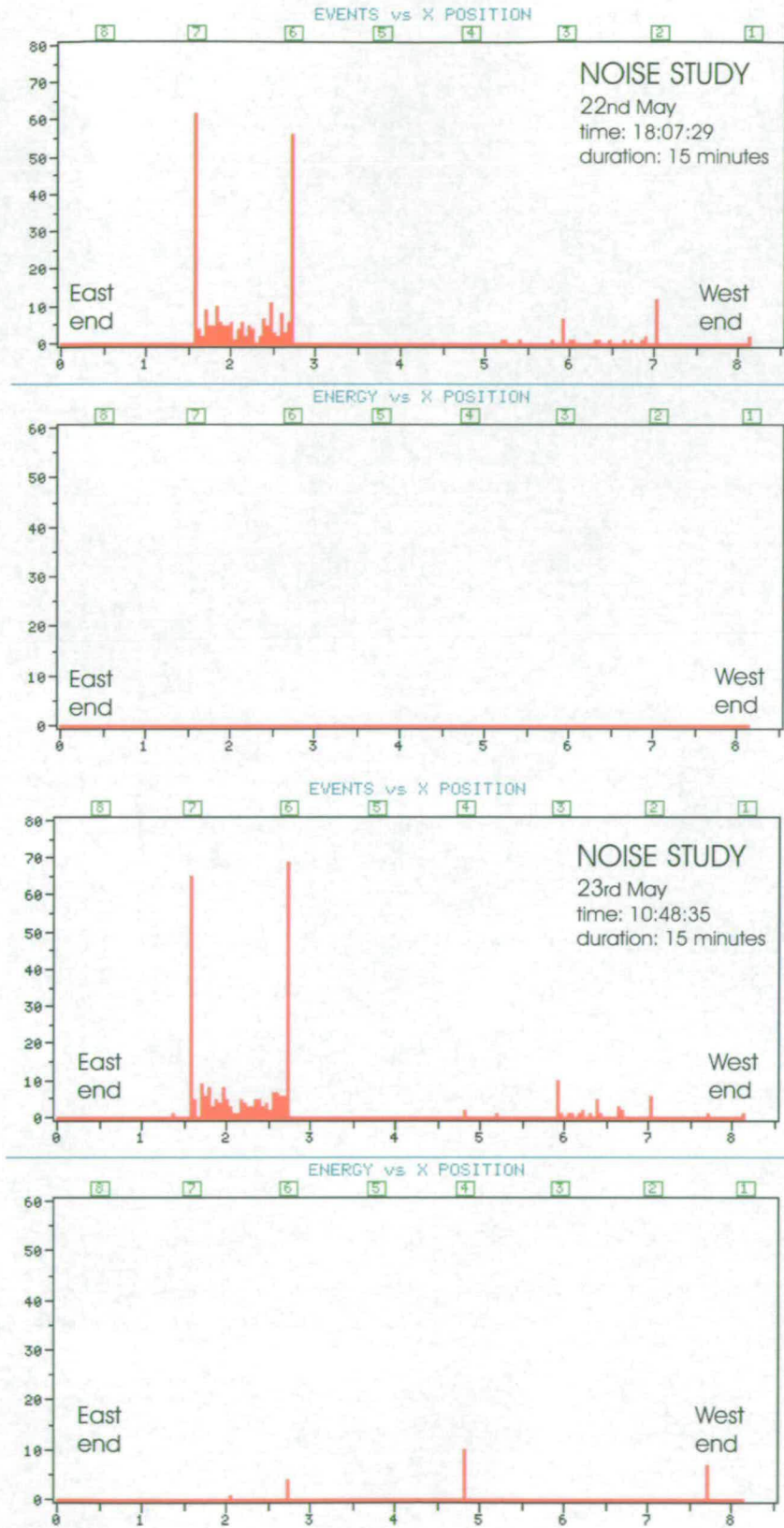


Figure 8.6: AE activity location: Noise study. The location along the beam is indicated on the x-axis in meters, whilst the green squares (on top) indicate the AE sensors.

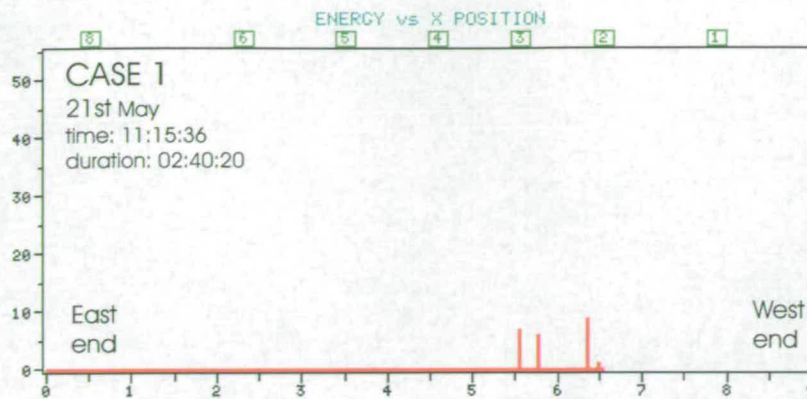


Figure 8.7: Boghall bridge. AE source location for Case 1, plotted as for Figure 8.6.

beam and that the process of corrosion is progressing. It has to be pointed out that a clearer pattern was observed on the 23rd and 30th of May, when a longer duration test was carried out. A longer monitoring time highlights the AE trend of the whole structure and minimises the influences due to single specific local events that can mislead the interpretation of the results. On the other hand long monitoring time would be less cost effective.

Case 3

Case 3 allowed a comparison between the behaviour of a badly damaged beam (Beam 1) and a beam that appeared to be in good condition (Beam 2). The results for the respective days of monitoring are shown in Figure 8.9. On the 24th May 2002, the wind was stronger (Figure 8.4) but this did not affect the results, showing that the use of cable holders and ties helped to prevent wind interference. Comparing the results to those obtained on Case 2, and taking into account the shorter duration of the test, much less AE activity was recorded in Case 3 - even if the volume of traffic (Figure 8.4) on those days appeared higher than during the previous days. Beam 1 did not show differences during the two monitoring days, as it was probably in a relatively stable condition. The results for Beam 2 showed very few emissions on the 24th of May, whilst more activity was recorded on the 29th of May. This can be explained by looking at the time of the recording. On the 24th of May the recording was made in the afternoon, when more traffic was travelling out of Edinburgh along the A697 thus running above Beam 1 (Figure 8.2). On the 29th, the data was acquired during

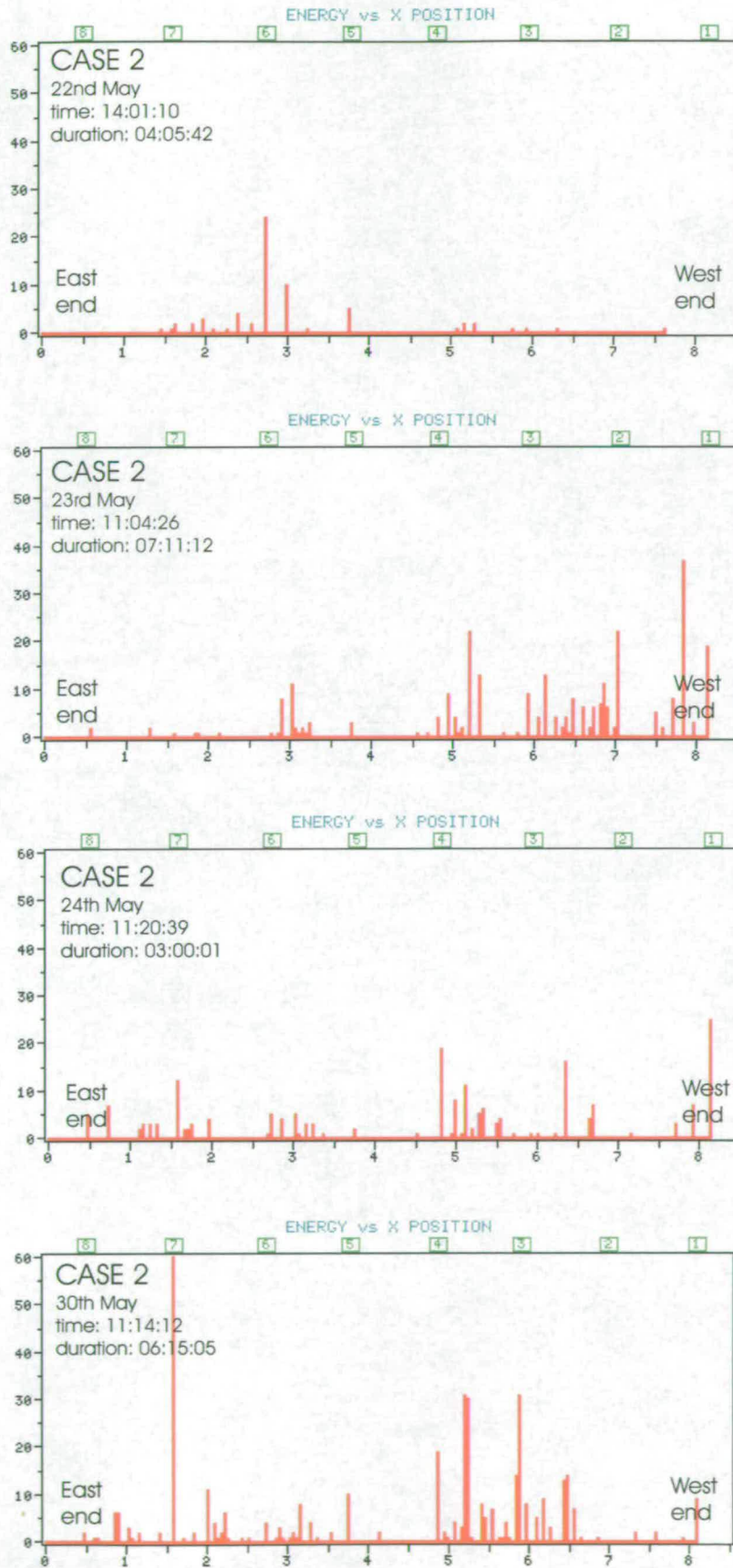


Figure 8.8: Boghall bridge. AE source location for Case 2, plotted as for Figure 8.6.

Case no.	Day	Total signals	Located signals	%
1	21st May	364	271	74%
2	22nd May	138	71	51%
2	23rd May	200	122	61%
2	24th May	79	44	56%
2	30th May	9	7	78%
3	24th May	173	64	37%
3	29th May	9	4	44%

Table 8.3: Boghall bridge: SP recorded and located signals.

lunchtime, when more vehicles were travelling towards Edinburgh and therefore over Beam 2. As Beam 2 appears to be in good condition and the east end of Beam 1 is already badly damaged (i.e. it does not generate high energy events), the structural response in terms of AE is limited and the traffic effect is relevant. This suggests that for totally reliable monitoring and easier comparisons the recordings should be done ideally at the same time and for the same duration. Once again, longer monitoring might have overcome the problem, allowing the identification of a pattern representing the structural behaviour of the beams.

8.4.4 AE Source Location - SP Data

A linear location of the data collected by the SP system was undertaken using the SP Analyst software and the results were plotted using Autocad. The filter developed during the TRL experiments (see section 7.4.1) was applied, but it led to a classification of all the signals as small cracks and therefore they were not located. For this reason, despite the time consuming nature of the undertaking, the signals were manually located for each case and each day of the monitoring. A summary of the total number of the recorded signals and the number of the located signals is shown in Table 8.3.

Case 1

Contrary to the results obtained from the PAC system, the largest number of signals were recorded when the sensors were located underneath the beam. The results (Figure 8.10) show that the majority of the AE activity was located on the east end with

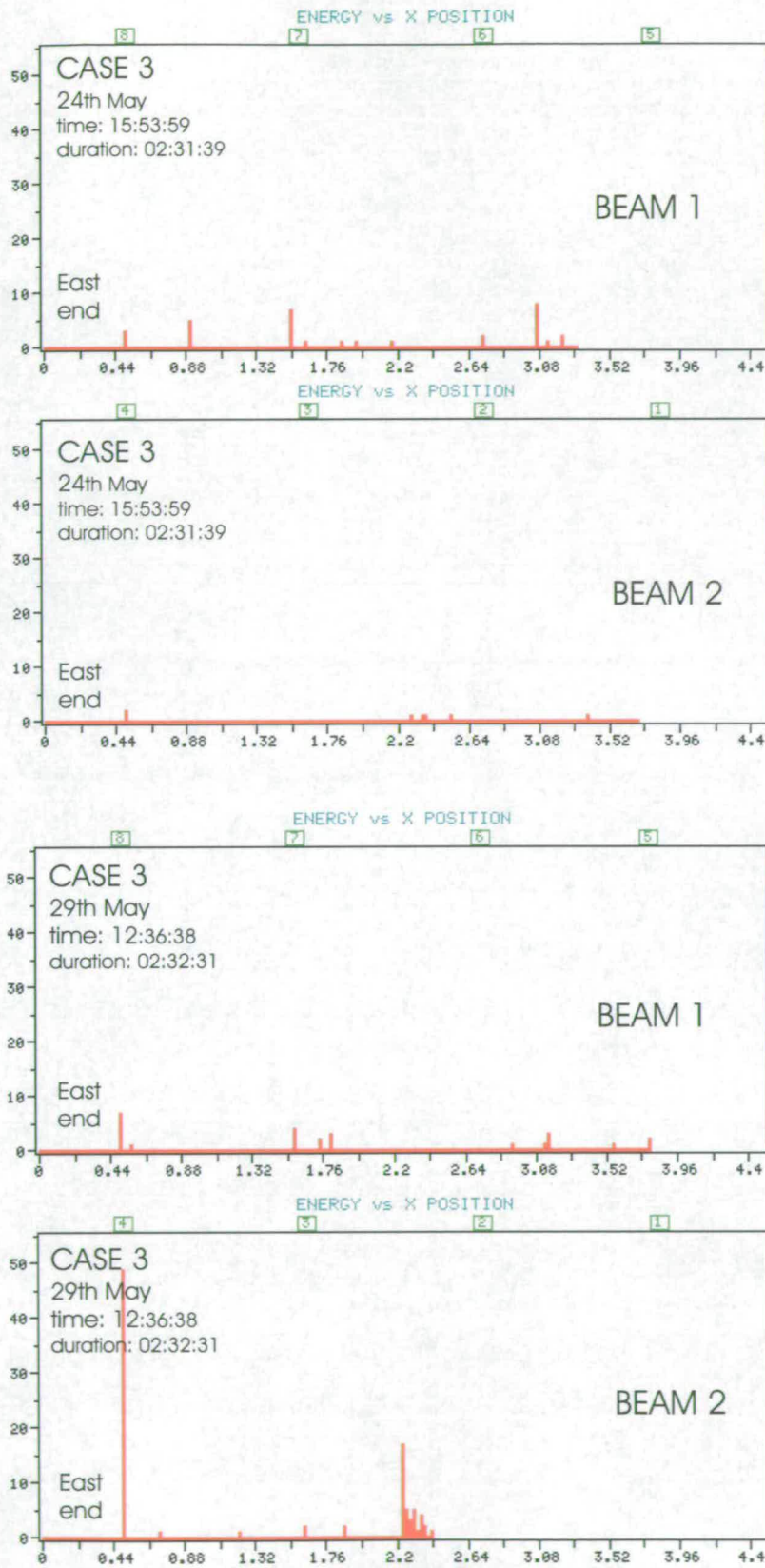


Figure 8.9: Boghall bridge. AE source location for Case 3, plotted as for Figure 8.6.



Figure 8.10: Boghall bridge. Location of the SP events, for Case 1. The green triangles represent the SP sensors, while the red circles show the located AE sources.

only 8% of the located signals derived from sources on the west end of the beam. A possible explanation is that as the SP sensors are more sensitive to low frequencies, their response is highly influenced by the noise derived from the existing cracks on the east area.

Case 2

The results of Case 2 (Figure 8.11) did not result in the emergence of any constant pattern during the three days of the monitoring. Once again this could be explained by the response and sensitivity of the SP transducers. As the SP sensors were located nearer to the bottom of the beam than the PAC's and thus nearer to the cracks, this might have amplified the influence of the existing cracks. No explanation could be found for the low number of events recorded on the last day. A visual analysis of the signals and their spectrum was performed in order to develop a filter, able to separate the signals coming from the two different sides of the beam - but no specific features needed for the filter could be identified.

Case 3

Fewer signals were located in relation to Case 3, and the AE sources were mainly coming from Beam 2 (Figure 8.12). Although the presence of low AE activity agrees in this case with the results obtained from the PAC system, it does not agree with the findings of the Case 2 as high activity on the cracked side of Beam 1 would be expected.

8.4.5 *b*-value Analysis

A *b*-value analysis of the PAC data was undertaken. The *b*-value was calculated using an interval range of amplitude of 3 dB for each day of monitoring and for each channel (see section 4.6). The results were plotted in Figure 8.13 and refer to the monitoring

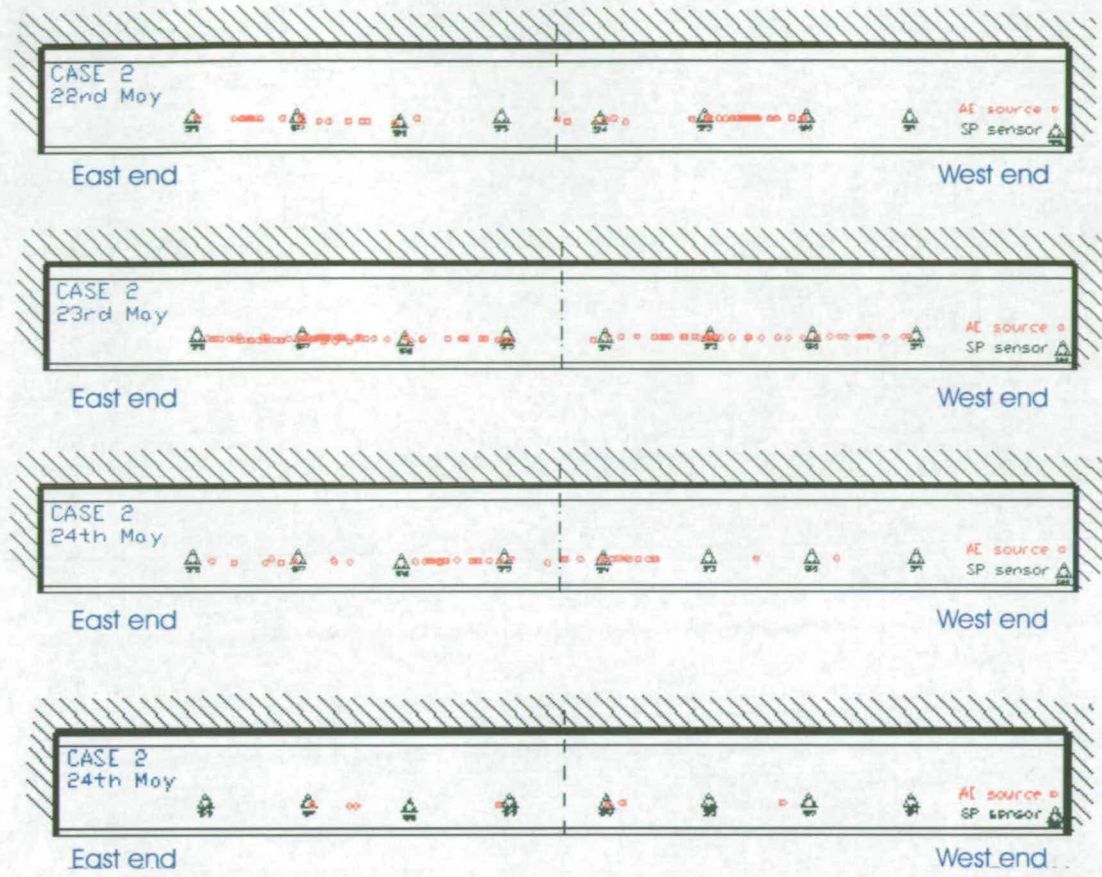


Figure 8.11: Boghall bridge. Location of the SP events, for Case 2, plotted as for Figure 8.10.



Figure 8.12: Boghall bridge. Location of the SP events, for Case 3, plotted as for Figure 8.10.

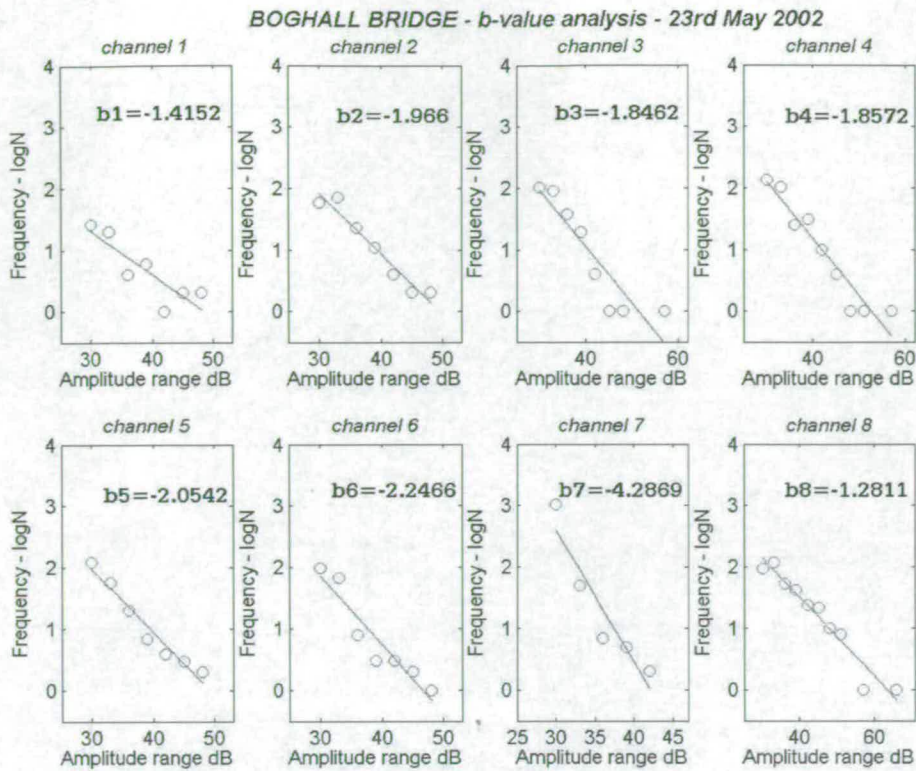


Figure 8.13: Boghall bridge: Frequency-magnitude plots and resulting b -value estimated on Beam 1.

of Case 2 on the 23rd of May. It can be seen that channels 5, 6 and 7 (east end) have a lower b -value than channels 1, 2, 3 and 4 (west end). This is due to the fact that the opening up of the existing cracks on the eastern end of the beam generated a large number of events but of small amplitude. Conversely, the possible formation of new cracks in the western areas created acoustic emissions of larger amplitude. Channel 8 showed a high b -value implying that the existing cracks may be growing also towards the western end of the beam, where it is possible that the corrosion is expanding and new cracks are occurring. The b -value analysis appears to support the results obtained from the previous data processing.

8.4.6 Old Monitoring Comparison

Monitoring of Boghall Bridge was undertaken at the beginning of 1999 using a PAC system and was reported by Shigeishi and associates [Shigeishi et al., 2001]. Although that research focused on the masonry arch, some data were collected from the concrete

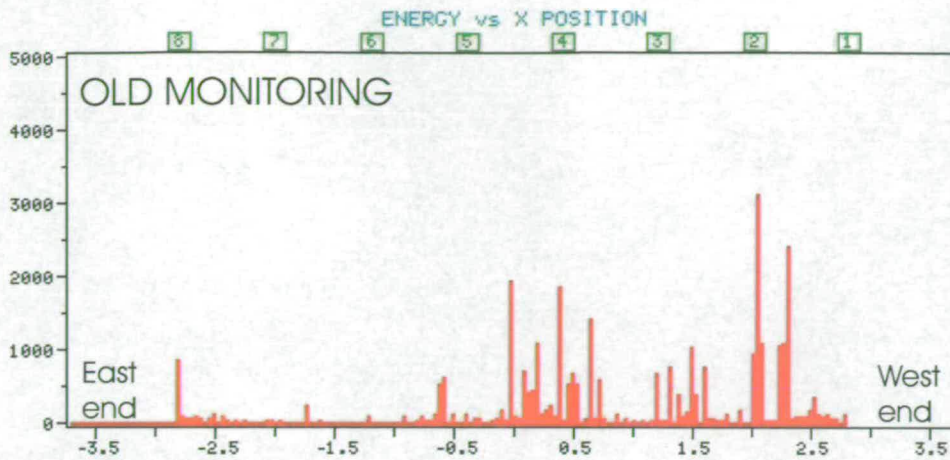


Figure 8.14: AE energy location: old monitoring results, plotted as for Figure 8.6.

beam (Beam 1 - side 1). The location of the AE energy activity from Shigeishi's study is shown in Figure 8.14. It shows that most of the AE activity was coming from the western end of the beam, suggesting that the cracks present on the eastern side were propagating into the opposite area. This observation agrees with the results obtained from the PAC system during the recent monitoring, suggesting that the damage situation has not changed and the beam has been stable during these years.

It must be pointed out that a larger number of events and larger amount of energy were recorded by the PAC system during the old monitoring study. This may be due to the fact that during 1999, a different type of sensor was used (R3I Resonant 30kHz Integral). As these transducers are resonant at a lower frequency, they were probably able to pick up a larger number of acoustic emissions. Since the earlier monitoring was carried out during winter, another possible explanation is that the heaviest rainfall occurred during that period together with the use of salt to avoid freezing - accelerating the rate of corrosion propagation and making the structure more acoustically active. However it remains more likely that the response can be attributed to the transducer sensitivity and frequency range.

8.5 Conclusions

This chapter provided an example and a detailed description of the application of the AE technique to a real structure. The AE method has proved to be a promising and effective means of investigating the condition of a concrete bridge. It allows one to

obtain an understanding of the structural condition of concrete bridge beams without any traffic disruption. From the undertaking of this study and the processing of the data, the following conclusions were drawn:

- A preliminary visual survey of the structure is always of fundamental importance to establish a first view of the state of the bridge.
- The presence of pre-existing cracks must be considered when deciding the sensor locations and when processing the data, as it affects the generation and detection of elastic waves.
- Environmental factors (rain, wind, temperature) as well as traffic volume must be considered in order to obtain a comprehensive understanding of the AE data.
- The cables should be clamped and fixed tightly in order to reduce wind interference.
- A preliminary study of the attenuation and noise can provide useful information about the condition of the structure.
- The location of the AE energy allows identification of the areas of highest activity, where possible damage is occurring, as visible cracking produces waves of low energy, whilst new internal cracks generate high energy signals.
- The monitoring should be repeated over time to allow verification of the results. For a more reliable comparison it is also advisable that such time is kept constant (both in terms of daily time and duration).
- A longer period of monitoring is preferred in order to obtain a realistic pattern of the AE activity and to minimise the effects of single events that can lead to misinterpretation of the data.
- The SoundPrint system was able to record AE activity on a real concrete structure but the response of the transducers was highly affected by the existing cracks. Some of the SP results were contradictory and at this stage a final conclusion about their significance could not be reached.
- The *b*-value analysis can be successfully applied on a real structure to distinguish between areas where macrocracking and/or microcracking are occurring.

- The existence of previous monitoring data is a useful feature in order to have an overview of the behaviour of the bridge over a period of years. Thus in order to verify the stability of a bridge's condition and to confirm and support the findings from AE work; the creation of a database containing information about the bridge stock should be developed.

The field work represented the last stage of this research. The next chapters will provide overall discussions and conclusions from this thesis.

Chapter 9

Overall Discussion

This chapter presents an overall discussion of the research reported in this thesis. As detailed discussions were already included in each of the previous chapters, only a few critical points are discussed herein and emphasis is mainly put on discussing the further work that could be carried out to continue the study presented herein.

This thesis investigated the feasibility of the Acoustic Emission (AE) technique to evaluate the structural condition of concrete bridges. The study consisted of two main stages - (1.) how to carry out an AE test in order to acquire useful data - (2.) how to analyse and interpret the AE data. The two phases are strongly interdependent, without correctly collected data the processing will rarely be successful. Vice-versa, if the aim and type of analysis required is not known, the recording of useful data is unlikely. Not all the data are suitable for certain types of analysis and thus the way they are recorded and the instrumentation settings that are used need to be determined in accordance with the required type of processing.

An experimental protocol was drafted for AE monitoring of bridges (section 5.6). It however should be pointed out that it merely provides general guidelines that identify the main steps to should be taken into consideration during an AE testing. Each bridge is a unique structure and thus has to be singly and specifically evaluated. Moreover as for most of the non-destructive methods, a complementary use of AE and other NDT techniques is desirable to support and strengthen the respective findings. One of the reasons for the mistrust that is sometimes related to NDT is caused by the lack of knowledge about the real possibilities and limits of

their applications. For this reason, during the thesis, emphasis was put on clearly stating the advantages and disadvantages of the AET and of the different analysis that were studied. Once again, a complementary use of NDT methods could overcome some of the disadvantages, as other techniques may be successful where the AET is not.

From an analysis of the AE literature (Chapter 3), several varied ways of analysing the data were found and few of them were personally applied to the data obtained from the experiments. Not all the attempted types of analysis have been included herein, only the ones that led to successful results and/or seem to be promising, have been reported. As the aim of this thesis was always very practical, the choice of processing was based on “practical” considerations, i.e. could it realistically be applied on real structures.

The proposed *b*-value analysis (section 7.1) appeared very promising but at this stage its application implies a continuous monitoring, possibly starting as soon as the bridge is built and it could therefore prove to be expensive for the owner of the bridge. Further work is needed to address this issue.

The AE source location analysis (section 7.2.1) is quick, easy, totally automatic and it has the significant advantage of being able to be carried out in real time. Its main drawback is that it provides only qualitative information, i.e. it can identify areas where acoustic emission is present and where damage may be occurring, but it cannot establish how serious that damage would be. On the other hand, this analysis can pinpoint areas acoustically active that can be investigated further with different AE analysis and/or NDT techniques.

The Relaxation ratio analysis (section 7.3) was proposed and it appeared to be very promising for practical applications. The novelty of this analysis lies in the use of the AE energy released during the unloading phase of a AE loading test, and which is generally not taken into consideration. However, the results obtained during the experiments suggested that the properties of the concrete and the loading rate affects the results. Notwithstanding the large amount of publications about AE work on concrete, no specific study was found about the correlation between the strength of

the concrete and the generated acoustic emissions or between the loading rate and the derived AE activity. The subject appeared very interesting and worthy of further investigation. Such an investigation should consist of testing several samples, changing one of the test features or concrete characteristics at the time. Data from field work are desirable at this stage. The procedure, based on this study and suggested to be applied to assess a bridge, needs further implementation once the possibilities and limits of the method have been clearly established. Only at this point, can one estimate the exact way of loading the bridge, the number of cycles required and the level of the applied load estimated. A cost effective analysis could then be carried out. Compared to the passive monitoring undertaken on Boghall bridge (Chapter 8) this type of AE testing would require a partial closure of the bridge. No closure is required during the installation of the system and the loading procedure could be done at night time, limiting the traffic disruption. Also, the bridge would not need to be tested all at once, so that partial lane closures only are needed.

The potential of the SoundPrint system to detect cracking in the concrete was investigated. Positive results were obtained, but at this stage some software modifications should be considered to better adapt it to deal with the large amount of AE events, that are usually generated during the fracture process. The filter utility incorporated within the existing software is however a powerful tool, and further investigation to verify if it could be able to distinguish between different types of crack is worth of study.

The Moment Tensor Analysis (section 7.5) is the method able to provide the most complete type of information. However its complex procedure and time consuming analysis are considered serious limitations towards its practical commercial application. The experiment reported in section 7.5 is a preliminary example to show the validity and high potential of the method. Due to the drawbacks, as well as time restrictions, no further experiments were carried out, although a field application would be highly desirable to test the MTA feasibility on-site. Further work to implement the software and increase the automation is needed and it is known that steps in this direction are currently being taken at Kumamoto University.

Working on-site always represents an interesting challenge. It starts from the necessity to find power sources in remote regions and continues through the need of data transfer, safely transporting the equipment and protecting it throughout the whole investigation. The case of the Boghall bridge described in Chapter 8 highlighted the issue of moving the systems. The SoundPrint is equipped with wheels that make its transportation on “asphalt like” roads very simple. Conversely, in the case of rough terrain (as for Boghall bridge) it needs to be lifted and its heavy weight represents an obstacle. Conversely, the PAC system is lighter but it has to be lifted in all circumstances. This sometimes created problems, such as the shifting of some of the internal hardware boards out of position and fixing on site. Work is necessary to improve these aspects of the systems. The safety of the instrumentation in relation to environmental factors as well as to human vandalism is a fundamental issue that needs to be taken into account, especially when permanent monitoring is required. It needs to be stressed that the collection of on-site data is a critical step to assess the real feasibility of the AE method.

The following chapter summarises the overall conclusions reached during the undertaking of this research project.

Chapter 10

Overall Conclusions

This chapter provides a summary overview of the conclusions reached during this research and already described in detail in the previous chapters.

10.1 Bridges

- Bridges represent a fundamental part of the asset of a country and their maintenance is a critical issue. Throughout the history of their development, their aspect evolved, their structural characteristics were modified and different problems arose (section 2.1). Concrete bridges constitute a particular type of bridge with its specific features and problems (section 2.2) and recently, as a consequence of their age:

- UK bridges: 25-35 year old
- USA bridges: 30-45 year old

they have started to show signs of distress. The necessity to assess their safety is thus a matter of concern (section 2.3). This thesis investigated the feasibility to use the Acoustic Emission (AE) technique to evaluate the structural integrity of concrete bridges.

10.2 AE Method

- The AE method was not born as a civil engineering tool and its application to concrete started in the 1960s. A review of AE work on concrete was undertaken

(section 3.2) to gain an understanding of the theory, instrumentation and different factors that influence and have to be taken into account during an AE test (Chapters 4 and 5). Although the AET started to be used on steel bridges in the 70s and a few years later on concrete bridges (section 3.4), no “standardised procedure” for its application to bridges existed in the UK (sections 3.5 and 5.6) prior to that suggested in this thesis on the basis of the author’s experience.

Two main and intercorrelated phases of an AE test were identified and investigated:

- (a) - the acquisition of AE data
- (b) - the processing of the AE data.

The investigation required the undertaking of several experiments, during which two different types of AE systems were used, the PAC and the SoundPrint system. The laboratory tests included six RC beams at the University of Edinburgh (Scotland), two full scale RC beams at the Transport Research Laboratory (England), plus six RC beams and a concrete sample at Kumamoto University (Japan). An on-site monitoring of a RC bridge in the Scottish Borders was also carried out (Chapter 8).

- An experiment on different couplant materials was carried out. Plasticine (2 mm thick) was seen to be a valid alternative to superglue, when temporary monitoring is required.
- In relation to the first above mentioned stage the results and experience gained throughout the undertaking of both the laboratory and the on-site tests identified some key factors that have to be taken into account before and during an AE testing:
 - preliminary survey
 - aim of the test
 - choice of sensor
 - sensor location
 - sensor mounting
 - instrumentation settings
 - sensor calibration

- noise and attenuation study
- complementary measurements and environment

If correctly considered these factors would lead to useful AE data and therefore to a successful analysis and results. From the above, an experimental protocol was drafted (section 5.6).

10.3 Analysis

The analysis and interpretation of the AE data, which represents the second stage of an AE test, is often not a trivial matter. To address this issue, different types of processing were investigated and alternative ways of analysis of the data were developed.

10.3.1 *b*-value Analysis

A conventional *b*-value analysis was applied and proposed (section 7.1).

- The trend of the *b*-value showed good agreement with the cracking appearing during the test, confirming that the *b*-value is correlated to the fracture process of the concrete and to the degree of localisation of damage and it is able to distinguish between the formation of macrocracks and microcracks growth.
- The use of the *b*-value analysis to interpret data obtained by “local monitoring” of concrete bridges was suggested, although the need for further work to make the *b*-value suitable for practical use was highlighted.

10.3.2 Source Location

An AE source location analysis was undertaken to investigate the relationship between the AE events and AE energy locations and the cracks as they appeared on the beams (section 7.2.1).

- The located activity showed a good agreement with the crack pattern mapped on the beams although its accuracy was higher in the early cycles when less cracks were present.
- The AE activity/crack correlation was stronger in term of AE energy than AE events, especially in relation to the formation of new cracks.

- The located energy showed concentrations of activity where cracks were not visibly present, but subsequently appeared and thus the AE energy can be considered a precursor of the failure and an effective parameter to indicate and anticipate the damage of a concrete structure.

This type of analysis is relatively quick and easy to interpret, but it only provides a qualitative assessment of a structure and no quantitative information about the state of damage can be obtained.

10.3.3 Relaxation Ratio

The issue of a quantitative assessment method was addressed by developing a new type of analysis, based on the definition of a new parameter, the “relaxation ratio” (section 7.3). Some disagreements, between the results obtained from different samples were found, so that only preliminary conclusions can be drawn at this stage.

- The method of analysis seemed very promising to define the state of damage of concrete beams - as structurally serious damage condition should result in the relaxation phase being dominant and thus a relaxation ratio greater than one.
- The results were affected by the different properties of the concrete (type and strength) and the loading rate used during the experiments.
- The successful results obtained at this stage were supported by comparison with the NDIS assessment procedure.
- On the basis of these results a full load test procedure for a real bridge was suggested, although further analysis is needed to define the limits of the method.

10.3.4 SoundPrint

The SoundPrint system was not originally designed to detect cracking in concrete and work focused on evaluating the potential of the system to address this task during the small and full scale experiments (section 7.4).

- In both the small and full scale experiments, the system was able to: (a) record AE data generated by concrete cracking, and (b) to identify acoustically active regions and thus locate AE events corresponding to the visible cracks. A clear

pattern of the AE activity generally emerged when approximately 50-60% of the ultimate load was reached.

- In the small scale tests the location process was affected by the number of cracks, as fewer events were located when a large amount of cracks were formed, i.e. during the last cycles of the experiments. The location of the events had to be done using the manual option of the SP software as the Decision Tree classified all the events as “small cracks” and thus did not locate them. The process was therefore very time consuming.
- On the full scale tests, the accuracy of the longitudinal location was greater than the vertical one.
- The results, in terms of energy, of the full scale tests obtained with the PAC and SP systems agreed with each other and, as previously found during the AE location study, high energy characterized serious structure damage.
- The differences and similarities of the SP and PAC systems were discussed, in terms of equipment, settings, filtering and targets.

10.3.5 Moment Tensor Analysis

The MTA was studied and the MTA procedure was discussed, summarized and applied (section 7.5).

- The results obtained by the MT experiment provided complete information about the location, type and orientation of the cracks, in good agreement with the failure of the sample. The validity of the method was thus confirmed, although only approximately 6% of the data collected could be processed through all the stages of the analysis.
- A few drawbacks were identified:
 - The analysis is highly time consuming, as many steps have to be undertaken manually. This manual aspect makes both the quantity and the quality of the results dependent on the individual skills of the operator, whilst being time consuming, making it “non-commercial”.

- The final visualization step of the procedure is at this stage incompatible with non Japanese software.
- During the test, one of the AE sensors has to be positioned near to the expected failure and this implies a knowledge of where the failure will occur.

10.3.6 Full - Scale Field Test

Finally, a field monitoring of a real concrete bridge was carried out. The AET proved to be a promising and effective means of investigating the condition of the bridge, allowing one to obtain an understanding of the structural condition of concrete bridge beams without any traffic disruption (Chapter 8).

- After a survey of the structure, a number of factors were identified which would affect the AE investigation: the presence of pre-existing cracks; environmental factors (rain, wind, temperature) as well as traffic; the need to use clamps and cable holder and ties to reduce wind interference; the need to undertake a study of the attenuation and noise to obtain preliminary information about the general condition of the structure.
- The AE energy locations pinpointed areas of highest activity, where possible damage was occurring.
- The monitoring was repeated over time to allow verification of the results. Also, a longer period of monitoring was found to provide a more realistic pattern of the AE activity and to minimise the effects of single events that can lead to misinterpretation or distortion of the data.
- The SoundPrint system was able to record AE activity but the response of the transducers was highly affected by the existing cracks. Some results were contradictory and a final conclusion could not be reached.
- The *b*-value analysis was successfully applied and it distinguished between areas where macrocracking and/or microcracking was occurring.
- The existence of previous monitoring data was a useful feature to obtain an overview of the behaviour of the bridge over a period of years. A database containing information about the bridge stock should therefore be created.

Overall, the feasibility and potential of the application of the AE method to assess concrete bridges was demonstrated in a positive way. An experimental protocol was drafted and alternative and new ways of data processing and interpretation were discussed and proposed.

10.4 Further Work

Further work is desirable to implement the conclusions reached at this stage.

1. Work is needed to make the b -value suitable for practical use. More in-situ data are desirable as well as the creation of a database that would allow an analysis of the variation of the b -value trend over a period of time. A reduction of the equipment cost is desirable, as this would make the installation of a continuous AE monitoring system on significant bridges easier. On continuous data, the b -value analysis could then provide vital information about the condition of a bridge.
2. Further experiments are needed to establish in which exact conditions the relaxation ratio analysis is successful. The limits of its application and the confirmation of its validity need to be investigated. These experiments should consider a large variety of samples tested in different ways with one parameter changing at a time. Particular emphasis should be placed on studying the effect of different loading rates and different types and strength of concrete. On site trials would also be indispensable. Once this stage would be concluded, a final procedure to apply this type of analysis to bridge loading test could be drafted.
3. Further work on the SoundPrint system is necessary. This should include alterations to the system software, in order to be able to automatically deal with large amounts of data. Field data are needed to confirm its feasibility to detect and distinguish concrete cracking on a real structure.
4. Effort needs to be expended to spread the application of the Moment Tensor method. In order to achieve this, the automation of the whole process of the analysis needs to be implemented.

5. Finally a full field trial on a representative sample of bridges of different ages, designs and locations is highly desirable.

References

- [Beckett, 1969] Beckett, D. (1969). *Bridges*. Hamlyn Publishing Group Ltd. pp. 191.
- [Berthelot et al., 1993] Berthelot, J. M., Souda, M. B., and Robert, J. L. (1993). Frequency analysis of acoustic emission signals in concrete. *Journal of Acoustics*, 11(1):11–18.
- [Bordyugov and Erminson, 1993] Bordyugov, D. M. and Erminson, A. L. (1993). Acoustic emission energy in fracture of concrete. *Russian Journal of Nondestructive Test*, 28(9):534–537.
- [Bradshaw et al., 2002] Bradshaw, T., Holford, K., Cole, P., and Davies, A. (2002). Ball bearing calibration of concrete structures using acoustic emission. In Mazal, P., editor, *Proc. of the EWGAE 2002- 25th European Conf. on Acoustic Emission Testing*, volume I, pages 91–97, Prague, Czech Republic. Czech Society for Non-destructive Testing.
- [Brunner and Bohse, 2002] Brunner, A. J. and Bohse, J. (2002). Acoustic emission standards and guidelines 2002: a comparative assessment and perspectives. *www.NDT.net*, 7(09):1–8.
- [BS, 1986a] BS (1986a). *British Standards 1881: Part 201: 1986 Guide to the use of non-destructive methods of test for hardened concrete*. Standards Committee.
- [BS, 1986b] BS (1986b). *British Standards 1881: Part 203: 1986 Recommendations for measurement of velocity of ultrasonic pulses in concrete*. Standards Committee.
- [BS, 2000] BS (2000). *British Standards EN 1330-9:2000 Non Destructive Testing Terminology - Part 9: Terms used in acoustic emission testing*. Standards Committee.
- [Bungey and Millard, 1996] Bungey, J. H. and Millard, S. G. (1996). *Testing of concrete structures*. Chapman & Hall. pp. 47–74.

- [Carter and Holford, 1996] Carter, D. C. and Holford, K. M. (1996). I.M.A.G.I.N.E: letting bridges do the talking. *Insight*, 38(11):775–779.
- [Carter and Holford, 1998] Carter, D. C. and Holford, K. M. (1998). Strategic considerations for the AE monitoring of bridges - a discussion and a case study. *Insight*, 40(2):103–109.
- [Chubb, 2000] Chubb, M. S. (2000). The bridge assessment and strengthening programme: the maintaining agent's views. In *ICE 2000 Conf. "Bridge Rehabilitation in the UK: review of the current programme and preparing for the next" 2-3 Oct. 2000*, London, UK. The Institution of Civ. Eng.
- [Collact, 1985] Collact, R. A. (1985). *Structural Integrity Monitoring*. Chapman and Hall Ltd. Ch.11, pp.386-411.
- [Colombo, 1999] Colombo, S. (1999). *Application of NDT to the investigation of masonry structures*. Politecnico di Milano - Dott. Ing. Thesis, Italy.
- [Colombo and Forde, 2001] Colombo, S. and Forde, M. C. (2001). AE experiments on concrete beams: general overview and research in progress on bridges. In Forde, M., editor, *Proc. of the Int. Conf. on Structural Faults + Repairs - 2001*, volume Cd-rom, London.
- [Colombo et al., 2000] Colombo, S., Forde, M. C., and Das, P. C. (2000). Improving impact echo and radar NDT data interpretation using uncertainty analysis technique. In *ICE 2000 Conf. "Bridge Rehabilitation in the UK: review of the current programme and preparing for the next" 2-3 Oct.2000*, London, UK. The Institution of Civ. Eng.
- [Colombo et al., 2002] Colombo, S., Main, I. G., Forde, M. C., and Halliday, J. (2002). AE on bridges: experiments on concrete beams. In Mazal, P., editor, *Proc. of the EWGAE 2002 - 25th European Conf. on Acoustic Emission Testing*, volume I, pages 127–134, Prague, Czech Republic. Czech Society for Non-destructive Testing.
- [Costin, 1989] Costin, L. S. (1989). *Fracture Mechanics of rock*. Academic Press Inc London. Ch. 5, pp. 167–203.
- [Cox and Meredith, 1993] Cox, S. J. D. and Meredith, P. G. (1993). Microcrack formation and material softening in rock measured by monitoring acoustic emission. *Int J. Rock Mech Min Sci & Geomech*, 30(1):11–21.

- [Cullington et al., 1999] Cullington, D. W., MacNeil, D., Paulson, P., and Elliot, J. (1999). Continuous acoustic monitoring of grouted post-tensioned concrete bridges. In Forde, M., editor, *Proc. 8th Int. Conf. Structural Faults + Repair - 1999.*, London.
- [Das, 2000] Das, P. C. (2000). Background to the current bridge rehabilitation programme and future needs - estimating uncertainty in bridge assessments. In *ICE 2000 Conf. "Bridge Rehabilitation in the UK: review of the current programme and preparing for the next" 2-3 Oct. 2000*, London, UK. The Institution of Civ. Eng.
- [Drouillard, 1986] Drouillard, T. F. (1986). AE Literature - Concrete. *J. Acoustic Emission*, 5(2):103–109.
- [Dunegan and Harris, 1969] Dunegan, H. L. and Harris, D. O. (1969). Acoustic emission - a new nondestructive testing tool. *Ultrasonics*, 7(3):160–166.
- [Dunegan et al., 1968] Dunegan, H. L., Harris, D. O., and Tatro, C. A. (1968). Fracture analysis by use of acoustic emission. *Engineering Fracture Mechanics*, 7(3).
- [Dunegan and Tatro, 1967] Dunegan, H. L. and Tatro, C. A. (1967). Passive pressure transducer utilizing acoustic emission. *Review of Scientific Instruments*, 38:1105–1147.
- [Elliot et al., 2002] Elliot, J., le Diouren, T., and Stubler, J. (2002). Continuous remote acoustic health monitoring of tensioned elements in structures. In *Proc. of the 1st Fib Congress*, volume CD-rom, Osaka, Japan.
- [Encyclopedia, 1980] Encyclopedia (1980). *Contemporary Architects*. Muriel Emanuel Ed. - The Macmillan Press Ltd. pp. 260-261.
- [Farid, 2001] Farid, U. A. K. M. (2001). *Fracture toughness of concrete and analysis of crack propagation*. Master's thesis, Graduate School of Science and Technology Kumamoto University, Japan.
- [Farid and Ohtsu, 2002] Farid, U. A. K. M. and Ohtsu, M. (2002). BEM analysis of mixed-mode crack propagation due to corrosion of reinforcement in concrete. *J. Materials, Conc. Struct. Pavements, JSCE*, 55(704):271–280.
- [Finck et al., 2002] Finck, F., Grosse, C. U., Reinhardt, H. W., Motz, M., and Kroplin, B. H. (2002). Integrated interpretation and visualization of a pull-out test using

- finite element modelling and quantitative acoustic emission analysis. *www.NDT.net*, 7(09):1-10.
- [Finegan and Hogg, 2000] Finegan, N. and Hogg, V. (2000). The next Steady State Bridge Programme. In *ICE 2000 Conf. "Bridge Rehabilitation in the UK: review of the current programme and preparing for the next" 2-3 Oct. 2000*, London, UK. The Institution of Civ. Eng.
- [Forde, 1992] Forde, M. C. (1992). Non-destructive evaluation of bridges: research in progress. CPD Course Note - The University of Edinburgh - UK.
- [Frangopol and Kong, 2001] Frangopol, D. M. and Kong, J. S. (2001). Bridge management based on reliability states and whole life costing: from theory to implementation. In Forde, M., editor, *Proc. of the Int. Conf. on Structural Faults + Repairs - 2001*, volume CD-rom, London.
- [Fugro, 2000a] Fugro (2000a). Soundprint acoustic monitoring - A453 River Soar Bridge. Fugro structural monitoring - confidential proposal report, Fugro, UK.
- [Fugro, 2000b] Fugro (2000b). Soundprint acoustic monitoring - Mossband viaduct - Cumbria. Fugro structural monitoring - confidential proposal report, Fugro, UK.
- [Gong et al., 1992] Gong, Z., Nyborg, E. O., and Oommen, G. (1992). Acoustic emission monitoring of steel railroad bridges. *Material Evaluation*, 50(7):883-887.
- [Green, 1970] Green, A. T. (1970). Stress wave emission and fracture of prestressed concrete reactor vessel materials. In ASME, editor, *Proc. 2nd InterAmerican Conference Materials Technology*, volume 1, pages 635-649.
- [Grosse, 2002] Grosse, C. U. (2002). Editorial: Special issue on acoustic emission. *www.NDT.net*, 7(09).
- [Grosse et al., 1995] Grosse, C. U., Reinhardt, H., and Dahm, T. (1995). Localisation and classification of fracture types in concrete with quantitative acoustic emission measurement. In Schickert, G. and Wiggenger, H., editors, *International Symposium Non-Destructive Testing in Civil Engineering NDT-CE*, volume 1, pages 605-612, Berlin, Germany.

- [Grosse et al., 2002] Grosse, C. U., Reinhardt, H. W., Motz, M., and Kroplin, B. H. (2002). Signal conditioning in acoustic emission analysis using wavelets. *www.NDT.net*, 7(09):1–9.
- [H-A, 2002] H-A (2002). Non-destructive evaluation of bridges: research in progress. Highways Agency Internal Draft Report, Ch.7, “private communication, unpublished”.
- [Hansford et al., 2001] Hansford, M., Paranhos, P., and Chrimes, M. (2001). Portuguese bridge disaster blamed on illegal dredging. *New Civil Engineer*, pages 5–6.
- [Hayter, 2000] Hayter, G. (2000). The 15 Year Bridge rehabilitation programme of the Highways Agency: lessons for the future. In *ICE 2000 Conf. “Bridge Rehabilitation in the UK: review of the current programme and preparing for the next” 2-3 Oct. 2000*, London, UK. The Institution of Civ. Eng.
- [Henning, 1988] Henning, D. (1988). Josef Kaiser: His achievements in acoustic emission research. *Materials Evaluation*, 46:193–195.
- [Hick et al., 1992] Hick, H., Willer, H., and Winter, E. (1992). Acoustic emission measurement on bridges. *Acoustic Emission*, 10(3/4):67–70.
- [Hill et al., 2002] Hill, M. E., Bradbury, T., and Cullington, D. W. (2002). Acoustic monitoring of concrete bridges - TRL beam trials. Technical report, TRL. pp.1-24.
- [Hodgson, 1942] Hodgson, E. A. (1942). Velocity of elastic waves and structure of the crust in the vicinity of Ottawa, Canada. *Bulletin of the Seismology Society of America*, 32(4):249–255.
- [Iwanami et al., 1997] Iwanami, M., Kamada, T., and Nagataki, S. (1997). Application of acoustic emission technique for crack monitoring in RC beam. In *JCA Proceedings of cement & concrete*, number 51, pages 192–197.
- [Kamada et al., 2000] Kamada, T., Asano, M., Lim, S., Kunieda, M., and Rokugo, K. (2000). Evaluation of fracture in concrete joint by acoustic emission. *Progress in Acoustic Emission X - The Japanese Society for NDI*, pages 207–212.

- [Keru et al., 2000] Keru, W., Chen, B., and Yao, W. (2000). Study on the AE characteristics of fracture process of mortar, concrete and steel-fiber reinforced concrete beams. *Cement and Concrete Research*, 30:1495–1500.
- [Kishinouye, 1934] Kishinouye, F. (1934). An experiment on the progress of fracture (A preliminary report). *Jishin*, 6:25–31. In Japanese.
- [Knopoff and Randall, 1970] Knopoff, L. and Randall, M. J. (1970). The compensated linear-vector dipole: A possible mechanism for deep earthquakes. *J. Geophys. Res.*, 75(26):4957–4963.
- [Koppel and Vogel, 2000] Koppel, S. and Vogel, T. (2000). Localisation and identification of cracking mechanism in reinforced concrete using acoustic emission. In M.J. Ryall, G. P. and j.E. Harding, editors, *Bridge Management 4*, pages 88–95. Dept. Civ, Eng. University of Surrey, UK, Thgomas Telford.
- [Lawn, 1993] Lawn, B. (1993). *Fracture of brittle solids - 2nd Edition*. Cambridge University Press. pp.378.
- [Leaird, 1984] Leaird, J. D. (1984). A report on the pulsed acoustic emission technique applied to masonry. *Journal of Acoustic Emission*, 3(4):204–210.
- [L'Hermite, 1960] L'Hermite, R. G. (1960). Volume changes of concrete. In *Fourth International Symposium on the Chemistry of Cement*, pages 659–694, Washington D.C.
- [Li and Xi, 1995] Li, Z. and Xi, Y. (1995). Application of acoustic emission technique to detection of concrete cracking and rebar corrosion. In G.Schickert and Wiggendauser, H., editors, *International Symposium Non-Destructive testing in Civil Engineering NDT- CE*, volume 1, pages 613–620, Berlin, Germany.
- [Liebenberg, 1992] Liebenberg, A. C. (1992). *Concrete Bridges: Design and Construction*. Longman Scientific and Technical. pp.280.
- [Lynn and Fuerst, 1989] Lynn, P. A. and Fuerst, W. (1989). *Digital Signal Processing with Computer Applications*. John Wiley & Sons Anchor Press Ltd. pp.359.
- [Main, 1991] Main, I. G. (1991). A modified Griffith criterion for the evolution of damage with a fractal distribution of crack lengths: application to seismic event rates and *b*-values. *Geophys. J. Int.*, 107(353–362).

- [Main and Meredith, 1991] Main, I. G. and Meredith, P. G. (1991). Stress corrosion constitutive laws as a possible mechanism of intermediate-term and short-term seismic quiescence. *Geophys. J. Int.*, 107(363–372).
- [Main et al., 1993] Main, I. G., Sammonds, P. R., and Meredith, P. G. (1993). Application of a modified Griffith criterion to the evolution of fractal damage during compressional rock failure. *Geophys. J. Int.*, 115(367–380).
- [Mallet, 1994] Mallet, G. P. (1994). *Repair of concrete bridges*. TRL - Thomas Telford Services Ltd. pp.194.
- [Manthei et al., 2001] Manthei, G., Eisenblatter, J., and Dahm, T. (2001). Moment tensor evaluation of acoustic emission sources in salt rock. *Construction and Building Materials*, 15:297–309.
- [Manual, 2002] Manual (2002). *Laser Doppler Vibrometer - User Manual*. Polytec.
- [McCabe et al., 1976] McCabe, W. M., Koerner, R. M., and Load, Jr, A. E. (1976). Acoustic emission behaviour of concrete laboratory specimens. *ACI Journal*, 13:367–371.
- [McGown et al., 2000] McGown, A., Telford, I., and Johnstone, R. (2000). The choice and performance of the instrumentation used to monitor the Kingston Bridge complex, Glasgow. *Structural Monitoring BSSM Workshop - University of Strathclyde - Glasgow*. 1st Nov 2000.
- [Miller et al., 1987] Miller, A., Richards, J. M., Browitt, C. W. A., and McCann, D. M. (1987). Preliminary studies of microseismic activity in an abandoned limestone mine. In Forde, M., editor, *Proceedings International Conference on Foundations and Tunnels*, volume 2, pages 50–59, University of London, Goldsmith College. Engineering Technics Press.
- [Mindess, 1982] Mindess, S. (1982). Acoustic emission and ultrasonic pulse velocity of concrete. *The International Journal of Cement Composites and Lightweight Concrete*, 4(3):173–179.
- [Mock, 1949] Mock, E. B. (1949). *The architecture of bridges*. The museum of Modern Art, New York. pp. 127.

- [Moczko et al., 1995] Moczko, A., Pszonka, A., and Stroeven (1995). Acoustic emission as a useful tool for reflecting cracking behaviour of concrete composites. In G. Schickert and W. Wigggenhauser, H., editors, *International Symposium Non-Destructive testing in Civil Engineering NDT-CE*, volume 1, pages 805–812, Berlin, Germany.
- [Mori and Obata, 1988] Mori, Y. and Obata, Y. (1988). Characteristics of acoustic emission source in a fatigue crack. *Nondestructive Testing Communications*, 4:11–21.
- [Munwam and Ohtsu, 1999] Munwam, M. C. and Ohtsu, M. (1999). Stress intensity factors in concrete by moment tensor analysis of acoustic emission. *Materials evaluation*, pages 1178–11182.
- [Muravin and Lezvinsky, 1995] Muravin, G. and Lezvinsky, L. (1995). Investigation of concrete structural and mechanical characteristics by acoustic emission method. In Schickert, G. and W. Wigggenhauser, H., editors, *International Symposium Non-Destructive testing in Civil Engineering NDT-CE*, volume 1, pages 597–604, Berlin, Germany.
- [Muravin et al., 2000] Muravin, G., Muravin, B., Kravetz, G., and Lezvinsky, L. (2000). Delayed fracture of stainless steel and peculiarities of associated acoustic emission. In *Progress in Acoustic Emission X*, pages 153–158. The Japanese Society for NDI.
- [Nesvijski, 1997] Nesvijski, E. G. (1997). Failure forecast and the acoustic emission “silence effect” in concrete. In *ASNT’s Spring Conference*, pages 108–110, Houston, Texas.
- [Nesvijski and Sarkis, 2000] Nesvijski, E. G. and Sarkis, P. J. (2000). Acoustic emission and failure prediction of composites. *www.NDT.net*, 5(3):1–10.
- [Neville, 1995] Neville, A. M. (1995). *Properties of concrete - 4th Edition*. Longman Group Ltd London. pp.844.
- [Obert, 1941] Obert, L. (1941). Use of subaudible noises for prediction of rock bursts. Technical report, *United States Department of the Interior - Bureau of mines*. pp.4.
- [O’Connor, 1993] O’Connor, C. (1993). *Roman Bridges*. Cambridge University Press. pp. 235.

- [Ohtsu, 1982] Ohtsu, M. (1982). Source mechanism and waveform analysis of acoustic emission in concrete. *Journal of Acoustic Emission*, 1(2):103–112.
- [Ohtsu, 1984] Ohtsu, M. (1984). A generalized theory of acoustic emission and Green's functions in half-space. *Journal of Acoustic Emission*, 3(1):27–40.
- [Ohtsu, 1987] Ohtsu, M. (1987). Determination of crack orientation by acoustic emission. *Materials Evaluation*, 45(9):1070–1075.
- [Ohtsu, 1991] Ohtsu, M. (1991). Simplified moment tensor analysis and unified decomposition of acoustic emission source: Application to in situ hydrofracturing test. *Journal of Geophysical Research*, 96(B4):6211–6221.
- [Ohtsu, 1995] Ohtsu, M. (1995). The history and the development of acoustic emission in concrete engineering. *The Concrete Library of the Japan Society for Civil Engineers*, (25):121–134.
- [Ohtsu, 1999a] Ohtsu, M. (1999a). Estimation of crack and damage progression in concrete by quantitative acoustic emission analysis. *Materials Evaluation*, pages 521–525.
- [Ohtsu, 1999b] Ohtsu, M. (1999b). Theoretical background of the SiGMA code for moment tensor analysis of AE. pp.48, “private communication, unpublished”.
- [Ohtsu, 2000] Ohtsu, M. (2000). Moment tensor analysis of AE and SiGMA code. In Kishi T, O. M. and S, Y., editors, *Acoustic Emission - Beyond the Millennium*, pages 19–34, Tokyo, Japan. Elsevier.
- [Ohtsu, 2002] Ohtsu, M. (2002). Generation of acoustic emission waves and moment tensor analysis. “private communication, unpublished”.
- [Ohtsu et al., 1994] Ohtsu, M., Arao, K., and Yuyama, S. (1994). Post-analysis of SiGMA solutions for error estimation in reinforced concrete members. In *Progress in AE VII*, pages pp.411–416. The Japanese Society for NDI.
- [Ohtsu and Iida, 2001] Ohtsu, M. and Iida, T. (2001). Quantitative damage evaluation of concrete core samples by acoustic emission. In Green, R. E., Kishi, T., Saito, T., Takeda, N., and Djordjevic, B. B., editors, *Nondestructive Characterization of Materials X*, pages 257–271, Karuizawa, Japan. Elsevier.

- [Ohtsu et al., 1998a] Ohtsu, M., Okamoto, T., and Yuyama, S. (1998a). Moment tensor analysis of acoustic emission for cracking mechanisms in concrete. *ACI Structural Journal*, pages 87–95.
- [Ohtsu and Shigeishi, 2002] Ohtsu, M. and Shigeishi, M. (2002). Three-dimensional visualization of moment tensor analysis by SiGMA-AE analysis. *www.ndt.net*, 07(09).
- [Ohtsu et al., 1998b] Ohtsu, M., Shigeishi, M., and Sakata, Y. (1998b). Non destructive evaluation of defects in concrete by quantitative acoustic emission and ultrasonic. *Ultrasonics*, (36):187–195.
- [Ohtsu et al., 2002] Ohtsu, M., Uchida, M., Okamoto, T., and Yuyama, S. (2002). Damage assessment of reinforced concrete beams qualified by acoustic emission. *ACI Structural Journal*, 99(04):411–417.
- [Ohtsu and Watanabe, 2001] Ohtsu, M. and Watanabe, H. (2001). Quantitative damage estimation of concrete by acoustic emission. *Construction and Building Materials*, 15:217–224.
- [Ohtsu and Yuyama, 2000] Ohtsu, M. and Yuyama, S. (2000). Recommended practice for insitu monitoring of concrete structures by acoustic emission. In *Progress in AE X*, pages 263–268.
- [Ono, 2000] Ono, K. (2000). New goals for acoustic emission in materials research. In Kishi T., O. M. and S., Y., editors, *Acoustic Emission - Beyond the Millenium*, pages 57–75, Tokyo, Japan. Elsevier.
- [PAC, 1995] PAC (1995). *MISTRAS-2001 AEDSP-32/16 User's manual*. Physical Acoustic Corporation Part number 6300-100, Princeton, New Jersey, USA.
- [PAC, 1997a] PAC (1997a). Acoustic emission sensors - product bulletin. Technical report, Physical Acoustic Corporation PAC, Princeton, New Jersey, USA. pp.4.
- [PAC, 1997b] PAC (1997b). *Moment Tensor Analysis Software - User's manual*. Physical Acoustic Corporation, Princeton, New Jersey, USA.
- [PAC, 2001] PAC (2001). AE Short Notes course. Technical report, Physical Acoustic Corporation PAC, Cambridge, UK.

- [Paulson, 1998] Paulson, P. O. (1998). United States Patent 5798457. Technical report, US Patent & Trademark Office, USA.
- [Paulson et al., 2001] Paulson, P. O., Tozser, O., and Youdan, D. (2001). The use of acoustic monitoring to manage concrete structures in the nuclear industry. In Forde, M., editor, *Proc. of the Int. Conf. on Structural Faults + Repairs - 2001*, volume CD-rom, London.
- [Pazdera, 2001] Pazdera, L. (2001). Basically knowledge about acoustic emission method. In <http://cmsnt.fme.vutbr.cz/uk/odbory/vav/AE2001/contrib/pazdera.html>, pages 1–9, International Conference on Internet. Czech Society for Non-destructive Testing.
- [PCB, 2000] PCB, P. (2000). *Sensors for Acceleration, Shock and Vibration*. PCB Group Inc. pp.2.
- [Pollock, 1969] Pollock, A. A. (1969). Stress-wave emission in ndt. *Non-destructive testing*, 2:178–182.
- [Pollock, 1981] Pollock, A. A. (1981). Acoustic Emission amplitude distributions. *International Advances in Nondestructive Testing*, 7:215–239.
- [Pollock, 1986] Pollock, A. A. (1986). Classical wave theory in practical AE testing. *Progress in Acoustic Emission III*, pages 215–239.
- [Pollock, 1989] Pollock, A. A. (1989). Acoustic emission inspection. *Metals Handbooks*, 17 ASM International(Ninth Edition):278–294.
- [Pollock and Smith, 1972] Pollock, A. A. and Smith, B. (1972). Stress-wave emission monitoring of a military bridge. *Non-destructive testing*, 5(6):348–353.
- [Prine and Hopwood, 1985] Prine, D. W. and Hopwood, T. (1985). Improved structural monitoring with acoustic emission pattern recognition. In *Proceedings of the 14th Symposium on Nondestructive Evaluation*, pages 429–439, San Antonio, TX. Southwest Research Institute.
- [Pure, 1996] Pure (1996). *SoundPrint Analyst-Data Analysis and reporting Software Manual*. Pure Technologies Ltd, Calgary, Canada. pp.39.
- [Raina, 1994] Raina, V. K. (1994). *Concrete bridges*. McGraw-Hill. pp.493.

- [Robins, 1948] Robins, F. W. (1948). *The story of the bridge*. Cornish Bros Ltd Publisher. pp.255.
- [Robinson, 1965] Robinson, G. S. (1965). Methods of detecting the formation and propagation of microcracks in concrete. In *Proceedings of an Int. Conf. The Structure of Concrete*, pages 131–145, London. Concrete materials research group.
- [Roca, 1997] Roca, L. O. V. (1997). *Acoustic Emission examination of high strength prestressed concrete girders*. PhD thesis, Graduate School of the University of Texas, Austin.
- [Royles and Hendry, 1991] Royles, R. and Hendry, A. W. (1991). Model tests on masonry arches. In *Proc. Instn Civ. Engrs*, volume 91, pages 299–321.
- [Rusch, 1959] Rusch, V. H. (1959). Physical problems in the testing of concrete. *Zement - Kalk - Gips*, (12):1–9.
- [Sammonds et al., 1994] Sammonds, P. R., Meredith, P. G., Murrell, S. A. F., and Main, I. G. (1994). Modelling the damage evolution in rock containing pore fluid by acoustic emission. *Eurock'94*, (897–904).
- [Sansalone and Streett, 1997] Sansalone, M. J. and Streett, W. B. (1997). *Impact-Echo: Nondestructive Evaluation of Concrete and Masonry*. Bullbrier Press. pp.339.
- [Scholz, 2002] Scholz, C. H. (2002). *The mechanics of Earthquakes and Faulting - 2nd Edition*. Cambridge University Press. pp.224-228.
- [Scott, 1991] Scott, I. G. (1991). *Basic Acoustic Emission - Non Destructive testing monographs and tracts*, volume 6. Gordon and Breach Science Publishers. pp.241.
- [Shearer, 1999] Shearer, P. M. (1999). *Introduction to Seismology*. Cambridge University Press. pp.250.
- [Sheriff and Geldart, 1995] Sheriff, R. E. and Geldart, L. (1995). *Exploration Seismology*. Cambridge University Press, 2nd edition. pp. 592.
- [Shigeishi, 1998] Shigeishi, M. (1998). Application of acoustic emission technique to concrete structure diagnosis. In Srivastava, editor, *Structural Engineering World Wide 1998 - CD-rom*, T180-6. Elsevier Science Ltd.

- [Shigeishi et al., 2001] Shigeishi, M., Colombo, S., Broughton, K. J., Rutledge, H., Bachelor, A. J., and Forde, M. C. (2001). Acoustic emission to assess and monitor the integrity of bridges. *Construction and Building Materials*, 15:35–49.
- [Shigeishi and Forde, 2001] Shigeishi, M. and Forde, M. C. (2001). Basic study on Acoustic Emission from masonry. In Forde, M., editor, *Proc. of the Int. Conf. on Structural Faults + Repairs - 2001*, volume CD-rom, London.
- [Shigeishi et al., 2002] Shigeishi, M., Makizumi, T., Jo, H., and Sonoda, Y. (2002). Acoustic emission monitoring of a reinforced concrete road bridge which served for 45 years. In *2nd Structural Engineers World Congress*, Yokohama, Japan.
- [Shigeishi et al., 1999a] Shigeishi, M., Masaki, Y., Jo, H., Fujimoto, S., Makizumi, T., and Matsushita, H. (1999a). Acoustic emission on a 60 years old bridge beam under bending test. In *Proc. of the Int. Conf. on the Current and the future trends in bridge design construction and aesthetics*, pages 436–445, Singapore.
- [Shigeishi and Ohtsu, 1997] Shigeishi, M. and Ohtsu, M. (1997). Acoustic emission generated by cyclic bending in damaged RC beam. In M.C.Forde, editor, *Proc. of the Int. Conf. on Structural Faults + Repair - 1997*, volume 2, pages 375–382, Edinburgh. Engineering Technics Press.
- [Shigeishi and Ohtsu, 1998] Shigeishi, M. and Ohtsu, M. (1998). Identification of AE source by using sigma-2D moment tensor analysis. Technical report, *Acoustic Emission: Standards and Technology Update, ASTM STP 1353- American Society for Testing and Materials*. S.J. Vahavilos Ed., pp.1-12.
- [Shigeishi and Ohtsu, 2001] Shigeishi, M. and Ohtsu, M. (2001). Acoustic emission moment tensor analysis: development for crack identification in concrete materials. *Construction and Building Materials*, 15:311–319.
- [Shigeishi et al., 1999b] Shigeishi, M., Ohtsu, M., and Forde, M. C. (1999b). Monitoring of fracture process in concrete using acoustic emission moment tensor analysis. In *Create with concrete*. The University of Dundee, Concrete Technology Unit.

- [Shigeishi et al., 2000] Shigeishi, M., Shiotani, T., and Ohtsu, M. (2000). A consideration about the rainy influence in field AE measurement. *Progress in Acoustic Emission X - The Japanese Society for NDI*, pages 177–182.
- [Shinomiya et al., 2002] Shinomiya, M., Y, Y. N., Morishima, H., and Shiotani, T. (2002). Damage diagnosis technique for brick structures using Acoustic Emission. In Mazal, P., editor, *Proc. of the EWGAE 2002- 25th European Conf. on Acoustic Emission Testing*, volume II, pages 141–148, Prague, Czech Republic. Czech Society for Non-destructive Testing.
- [Shiotani et al., 1994] Shiotani, T., Fujii, K., Aoki, T., and Amou, K. (JSNDI 1994). Evaluation of progressive failure using AE sources and improved b -value on slope model tests. *Prog. Acout. Emiss VII*, 7:529–534.
- [Shiotani et al., 2001a] Shiotani, T., Keisuke, I., and Otsu, M. (2001a). Damage evaluation of concrete structures by AE/UT technique. In Forde, M., editor, *Proc. of the Int. Conf. on Structural Faults + Repairs - 2001*, volume CD-rom, London.
- [Shiotani et al., 2000a] Shiotani, T., Miwa, S., Ichimura, Y., and Ohtsu, M. (2000a). Damage diagnosis of concrete piles by machinery-induced acoustic emission. *Progress in Acoustic Emission X - The Japanese Society for NDI*, pages 213–218.
- [Shiotani et al., 2001b] Shiotani, T., Ohtsu, M., and Ikeda, K. (2001b). Detection and evaluation of AE waves due to rock deformation. *Construction and Building Materials*, 15(5):235–246.
- [Shiotani et al., 2000b] Shiotani, T., Yuyama, S., Li, Z. W., and Ohtsu, M. (2000b). Quantitative evaluation of fracture process in concrete by the use of improved b -value. In Uomoto, T., editor, *5th Int Symposium Non-Destructive Testing in Civil Eng*, pages 293–302, Amsterdam. Elsevier Science.
- [Shiotani et al., 2000c] Shiotani, T., Yuyama, S., Zi, L. W., and Ohtsu, M. (2000c). Application of the AE improved b -value to quantitative evaluation of fracture processes in concrete materials. *Progress in Acoustic Emission X - The Japanese Society for NDI*, pages 201–206.

- [Sison et al., 1996] Sison, M., Duke, J. C. J., Clemena, G., and Lozev, M. G. (1996). Acoustic emission: A tool for the bridge engineer. *Materials Evaluation - ASNT*, pages 888–902.
- [SoundPrint, 1996] SoundPrint (1996). *SoundPrint-structural Monitoring Systems-Installation and Operations Manual*. Pure Technologies Ltd, Calgary, Canada. pp.40.
- [Spanner, 1981] Spanner, J. C. (1981). Acoustic emission: Who needs it? - and why? In Dunegan, H. L. and Ed., W. F. H., editors, *Proc. of the Int. Conf. on Acoustic Emission*, pages 1–14, Anaheim, California. Dunhart Publishers, Knoxville Tennessee.
- [Stephens and Pollock, 1971] Stephens, R. W. B. and Pollock, A. A. (1971). Waveforms and frequency spectra of acoustic emissions. *Journal of the Acoustical Society of America*, 50(3):904–910.
- [Takemoto et al., 2000] Takemoto, M., Nishino, H., and Ono, K. (2000). Wavelet transform - Application to AE signals analysis. In Kishi T, Ohtsu M., Y. S., editor, *Acoustic Emission - Beyond the Millennium*, pages 35–56, Tokyo, Japan. Elsevier.
- [Tsuji et al., 2000] Tsuji, N., Uchida, M., Okamoto, T., and Ohtsu, M. (2000). Application of acoustic emission technique to evaluation of cracking in concrete structures. *Progress in Acoustic Emission X - The Japanese Society for NDI*, pages 189–194.
- [Uomoto, 2000] Uomoto, T. (2000). Maintenance of concrete structures and application of non-destructive inspection in Japan. In Uomoto, T., editor, *Non-Destructive Testing in Civil Engineering - Seiken Symposium No.26*, pages 1–11, Tokyo, Japan. Elsevier.
- [ACI, 1998] ACI (1998). *Nondestructive Test Methods for Evaluation of Concrete in Structures - ACI 228.2R-98*. American Concrete Institute.
- [von Kaiser, 1953] von Kaiser, J. (1953). Knowledge and research on noise measurements during the tensile stressing of metals. *Archiv fur das Eisenhüttenwesen*, 24(1335):43–45. in German.
- [Watson and Cole, 2001] Watson, J. R. and Cole, P. T. (2001). Acoustic emission monitoring of half joints on Borrowbeck Bridge. Technical report, PAC. “Confidential for the Highways Agency”.

- [Watson et al., 2000] Watson, J. R., Holford, K. M., Davies, A. W., and Cole, P. T. (2000). Boxmap - non invasive detection of cracks in steel box girders. In M.J. Ryall, G. P. and Harding, J., editors, *Bridge Management 4*, pages 80–87. Dept. Civ, Eng. University of Surrey, UK, Thomas Telford.
- [Watson et al., 1999] Watson, J. R., Yuyama, S., and Johnson, D. (1999). Remote detection and assessment of damage in bridges. In Forde, M., editor, *Proc. of the Int. Conf. on Structural Faults + Repairs - 1999*, volume CD-rom, London.
- [Wells, 1970] Wells, D. (1970). An acoustic apparatus to record emissions from concrete under strain. *Nuclear Engineering and Design*, 12:80–88.
- [Williams, 1980] Williams, R. V. (1980). *Acoustic Emission*. Adam Hilger Ltd. pp.116.
- [Woodward, 1983] Woodward, R. J. (1983). Cracks in a concrete bridge. *Concrete*, 17(7):40–45.
- [Woodward, 1989] Woodward, R. J. (1989). Non destructive testing methods for concrete bridges. Technical report, Transport and Road Research Laboratory. Research Report 250.
- [Young, 2000] Young, M. (2000). The current bridge strengthening programme: local authorities' experience. In *ICE 2000 Conf. "Bridge Rehabilitation in the UK: review of the current programme and preparing for the next" 2-3 Oct. 2000*, London, UK. The Institution of Civ. Eng.
- [Yuyama and Li, 2000] Yuyama, S. and Li, Z. W. (2000). Evaluation of fatigue damage in reinforced concrete slab by acoustic emission. In *Non-Destructive Testing in Civil Engineering-2000*, Tokyo, Japan. pp 51–57.
- [Yuyama et al., 2000] Yuyama, S., Li, Z. W., Yoshizawa, M., Tomokiyo, T., and Uomoto, T. (2000). Acoustic emission evaluation during fatigue processes in reinforced concrete slabs. *Progress in Acoustic Emission X - The Japanese Society for NDI*, pages 195–206.
- [Yuyama et al., 1994] Yuyama, S., Okamoto, T., and Nagataki, S. (1994). Acoustic emission evaluation of structural integrity in repaired reinforced concrete beams. *Materials Evaluation*, 52(Part 1):86–90.

- [Yuyama et al., 1995a] Yuyama, S., Okamoto, T., Shigeishi, M., and Ohtsu, M. (1995a). Acoustic emission generated in corners of reinforced concrete rigid frame under cyclic loading. *Materials Evaluation*, 53(Part 3):409–412.
- [Yuyama et al., 1995b] Yuyama, S., Okamoto, T., Shigeishi, M., and Ohtsu, M. (1995b). Quantitative evaluation and visualization of cracking process in reinforced concrete by a moment tensor analysis of acoustic emission. *Materials Evaluation*, 53(Part 6):751–756.
- [Yuyama et al., 1998] Yuyama, S., Okamoto, T., Shigeishi, M., Ohtsu, M., and Kishi, T. (1998). A proposed standard for evaluating structural integrity of reinforced concrete beams by acoustic emission. Technical report, Acoustic Emission: Standards and Technology Update, ASTM STP 1353- American Society for Testing and Materials. S.J. Vahavilos Ed., pp.1-12.
- [Zietlow and Labuz, 1998] Zietlow, W. K. and Labuz, J. F. (1998). Measurement of the intrinsic process zone in rock using acoustic emission. *Int. J. Rock Mech. Min. Sci.*, 35(3):291–299.

Appendix A

Design Calculations of RC Beams

The design calculations of the RC beams tested in Edinburgh were based on BS 8110: Part1: 1997 - Section 3. The calculations given below illustrate an example of the steps followed for the design of the singly reinforced beams and they specifically refer to beam BF3. Beams BF1, BF2 and BF4 were designed following the exact same procedure. The design of beam BF5 was based on the same calculations but the shear links were omitted to assure a shear failure. Once again these basic calculation were considered in designing beam BF6 but the failure load was calculated following the procedure described in Appendix B. For each beam the calculation was carried out according to the specific load configuration.

Design of beam BF3

Dimensions

Span of the beam = $L = 3000$ mm

Depth of section = $d = 275$ mm

Width of section = $b = 200$ mm

Properties

Characteristic concrete cube strength = f_{cu} assumed = 25 N/mm^2

Yield stress of reinforcement = $f_y = 460 \text{ N/mm}^2$

Yield stress of link reinforcement = $f_{yv} = 250 \text{ N/mm}^2$

Max. size of aggregate = 20 mm

Max. bar size assumed = 16 mm

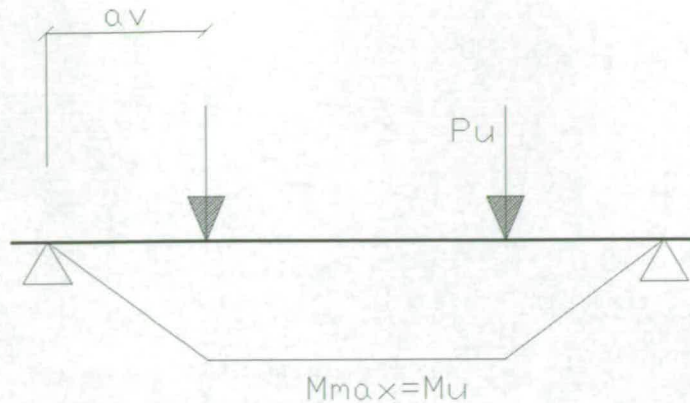
Min. size of link assumed = 8 mm

Exposure condition = mild

Fire resistance required = 1 hr therefore cover = 25 mm

Effective depth of tension reinforcement = $d_{eff} = 275 - 25 - (16/2) - 8 = 234$ mm

Assumed load configuration



$$\text{Load} = P = 50 \text{ kN}$$

$$\text{Shear span} = a_v = 0.75 \text{ m}$$

$$\text{Max bending Moment} = M_{max} = P \times a_v = 37.5 \text{ kN}$$

$$\text{Max shear force at face of support} = 50 \text{ kN}$$

Check slenderness of the beam

$$60b = 60 \times 200 = 1200 \text{ mm} = 1.2 \text{ m}$$

$$\frac{250b^2}{d} = \frac{250 \times 200^2}{234} = 42735.04 \text{ mm} = 42.74 \text{ m}$$

$$L = 3 \text{ m} \leq 60b \leq \frac{250b^2}{d} \dots \text{slenderness is OK.}$$

Calculate K

$$K = \frac{M}{f_{cu} b d_{eff}^2} = \frac{37.5 \times 10^6 \text{ (Nmm)}}{25 \times 200 \times 234^2 \text{ (Nmm)}} = 0.137$$

as $K \leq K' = 0.156 \dots$ NO compression reinforcement is required.

Design for flexure

Calculate the lever arm z :

$$z/d = \left[0.5 + \sqrt{0.25 - \frac{K}{0.9}} \right] = 0.81$$

as it is not greater than $0.95d$ then $z = 190 \text{ mm}$

and the required cross-sectional area of tension reinforcement is:

$$A_s = \frac{M}{0.95 f_y z} = \frac{37.5 \times 10^6 \text{ (Nmm)}}{0.95 \times 460 \times 190 \text{ (N/mm)}} = 451 \text{ mm}^2$$

Using $2\Phi 16 \text{ mm}$ bars provide an area of 402 mm^2 so to have an under-reinforced beam.

Design for shear

$$\text{Design shear stress at a cross section} = v = \frac{V}{b d_{eff}} = \frac{50 \times 10^3}{200 \times 234} = 1.068 \text{ N/mm}^2$$

Check that $v \leq 0.8\sqrt{f_{cu}} = 4$ and $v \leq 5.0 \text{ N/mm}^2 \dots$ OK

Being the ratio R $R = \frac{100A_s}{bd_{eff}} = \frac{100 \times 402}{200 \times 234} = 0.86$

from Table 3.8 of the BS 8110: Part1: 1997 - Section 3 it derives that:

Design concrete shear stress = $v_c = 0.68 \text{ N/mm}^2$

It can be seen that:

$$0.34 = 0.5v_c \leq v = 1.068 \leq (v_c + .4) = 1.08$$

then the minimum links have to be provided, i.e. web reinforcement that will provide a shear resistance, $v - v_c$, of at least 0.4 N/mm^2

Checking the maximum allowable spacing $s_{v \max} = 0.75d = 175.5 \text{ mm}$ and therefore assuming a link spacing $s_v = 175 \text{ mm}$

the cross sectional area of the web reinforcement is then calculated from:

$$A_{sv} = \frac{0.4bs_v}{0.95f_{yv}} = \frac{0.4 \times 200 \times 175}{0.95 \times 250} = 58.95 = 59 \text{ mm}^2$$

thus $\phi 8 \text{ mm}$ links @175mm spacing will satisfy the request.

Design Stress block

Assuming the characteristics of the simplified design stress blocks as:

$$k_1 = 0.9 \times \frac{0.67}{\gamma_m} = 0.9 \times 0.671.5 = 0.402$$

$$k_2 = 0.45$$

then the position of the neutral axis x is calculated as:

$$k_1 f_{cu} b x = A_s f_s \dots 0.402 \times 25 \times 200 \times x = 402 \times 460 \dots x = 82.19 \text{ mm}$$

and $x/d = 0.351 \geq 0.2 \dots$ therefore OK

while the tension steel ratio results:

$$\rho = \frac{A_s}{bd} = 0.0086$$

Calculate ultimate bending Moment

The ultimate moment of resistance for under-reinforced beams is calculated as:

$$M_u = A_s \left(\frac{f_y}{\gamma_m} \right) \left(1 - \rho \frac{k_2}{k_1} \frac{f_y}{f_{cu}} \right) d_{eff} = 402 \left(\frac{460}{1.5} \right) \left(1 - 0.0086 \frac{0.45}{0.402} \frac{460}{25} \right) 234 = 25.44 \text{ kNm}$$

where $\gamma_m = 1.5$ is the partial factor of safety.

The ultimate axial load thus results to be:

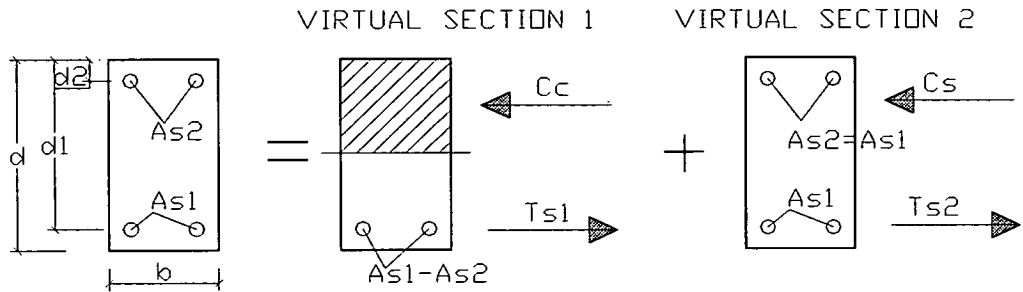
$$P_u = \frac{M_u}{a_v} = 33.92 \text{ kN}$$

Appendix B

Failure Load Calculations of Kumamoto Beams

The failure load for beams K1 to K4 was computed on the basis of the following general procedure.

The doubly reinforced section of a beam can be subdivided into two virtual sections as shown in the diagram below:



For the equilibrium of the virtual section 1 it is:

$$\bar{C}_c + \bar{T}_{s1} = 0$$

$$\bar{C}_c = -\bar{T}_{s1} = (A_{s1} - A_{s2}) f_y$$

where C = resultant of compression

T = resultant of tension.

The ultimate Moment results to be:

$$M_{u1} = (A_{s1} - A_{s2}) f_y \left(d_1 - \frac{d}{2} \right)$$

For the equilibrium of the virtual section 2 it is:

$$\bar{C}_s = \bar{T}_{s2} = A_{s2} f_y$$

and the ultimate Moment is:

$$M_{u2} = A_{s2} f_y (d_1 - d_2)$$

Therefore the total ultimate Moment M_u is:

$$M_u = M_{u1} - M_{u2} = (A_{s1} - A_{s2}) f_y \left(d_1 - \frac{d}{2} \right) + A_{s2} f_y (d_1 - d_2)$$

In the case of beams K1 to K4, the compression and tension reinforcement are symmetrical and therefore:

$$A_{s1} = A_{s2} \text{ and } (A_{s1} - A_{s2}) = 0$$

thus:

$$M_u = A_{s2} f_y (d_1 - d_2)$$

Assuming the same four points load configuration shown in Appendix A, the failure load is calculated as:

$$P_u = \frac{M_u}{a_v}$$

The failure loads were calculated for all four beams using the following values:

$$f_y = 295 \text{ N/mm}^2$$

$$(d_1 - d_2) = 218.5 \text{ mm}$$

$$A_{s2} = 265.33 \text{ mm}^2$$

The results were as follows:

$$\text{Beam K1: } \dots P_u = 30 \text{ kN}$$

$$\text{Beam K2: } \dots P_u = 31.5 \text{ kN}$$

$$\text{Beam K3: } \dots P_u = 50 \text{ kN}$$

$$\text{Beam K4: } \dots P_u = 81 \text{ kN}$$

For the simply reinforced beams KL1 and KL2 the calculations described in Appendix A were used and the results were as follows:

$$\text{Beam KL1: } \dots P_u = 23 \text{ kN}$$

$$\text{Beam KL2: } \dots P_u = 60 \text{ kN}$$

Appendix C

P-wave Velocity Calculations for Kumamoto Beams

During the experiments in Kumamoto, the velocity of the P-wave was computed using equation 4.3, where the static modulus E was used instead of the Bulk modulus. The static modulus of elasticity of the concrete was established using The Japan Industrial Standard JIS A 1149:2001 “*Method of test for static modulus of elasticity of concrete*”. The method consisted of carrying out a compression test on a concrete cylinder, 200 mm high and 100 mm diameter, during which two couples of strain gauges were mounted on the sample, each of them comprised a horizontal strain gauge and a vertical strain gauge. They measured the strains ϵ_1 and ϵ_2 respectively. The following steps were undertaken:

- During the compression test, the load and the strains were recorded by means of a data logger and thus the average vertical strain ϵ between the two couples of strain gauges and the stress σ (=Applied Load/Area) were calculated.
- The value of σ_1 was calculated as: $\sigma_1 = \frac{P_{max}/3}{A}$ where P_{max} was the maximum applied load and A was the area of the sample.
- The value of σ_2 was calculated as the value of stress corresponding to an average basic vertical strain ϵ_2 of 50×10^{-6} .
- The data interval between the above calculated values σ_1 and σ_2 was then used to obtain the best fit graph of “ ϵ' vs σ' ”, where the apex indicates the values on the fitting line.
- From the best fit graph, the following pairs of values were obtained: (σ_1, ϵ'_1)
 (σ'_2, ϵ_2)
- The above values were then used to calculate the static modulus using the formula:

$$E = \frac{\sigma_1 - \sigma'_2}{\epsilon'_1 - \epsilon_2}$$

It is interesting to note that the above Japanese procedure is similar to the procedure described in the British Standard BS 1881: Part 121:1983 “*Method for determination of static modulus of elasticity in compression*”, which instead of

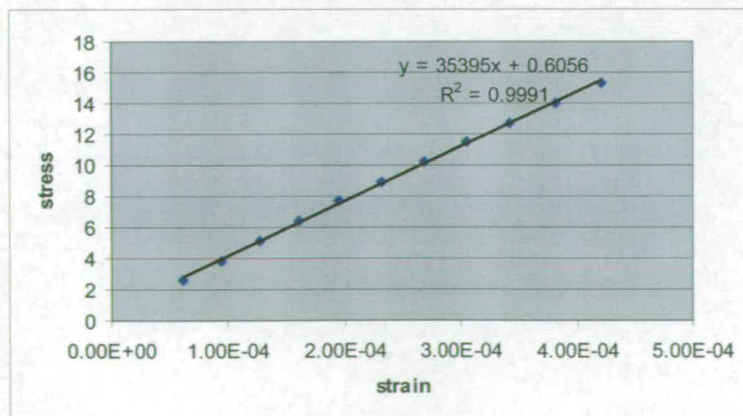
referring to a basic strain of 50×10^{-6} , refers to a basic stress of 0.5 N/mm^2 .

The results of the numerical calculations carried out for a cylinder tested in Kumamoto are reported herein. The following table includes: the applied load; the values of strain recorded by the strain gauges - $\epsilon_{1'}$, $\epsilon_{2'}$ from the first pair and $\epsilon_{1''}$, $\epsilon_{2''}$ from the second pair; the average strain is calculated in the 6th column and the applied stress is computed in the 7th column. The double horizontal line in the table identifies the group of data that were used to obtain the ensuing fitting graph.

Load tf	$\epsilon_{2'}$ 10^{-6}	$\epsilon_{2''}$ 10^{-6}	$\epsilon_{1'}$ 10^{-6}	$\epsilon_{1''}$ 10^{-6}	Avg. ϵ_{vert}	Stress N/mm^2
0	0	0	0	0	0	0
1.01	34	24	7	15	0.000029	1.29
2.01	75	47	12	25	6.10×10^{-5}	2.56
3.01	114	74	19	34	9.40×10^{-5}	3.83
4.01	152	102	25	45	1.27×10^{-4}	5.12
5	189	132	33	54	1.61×10^{-4}	6.37
6.01	228	163	41	64	1.96×10^{-4}	7.67
7.01	266	196	47	74	2.31×10^{-4}	8.93
8.01	307	229	56	85	2.68×10^{-4}	10.20
9.01	348	262	63	94	3.05×10^{-4}	11.48
10	387	297	71	105	3.42×10^{-4}	12.74
11.01	429	335	80	114	3.82×10^{-4}	14.03
12.03	472	370	89	125	4.21×10^{-4}	15.32
13.03	514	408	96	136	4.61×10^{-4}	16.60
14.01	559	445	105	147	5.02×10^{-4}	17.85
15.03	604	484	113	158	5.44×10^{-4}	19.15
16.03	647	525	123	169	5.86×10^{-4}	20.42
17.03	690	568	133	180	6.29×10^{-4}	21.69
18.03	734	614	143	191	6.74×10^{-4}	22.97
19.02	777	660	154	202	7.19×10^{-4}	24.23
20.02	821	708	166	215	7.65×10^{-4}	25.50
21.02	867	759	179	226	8.13×10^{-4}	26.78

Load tf	ϵ_2' 10^{-6}	ϵ_2'' 10^{-6}	ϵ_1' 10^{-6}	ϵ_1'' 10^{-6}	Avg. ϵ_{vert}	Stress N/mm^2
22.03	913	811	192	238	$8.62 \cdot 10^{-4}$	28.06
23.02	960	864	206	250	$9.12 \cdot 10^{-4}$	29.32
24.02	1008	919	221	263	$9.64 \cdot 10^{-4}$	30.60
25.02	1058	974	239	277	$1.02 \cdot 10^{-3}$	31.87
26.02	1110	1031	259	292	$1.07 \cdot 10^{-3}$	33.15
27.03	1167	1091	278	308	1.1310^{-3}	34.43
28.03	1225	1153	302	324	$1.19 \cdot 10^{-3}$	35.70
29.03	1285	1215	327	342	$1.25 \cdot 10^{-3}$	36.98
30.03	1349	1281	358	362	$1.32 \cdot 10^{-3}$	38.25
31.02	1414	1350	394	383	$1.38 \cdot 10^{-3}$	39.52
32.02	1485	1425	436	404	$1.46 \cdot 10^{-3}$	40.79
33.02	1559	1503	489	429	$1.53 \cdot 10^{-3}$	42.06
34.02	1639	1589	563	457	$1.61 \cdot 10^{-3}$	43.34
35.04	1725	1684	663	491	$1.70 \cdot 10^{-3}$	44.64
36.02	1820	1791	808	536	$1.81 \cdot 10^{-3}$	45.89
37.02	1934	1921	1028	608	$1.93 \cdot 10^{-3}$	47.16
38	2135	2124	1701	844	$2.13 \cdot 10^{-3}$	48.41
38.05	2170	2160	1888	912	$2.17 \cdot 10^{-3}$	48.47

Using the above specified data interval of the table, the following best fit line was obtained:



From the above best fit graph and its relative equation the following values were obtained:

$$\epsilon'_1 = 4.9028 \times 10^{-4}, \text{ corresponding to } \sigma_1 = \frac{P_{max}/3}{A} = 16.16 \text{ N/mm}^2$$

$$\sigma'_2 = 2.1460 \times 10 \text{ N/mm}^2, \text{ corresponding to } \epsilon_2 = 50 \times 10^{-6}$$

and then:

$$E = 3.194 \times 10^{+04}$$

The velocity of the P-wave was thus calculated:

Sample no.	Weight kg	Radius mm	Height mm	Volume mm^3	Density g/mm^3	Static Modulus N/mm^2	Static Modulus kgf/cm^2	Velocity m/sec
2	3.87	50	200	1570000	0.002465	$3.19 \cdot 10^3$	$3.13 \cdot 10^3$	3599.61

Appendix D

MATLAB Programs

channels.m

%prg that reads the data file with all the recorded parameters
%and creates a different vector ch1, ch2, ch3 etc for each channels and then
%a vector with the time as well, t1,t2,t3 etc.

```
fn= input('insert the name (or path) of the file containing all the AE parameters for all the channels(no file  
extension) ','s');  
s=load(['fn'.txt']);  
format long g %to visualise all the decimals
```

```
dim=size(s); %calculates the dimension of the initial file  
hits=dim(1,1); %total number of hits=number of rows  
par=dim(1,2); %total number of columns
```

```
ch1=zeros(1,par); %initialise file  
ch2=zeros(1,par);  
ch3=zeros(1,par);  
ch4=zeros(1,par);  
ch5=zeros(1,par);  
ch6=zeros(1,par);  
ch7=zeros(1,par);  
ch8=zeros(1,par);
```

```
for k=1:hits %create separate file for each channel  
switch s(k,2)  
case 1  
ch1=[ch1;s(k,:)];  
case 2  
ch2=[ch2;s(k,:)];  
case 3  
ch3=[ch3;s(k,:)];  
case 4  
ch4=[ch4;s(k,:)];  
case 5  
ch5=[ch5;s(k,:)];  
case 6  
ch6=[ch6;s(k,:)];  
case 7  
ch7=[ch7;s(k,:)];  
case 8  
ch8=[ch8;s(k,:)];  
otherwise  
error('This is impossible');  
end  
end
```

```
t=s(:,1); %create a vector with all time  
t1=ch1(:,1); %create a vector for each time of each channel  
t2=ch2(:,1);  
t3=ch3(:,1);  
t4=ch4(:,1);  
t5=ch5(:,1);  
t6=ch6(:,1);  
t7=ch7(:,1);  
t8=ch8(:,1);
```

Amplitude_ver2.m

```
%prg that creates the column vectors a1 a2 a3... with the amplitude of the signals in dB
%need to run prg channels.m first, so that
%the input data are already there
%it verifies that no hits was lost in the process

events=input('insert the number of AE events: '); %ask for number of events I want to use

a1=ch1(:,10); %create a file with signals amplitude for each channel
a2=ch2(:,10); %first row are zeros
a3=ch3(:,10);
a4=ch4(:,10);
a5=ch5(:,10);
a6=ch6(:,10);
a7=ch7(:,10);
a8=ch8(:,10);
dim1=size(a1);
dim2=size(a2);
dim3=size(a3);
dim4=size(a4);
dim5=size(a5);
dim6=size(a6);
dim7=size(a7);
dim8=size(a8);
da1=fix(length(a1)/events); %number of intervals
da2=fix(length(a2)/events);
da3=fix(length(a3)/events);
da4=fix(length(a4)/events);
da5=fix(length(a5)/events);
da6=fix(length(a6)/events);
da7=fix(length(a7)/events);
da8=fix(length(a8)/events);
N1=zeros(14,da1(1,1));
N2=zeros(14,da2(1,1));
N3=zeros(14,da3(1,1));
N4=zeros(14,da4(1,1));
N5=zeros(14,da5(1,1));
N6=zeros(14,da6(1,1));
N7=zeros(14,da7(1,1));
N8=zeros(14,da8(1,1));

%CHANNEL 1
ev=0;
T1t=zeros(1,1);
for i=1:da1
    n=0;
    m=35;
    while m<100
        n=n+1;
        q=a1((2+ev):(events+1+ev),1)>(m-1) & a1((2+ev):(events+1+ev),1)<(m+5);
        A1=a1(q,1);
        N1(n,i)=length(A1);
        m=m+5;
        clear q;
        clear A1;
    end
end
```

```

clear q;
end
%I have the vector b with all the b-values during all the time for this channel
%now I can draw the chart with the trend of the b-values during the recording time
B2=b2*-20; %multiply the b-values by 20 (as this is the sismic value) and I made it positive as well
q=T2t(1,:)>0;
T2=T2t(1,q); %vector of the time to be plotted
figure %plot the chart
plot(T2,B2,'-',T2,B2,'o');
axis([0 T2(1,da2(1,1))+10 0 2.5])
xlabel('time sec')
ylabel('b-value')
title('Trend of b-values CHANNEL 2')

%FOR CHANNEL 3
for n=1:da3(1,1)
    q=N3(:,n)>0;
    N3b=N3(q,n);
    A3=A(q,1);
    if length(A3)>3
        N3L=LOG10(N3b);
        p=polyfit(A3,N3L(:,1),1);
        p3=polyval(p,A3);
        b3(1,n)=p(1,1);
    else
        b3(1,n)=NaN;
    end
    clear q;
end
B3=b3*-20;
q=T3t(1,:)>0;
T3=T3t(1,q);
figure
plot(T3,B3,'-',T3,B3,'o');
axis([0 T3(1,da3(1,1))+10 0 2.5])
xlabel('time sec')
ylabel('b-value')
title('Trend of b-values CHANNEL 3')

%FOR CHANNEL 4
for n=1:da4(1,1)
    q=N4(:,n)>0;
    N4b=N4(q,n);
    A4=A(q,1);
    if length(A4)>3
        N4L=LOG10(N4b);
        p=polyfit(A4,N4L(:,1),1);
        p4=polyval(p,A4);
        b4(1,n)=p(1,1);
    else
        b4(1,n)=NaN;
    end
    clear q;
end
B4=b4*-20;
q=T4t(1,:)>0;

```

```

A4=a4(q,1);
  N4(n,i)=length(A4);
  m=m+5;
  clear q;
  clear A4;
end
T4t=[T4t,t4(events+1+ev,1)];
ev=ev+events;
end

%CHANNEL 5
ev=0;
T5t=zeros(1,1);
for i=1:da5
  n=0;
  m=35;
  while m<100
    n=n+1;
    q=a5((2+ev):(events+1+ev),1)>(m-1) & a5((2+ev):(events+1+ev),1)<(m+5);
    A5=a5(q,1);
    N5(n,i)=length(A5);
    m=m+5;
    clear q;
    clear A5;
  end
  T5t=[T5t,t5(events+1+ev,1)];
  ev=ev+events;
end

%CHANNEL 6
ev=0;
T6t=zeros(1,1);
for i=1:da6
  n=0;
  m=35;
  while m<100
    n=n+1;
    q=a6((2+ev):(events+1+ev),1)>(m-1) & a6((2+ev):(events+1+ev),1)<(m+5);
    A6=a6(q,1);
    N6(n,i)=length(A6);
    m=m+5;
    clear q;
    clear A6;
  end
  T6t=[T6t,t6(events+1+ev,1)];
  ev=ev+events;
end

%CHANNEL 7
ev=0;
T7t=zeros(1,1);
for i=1:da7
  n=0;
  m=35;
  while m<100
    n=n+1;

```

```

q=a7((2+ev):(events+1+ev),1)>(m-1) & a7((2+ev):(events+1+ev),1)<(m+5);
A7=a7(q,1);
N7(n,i)=length(A7);
m=m+5;
clear q;
clear A7;
end
T7t=[T7t,t7(events+1+ev,1)];
ev=ev+events;
end

%CHANNEL 8
ev=0;
T8t=zeros(1,1);
for i=1:da8
n=0;
m=35;
while m<100
n=n+1;
q=a8((2+ev):(events+1+ev),1)>(m-1) & a8((2+ev):(events+1+ev),1)<(m+5);
A8=a8(q,1);
N8(n,i)=length(A8);
m=m+5;
clear q;
clear A8;
end
T8t=[T8t,t8(events+1+ev,1)];
ev=ev+events;
end

```

b-value_ver2.m

```
%prg to calculate the b-values
%i need to have already the data loaded
%i.e. : I need to run prg amplitudes_ver2 first.
%i do not call that prg from here 'cos in this way I can choose which
%time interval to use and run the relative amplitude prg.

A=[35:5:100];
A=A';
b1=zeros(1,da1(1,1));
b2=zeros(1,da2(1,1));
b3=zeros(1,da3(1,1));
b4=zeros(1,da4(1,1));
b5=zeros(1,da5(1,1));
b6=zeros(1,da6(1,1));
b7=zeros(1,da7(1,1));
b8=zeros(1,da8(1,1));

%FOR CHANNEL 1
for n=1:da1(1,1)
    q=N1(:,n)>0;
    N1b=N1(q,n);
    A1=A(q,1);
    if length(A1)>3
        N1L=LOG10(N1b);
        p=polyfit(A1,N1L(:,1),1);
        p1=polyval(p,A1);
        b1(1,n)=p(1,1);
    else
        b1(1,n)=NaN;
    end
    clear q;
end
B1=b1*-20;
q=T1f(1,:)>0;
T1=T1f(1,q);
figure
plot(T1,B1,'-',T1,B1,'o');
axis([0 T1(1,da1(1,1))+10 0 2.5])
xlabel('time sec')
ylabel('b-value')
title('Trend of b-values CHANNEL 1')

%FOR CHANNEL 2
for n=1:da2(1,1)
    q=N2(:,n)>0; %delete zeros from N2 'cos otherwise the log goes mad. Use the logical variable
    q. %cycle for each column. da2(1,1) is the number of columns of N2
    N2b=N2(q,n);
    A2=A(q,1);
    if length(A2)>3 %fitting curve only if I have at least 4 values!
        N2L=LOG10(N2b); % create a new vector N2L, with the log of the frequency.
        p=polyfit(A2,N2L(:,1),1);
        p2=polyval(p,A2);
        b2(1,n)=p(1,1); %put the b-value in the b vector
    else
        b2(1,n)=NaN;
    end
end
```

```

clear q;
end
%I have the vector b with all the b-values during all the time for this channel
%now I can draw the chart with the trend of the b-values during the recording time
B2=b2*-20; %multiply the b-values by 20 (as this is the sismic value) and I made it positive as well
q=T2t(1,:)>0;
T2=T2t(1,q); %vector of the time to be plotted
figure %plot the chart
plot(T2,B2,'-',T2,B2,'o');
axis([0 T2(1,da2(1,1))+10 0 2.5])
xlabel('time sec')
ylabel('b-value')
title('Trend of b-values CHANNEL 2')

%FOR CHANNEL 3
for n=1:da3(1,1)
    q=N3(:,n)>0;
    N3b=N3(q,n);
    A3=A(q,1);
    if length(A3)>3
        N3L=LOG10(N3b);
        p=polyfit(A3,N3L(:,1),1);
        p3=polyval(p,A3);
        b3(1,n)=p(1,1);
    else
        b3(1,n)=NaN;
    end
    clear q;
end
B3=b3*-20;
q=T3t(1,:)>0;
T3=T3t(1,q);
figure
plot(T3,B3,'-',T3,B3,'o');
axis([0 T3(1,da3(1,1))+10 0 2.5])
xlabel('time sec')
ylabel('b-value')
title('Trend of b-values CHANNEL 3')

%FOR CHANNEL 4
for n=1:da4(1,1)
    q=N4(:,n)>0;
    N4b=N4(q,n);
    A4=A(q,1);
    if length(A4)>3
        N4L=LOG10(N4b);
        p=polyfit(A4,N4L(:,1),1);
        p4=polyval(p,A4);
        b4(1,n)=p(1,1);
    else
        b4(1,n)=NaN;
    end
    clear q;
end
B4=b4*-20;
q=T4t(1,:)>0;

```

```

T4=T4f(1,q);
figure
plot(T4,B4,'-',T4,B4,'o');
axis([0 T4(1,da4(1,1))+10 0 2.5])
xlabel('time sec')
ylabel('b-value')
title('Trend of b-values CHANNEL 4')

%FOR CHANNEL 5
for n=1:da5(1,1)
    q=N5(:,n)>0;
    N5b=N5(q,n);
    A5=A(q,1);
    if length(A5)>3
        N5L=LOG10(N5b);
        p=polyfit(A5,N5L(:,1),1);
        p5=polyval(p,A5);
        b5(1,n)=p(1,1);
    else
        b5(1,n)=NaN;
    end
    clear q;
end
B5=b5*-20;
q=T5f(1,:)>0;
T5=T5f(1,q);
figure
plot(T5,B5,'-',T5,B5,'o');
axis([0 T5(1,da5(1,1))+10 0 2.5])
xlabel('time sec')
ylabel('b-value')
title('Trend of b-values CHANNEL 5')

%FOR CHANNEL 6
for n=1:da6(1,1)
    q=N6(:,n)>0;
    N6b=N6(q,n);
    A6=A(q,1);
    if length(A6)>3
        N6L=LOG10(N6b);
        p=polyfit(A6,N6L(:,1),1);
        p6=polyval(p,A6);
        b6(1,n)=p(1,1);
    else
        b6(1,n)=NaN;
    end
    clear q;
end
B6=b6*-20;
q=T6f(1,:)>0;
T6=T6f(1,q);
figure
plot(T6,B6,'-',T6,B6,'o');
axis([0 T6(1,da6(1,1))+10 0 2.5])
xlabel('time sec')
ylabel('b-value')

```



```
title('Trend of b-values CHANNEL 6')
```

```
%FOR CHANNEL 7
for n=1:da7(1,1)
    q=N7(:,n)>0;
    N7b=N7(q,n);
    A7=A(q,1);
    if length(A7)>3
        N7L=LOG10(N7b);
        p=polyfit(A7,N7L(:,1),1);
        p7=polyval(p,A7);
        b7(1,n)=p(1,1);
    else
        b7(1,n)=NaN;
    end
    clear q;
end
B7=b7*-20;
q=T7t(1,:)>0;
T7=T7t(1,q);
figure
plot(T7,B7,'-',T7,B7,'o');
axis([0 T7(1,da7(1,1))+10 0 2.5])
xlabel('time sec')
ylabel('b-value')
title('Trend of b-values CHANNEL 7')
```

```
%FOR CHANNEL 8
for n=1:da8(1,1)
    q=N8(:,n)>0;
    N8b=N8(q,n);
    A8=A(q,1);
    if length(A8)>3
        N8L=LOG10(N8b);
        p=polyfit(A8,N8L(:,1),1);
        p8=polyval(p,A8);
        b8(1,n)=p(1,1);
    else
        b8(1,n)=NaN;
    end
    clear q;
end
B8=b8*-20;
q=T8t(1,:)>0;
T8=T8t(1,q);
figure
plot(T8,B8,'-',T8,B8,'o');
axis([0 T8(1,da8(1,1))+10 0 2.5])
xlabel('time sec')
ylabel('b-value')
title('Trend of b-values CHANNEL 8')
```

bvaluech2_ver7.

```
%prg that creates a graph for a single channel
%with the trends of bvalues for different groups of events
%need to run prg channels.m first

events=input('insert the number of AE events: '); %ask for number of events I want to use
a2=ch2(:,10);
dim2=size(a2);
A=[35:5:100];
A=A';

    da2=fix(length(a2)/events); %calculates with "events" number of events
    N2=zeros(14,da2(1,1));
    ev=0;
    T2t=zeros(1,1);
for i=1:da2
    n=0;
    m=35;
    while m<100
        n=n+1;
        q=a2((2+ev):(events+1+ev),1)>(m-1) & a2((2+ev):(events+1+ev),1)<(m+5);
        A2=a2(q,1);
        N2(n,i)=length(A2);
        m=m+5;
        clear q;
        clear A2;
    end
    T2t=[T2t,t2(events+1+ev,1)];
    ev=ev+events;
end

for n=1:da2(1,1)
    q=N2(:,n)>0;
    N2b=N2(q,n);
    A2=A(q,1);
    if length(A2)>3
        N2L=LOG10(N2b);
        p=polyfit(A2,N2L(:,1),1);
        p2=polyval(p,A2);
        b2(1,n)=p(1,1);
    else
        b2(1,n)=NaN;
    end
    clear q;
end

B2=b2*-20;
q=T2t(1,:)>0;
T2=T2t(1,q);
figure
plot(T2,B2,'k+-');
hold on
axis([0 T2(1,da2(1,1))+10 0 2.5])
xlabel('time sec')
ylabel('b-value')
title('Trend of b-values CHANNEL 2')
```

```

clear T2t;
clear T2;
clear b2;
clear B2;

events=events+30;
da2=fix(length(a2)/events); %calculate with "events+30" events
N2=zeros(14,da2(1,1));
ev=0;
T2t=zeros(1,1);
for i=1:da2
n=0;
m=35;
while m<100
n=n+1;
q=a2((2+ev):(events+1+ev),1)>(m-1) & a2((2+ev):(events+1+ev),1)<(m+5);
A2=a2(q,1);
N2(n,i)=length(A2);
m=m+5;
clear q;
clear A2;
end
T2t=[T2t,t2(events+1+ev,1)];
ev=ev+events;
end

for n=1:da2(1,1)
q=N2(:,n)>0;
N2b=N2(q,n);
A2=A(q,1);
if length(A2)>3
N2L=LOG10(N2b);
p=polyfit(A2,N2L(:,1),1);
p2=polyval(p,A2);
b2(1,n)=p(1,1);
else
b2(1,n)=NaN;
end
clear q;
end

B2=b2*-20;
q=T2t(1,:)>0;
T2=T2t(1,q);
plot(T2,B2,'r+');
hold on
axis([0 T2(1,da2(1,1))+10 0 2.5])
clear T2t;
clear T2;
clear b2;
clear B2;

events=events-60;
da2=fix(length(a2)/events); %calculate with "events-30" events
N2=zeros(14,da2(1,1));
ev=0;

```

```

    T2t=zeros(1,1);
for i=1:da2
    n=0;
    m=35;
    while m<100
        n=n+1;
        q=a2((2+ev):(events+1+ev),1)>(m-1) & a2((2+ev):(events+1+ev),1)<(m+5);
        A2=a2(q,1);
        N2(n,i)=length(A2);
        m=m+5;
        clear q;
        clear A2;
    end
    T2t=[T2t,t2(events+1+ev,1)];
    ev=ev+events;
end

for n=1:da2(1,1)
    q=N2(:,n)>0;
    N2b=N2(q,n);
    A2=A(q,1);
    if length(A2)>3
        N2L=LOG10(N2b);
        p=polyfit(A2,N2L(:,1),1);
        p2=polyval(p,A2);
        b2(1,n)=p(1,1);
    else
        b2(1,n)=NaN;
    end
    clear q;
end

B2=b2*-20;
q=T2t(1,:)>0;
T2=T2t(1,q);
plot(T2,B2,'c+');
hold on
axis([0 T2(1,da2(1,1))+10 0 2.5])
clear T2t;
clear T2;
clear b2;
clear B2;

```

b-value_fullcycle.m

%prg to calculate the b-value for all cycle
%done for all channels, but this is only one of them!

```
channels
a1=ch1(:,10);
dim1=size(a1);
N1=zeros(14,1);
%CHANNEL 1
n=0;
m=35;
while m<100
    n=n+1;
    q=a1>(m-1) & a1<(m+5);
    A1=a1(q,1);
    N1(n,1)=length(A1);
    m=m+5;
    clear q;
    clear A1;
end
A=[35:5:100]; %now I can calculate the b-values
A=A';
b1=0;
%FOR CHANNEL 1
q=N1(:,1)>0;
N1b=N1(q,1);
A1=A(q,1);
if length(A1)>3
    N1L=LOG10(N1b);
    p=polyfit(A1,N1L(:,1),1);
    p1=polyval(p,A1);
    b1=p(1,1);
    figure
    subplot(2,4,1)
        plot(A1,p1,'-',A1,N1L,'o')
        axis([30 A1(length(A1),1)+5 -0.5 4])
        xlabel('Amplitude range dB')
        ylabel('Frequency - logN')
        title('CHANNEL 1')
    text1=num2str(b1(1,1)*20);
    out1=['b1 = ' text1];
    text(35,1,out1);
else
    b1=NaN;
end
clear q;

%when it contains all the channel I can
%overlap of all the curves for all the channels!
figure
plot(A1,p1,'r-',A2,p2,'c-',A3,p3,'y-',A4,p4,'g-',A5,p5,'b-',A6,p6,'b-', A7,p7,'m-',A8,p8,'r:');
axis([30 A8(length(A8),1)+5 -0.5 5])
xlabel('Amplitude range dB')
ylabel('Frequency - logN')
title('Frequency vs Amplitude - Beam BF2 - Cycle 05')
legend('Ch1','Ch2','Ch3','Ch4','Ch5','Ch6','Ch7','Ch8');
```

Bar_err_bf2ch7.m

```
%prg to draw the error bar on a figure already created
%need to have the figure already up in matlab
%created for the trend of the b-value
%specifically for beam BF2
%it does one channel at the time
%so this is for channel 7
%need to have the txt file created from the excel spreadsheet for the right channel
%run first the bvalues_ver2, which creates the vectors T7 and B7

fn= input('insert the name (or path) of the file containing all min-max errors(no file extension) ','s');
bar7=load([fn '.txt']);
format long g
hold on
xx=[T7-7;T7+7];      %create the vector to draw the horizontal bar
for i=1:length(T7)
    TT7=[T7(1,i) T7(1,i)];
    BAR7=[bar7(i,1) bar7(i,2)];
    plot(TT7,BAR7,'c-')
    XX=[xx(1,i) xx(2,i)];
    BB7=[bar7(i,1) bar7(i,1)];
    plot(XX,BB7,'c-')
    BBB7=[bar7(i,2) bar7(i,2)];
    plot(XX,BBB7,'c')
end
```

b-value_fitcurve_ch7.m

```
%prg to calculate the b-values
%I need to have already the data loaded
%i.e. : I need to run prg amplitudes_ver2 first.
%I do not call that prg from here 'cos in this way I can choose which
%time interval to use and run the relative amplitude prg.

A=[35:5:100];      %create the vector with the amplitude range from 35dB to 100dB
A=A';      %transposition to make it a column vector
b7=zeros(1,da7(1,1)); %initialise vectors b, where I'll put all the b-values. A vector for each channel
%FOR CHANNEL 7
for n=1:da7(1,1)      %cycle for each column. da2(1,1) is the number of columns of N2
    q=N7(:,n)>0;      %delete zeros from N2 'cos otherwise the log goes mad. Use the logical variable q.
    N7b=N7(q,n);      %create temporary var N2b without zeros. It re-writes it every cycle for the other column so it's
    always a one column vector
    A7=A(q,1);      %cut zeros in range di amplitude. still re-write it at every cycle
    if length(A7)>3      %fitting curve only if I have at least 4 values!
        N7L=LOG10(N7b);      % create a new vector N2L, with the log of the frequency.
        %re-write at every cycle; always one column
        p=polyfit(A7,N7L(:,1),1); %create the variable p with 2 elements:
        %the 1st is the b_value the second is the a of the curve
        p7=polyval(p,A7);      %calculate the values on the curve
        b7(1,n)=p(1,1);      %put the b-value in the b vector
        figure
        plot(A7,p7,'-',A7,N7L,'o');
        axis([30 A7(length(A7),1)+5 0 2.5])
        xlabel('Amplitude range dB')
        ylabel('Frequency - logN')
        title('Frequency vs Amplitude. CHANNEL 7')
    else
        b7(1,n)=NaN;
    end
    clear q;      %at the end of the cycle delete q, or create pb for next step
end
```

Damage_parameter.m

```
%prg to calculate the damage parameter D
%done for beam BF2
%it recalls the prg channels to load up data
%it calculates the damage parameter each 'n' events, where I tell it how many is 'n'
%it calculates the maximum value of the damage parameter Dmax
%it plots the trend of D normalized by Dmax over the time of the cycle
%one plot for each channel

channels          %load up data
events=input('insert the number of AE events: '); %ask for number of events I want to use
c=input('insert the value of the factor c '); %ask for the value of the factor c that I want to use

a1=ch1(:,10);      %create a filewith the amplitude of the signals, for each channel
a2=ch2(:,10);      %the first row is all zeros!
a3=ch3(:,10);
a4=ch4(:,10);
a5=ch5(:,10);
a6=ch6(:,10);
a7=ch7(:,10);
a8=ch8(:,10);

dim1=size(a1);    %calculate the dimensions of the vectors for each channel
dim2=size(a2);    %NB it is not the number of hits... it's the number of hits plus 1!
dim3=size(a3);    % NB these are the dimensions of the vectors 'a' and 't'
dim4=size(a4);
dim5=size(a5);
dim6=size(a6);
dim7=size(a7);
dim8=size(a8);

da1=fix(length(a1)/events); %calculate number of intervals, with "events" number of events
da2=fix(length(a2)/events);
da3=fix(length(a3)/events);
da4=fix(length(a4)/events);
da5=fix(length(a5)/events);
da6=fix(length(a6)/events);
da7=fix(length(a7)/events);
da8=fix(length(a8)/events);

%calculate Dmax for each channel

b1=10*ones(size(a1));
c1=b1.^(c*a1);
D1max=sum(c1)-1; %need to subtract 1 'cos the amplitude vectors have the first row of zeros!
b2=10*ones(size(a2));
c2=b2.^(c*a2);
D2max=sum(c2)-1;
b3=10*ones(size(a3));
c3=b3.^(c*a3);
D3max=sum(c3)-1;
b4=10*ones(size(a4));
c4=b4.^(c*a4);
D4max=sum(c4)-1;
b5=10*ones(size(a5));
c5=b5.^(c*a5);
```

```

D5max=sum(c5)-1;
b6=10*ones(size(a6));
c6=b6.^(c*a6);
D6max=sum(c6)-1;
b7=10*ones(size(a7));
c7=b7.^(c*a7);
D7max=sum(c7)-1;
b8=10*ones(size(a8));
c8=b8.^(c*a8);
D8max=sum(c8)-1;

%calculate D for 'tot' events and plot them
%explanation is next to channel 2

%channel 1
T1t=zeros(1,1);
D1=zeros(1,1);
D1t=zeros(1,1);
for i=2:(da1+1)
    if i<(da1+1)
        format long g
        A1=a1((events*(i-1))-(events-2):events*(i-1)+1);
        B1=10*ones(size(A1));
        C1=B1.^(c*A1);
        D1(i,1)=sum(C1)+D1(i-1,1);
        D1t(i,1)=D1(i,1)/D1max;
        T1t=[T1t,t1(events*(i-1)+1,1)];
    else A1=a1((events*(i-1))-(events-2):end);
        B1=10*ones(size(A1));
        C1=B1.^(c*A1);
        D1(i,1)=sum(C1)+D1(i-1,1);
        D1t(i,1)=D1(i,1)/D1max;
        T1t=[T1t,t1(end,1)];
    end
end
figure
plot(T1t,D1t,'r');
title('Evolution of the Damage Parameter D - Ch.1')
axis([0 T1t(1,end)+10 0 1.1])
xlabel('time sec')
ylabel('damage parameter D')

%channel 2
T2t=zeros(1,1);
D2=zeros(1,1);
D2t=zeros(1,1);
for i=2:(da2+1)
    if i<(da2+1)
        format long g
        A2=a2((events*(i-1))-(events-2):events*(i-1)+1);
        B2=10*ones(size(A2));
        C2=B2.^(c*A2);
        D2(i,1)=sum(C2)+D2(i-1,1);
        D2t(i,1)=D2(i,1)/D2max;
        T2t=[T2t,t2(events*(i-1)+1,1)];
    else A2=a2((events*(i-1))-(events-2):end); %need two cases, 'cos the last interval does not have

```



```

        B2=10*ones(size(A2));           %an exact number of events according to the step I set up
        C2=B2.^(c*A2);
        D2(i,1)=sum(C2)+D2(i-1,1);
        D2t(i,1)=D2(i,1)/D2max;
        T2t=[T2t,t2(end,1)];
    end
end
figure
plot(T2t,D2t,'r');
title('Evolution of the Damage Parameter D - Ch.2')
axis([0 T2t(1,end)+10 0 1.1])
xlabel('time sec')
ylabel('damage parameter D')

%channel 3
T3t=zeros(1,1);
D3=zeros(1,1);
D3t=zeros(1,1);
for i=2:(da3+1)
    if i<(da3+1)
        format long g
        A3=a3((events*(i-1))-(events-2):events*(i-1)+1);
        B3=10*ones(size(A3));
        C3=B3.^(c*A3);
        D3(i,1)=sum(C3)+D3(i-1,1);
        D3t(i,1)=D3(i,1)/D3max;
        T3t=[T3t,t3(events*(i-1)+1,1)];
    else A3=a3((events*(i-1))-(events-2):end);
        B3=10*ones(size(A3));
        C3=B3.^(c*A3);
        D3(i,1)=sum(C3)+D3(i-1,1);
        D3t(i,1)=D3(i,1)/D3max;
        T3t=[T3t,t3(end,1)];
    end
end
figure
plot(T3t,D3t,'r');
title('Evolution of the Damage Parameter D - Ch.3')
axis([0 300 0 1.1])
xlabel('time sec')
ylabel('damage parameter D')

%channel 4
T4t=zeros(1,1);
D4=zeros(1,1);
D4t=zeros(1,1);
for i=2:(da4+1)
    if i<(da4+1)
        format long g
        A4=a4((events*(i-1))-(events-2):events*(i-1)+1);
        B4=10*ones(size(A4));
        C4=B4.^(c*A4);
        D4(i,1)=sum(C4)+D4(i-1,1);
        D4t(i,1)=D4(i,1)/D4max;
        T4t=[T4t,t4(events*(i-1)+1,1)];
    else A4=a4((events*(i-1))-(events-2):end);

```

```

        B4=10*ones(size(A4));
        C4=B4.^(c*A4);
        D4(i,1)=sum(C4)+D4(i-1,1);
        D4t(i,1)=D4(i,1)/D4max;
        T4t=[T4t,t4(end,1)];
    end
end
figure
plot(T4t,D4t,'r');
title('Evolution of the Damage Parameter D - Ch.4')
axis([0 T4t(1,end)+10 0 1.1])
xlabel('time sec')
ylabel('damage parameter D')

%channel 5
T5t=zeros(1,1);
D5=zeros(1,1);
D5t=zeros(1,1);
for i=2:(da5+1)
    if i<(da5+1)
        format long g
        A5=a5((events*(i-1))-(events-2):events*(i-1)+1);
        B5=10*ones(size(A5));
        C5=B5.^(c*A5);
        D5(i,1)=sum(C5)+D5(i-1,1);
        D5t(i,1)=D5(i,1)/D5max;
        T5t=[T5t,t5(events*(i-1)+1,1)];
    else A5=a5((events*(i-1))-(events-2):end);
        B5=10*ones(size(A5));
        C5=B5.^(c*A5);
        D5(i,1)=sum(C5)+D5(i-1,1);
        D5t(i,1)=D5(i,1)/D5max;
        T5t=[T5t,t5(end,1)];
    end
end
figure
plot(T5t,D5t,'r');
title('Evolution of the Damage Parameter D - Ch.5')
axis([0 T5t(1,end)+10 0 1.1])
xlabel('time sec')
ylabel('damage parameter D')

%channel 6
T6t=zeros(1,1);
D6=zeros(1,1);
D6t=zeros(1,1);
for i=2:(da6+1)
    if i<(da6+1)
        format long g
        A6=a6((events*(i-1))-(events-2):events*(i-1)+1);
        B6=10*ones(size(A6));
        C6=B6.^(c*A6);
        D6(i,1)=sum(C6)+D6(i-1,1);
        D6t(i,1)=D6(i,1)/D6max;
        T6t=[T6t,t6(events*(i-1)+1,1)];
    else A6=a6((events*(i-1))-(events-2):end);

```

```

        B6=10*ones(size(A6));
        C6=B6.^(c*A6);
        D6(i,1)=sum(C6)+D6(i-1,1);
        D6t(i,1)=D6(i,1)/D6max;
        T6t=[T6t,t6(end,1)];
    end
end
figure
plot(T6t,D6t,'r');
title('Evolution of the Damage Parameter D - Ch.6')
axis([0 T6t(1,end)+10 0 1.1])
xlabel('time sec')
ylabel('damage parameter D')

%channel 7
T7t=zeros(1,1);
D7=zeros(1,1);
D7t=zeros(1,1);
for i=2:(da7+1)
    if i<(da7+1)
        format long g
        A7=a7((events*(i-1))-(events-2):events*(i-1)+1);
        B7=10*ones(size(A7));
        C7=B7.^(c*A7);
        D7(i,1)=sum(C7)+D7(i-1,1);
        D7t(i,1)=D7(i,1)/D7max;
        T7t=[T7t,t7(events*(i-1)+1,1)];
    else A7=a7((events*(i-1))-(events-2):end);
        B7=10*ones(size(A7));
        C7=B7.^(c*A7);
        D7(i,1)=sum(C7)+D7(i-1,1);
        D7t(i,1)=D7(i,1)/D7max;
        T7t=[T7t,t7(end,1)];
    end
end
figure
plot(T7t,D7t,'r');
title('Evolution of the Damage Parameter D - Ch.7')
axis([0 T7t(1,end)+10 0 1.1])
xlabel('time sec')
ylabel('damage parameter D')

%channel 8
T8t=zeros(1,1);
D8=zeros(1,1);
D8t=zeros(1,1);
for i=2:(da8+1)
    if i<(da8+1)
        format long g
        A8=a8((events*(i-1))-(events-2):events*(i-1)+1);
        B8=10*ones(size(A8));
        C8=B8.^(c*A8);
        D8(i,1)=sum(C8)+D8(i-1,1);
        D8t(i,1)=D8(i,1)/D8max;
        T8t=[T8t,t8(events*(i-1)+1,1)];
    else A8=a8((events*(i-1))-(events-2):end);

```

```

B8=10*ones(size(A8));
C8=B8.^(c*A8);
D8(i,1)=sum(C8)+D8(i-1,1);
D8t(i,1)=D8(i,1)/D8max;
T8t=[T8t,t8(end,1)];
end
end
figure
plot(T8t,D8t,'r');
title('Evolution of the Damage Parameter D - Ch.8')
axis([0 T8t(1,end)+10 0 1.1])
xlabel('time sec')
ylabel('damage parameter D')

```

b-value_boghall.m

%prg for the b-value analysis
%of Boghall bridge data

```
channels_ver2
a1=ch1(:,7);
a2=ch2(:,7);
a3=ch3(:,7);
a4=ch4(:,7);
a5=ch5(:,7);
a6=ch6(:,7);
a7=ch7(:,7);
a8=ch8(:,7);
dim1=size(a1);
dim2=size(a2);
dim3=size(a3);
dim4=size(a4);
dim5=size(a5);
dim6=size(a6);
dim7=size(a7);
dim8=size(a8);
N1=zeros(16,1); %create vector with the frequency. It's just one column!
N2=zeros(16,1); %'cos it's with all the events of the cycle
N3=zeros(16,1);
N4=zeros(16,1);
N5=zeros(16,1);
N6=zeros(16,1);
N7=zeros(16,1);
N8=zeros(16,1);

%CHANNEL 1
n=0;
m=30;
while m<76
    n=n+1;
    q=a1>(m-1) & a1<(m+3);
    A1=a1(q,1);
    N1(n,1)=length(A1);
    m=m+3;
    clear q;
    clear A1;
end

%CHANNEL 2
n=0;
m=30;
while m<76
    n=n+1;
    q=a2>(m-1) & a2<(m+3);
    A2=a2(q,1);
    N2(n,1)=length(A2);
    m=m+3;
    clear q;
    clear A2;
end
```

```

%CHANNEL 3
n=0;
m=30;
while m<76
    n=n+1;
    q=a3>(m-1) & a3<(m+3);
    A3=a3(q,1);
    N3(n,1)=length(A3);
    m=m+3;
    clear q;
    clear A3;
end

```

```

%CHANNEL 4
n=0;
m=30;
while m<76
    n=n+1;
    q=a4>(m-1) & a4<(m+3);
    A4=a4(q,1);
    N4(n,1)=length(A4);
    m=m+3;
    clear q;
    clear A4;
end

```

```

%CHANNEL 5
n=0;
m=30;
while m<76
    n=n+1;
    q=a5>(m-1) & a5<(m+3);
    A5=a5(q,1);
    N5(n,1)=length(A5);
    m=m+3;
    clear q;
    clear A5;
end

```

```

%CHANNEL 6
n=0;
m=30;
while m<76
    n=n+1;
    q=a6>(m-1) & a6<(m+3);
    A6=a6(q,1);
    N6(n,1)=length(A6);
    m=m+3;
    clear q;
    clear A6;
end

```

```

%CHANNEL 7
n=0;
m=30;
while m<76

```

```

n=n+1;
    q=a7>(m-1) & a7<(m+3);
    A7=a7(q,1);
    N7(n,1)=length(A7);
    m=m+3;
    clear q;
    clear A7;
end

%CHANNEL 8
n=0;
m=30;
while m<76
    n=n+1;
    q=a8>(m-1) & a8<(m+3);
    A8=a8(q,1);
    N8(n,1)=length(A8);
    m=m+3;
    clear q;
    clear A8;
end

    %now calculate the b-values
A=[30:3:75]; %create the vector with the amplitude range from 35dB to 100dB
A=A'; %transposition to make it a column vector

b1=0; %initialise vectors b, where I'll put all the b-values
b2=0;
b3=0;
b4=0;
b5=0;
b6=0;
b7=0;
b8=0;

%FOR CHANNEL 1
q=N1(:,1)>0;
N1b=N1(q,1);
A1=A(q,1);
if length(A1)>2
    N1L=LOG10(N1b);
    p=polyfit(A1,N1L(:,1),1);
    p1=polyval(p,A1);
    b1=p(1,1);
    figure
    subplot(2,4,1)
        plot(A1,p1,'-',A1,N1L,'o')
        axis([25 A1(length(A1),1)+5 -0.5 4])
        xlabel('Amplitude range dB')
        ylabel('Frequency - logN')
        title('channel 1')
    text1=num2str(b1(1,1)*20);
    out1=['b1 = ' text1];
    text(35,1,out1,'FontSize',12,'FontWeight','bold','FontName','serifa BT');
else
    b1=NaN;
end

```

```

end
clear q;

%FOR CHANNEL 2
q=N2(:,1)>0;
N2b=N2(q,1);
A2=A(q,1);
if length(A2)>2
    N2L=LOG10(N2b);
    p=polyfit(A2,N2L(:,1),1);
    p2=polyval(p,A2);
    b2=p(1,1);
    subplot(2,4,2)
        plot(A2,p2,'-',A2,N2L,'o')
        axis([25 A2(length(A2),1)+5 -0.5 4])
        xlabel('Amplitude range dB')
        ylabel('Frequency - logN')
        title('channel 2')
    text2=num2str(b2(1,1)*20);
    out2=['b2=' text2];
    text(35,1,out2,'FontSize',12,'FontWeight','bold','FontName','serifa BT');
else
    b2=NaN;
end
clear q;

%FOR CHANNEL 3
q=N3(:,1)>0;
N3b=N3(q,1);
A3=A(q,1);
if length(A3)>2
    N3L=LOG10(N3b);
    p=polyfit(A3,N3L(:,1),1);
    p3=polyval(p,A3);
    b3=p(1,1);
    subplot(2,4,3)
        plot(A3,p3,'-',A3,N3L,'o')
        axis([25 A3(length(A3),1)+5 -0.5 4])
        xlabel('Amplitude range dB')
        ylabel('Frequency - logN')
        title('channel 3')
    text3=num2str(b3(1,1)*20);
    out3=['b3=' text3];
    text(35,1,out3,'FontSize',12,'FontWeight','bold','FontName','serifa BT');
else
    b3=NaN;
end
clear q;

%FOR CHANNEL 4
q=N4(:,1)>0;
N4b=N4(q,1);
A4=A(q,1);
if length(A4)>2
    N4L=LOG10(N4b);
    p=polyfit(A4,N4L(:,1),1);

```



```

        p4=polyval(p,A4);
        b4=p(1,1);
        subplot(2,4,4)
            plot(A4,p4,'-',A4,N4L,'o')
            axis([25 A4(length(A4),1)+5 -0.5 4])
            xlabel('Amplitude range dB')
            ylabel('Frequency - logN')
            title('channel 4')
        text4=num2str(b4(1,1)*20);
        out4=['b4=' text4];
        text(35,1,out4,'FontSize',12,'FontWeight','bold','FontName','serifa BT');
    else
        b4=NaN;
    end
    clear q;

%FOR CHANNEL 5
    q=N5(:,1)>0;
    N5b=N5(q,1);
    A5=A(q,1);
    if length(A5)>2
        N5L=LOG10(N5b);
        p=polyfit(A5,N5L(:,1),1);
        p5=polyval(p,A5);
        b5=p(1,1);
        subplot(2,4,5)
            plot(A5,p5,'-',A5,N5L,'o')
            axis([25 A5(length(A5),1)+5 -0.5 4])
            xlabel('Amplitude range dB')
            ylabel('Frequency - logN')
            title('channel 5')
        text5=num2str(b5(1,1)*20);
        out5=['b5=' text5];
        text(35,1,out5,'FontSize',12,'FontWeight','bold','FontName','serifa BT');
    else
        b5=NaN;
    end
    clear q;

%FOR CHANNEL 6
    q=N6(:,1)>0;
    N6b=N6(q,1);
    A6=A(q,1);
    if length(A6)>2
        N6L=LOG10(N6b);
        p=polyfit(A6,N6L(:,1),1);
        p6=polyval(p,A6);
        b6=p(1,1);
        subplot(2,4,6)
            plot(A6,p6,'-',A6,N6L,'o')
            axis([25 A6(length(A6),1)+5 -0.5 4])
            xlabel('Amplitude range dB')
            ylabel('Frequency - logN')
            title('channel 6')
        text6=num2str(b6(1,1)*20);
        out6=['b6=' text6];
    end

```

```

text(35,1,out6,'FontSize',12,'FontWeight','bold','FontName','serifa BT');
else
    b6=NaN;
end
clear q;

%FOR CHANNEL 7
q=N7(:,1)>0;
N7b=N7(q,1);
A7=A(q,1);
if length(A7)>2
    N7L=LOG10(N7b);
    p=polyfit(A7,N7L(:,1),1);
    p7=polyval(p,A7);
    b7=p(1,1);
    subplot(2,4,7)
        plot(A7,p7,'-',A7,N7L,'o')
        axis([25 A7(length(A7),1)+5 -0.5 4])
        xlabel('Amplitude range dB')
        ylabel('Frequency - logN')
        title('channel 7')
    text7=num2str(b7(1,1)*20);
    out7=['b7=' text7];
    text(35,1,out7,'FontSize',12,'FontWeight','bold','FontName','serifa BT');
else
    b7=NaN;
end
clear q;

%FOR CHANNEL 8
q=N8(:,1)>0;
N8b=N8(q,1);
A8=A(q,1);
if length(A8)>2
    N8L=LOG10(N8b);
    p=polyfit(A8,N8L(:,1),1);
    p8=polyval(p,A8);
    b8=p(1,1);
    subplot(2,4,8)
        plot(A8,p8,'-',A8,N8L,'o')
        axis([25 A8(length(A8),1)+5 -0.5 4])
        xlabel('Amplitude range dB')
        ylabel('Frequency - logN')
        title('channel 8')
    text8=num2str(b8(1,1)*20);
    out8=['b8=' text8];
    text(35,1,out8,'FontSize',12,'FontWeight','bold','FontName','serifa BT');
else
    b8=NaN;
end
clear q;

```

dataHB2.m

```
%prg for processing of beam HB2
%so I only have channels 1 2 5 6 7 8
%prg that reads all the data files related to the beam HB2
%after reading the file, as first thing it selects only the signals
%with amplitude above 60dB, to make all the cycles comparable
%! load all the 4 cycles all the time
%!it plots the energy in the different load intervals and as function of sensors location

s=cell(4,1); %create the cell array to put in all the data files
ch1=cell(4,1); %create the cell array for the data of channel 1
ch2=cell(4,1);
ch5=cell(4,1);
ch6=cell(4,1);
ch7=cell(4,1);
ch8=cell(4,1);
cumenergy=cell(4,1); %cell array only with the total energy for each cycle and for each
ch
energy=cell(4,1); %create cell array with the cum energy for each ch (columns) and for
each cycle (4)
CH1=cell(4,1); %create cell array with data for ch 1 up to a certain load
CH2=cell(4,1);
CH5=cell(4,1);
CH6=cell(4,1);
CH7=cell(4,1);
CH8=cell(4,1);
colour=cell(5,1); %create the cell with the string to define the line type and colour of
the plots
legenda=cell(11,1); %create the cell with the possible legend
CH=[1 2 5 6 7 8]; %need to have the vector for x-axis

colour{1}='b';
colour{2}='g';
colour{3}='y';
colour{4}='r';
colour{5}='m';

legenda{1}='cycle no.1';
legenda{2}='cycle no.4';
legenda{3}='cycle no.6';
legenda{4}='cycle no.7';
legenda{5}='all the test';
legenda{6}='up to 60kN';
legenda{7}='up to 120kN';
legenda{8}='up to 140kN';
legenda{9}='up to 160kN';
legenda{10}='up to 190kN';
legenda{11}='up to failure';

%INSERT DATA
for i=1:4
    fn= input('insert the name (or path) of the file containing all the AE parameters for all the channels(no
file extension) ','s');
    s{i}=load([fn '.txt']);
    format long g
    q=s{i}(:,7)>59; %to keep only signals above 60dB
    s{i}=s{i}(q,:);
```

```

dim=size(s{i});
for k=1:dim(1,1)      %create cells for each channel
    switch s{i}(k,2)
        case 1
            ch1 {i}=[ch1 {i};s{i}(k,:)];
        case 2
            ch2{i}=[ch2{i};s{i}(k,:)];
        case 5
            ch5{i}=[ch5{i};s{i}(k,:)];
        case 6
            ch6{i}=[ch6{i};s{i}(k,:)];
        case 7
            ch7{i}=[ch7{i};s{i}(k,:)];
        case 8
            ch8{i}=[ch8{i};s{i}(k,:)];
        otherwise
            error('This is impossible');
        end
    end
end

%CALCULATE DIMENSIONS OF CH1 {i}
dim1 =cell(4,1);
dim2=cell(4,1);
dim5=cell(4,1);
dim6=cell(4,1);
dim7=cell(4,1);
dim8=cell(4,1);
for i=1:4
    dim1 {i}=size(ch1 {i});
    dim2{i}=size(ch2{i});
    dim5{i}=size(ch5{i});
    dim6{i}=size(ch6{i});
    dim7{i}=size(ch7{i});
    dim8{i}=size(ch8{i});
end

%CALCULATE THE TOTAL CUM ENERGY FOR EACH CHANNEL & FOR EACH CYCLE
for i=1:4
    if size(ch1 {i})>0
        cumenergy{i}(1,1)=sum(ch1 {i}(:,5));
    else cumenergy{i}(1,1)=0;          %if in that channel there are no events it assigns zero
    energy
    end
    if size(ch2{i})>0
        cumenergy{i}(1,2)=sum(ch2{i}(:,5));
    else cumenergy{i}(1,2)=0;
    end
    if size(ch5{i})>0
        cumenergy{i}(1,3)=sum(ch5{i}(:,5));
    else cumenergy{i}(1,3)=0;
    end
    if size(ch6{i})>0
        cumenergy{i}(1,4)=sum(ch6{i}(:,5));
    else cumenergy{i}(1,4)=0;
    end
end

```

```

if size(ch7{i})>0
cumenergy{i}(1,5)=sum(ch7{i}{:},5);
else cumenergy{i}(1,5)=0;
end
if size(ch8{i})>0
cumenergy{i}(1,6)=sum(ch8{i}{:},5);
else cumenergy{i}(1,6)=0;
end
end

%PLOT THE CUM ENERGY OF EACH CHANNEL FOR EACH CYCLE
%IN TWO WAYS: ONE CYCLE NEXT TO THE OTHER OR ONE CYCLE ON THE TOP OF THE OTHER

CUMENERGY=[cumenergy{1}; cumenergy{2}; cumenergy{3}; cumenergy{4}];
figure
bar(CH,transpose(CUMENERGY));           %one next to the other
title('CUMULATIVE ENERGY','FontSize',12,'FontWeight','bold','FontName','serifa BT')
axis([0 9 0 max(max(CUMENERGY))+50])
xlabel('channel','FontSize',12,'FontName','serifa thin BT')
ylabel('energy','FontSize',12,'FontName','serifa thin BT')
legend(legenda{1:4})
figure
bar(CH,transpose(CUMENERGY),'stack');   %on the top
title('CUMULATIVE ENERGY','FontSize',12,'FontWeight','bold','FontName','serifa BT')
axis([0 9 0 max(max(CUMENERGY))*3])
xlabel('channel','FontSize',12,'FontName','serifa thin BT')
ylabel('energy','FontSize',12,'FontName','serifa thin BT')
legend(legenda{1:4})

%CONSIDERING THE DATA OF ALL 4 CYCLES
%DIVIDE THE ENERGY FOR GROUPS OF LOAD - 60-120-140-160-190-FAIL
%AND FOR EACH CHANNEL
%STACK THE DIFFERENT GROUPS ON THE TOP OF EACH OTHER
%the vectors t60,... contains the time when the relative load is reach in each cycle

t60=[1 2335 1742 210];           %1 stands for ALL CYCLE!
t120=[0 0 1 2340];              %0 stands for no contributions of that cycle
t140=[0 0 0 3720];
t160=[0 0 0 5520];
t190=[0 0 0 6270];
tfail=[0 0 0 1];

%for 60kN
%for channel 1
if size(ch1{2})>0
p=ch1{2}{:,1}<2335;
CH1{2}=ch1{2}(p,:);
else CH1{2}=zeros(1,5);
end
if size(ch1{3})>0
p=ch1{3}{:,1}<1742;
CH1{3}=ch1{3}(p,:);
else CH1{3}=zeros(1,5);
end

```

```

end
if size(ch1{4})>0
p=ch1{4}(:,1)<210;
CH1{4}=ch1{4}(p,:);
else CH1{4}=zeros(1,5);
end
energy60=[(sum(ch1{1}(:,5)))+(sum(CH1{2}(:,5)))+(sum(CH1{3}(:,5)))+(sum(CH1{4}(:,5)))]);
%for channel 2
if size(ch2{2})>0
p=ch2{2}(:,1)<2335;
CH2{2}=ch2{2}(p,:);
else CH2{2}=zeros(1,5);
end
if size(ch2{3})>0
p=ch2{3}(:,1)<1742;
CH2{3}=ch2{3}(p,:);
else CH2{3}=zeros(1,5);
end
if size(ch2{4})>0
p=ch2{4}(:,1)<210;
CH2{4}=ch2{4}(p,:);
else CH2{4}=zeros(1,5);
end
energy60(1,2)=sum(ch2{1}(:,5))+sum(CH2{2}(:,5))+sum(CH2{3}(:,5))+sum(CH2{4}(:,5));
%for channel 5
if size(ch5{2})>0
p=ch5{2}(:,1)<2335;
CH5{2}=ch5{2}(p,:);
else CH5{2}=zeros(1,5);
end
if size(ch5{3})>0
p=ch5{3}(:,1)<1742;
CH5{3}=ch5{3}(p,:);
else CH5{3}=zeros(1,5);
end
if size(ch5{4})>0
p=ch5{4}(:,1)<210;
CH5{4}=ch5{4}(p,:);
else CH5{4}=zeros(1,5);
end
energy60(1,3)=sum(ch5{1}(:,5))+sum(CH5{2}(:,5))+sum(CH5{3}(:,5))+sum(CH5{4}(:,5));
%for channel 6
if size(ch6{2})>0
p=ch6{2}(:,1)<2335;
CH6{2}=ch6{2}(p,:);
else CH6{2}=zeros(1,5);
end
if size(ch6{3})>0
p=ch6{3}(:,1)<1742;
CH6{3}=ch6{3}(p,:);
else CH6{3}=zeros(1,5);
end
if size(ch6{4})>0
p=ch6{4}(:,1)<210;
CH6{4}=ch6{4}(p,:);
else CH6{4}=zeros(1,5);
end

```

```

end
energy60(1,4)=sum(ch6{1}{:,.5})+sum(CH6{2}{:,.5})+sum(CH6{3}{:,.5})+sum(CH6{4}{:,.5});
%for channel 7
if size(ch7{2})>0
p=ch7{2}{:,.1}<2335;
CH7{2}=ch7{2}(p,:);
else CH7{2}=zeros(1,5);
end
if size(ch7{3})>0
p=ch7{3}{:,.1}<1742;
CH7{3}=ch7{3}(p,:);
else CH7{3}=zeros(1,5);
end
if size(ch7{4})>0
p=ch7{4}{:,.1}<210;
CH7{4}=ch7{4}(p,:);
else CH7{4}=zeros(1,5);
end
energy60(1,5)=sum(ch7{1}{:,.5})+sum(CH7{2}{:,.5})+sum(CH7{3}{:,.5})+sum(CH7{4}{:,.5});
%for channel 8
if size(ch8{2})>0
p=ch8{2}{:,.1}<2335;
CH8{2}=ch8{2}(p,:);
else CH8{2}=zeros(1,5);
end
if size(ch8{3})>0
p=ch8{3}{:,.1}<1742;
CH8{3}=ch8{3}(p,:);
else CH8{3}=zeros(1,5);
end
if size(ch8{4})>0
p=ch8{4}{:,.1}<210;
CH8{4}=ch8{4}(p,:);
else CH8{4}=zeros(1,5);
end
energy60(1,6)=sum(ch8{1}{:,.5})+sum(CH8{2}{:,.5})+sum(CH8{3}{:,.5})+sum(CH8{4}{:,.5});

%for up to 120kN
%for channel 1
if size(ch1{2})>0
p=ch1{2}{:,.1}>2334;
CH1{2}=ch1{2}(p,:);
else CH1{2}=zeros(1,5);
end
if size(ch1{3})>0
p=ch1{3}{:,.1}>1741;
CH1{3}=ch1{3}(p,:);
else CH1{3}=zeros(1,5);
end
if size(ch1{4})>0
p=ch1{4}{:,.1}>209 & ch1{4}{:,.1}<2340;
CH1{4}=ch1{4}(p,:);
else CH1{4}=zeros(1,5);
end
energy120=[sum(CH1{2}{:,.5})+sum(CH1{3}{:,.5})+sum(CH1{4}{:,.5})];
%for channel 2

```

```

if size(ch2{2})>0
    p=ch2{2}{:,1}>2334;
    CH2{2}=ch2{2}(p,:);
else CH2{2}=zeros(1,5);
end
    if size(ch2{3})>0
        p=ch2{3}{:,1}>1741;
        CH2{3}=ch2{3}(p,:);
else CH2{3}=zeros(1,5);
end
    if size(ch2{4})>0
        p=ch2{4}{:,1}>209 & ch2{4}{:,1}<2340;
        CH2{4}=ch2{4}(p,:);
else CH2{4}=zeros(1,5);
end
energy120(1,2)=[sum(CH2{2}{:,5})+sum(CH2{3}{:,5})+sum(CH2{4}{:,5})];
    %for channel 5
if size(ch5{2})>0
    p=ch5{2}{:,1}>2334;
    CH5{2}=ch5{2}(p,:);
else CH5{2}=zeros(1,5);
end
    if size(ch5{3})>0
        p=ch5{3}{:,1}>1741;
        CH5{3}=ch5{3}(p,:);
else CH5{3}=zeros(1,5);
end
    if size(ch5{4})>0
        p=ch5{4}{:,1}>209 & ch5{4}{:,1}<2340;
        CH5{4}=ch5{4}(p,:);
else CH5{4}=zeros(1,5);
end
energy120(1,3)=[sum(CH5{2}{:,5})+sum(CH5{3}{:,5})+sum(CH5{4}{:,5})];
    %for channel 6
if size(ch6{2})>0
    p=ch6{2}{:,1}>2334;
    CH6{2}=ch6{2}(p,:);
else CH6{2}=zeros(1,5);
end
    if size(ch6{3})>0
        p=ch6{3}{:,1}>1741;
        CH6{3}=ch6{3}(p,:);
else CH6{3}=zeros(1,5);
end
    if size(ch6{4})>0
        p=ch6{4}{:,1}>209 & ch6{4}{:,1}<2340;
        CH6{4}=ch6{4}(p,:);
else CH6{4}=zeros(1,5);
end
energy120(1,4)=[sum(CH6{2}{:,5})+sum(CH6{3}{:,5})+sum(CH6{4}{:,5})];
    %for channel 7
if size(ch7{2})>0
    p=ch7{2}{:,1}>2334;
    CH7{2}=ch7{2}(p,:);
else CH7{2}=zeros(1,5);
end

```



```

if size(ch7{3})>0
    p=ch7{3}{:,1}>1741;
    CH7{3}=ch7{3}(p,:);
else CH7{3}=zeros(1,5);
end
if size(ch7{4})>0
    p=ch7{4}{:,1}>209 & ch7{4}{:,1}<2340;
    CH7{4}=ch7{4}(p,:);
else CH7{4}=zeros(1,5);
end
energy120(1,5)=[sum(CH7{2}{:,5})+sum(CH7{3}{:,5})+sum(CH7{4}{:,5})];
    %for channel 8
if size(ch8{2})>0
    p=ch8{2}{:,1}>2334;
    CH8{2}=ch8{2}(p,:);
else CH8{2}=zeros(1,5);
end
if size(ch8{3})>0
    p=ch8{3}{:,1}>1741;
    CH8{3}=ch8{3}(p,:);
else CH8{3}=zeros(1,5);
end
if size(ch8{4})>0
    p=ch8{4}{:,1}>209 & ch8{4}{:,1}<2340;
    CH8{4}=ch8{4}(p,:);
else CH8{4}=zeros(1,5);
end
energy120(1,6)=[sum(CH8{2}{:,5})+sum(CH8{3}{:,5})+sum(CH8{4}{:,5})];

    %for up to 140
%for channel 1
if size(ch1{4})>0
    p=ch1{4}{:,1}>2339 & ch1{4}{:,1}<3720;
    CH1{4}=ch1{4}(p,:);
else CH1{4}=zeros(1,5);
end
energy140=[sum(CH1{4}{:,5})];
    %for channel 2
if size(ch2{4})>0
    p=ch2{4}{:,1}>2339 & ch2{4}{:,1}<3720;
    CH2{4}=ch2{4}(p,:);
else CH2{4}=zeros(1,5);
end
energy140(1,2)=[sum(CH2{4}{:,5})];
    %for channel 5
if size(ch5{4})>0
    p=ch5{4}{:,1}>2339 & ch5{4}{:,1}<3720;
    CH5{4}=ch5{4}(p,:);
else CH5{4}=zeros(1,5);
end
energy140(1,3)=[sum(CH5{4}{:,5})];
    %for channel 6
if size(ch6{4})>0
    p=ch6{4}{:,1}>2339 & ch6{4}{:,1}<3720;
    CH6{4}=ch6{4}(p,:);
else CH6{4}=zeros(1,5);
end

```

```

end
energy140(1,4)=[sum(CH6{4}{:,5})];
%for channel 7
if size(ch7{4})>0
    p=ch7{4}{(:,1)}>2339 & ch7{4}{(:,1)}<3720;
    CH7{4}=ch7{4}{p,:};
else CH7{4}=zeros(1,5);
end
energy140(1,5)=[sum(CH7{4}{:,5})];
%for channel 8
if size(ch8{4})>0
    p=ch8{4}{(:,1)}>2339 & ch8{4}{(:,1)}<3720;
    CH8{4}=ch8{4}{p,:};
else CH8{4}=zeros(1,5);
end
energy140(1,6)=[sum(CH8{4}{:,5})];

%up to 160kN
%for channel 1
if size(ch1{4})>0
    p=ch1{4}{(:,1)}>3719 & ch1{4}{(:,1)}<5520;
    CH1{4}=ch1{4}{p,:};
else CH1{4}=zeros(1,5);
end
energy160=[sum(CH1{4}{:,5})];
%for channel 2
if size(ch2{4})>0
    p=ch2{4}{(:,1)}>3719 & ch2{4}{(:,1)}<5520;
    CH2{4}=ch2{4}{p,:};
else CH2{4}=zeros(1,5);
end
energy160(1,2)=[sum(CH2{4}{:,5})];
%for channel 5
if size(ch5{4})>0
    p=ch5{4}{(:,1)}>3719 & ch5{4}{(:,1)}<5520;
    CH5{4}=ch5{4}{p,:};
else CH5{4}=zeros(1,5);
end
energy160(1,3)=[sum(CH5{4}{:,5})];
%for channel 6
if size(ch6{4})>0
    p=ch6{4}{(:,1)}>3719 & ch6{4}{(:,1)}<5520;
    CH6{4}=ch6{4}{p,:};
else CH6{4}=zeros(1,5);
end
energy160(1,4)=[sum(CH6{4}{:,5})];
%for channel 7
if size(ch7{4})>0
    p=ch7{4}{(:,1)}>3719 & ch7{4}{(:,1)}<5520;
    CH7{4}=ch7{4}{p,:};
else CH7{4}=zeros(1,5);
end
energy160(1,5)=[sum(CH7{4}{:,5})];
%for channel 8
if size(ch8{4})>0
    p=ch8{4}{(:,1)}>3719 & ch8{4}{(:,1)}<5520;

```

```

    CH8{4}=ch8{4}(p,:);
else CH8{4}=zeros(1,5);
end
energy160(1,6)=[sum(CH8{4}{:,5})];

%up to 190kN
%for channel 1
if size(ch1{4})>0
    p=ch1{4}{:,1}>5519 & ch1{4}{:,1}<6270;
    CH1{4}=ch1{4}(p,:);
else CH1{4}=zeros(1,5);
end
energy190=[sum(CH1{4}{:,5})];
%for channel 2
if size(ch2{4})>0
    p=ch2{4}{:,1}>5519 & ch2{4}{:,1}<6270;
    CH2{4}=ch2{4}(p,:);
else CH2{4}=zeros(1,5);
end
energy190(1,2)=[sum(CH2{4}{:,5})];
%for channel 5
if size(ch5{4})>0
    p=ch5{4}{:,1}>5519 & ch5{4}{:,1}<6270;
    CH5{4}=ch5{4}(p,:);
else CH5{4}=zeros(1,5);
end
energy190(1,3)=[sum(CH5{4}{:,5})];
%for channel 6
if size(ch6{4})>0
    p=ch6{4}{:,1}>5519 & ch6{4}{:,1}<6270;
    CH6{4}=ch6{4}(p,:);
else CH6{4}=zeros(1,5);
end
energy190(1,4)=[sum(CH6{4}{:,5})];
%for channel 7
if size(ch7{4})>0
    p=ch7{4}{:,1}>5519 & ch7{4}{:,1}<6270;
    CH7{4}=ch7{4}(p,:);
else CH7{4}=zeros(1,5);
end
energy190(1,5)=[sum(CH7{4}{:,5})];
%for channel 8
if size(ch8{4})>0
    p=ch8{4}{:,1}>5519 & ch8{4}{:,1}<6270;
    CH8{4}=ch8{4}(p,:);
else CH8{4}=zeros(1,5);
end
energy190(1,6)=[sum(CH8{4}{:,5})];

%up to failure
%for channel 1
if size(ch1{4})>0
    p=ch1{4}{:,1}>6269;
    CH1{4}=ch1{4}(p,:);
else CH1{4}=zeros(1,5);
end

```

```

energyfail=[sum(CH1{4}{:,.5})];
    %for channel 2
if size(ch2{4})>0
    p=ch2{4}{:,1}>6269;
    CH2{4}=ch2{4}(p,:);
else CH2{4}=zeros(1,5);
end
energyfail(1,2)=[sum(CH2{4}{:,.5})];
    %for channel 5
if size(ch5{4})>0
    p=ch5{4}{:,1}>6269;
    CH5{4}=ch5{4}(p,:);
else CH5{4}=zeros(1,5);
end
energyfail(1,3)=[sum(CH5{4}{:,.5})];
    %for channel 6
if size(ch6{4})>0
    p=ch6{4}{:,1}>6269;
    CH6{4}=ch6{4}(p,:);
else CH6{4}=zeros(1,5);
end
energyfail(1,4)=[sum(CH6{4}{:,.5})];
    %for channel 7
if size(ch7{4})>0
    p=ch7{4}{:,1}>6269;
    CH7{4}=ch7{4}(p,:);
else CH7{4}=zeros(1,5);
end
energyfail(1,5)=[sum(CH7{4}{:,.5})];
    %for channel 8
if size(ch8{4})>0
    p=ch8{4}{:,1}>6269;
    CH8{4}=ch8{4}(p,:);
else CH8{4}=zeros(1,5);
end
energyfail(1,6)=[sum(CH8{4}{:,.5})];

%NOW PLOT THE DATA FOR EACH CHANNEL
%DIVIDED BY INTERVAL OF LOAD :60-120-140-160-190-failure

ENERGYLOAD=[energy60; energy120; energy140; energy160; energy190; energyfail];
figure
bar(CH,transpose(ENERGYLOAD),'stack');
title('CUMULATIVE ENERGY','FontSize',12,'FontWeight','bold','FontName','serifa BT')
axis([0 9 0 max(max(ENERGYLOAD))*2])
xlabel('channel','FontSize',12,'FontName','serifa thin BT')
ylabel('energy','FontSize',12,'FontName','serifa thin BT')
legend(legenda{6:11})

%PLOT DIVIDE FOR SIDE AND PROPER LOCATION
x=[5000 5000 8171 8171 5421 5000];
y=[500000 1500000 1500000 750000 750000 500000];
figure
subplot(2,1,1)

```

```

CUMENERGYSIDE1=[CUMENERGY(:,5) CUMENERGY(:,2) CUMENERGY(:,1)];
X1=[5936 6536 7146];
bar(X1,transpose(CUMENERGYSIDE1));           %one next to the other
title('CUMULATIVE ENERGY - beam HB2- SIDE
1','FontSize',12,'FontWeight','bold','FontName','serifa BT')
axis([5000 81 71 0 max(max(CUMENERGY))+50])
xlabel('x positon','FontSize',12,'FontName','serifa thin BT')
ylabel('energy','FontSize',12,'FontName','serifa thin BT')
legend(legenda{1:4})
hold on
subplot(2,1,1)
plot(x,y)
subplot(2,1,2)
CUMENERGYSIDE2=[CUMENERGY(:,6) CUMENERGY(:,4) CUMENERGY(:,3)];
X2=[5276 5846 7291];
bar(X2,transpose(CUMENERGYSIDE2));           %one next to the other
title('CUMULATIVE ENERGY - beam HB2 -SIDE
2','FontSize',12,'FontWeight','bold','FontName','serifa BT')
axis([5000 81 71 0 max(max(CUMENERGY))+50])
xlabel('x positon','FontSize',12,'FontName','serifa thin BT')
ylabel('energy','FontSize',12,'FontName','serifa thin BT')
legend(legenda{1:4})
hold on
subplot(2,1,2)
plot(x,y)

```

Appendix E

Prize awarded, Publications submitted and Certificates obtained during this thesis

Prize:

- Joint Third Prize at the Young Researchers' Conference, Institution of Structural Engineers, London, UK, 2002.

Journal Papers:

- Colombo S., Main I.G., Forde M.C. (2003), Assessing Damage of Reinforced Concrete Beam using "b-value" Analysis of Acoustic Emission Signals, *Journal of Materials in Civil Engineering*, ASCE, "in press".
- Shigeishi M., Colombo S., Broughton K.J., Rutledge H., Bachelor A.J., Forde M.C. (2001), Acoustic Emission to assess and monitor the integrity of bridges, *Construction and Building Materials*, Vol.15, pp.35-49.
- Colombo S., Forde M.C., Halliday J., Kavanagh J., AE monitoring of concrete bridge beams in situ, *The Structural Engineer*, IStructE, "in press".

Conference Papers:

- Colombo S., Forde M.C., Das P.C. (2000), Improving Impact Echo and Radar NDT data interpretation using uncertainty analysis technique, ICE 2000 Conf. "Bridge Rehabilitation in the UK: review of the current programme and preparing for the next" 2-3 Oct.2000.
- Colombo S., Forde M.C. (2001), AE experiments on concrete beams: general overview and research in progress on bridges, *Proc. of the Int. Conf. on Structural Faults + Repairs - 2001*, M. Forde Ed., CD-Rom, London July 2001.
- Shigeishi M., Colombo S., Forde M.C., (2001), Acoustic Emission application to masonry structure, On site control and non destructive evaluation of masonry structures and materials, *RILEM Technical Committee International Workshop*, 13-14 November 2001, Mantova, Italy, "in press".

- Colombo S., Main I.G., Forde M.C., Halliday J. (2002), AE on bridges: experiments on concrete beams, *Proc. of the EWGAE 2002- 25th European Conf on Acoustic Emission Testing*, P.Mazal Ed, Czech Society for Non-destructive Testing, Prague, 11-13 September 2002, pp.127-134.
- Colombo S., Main I.G., Forde M.C., Halliday J., Shigeishi M. (2003), AE Energy analysis on concrete bridge beams, *NDT-CE Conference*, BAM, Berlin, 16-19 September 2003, "in press".

Certificates:

- 15th Annual Short Course on Acoustic Emission, Cambridge, UK, 16-19 July 2001.
- Advanced Course of the Acoustic Emission Structural Diagnosis Technique, AcoustWorks Lab, Graduate School of Science and Technology, Kumamoto University, Japan, 2002 (English and Japanese Version).

INSTITUTION OF STRUCTURAL ENGINEERS

YOUNG RESEARCHERS' CONFERENCE

20th March 2002



JOINT THIRD PRIZE

This is to certify that

Sabrina Colombo

of

University of Edinburgh

was awarded *Joint Third Prize* for delivering a presentation on

Acoustic Emission Monitoring of Concrete Bridges

Official Position President

Date 20th March 2002

Official Signature

A handwritten signature in dark ink, appearing to read "D. Bloch", is written over a horizontal line. The signature is fluid and cursive.

establishing the static state of material in a soil filled masonry bridge. This includes selective coring to determine material composition, chemical analysis of masonry or fill and laboratory investigation of the mechanical properties of samples obtained from coring. Condition assessment of the structure can be enhanced by techniques such as external crack monitoring to detect movement, conductivity, resistivity profiling, acoustic impact-echo and ground probing radar to detect water ingress and construction anomalies. It is often a prerequisite that a bridge remain open to traffic whilst a condition assessment survey is carried out. This prevents or limits the use of some techniques, as access to the bridge deck is severely limited. Furthermore, these methods are time consuming and labour intensive and can be costly.

Another aspect of bridge assessment that needs consideration is the dynamic behaviour of the structure under load. This is difficult and expensive to determine. One method is to install displacement or strain gauges on the structure and apply a large, quantifiable, dynamic load to the deck. This method requires closure of the bridge to traffic. None of the techniques described so far are capable of detecting seasonal and longer-term ageing factors that may alter the behaviour of the structure. To do this would require that many surveys be carried out on a continuous basis, which is not presently cost effective.

The focus of the work described in this paper has been to evaluate the potential for the introduction of acoustic emission (AE) monitoring to provide cost effective in situ long-term monitoring of bridge condition. The AE technique uses the dynamic response of a structure to traffic loading. In effect vehicles become the signal excitation and the AE equipment monitors the response of the bridge to the excitation. Acoustic energy is emitted from materials within the bridge whenever there is movement due to changes in loading. An array of acoustic sensors is used to record the response and facilitate location of the noise sources within the structure.

The AE technique is used widely in Japan for the in situ monitoring of reinforced concrete bridges. AE has the potential to provide cost effective condition monitoring for UK bridges because:

1. it does not interfere with the flow of traffic or require closure of the bridge;
2. it is relatively quick and easy to install;
3. it is not labour intensive and can be linked via telemetry to provide remote data collection;
4. it provides continuous monitoring; and
5. it can be retrofitted to existing structures and adapted to existing topologies.

Although theoretical and experimental work in the



Fig. 1. Boghall Bridge viewed from the north side.

AE technique has been progressing for many years, the use of AE for civil engineering applications has only become a practical reality within the last 30 years [1–3]. The introduction of portable equipment based on personal computer components and using digital signal processing techniques has paved the way for cost-effective implementations [4,5]. Encouraging results have been obtained working on concrete structures [6] although AE has rarely been applied to masonry structures [7] and no precedent exists for the application of full signal analysis of AE data from masonry arch bridges.

2. Experimental programme

The work described in this paper was performed on a bridge, chosen to be representative of both masonry and reinforced concrete construction methods, located in the Scottish Borders on the A697. Boghall Bridge is an old flat masonry arch bridge (shown in Fig. 1). It is located just south of Carfraemill, north-east of Lauder. Records provided by the Scottish Borders Council date the construction to 1793. More recently, the bridge was widened by the addition of a cast in situ reinforced concrete deck and beams alongside the masonry arch as seen in Fig. 2. The original parapet has been repositioned.

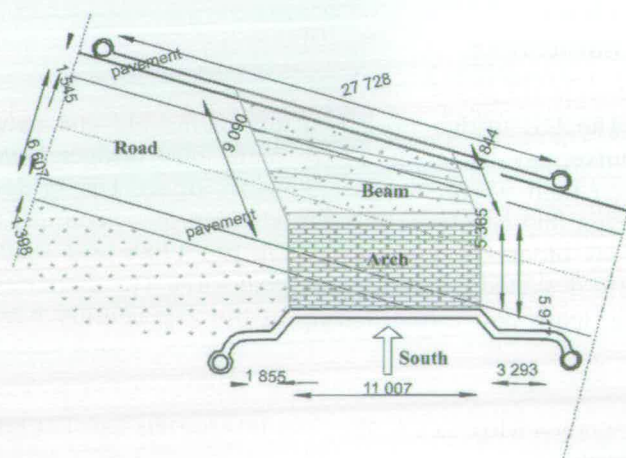


Fig. 2. Plan view of Boghall bridge showing construction detail.

Acoustic emission to assess and monitor the integrity of bridges

M. Shigeishi^a, S. Colombo^b, K.J. Broughton^{b,*}, H. Rutledge^b, A.J. Batchelor^b,
M.C. Forde^b

^aKumamoto University, Department of Civil Engineering and Architecture, 39-1 Kurokami 2-cyome, Kumamoto 860-8555, Japan

^bUniversity of Edinburgh, School of Civil & Environmental Engineering, The Kings Buildings, Edinburgh EH9 3JN, Scotland, UK

Received 6 March 2000; received in revised form 26 May 2000; accepted 20 August 2000

Abstract

Increased axle loads and traffic density necessitate strengthening and widening of traditional masonry arch bridges. The question remains as to how to evaluate the condition of a bridge and assess the effect of modern traffic on its serviceability? The focus of this paper has been the evaluation of the potential for the acoustic emission technique to provide cost effective in-situ long term monitoring of bridge condition. The work was performed on a bridge chosen to be representative of both masonry and reinforced concrete construction methods. The results demonstrate that acoustic emission technique can be applied to condition assessment of bridges. These results confirm that strong acoustic emission signals are obtained from reinforced concrete structures and demonstrate that acoustic emissions can be detected in masonry structures but at lower energy levels. The experimental programme has shown that AE is useful in detecting crack growth and determining the position of the crack tips at a much earlier stage in their development, before they are noticed during visual inspection © 2001 Elsevier Science Ltd. All rights reserved.

Keywords: Acoustic emission; Masonry; Reinforced concrete; Bridges

1. Introduction

The UK bridge stock is a mix of the old and new. Unlike, say in Japan, where many new bridges have been built within the last 50 years or so, UK bridge design and construction methods span many centuries. Many older UK bridges built in the 1700s and 1800s were designed to carry horses and carts. The increased axle loads and traffic density of the 21st century have

necessitated strengthening and widening of traditional masonry arch bridges. Modern constructions are predominantly of reinforced concrete and steel.

The assessment of design life and structural integrity of older bridges is problematic. Quite often historical records of design and construction method give sparse detail or have been lost. It is probably safe to assume that, of all bridges built over 100 years ago, what remains are the more robust and better engineered examples; the rest having fallen down or been rebuilt. The question is how to evaluate the condition of those that remain and assess the effect of modern traffic on their serviceability.

A range of diagnostic techniques exists to assist in

* Corresponding author. Tel.: +44-131-650-5791; fax: +44-131-650-7167.

E-mail address: kevin@srv0.civ.ed.ac.uk (K.J. Broughton).

3. All sensors mounted horizontally facing south on the north side of the beam.
4. A combination of vertical and horizontal beam mounted sensors.
5. All sensors mounted vertically facing up on the underside of the masonry arch.
6. A combination of beam and arch mounted sensors.
7. Sensors mounted horizontally along the west masonry spring wall of the arch.
8. A combination of spring wall and arch mounted sensors.

For signal detection, it is necessary to have a good acoustic coupling between the sensors and the material surface. This was easily achieved on the relatively flat surface of the concrete beam but difficulties were experienced with attachment to the rough and uneven facing of the sandstone masonry. Cyanoacrylate adhesive was used to bond the sensors to the concrete. Attachment to the masonry required surface preparation with a rotary sander prior to fixing. On very rough surfaces it was found necessary to ‘fill in’ large indentations with quick setting mortar, to ensure that the adhesive remained on the protruding stone surface and did not flow away from the intended bonding site before it had cured. On some occasions, particularly after heavy overnight rainfall, the sandstone on the underside of the arch became saturated and it was necessary to re-locate sensors to prevent them being ‘washed off’.

The AE events, generated by dynamic loading due to traffic on the bridge, were recorded and analysed parametrically by the MISTRAS system. Although the entire sensor waveform can be digitised and stored for calibration and verification of system operation, it is

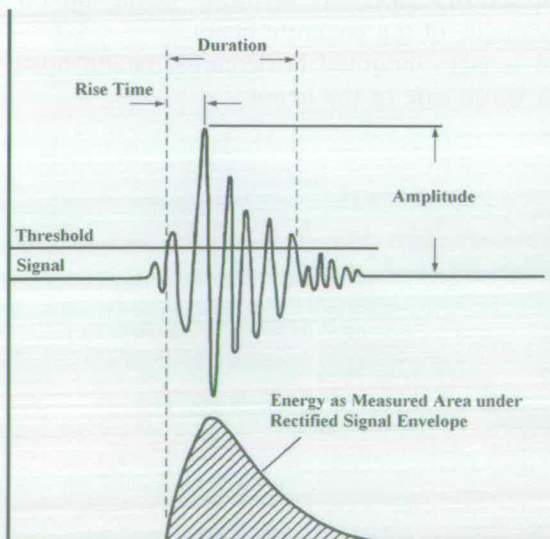


Fig. 5. Relationship of threshold, energy and amplitude for a recorded event.

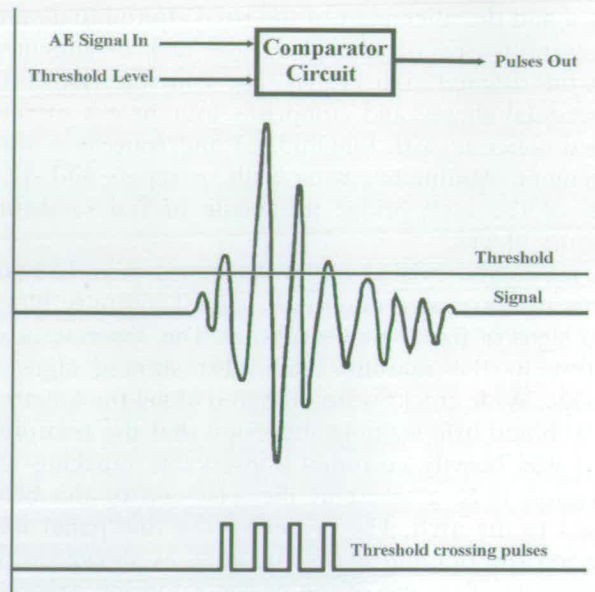


Fig. 6. Relationship of threshold and hit counts for a recorded event.

not stored during tests because the large number of samples needed to provide a typical 1 MHz bandwidth on all sensor channels would rapidly fill the storage capacity of the analyser. The MISTRAS system uses parallel channels (one for each sensor) of real time digital signal processing to pre-process the received waveform. They describe its characteristics using a small number of quantitative numerical parameters that closely relate to the waveform energy (see Figs. 5 and 6) as expressed in both the time and frequency domains. By storing only the processed parameters, the MISTRAS system can record a large number of events over long periods without excessive data redundancy, whilst providing sufficient information of interest at low bandwidth.

The source location of AE events was used to plan a complementary ground probing radar survey using a GSSI SIR10C at frequencies of 500 and 900 MHz, shown in Fig. 7. It was intended that the radar survey



Fig. 7. SIR10A impulse surface probing radar system.

tioned and the alignment of the road altered to assume the current aspect—this explains the lack of alignment with the original arch bridge. The concrete slab has a trapezoidal shape, and comprises four beams of reinforced concrete with longitudinal and transverse reinforcement. Abutments, wing walls, parapets and spandrels of the arch bridge are made of red sandstone masonry blocks.

A preliminary visual survey was performed. In many places mortar has eroded and several masonry blocks show signs of freeze-thaw cracking. The concrete beam nearest to the masonry arch also showed signs of damage. Wide cracks were observed along the length of the web and iron staining suggested that the reinforcement was heavily corroded. Observable cracking and corrosion were greatest at the east end of the beam closest to the arch. The presence of a thin paper joint between the old and new structures, as shown on the engineering diagrams of the bridge extension, was confirmed. It was decided to concentrate efforts around the interface between the concrete beam and the masonry arch as it was assumed that the amplitude of acoustic emissions associated with any interaction between the beam and the arch would be most easily detected close to this interface.

A series of experimental tests, each lasting between 2 and 6 h, were carried out over a period of 3 weeks during the Spring of 1999. Air shade temperature did not vary much between tests but wind velocity was highly variable, ranging from dead calm to gusts of force 4–5. Precipitation also varied. Although rainfall did not have a direct effect on measurements, changes in the degree of saturation of the bridge fabric, from test to test, were noticeable.

3. Experimental objectives

The aims of the experimental program were to:

1. Investigate the effectiveness of applying AE to a masonry structure, by comparison of the different responses of masonry and concrete.
2. Investigate the behaviour of the reinforced concrete beams by recording the AE response.
3. Determine from the AE data what, if any, interaction occurs between the concrete beam and the masonry arch.
4. Determine the reliability of the AE data by using ground probing radar to verify the results.

4. Experimental method

The results presented in this paper were obtained



Fig. 3. Mistras data acquisition and analysis system.

using a Physical Acoustics Corporations MISTRAS-2001 (*Massively Instrumented Sensor Technology for Received Acoustic Signals*) fitted with DSP-32/16 signal processing devices (shown in Fig. 3). The parallel processing architecture used for computerised AE was configured to simultaneously perform signal measurement on eight channels. Eight AE sensors of Type R3I were used. These transducers of 30 mm diameter by 40 mm high incorporated a built in pre-amplifier of 40 dB and had a low resonant frequency of approximately 30 kHz and operated in the 100 Khz to 1 Mhz frequency range.

The equipment was mounted beneath the arch on a low scaffold platform to raise it clear of the stream, as shown in Fig. 4. The equipment was powered from a 600 W inverter operating from 24 V. In all tests one sensor was configured as a trigger to initiate event recording on all channels. The positions of the AE sensors were varied for each test to try to establish the best positioning strategy for detection of AE events. This included:

1. All sensors mounted vertically facing up on the underside of the concrete beam.
2. All sensors mounted horizontally facing north on the south side of the beam.

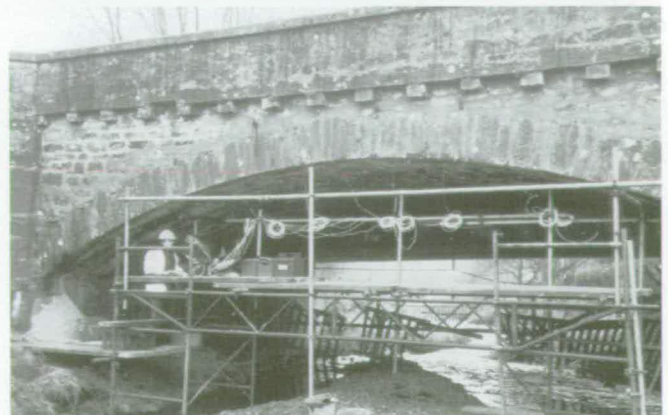


Fig. 4. South facing view of experimental installation under bridge.

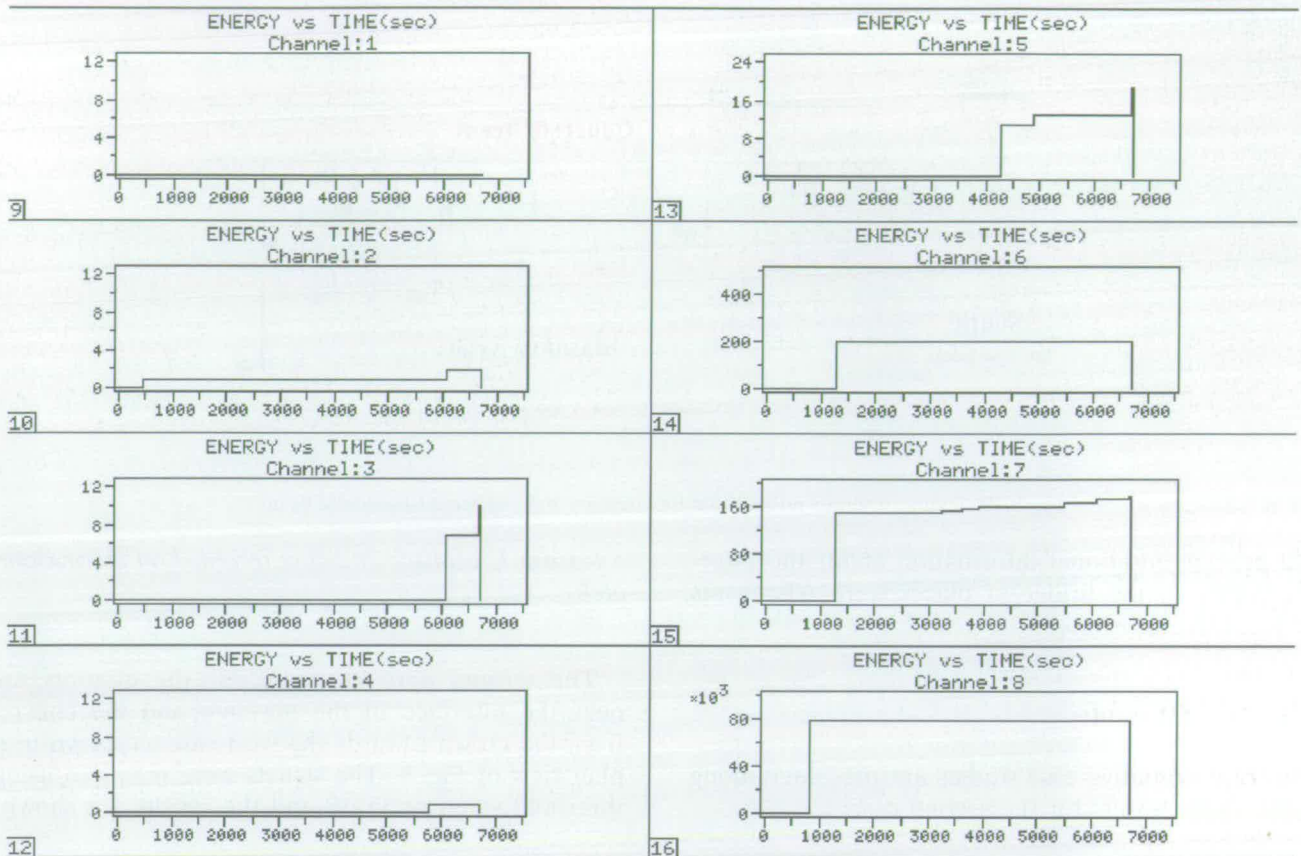


Fig. 10. Case 1: recorded energy for all channels on the arch.

Figs. 9–11. Fig. 9 shows one chart for each of the eight transducers. In the vertical axis the number of hits, that is the number of detected signals that cross the threshold value, have been shown, whilst the recording time is on the horizontal axis. The low amplitude and flat response lines indicate that very few events are detected, with the exception of channels six and seven. In Fig. 10 there are also eight charts, one for each channel. The time is on the horizontal axis, whilst the energy, which is related to the amplitude of the signal, is on the vertical axis. The large amplitude recorded on channel eight is attributed to the impact of a hammer used to test the transducers at the beginning of the test and is not significant. Channels six and seven show a large amplitude response. Fig. 11 shows the hits response of every channel. A logarithmic vertical scale has been used. Sensors six and seven show a large energy response.

5.2. Case 2: acoustic emission recorded on the west spring wall

The sensors were located along the west spring wall of the masonry arch as shown in Figs. 12–14. From previous tests it had been determined that a good

signal-to-noise ratio at this position allowed for a lower threshold value of 28 dB. The results are shown in Figs. 15 and 16. Fig. 15 shows that compared with case 1, a larger number of hits can be detected. Channels seven and eight in particular gave a frequent response. Although the number of hits increased in all channels, the energy of the recorded events remained low in the first six channels as shown in Fig. 16.

5.3. Case 3: acoustic emission and connectivity of the masonry arch and concrete beam

Seven of the sensors were located along the west

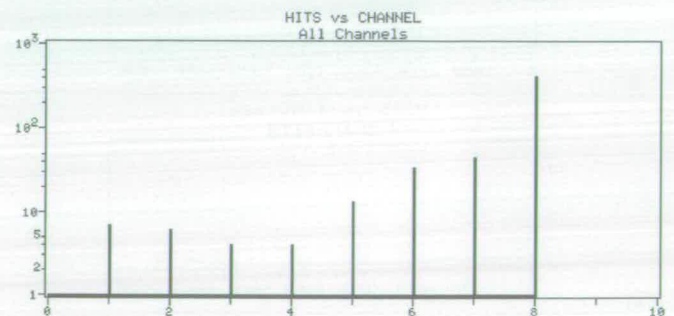


Fig. 11. Case 1: cumulative total hits for each channel on the arch.

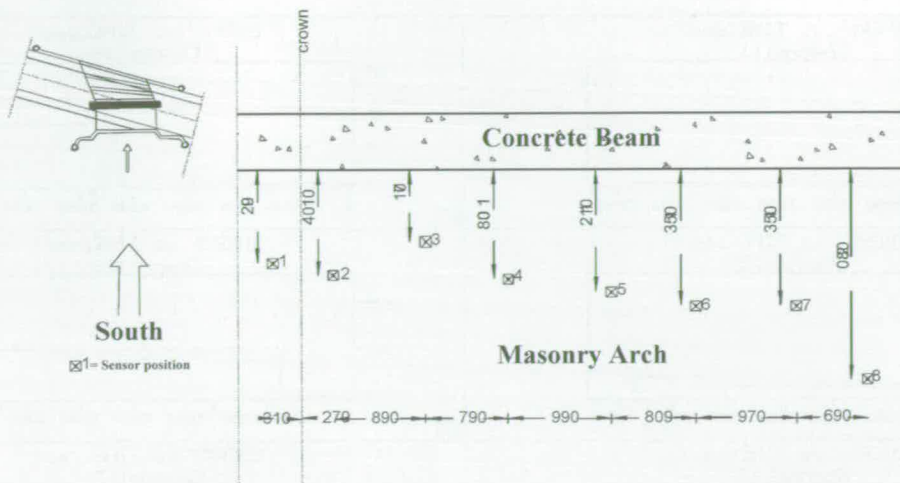


Fig. 8. Plan view of sensor positions on the masonry arch, adjacent to concrete beam.

would provide additional information about the internal structure of the bridge at places where AE events were recorded most often.

5. Experimental results

Four representative case studies are presented along with the radar results for the second case.

5.1. Case 1: acoustic emission recorded on the masonry arch

The sensors were located along the masonry arch, near the interface of the masonry and the concrete, from the crown towards the west side as shown in the plan view of Fig. 8. The signals were recorded using a threshold value of 35 dB and the results are shown in

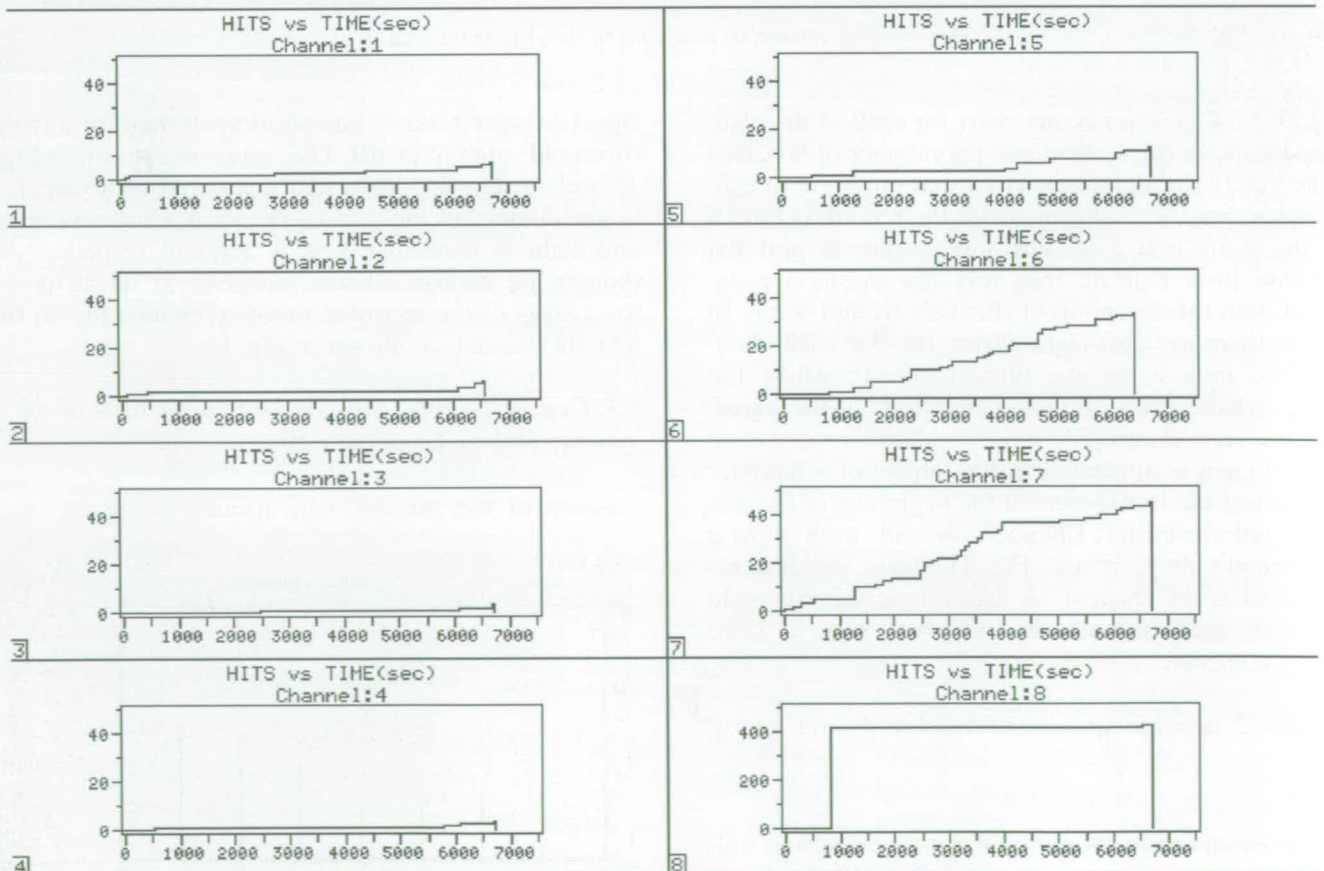


Fig. 9. Case 1: recorded hits for all channels on the arch.

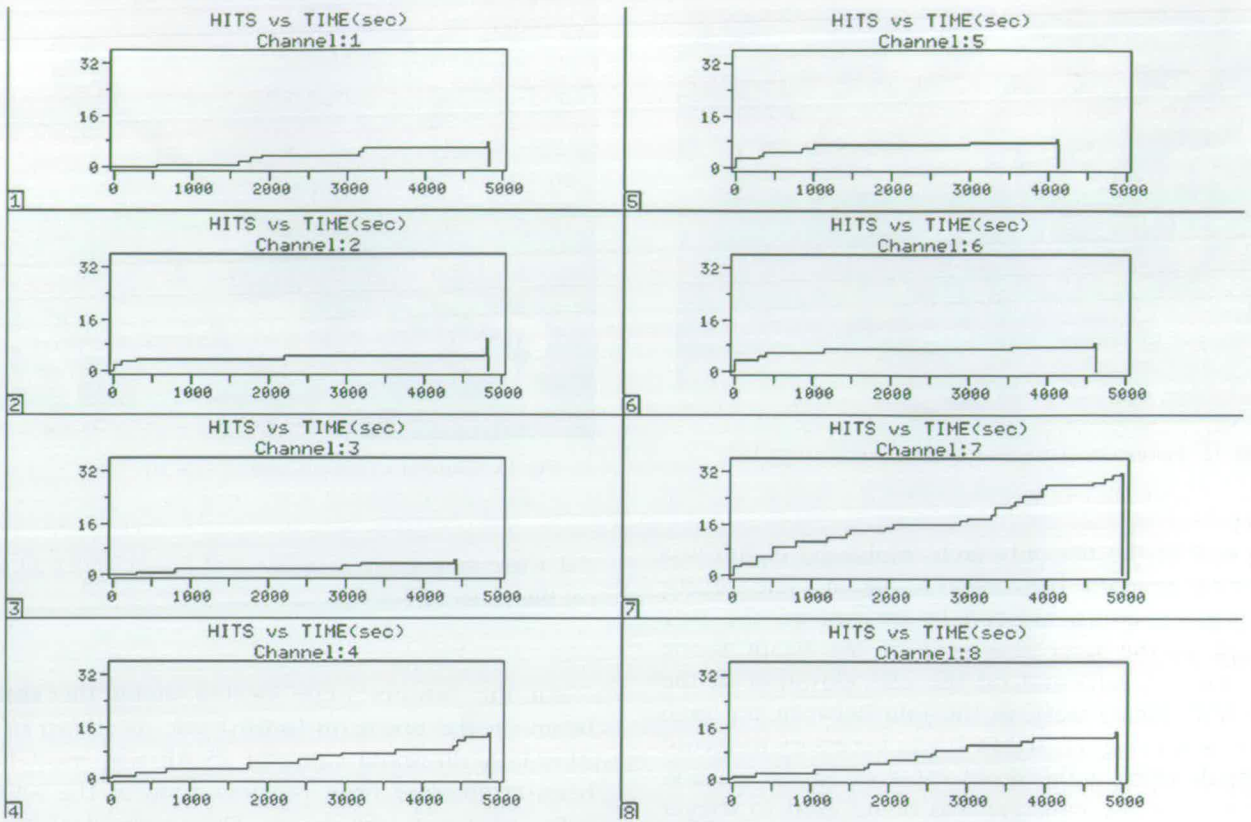


Fig. 15. Case 2: recorded hits for all channels on the spring wall.

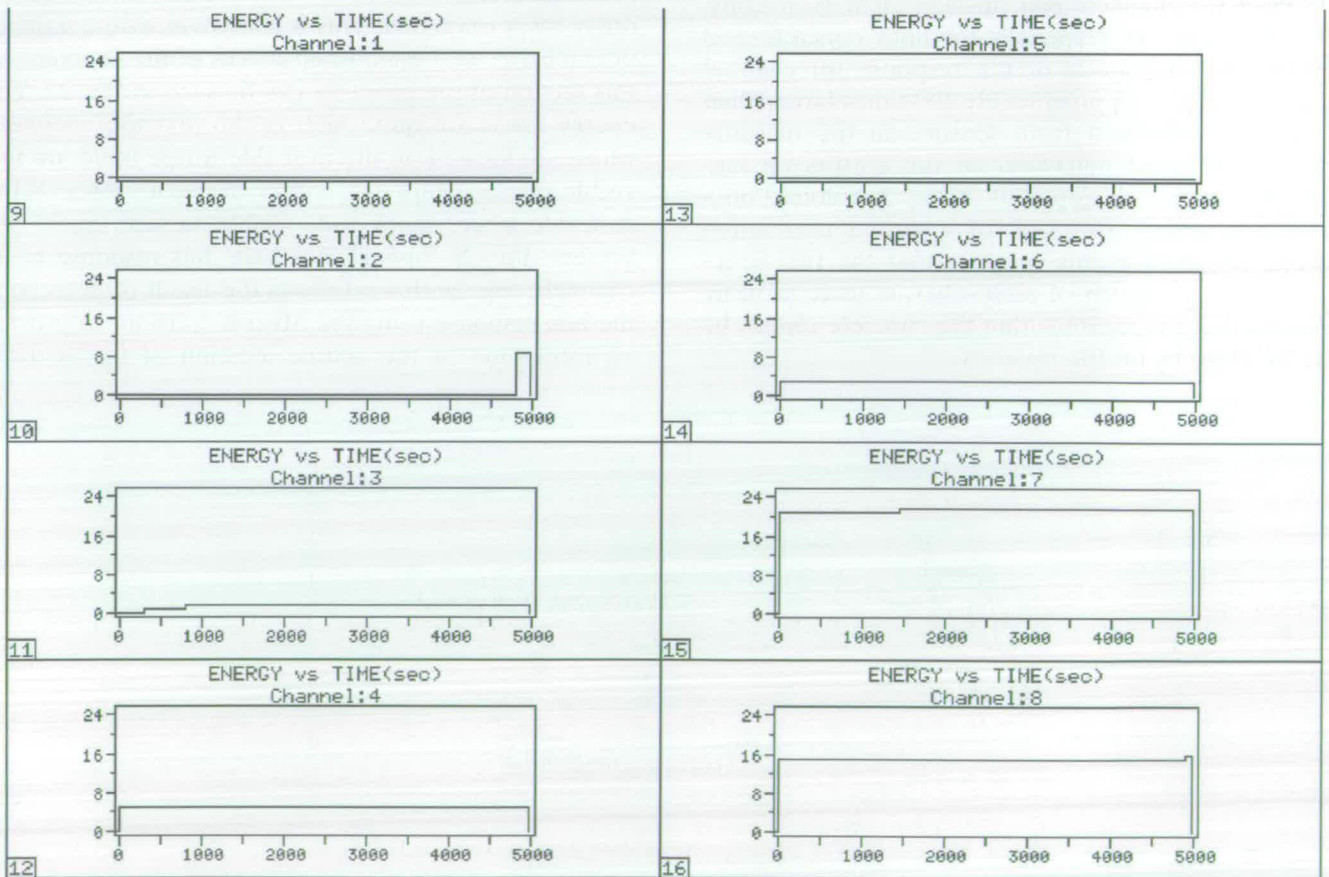


Fig. 16. Case 2: recorded energy for all channels on the spring wall.

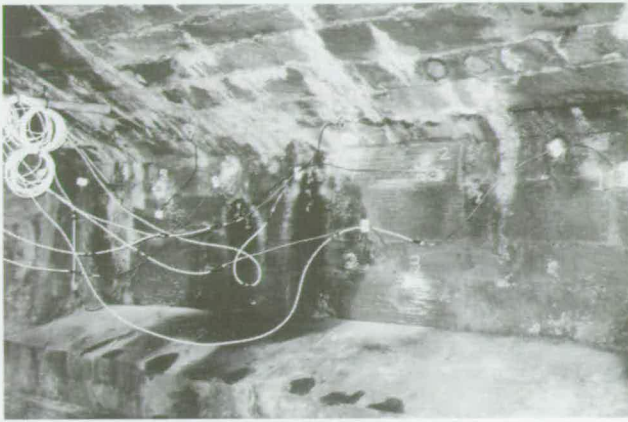


Fig. 12. Sensors fixed to west spring wall of masonry arch.

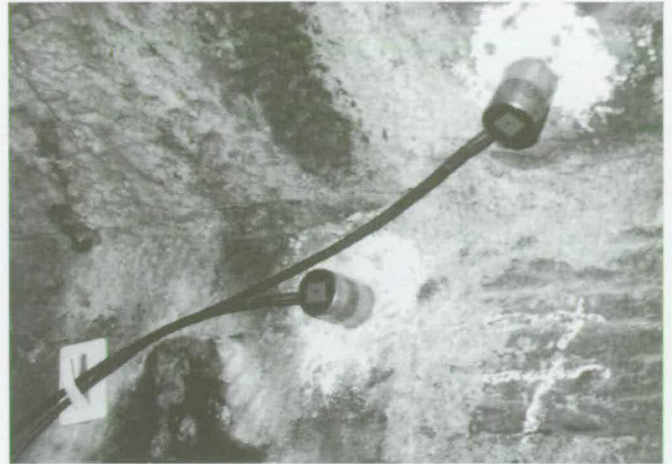


Fig. 13. Close-up of sensors mounted on arch and spring wall.

spring wall of the masonry arch, whilst the eighth was positioned beneath the concrete beam. The sensor positions are shown marked by crosses on the side elevation of the west abutment of the beam facing north (Fig. 17, left) and on the end elevation of the spring wall, facing west, at the join between the arch and the beam (Fig. 17, right). It was necessary to record the signals using a threshold value of 35 dB because the sensor on the concrete was being used to trigger event capture. The results are shown in Figs. 18–20. The scale used for channel one is thousands and the scale used for channels two through eight is in units. Although there are responses for both concrete and masonry, the magnitude of the response for channel one on concrete is approximately 100 times larger than the response obtained from sensors on the masonry arch. The different behaviour of the sensors on masonry and concrete is apparent in Fig. 20 (plotted on a logarithmic scale). The lack of a strong correlation between observed events suggests that the two structures act independently of each other, as large acoustic emissions that propagate within the concrete cannot be detected close by on the masonry.

5.4. Case 4: acoustic emission and linear source location on the concrete beam

All the sensors were located along the concrete beam on the upstream (north) side as shown in Figs. 21–23. A threshold value of 35 dB was used, having been established from previous tests as the optimum value to use on this beam. The results are shown in Figs. 24–26. Fig. 24 demonstrates a larger number of detected events than have been present in any of the other cases examined. This is consistent with a number of extensive, well-established cracks in the concrete on this section of the beam, as can be seen in Fig. 27. The energy levels are quite high in the first five channels, which are located on the west side where there are few visible cracks, whilst the energy decreases towards the east side where many wide visible surface cracks are present. Fig. 26 (upper) shows the hits response of all channels. Fig. 26 (lower) shows the result of processing the hits response using the Mistras software to provide an estimation of the source location of the acoustic

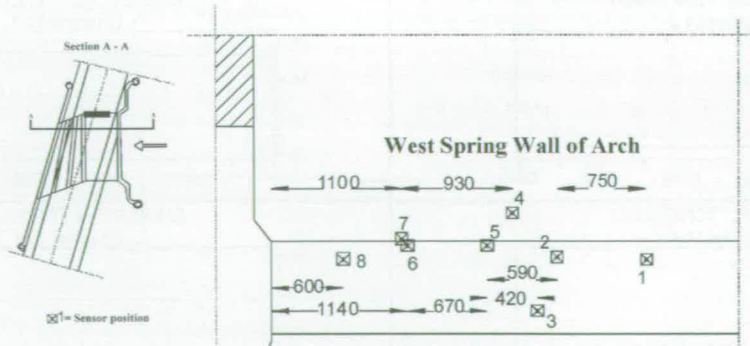


Fig. 14. Side elevation of sensors positions along the west spring wall of the arch.

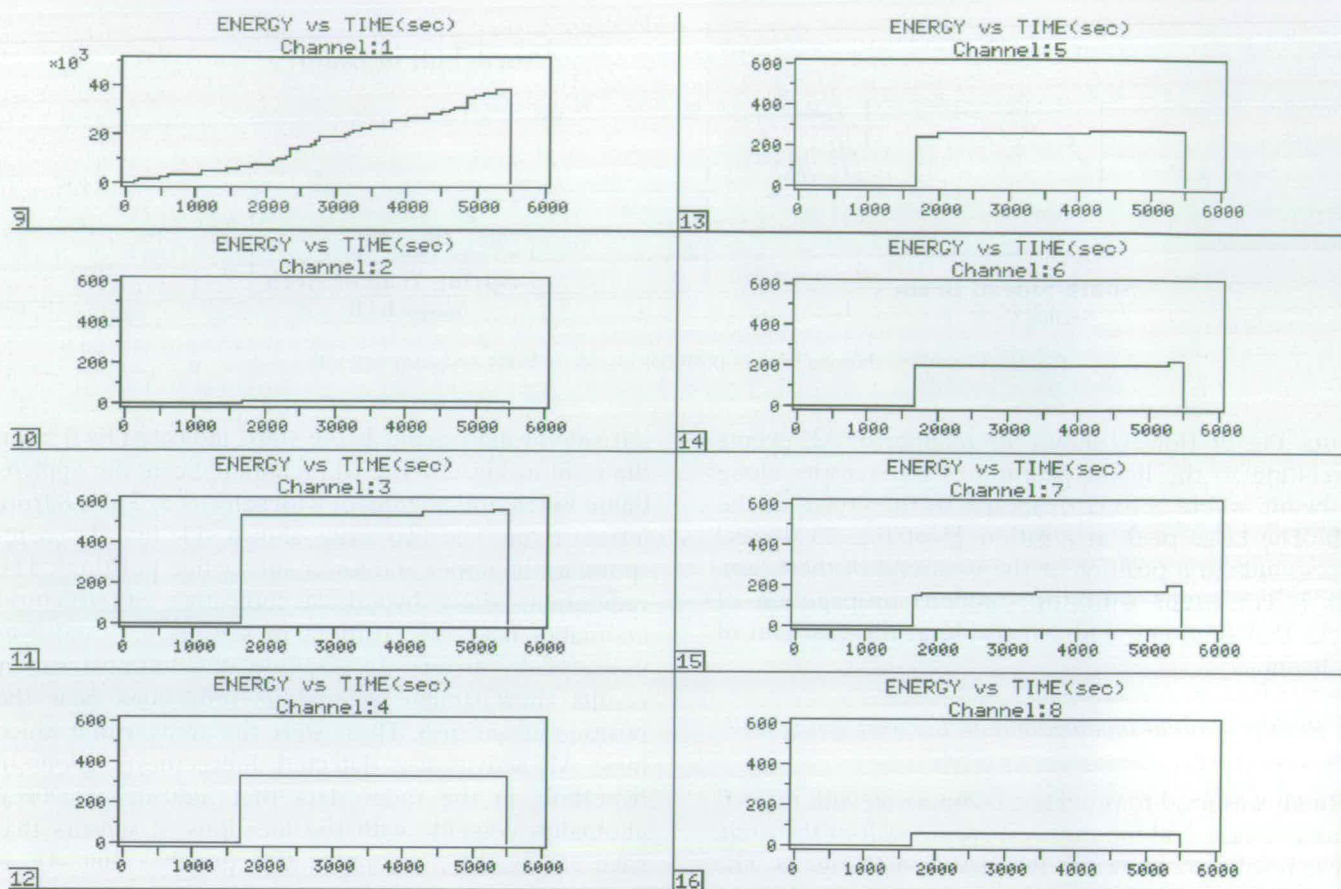


Fig. 19. Case 3: recorded energy for all channels.

related to structural composition at these positions (Fig. 29).

6. Discussion

Coupling and bonding of sensors to bridge materials needs further consideration. In these tests which were of short duration and exploratory, sensor placement was temporary and the limitations of the fixing method

were not considered to be significant. For extended tests and semi-permanent placement it will be necessary to develop standardised fixing methods that can be adapted and applied to the range of materials that are commonly found in constructions. In particular, any fixing method must be capable of operating and of being deployed in both wet and dry conditions.

Both sensors and cables need to be securely fixed. It was found that gusting wind blowing against loose cables could couple acoustic energy to the sensors.

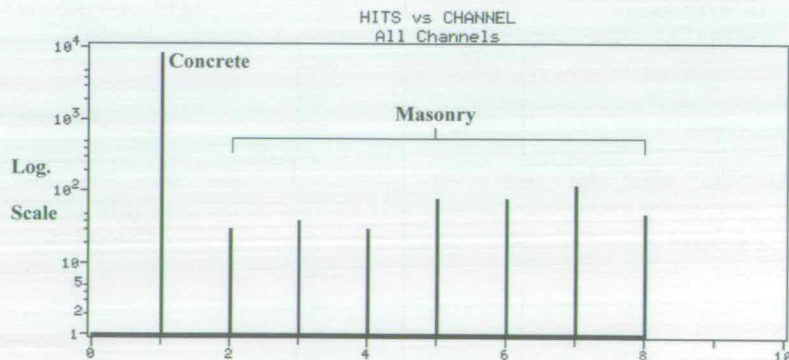


Fig. 20. Case 3: cumulative total hits for each channel.

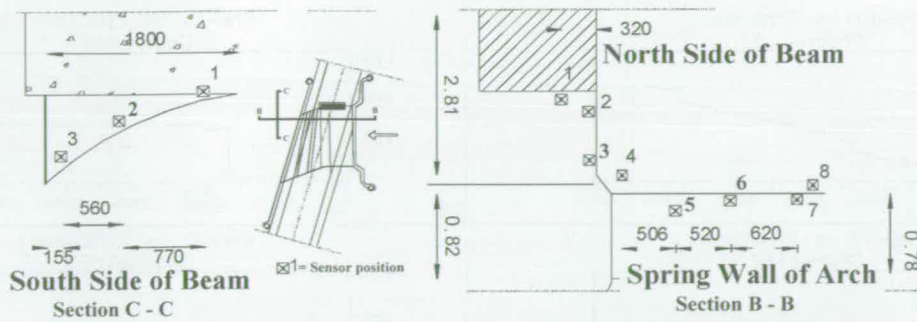


Fig. 17. Elevations showing sensors positions on side of beam and on spring wall.

events. Fig. 26 (lower) shows the number of AE events in relation to the linear position of the sensors along the beam, where zero corresponds to the crown of the arch. The large peak at position 25 of Fig. 26 (lower) corresponds to a position at the west-end of the beam. This is consistent with the (hidden) propagation of cracks that originate and are visible at the east-end of the beam.

5.5. Results of radar investigation on the west spring wall

Radar was used to provide a comparison with the AE results of case 2 along the west spring wall of the arch. These results are shown in the elevation of Fig. 29. The

left side of these scans is the start, indicated by 0 m on the right in Fig. 28. The white bars indicate the approximate horizontal alignment with sensors 5, 7 and 8 from left to right. The two scans shown side-by-side correspond to the upper and lower survey line positions. The radiograms show hyperbola indicative of structural anomalies near the positions of sensors 4, 5 and 7 as indicated by arrows. In addition, the leftmost survey results show similar anomalous reflections near the position of sensor 8. These were the areas within which most AE activity was detected. Since the positions of hyperbola in the radar data that indicate structural anomalies coincide with the locations of sensors that gave strong AE responses, it is possible that AE is

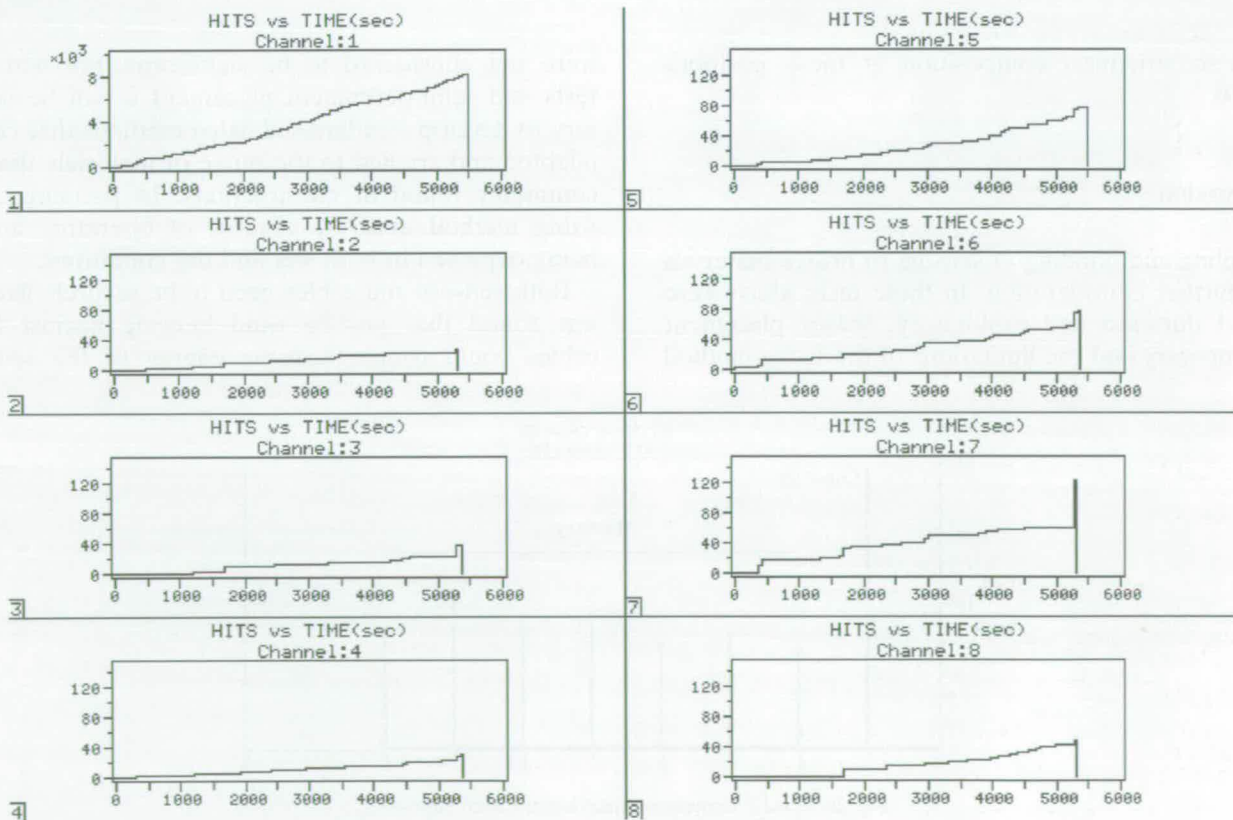


Fig. 18. Case 3: recorded hits for all channels.

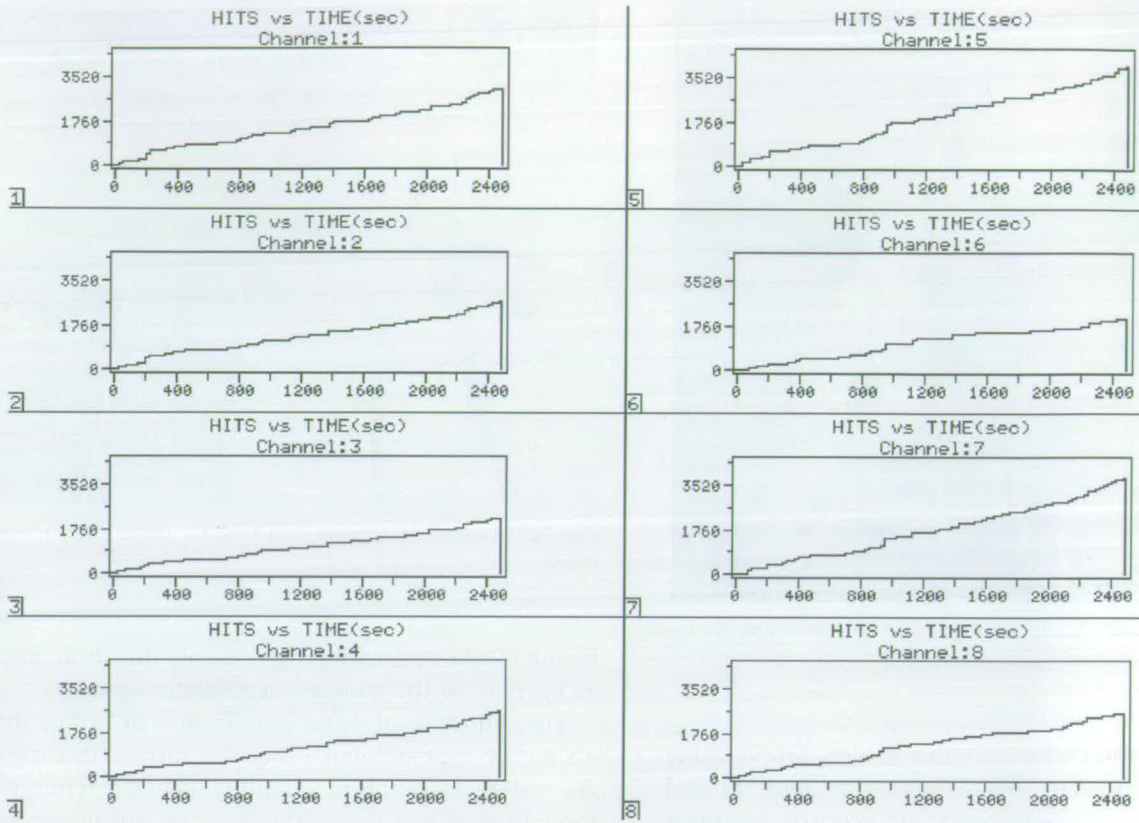


Fig. 24. Case 4: recorded hits for all channels on the beam.

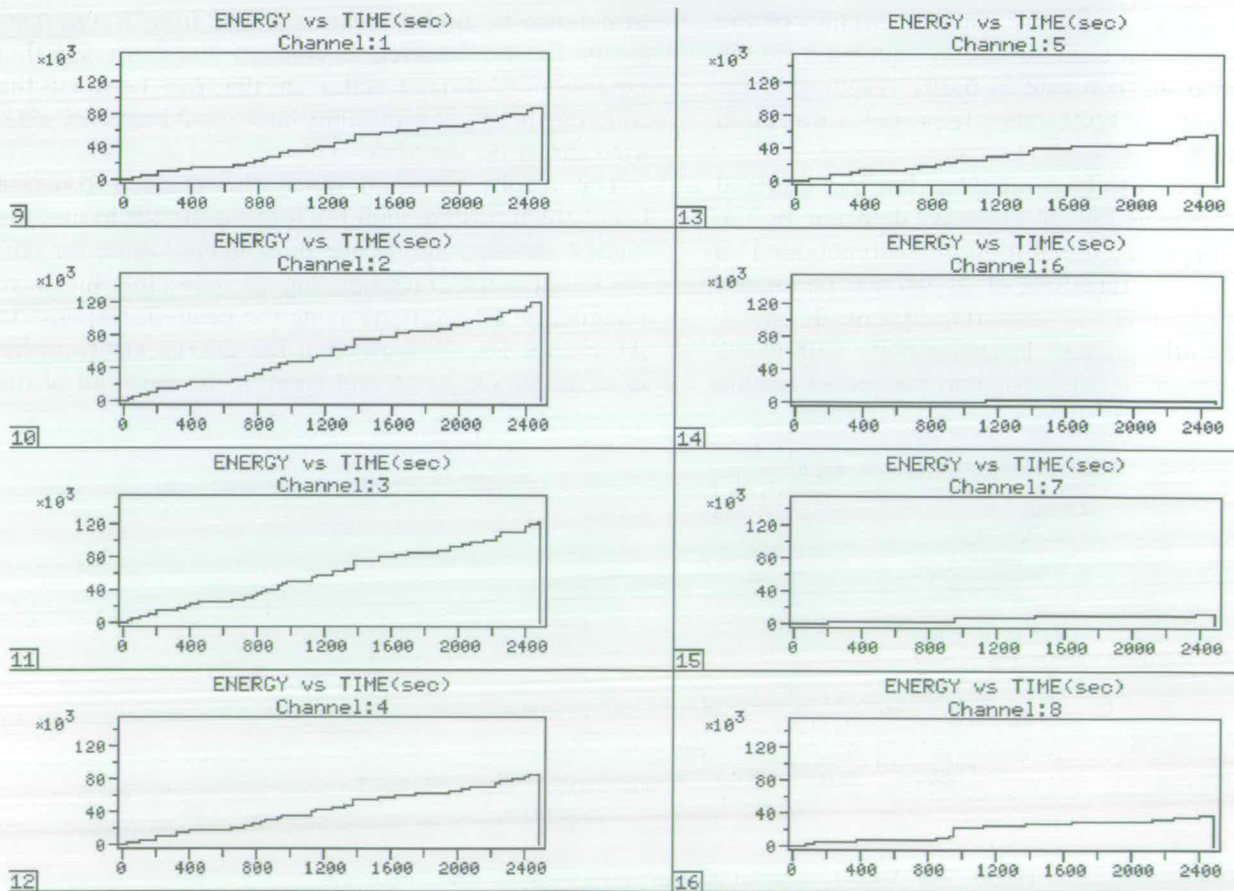


Fig. 25. Case 4: recorded energy for all channels on the beam.

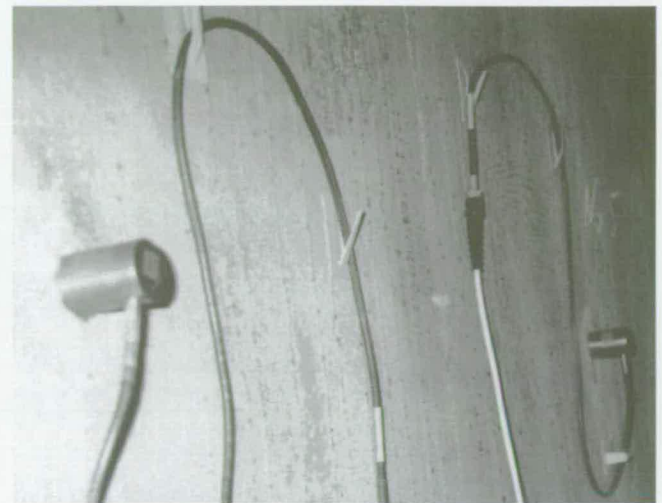


Fig. 22. Close-up of sensors mounted on south side of concrete beam.

facing blocks and within fill material are thought to act as barriers to the passage of acoustic signals.

The influence of water penetration of bridge materials on the measurements requires further investigation. As water is useful in coupling acoustic energy it is thought that wet conditions may be advantageous for AE techniques. Conversely, it may be difficult to obtain results from air voided structures in dry conditions. It would also be useful to know if AE from freeze-thaw events can be detected as concern was expressed that expansion of frozen water in the gap between the concrete beam and masonry arch could exert a sideways thrust on the arch.

The results obtained along the cracked concrete beam are consistent with fracture mechanics in that the highest stresses, and hence most likely source for AE, are found at the crack tips. Fig. 24 shows that hits were recorded at all positions along the beam in response to AE events. Fig. 25 shows that low energy was recorded in channels six, seven and eight at the east-end of the

Fig. 21. Sensors fixed on the north side of the west end of the concrete beam.

Securing the cables close to the bridge fabric using cable clips can prevent this, as shown in Figs. 13 and 22. Another unintended source of acoustic coupling was the water flowing in the stream under the bridge. Stones thrown into the water were observed to generate acoustic events within the concrete section of the bridge. It may be that acoustic energy coupled from the water flow into the concrete is partly responsible for the poorer signal to noise ratio, requiring a threshold setting of 35 dB.

Concrete appears to be a relatively low loss material for at least some of the frequencies detected by the sensors. The improved signal-to-noise ratio obtained on masonry (allowing a threshold of 28 dB) may be related to greater attenuation and scattering of acoustic energy due to inherently greater inhomogeneity within the masonry construction. In particular, air spaces behind

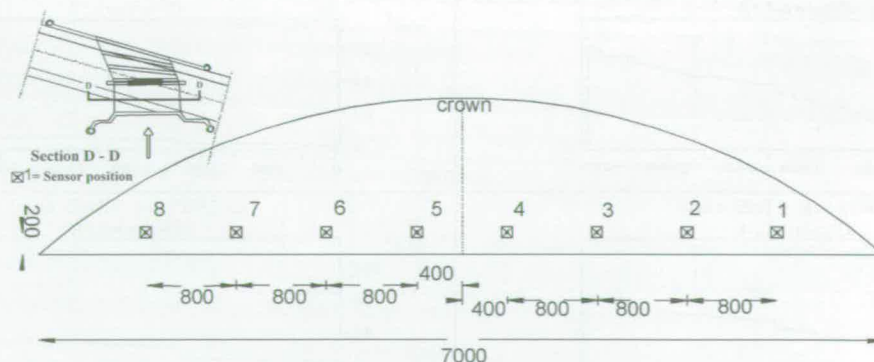


Fig. 23. Side elevation of sensor positions along the north side of the beam.

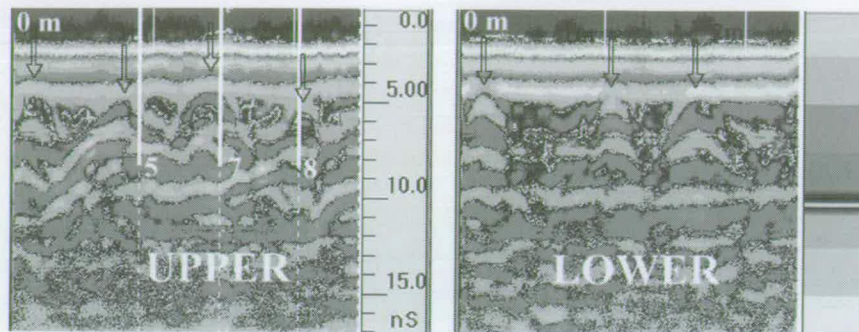


Fig. 29. Results of 900 MHz radar survey on west spring wall of arch.

alignment of the arch it could be that the higher number of acoustic events occurring towards the west side of the bridge simply reflects the closer proximity of the signal excitation. Results from sensors mounted on the west spring wall and, therefore, further away from the traffic contradict the assumption that closeness to the excitation source is the primary determinant of acoustic activity. The results of the radar survey were helpful in confirming that anomalies existed behind the spring wall that could account for the acoustic signals detected.

Although the acoustic signals detected on masonry were much lower in energy than those obtained on concrete, their presence indicates that further investigations may be worthwhile.

The equipment used was found to be easy to set up, despite its computational complexity. It took between 30 and 60 min to install and activate. Unlike other survey methods that require the constant attendance of one or more operators, it was possible to leave the equipment recording without human intervention for several hours. Employing personnel to operate equipment is a large proportion of the direct costs of any survey, thus the ability to perform unattended data collection and analysis has favourable cost implications. The use of compressed, parameterised data recording makes it feasible to provide remote telemetry for automated downloading of data at intervals of days or weeks. Although the equipment is expensive to purchase, it may be that savings that accrue over the lifetime of the structure (through reductions in costs due to the ability to provide planned maintenance rather than reactive repairs) could be factored in to offset the initial capital cost of the equipment.

7. Conclusions

The results of this experimental program demonstrated that:

1. AE can be applied to condition assessment of bridges;
2. strong AE signals are obtained from reinforced concrete structures;
3. AE can be detected in masonry structures but at lower energy levels than those obtained from concrete structures;
4. large, wide, visible cracks do not release much AE energy, whilst invisible internal ones do; and
5. AE is useful in detecting crack growth and determining the position of the crack tips at a much earlier stage in their development, before they are noticed during visual inspection.

Acknowledgements

The authors acknowledge the facilities of the University of Edinburgh. The financial support of the Highways Agency, London is gratefully acknowledged. The first author gratefully acknowledges the Japan Society for the Promotion of Science, and the Royal Society, London for supporting his sabbatical visit in Edinburgh to enable the research collaboration. The authors thank Physical Acoustics Ltd for technical help and loan of sensors; Holequest Ltd, Galashiels for the provision of scaffolding and Scottish Borders Regional Council for allowing access to the bridge.

References

- [1] Wells D. An acoustic apparatus to record emissions from concrete under strain. *Nucl Eng Des* 1970;12:80–88.
- [2] McCabe MW, Koerner RM, Lord AE. Acoustic emission behaviour of concrete laboratory specimens. *J Am Conc Inst*, July 1976;73:367–371.
- [3] Chabowski AJ, Bowyer WH, Cook JM, Peters CT. Complementary methods for assessing the strength of high alumina cement concrete structures. *Proceedings of the Eighth World Conference on Non-destructive Testing, Cannes, 1977.*

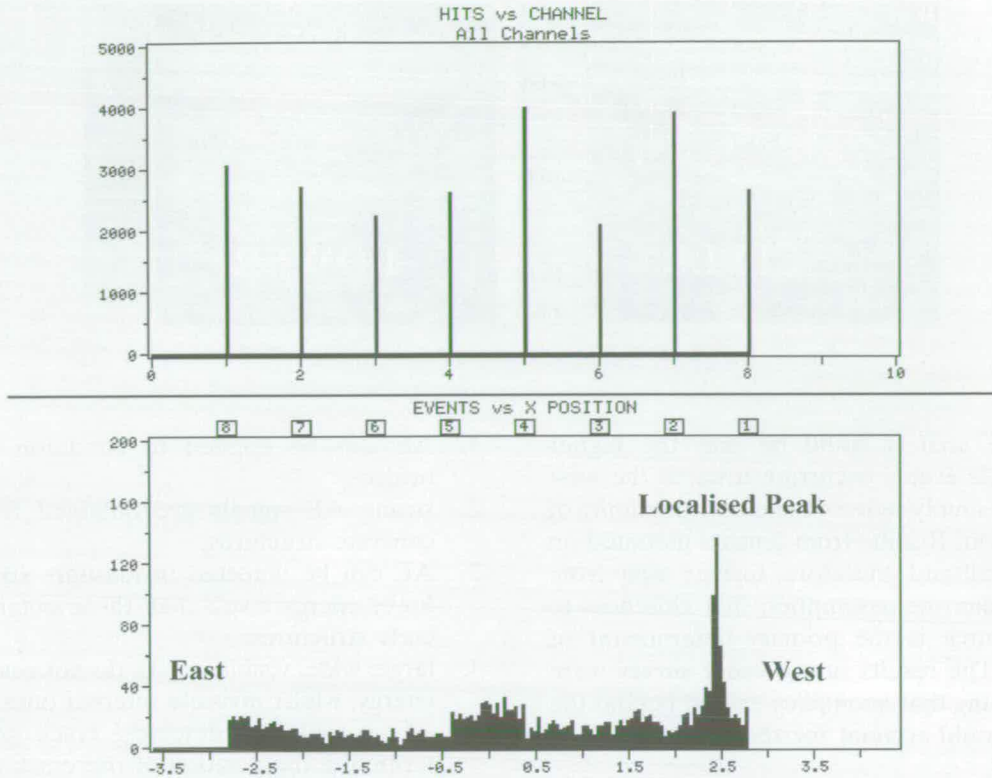


Fig. 26. Case 4: cumulative total hits for each channel and analysis of event location.

beam where large visible cracks were evident (Fig. 27). Fig. 25 also shows that the highest energy was recorded in channels one, two and three at the west-end of the beam where visible surface cracking was not evident (Fig. 21). These results show that large, wide, visible cracks do not release much energy, whilst invisible internal ones do. This suggests that the state of damage on the east side of the concrete beam resulting from reinforcement corrosion and fatigue loading has stabilised. However, the west side is gradually corroding and cracks are propagating into this area unseen. In

this situation AE is useful in detecting crack growth and determining the position of the crack tips at a much earlier stage in the development of cracks, before they are noticed during visual inspection. The implications of this for bridge maintenance are that earlier detection allows for planned monitoring and scheduled preventative maintenance rather than urgent and expensive reactive repair work.

As the alignment of the road does not match the

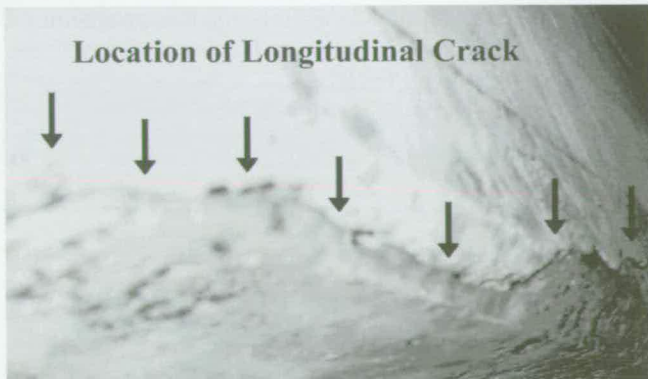


Fig. 27. Cracking at east end along base and north side of concrete beam.

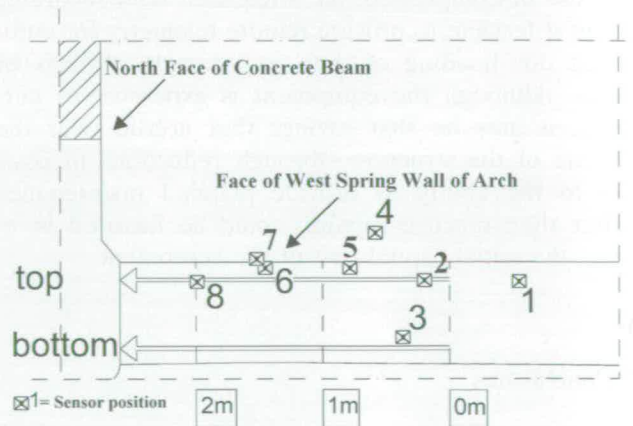


Fig. 28. Elevation of radar survey lines along west spring wall of arch.

- [4] Woodward RJ. Cracks in a concrete bridge, *Concrete*. July 1983;17(7):40–45.
- [5] Vahaviolos SJ, Third generation AE instrumentation techniques for high fidelity and speed of data acquisition, in *Progress in Acoustic Emission III, Proceedings of the Eight International Acoustic Emission Symposium, The Japanese Society for Non-destructive Inspection, 1986, 102–116.*
- [6] Ohtsu M. The history and development of acoustic emission in concrete engineering. *Mag Concr Res* 1996;48(177):321–330.
- [7] Royles R, Hendry AW. Model tests on masonry arches. *Proc Inst Civil Eng Res Theory* 1991;91:299–321.

Assessing Damage of Reinforced Concrete Beam Using "b-value" Analysis of Acoustic Emission Signals

Ing. S. Colombo¹; I. G. Main²; and M. C. Forde³

Abstract: Concrete bridges in the United Kingdom represent a major legacy and they are starting to show signs of distress. Therefore, the need for monitoring them is an urgent task. The acoustic emission (AE) technique was proposed as a valid method for monitoring these bridges but more study is needed to develop methods of analyzing the data recorded during the monitoring. The writers would like to propose a *b*-value analysis as a possible way to process AE data obtained during a local monitoring. The *b*-value is defined as the log-linear slope of the frequency-magnitude distribution of acoustic emission. This paper presents the results of a *b*-value analysis carried out on data recorded during a laboratory test on a reinforced concrete beam designed as representative of a bridge beam. During the experiment, the specimen was loaded cyclically and it was continuously monitored with an AE system. The data obtained were processed and a *b*-value analysis was carried out. The *b*-value was compared with the applied load, with a damage parameter, and with the cracks appearing on the beam. The damage parameter represents the cumulative damage in terms of total sum of acoustic emissions. The results showed a good agreement with the development of the fracture process of the concrete. From a study of the *b*-value calculated for a whole loading cycle and for each channel, some quantitative considerations were also drawn. Further development work is needed to make the *b*-value technique suitable for practical use on a real bridge.

DOI: 10.1061/(ASCE)0899-1561(2003)15:3(1)

CE Database subject headings: Acoustic detection; Concrete, reinforced; Cracking; Beams.

Introduction

Concrete bridges represent the majority of the U.K. motorways and trunk roads stock bridges. As their age is of the order of 25–35 years they are starting to show signs of deterioration. This compares with the U.S. bridge stock, which is commonly approaching 40 years old. Consequently, the necessity to monitor and verify their performance and safety is a matter of urgent concern. Acoustic emission (AE) can be used to monitor these bridges and to gain a better understanding of their conditions (Yuyama et al. 1998). Two types of monitoring are possible: A global monitoring which is intended to yield general information on the state of the whole structure and a local monitoring which yields a more detailed understanding of a certain area of the bridge. The writers consider that work needs to be done in order to find alternative ways to process and interpret the AE data obtained during monitoring. As a first stage in this direction, some experiments on reinforced concrete (RC) beams have been under-

taken and a *b*-value analysis is presented and proposed as a method to study the development of the fracture process of the concrete.

Different types of cracks generate different types of AE signals with varying frequency ranges and amplitudes. These differences can be related to the degree of damage of the structure. Microcracks generate a large number of events of a small amplitude while macrocracks generate fewer events but of a larger amplitude. When the cracks are opening up, as most of the energy has already been released, many events are created, but of a small amplitude. Furthermore, tensile cracks spawn large amplitude events while shear cracks create smaller amplitude signals (Li and Xi 1995; Iwanami et al. 1997).

The *b*-value analysis can take all these factors into account and it could then be used as an alternative way to process and interpret data recorded during a local AE monitoring.

b-value Analysis

In earthquake seismology, events of larger magnitude occur less frequently than events of smaller magnitude. This fact can be quantified in terms of a magnitude-frequency relationship, for which Gutenberg and Richter proposed the empirical formula:

$$\log_{10} N = a - bM_L \quad (1)$$

where M_L = Richter magnitude of the events; N = incremental frequency (i.e., the number of events with magnitudes in the range of $M_L \pm \Delta M/2$); and a and b = empirical constants (Shearer 1999).

The Richter magnitude M_L is proportional to the logarithm of the maximum amplitude A_{max} recorded in a seismic trace, corrected for the attenuation in amplitude with distance due to wave propagation and inelastic absorption. The magnitude is proportional to the logarithm of source rupture area S

¹School of Engineering and Electronics, The Univ. of Edinburgh, Crew Building-King's Buildings, Scotland, UK. E-mail: s.colombo@ed.ac.uk

²Professor, Dept. of Geology and Geophysics, The Univ. of Edinburgh, King's Buildings, Scotland, UK.

³Professor, School of Engineering and Electronics, The Univ. of Edinburgh, Crew Building-King's Buildings, Scotland, UK.

Note. Associate Editor: John S. Popovics. Discussion open until November 1, 2003. Separate discussions must be submitted for individual papers. To extend the closing date by one month, a written request must be filed with the ASCE Managing Editor. The manuscript for this paper was submitted for review and possible publication on May 7, 2002; approved on December 4, 2002. This paper is part of the *Journal of Materials in Civil Engineering*, Vol. 15, No. 3, June 1, 2003. ©ASCE, ISSN 0899-1561/2003/3-1-7/\$18.00.

$$M_L \propto \frac{2}{3} c \log_{10} A_{\max} \propto \frac{2}{3} c \log_{10} S \quad (2)$$

where the factor c varies depending on the transducer. If the sensor is acting as a strainmeter then $c = 1$; while if it is acting as a velocity transducer, $c = 1.5$; and finally $c = 3$ in the case of an accelerometer.

The same principle can be applied to the AE method to study the scaling of the "amplitude distribution" of the acoustic emission waves generated during the cracking process in the laboratory or in engineering structures. From relationship (1), the b -value is the negative gradient of the log-linear AE frequency/magnitude plot and hence it represents the slope of the amplitude distribution. The b -value changes systematically with the different stages of fracture growth (Sammonds et al. 1994), so it could be used to estimate the development of fracture process. In terms of AE technique, the Gutenberg-Richter formula can be modified as

$$\log_{10} N = a - b' A_{dB} \quad (3)$$

where now A_{dB} = peak-amplitude of the AE events in decibels

$$A_{dB} = 10 \log_{10} A_{\max}^2 = 20 \log_{10} A_{\max} \quad (4)$$

Comparing Eqs. (2) and (4), the b -value obtained with this relationship should be multiplied by a factor of 20 to be comparable with the one used in seismology (Shiotani et al. 2001).

In general terms, when the distributed microcracks are occurring in the early stages of damage, the b -value is high and when the macrocracks begin to localize the b -value is low (Sammonds et al. 1994).

Although the analysis of the b -value is well known in rock mechanics and seismology, very little work has been done on concrete and civil engineering structures. In the work of Sammonds et al. on damage evolution in rock, the trend of the b -value over time is plotted and a single minimum is observed just prior to dynamic failure. The decrease in b -value leads directly to dynamic failure immediately following minimum b -value (Sammonds et al. 1994).

An 'improved' lb -value was proposed and applied to the evaluation of slope failure by Shiotani et al. (1994). The lb -value was defined as

$$lb = \frac{\log N(\mu - \alpha_1 \sigma) - \log N(\mu - \alpha_2 \sigma)}{(\alpha_1 + \alpha_2) \sigma} \quad (5)$$

where σ = standard deviation; μ = mean value of the amplitude distribution; α_1 = coefficient related to the smaller amplitude; and α_2 = coefficient related to the fracture level. The variation of the lb -value was found to be in significant agreement with the progressive failure of the slope model, suggesting that the lb -value has the possibility to be a precursor for slope failure (Shiotani et al. 1994), just as it is in the laboratory to rock failure.

The use of the improved lb -value was later on applied by Shiotani et al. (2000) to evaluate the fracture process in concrete. The work showed that the lb -value analysis was successful in evaluating fracture process of concrete specimens (Shiotani et al. 2000).

In this work, a conventional b -value analysis was applied on the data recorded on a reinforced concrete beam, using relationship (3) and assuming

$$b = b' * 20. \quad (6)$$

The trend of the b -value was then compared with the development of the fracture process of the beam observed during the test.

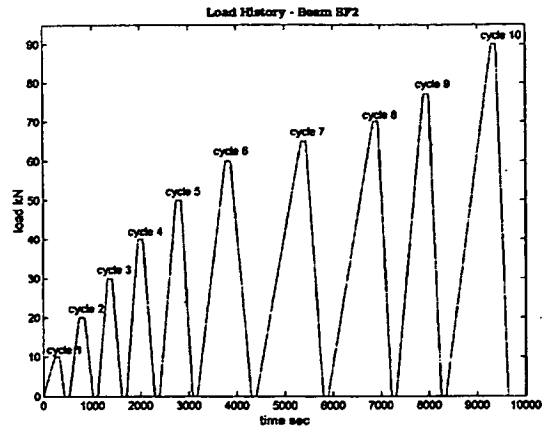


Fig. 1. Beam BF2-representation of load history cycles. Time on x-axis is only representative and it does not correspond to real time during test.

Test Description

All the data reported in this work refer to an experiment carried out on an RC beam in the Structures Laboratory of the University of Edinburgh. The beam (named beam BF2) was designed based on the BS 8110: Part 1997 to represent the behavior of a beam belonging to a real bridge. The beam was 125 mm wide, with an overall height of 270 mm; it was 2.16 m long and simply reinforced with a 16 mm diameter deformed steel bar. The beam was designed to be under-reinforced in order to have extensive cracking of the concrete and substantial deflection. The extensive cracking was then expected to generate a large amount of acoustic emission.

During the test, the beam was simply supported, using rollers, over a span of 2 m. The load was applied at two points using two hydraulic jacks. A small layer of rubber material was placed under the jack during the test of the beam to reduce the noise due to the jack itself. The load was applied in 5 kN steps and measured via two 100 kN load cells, connected to a voltmeter. The load cycles are shown in Fig. 1: At the end of each loading and off-loading cycle, the load was held just for the time that the beam needed to stabilize (i.e., no more acoustic emissions were recorded). At the end of the last cycle the beam was seriously damaged but it did not fail completely and no higher load could be applied due to the maximum load limitations of the loading equipment.

During the test the beam was monitored using a Physical Acoustic Corporation (PAC) MiStras system. Eight PAC R61 sensors (Resonant 60 kHz Integral sensor) were mounted on the beam using plasticine. The AE threshold was set to be 35 dB. This allowed us to eliminate the background noise and record only the emissions due to the cracking of the concrete. All the transducers were calibrated at the beginning and at the end of the test using a hammer and a pencil lead break (BS EN 1339-9:2000—section 6.8). The exact location of all sensors can be seen in Fig. 2. The test rig and the instrumented beam are shown in Fig. 3.

During the test the cracks were marked with numbers referring to the load cycle number in which they appeared. It was possible to identify different stages of cracking:

- Cycle 01: no cracks,
- Cycle 02 to cycle 05: Cracks forming and the appearance of tensile cracks along the whole span of the beam,

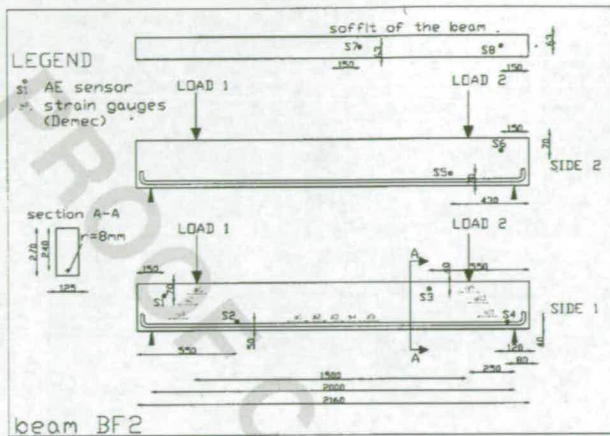


Fig. 2. Designing details—load configuration and AE sensors location on beam. AE sensors are labeled S1–S8. All measurements are in millimeters.

- Cycle 06: Appearance of shear cracks at the two ends of the beam, and
- After Cycle 06: No new cracks growing; the old cracks opened up.

Analyses and Results

The raw data recorded with the PAC Mistras system were processed using *Matlab* in order to carry out a *b*-value analysis. During all the processing the first cycle was ignored as the numbers of AE events was not significant. First the range of amplitude was decided, going from a threshold of 35 dB to a maximum of 100 dB in steps of 5 dB. Then the total number of events during a loading cycle was divided in groups. For each group the log-frequency–magnitude graph was plotted and their linear trend calculated using the least-squares method of fitting curves. The slopes of such graphs represented then the *b*-values (an example of some of these graphs and their relative *b*-values can be seen in Fig. 4). These *b*-values, during a whole cycle, were then plotted versus time (which corresponded to the final time in seconds of

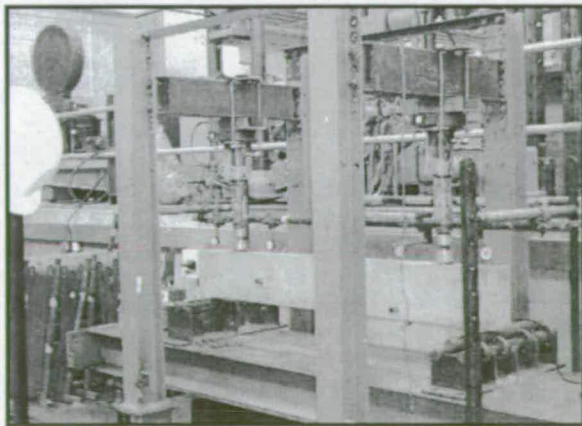


Fig. 3. Test rig and instrumented beam in structural laboratory of the University of Edinburgh

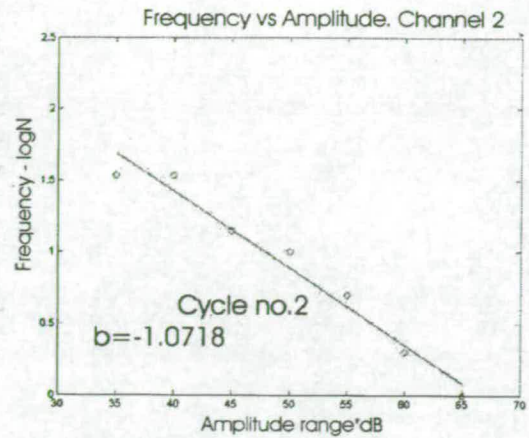


Fig. 4. Example of calculation of *b*-values for Channel 2 during loading cycle Number 2. *b*-value is calculated for groups of events during whole cycle. Graph represents log-frequency–magnitude chart and its relative curve fitting and *b*-value calculation for group of 100 events.

the time-range in which the relative group of events happened during the test). This was done for each loading cycle and for each channel. It was necessary to determine the number of events forming the groups on which the calculations were based. In order to do this, the whole calculation process was repeated using groups formed by different numbers of events. The trends of *b*-value values were then plotted for each case and overlapped. The results (see Fig. 5) showed that using groups formed by a number of events between 70 and 130 did not substantially modify the final trend. It was then decided to use an intermediate value of 100 events. This whole process allowed verification that the choice of the number of events on which the *b*-value calculation would be based does not effect the results.

The trend of the *b*-value was then calculated and plotted for each cycle of the test and for each channel. The pattern was clearer in the early cycles when the cracks were forming. The

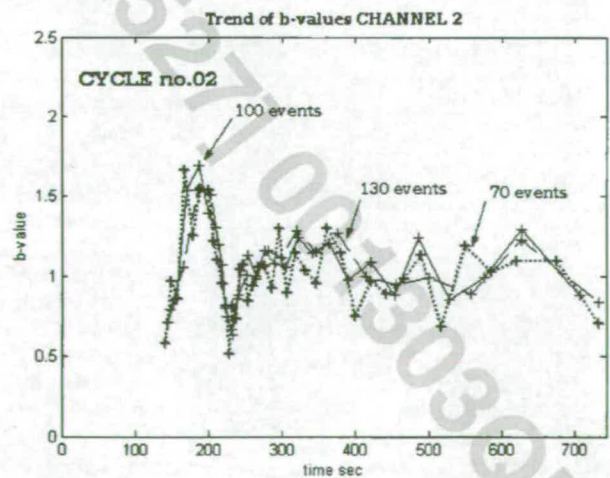


Fig. 5. *b*-value over time calculated with using groups of, respectively, 70 (dotted line), 100 (continuous line), and 130 (dashed line) numbers of events to verify independence of final results from number of events chosen for calculation

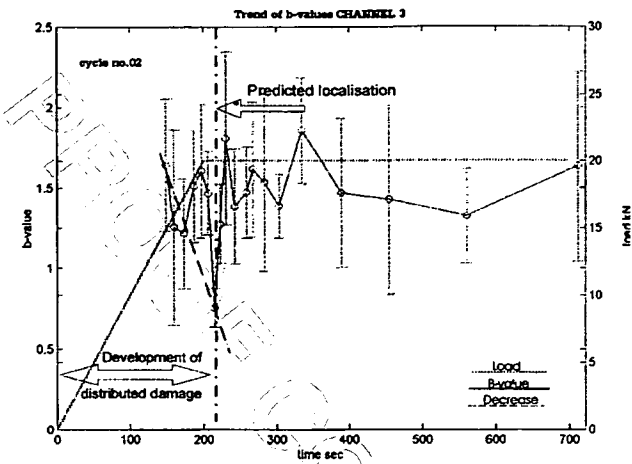


Fig. 6. *b*-value over time for Channels 3 (top) and 7 (bottom) during load cycle Number 2—load is shown on vertical axis on right. Localization predicted on basis of minimum *b*-value is shown by arrow. Bar errors of statistical calculation are shown.

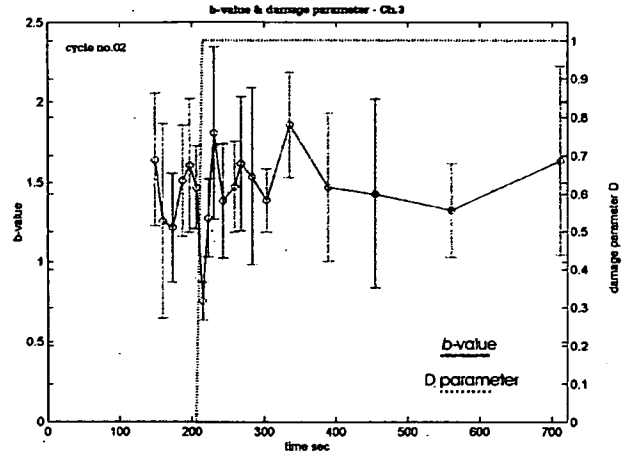


Fig. 8. Overlapping of *b*-value (left vertical axis) and normalized damage parameter (right vertical axis) for Channels 3 (top) and 7 (bottom) during load cycle Number 2. Bar errors of statistical calculation are shown.

presence of a large number of concentrated microcracks creates a clear pattern. However once the external macrocracks are formed (the beam is failing) the AE sources are fewer and more scattered so the pattern is less clear. This might imply that the analysis of the *b*-value is meaningful on good structures as it provides information between the microcracking beginning up to the stage where macrofractures occur by localization (i.e., the number of microcracks is high and they join creating a localized macrocrack). The trend of the *b*-value for Channels 3 and 7 during the second cycle of the test are shown in Figs. 6 and 7; the load over time is shown on the same graph (dotted line). As the two sensors were located, respectively, on the end and on the middle area of the beam they can be considered to give a whole representation of the full beam. Notwithstanding the presence of “up and down” in the trend (due to the presence of reinforcement bars in the concrete), it is possible to see in both cases a pattern showing a

decrease at the beginning (the dashed line in the chart) when the load is going up, and then a transient during the relaxation when the load is held constant. The *b*-value decrease corresponds then to the phase of the test (the loading up) when the cracking is happening and it reaches its minimum when the load and the damage on the beam are maximum, giving consequentially a good representation of what is really happening on the beam.

The trend of the *b*-value was also compared with the damage parameter *D*. This parameter was derived by the study of Cox and Meredith on the microcrack formation in rock [Cox and Meredith 1993]. The accumulated state of damage in a material can be analyzed in terms of acoustic emissions by defining a damage parameter

$$D = \sum 10^{c_m} \quad (7)$$

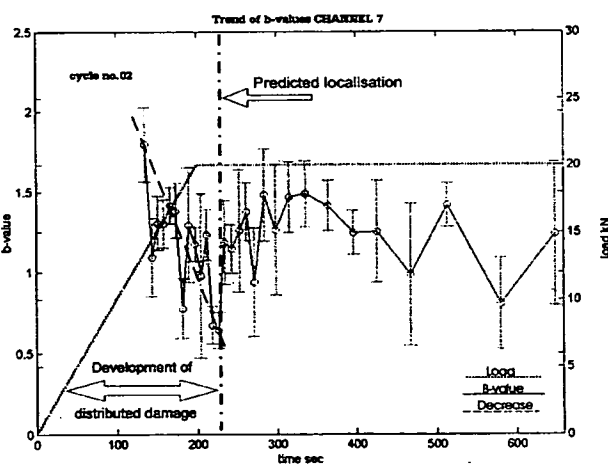


Fig. 7. *b*-value over time for Channels 3 (top) and 7 (bottom) during load cycle Number 2—load is shown on vertical axis on right. Localization predicted on basis of minimum *b*-value is shown by arrow. Bar errors of statistical calculation are shown.

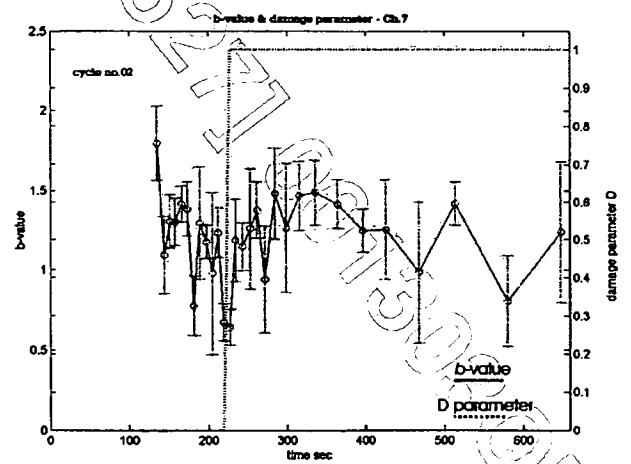


Fig. 9. Overlapping of *b*-value (left vertical axis) and normalized damage parameter (right vertical axis) for Channels 3 (top) and 7 (bottom) during load cycle Number 2. Bar errors of statistical calculation are shown.

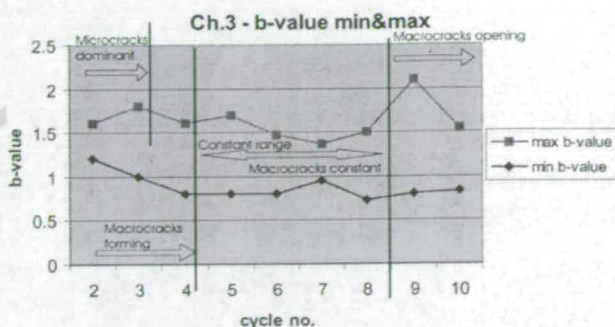


Fig. 10. Variation of maximum and minimum b -value for Channels 3 (top) and 7 (bottom) during all cycles of whole experiment. Vertical lines show different identified cracking stages indicated by arrows.

where m =seismic magnitude and $c=3$ here because the instrument acts as an accelerometer. In terms of AE, m can be computed as the AE event amplitude in dB/20. Such a parameter is proportional to cube of the mean of the crack length [Cox and Meredith 1993]. The parameter is descriptive of a damage and then by definition is related to the volume of the cracks, i.e., to a change of porosity in the concrete. The latter fails due to dilatant cracking, just like rocks, although the evolution of the damage itself might be different for both materials.

The use of this parameter was applied to the tested concrete beam. D was calculated for each loading cycle, using intervals of 100 events as for the b -value. The whole damage parameter was normalized to one, so that one was equal to the maximum damage at the end of each cycle. The results were compared with the b -value trend and they are shown in Figs. 8 and 9 where the continuous line is the b -value trend, while the dotted line represents the damage parameter. The graph shows how the minimum of the b -value corresponds to the sudden increase of damage on the beam represented by the D parameter. Such an increase of damage corresponds to the final stage of the loading up when the visual observations during the experiment confirmed the appearance of the cracking on the beam.

In a postfailure phase, the minimum and maximum values of the b -value were considered, for each cycle and for each channel. The trend of the range during the whole cycle and for each channel was then plotted. Due to the relationship mentioned earlier in the paper between the increasing and decreasing of the b -value

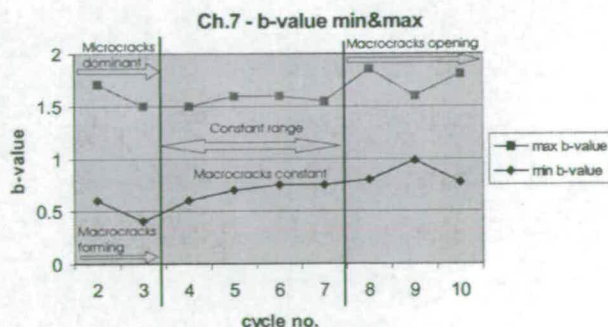


Fig. 11. Variation of maximum and minimum b -value for Channels 3 (top) and 7 (bottom) during all cycles of whole experiment. Vertical lines show different identified cracking stages indicated by arrows.

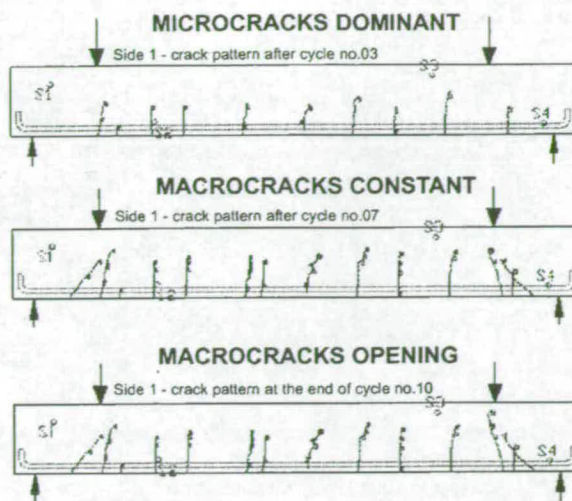


Fig. 12. Fracture process developments during different stages of loading. Dotted line outlines steel reinforcement.

and the micro- and macro-cracking, the minimum b -value trend suggests macrocracks have formed, while the maximum b -value trend implies microcrack growth. The chart of the trend for Channels 3 and 7 during the whole experiment is shown in Figs. 10 and 11.

When examining the results for Channel 3 (which is located near to the end of the beam, see Fig. 2), the maximum trend is increasing from cycle Number 2 to 3, implying that microcracks are forming. During the experiment it was actually in these early stages that the cracking appeared and could be mapped on the beam. A peak of the trend appears in cycle Number 9: at this time of the experiment, all the cracks were already been formed but the shear cracks at the end of the beam were visibly opening up, just before the failure that happened in the following cycle. The minimum trend is decreasing in the early stages, reaching a minimum in cycle Number 4, suggesting the existence of macrocracks: it was indeed possible to observe that at this stage all the macrocracks had appeared on the beam. Therefore from this point onward the minimum trend is constant as no major changes of dam-

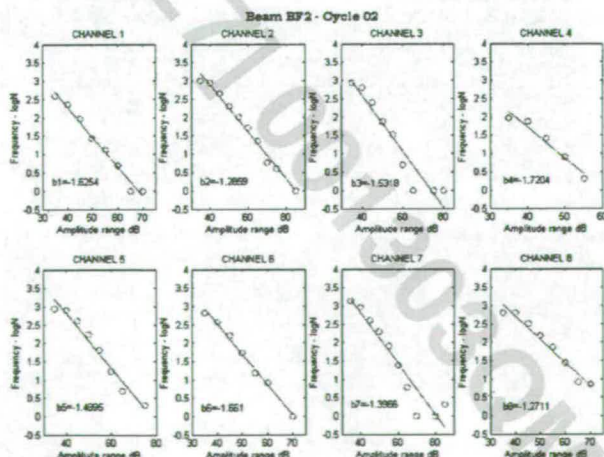


Fig. 13. Frequency versus amplitude charts and b -values during whole cycle Number 2 for each channel

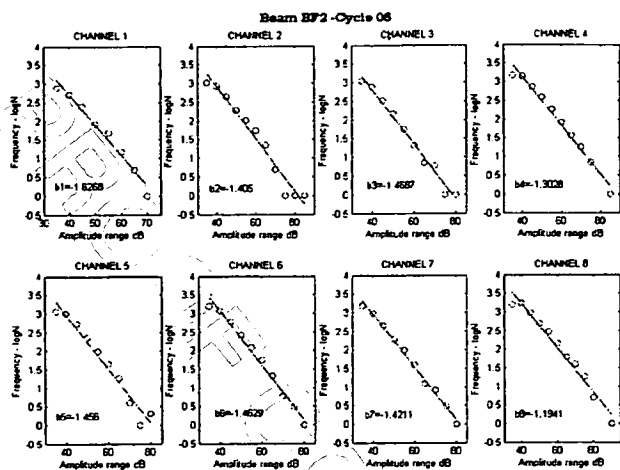


Fig. 14. Frequency versus amplitude charts and *b*-values during whole cycle Number 6 for each channel

age could be observed on the beam. The *b*-value evolution is in good agreement with the damage observed independently on the beam.

Looking at the results for Channel 7 (which is located in the middle of the beam), the maximum trend still decreases at the beginning, implying that microcracks are forming; once again this corresponds to the stage of the test when the microcracking was happening. After this phase, the trend remains constant as at this point the cracks could be seen uniformly spread along the beam. The peak at the end (shown in the results from Channel 3) is unclear now, as this channel is located too far from the end of the beam where the shear cracks are opening to be affected strongly by them. The minimum trend is decreasing in the first cycle as macrocracks started to be visible on the beam and it stabilizes afterwards when all the macrocracks had appeared on the beam and no more new cracks could be seen.

In both cases, three stages of the fracture process can be identified. A first stage is where the microcracks are dominant and the macrocracks are starting to appear. This corresponded to the early stages of loading when the cracking could be seen starting to appear on the beam. A second phase of constant range when the macrocracks are constant and uniformly distributed all along the beam can then be recognized during the middle phase of the loading when visually no new cracks could be seen appearing on the beam. After this stage the cracks do not grow toward the top part of the beam (as the concrete is in compression) so a last stage can be identified when the macrocracks are opening up as the beam is failing. The crack pattern during these phases as it appeared on the beam is represented in Fig. 12. The stress level related to the fracture stages could not be estimated exactly as the data obtained using a Demec gauge are not reliable once macrocracks appeared.

Finally, the *b*-value was calculated considering all the events (instead of groups of 100 events) of a whole cycle and for all channels, to compare the slopes of each channel. The results of these *b*-value calculations for two of the loading cycles (Numbers 2 and 6) are shown in Figs. 13 and 14. By comparing the numerical values obtained in all cycles for all eight sensors with the location of the sensors themselves and the appearance of the cracks on the beam some quantitative considerations were drawn and they are summarized in Table 1. At this stage, the results confirm observations from earthquake aftershocks, slope stability

Table 1. *b*-value Quantitative Results

$1.0 < b\text{-value} < 1.2$	Implies that the channel is very near to a large crack; i.e., macrocracks forming
$1.2 < b\text{-value} < 1.7$	Uniformly distributed cracking; i.e., macrocracks are constant
$b\text{-value} > 1.7$	Microcracks are dominant or macrocracks are opening

studies, and laboratory rock mechanics, that the *b*-value is correlated with the degree of localization of damage (Sammonds et al. 1994).

Practical Significance

The significance of this work is that the *b*-value analysis possibly provides a tool to enable an engineer to diagnose the degree and type of degradation of a concrete beam from remote monitoring of sensors mounted on the structure. The specific practical application that motivated this project related to the monitoring on concrete bridge beams. These are instances when a concrete bridge is showing signs of deterioration and the bridge engineer is faced with the choice of “pass” or “fail.” To “fail” the bridge implies one of the following options:

- Closure,
- Weight restriction, and
- Lane closure.

All of the above options are undesirable for the bridge owner. Thus a third option of “monitoring” would be highly desirable—provided that the monitoring procedure gave real confidence regarding its accuracy re: deterioration progress. This work to date is a valuable step in providing the bridge engineer with another quantitative monitoring tool. The installation of the AE monitoring on a bridge would provide information on changes in the cracking forming in the structure, although at this stage the monitoring should be applied continuously and at an early age of the structure to be really effective.

Conclusions

The paper presents the results from a laboratory experiment on a RC beam. The beam was loaded in cycles and the acoustic emissions were recorded during the test. A conventional *b*-value analysis was applied on the AE data obtained from the beam and the trend of the *b*-value was then compared with the development of the fracture process of the beam observed during the experiment:

- A good relationship was found between the trend of the *b*-value and the microcracking and macrocracking appearing during the test,
- The results confirmed that the *b*-value is correlated to the fracture process of the concrete and to the degree of localization of damage,
- The minimum *b*-value trend suggests macrocracks have formed, whilst the maximum *b*-value trend implies microcrack growth, and
- This study suggests that a *b*-value analysis could be used to interpret data obtained by a “local monitoring” of concrete bridges, although further work is needed in order to consolidate the results that were found and to make the *b*-value suitable for practical use.

Acknowledgments

The writers acknowledge the facilities of the University of Edinburgh and the financial support for this work of the Highways Agency (London), Contract No. 3/320. Thanks are also due to the technical and support staff of the University for their help.

References

- Cox, S. J. D., and Meredith, P. G. (1993). "Microcrack formation and material softening in rock measured by monitoring acoustic emission." *Int. J. Rock Mech. Min. Sci. Geomech. Abstr.*, 30(1), 11–21.
- Iwanami, M., Kamada, T., and Nagataki, S. (1997). "Application of acoustic emission technique for crack monitoring in RC beams." *JCA Proc. of Cement and Concrete*, ■, ■, 51, 192–197.
- Li, Z., and Xi, Y. (1995). "Application of acoustic emission technique to detection of concrete cracking and rebar corrosion." *NDT-CE: Int. Symposium Non-Destructive Testing in Civil Engineering*, Sept. 28

- 1995, Berlin, Germany, 613–620.
- Sammonds, P. R., Meredith, P. G., Murrel, S. A. F., and Main, I. G. (1994). "Modelling the damage evolution in rock containing pore fluid by acoustic emission." *Eurock '94*, Balkema, Rotterdam.
- Shearer, P. M. (1999). *Introduction to seismology*, Cambridge University Press., Cambridge, England, 1–189.
- Shiotani, T., Fujii, K., Aoki, T., and Amou, K. (1994). "Evaluation of progressive failure using AE sources and improved b-value on slope model tests." *Prog. Acoust. Emiss VII*, 7, 529–534.
- Shiotani, T., Yuyama, S., Li, Z. W., and Ohtsu, M. (2000). "Quantitative evaluation of fracture process in concrete by the use of improved b-value." *5th Int. Symposium Non-Destructive Testing in Civil Engineering*, T. Uohoto, ed., Elsevier Science, Amsterdam, 293–302.
- Shiotani, T., Ohtsu, M., and Ikeda, K. (2001). "Detection and evaluation of AE waves due to rock deformation." *Constr. Build. Mat.*, 15(5–6), 235–246.
- Yuyama, S., Okamoto, T., Shigeishi, M., Ohtsu, M., and Kishi, T. (1998). "A proposed standard for evaluating structural integrity of reinforced concrete beams by acoustic emission." *Acoustic emission: Standards and technology update*, ASTM STP 1353, S. J. Vahavilos, ed., American Society for Testing and Materials, Philadelphia, 1–12.

PhD student Sabrina Colombo was Joint 3rd Prize Winner at the IStructE Young Researcher of the Year Conference 2002.

AE monitoring of concrete bridge beams *in situ*

Synopsis

Concrete bridges were built originally to have a cost-effective maintenance free life of 120 years, but work in the UK and USA shows that substantial maintenance is required after 20 to 30 years. This paper presents the description and results of an acoustic emission (AE) monitoring exercise on concrete bridge beams *in situ*, as part of a larger project aimed to develop an Advice Note on the use of AE to evaluate the structural conditions of concrete bridges.

The fieldwork focussed on the concrete beams on Boghall Bridge, which is located in the Scottish Borders, south of Carfraemill on the A697. The AE processing described in this paper includes location of the AE sources in terms of the recorded energy and a b-value analysis. From the results one is able to distinguish between the different structural behaviour of the beams – thus showing that the AE method is a promising way to evaluate the condition of an *in-situ* structure.

Introduction

From the late 1960s to late 1970s the motorway construction boom in the UK gave rise to a large number of new highway bridges. Concrete was mainly chosen as the building material as it was perceived to be 'maintenance free' and was thought to give bridges a cost-effective life span of 120 years. As a result, concrete bridges represent the majority of the UK motorway and trunk road bridge stock. As of now their average age is of the order of 25-35 years and they are starting to show signs of deterioration, due to varied construction defects and general wear and tear. The original designers' expectation thus has been demonstrated to be too optimistic. The US bridge stock is older and faces a similar situation with concrete road bridges that are typically 40 years old and are approaching the end of their useful life. Concrete bridges frequently require major maintenance after 20 to 30 years in order to extend their life by a further 20 years. The scale of the rate of deterioration is related to the increased axle loads dictated by European Standards and the increased volume of modern traffic – neither of which was envisaged at the time of the original design. There is therefore a necessity to verify their serviceability under the new conditions that have arisen.

Authorities and engineers are faced with the assessment of these structures to verify their structural integrity. Long term plans¹ and a range of diagnostic techniques have been proposed and developed to assist the undertaking of this task, but the question of how to cost-effectively evaluate concrete bridges still remains.

The standard bridge assessment provides a 'pass' or 'fail' answer to that question but lately a third option of 'monitoring' has been proposed² for those bridges that fail the assessment by a small margin. A long or short term monitoring would provide information on defects, damage or deficiencies and their relative degree of risk for the structure. A reliable evaluation should take into account a combination of factors (materials, design, construction methodology, structural history) that would give a comprehensive knowledge of the bridge and its actual condition. A distinction can be made between 'global' monitoring aiming to obtain an understanding of the whole bridge and 'local' monitoring which addresses a very specific problem generally concerning components or smaller areas of the bridge. At the moment in the UK, no Standards or procedures to monitor concrete bridges exist.

This research is part of a project sponsored by the Highways Agency (London) to verify the feasibility of the acoustic emission (AE) technique as a valid method of monitoring concrete bridges. The acoustic emission technique (AET) is a passive, non-intrusive, method that allows monitoring of concrete structures. Its basic principle, derived from the theory of

elastic waves, is very similar to that used for earthquakes in seismology. The term acoustic emission encompasses all phenomena where elastic waves are generated by the release of energy from localised sources. In every solid body subjected to stress – the occurrence of cracking, corrosion, slip or friction is followed by a release of stored strain energy that generates elastic waves, which is referred to as acoustic emission. Acoustic emission testing was largely used in the nuclear and the oil industries to remotely monitor critical structures such as pressure vessels and storage tanks. Lately, the technique has started to be used in a broader range of fields such as in the research of material properties, fracture mechanics, rock corrosion studies, the aircraft industry and finally civil engineering³.

One possibility is that AE might give the bridge engineer confidence about the mechanism of deterioration of individual members of a bridge already showing signs of significant distress. The eventual plan is to write an Advice Note on the use of AE on concrete bridges. The work presented here puts into practice on a real structure, information and results obtained in previous laboratory experiments. This will permit verification of their applicability for *in situ* monitoring. The bridge investigated in this research is a composite masonry arch/RC beam bridge. It was chosen on the basis of its characteristics (dimensions, materials, and degree of distress), location (easy access, safe location and environment) as well as the fact that it had already been monitored during 1999⁴. This allowed a comparison between the earlier findings and the actual current state of the bridge and comparisons to be drawn.

The Boghall bridge

The Boghall Bridge is located in the Scottish Borders, south of Carfraemill on the A697. The original bridge was a flat masonry arch built, according to the Council records, in 1793. Later on, the road was widened and a trapezoidal cast *in situ* concrete slab was placed alongside the masonry arch. The concrete slab consists of four beams, whilst the masonry arch was built using red sandstone blocks. The road orientation was also altered explaining the lack of alignment. This work focuses on the concrete side of the bridge. Construction details of the bridge and its actual aspect can be seen in Fig 1 and 2.

Monitoring description

Preliminary investigation

Initially a visual survey was undertaken. The most northerly of the four concrete beams (named beam 1) shows extensive visible cracking on both sides, and concentrated mainly on

Ing. S. Colombo

Qualifications?

Prof. M. C. Forde

FREng, Other Qualifications?

Both University of Edinburgh, The King's Buildings, Edinburgh EH9 3JN, Scotland, UK

Jack Halliday

Qualifications?

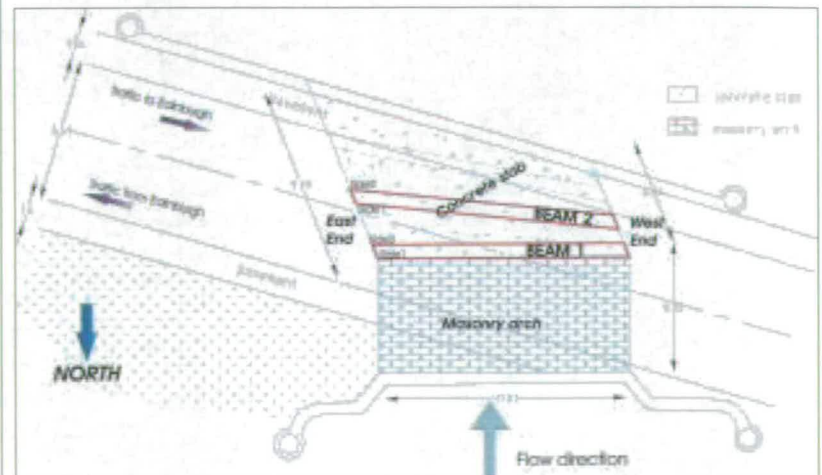
The Highways Agency, St. Christopher House, Southwark Street, London SE1 0TE, UK

Received: 08/02

Accepted: 04/03

Keywords: Acoustic emission, Monitoring, Boghall Bridge, Scotland Concrete Beams, In situ

Fig 1. Plan view of Boghall bridge





Sample rate	1 MHz
Hil length	2K
Threshold	30dB
PDT	500
HDT	1000
HLT	65534



Fig 2. (above) Boghall bridge: masonry and concrete side; pre-existing cracks

Fig 3. (left) Settings values of AE system and PAC system

points were positioned (in nine locations) on either side of the cracks and the distance between them measured using a digital Vernier caliper. This allowed recording any variation in crack width throughout the whole monitoring. The length of the cracks was recorded as well at the beginning and at the end of the study.

- Excessive movements and vibrations of the bridge could affect the AE data by generating misleading signals. A laser vibrometer was used to measure the displacements of the bridge; it was set on the river bank with the laser pointing at the mid-span of beam 1. The instrument allows displacement measurements to be made over a range of 0.08µm to 80mm with a frequency range of up to 1500kHz (1.5GHz). The laser vibrometer was connected to a data logger and to a laptop, where the data were recorded and stored using Matlab software.
- Acoustic emissions are generated by stress release deriving from applied load. To avoid any road closure or disruption, a passive monitoring was adopted using normal traffic condition as load to induce AE. A video camera was positioned on the deck of the bridge to film the flow of traffic during the monitoring period. The number of vehicles passing per minute for each 30 minutes period was established, indicating the volume of traffic.
- A previous study⁶ showed that environmental factors may influenced the AE readings. Meteorological data were obtained from the Meteorological Office, Charterhall station, 23.1km east of Boghall bridge. Due to the distance of the meteorological office station from Boghall Bridge, it was anticipated that the information might not be totally accurate, but would still provide an understanding of the meteorological situation. This information would then be integrated with the field observations.

the eastern end of the beam (Fig 2). This cracking is probably due to the corrosion of the reinforcement, as iron staining can be clearly observed on the beam. As there is no joint present between the masonry arch and the concrete slab, water can penetrate freely and cause such corrosion. Salt, commonly spread on roads to avoid ice can also be dissolved in water and infiltrated through the bridge – accelerating the rate of corrosion. The other three beams appear in good condition. At the beginning of this preliminary investigation it was decided to focus the monitoring on the visibly damaged beam (beam 1) and on the one in good condition beside it (named beam 2).

Experimental objectives

- The main objectives of this research were:
- to investigate the feasibility of the AE technique on a real concrete bridge;
 - to investigate the different factors that can influence the AE data during *in situ* monitoring, such as: wind, temperature, rain, traffic, displacements, presence of cracks, and so on.
 - to compare the response from a beam in visibly poor condition to one that shows little deterioration and to gain an understanding of the bridge condition;
 - to compare the actual results with the findings obtained in the previous monitoring in 1999.

Recorded data & equipment

During the monitoring, different sets of data were recorded in order to obtain a comprehensive understanding of the bridge. Acoustic emission data were recorded using the PAC Mistras equipment detecting frequencies above 25 kHz. The settings used for the system are summarised in Fig 3. Eight PAC R61 (Resonant 60kHz Integral) were used in conjunction with the system.

Pre-existing cracks can generate acoustic emissions and their presence has to be taken into great account. The cracks visible on beam 1 were mapped and measured. Metal base

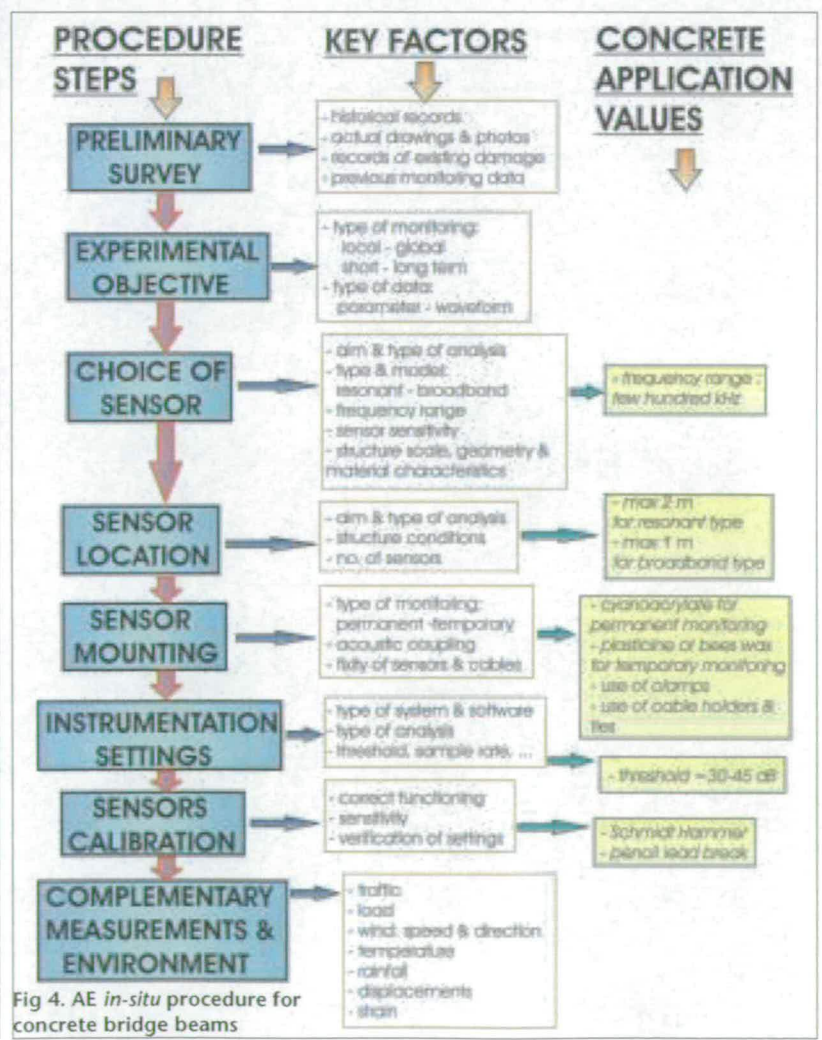


Fig 4. AE *in-situ* procedure for concrete bridge beams

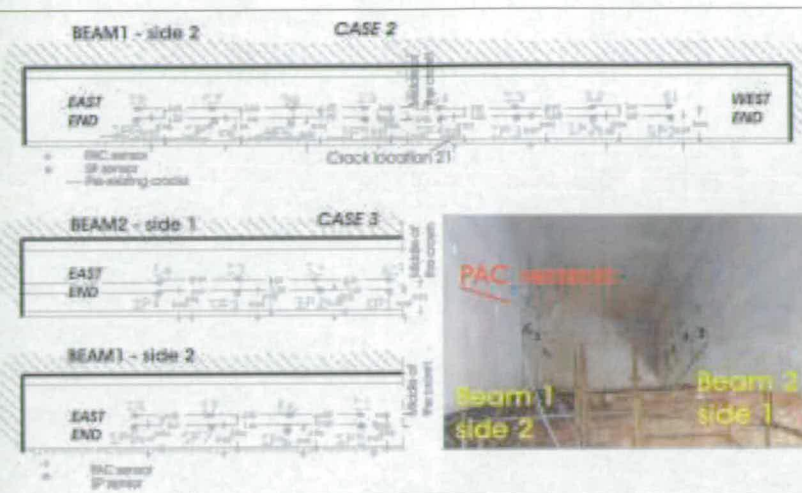


Fig 5. Sensors location: case 2 (a) and case 3 (b/c)

Sensors mounting & calibration

All the sensors were mounted on the surface of the beam using metals clamps to hold them in place. Plasticine was used as acoustic couplant. The cables connecting the sensors to the acquisition system were secured using cable holders and ties to prevent movements and/or interference. Every day before recording commenced, the transducers were calibrated. The calibration consisted of:

- Generating some high energy elastic waves using a Schmidt Hammer, to verify the functionality of all the sensors;
- Breaking a 0.5mm pencil lead [British Standards EN 1330-9:2000 *Non Destructive Testing Terminology - Part 9*] near to each sensor to verify their sensitivity.

AE monitoring procedure

A simplified sketch of the AE procedure followed during this work has been summarised in Fig 4 and it included the following steps:

- Preliminary survey
- Aim of the test
- Choice of sensor

- Sensor location
- Sensor mounting
- Instrumentation settings
- Sensors calibration
- Complementary measurements and environment

Case study

Three different cases were investigated. Firstly, the sensors were placed underneath beam 1 (case 1). Due to the poor quality data recorded using this location, the sensors were removed and located alongside beam 1 on side 2 (case 2, Fig 5a). Finally (case 3, Fig 5b, Fig 5c), half of the sensors were placed on beam 1 (side 2) and the other half on beam 2 (side 1), to compare the response of beams in a different state of deterioration. The exact location of the sensors for case 2 and case 3 is shown in the drawings of Fig 5.

The bridge was monitored over a period of about 10 days. The exact monitoring time for each case is shown in Fig 6. The figure also includes a summary of the meteorological and traffic data.

Data processing

Crack and displacements measurements

The measurements showed that the cracks did not grow in length during the monitoring period. Little variation (Fig 7a) in their width was recorded between the start and the end of each day; and this small variation was probably due to temperature conditions or instrument inaccuracy. Only one discrepancy is noticeable - on the 23rd May 2002 - but it is believed to be due to an error in the reading as on the following day the recorded crack width was returned to the previously recorded value.

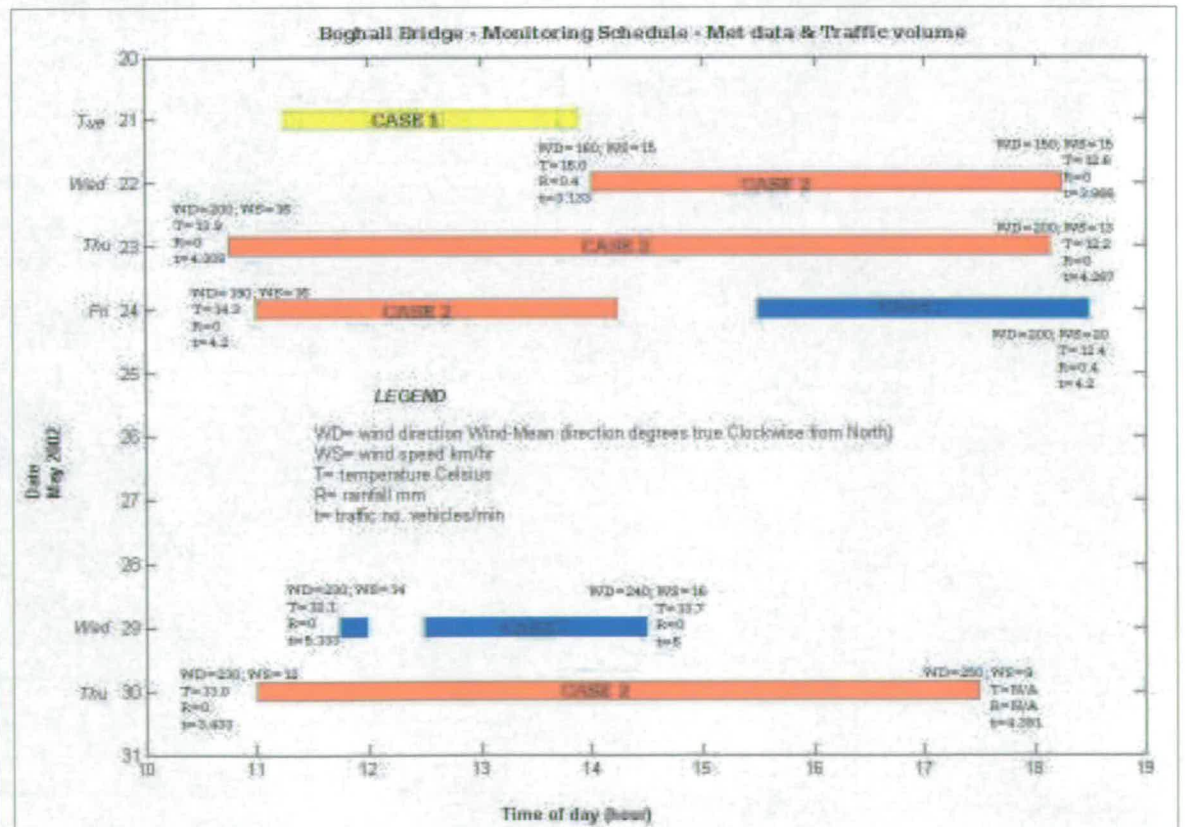
The laser measurements showed that the displacements were limited (about 1mm) following a regular trend (Fig 7b). It can then be assumed that they should not have affected the AE readings.

AE results

AE location

The analysis of the AE location consists in locating the AE sources. These sources can then be related to development or

Fig 6. Monitoring schedule and meteorological data



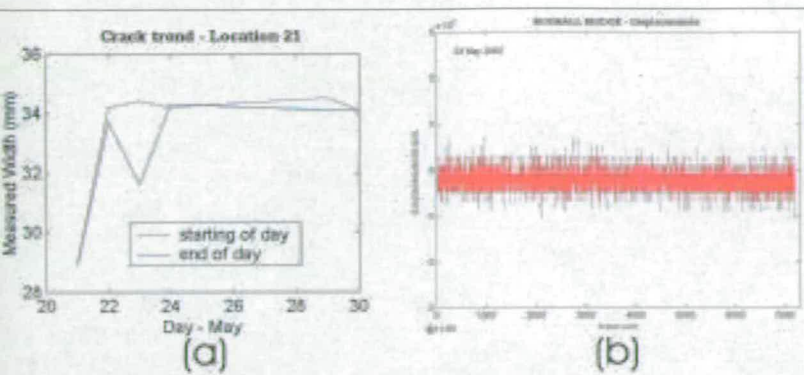


Fig 7. a) Measured crack width trend in location 21 during the monitoring days. b) Bridge displacements

existence of cracks pattern on the beams. A linear location (alongside the beams) was carried out using the Mistras (PAC) software. The sources were located with reference both to the recorded events and energy but only the second ones are shown here as it is energy that can be then considered as an effective parameter to indicate the damage of a structure⁶. Events generated by reflections, noise or interference can be located but the energy associated with them is irrelevant. On the other hand, structurally meaningful events are characterised by a relevant amount of energy. The energy is calculated as the area under the envelope of the AE signal. Figs 8, 9 and 10 in the following paragraphs show the sensors (represented by the green squares) on the top horizontal axis and their distance in metres on the beam on the bottom horizontal axis; the located energy is shown on the vertical axis.

Case 1: On a bridge beam, it is the bottom part that is in tension and then that is the area where the cracks and the acoustic emissions are generally expected to develop from. For this reason, in the first case study, all the sensors were placed underneath beam 1. Very few AE activities were recorded and it was confined to the western area of the beam (Fig 8). This was thought to be due to the presence of large visible cracks propagating alongside the eastern area. The

Fig 8. AE energy location - Case 1

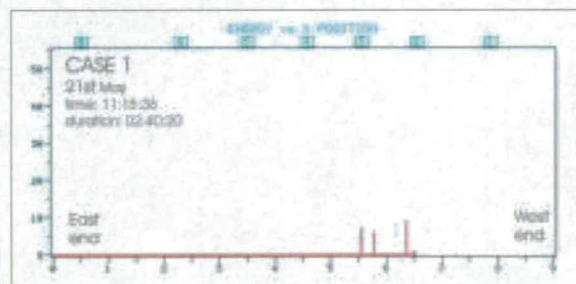
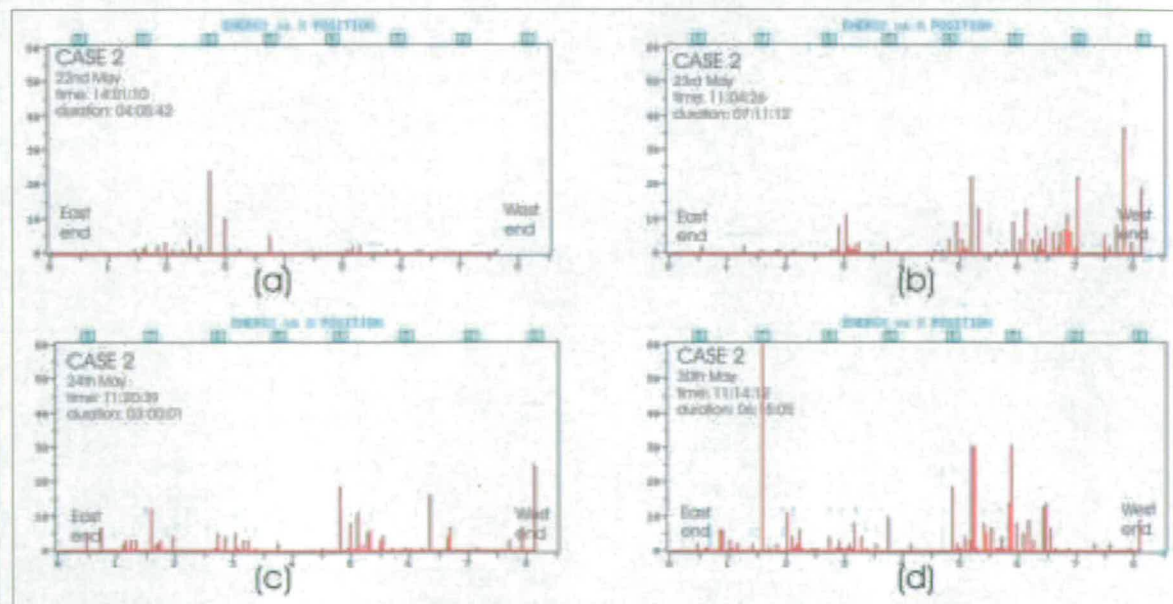


Fig 9. AE energy location - Case 2



existence of these cracks prevented the elastic waves from travelling through the concrete and reaching the sensors located on the underneath of the beam. The sensors were then moved to another location.

Case 2: Beam 1 was monitored for about 4 days and the results are shown in Fig 9. In 3 out of the 4 days (Figs 9 b, c, d) the location shows consistently that the majority of the AE activity was occurring on the western side of the beam. The cracks already visible on the eastern side generated acoustic emission but of lower energy as the opening up of existing cracks creates AE events of smaller amplitude and energy. Most of the energy is usually released during the forming and localisation of new microcracks. This suggests that the existing cracks on the west side are propagating towards the opposite side of the beam and that the process of corrosion is progressing. It has to be pointed out that the clearer pattern appeared in Fig 9b and Fig 9d when a longer duration was involved. A longer monitoring time highlights the AE trend of the whole structure and minimises the influences due to single specific local events that can mislead the interpretation of the results.

Case 3: Case 3 allowed a comparison between the behaviour of a badly damaged beam (beam1) and a beam that appeared to be in good condition (beam 2). The results for the relative days of monitoring are shown in Fig 10. On the 24th May 2002 the wind was stronger (Fig 6) but this did not affect the results, showing that the use of cable holders and tie helped to prevent wind interference. Comparing the results to those obtained on case 2, and even taking into account the shorter duration, much less AE activity was recorded in case 3 - even if the volume of traffic (Fig 6) on those days appeared higher than during the previous days. Beam 1 did not show differences during the two monitoring days, as it was probably in a quite stable condition. The results for beam 2 (Fig 10) showed few emissions on the 24th May, but some activity was recorded on the 29th May. This can be explained by looking at the time of the recording. On the 24th May the recording was made in the afternoon, when more traffic was travelling out of Edinburgh along the A697 and then running above beam 1 (Fig 1). On the 29th, the data were acquired during lunchtime, when more vehicles were travelling towards Edinburgh and then over beam 2. As beam 2 appears to be in good condition and the east end of beam 1 is already badly damaged (i.e.: it does not generate high energy events) the structural response in terms of AE is limited and the traffic effect is relevant. This suggests that for totally reliable monitoring and easier comparison, the recordings should be done ideally at the same time and for the same duration. Once again, a longer monitoring might have overcome the problem, allowing the identification of a pattern representing the structural

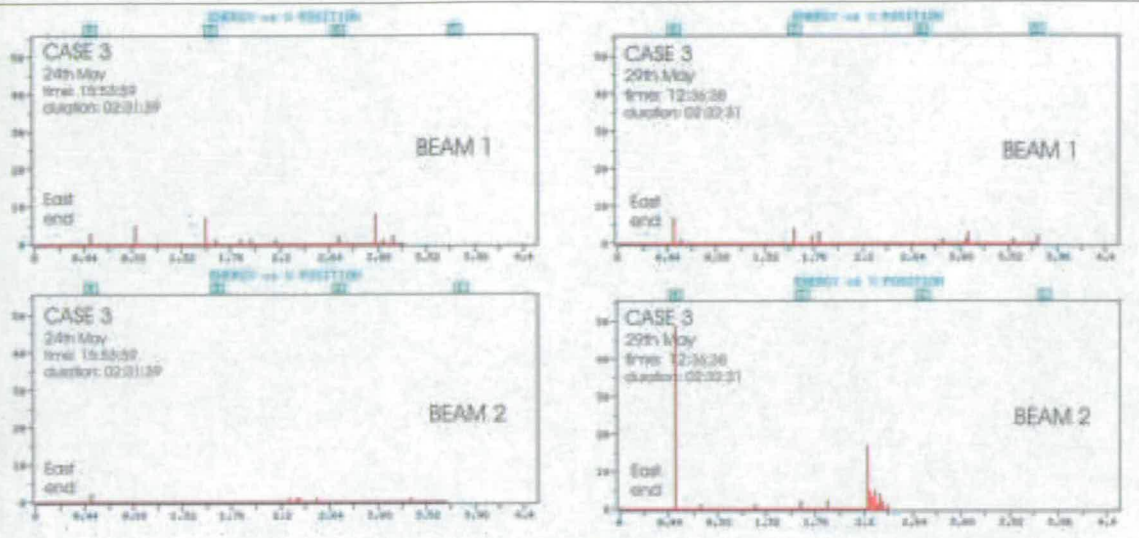


Fig 10. AE energy location – Case 3

behaviour of the beams.

b-value analysis

A challenge with the AE technique is to decide how best to analyse and present the data in a meaningful way. One way of doing this is to look at a frequency-magnitude plot and a technique for this can be borrowed from seismic engineering which is also about vibration emissions (from the fault) of varying magnitude and at variable intervals. In the light of this a *b*-value analysis of the data was undertaken. The *b*-value is the negative gradient of the log-linear AE frequency/magnitude plot and hence it represents the slope of the amplitude distribution. It is defined by the following empirical formula proposed by Gutenberg and Richter:

$$\log_{10} N = a - bM_L \quad \dots(1)$$

where M_L is the Richter magnitude of the events, N is the incremental frequency (i.e. the number of events with magnitudes in the range of $(M_L \pm \Delta M)$), and a and b are empirical constants⁷. The Richter magnitude M_L is proportional to the logarithm of the maximum amplitude A_{max} recorded in a seismic trace, corrected for the attenuation in amplitude with distance due to wave propagation and inelastic absorption. Equation (1) defines the fact that in earthquake seismology, events of larger magnitude occur less frequently than events of smaller magnitude.

The same principle can be applied to the AE method to study the scaling of the 'amplitude distribution' of the acoustic

emission waves generated during the cracking process in the laboratory or in engineering structures. The *b*-value changes systematically with the different stages of fracture growth⁷, so it could be used to estimate the development of the fracture process. In terms of the AE technique, the Gutenberg-Richter formula can be modified as:

$$\log_{10} N = a - b'A_{dB} \quad \dots(2)$$

where now A_{dB} is the peak-amplitude of the AE events in decibels:

$$A_{dB} = 10 \log_{10} A_{max}^2 = 20 \log_{10} A_{max} \quad \dots(3)$$

The *b*-value obtained with this relationship should be then multiplied by a factor of 20 to be comparable with the one used in seismology⁶.

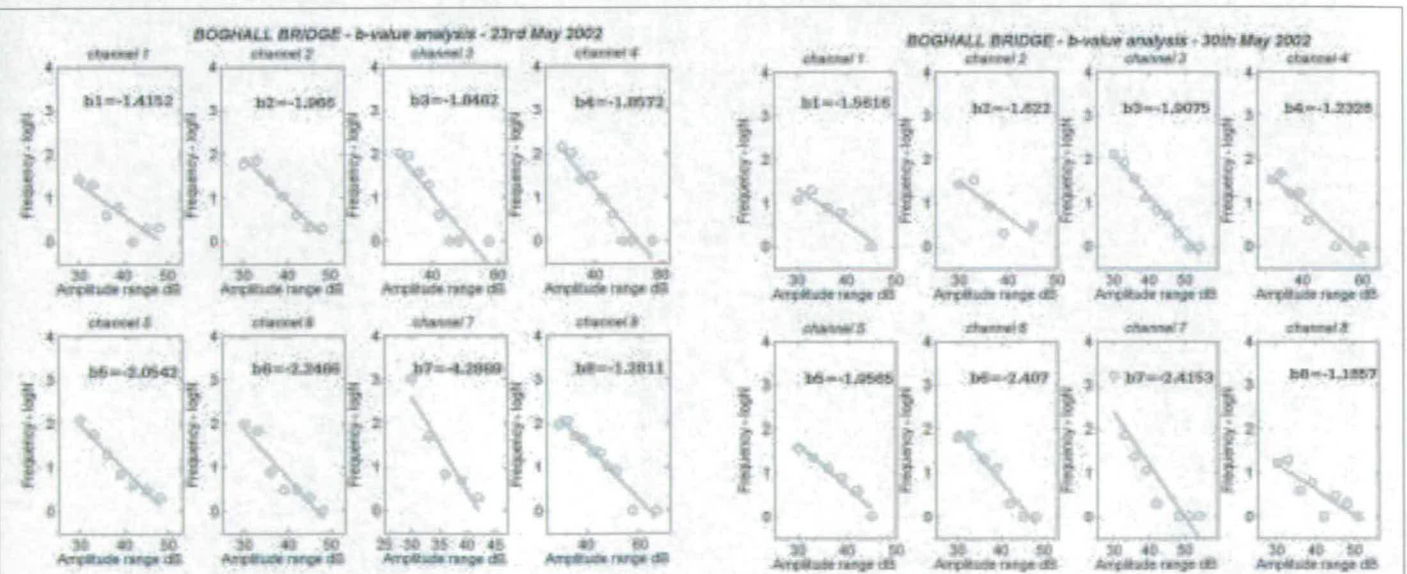
In general terms, when the distributed microcracks are occurring in the early stages of damage, the *b*-value is high and when the macrocracks begin to localise or to open up the *b*-value is low.

In the analysis presented in this paper, a conventional *b*-value analysis was applied on the data recorded on the bridge beam 1, using the relationship (2) and assuming:

$$b = b' * 20$$

The *b*-value was calculated using the least squares method and interval range of amplitude of 3dB for each day of moni-

Fig 11. *b*-value results on beam 1



ring and for each channel. The results were plotted in Fig 11, which refer to the two full days of monitoring of case 2.

It can be seen, in both days, that channels 5, 6 and 7 (east side) have a lower b -value than channels 1, 2, 3 and 4 (west side). This is due to the fact that the opening up of the existing cracks on the eastern end of the beam generated a large number of events but of small amplitude. On the contrary, the possible formation of new microcracks in the western areas created less acoustic emissions but of larger amplitude. Channel 8 showed again a high b -value implying that the existing cracks may be growing also towards the western end of the beam, where it is possible that the corrosion is expanding and new cracks are localising.

The b -value analysis appears to support the results obtained by the previous data processing.

Comparison with earlier monitoring

Monitoring of Boghall Bridge was undertaken at the beginning of 1999 and reported in Shigeishi *et al*⁸. Although that research focused on the masonry arch, some data were collected on the concrete beam (beam 1 – side 1) as well. The location (Fig 12) of the AE activity was quantified in terms of AE events instead of energy. It did show that the most of the AE activity was coming from the western end of the beam, suggesting that the cracks present on the eastern side were propagating into the opposite area. This observation agrees with the results obtained during the recent monitoring. Therefore it must be pointed out that it appeared that a larger amount of events were recorded by the PAC system during the monitoring study. This may be due to the fact that during 1999 a different type of sensor was used (R3I Resonant 30kHz Integral). As those transducers were resonant at a lower frequency, they were probably able to pick up a larger number of acoustic emissions. Since the earlier monitoring was carried out during winter, a possible explanation is that the heaviest rainfall happening during that period together with the use of salt to avoid freezing - accelerated the rate of corrosion propagation and made the structure more acoustically active. However it remains more likely that the response can be attributed to the transducer sensitivity and range.

Conclusions

The AE method has proved to be a promising and effective means of investigating the condition of concrete bridges. It can be used as a trend tool to obtain an understanding of the structural condition of concrete bridge beams without any traffic disruption. An AE testing can provide physical measure of whether a situation is getting worse with time and so alert the authorities and bridge engineers that it is time to intervene on the structure. If the testing is repeated in time, it can also show if the state of the structure is stable, i.e. if it is getting worse or can be lived with.

The procedure followed during the study has been presented.

From the undertaking of this work and the processing of the data, the following conclusions were drawn:

- A preliminary visual survey of the structure is always of fundamental importance to establish a first view of the state of the bridge;
- The presence of pre-existing cracks must be considered when deciding the sensors locations and during the data processing, as it affects the generation of elastic waves;
- Environmental factors (rain, wind, temperature) as well as traffic volume must be considered in order to obtain a comprehensive understanding of the AE data;
- The cables should be clamped and fixed tightly in order to reduce wind interference;
- The location of the AE energy allows identification of the areas of highest activity, where possible damage is occurring; visible cracking produces waves of low energy, whilst new internal cracks generate high energy signals;
- The monitoring should be repeated in time to allow verification of the results; for a more reliable comparison it is also advisable that such a time is kept constant (both in terms of daily time and duration);

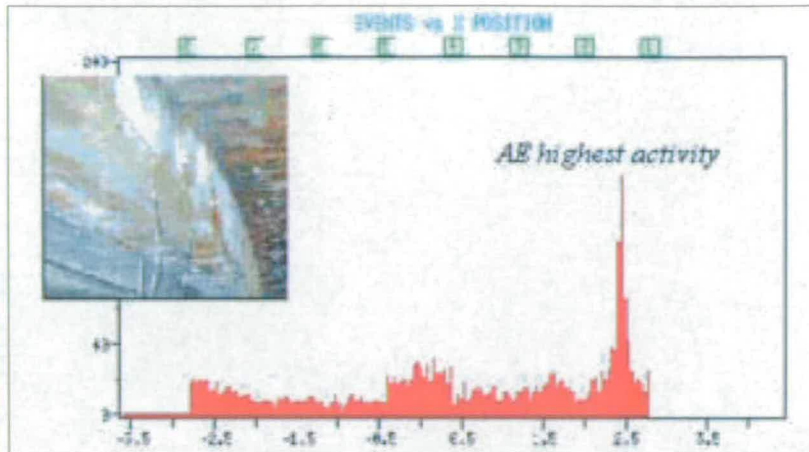


Fig 12. AE energy location on beam 1, during February 1999

- A longer period of monitoring is preferred in order to obtain a realistic pattern of the AE activity and to minimise the effects of single events that can mislead the data interpretation;
- The b -value analysis can be successfully applied on a real structure to distinguish areas where macrocracking and/or microcracking is occurring;
- The existence of previous monitoring data is a useful feature in order to have an overview of the behaviour of the bridge over a period of years - in order to verify the stability of its condition and to confirm and support the findings from AE work; the creation of a database containing information about the bridge stock should be developed.

Acknowledgments

This work was presented at the IStructE Young Researchers Conference, 2002, where Sabrina Colombo received a joint Third Prize. This research is part of a PhD study sponsored by the Highways Agency (London), contract no. 3/320 and whose financial support is greatly acknowledged. Thanks are due to Mr A. J. Batchelor, Holequest Ltd, Galashiels for providing the scaffolding, to the Scottish Borders Council for allowing access to the bridge and to Mr. G. Hood of the Meteorological Office for providing the meteorological data. The first author wishes to thank Assoc Prof. M. Shigeishi, Kumamoto University, Japan for his invaluable advice and support, and also the academic staff of the University of Edinburgh.

REFERENCES

1. Das, P. C.: 'Background to the current bridge rehabilitation programme and future needs – estimating uncertainty in bridge assessments', *Bridge Rehabilitation in the UK, Proc of ICE Conf.*, 2-3 Oct 2000, London, UK, Paper 1, p 1-15.
2. Colombo, S., Forde, M. C., Das, P. C.: 'Improving impact echo and radar NDT data interpretation using uncertainty analysis technique', *Bridge Rehabilitation in the UK, Proc of ICE Conf.*, 2-3 Oct 2000, London, UK, Paper 20, p 1-14.
3. Ohtsu, M.: 'The history and the development of acoustic emission in concrete engineering', *The Concrete Library of the Japan society for Civil Engineers*, 25, p 121-134.
4. Shigeishi, M., Colombo, S., Broughton, K. J., Rutledge, H., Batchelor, A. J., Forde, M. C.: 'Acoustic emission to assess and monitor the integrity of bridges', *Construction and Building Materials*, 15, p 35-49.
5. Shigeishi, M., Shiotani, T., Ohtsu, M. (2000) 'A consideration about the rainy influence in field AE measurements', *Progress in Acoustic Emission X*, The Japanese society for NDI, p 177-182.
6. Colombo, S., Main, I. G., Forde, M. C., Halliday, J.: 'Acoustic emissions on bridges: experiments on concrete beams', *EWGAE 2002*, 11-13 Sept, 2002, Prague.
7. Shearer, P. M.: *Introduction to Seismology*, (1999), Cambridge University Press, p 189, ISBN 0 521 669537
8. Shiotani T., Yuyama S., Li Z.W., Ohtsu M.: 'Quantitative evaluation of fracture process in concrete by the use of improved b -value'. *5th Int. Symposium Non-Destructive Testing in Civil Eng.*, Ed. T. Uomoto, Amsterdam, Elsevier Science, 2000, 293-302, ISBN 0080437176.
9. Shiotani, T., Ohtsu, M., Ikeda, K.: 'Detection and evaluation of AE waves due to rock deformation'. *Construction and Building Materials*, Elsevier Science, Vol 15/5-6, 2001, p 235-246

IMPROVING IMPACT ECHO AND RADAR NDT DATA INTERPRETATION USING UNCERTAINTY ANALYSIS

Ing. S Colombo
School of Civil and Environmental Engineering
University of Edinburgh

Prof. Michael C Forde, PhD, FREng, CEng, FICE, FIEE
Carillion Professor of Civil Engineering Construction
School of Civil and Environmental Engineering
University of Edinburgh

Prof. Parag C Das, OBE, PhD, CEng, FICE
Project Director Bridge Management
Highways Agency

INTRODUCTION

Non-destructive test (NDT) methods such as the impact echo (I-E), ground probing radar (GPR) and acoustic emission (AE) techniques have been used increasingly in recent years for investigating structural integrity. Although these methods have sometimes been used for bridge investigations, such uses have been mainly confined to research related or trial applications. It has not so far been possible to use these methods directly in the structural assessment of bridges because of the qualitative nature of the results.

Nevertheless, the current national bridge assessment and strengthening programme has highlighted the fact that the results of conventional assessments can be uncertain to varying degrees. It has been discussed elsewhere [1] that, even for structurally simple bridges where assessments ought to be precise, the uncertainties in some of the input parameters are such that it will be more rational for the assessment results to be qualified with confidence levels for taking important decisions. This can be achieved through uncertainty analysis using methods such as fuzzy set theory and Bayesian updating.

In addition, there are certain older bridge types such as the masonry arch bridges, for which the factors influencing structural behaviour are not amenable to precise analysis. For such bridges, instead of the "pass or fail" type of results from the assessments, it may be more logical to allow a graduated "pass, fail or monitor" type of result. The monitor option could be used when a bridge passes or fails a conventional assessment by a small margin but may have features or faults which are likely to influence structural capacity, which cannot be taken into account in the calculations.

There is a third group of bridges, for example the post-tensioned concrete bridges or bridges over waterways, for which conventional assessment of structural capacity is only a part of the overall risk assessment, which has to take into account many factors that do not enter into the calculation of capacity. These factors are generally of a 'fuzzy' nature, and hence for these bridges, uncertainty analysis would be appropriate for defining the potential risk levels.

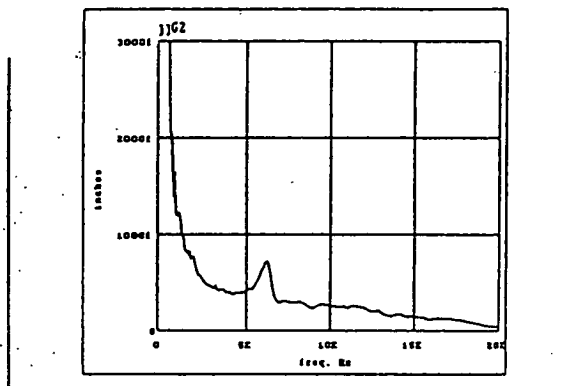
Non-destructive testing methods such as the sonar, radar or the dynamic methods could be of great value in carrying out the uncertainty analysis desirable in the above situations. Furthermore, once the monitor option is decided upon, some of these methods could also be used for examining the bridge periodically to see if any significant structural deterioration is taking place.

The purpose of this paper is to highlight the areas of bridge assessment and management where non-destructive testing techniques, particularly the impulse radar and impact echo methods, could be fruitfully used in conjunction with uncertainty analysis.

METHODS

NDT methods such as radar, impact echo and acoustic emission techniques are being used increasingly to investigate structural faults and hidden features. The following are a few examples of such applications, presented in brief here in order to give a broad overview of typical results.

Olson et al [2] have carried out an investigation of the integrity of the raised terrace concrete slabs at the Lincoln Memorial in Washington, D.C.. They used the impact echo technique and an example of the test results is shown in Fig.1.



Note: 1f inch = 1 femtoinch = 1E-15 inches

Notes:

- 1. Backside Echo Peak = $f_1 = 6.2 \text{ kHz}$
- 2. Concrete thickness = $T = 10.8'' = 0.9'$
- 3. Velocity $V_c = T * f_1 * 2 = 0.9 * 6.2 * 2 = 11.2 \text{ kfps}$
- 4. This location is indicated to be sound, with a backside echo and no other distinct peaks.

Figure 1. Impact Echo test record [2].

The results show the transducer displacements against frequency. They indicate a resonance at 6.2 kHz corresponding to a slab thickness of 27.4 cm (10.8 inches).

Another example is a radar application on the surface of a masonry wall of the Torrazzo tower (Cremona, Italy) [3]. The radar image shown in Fig.2 indicates the presence of a superficial detachment in the masonry wall.

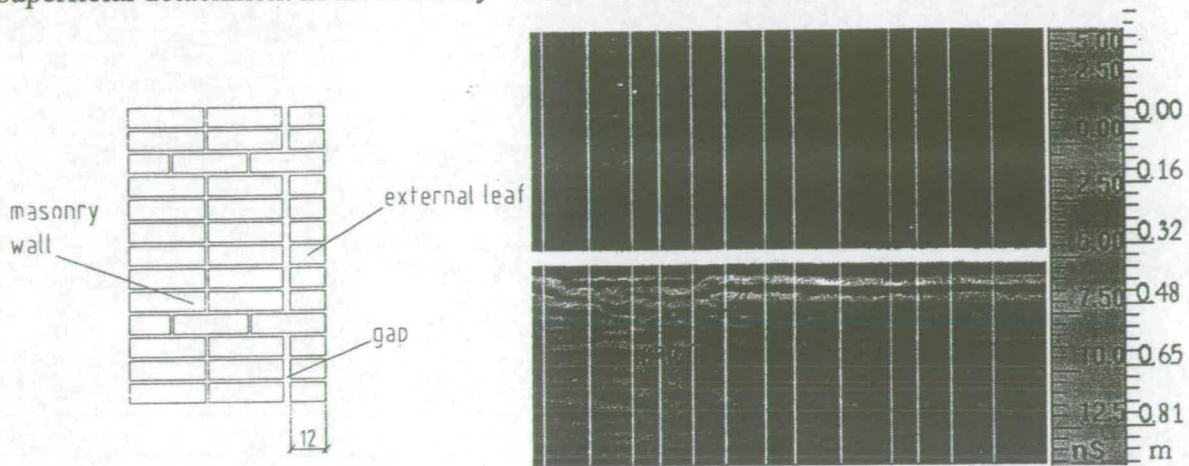


Figure 2. Radar image of a masonry wall [3].

An example of the application of acoustic emission monitoring is given by Shigeishi et al [4]. In this work, a reinforced concrete beam of 400mm length, with a notch as shown in Fig.3, was monitored. The beam was first tested under a static load and then was put under cyclic loading. As the cracks developed in the tests, 'events' were recorded (see Fig.4), and these records were then used to determine the progress and the extent of the cracks.

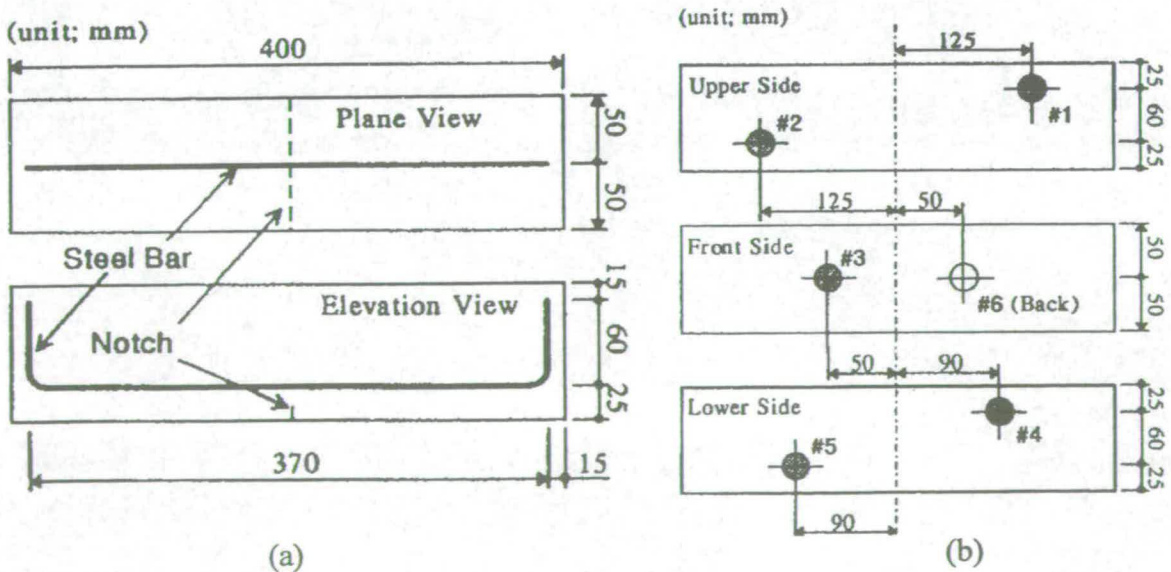


Figure 3. RC beam subjected to acoustic emission monitoring (a) and arrangement of AE sensors (b)[4].

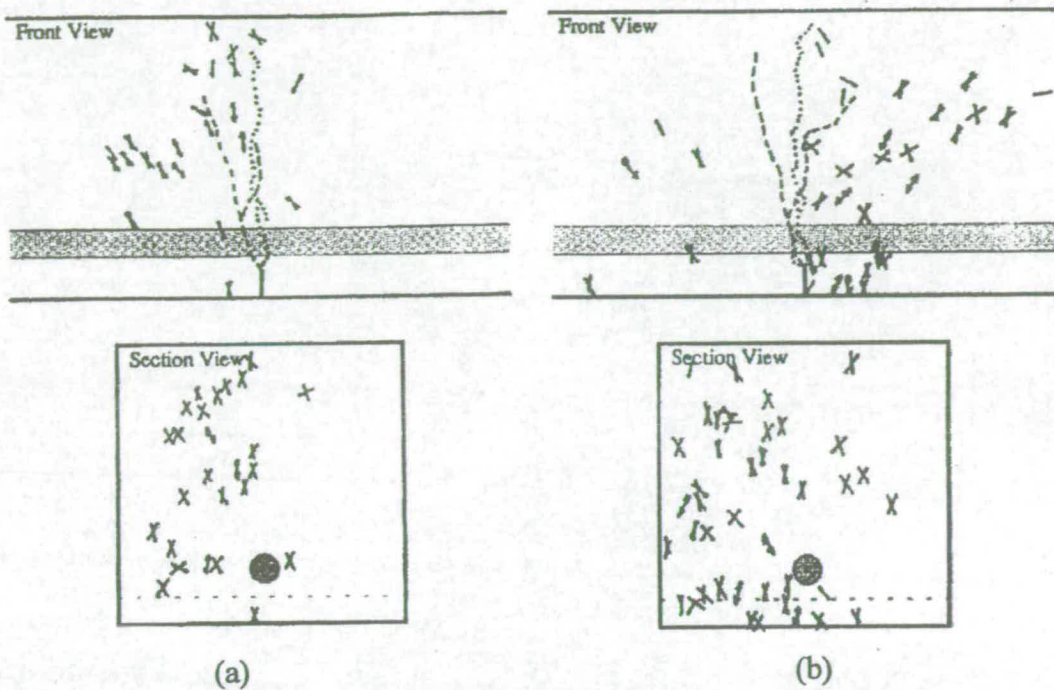


Figure 4. Results from acoustic emission monitoring: microcracks generated by static pre-loading (a) and cycling loading (b) in RC beam specimen "Type B" [4].

It can be seen from these examples that the recorded results from NDT techniques can be very vague, and any quantitative information will at best be approximate. This is primarily the reason why these methods have not found routine use in bridge engineering applications.

The important advantage of such NDT methods is however in the very fact that they provide qualitative information without incurring great costs or traffic disruption. The information gathered can be not only extensive but also of considerable significance as far as structural capacity is concerned. If applied in conjunction with appropriate uncertainty analysis methods, these techniques will prove to be valuable tools in the armoury of the bridge engineer.

EXAMPLE OF UNCERTAINTY ANALYSIS

The following is an example of how such methods could contribute to the confidence (or lack of it) in an assessment.

In this example, let us consider a brick wall which has been assessed as being without any fault. A radar investigation reveals the possibility that there may be some de-lamination. A fuzzy set analysis is carried out to determine the appropriate confidence levels of the assessed result in the light of the NDT finding. The analysis is carried out in two stages as shown in Figures 5 and 6. In Stage 1, the uncertainty (confidence levels) of the actual length of de-

lamination is determined. In Stage 2, the confidence levels in respect to the possible assessment errors are calculated using the Stage 1 results as input. The calculations are carried out using the following methodology.

Referring to Fig.5, X is a set of five numbers representing five lengths of de-lamination which may be observed from the tests. Similarly, Y is a set of five de-lamination lengths which may be actually present in the structure.

μ _{A(x)} =recorded membership levels	X=Length of delamination	R=Relation Matrix between estimated delamination and actual				
0.4	500mm	0	0.1	0.4	0.8	1
1	400mm	0.1	0.4	0.8	1	1
0.3	300mm	0.3	0.8	1	1	0.6
0.1	200mm	0.8	1	1	0.6	0.1
0	100mm	1	1	0.6	0.1	0

Figure 5. Fuzzy set analysis of error involved in the estimation of de-lamination from a radar survey.

R is the relation between X and Y, the membership levels of which (1, 0.1 etc.) represent the confidence levels with which the different elements y (i.e. 100mm to 500mm) of Y are related to each element x (i.e. 100mm, 200mm, etc.) of X.

A is a subset of X, representing a particular de-lamination observation, the relation of which with X is defined as follows :-

$$A = 0.4 \ 500, 1 \ 400, 0.3 \ 300, 0.1 \ 200$$

where 0.4, 1, 0.3 and 0.1 are membership levels of A corresponding to when x is 500, 400, 300 and 200mm respectively. A thus represents an estimated de-lamination length of 'about' 400mm.

$\mu_A(x)$ = True membership levels	X=Length of delamination	R=Relation Matrix between true delamination and assessment error levels				
1	500mm	1	0.4	0.1	0	0
1	400mm	1	1	0.5	0.1	0
0.8	300mm	0.8	1	0.8	0.3	0.1
0.4	200mm	0.4	0.8	1	1	0.8
0.3	100mm	0	0.1	0.4	0.8	1
	$\mu_B(y)$	0.3	0.4	0.8	1	1
	$\mu_{B^c}(y)$	0.7	0.6	0.2	0	0

Figure 6. Fuzzy set analysis of assessment error after the identification of d-lamination from a radar survey.

The membership levels of the fuzzy subset A in X are expressed as $\mu_A(x)$.

For the given relation R between X and Y, and for a given subset A of X, it is possible to find a subset B of Y the membership of which are obtained by :

first, for each x, taking the minimum of the membership of A and the corresponding membership in R, and then taking the maximum of the resulting column of membership for each y. This will give the membership of B in Y.

As shown in Fig.5, in the example concerned,

$$B = 0.3 \ 100, 0.4 \ 200, 0.8 \ 300, 1 \ 400, 1 \ 500$$

which indicates that the actual de-lamination length can be anything from 100mm to 500mm, but most likely to be 400-500mm.

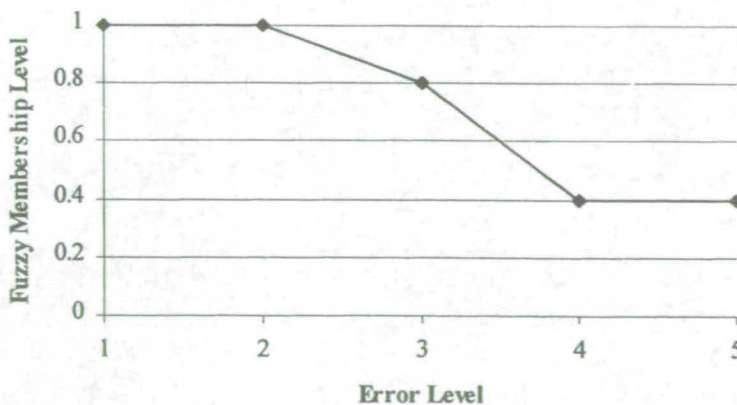


Figure 7. Error levels based on fuzzy analysis of radar investigation of a brick arch bridge with de-lamination.

The Stage 2 analysis, which is shown in Fig.6, is carried out using the same procedure. The resulting confidence levels in the assessment in respect of the different error levels are shown

in Fig.7. In this example the finding of de-lamination has meant that the already carried out assessment has now become less safe. Of course, it may be possible to carry out another assessment using analysis methods which can take into account de-lamination. In that case a different relation matrix R will be appropriate for Stage 2.

Finally, it should be noted that some features can actually indicate greater strength than assumed in an assessment, and therefore will make the assessment more conservative. In such cases, if such features could be identified using NDT, an uncertainty analysis as described here will give a measure of the conservatism in the assessment.

POTENTIAL AREAS OF APPLICATION

Masonry Arch bridges

Masonry arch bridges form a large proportion of the existing national bridge stock in the UK. Periodic structural assessment of these bridges is therefore very important for the authorities to ensure their continued safety and serviceability.

It has been observed from full scale tests and theoretical investigations that, under extreme load conditions, masonry arch bridges can fail in a manner in between the two following modes [5] :-

- (1) If the bridge is very flexible, it will fail by forming a 'mechanism', i.e. by the line of thrust moving outside the arch ring.
- (2) If the bridge is very rigid, it will fail by compressive failure of the ring material.

How close the actual failure will be to either of these modes will depend upon the interaction between a large number of factors, which can be broadly itemised as :-

- (1) Geometrical and material properties of the arch ring material
- (2) Geometrical and material properties of the surrounding fill
- (3) Lateral resistance of the fill
- (4) Rigidity of the supports
- (5) Condition and the material of the joints
- (6) General condition i.e. permanent deformation etc.

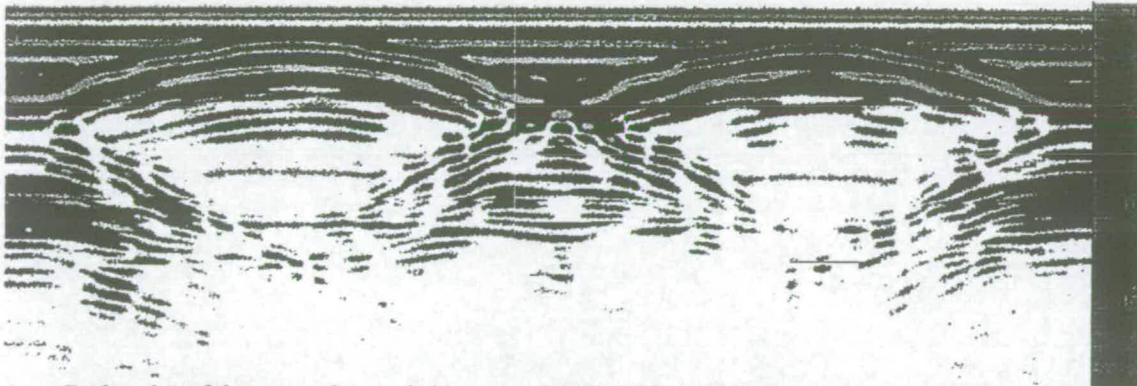
Most of these parameters cannot be determined with any certainty and should indeed be considered as 'fuzzy' parameters. The MEXE method of arch bridge assessment, described in BA 16 [6], takes into account all these factors in a series of numerical modifying factors. The modifying factors are multiplied to a 'provisional axle load' (PAL) in order to obtain the 'allowable axle load' (AAL) which corresponds to the vehicles to be permitted on the bridge. The 'provisional axle load' is determined from a nomogram, which is believed to be based on the elastic analysis of an arch ring [7]. A number of other more precise methods have been developed in recent years. However, due to the uncertainty involving the above factors, the results from these do not seem to be any better than those derived from MEXE when compared to the collapse loads from a number of full scale tests [6].

A more rational approach would be to express the MEXE AAL as a probable range of allowable

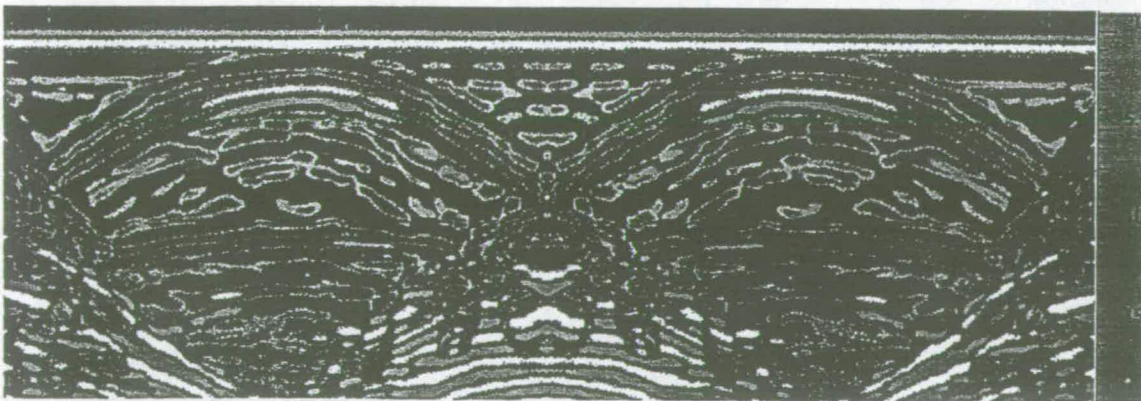
axle loads and the confidence levels for these could be determined by fuzzy set analysis as illustrated earlier in the paper, using the input MEXE 'modifying factors' as fuzzy subsets. Once the probable range of AAL is determined with its confidence levels, an appropriate 'pass', 'fail' or 'monitor' decision could be taken.

To apply such a procedure, it will be necessary to determine the confidence levels of each of the input modifying factors. For some of these factors, NDT methods can be a quick and cost effective way of obtaining qualitative information. For example, such information has been obtained during a research study carried out by Colla at Edinburgh University [8] to investigate the feasibility of using radar on a masonry bridge model to determine various parameters. Fig.8 shows two radar images of the model with and without any fill. Colla determines the fill depth above the crown as well as the presence of fill from this investigation.

Clearly such investigations can be very useful in determining the likely range of a MEXE 'modifying factor' and its confidence levels for inputting into an uncertainty analysis of the allowable axle load of a masonry arch bridge.



Radar plot of the empty 2-span bridge model (900 MHz and 20ns).



Radar plot of the sand filled 2-span bridge model (900 MHz and 20ns).

Figure 8. Radar images of a two arch bridge model [8].

Scour under flood conditions is the most frequent cause of bridge failure. It is therefore very important to assess the bridges over waterways for their potential of failure under such conditions. In such assessments, many factors in addition to their existing structural adequacy need to be considered. The Draft Advice Note BA 73 [9] recommends a risk assessment procedure, which involves determining two parameters - 'relative scour depth' D_R and 'priority factor' P_F . These parameters are based on the following factors :-

- Depth of scour
- Depth to the underside of the foundation
- Foundation type - piled or spread
- History of scour
- Foundation material
- Type of river - mountain, estuary etc.

The priority (risk) rating is then determined from a graph using D_R and P_F . Based on the priority rating (from 5 possible ratings), the suggested action can be determined.

Most of the factors listed above cannot be determined precisely, hence the whole process of risk assessment is 'fuzzy'. Uncertainty analysis will therefore be very appropriate for such risk assessment of bridges over waterways.

Some of the factors, such as the depth to the underside of foundation and foundation material are amenable for radar investigation. Indeed, Davidson et al [10] at Edinburgh University have conducted impulse radar surveys for scour at two sites to obtain such information. In addition to the radar equipment a sonar device was used to detect the river bed profile. A dingy carrying the transceivers was towed behind a small boat which contained the instrumentation. Various traverses, across and up and down the river, were then made in the vicinity of the bridge. The whole procedure was recorded on video to provide information on the position of the boat during traverses.

From these investigations it was found that the nature of the river bed affected the strength of signals returned from within the bed. At the site of a bridge crossing a river with a gravel bed only the surface of the bed was shown on the radar section, demonstrated in Fig.9. However, the texture of the bed was resolved indicating the position of rock armour around the piers. In the case of a river with a sandy bed, see Fig.10, signals from the bed itself and subsurface interfaces were received. This allowed a proposal for the history of scour formed during past floods to be put forward (Fig.11). This information allows the extent to which the hole may be opened up during subsequent flood events to be predicted and the risk of failure assessed.

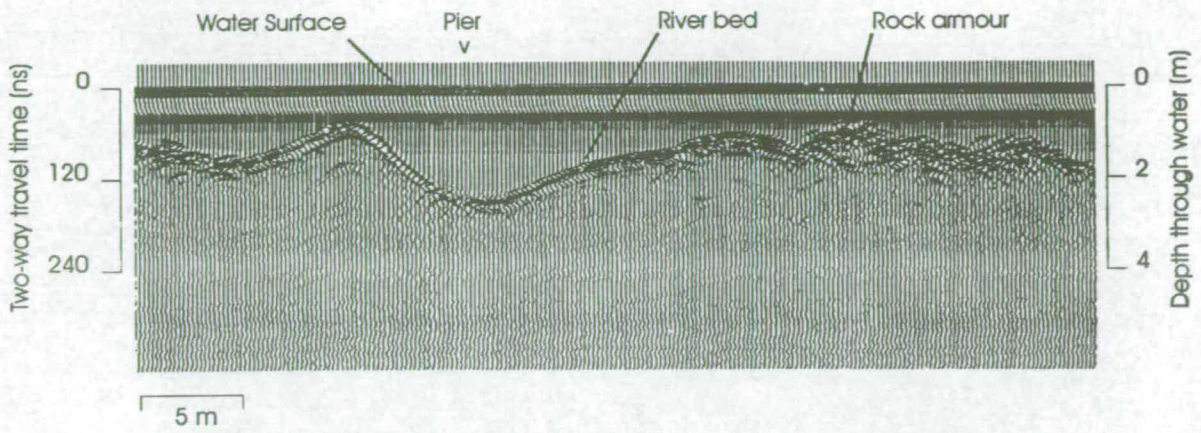


Figure 9. Radargram of river bed with gravel bed and rock armour [10].

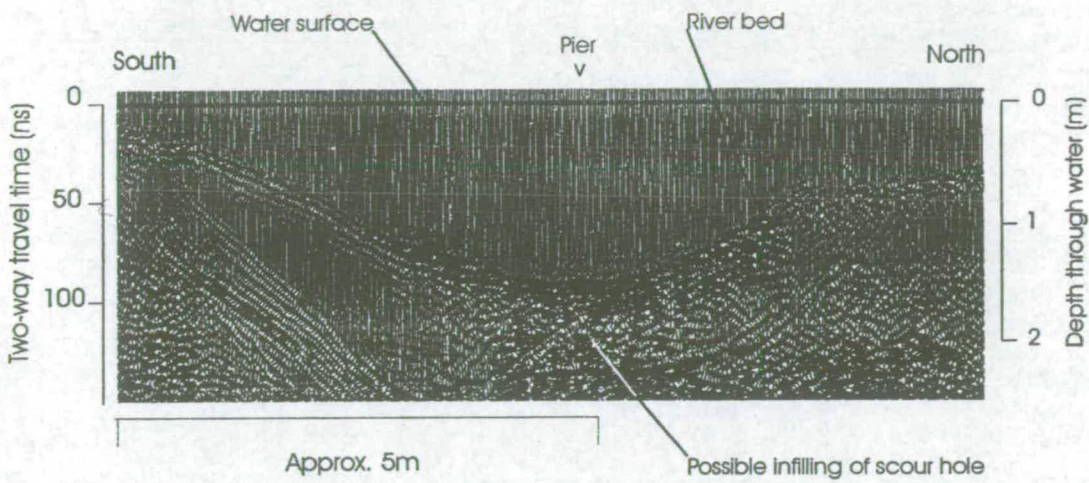


Figure 10 Radargram of sandy river bed showing penetration [10].

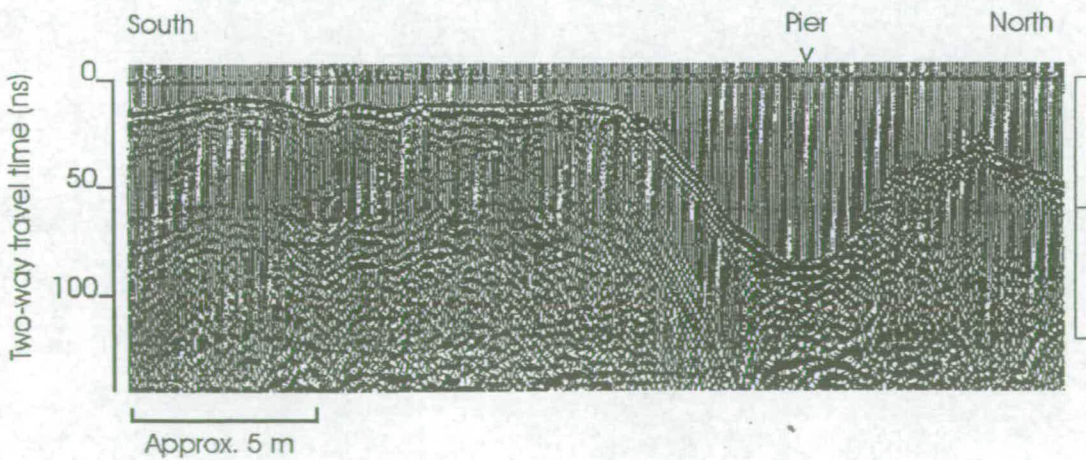


Figure 11 GPR data showing an "infilled" scour hole in a sandy riverbed [10].

The research has shown that impulse radar produces useful, accurate information when applied to the problem of bridge scour. Such information can be used as 'fuzzy set' input into an uncertainty analysis of the BA 73 recommended risk assessment of a bridge.

POST-TENSIONED CONCRETE BRIDGES

A number of post-tensioned concrete bridges have collapsed in service in the UK and abroad, and many have been found to have corrosion in the prestressing components. As a result the safety of such bridges is a subject of concern. Indeed, the construction of grouted duct bridges was banned in the UK for some time. Although, following the development of better specification and quality control procedures such bridges are now permitted to be constructed, the risk assessment of the existing bridges is likely to be an on-going process.

Advice Note BA 50 [11] recommends two stages of risk assessment, first based on the existing information, and the second following detailed inspection and testing. Lindsell [12] lists the factors to be considered in these two stages as follows :-

Initial risk assessment

- structural form
- articulation
- joints
- prestressing system
- grouting material and extent
- reinforcement
- past maintenance

Final risk assessment

- general condition - leakage, cracks
- condition at critical sections - extent of voids etc
- concrete corrosion agents
- rebar corrosion
- structural capacity.

Following a risk assessment, one or more of the following actions need to be considered :-

- Inspection
- Maintenance only
- Monitoring
- Traffic control
- Propping
- Strengthening or replacement.

Clearly such risk analysis and the subsequent choice of action are likely to be very approximate or 'fuzzy' since most of the risk factors listed above cannot be determined precisely for an

existing bridge. In such cases, uncertainty analysis based risk assessment would be more rational than choosing arbitrary numbers as precise measures of these factors. Here again, NDT methods can assist in determining some of the factors, such as the presence and extent of voids in ducts, in a quick and qualitative process. Martin et al [13 & 14] at Edinburgh University have carried out laboratory tests on grouted and voided duct samples (Fig.12) to examine the feasibility of using the 'impact echo' method to identify voids in post-tensioned concrete bridges. Some of the results are shown in Fig.13.

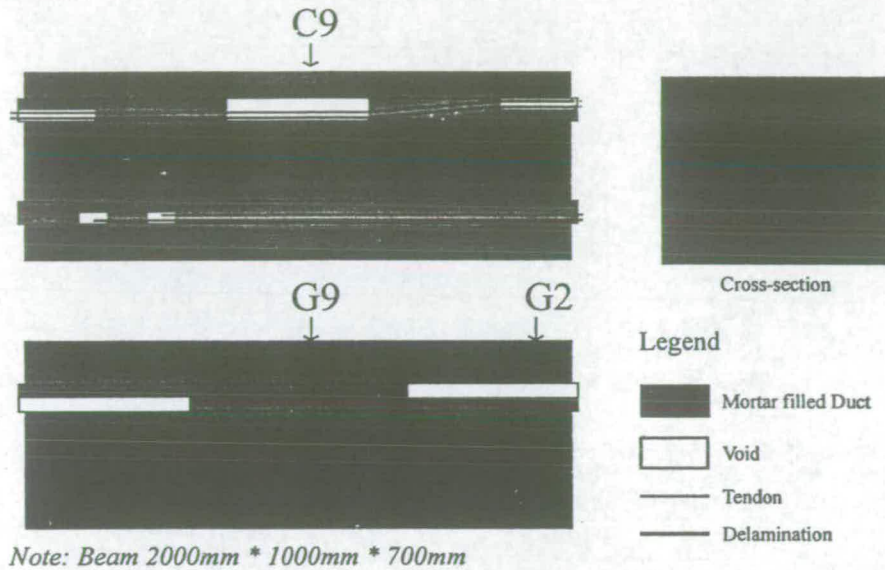


Figure 12. Post-tensioned concrete beam model [13].

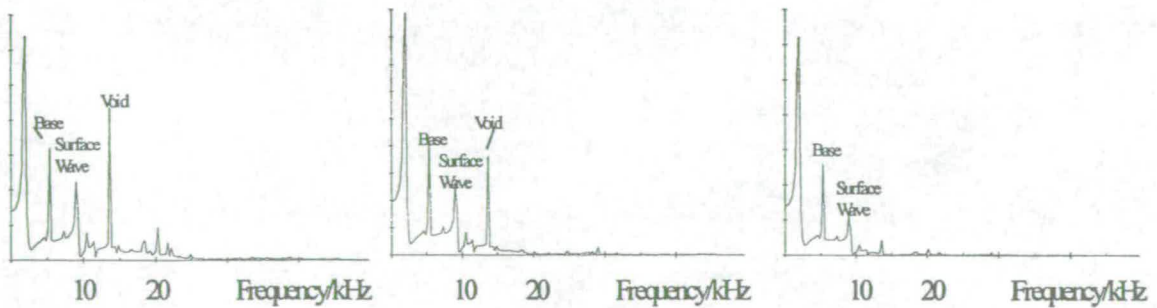


Figure 13. Comparison of results from impact echo tests on grouted and voided sections [13].

The trial investigation showed that impact echo testing can be used to detect voids in ducts in post tensioned concrete beams. The test model was simple and an actual bridge is likely to be more complex. But the tests showed that the technique could reliably produce useful, accurate information when applied to the problem of voided ducts. Such information can potentially be used as 'fuzzy set' input into an uncertainty analysis of the risk assessment of a post-tensioned concrete bridge.

CONCLUSIONS

However rigorously the bridge assessment calculations are carried out, the assessment process will always contain an element of uncertainty. This means that the assessment results cannot be taken as absolute, and hence need to be qualified by confidence levels. In addition, there are bridge types such as masonry arch bridges and bridges over waterways, where structural assessment is only a part of the risk assessment process, which itself is based on 'fuzzy' parameters. The paper demonstrates that in such cases, NDT methods have the potential for useful application in conjunction with uncertainty analysis techniques such as the fuzzy set theory and Bayesian updating.

ACKNOWLEDGEMENTS

This paper is being presented with the kind permission of the Chief Executive of the Highways Agency. The authors acknowledge the contributions of Dr C Colla, Dr NC Davidson, Prof. L. Binda and Mr KJ Broughton. The facilities of the University of Edinburgh and the financial support of the Highways Agency are gratefully acknowledged.

REFERENCES

1. Das, P.C. Background to the current bridge rehabilitation programme and future needs. *Conference: Bridge Rehabilitation in the UK*. Institution of Civil Engineers, London, 2000.
2. Olson, L.D, Sack D.A. and Fidelman D. Comparison of the performance of several impact echo transducers and application of impact echo NDT to the Lincoln Memorial in Washington D.C. *Proceedings of the 7th International Conference on Structural Faults and Repair-97*, M.C.Forde (ed). Engineering Technics Press, Edinburgh, 1997, Vol.3, 417-424.
3. Colombo S., *Applications of NDT to the investigation of masonry structures*, Dott Ing Degree Thesis at Politecnico di Milano, 1999, pp.196, 209.
4. Shigeishi, M. and Ohtsu, M. Acoustic emission generated by cyclic bending in damaged RC beam. *Proceedings of the 7th International Conference on Structural Faults and Repair-97*, M.C.Forde (ed). Engineering Technics Press, Edinburgh, 1997, Vol.2 375-382.
5. Das, P.C. An examination of masonry arch assessment methods. *Proceedings IABSE Symposium: Structural Preservation of the Architectural Heritage*. IABSE, Rome, 1993, 385-392
6. BA 16. *The assessment of highway bridges and structures. Design Manual for Roads and Bridges*. The Stationery Office, London, 1993.
7. Pippard, A.J.S. The approximate estimation of safe loads on masonry bridges. *Civil Engineers at War*. The Institution of Civil Engineers, London, 1948.
8. Colla, C. *Non destructive testing of masonry arch bridges*. Ph.D. Thesis. University of Edinburgh, 1997.
9. BA 73 (Draft). *Assessment of scour at highway bridges*. The Highways Agency, London, 2000.
10. Davidson, N.C., Forde M.C., Hardy M.S.A., McCann D.M., Colla C., Clark M., Broughton K.J., Das P.C. Field trials to establish accuracy of radar for scour detection.

- Conference proceedings: Structural Faults and Repair-97*, (Ed. M.C.Forde). Engineering Technics Press, Edinburgh, 1997, Vol.1, 171-178.
11. BA 50. *Post-tensioned concrete bridges- planning, organisation and methods for carrying out special inspections*. Design Manual for Roads and Bridges. The Stationery Office, London, 1993.
 12. Lindsell, P. and Buchner, S.H. Evaluating the risks and durability of post-tensioned concrete bridges. *Conference proceedings: Structural Faults and Repair-97*, (Ed. M.C.Forde). Engineering Technics Press, Edinburgh, 1997, Vol.1, 395-400.
 13. Martin, J., Hardy M.S.A., Usmani A.S., Forde M.C. Impact-echo assessment of post-tensioned concrete bridge beams. *Conference proceedings: Structural Faults and Repair-97*, (Ed. M.C.Forde). Engineering Technics Press, Edinburgh, 1997, Vol.1, 341-354.
 14. Martin, J, Hardy, MSA, Usmani, AS & Forde, MC, (1998) Accuracy of NDE in bridge assessment, *Engineering Structures*, Vol 20, No. 11, 979-984.

AE EXPERIMENTS ON CONCRETE BEAMS: GENERAL OVERVIEW AND RESEARCH IN PROGRESS ON BRIDGES

Ing S Colombo & Prof MC Forde
University of Edinburgh
School of Civil & Envl Eng
The Kings Buildings
Edinburgh EH9 3JN
Scotland, UK.

Prof PC Das, OBE
The Highways Agency, UK
Bridge Management Advisor
TRL
Crowthorne
UK

Jack Halliday
The Highways Agency
St Christopher House
Southwark Street
London
UK

KEYWORDS: Acoustic Emission (AE), non-destructive technique (NDT), concrete bridges.

ABSTRACT

The average age of concrete highway bridges in the UK is approximately 25-35 years and they are starting to show signs of deterioration. The investigation of these bridges is then a matter of topical concern and a third category of "monitoring" has been proposed to be added to the two "passed" or "failed" categories in order to evaluate a bridge.

This article gives a general overview on the Acoustic Emission (AE) technique: how it works, its applications, advantages and drawbacks to try to understand if, why and when this method can be used.

Several types of non-destructive techniques (NDT) can be used during the monitoring of a bridge. The choice of the right method is a key point in order to obtain successful results. A research in progress at the University of Edinburgh (sponsored by The Highways Agency) concerning the feasibility of Acoustic Emission to monitor concrete bridges is outlined.

BACKGROUND

Concrete bridges represent a large part of the UK bridge stock (Figure 1). The average age of the concrete highway bridges in the UK is of the order of 25-35 years. Concrete bridges in particular are starting to show signs of deterioration. As a consequence of this situation, the investigation of these bridges is a matter of topical concern. The WS Atkins Consultants Ltd, reported that 10% of the Highways Agency bridges failed assessment and 30% of other bridges failed as well. This gives a total amount of about 30,000 bridges, but as there are no reports of bridges failing in service, this suggests that the assessment standards are too conservative (Chubb, 2000). Particular effort has then been made to increase the accuracy of the assessment, so that the answer to whether a structure is safe or not is not a simple pass or fail (Das, 2000).

Until recently, the common strategy for bridge inspection was, for the appropriate authorities, to undertake an inspection and then evaluate if a bridge either "passed" or "failed" that inspection. A third category of "monitoring" has been proposed to be applied when a bridge passes or fails by a small margin (Colombo, Forde & Das, 2000). In this case the monitoring might be undertaken using NDT methods as they can provide qualitative information without great cost and disruption.

Research is being carried out at the University of Edinburgh, sponsored by the Highways Agency in order to understand if, between all the different types of NDT, the Acoustic Emission technique could be a valid alternative to monitor concrete bridges.

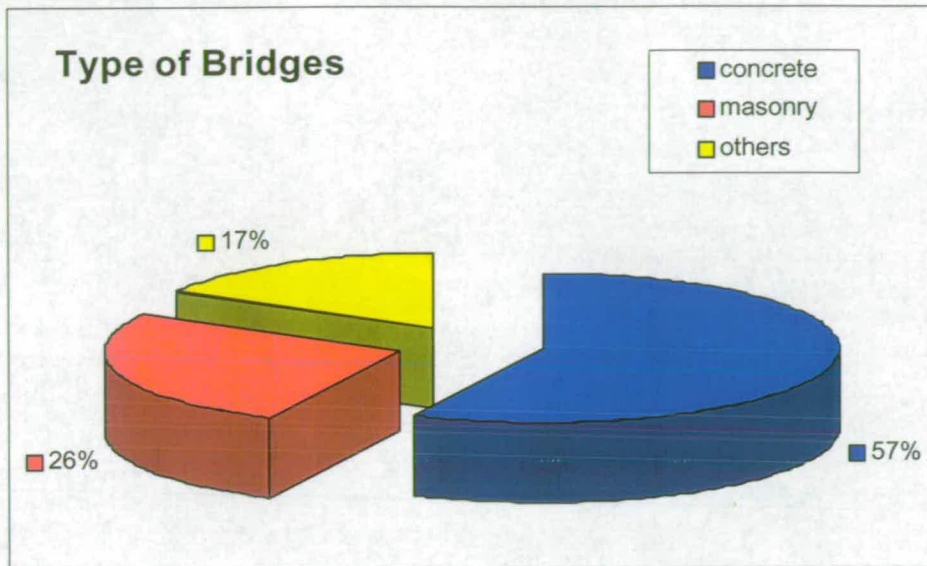


Figure 1. Type of bridges in the UK. The data includes England, Scotland and Northern Ireland.

AE TECHNIQUE

Literature Review

As with all the other non-destructive methods, the Acoustic Emission technique was not born as a “civil engineering” tool. T. F. Drouillard (Ohtsu, 1995) found that the first report on a planned acoustic emission experiment was published in 1934 by F. Kishinouya on AE on fractures in wood. Studies were carried out by Obert in 1941 and by Hodgson in 1942 (McCabe et al, 1976) using acoustic emission to predict rock bursts in mines, generated during the excavation process. They formulated the basic ideas of AE monitoring.

A key contribution was provided by Kaiser’s studies (McCabe et al, 1976) in the early 1950s on AE in metals (copper, steel, lead, zinc and aluminium). He noticed the “irreversibility” of acoustic emissions (today known as the Kaiser effect), i.e. emissions are not generated in a material until it is stressed beyond its prior stress states. Several studies have been then developed especially in areas where safety is of prime concern (i.e. nuclear energy) (McCabe et al, 1976). Acoustic Emission work also continues to be active in the study of metals structures and rocks.

The first Acoustic Emission research in concrete started in 1959 (Ohtsu, 1995; McCabe et al, 1976). In that year, Rush produced preliminary observations on noises produced by stressed concrete and the confirmation of the Kaiser effect for stresses up to 70-85% of the fracture load. In the same year, l’Hermite reported a study on the noises generated during concrete deformation, simply using a microphone and an amplifier. He found out that the noises occurred and increased in relation to a significant volumetric change in the concrete structure. Besides, a sudden increase of the Poisson’s ratio and a sharp decrease of the velocity of noise propagation accompanied a great increase of acoustic emissions (McCabe et al, 1976). Studies on AE in mortar and concrete of different sizes and aggregates were undertaken in 1965 by Robinson. They proved that the Acoustic Emission method gives information about structural changes, before the Poisson’s ratio and the propagation velocity were affected (McCabe et al, 1976). In 1970, Wells recorded acoustic emissions from concrete under strain in a range of frequency between 2 and 20 kHz. In the same year, Green undertook one of the most comprehensive studies on concrete, up to that time. Using better instrumentation he was able to record acoustic emissions on cylindrical specimens of frequency up to

100 kHz. His studies also confirmed, once again, the Kaiser effect and a source location method was used in order to localise defects (McCabe et al, 1976).

More references can be found in the bibliography published in 1986 by Thomas F. Drouillard (Drouillard, 1986). It contains a list of 76 references specifically about acoustic emission on concrete. Although not completely exhaustive, the list gives a useful compilation of the word literature published on this subject from 1959 to the date of the article.

More recently, thanks to technological improvements, researchers have examined the application of AE to civil engineering structures.

An application on high strength pre-stressed concrete girders has been carried out in the laboratory of the University of Texas, by L. O. Y. Roca (Roca, 1997). A parametric analysis, source location and moment tensor analysing was reported. The test showed clear warning signs prior to the appearance of the cracks at the surface and a good agreement with the crack pattern visible on the surface.

Another application (Yuyama et al, 1998) on different conditions of reinforced concrete beams, subjected to cyclic loading has found interesting conclusions. It suggested a criterion to measure and evaluate the degree of damage for these RC beams, based on the CBI (concrete beam integrity) ratio:

$$\text{CBI} = \text{load at onset of acoustic emission}/\text{maximum prior load}$$

so that a $\text{CBI} < 1$ indicates the presence of damage.

An analysis of AE generated by cyclic bending in damaged RC beam was undertaken and it provided helpful information about the damaging process of the material structure (Shigeishi & Otshu, 1997). AE measurements were carried out on a 60 year old RC bridge beam under a bending test to confirm the results obtained on small scale RC beam specimens (Shigeishi et al., 1999).

Principles

The Acoustic Emission technique was derived from the theory of elastic waves and by 1970 it was widespread in concrete engineering applications. This method of investigation differs from most other non-destructive method in two points. Firstly, the signal has its origin in the material itself, not in an external source. Secondly, acoustic emission detects movements, whilst most other methods detect existing geometrical discontinuities.

Acoustic emission is the term used to indicate all those phenomena in which elastic waves are generated by the release of energy from localised sources. Every rapid dislocation of mass, such as crack formation, corrosion, slips or friction, in every solid body subjected to stress is followed by the release of stored strain energy, and emits transient elastic waves which are called acoustic emissions. After having been generated, these waves propagate through the material and can be detected by AE sensors, previously mounted on the surface of the material (Figure 2). The sensors detect the waves and then turn the vibrations into an electrical signal that can be subsequently analysed and interpreted. As the source of the AE energy is the elastic stress in the material, without stress there is no emission. Therefore, an acoustic inspection is usually carried out during a controlled loading of the structure.

AE research implies then an understanding of physics, fracture mechanics and mechanical behaviour.

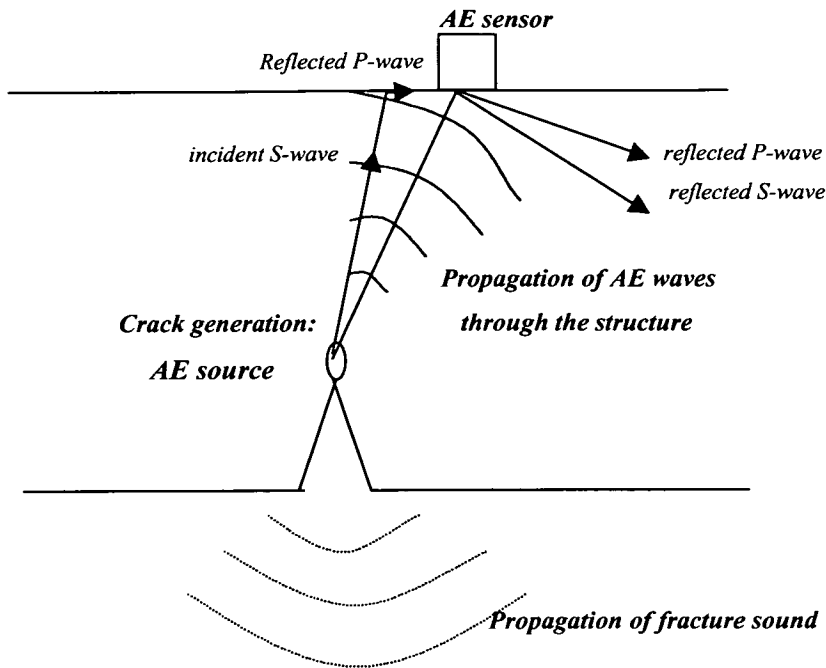


Figure 2. Acoustic Emission Principle.

WHY AE?

Why between all the different available non-destructive methods, could the Acoustic Emission technique be feasible to monitor concrete bridges? As a general rule, the type of NDT that needs to be used during a survey, should take into account several aspects, such as the aim of the survey, the type of structure and material, and the environment. The different kind of techniques do not exclude each other, but on the contrary have to be thought of as complementary in order to improve and increase the acquirable data.

The choice of the right method is a key point in order that the survey is successful.

Infrared termography can be used to detect delamination and cracks on bridges, whilst GPR was successfully used for scour detection (Forde et al, 1999) and it can be used to detect voids in post-tensioned concrete bridges. Both radar and sonic tomography can help to identify the presence of defects or anomalies inside of a structure. However, none of these methods can determine the presence of microcracks inside a structure before they become externally visible. For this reason and for the characteristics of the technique itself, the Acoustic Emission technique has been considered as a possibility.

The disadvantages of the AE technique are:

- The technique is dependent by the loading method, as if an area is unstressed it is not possible to detect acoustic emission;
- The results are dependent on the geometry of the structure and on the attenuation;
- There is not yet a standardised procedure for data interpretation;
- The technique does not allow to detect the size of the flaw.

The disadvantages of the AE technique are:

- It collects data quickly;
- It does not interfere with the flow of traffic or require closure of the bridge.
- It is not labour intensive and can be linked via telemetry to provide remote data collection.

- It provides continuous monitoring.
- It can be retrofitted to existing structures and adapted to existing topologies;
- It can predict the presence of cracks before they are visible.

RESEARCH IN PROGRESS

Research is in progress at Edinburgh University concerning the “non destructive testing and monitoring of concrete bridges using Acoustic Emission”. The main aim of the project is to obtain a better understanding of Acoustic Emission (AE) monitoring of bridges in order to provide more confidence to engineers concerned about the safety of bridges. A draft Advisory Note will be delivered on the use of Acoustic Emission testing to assess concrete bridges, based on the evaluation of generically different systems.

The project consists of:

- Small scale laboratory tests on concrete beams;
- Full scale laboratory tests on concrete beams;
- Monitoring of an existing bridge in Scotland or England.

The research will be carried out using two different acoustic emission systems: the Physical Acoustic Corporation (PAC) Mistras system and the Pure Technologies Ltd (PTL) SoundPrint[®] system (Figure 3).

SoundPrint[®] System

The SoundPrint[®] system was originally developed by Pure Technologies Ltd for the detection of the failure of unbonded tendons in car parks and buildings. The System is composed of low-cost data acquisition, computing hardware, analytical and data management software and an array of sensors that are low-cost piezo-electric accelerometers. The System measures and records the dynamic response of a structure and it transmits the data automatically to the headquarters of Pure Technologies by means of an Internet file transmission protocol (FTP) (Cullington et al, 1999). The System is currently used in Canada to monitor buildings and to detect wire breaks. In the UK it was adopted to continuously monitor the Railway Viaduct at Huntingdon. Work will be carried out using this System in collaboration with the Transport Research Laboratory (TRL).

Mistras Physical Acoustic System

The MISTRAS-2001 (Massively Instrumented Sensor Technology for Received Acoustic Signals), PAC’s (Physical Acoustic Corporation) is a DSP-32/16 new parallel processing AE architecture for (2-256) digital channels. The system performs waveform and signal measurement and stores and displays resulting data.



Figure 3. Mistras System (left), and SoundPrint[®] System (right).

Test Procedure

In terms of an AE test in the UK it does not exist a standardised procedure. However, it is possible to identify two main steps during an AE test:

1. Acquiring AE data;
2. Processing/analysing AE data.

The first step is of crucial importance if the second step is to be successful. Only by recording good quality AE data is it possible to obtain meaningful results during the processing. On the other hand, the type and data that need to be acquired depends on the kind of analysis and information that are expected. The two steps are then mutually influenced. Generally, it is possible to identify the following factors that need to be taken into considerations:

- Choice of the right sensor - it is affected by the signal attenuation, the structure material and geometry, the sensitivity and the frequency range. Working with small samples or small scale it implies working with a wider range of frequencies, whilst for larger structures the range of frequency is reduced (Figure 4);
- Location of the sensors- the distance and the position of the sensors have to be chosen taking into account the attenuation of the signal through the structure and the area that is needed to be monitored;
- Environment.

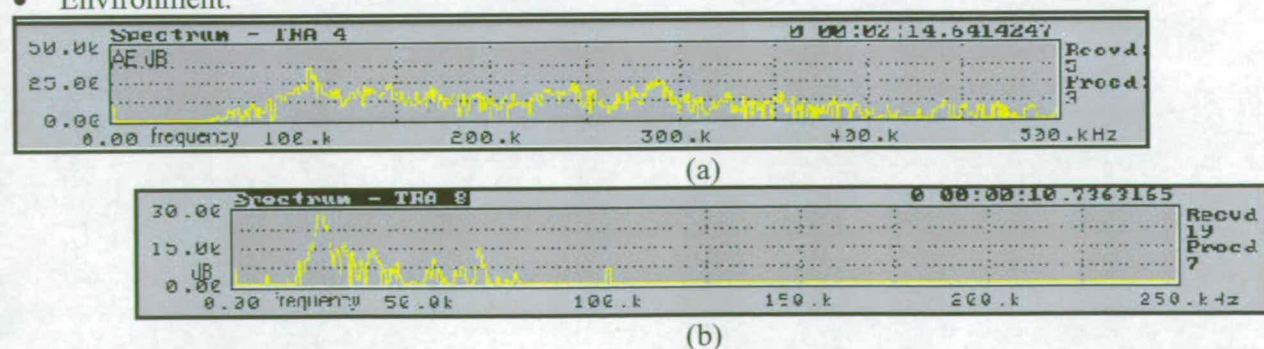


Figure 4. Frequency spectrum of a signal recorded during a compression test on the concrete cube (a) and of a signal acquired on a concrete beam of the Boghall Bridge (b) (Shigeishi et al, 2000).

With reference to the PAC system, the AE signals can be analysed in an analog way or in a digital way. The analog analysis consists of a parametric test, whilst the digital one of a moment tensor analysis. The parametric test analysis allows the determination of several AE parameters (i.e.: amplitude, duration, AE counts, arrival time...), which are correlated with the fracture process. Examples can be seen in Figure 5. The two charts represents the events and energy location of the data recorded on a masonry arch/RC beam Scottish Bridge (Shigeishi et al., 2000). The area with the highest AE activity can be easily localised.

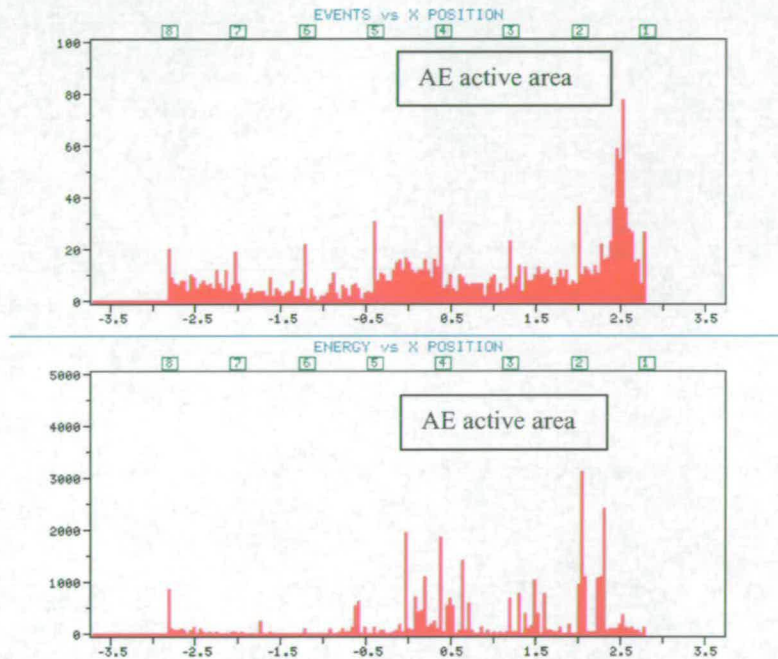
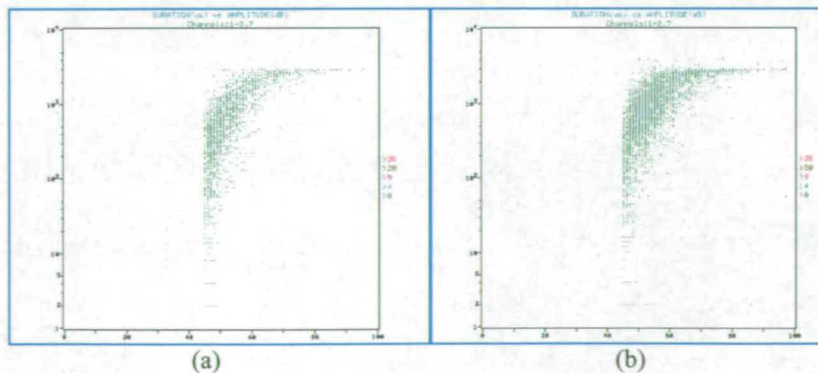


Figure 5. Events and energy location of AE data collected on the concrete beam of a Scottish bridge (Shigeishi et al., 2000).

Figure 6 shows an example of a different type of chart: duration of the signal vs amplitude. The data refers to a test carried out at TRL on a hinge beam. The charts refer to 4 cycles of loading: from 0 to 40kN, from 0 to 80kN, from 0 to 120kN and from 0 up to failure. It is possible to see the presence of truncated hits, which increases with the load and deterioration of the beam giving an indication of the state of the beam.



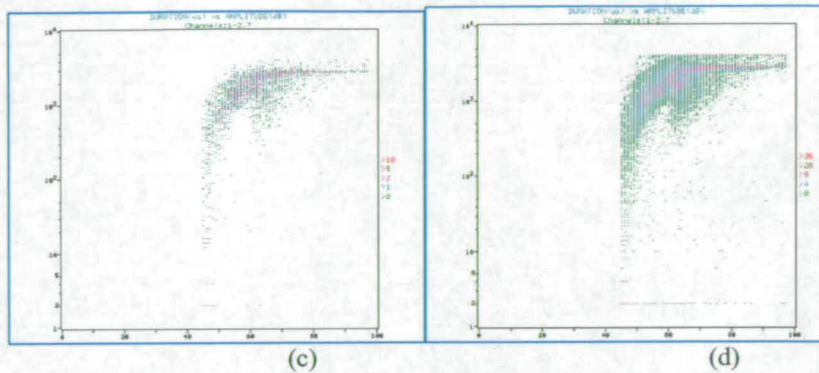


Figure 6. Duration vs Amplitude charts of the hinge beam tested at TRL, during 4 different cycles of loading: 0→40kN (a); 0→80kN (b); 0→120kN (c); 0→failure (d).

The waveform analysis is about looking at the shape of the waves, at the frequency response and to apply the Moment Tensor Analysis. The latter is a technique developed by M. Ohtsu and based on the measurement of P waves amplitudes and it can provide quantitative three-dimensional information on the cracks location, type and orientation.

The parametric analysis appears to be quick and cost-effective to monitor structure, whilst the wave analysis is more time consuming. On the other hand the latter can provide more detailed information. The parametric analysis could then be used in the first instance to pinpoint the critical areas of a structure. On these areas, subsequently a waveform analysis could be performed.

CONCLUSION

The investigation of concrete bridges in the UK is a matter of topical concern. The use and development of new methods capable of providing useful information and monitoring concrete bridges is needed. Amongst the non-destructive methods, the AE technique appears to have good potential in order to monitor concrete bridges. Research is in progress at the University of Edinburgh to obtain a better understanding of AE testing and to develop a standardised procedure for its applicability to concrete bridges.

ACKNOWLEDGEMENTS

The authors gratefully acknowledge the facilities of the University of Edinburgh and the sponsorship of the Highways Agency under contract No.3/320. Collaboration with the Transport Research Laboratory, Crowthorne; Physical Acoustic Ltd and Pure Tecnologies Ltd are also acknowledged. Thanks are due to Professor M Shigeishi, Kumamoto University, Kevin Broughton & Dr. A. Giannopoulos, University of Edinburgh and Dr D Cullington & Mike Hill, TRL for their help, advice and support.

REFERENCES

- Chubb M.S. (2000), "The bridge assessment and strengthening programme: the maintaining agent's views", *ICE 2000 Conf. "Bridge Rehabilitation in the UK: review of the current programme and preparing for the next"*. 2-3 Oct. 2000 at the Institution of Civ. Eng., London,UK
- Colombo S., Forde M.C., Das P.C. (2000), "Improving Impact Echo and Radar NDT data interpretation using uncertainty analysis technique", *ICE 2000 Conf. "Bridge Rehabilitation in the UK: review of the current programme and preparing for the next"*. 2-3 Oct. 2000 at the Institution of Civ. Eng., London,UK

- Cullington D.W., MacNeil D., Paulson P., Elliot J., (1999), "Continuous Acoustic Monitoring of Grouted Post-tensioned Concrete Bridges", *Proc. 8th International Structural Faults and Repair Conference*, London, 13th July.
- Das P.C. (2000), "Background to the current bridge rehabilitation programme and future needs-estimating uncertainty in bridge assessments", *ICE 2000 Conf. "Bridge Rehabilitation in the UK: review of the current programme and preparing for the next"*. 2-3 Oct. 2000 at the Institution of Civ. Eng., London, UK.
- Drouillard T.F. (1986). "AE Literature- Concrete", *J. Acoustic Emission*, Vol.5, No.2, pp. 103-109.
- Forde, MC, McCann, DM, Clark, MR, Broughton, KJ, Fenning, PJ & Brown, A (1999) Radar measurement of bridge scour, *NDT&E International*, Vol 32, No 8, 481-492.
- McCabe W.M., Koerner R.M., Load A.E. Jr, (1976). "Acoustic Emission behaviour of concrete Laboratory Specimens", *ACI Journal*, Vol.13, pp.367-71.
- Ohtsu M. (1995). "The history and the development of acoustic emission in concrete engineering", *The concrete Library of the Japan society for Civil Engineers*, No.25, pp.121-134.
- Roca L.O.V., (1997). "Acoustic emission examination of high strength prestressed concrete girders", Thesis presented at Faculty of the Graduated School of the University of Texas as Austin, pp. 1-96.
- Shigeishi M., Colombo S., Broughton, K.J., Rutledge, H., Batchelor A.J., Forde M.C., (2000), "Acoustic Emission to assess and monitor the integrity of bridges", *Construction and Building Materials*, Vol.15, pp.35-49.
- Shigeishi M., Masaki Y., Jo H., Fujimoto S., Makizumi T., Matsushita H. (1999). "Acoustic emission on a 60 years old bridge beam under bending test", *Proc. of the Int. Conf. on the Current and the future trends in bridge design construction and aesthetics*, 4-5 October 1999 Singapore.
- Shigeishi M., Ohtsu M., (1997) "Acoustic Emission generated by cyclic bending in damaged RC beam", *Proc. Of the Int. Conf. On Structural Faults and Repair*, M.C.Forde(ed.), Engineering Technics Press, Edinburgh 1997.
- Yuyama S., Okamoto T., Shigeishi M., Ohtsu M., Kishi T. (1998). "A proposed standard for evaluating structural integrity of reinforced concrete beams by acoustic emission", *Acoustic Emission: Standards and Technology Update*, ASTM STP 1353, S.J. Vahavilos, Ed., American Society for Testing and Materials, pp.1-12.

ACOUSTIC EMISSION ON BRIDGES: EXPERIMENTS ON CONCRETE BEAMS

*S. Colombo &
I.G.Main & M.C.Forde*
University of Edinburgh
The King's Buildings
Edinburgh EH9 3JN
Scotland, UK

Jack Halliday
The Highways Agency
St. Christopher House
Southwark Street
London SE1 0TE
UK

KEYWORDS: Acoustic Emission (AE), concrete bridges, AE parameter, *b*-value.

ABSTRACT

Bridges in the UK represent a huge legacy and concrete bridges are the majority of this estate. As the average age of these bridges is of the order of 25-35 years, they are starting to show signs of deterioration. Therefore there is a need to monitor and verify their performance and safety for ongoing usage.

The questions that will be addressed are: could the Acoustic Emission technique be a possible and effective way of monitoring and evaluating the safety of concrete bridges; and if so, how would it be used and applied? The Highways Agency (London, UK) has sponsored a research project, currently in progress at the University of Edinburgh, to verify the feasibility of the AE method.

This paper concerns the first stage of that project and it describes the experiments undertaken in the laboratory on concrete beams. Some key points are drawn and discussed about the different features that influence an AE test and about the procedure to carry it out.

The data recorded during the tests are presented. A parametric analysis was undertaken in order to process the data. The relationships between some of the AE parameters and the structural behaviour and cracking of the beams are discussed. A comparison of the AE activity and AE energy showed that the energy appears to be the most effective parameter to identify structural damage. A *b*-value analysis is also presented; the *b*-value was compared with the applied load and with the cracks appearing on the beam. The results showed a good agreement with the development of the fracture process of the concrete.

INTRODUCTION

Concrete bridges represent the majority of the UK motorways and trunk roads stock bridges. As their age is of the order of 25-35 years they are starting to show signs of deterioration. This compares with the US bridges stock, which is around 40 years old. Consequently, the necessity to monitor and verify their performance and safety is a matter of urgent concern. When faced with the choice of “pass” or “fail” for a bridge, the Bridge Engineer knows that the “fail” option implies one of the following consequences: closure, weight restriction or lane closure. All the above options are undesirable for the bridge owner. Thus a third option of “monitoring” would be highly desirable. The Acoustic Emission (AE) technique has been proposed [1] as a valid method for monitoring these bridges. However more study is needed to develop a standard procedure for undertaking an AE investigation as well as to find out alternative methods of processing and interpreting the obtained data.

As a first stage in this direction, some experiments on reinforced concrete (RC) beams have been undertaken and some key points on the factors that influenced, and have to take into account during, an AE investigation are discussed. Two types of monitoring are possible: a “global” monitoring which is intended to yield general information on the state of the whole structure and “local” monitoring which yields a more detailed understanding of a certain area of the bridge. Two parametric ways of data processing, representative of the two monitoring methods, are shown in the paper: location of the AE activity as a way of “global” monitoring and a *b*-value analysis as a mean for “local” monitoring of the structure.

AE PROCEDURE

In the UK there is no standardised procedure for the AE method applied to civil engineering structures. However, acquiring meaningful data during a test it is of crucial importance in order to obtain useful results [2]. Generally, it is possible to identify some key factors that need to be taken into consideration:

- Choice of sensor – it is affected by the signal attenuation, the structure material and geometry, the sensitivity and the frequency range;
- Sensor locations – the distance apart and position of the sensors depends on the structure itself and the aim of the study (“local” or “global” monitoring). For concrete a maximum interspacing of 2 metres is usually reasonable. The choice of the right couplant is fundamental: while Cyanoacrylate adhesive glue can be very good for permanent monitoring, other solutions have to be found when the sensors need to be removed. Plasticine proved to be a good option. The use of clamps to hold the sensors in place is also advisable;
- Sensor calibration – the sensors need to be calibrated at the beginning and at the end of the test. The Schmidt Hammer is a quick and easy way to verify that all the transducers are working, whilst a pencil lead break [3] near to each sensor provides confidence on the sensitivity of the transducers.
- Condition of the structure – the presence of pre-existing crack or damage can affect the signal and its propagation and therefore has to be taken into account;
- Environment – less influencing when working in a lab, it becomes important when monitoring on-site. Factors such as wind and rain can heavily affect the recording and have to be considered when setting the threshold. In lab environment a threshold between 30-35dB is generally acceptable for concrete.

A summary of all the main factors can be seen in the sketch of Figure 1.

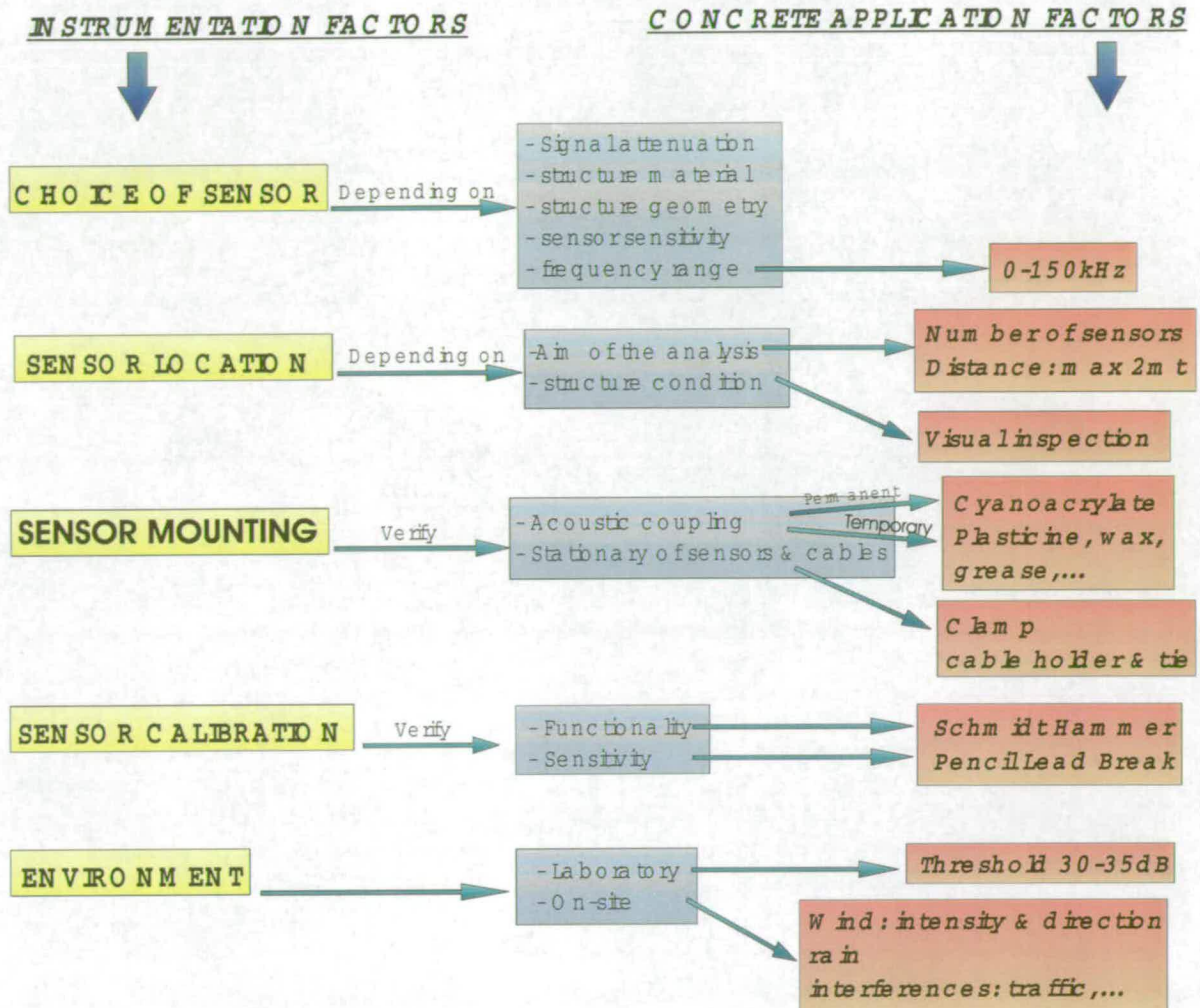


Figure 1. Sketch of the main factors influencing an AE test.

EXPERIMENT

The data refer to a test carried out on a RC beam in the Structures Laboratory of the University of Edinburgh. The beam (named beam BF2) was designed to represent the behaviour of a beam belonging to a real bridge. The experiment consisted of a four points load test of a simply supported beam. The load was applied in 10kN steps. During the test the beam was monitored using a Physical Acoustic (PAC) Mistras system. Eight PAC R61 sensors were mounted on the beam and set at a threshold of 35dB. The details of the beam and the sensor location can be seen in Figure 2.

During the test it was possible to identify different stages of cracking:

- cycle 01: no cracks;
- cycle 02 to cycle 05: cracks forming and the appearance of tensile cracks along the whole span of the beam;
- cycle 06: appearance of shear cracks at the two ends of the beam;
- after cycle 06: no new cracks growing; the old cracks opened up.

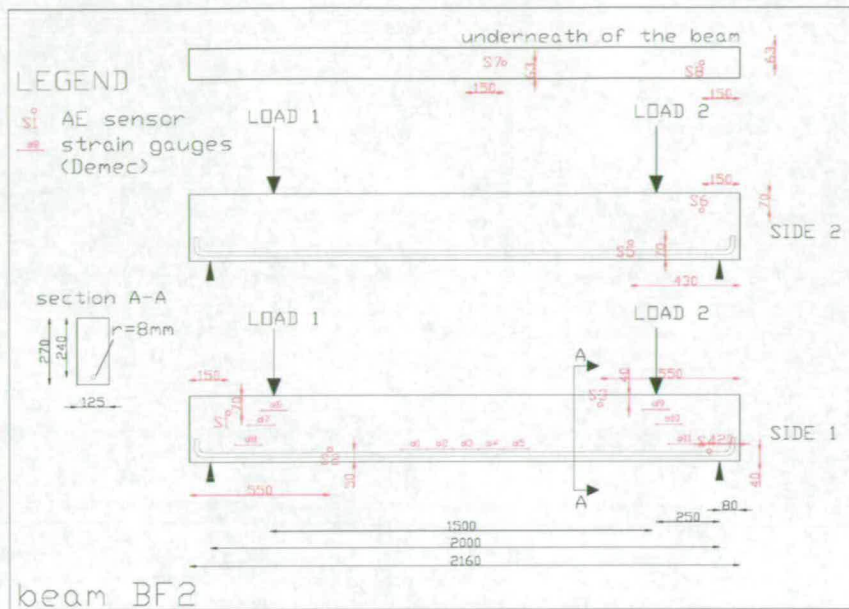


Figure 2. Designing details – Load configuration and AE sensors location on the beam. AE sensors are labelled S1-S8

AE ANALYSIS AND PROCESSING

Different types of damage and cracks generate different types of AE signals. These differences can be related to the degrees of damage of the structure and can be associated to different parameters of the AE data. The analysis presented in this paper focuses on some of these parameters and their interpretation.

AE LOCATION

The analysis of the AE location consists in locating the AE sources. These sources can then be compared with the crack pattern on the beam to see if there is any agreement.

A linear location (alongside the beam) was carried out using the Mistras software. The sources were located with reference both to the recorded events and energy and the results for two of the loading cycles are shown in Figure 3, where the black thick lines represent the cracks as they appeared on the specific cycle. The energy is calculated as the area under the envelope of the AE signal. A good relationship can be seen between the AE events and the cracks but it should be noted that the correlation with the cracks is stronger in terms of energy than events. This might be due to the fact that events generated by reflections, noise or interference can still be located but the energy associated with them is irrelevant. On the other hand, structurally meaningful events are characterised by a relevant amount of energy. The energy can be then considered as an effective parameter to indicate the damage of a structure.

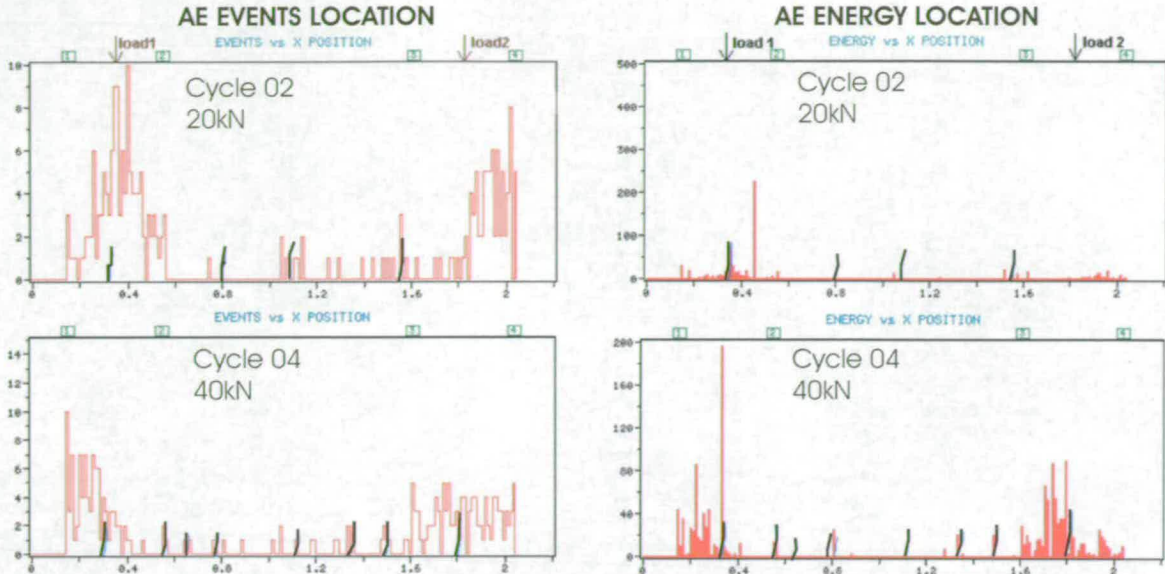


Figure 3. AE events and AE energy location during cycles 02 and 04.

B-VALUE ANALYSIS

In earthquake seismology events of larger magnitude occur less frequently than events of smaller magnitude. This fact can be quantified in terms of a magnitude-frequency relationship, for which Gutenberg and Richter proposed the empirical formula:

$$\log_{10} N = a - bM_L \quad (1)$$

where M_L is the Richter magnitude of the events, N is the incremental frequency (i.e. the number of events with magnitudes in the range of $M_L \pm \Delta M$), and a and b are empirical constants [4]. The Richter magnitude M_L is proportional to the logarithm of the maximum amplitude A_{max} recorded in a seismic trace, corrected for the attenuation in amplitude with distance due to wave propagation and inelastic absorption.

The same principle can be applied to the AE method to study the scaling of the "amplitude distribution" of the acoustic emission waves generated during the cracking process in the laboratory or in engineering structures. From the relationship (1), the b -value is the negative gradient of the log-linear AE frequency/magnitude plot and hence it represents the slope of the amplitude distribution. The b -value changes systematically with the different stages of fracture growth [5], so it could be used to estimate the development of fracture process. In terms of AE technique, the Gutenberg-Richter formula can be modified as:

$$\log_{10} N = a - b' A_{dB} \quad (2)$$

where now A_{dB} is the peak-amplitude of the AE events in decibels:

$$A_{dB} = 10 \log_{10} A_{max}^2 = 20 \log_{10} A_{max} \quad (3)$$

The b -value obtained with this relationship should be then multiplied by a factor of 20 to be comparable with the one used in seismology [6-7].

In general terms, when the distributed microcracks are occurring in the early stages of damage, the b -value is high and when the macrocracks begin to localise the b -value is low.

In the analysis presented in this paper, a conventional b -value analysis was applied on the data recorded on the RC beam, using the relationship (2) and assuming:

$$b = b' * 20.$$

The trend of the b -value was then compared with the development of the fracture process of the beam observed during the test.

The b -value was calculated using the least squares method for groups of 100 events during each loading cycle; the trend of the b -value was then plotted for each cycle and for each channel. The pattern was clearer in the early cycles when the cracks were forming as the presence of a large number of concentrated microcracks creates a clear pattern. However once the external macrocracks are formed (the beam is failing) the AE sources are fewer and more scattered so the pattern is less clear. This might imply that the analysis of the b -value is meaningful on good structures as it provides information between the microcracking beginning up to the stage where macro fractures occur by localisation.

The trend of the b -value for channels 3 and 7 during the second cycle of the test are shown in Figure 4; the load over time is shown on the same graph (dotted line). As the two sensors were located respectively on the end and on the middle area of the beam they can be considered to give a whole representation of the full beam. In both cases, the pattern shows a clear decrease at the beginning (the dashed line in the chart) when the load is going up, and then a transient during the relaxation when the load is held constant.

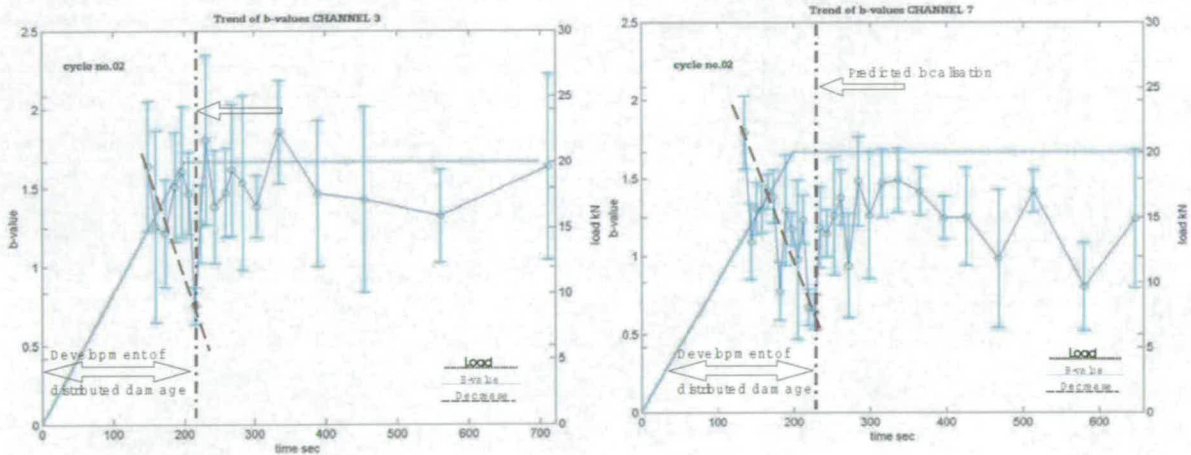


Figure 4. Trend of b -value over time for channel 3 (left) and 7 (right) during the load cycle number 2; the load is shown on the vertical axis on the right.

In a post-failure phase, the minimum and maximum value of the b -value was considered, for each cycle and for each channel. The trend of the range during the whole cycle and for each channel was then plotted. The minimum b -value trend suggests macrocracks have formed, whilst the maximum b -value trend implies microcrack growth. The chart of the trend for channel 3 and channel 7 during the whole experiment is shown in Figures 5.

The results for channel 3 (located near to the end of the beam) show that the maximum trend is increasing from cycle number 2 to 3, implying that microcracks are forming. A peak appears in cycle number 9 when all the cracks that formed in cycle number 2 are visibly opening up. The minimum trend is decreasing in the early stages, reaching a minimum in cycle number 4. When all the macrocracks had appeared on the beam, then from this point onwards the minimum trend is constant. The b -value evolution is in good agreement with the damage observed independently on the beam.

The results for channel 7 (located in the middle of the beam) show that the maximum trend decreases at the beginning, implying that microcracks are forming, but it then remains

constant as the cracks are uniformly spread. The peak at the end is unclear now, as this channel is too far from the shear cracks that are opening to be affected strongly by them. The minimum trend is decreasing in the first cycle and it stabilises afterwards when all the macrocracks had appeared on the beam.

In both cases, three stages of the fracture process can be identified. A first stage where the microcracks are dominant and the macrocracks are starting to appear. A second phase of constant range when the macrocracks are constant and uniformly distributed all along the beam. After this stage the cracks do not grow towards the top part of the beam (as the concrete is in compression) so a last stage can be identified when the macrocracks are opening up as the beam is failing.

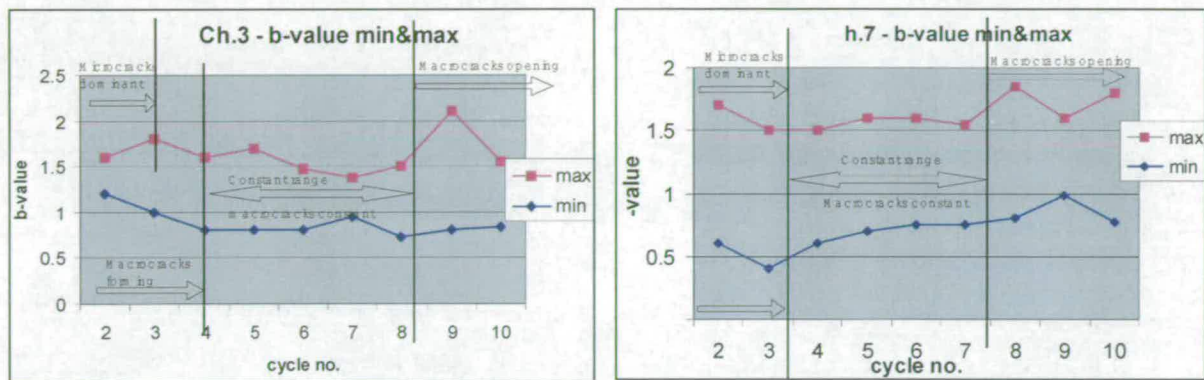


Figure 5. Trend of maximum & minimum b -value for channel 3 (left) and 7 (right) during the whole experiment.

CONCLUSIONS

The paper presents the results from a laboratory experiment on a RC beam. The beam was loaded in cycles and the acoustic emissions were recorded during the test.

- Some key points were drawn about the procedure to carry out an AE test.
- From a location of the AE sources, the AE energy appeared to be the most effective parameter to indicate the damage in a structure.
- A good relationship was found between the trend of the b -value and the microcracking and macrocracking observed during the test.
- The results confirmed that the b -value is correlated to the fracture process of the concrete and to the degree of localisation of damage.
- The minimum b -value trend suggests macrocracks have formed, whilst the maximum b -value trend implies microcrack growth.
- This study suggests that a b -value analysis could be used to interpret data obtained by a “local monitoring” of concrete bridges, although further work is needed in order to consolidate the results that were found and to make the b -value suitable for practical use.

ACKNOWLEDGEMENTS

The authors acknowledge the facilities of the University of Edinburgh and the financial support for this work of the Highways Agency (London), contract no. 3/320. Thanks are also due to the technical and support staff of the University for their help.

REFERENCES

1. Yuyama S., Okamoto T., Shigeishi M., Ohtsu M., Kishi T. (1998). "A proposed standard for evaluating structural integrity of reinforced concrete beams by acoustic emission", Acoustic Emission: Standards and Technology Update, ASTM STP 1353, S.J. Vahavilos, Ed., American Society for Testing and Materials, pp.1-12.
2. Colombo S., Forde M.C., Das P.C., Halliday J., (2001) "AE experiments on concrete beams: general overview and research in progress on bridges", Proceedings of the Structural Faults and Repair 2001, CD-ROM, 4-6 July 2001, London, ISBN 0947644474.
3. BS EN 1330-9:2000, "Non destructive testing – Terminology".
4. Shearer P.M.(1999), Introduction to Seismology. Cambridge University Press.,p189.ISBN 0 521 669537.
5. Sammonds P.R., Meredith P.G., Murrell S.A.F., Main I.G., (1994)"Modelling the damage evolution in rock containing pore fluid by acoustic emission", Eurock '94, Balkema, Rotterdam. ISBN 90 5410 502 X.
6. Shiotani T., Yuyama S., Li Z.W., Ohtsu M. (2000), "Quantitative evaluation of fracture process in concrete by the use of improved b-value". 5th Int. Symposium Non- Destructive Testing in Civil Eng, Ed. T. Uohoto, Amsterdam, Elsevier Science, 2000:293-302, ISBN 0080437176.
7. Shiotani T., Ohtsu M., Ikeda K. (2001), "Detection and evaluation of AE waves due to rock deformation". Construction and Building Material, Elsevier Science, Vol 15, No 5-6 2001:235-246.

ACOUSTIC EMISSION APPLICATION TO MASONRY STRUCTURE

Mitsuhiro Shigeishi

Kumamoto University, Japan

Sabrina Colombo & Michael C. Forde

University of Edinburgh, Scotland, United Kingdom

Keywords: acoustic emission, attenuation, bending, brickwork, cracking, fracture, frequency, in-situ monitoring, shear, stone masonry arch

Extended Abstract

In Europe, there are huge of masonry structures, built of brick or stone that represent great legacies but also significant problems for the countries. Most of them are at least a century old and they were built to carry traffic over railways, canals and rivers, which were very different from modern transport. The years have brought them to a new condition in which they have to support loads mostly greater and decidedly severer than those capacities. Consequently, there is now the necessity to control and verify their performance and safety, as well as intervene with strengthening works to avoid collapse

This paper reports basic consideration on applying of acoustic emission technique (AET) to masonry structure. To examine the characteristics of AE in masonry, brickwork test-pieces likened to the masonry structure were used in the first study. The frequency component and attenuating of the elastic wave that propagates the inside of brickwork were examined.

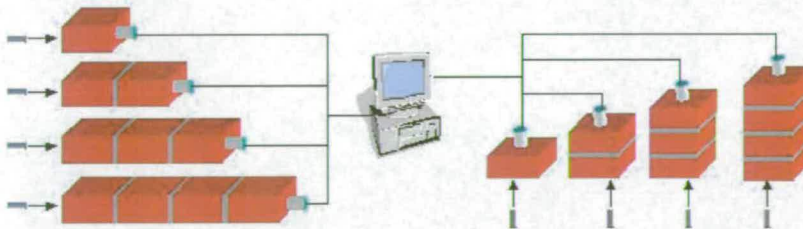


Figure 1. Experimental set-up for the detection of shock wave through brickwork

By the elastic collision between an aluminum small flying body and brick test-piece, the shock wave in bandwidth up to 200kHz can be inserted into the specimen. From the Fast Fourier Transformation results of the waveforms detected at other side by a calibrated seismic sensor, it is confirmed that the wave components in upper range were dumped and the significant frequency band for waveform analysis in brickwork was up to 100kHz. It was also confirmed that elastic wave in the band below 100kHz did not receive the attenuation by the existence of the joints.

To examine the possibility of the practical application of AET, AE from the specimens were observed while the brick structures were loaded. The difference between the cracking pattern could not be recognised, even if the loading arrangement was different. However, the result of AE source location clearly showed the difference in distribution of the AE sources.

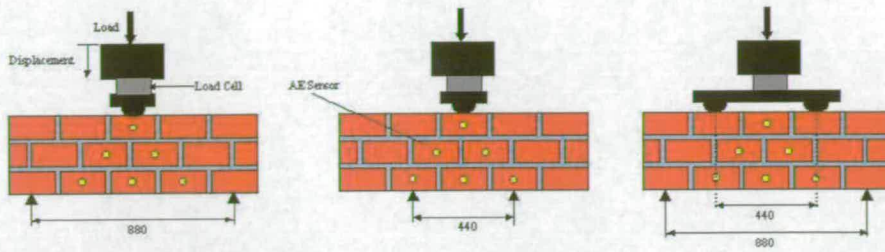


Figure 2. Load arrangements for bending (left), bending shear (middle) and four points bending (right)

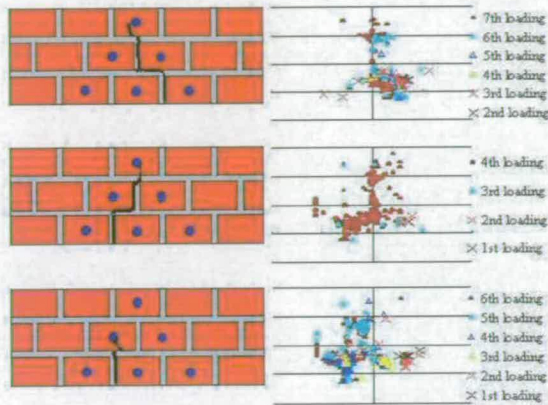


Figure 3. Cracking and AE source locations in case of the three point bending (top), the bending shear (middle) and the four points bending (bottom)

In the second, the possibility of Acoustic Emission (AE) method for application to the non-destructive inspection technique of masonry arch bridges was examined. Having become the object of AE measurement was the in-service masonry arch bridge combined with a reinforced concrete (RC) bridge in Scottish Borders, Scotland, United Kingdom.

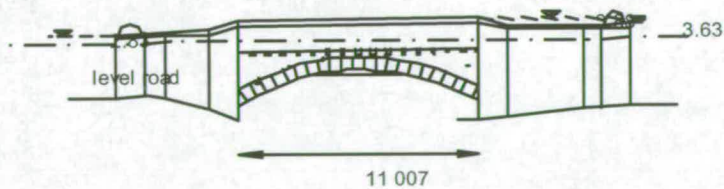


Figure 2. Elevation view of the Boghall Bridge.

Using 8-channels AE analyser, the measurements were carried out separately for some parts of the bridge under the usual traffic. Because it was a traffic situation made quiet, the generation behaviour of AE was small. However, when a large-scale vehicle passed, AE generation was observed. The AE generation behaviour in the part of concrete beam was clearly observed. The number of AE generated in the concrete beam largely exceeded the number of AE observed at the same time in the masonry arch rib. It could be suggest that this shows the displacement behaviour with different these two bridges relatively.

The results of linear AE source location applied to AE data on a RC beam shows that the distributions of AE sources agree with the area have been damaged. Radar investigation was also performed for the part of abutment and detected the faults nearby the areas of high AE activities observed.

ACOUSTIC EMISSION ON BRIDGES: EXPERIMENTS ON CONCRETE BEAMS

***S. Colombo &
I.G. Main & M.C. Forde***
University of Edinburgh
The King's Buildings
Edinburgh EH9 3JN
Scotland, UK

Jack Halliday
The Highways Agency
St. Christopher House
Southwark Street
London SE1 0TE
UK

KEYWORDS: Acoustic Emission (AE), concrete bridges, AE parameter, *b*-value.

ABSTRACT

Bridges in the UK represent a huge legacy and concrete bridges are the majority of this estate. As the average age of these bridges is of the order of 25-35 years, they are starting to show signs of deterioration. Therefore there is a need to monitor and verify their performance and safety for ongoing usage.

The questions that will be addressed are: could the Acoustic Emission technique be a possible and effective way of monitoring and evaluating the safety of concrete bridges; and if so, how would it be used and applied? The Highways Agency (London, UK) has sponsored a research project, currently in progress at the University of Edinburgh, to verify the feasibility of the AE method.

This paper concerns the first stage of that project and it describes the experiments undertaken in the laboratory on concrete beams. Some key points are drawn and discussed about the different features that influence an AE test and about the procedure to carry it out.

The data recorded during the tests are presented. A parametric analysis was undertaken in order to process the data. The relationships between some of the AE parameters and the structural behaviour and cracking of the beams are discussed. A comparison of the AE activity and AE energy showed that the energy appears to be the most effective parameter to identify structural damage. A *b*-value analysis is also presented; the *b*-value was compared with the applied load and with the cracks appearing on the beam. The results showed a good agreement with the development of the fracture process of the concrete.

INTRODUCTION

Concrete bridges represent the majority of the UK motorways and trunk roads stock bridges. As their age is of the order of 25-35 years they are starting to show signs of deterioration. This compares with the US bridges stock, which is around 40 years old. Consequently, the necessity to monitor and verify their performance and safety is a matter of urgent concern. When faced with the choice of “pass” or “fail” for a bridge, the Bridge Engineer knows that the “fail” option implies one of the following consequences: closure, weight restriction or lane closure. All the above options are undesirable for the bridge owner. Thus a third option of “monitoring” would be highly desirable. The Acoustic Emission (AE) technique has been proposed [1] as a valid method for monitoring these bridges. However more study is needed to develop a standard procedure for undertaking an AE investigation as well as to find out alternative methods of processing and interpreting the obtained data.

As a first stage in this direction, some experiments on reinforced concrete (RC) beams have been undertaken and some key points on the factors that influenced, and have to take into account during, an AE investigation are discussed. Two types of monitoring are possible: a “global” monitoring which is intended to yield general information on the state of the whole structure and “local” monitoring which yields a more detailed understanding of a certain area of the bridge. Two parametric ways of data processing, representative of the two monitoring methods, are shown in the paper: location of the AE activity as a way of “global” monitoring and a *b*-value analysis as a mean for “local” monitoring of the structure.

AE PROCEDURE

In the UK there is no standardised procedure for the AE method applied to civil engineering structures. However, acquiring meaningful data during a test it is of crucial importance in order to obtain useful results [2]. Generally, it is possible to identify some key factors that need to be taken into consideration:

- Choice of sensor – it is affected by the signal attenuation, the structure material and geometry, the sensitivity and the frequency range;
- Sensor locations – the distance apart and position of the sensors depends on the structure itself and the aim of the study (“local” or “global” monitoring). For concrete a maximum interspacing of 2 metres is usually reasonable. The choice of the right couplant is fundamental: while Cyanoacrylate adhesive glue can be very good for permanent monitoring, other solutions have to be found when the sensors need to be removed. Plasticine proved to be a good option. The use of clamps to hold the sensors in place is also advisable;
- Sensor calibration – the sensors need to be calibrated at the beginning and at the end of the test. The Schmidt Hammer is a quick and easy way to verify that all the transducers are working, whilst a pencil lead break [3] near to each sensor provides confidence on the sensitivity of the transducers.
- Condition of the structure – the presence of pre-existing crack or damage can affect the signal and its propagation and therefore has to be taken into account;
- Environment – less influencing when working in a lab, it becomes important when monitoring on-site. Factors such as wind and rain can heavily affect the recording and have to be considered when setting the threshold. In lab environment a threshold between 30-35dB is generally acceptable for concrete.

A summary of all the main factors can be seen in the sketch of Figure 1.

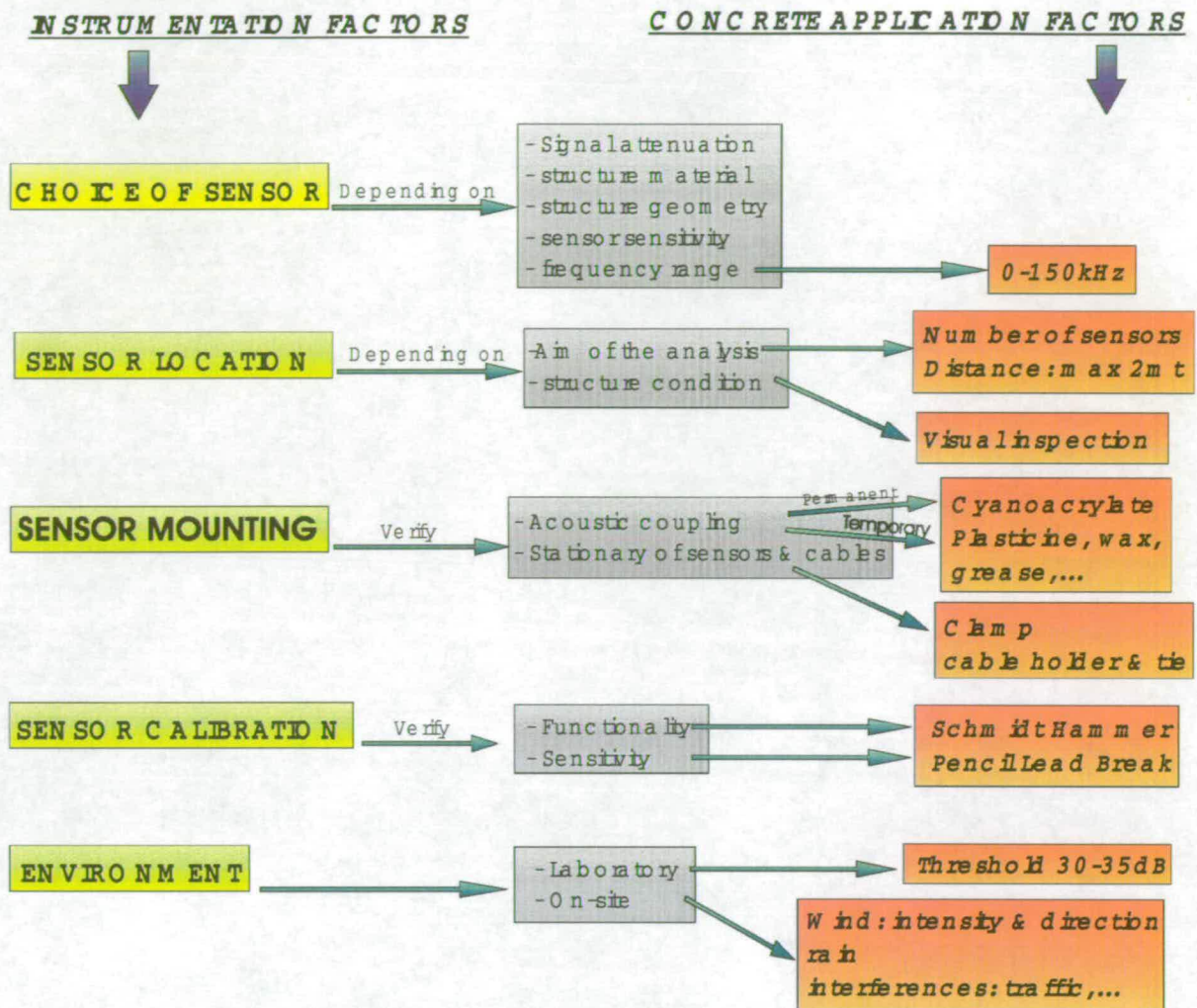


Figure 1. Sketch of the main factors influencing an AE test.

EXPERIMENT

The data refer to a test carried out on a RC beam in the Structures Laboratory of the University of Edinburgh. The beam (named beam BF2) was designed to represent the behaviour of a beam belonging to a real bridge. The experiment consisted of a four points load test of a simply supported beam. The load was applied in 10kN steps. During the test the beam was monitored using a Physical Acoustic (PAC) Mistras system. Eight PAC R6I sensors were mounted on the beam and set at a threshold of 35dB. The details of the beam and the sensor location can be seen in Figure 2.

During the test it was possible to identify different stages of cracking:

- cycle 01: no cracks;
- cycle 02 to cycle 05: cracks forming and the appearance of tensile cracks along the whole span of the beam;
- cycle 06: appearance of shear cracks at the two ends of the beam;
- after cycle 06: no new cracks growing; the old cracks opened up.

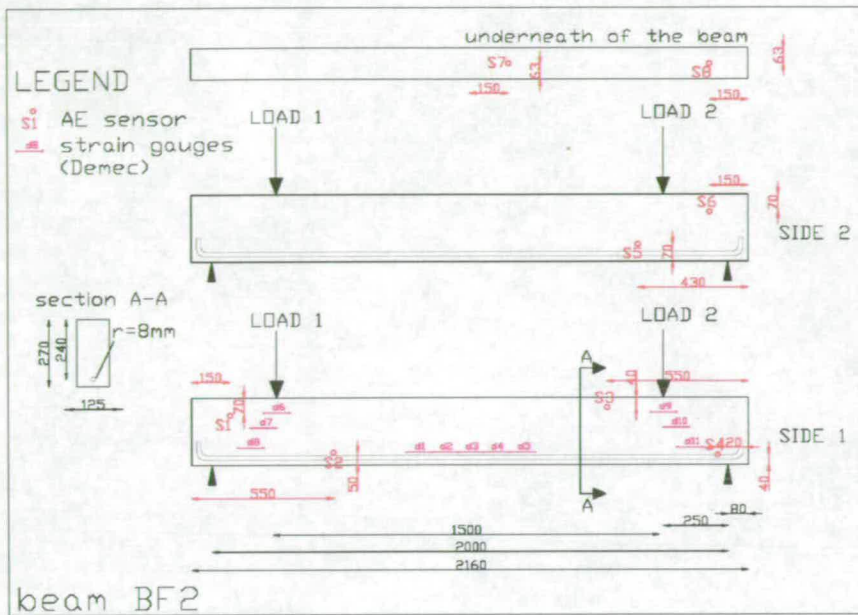


Figure 2. Designing details – Load configuration and AE sensors location on the beam. AE sensors are labelled S1-S8

AE ANALYSIS AND PROCESSING

Different types of damage and cracks generate different types of AE signals. These differences can be related to the degrees of damage of the structure and can be associated to different parameters of the AE data. The analysis presented in this paper focuses on some of these parameters and their interpretation.

AE LOCATION

The analysis of the AE location consists in locating the AE sources. These sources can then be compared with the crack pattern on the beam to see if there is any agreement.

A linear location (alongside the beam) was carried out using the Mistras software. The sources were located with reference both to the recorded events and energy and the results for two of the loading cycles are shown in Figure 3, where the black thick lines represent the cracks as they appeared on the specific cycle. The energy is calculated as the area under the envelope of the AE signal. A good relationship can be seen between the AE events and the cracks but it should be noted that the correlation with the cracks is stronger in terms of energy than events. This might be due to the fact that events generated by reflections, noise or interference can still be located but the energy associated with them is irrelevant. On the other hand, structurally meaningful events are characterised by a relevant amount of energy. The energy can be then considered as an effective parameter to indicate the damage of a structure.

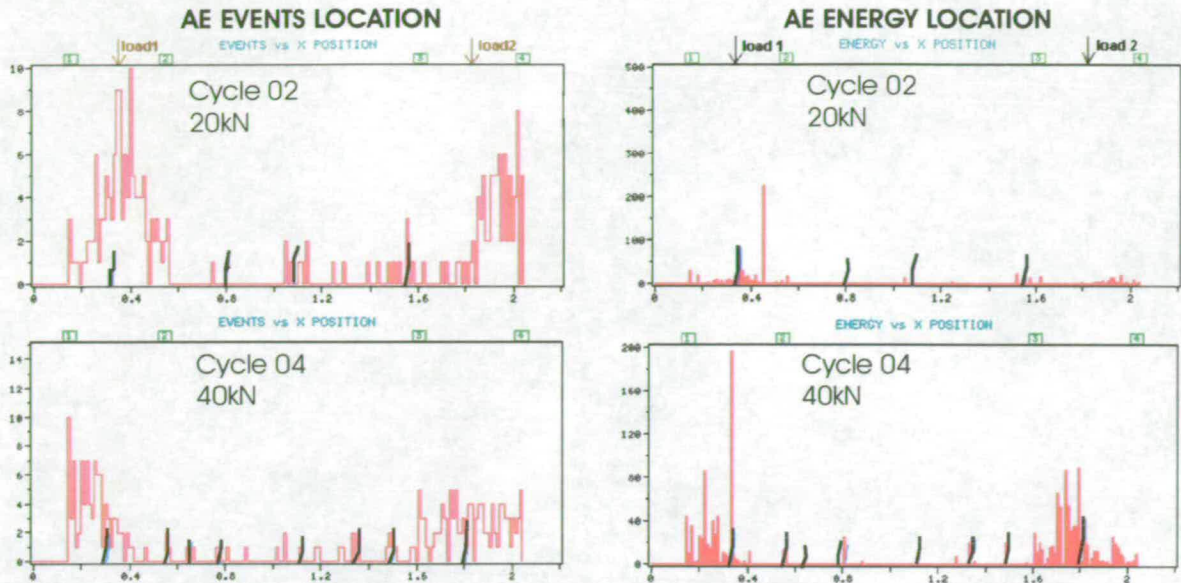


Figure 3. AE events and AE energy location during cycles 02 and 04.

B-VALUE ANALYSIS

In earthquake seismology events of larger magnitude occur less frequently than events of smaller magnitude. This fact can be quantified in terms of a magnitude-frequency relationship, for which Gutenberg and Richter proposed the empirical formula:

$$\log_{10} N = a - bM_L \quad (1)$$

where M_L is the Richter magnitude of the events, N is the incremental frequency (i.e. the number of events with magnitudes in the range of $M_L \pm \Delta M$), and a and b are empirical constants [4]. The Richter magnitude M_L is proportional to the logarithm of the maximum amplitude A_{max} recorded in a seismic trace, corrected for the attenuation in amplitude with distance due to wave propagation and inelastic absorption.

The same principle can be applied to the AE method to study the scaling of the "amplitude distribution" of the acoustic emission waves generated during the cracking process in the laboratory or in engineering structures. From the relationship (1), the b -value is the negative gradient of the log-linear AE frequency/magnitude plot and hence it represents the slope of the amplitude distribution. The b -value changes systematically with the different stages of fracture growth [5], so it could be used to estimate the development of fracture process. In terms of AE technique, the Gutenberg-Richter formula can be modified as:

$$\log_{10} N = a - b' A_{dB} \quad (2)$$

where now A_{dB} is the peak-amplitude of the AE events in decibels:

$$A_{dB} = 10 \log_{10} A_{max}^2 = 20 \log_{10} A_{max} \quad (3)$$

The b -value obtained with this relationship should be then multiplied by a factor of 20 to be comparable with the one used in seismology [6-7].

In general terms, when the distributed microcracks are occurring in the early stages of damage, the b -value is high and when the macrocracks begin to localise the b -value is low.

In the analysis presented in this paper, a conventional b -value analysis was applied on the data recorded on the RC beam, using the relationship (2) and assuming:

$$b = b' * 20.$$

The trend of the b -value was then compared with the development of the fracture process of the beam observed during the test.

The b -value was calculated using the least squares method for groups of 100 events during each loading cycle; the trend of the b -value was then plotted for each cycle and for each channel. The pattern was clearer in the early cycles when the cracks were forming as the presence of a large number of concentrated microcracks creates a clear pattern. However once the external macrocracks are formed (the beam is failing) the AE sources are fewer and more scattered so the pattern is less clear. This might imply that the analysis of the b -value is meaningful on good structures as it provides information between the microcracking beginning up to the stage where macro fractures occur by localisation.

The trend of the b -value for channels 3 and 7 during the second cycle of the test are shown in Figure 4; the load over time is shown on the same graph (dotted line). As the two sensors were located respectively on the end and on the middle area of the beam they can be considered to give a whole representation of the full beam. In both cases, the pattern shows a clear decrease at the beginning (the dashed line in the chart) when the load is going up, and then a transient during the relaxation when the load is held constant.

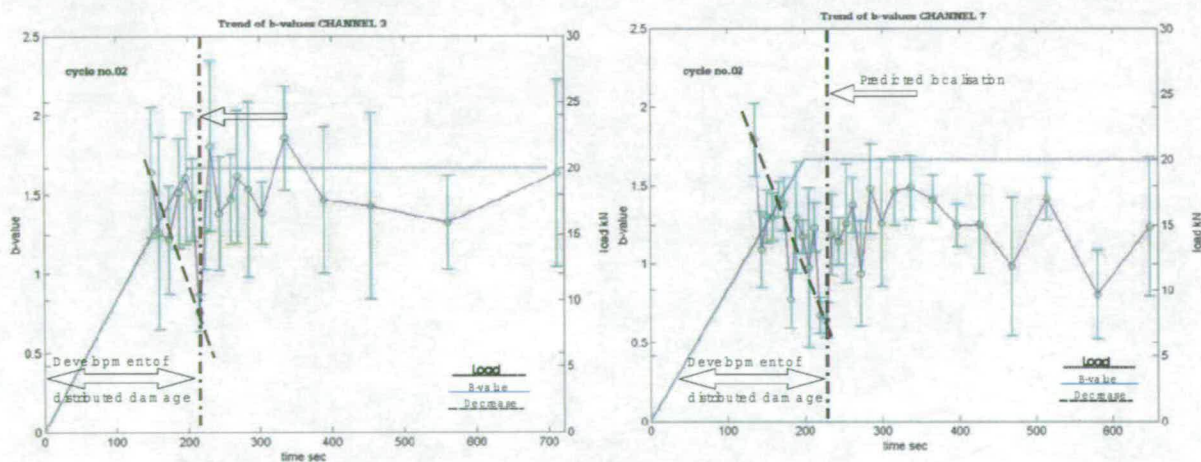


Figure 4. Trend of b -value over time for channel 3 (left) and 7 (right) during the load cycle number 2; the load is shown on the vertical axis on the right.

In a post-failure phase, the minimum and maximum value of the b -value was considered, for each cycle and for each channel. The trend of the range during the whole cycle and for each channel was then plotted. The minimum b -value trend suggests macrocracks have formed, whilst the maximum b -value trend implies microcrack growth. The chart of the trend for channel 3 and channel 7 during the whole experiment is shown in Figures 5.

The results for channel 3 (located near to the end of the beam) show that the maximum trend is increasing from cycle number 2 to 3, implying that microcracks are forming. A peak appears in cycle number 9 when all the cracks that formed in cycle number 2 are visibly opening up. The minimum trend is decreasing in the early stages, reaching a minimum in cycle number 4. When all the macrocracks had appeared on the beam, then from this point onwards the minimum trend is constant. The b -value evolution is in good agreement with the damage observed independently on the beam.

The results for channel 7 (located in the middle of the beam) show that the maximum trend decreases at the beginning, implying that microcracks are forming, but it then remains

constant as the cracks are uniformly spread. The peak at the end is unclear now, as this channel is too far from the shear cracks that are opening to be affected strongly by them. The minimum trend is decreasing in the first cycle and it stabilises afterwards when all the macrocracks had appeared on the beam.

In both cases, three stages of the fracture process can be identified. A first stage where the microcracks are dominant and the macrocracks are starting to appear. A second phase of constant range when the macrocracks are constant and uniformly distributed all along the beam. After this stage the cracks do not grow towards the top part of the beam (as the concrete is in compression) so a last stage can be identified when the macrocracks are opening up as the beam is failing.

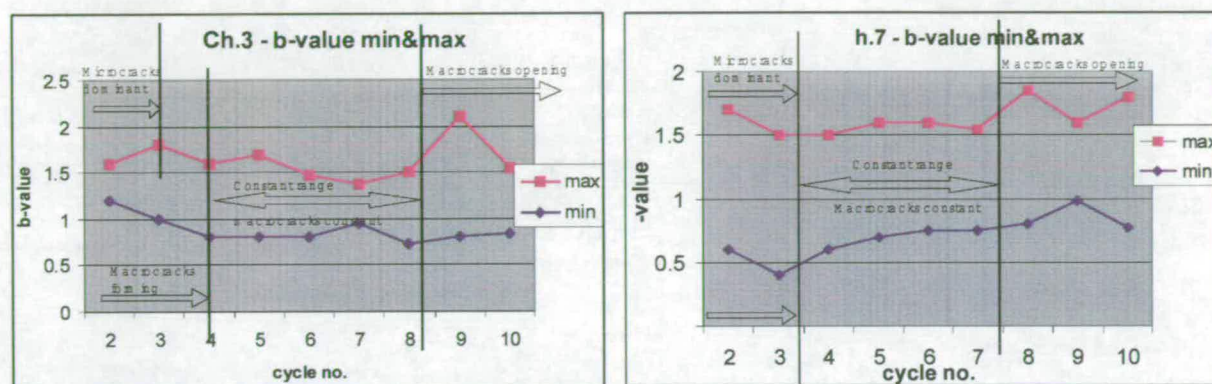


Figure 5. Trend of maximum & minimum b -value for channel 3 (left) and 7 (right) during the whole experiment.

CONCLUSIONS

The paper presents the results from a laboratory experiment on a RC beam. The beam was loaded in cycles and the acoustic emissions were recorded during the test.

- Some key points were drawn about the procedure to carry out an AE test.
- From a location of the AE sources, the AE energy appeared to be the most effective parameter to indicate the damage in a structure.
- A good relationship was found between the trend of the b -value and the microcracking and macrocracking observed during the test.
- The results confirmed that the b -value is correlated to the fracture process of the concrete and to the degree of localisation of damage.
- The minimum b -value trend suggests macrocracks have formed, whilst the maximum b -value trend implies microcrack growth.
- This study suggests that a b -value analysis could be used to interpret data obtained by a "local monitoring" of concrete bridges, although further work is needed in order to consolidate the results that were found and to make the b -value suitable for practical use.

ACKNOWLEDGEMENTS

The authors acknowledge the facilities of the University of Edinburgh and the financial support for this work of the Highways Agency (London), contract no. 3/320. Thanks are also due to the technical and support staff of the University for their help.

REFERENCES

1. Yuyama S., Okamoto T., Shigeishi M., Ohtsu M., Kishi T. (1998). "A proposed standard for evaluating structural integrity of reinforced concrete beams by acoustic emission", Acoustic Emission: Standards and Technology Update, ASTM STP 1353, S.J. Vahavilos, Ed., American Society for Testing and Materials, pp.1-12.
2. Colombo S., Forde M.C., Das P.C., Halliday J., (2001) "AE experiments on concrete beams: general overview and research in progress on bridges", Proceedings of the Structural Faults and Repair 2001, CD-ROM, 4-6 July 2001, London, ISBN 0947644474.
3. BS EN 1330-9:2000, "Non destructive testing – Terminology".
4. Shearer P.M.(1999), Introduction to Seismology. Cambridge University Press.,p189.ISBN 0 521 669537.
5. Sammonds P.R., Meredith P.G., Murrell S.A.F., Main I.G., (1994)"Modelling the damage evolution in rock containing pore fluid by acoustic emission", Eurock '94, Balkema, Rotterdam. ISBN 90 5410 502 X.
6. Shiotani T., Yuyama S., Li Z.W., Ohtsu M. (2000), "Quantitative evaluation of fracture process in concrete by the use of improved b-value". 5th Int. Symposium Non- Destructive Testing in Civil Eng, Ed. T. Uohoto, Amsterdam, Elsevier Science, 2000:293-302, ISBN 0080437176.
7. Shiotani T., Ohtsu M., Ikeda K. (2001), "Detection and evaluation of AE waves due to rock deformation". Construction and Building Material, Elsevier Science, Vol 15, No 5-6 2001:235-246.

AE ENERGY ANALYSIS ON CONCRETE BRIDGE BEAMS

Ing. S. Colombo & Prof. M. C. Forde
School of Engineering and Electronics
The University of Edinburgh - UK

J. Halliday
Highways Agency
London - UK

Prof. I.G. Main
School of GeoSciences
The University of Edinburgh - UK

Assoc. Prof. M. Shigeishi
Department of Civil Engineering
Kumamoto University - Japan

ABSTRACT

Concrete bridges were built originally to have a cost-effective maintenance free life of 120 years, however both in Europe and the USA this has proved to be totally optimistic. Concrete bridges require major maintenance after twenty to thirty years in order to extend their life. The Acoustic Emission technique has been successfully applied to monitor and provide information on the safety of concrete bridges, but the processing of the AE data is often not trivial. This paper proposes a method of AE analysis to assess concrete bridges based on the fact that the AE energy is one of the effective parameters to evaluate the damage of a concrete structure. Results from experiments on concrete with different design and loading configurations are presented. The beams were loaded in cycles and the energy during the loading and unloading phase was analysed. It was observed during the tests that none or very low energy activity was recorded during the unloading cycles. On the other hand such activity was increasing as the failure was approaching and the damage on the beams increased. In the light of these observations the energy recording during each loading up and loading off cycle was computed and a new parameter, the "relaxation ratio" was introduced. The final results were compared and combined and a proposed assessment criterion for the damage of concrete structures was obtained. It is argued that in some cases the state of damage of bridge beams can be estimated from the AE energy analysis when approximately 45% of the ultimate load has been applied. This criterion was then evaluated in relation to the quantitative assessment criterion recommended by the Japanese Society for Non-Destructive Inspection. Full laboratory data and analyses are given in the paper.

INTRODUCTION

Bridges represent a huge asset of a country with their importance lying in their functional and cultural significance. From the late 1960's to late 1970's the motorway construction boom in the UK gave rise to a large number of new concrete highway bridges, as concrete was perceived to be "maintenance free" and able to give bridges a 120 year life span. As a consequence, concrete bridges represent the majority of the UK motorway and trunk road bridge stock. Now that their average age is of the order of 25-35 years, they are starting to show signs of deterioration, demonstrating that the original construction expectation was too optimistic. The US bridge stock is older and faces a worse situation. Consequently, the necessity to monitor and verify the performance and safety for ongoing usage of concrete bridges is a matter of urgent concern. The Acoustic Emission (AE) technique has been successfully applied to monitor concrete bridges and to provide information about their structural condition, but the processing of the AE data is often not trivial. Moreover, during the evaluation of the safety of a bridge, it would be useful for the bridge engineer to be able to establish not only if the bridge is damaged, but also "how seriously" it is damaged. A quantitative way to assess the structural condition of a bridge is therefore highly desirable. The work presented herein approached this issue. A new type of parametric analysis of the AE data was developed on the base on a new defined parameter, the "relaxation ratio", that takes into account the AE energy recorded during the loading and unloading phase of an AE test. In the light of the results of this analysis, a criterion to assess the damage of concrete bridge beams was proposed. This criterion was then evaluated in comparison with the quantitative assessment procedure recommended by the Japanese Society for Non-Destructive Inspection (NDIS) (Ohtsu, 2002).

THE "RELAXATION RATIO" ANALYSIS

An AE test often consists of several load cycles, each of which generally includes two stages: a loading phase and an unloading phase. In the course of some experiments it was observed that during the early cycles of the tests, none or very low AE activity was recorded during the unloading of the specimens. The AE activity increased with the approach of failure and increasing damage of samples. In fact, AE activity observed during the unloading process is generally an indication of structural instability (Ohtsu, 2002).

A parallel can be drawn with earthquake sequences, recognised in seismology. Earthquakes generally are made up of *foreshock* and *aftershock* sequences which are closely associated with a larger event called the mainshock. A schematic illustration can be seen in Figure 1. Aftershocks follow the mainshock and are linearly proportional to the area of the mainshock rupture. Aftershocks typically begin immediately after the mainshock over the entire rupture area and its surroundings, or are generally concentrated around the rupture perimeter or in locations where the mainshock has newly produced high concentrations of stress. Therefore it can be said that aftershocks are a process of relaxing stress concentrations caused by the dynamic rupture of the mainshock. Foreshocks are smaller earthquakes that precede the mainshock. They generally occur in the vicinity of the mainshock hypocentre and are probably a part of the nucleation process (Scholz, 2002).

Keeping earthquake sequences in mind the failure of a specimen, or accumulated damage at the end of a load cycle, can be considered as the mainshock. The foreshocks and aftershocks can be seen as the acoustic emissions generated respectively during the loading and unloading phases. In the light of these preliminary observations, a "relaxation ratio" is proposed to quantify and compare the AE activity during the loading and unloading phases. As previous experiments had shown that the AE energy seems to be the most

effective parameter to describe the damage of a beam (Colombo *et al*, 2002) the relaxation ratio is expressed in terms of energy and defined as:

$RELAXATION\ RATIO = \text{average energy during unloading phase} / \text{average energy during loading phase}$

where the average energy is calculated as the cumulative energy recorded for each phase divided by the number of recorded hits. A relaxation ratio greater than one implies that the average energy recorded during the unloading cycle is higher than the average energy recorded during the corresponding loading cycle, therefore the relaxation (aftershock) is dominant. Vice-versa, the loading (foreshock) is dominant.

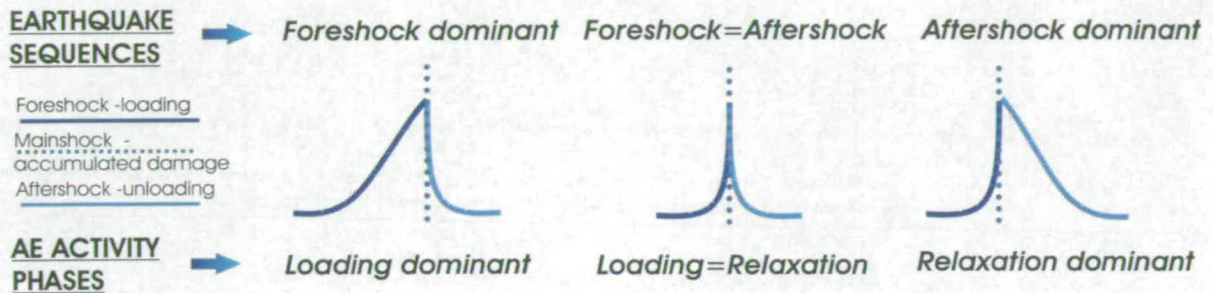


Figure 1. Schematic representation of earthquake sequences and AE activity phases.

NDIS ASSESSMENT PROCEDURE

The Japanese Society for Non-Destructive Inspection (NDIS) has recently proposed a criterion based on the Kaiser Effect to quantitatively assess concrete structures (Ohtsu, 2002). The criterion is based on the definition of two parameters:

$Load\ ratio = \text{load at the onset of AE activity in the subsequent loading} / \text{the previous load}$

$Calm\ ratio = \text{the number of cumulative AE activities during the unloading process} / \text{total AE activity during the last loading cycle up to the maximum.}$

The *Load ratio* is based on the concept of Kaiser Effect (Yuyama *et al*, 1998). A ratio greater than 1 is an indication of a structure in good condition, whilst a value less than 1 suggests the presence of damage. The *Calm ratio* refers to the generation of AE activity during unloading which is an indication of structural instability - as in a structure in good condition no acoustic emissions are generally recorded during this phase. The NDIS-2421 recommended an assessment chart based on a combination of these two parameters as shown in Figure 2.

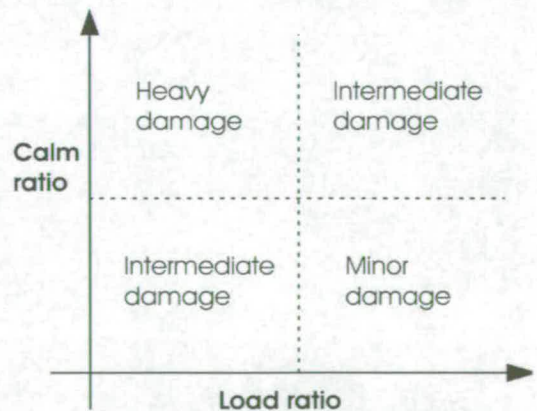


Figure 2. NDIS assessment Table.

The classification limits indicated by the dashed line in the figure need to be determined in advance, based on preliminary tests, in order to be used for practical applications (Ohtsu, 2002).

TEST DESCRIPTION

In order to have results representative of a significant variety of cases (in terms of type of failure, design, load configuration, concrete properties and type of sensor) the data related to several beams were analysed. Half of the beams were tested in Edinburgh (named beams BF2, BF3, BF2c, BF4, BF5 and BF6) whilst the remaining (named beams K1, K2, K3, K4, KL1 and KL2) were tested in Kumamoto, Japan. The beams were designed to be representative of the behaviour of concrete bridge beams. During the tests, they were simply supported and the load was applied at two points using hydraulic jacks that varied for the different specimens according to the type of failure that was to be achieved. The load was applied in cycles of varying steps, generally determined on the basis of the calculated designed failure load. A complete cycle consisted of two main sequential phases a loading up and an unloading phase. Beam BF2 was tested twice (renamed BF2c) - although it was seriously damaged it did not fail completely under the first load configuration. During the tests the beams were monitored using a PAC AE system and a varying number, location and type of sensors. A summarised description of all the tested beams is in Tables 1 and 2.

	<i>Section</i>	<i>Span</i>	<i>Reinf.</i>	<i>Concrete</i>	<i>wave vel.</i>	<i>Failure</i>	<i>Sensors</i>	<i>Threshold</i>
BF2	125x270	2m	Simply reinf.	25MPa	3800m/sec	shear	R6I	35dB
BF3	200x275	3m	Shear links at ends	25MPa	3700m/sec	shear	R6I	40dB
BF4	200x275	3m	Shear links at ends	25MPa	3300m/sec	bending	R6I & WD	35dB
BF2c	125x270	2m	Simply reinf.	Pre-damage	3300m/sec	shear	R6I & WD	35dB
BF5	200x275	3m	Simply reinf.	25MPa	3100m/sec	shear	R6I & WD	35dB
BF6	200x275	3m	Stirrups cage	25MPa	3100m/sec	bending	R6I & WD	35dB

Table 1. Summarised description of beam tested in Edinburgh.

	<i>Section</i>	<i>Span</i>	<i>Reinf.</i>	<i>Concrete</i>	<i>wave vel.</i>	<i>Failure</i>	<i>Sensors</i>	<i>Threshold</i>
K1	150x250	2.2m	Stirrups cage	45.99MPa	3600m/sec	bending	UT-1000	40dB
K2	150x250	2.2m	Stirrups cage	45.99MPa	3600m/sec	bending	UT-1000	43dB
K3	150x250	2.2m	Stirrups cage	45.99MPa	3600m/sec	bending	UT-1000	43dB
K4	150x250	2.2m	Stirrups cage	45.99MPa	3600m/sec	bending	UT-1000	43dB
KL1	150x250	2.2m	Simply reinf.	45.99MPa	3600m/sec	bending	UT-1000	43dB
KL2	150x250	2.2m	Simply reinf.	45.99MPa	3600m/sec	bending	UT-1000	43dB

Table 2. Summarised description of beam tested in Kumamoto.

RESULTS

The results are shown in Figures 3, 4 and 5. The dots on each graph represent the values of the relaxation ratio for each set of data and for all the cycles that composed the whole experiment relative to the specific sample. The number of the cycle is indicated on the horizontal axis, whilst the value of the relative relaxation ratio is shown on the vertical axis. The red horizontal line corresponds to a relaxation ratio equal to one. It therefore divides the area above the line, in which the relaxation phase is dominant, from the zone below the line, where the loading phase is dominant. According to the preliminary

observations, a dominance of the relaxation phase is then indicative of heavy damage on the beam.

Figure 3 shows the results related to the beams BF2, BF3, BF4 and BF2c. A common behaviour can be noted. Initially, the loading phase is dominant and the values of the relaxation ratio all lie below the red line. An inversion of trend occurs when the load reached a specific value of approximately 45% of the failure load of the sample and the relaxation phase then becomes dominant. The data related to the resonant sensors on beam BF2c indicate the change of trend at a lower percentage (36.9%). As the beam was pre-damaged, the resonant sensors might have been recorded more activity generated by the closing of the pre-existing crack during the relaxation phase. The general trend can be explained as a dominance of the primary AE activity (Iwanami *et al*, 1997) during the early stage of the fracture process when the cracks are forming and the damage is still restricted. Conversely, once the damage has seriously progressed, the secondary AE activity due to the friction of the existing cracks starts to prevail - manifesting itself during the relaxation phase of the tests.

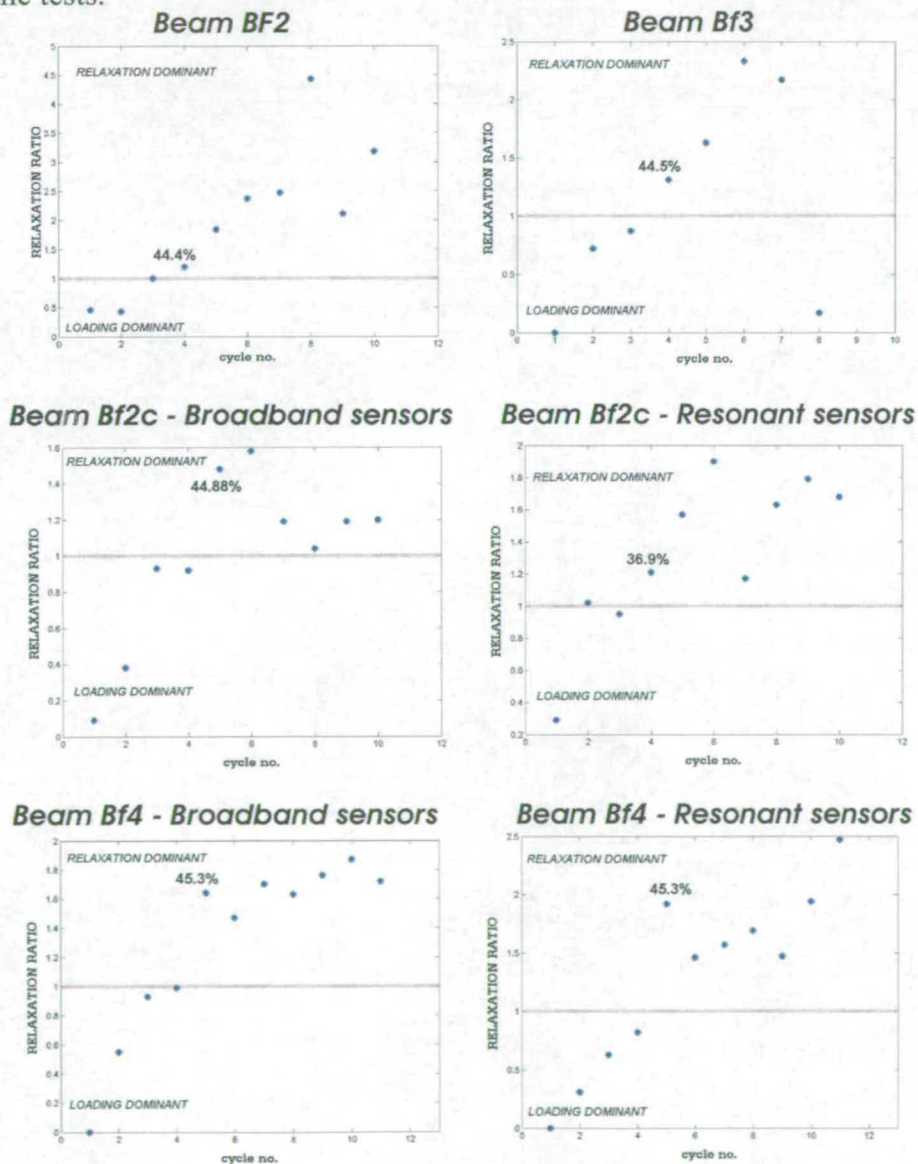


Figure 3. Relaxation ratio results for beams BF2, BF3, BF4 and BF2c.

Figure 4 illustrates the results of the data related to the beams K1, K2, K3, K4, KL1 and KL2. The data are more scattered and this is due to the fact that a higher threshold value was used than in the Edinburgh experiments (see Tables 1 and 2). The higher threshold generates a higher "noise to signal" ratio, resulting in the dispersion. However, no clear pattern can be identified in any of these six cases. In some graphs (beams K1, K4 and KL2), the relaxation ratio never exceeds the threshold value of one represented by the red line. In the remaining cases, some values go beyond the horizontal red line, but without a constant trend.

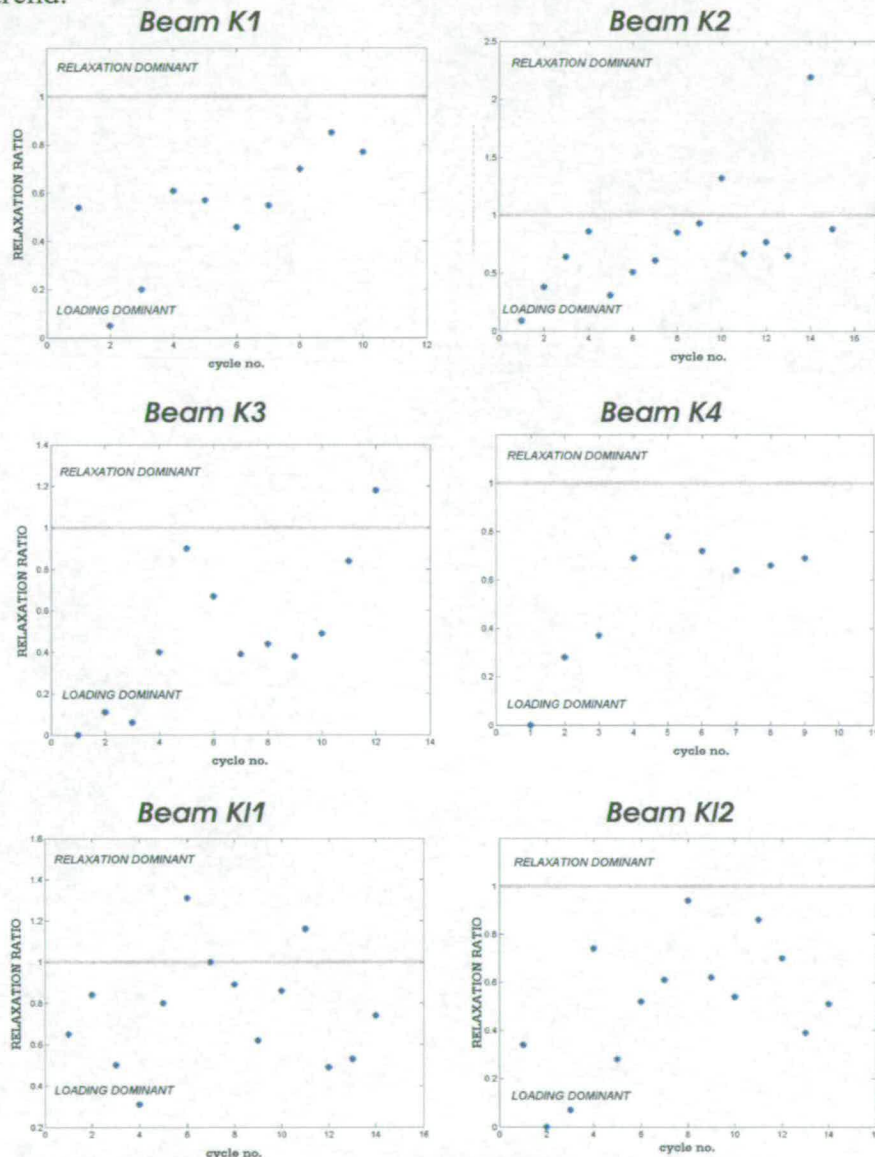


Figure 4. Relaxation ratio results for beams K1, K2, K3, K4, KL1 and KL2.

Two possible reasons can explain this different behaviour. The first possibility is related to the characteristics of the concrete. The concrete used in Japan had a much higher strength and thus it cracked at a higher level of stress. As AE derives from the energy released from the material, it seems reasonable to expect that higher stress should release a higher amount of energy. This could therefore be the reason for the dominance of activity recorded during crack nucleation and forming, i.e. during the loading phase. Secondly, the

load rate used in the test was different. An average value of loading rate was calculated by dividing the sum of the maximum load applied in each cycle for the total duration time of each cycle. An average value of approximately 0.06-0.07 kN/sec was found for the experiments carried out in Edinburgh, whilst a value of approximately 0.04-0.05 kN/sec was found for the experiments in Kumamoto. This could in fact have affected the generation of AE activity and therefore the results.

To have a further confirmation, the data related to the beams BF5 and BF6 were analysed and the results are shown in Figure 5. To verify the influence of the load rate, the load was applied and removed as slowly as possible. The average value of load rate was in fact calculated as approximately 0.04 kN/sec. By looking at the graphs referring to the resonant sensors, it is possible to note that a similar trend to the one observed in the previous Edinburgh experiments is present. The percentage of ultimate load to which the change of dominant phases occurs is however different, being 31.8% for beam BF6 and 83.6% for beam BF5. Looking at Table 1, the lower wave velocity measured on these beams suggests a lower quality of the concrete compared to all previous cases. The characteristics of the concrete and the lower load rate might have once again influenced the results.

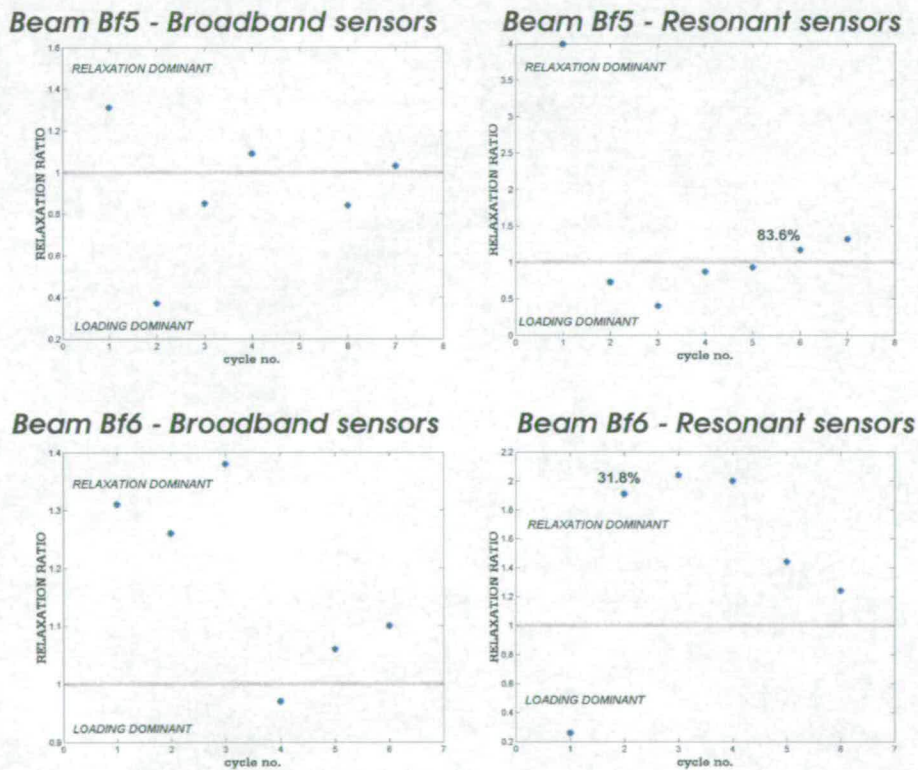


Figure 5. Relaxation ratio results for beams BF5 and BF6.

To evaluate the feasibility of the described analysis in the above section, a comparison with the quantitative assessment criterion proposed by the NDIS was carried out. Two cases were considered, beam BF4 for which the proposed method appeared to work and beam K2 for which it was not successful. The NDIS assessment procedure was then applied, using the data of the most active channel (number 5). The limits were determined graphically. The results are shown in Figure 6 with the load ratio and the calm

ratio indicated on the horizontal and vertical axes respectively. The number inside the circle represents the corresponding loading cycle number. For beam BF4, the change of trend during the relaxation analysis occurred during cycle number 5. It can be noted on the NDSI assessment table that that cycle corresponds to the last one falling into the intermediate damage area - after which serious damage takes place. The two results appear then to support each other.

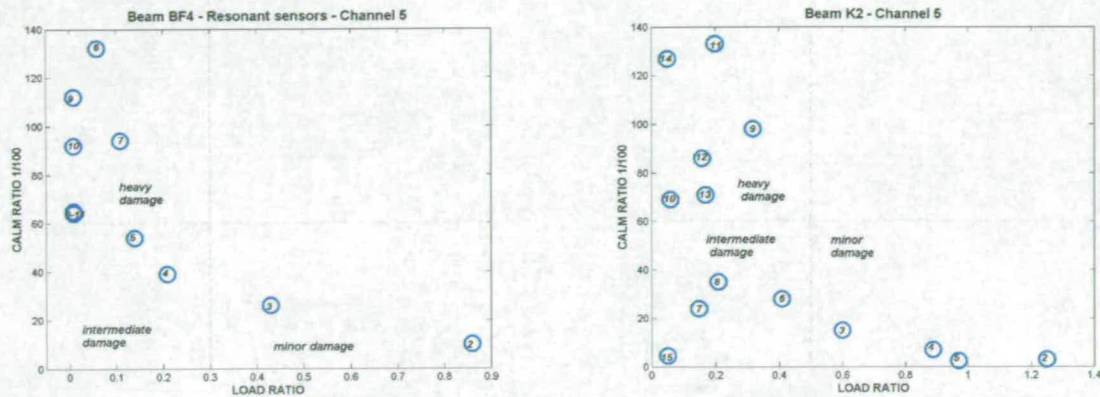


Figure 6. NDIS assessment results for beams BF4 and K2.

CONCLUSIONS

At this stage, only partial conclusions can be drawn. The method of analysis seems to be very promising and able to define the state of damage of concrete beams. A structurally serious damage condition should in fact result in the relaxation phase being dominant and thus a relaxation ratio greater than one. However, some of the results showed however a disagreement which is thought to be due to a combination of different properties of the concrete and load rate adopted during the tests. Further experiments are needed to evaluate in which specific conditions the analysis is successful and to establish the limits of its application. Once the limits are defined, a practical application to a full scale assessment load test on a real bridge is suggested. A new procedure is suggested using the AET and the relaxation ratio analysis. The assessment test would consist of cycles of loading and unloading, whilst monitoring it with an AE system. The load values should be based on the 45% of the expected ultimate load of the bridge where the significant change of trend would be expected. The relaxation ratio of each cycle should be calculated. A value greater than one would indicate serious damage, whilst a value minor than one would reassure about the condition of the bridge and its capacity to hold the expected load. Further work is needed to obtain final conclusions and thus confirm the feasibility of this type of analysis and eventual test procedure. On site trials would also be indispensable.

ACKNOWLEDGEMENTS

The authors acknowledge the facilities and the technical and support staff of the University of Edinburgh (UK) and of the University of Kumamoto (Japan). The financial support of Highways Agency (London) Contract No.3/320, the Small Project Grants of the University of Edinburgh Development Trust and the Academic Frontiers Student Exchange Promotion Program Scholarship of the Japanese Ministry of Education and Culture is greatly acknowledged.

REFERENCES


- Colombo S, Main I G, Forde M C, Halliday J, (2002), AE on bridges: experiments on concrete beams, Proc. of the EWAGAE 2002- 25th European Conf on Acoustic Emission Testing, Ed. P. Mazal, Czech Society for Non-destructive Testing, Prague, Czech Republic, 11-13 Sept., pp.127-134
- Iwanami M, Kamada T, Nagataki S, (1997), Application of acoustic emission technique for crack monitoring in RC beams, JCA Proc. of Cement and Concrete, Vol.51, pp.192-197.
- Ohtsu M , Uchida M, Okamoto T, Yuyama S, (2002), Damage assessment of Reinforced Concrete Beams Qualified by Acoustic Emission, ACI Structural Journal, Vol.99, No.4, pp.411-417.
- Scholz C H, (2002), The mechanics of Earthquakes and Faulting - 2nd Edition, Cambridge University Press, pp.224-228.
- Yuyama S, Okamoto T, Shigeishi M, Ohtsu M, Kishi T, (1998), A proposed standard for evaluating structural integrity of reinforced concrete beams by acoustic emission, Acoustic Emission: Standards and Technology Update, ASTM STP 1353- American Society for Testing and Materials, S.J. Vahavilos Ed., pp.1-12.

ACOUSTIC EMISSION TESTING


Short Course Attendance Certificate

This Certifies that Sabrina Colombo has been in attendance at the 15th Annual Short Course on Acoustic Emission held at Cambridge, United Kingdom, July 16 - 19, 2001 and has satisfactorily completed twenty-four hours of instruction in the scientific principles and technological applications of acoustic emission, and is hereby awarded this certificate in acknowledgment of knowledge and proficiency gained, and in recommendation of his acquirments.

In Witness Whereof, we have hereunto affixed our signatures and seal at Princeton, New Jersey, this 25th day of October, 2001.

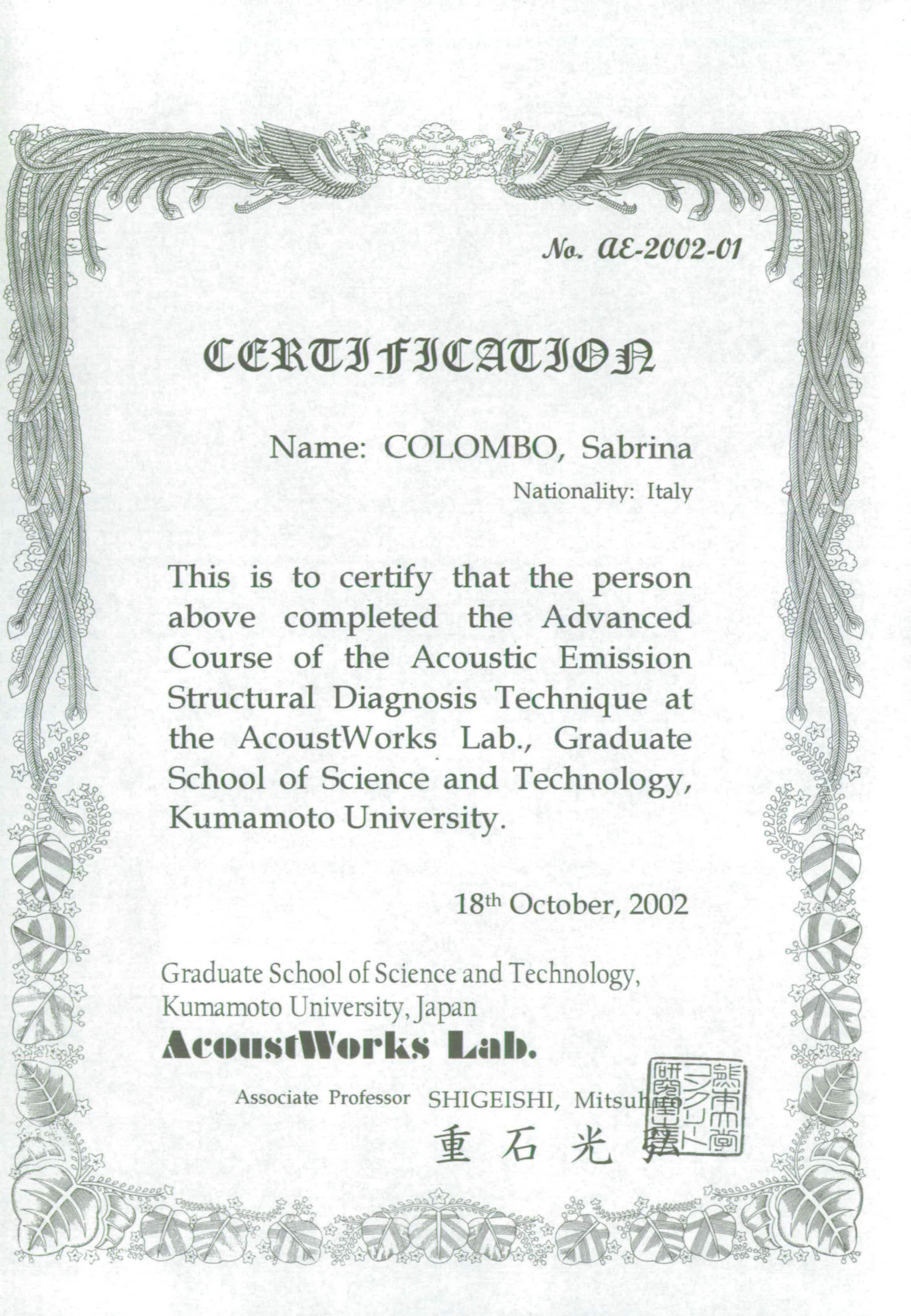

Adrian A. Pollock, Instructor


Phillip T. Cole, Instructor


Dr. Adrian A. Pollock, Director of Training,
PQ and Certification Programs

WORLD LEADER
IN
ACOUSTIC EMISSION

 **PHYSICAL
ACOUSTICS
CORPORATION**
A MISTRAS Holdings Company



No. AE-2002-01

CERTIFICATION

Name: COLOMBO, Sabrina

Nationality: Italy

This is to certify that the person above completed the Advanced Course of the Acoustic Emission Structural Diagnosis Technique at the AcoustWorks Lab., Graduate School of Science and Technology, Kumamoto University.

18th October, 2002

Graduate School of Science and Technology,
Kumamoto University, Japan

AcoustWorks Lab.

Associate Professor SHIGEISHI, Mitsuhiko

重石光彦



第二〇〇二一〇一号

修了証書

コロンボII

サブリナ殿

出身地 イタリア

あなたは熊本大学大学院
自然科学研究科において
AE構造診断学の全課程
を修了したことをここに
証明します

平成十四年十月十八日

熊本大学大学院自然科学研究科

重石光弘

